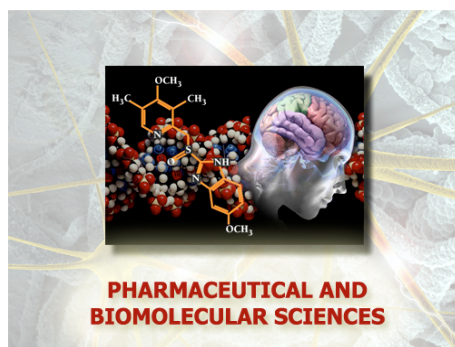


Università degli Studi di Torino



**Scuola di Dottorato in
Scienze della Natura e Tecnologie Innovative**

**Dottorato in
Scienze Farmaceutiche e Biomolecolari
(XXX ciclo)**



**Development of new therapeutic
approaches based on drug delivery, target
therapy and isolation of biomarkers**

Candidatoa: Benedetta Ferrara

**Tutor(s): Prof Roberto Fantozzi
Dr Chiara Dianzani**

Università degli Studi di Torino



**Dottorato in
Scienze Farmaceutiche e Biomolecolari**

**PHD THESIS CARRIED OUT AT:
Department of Drug Science and Technology**

**PHD CYCLE:
XXX**

**TITLE:
Development of new therapeutic approaches based on
drug delivery, target therapy and isolation of
biomarkers**

THESIS PRESENTED BY: Benedetta Ferrara

TUTOR(S): Prof. Roberto Fantozzi and Dr.ssa Chiara Dianzani

PHD COORDINATOR: Prof. Gianmario Martra

ACADEMIC PERIOD: 2014-2017

SCIENTIFIC FIELD: Pharmacology

Summary

AIM.....	3
BACKGROUND	7
Cancer	8
Cancer incidence.....	8
Cancer causes.....	9
Cancer features.....	12
Therapeutic approaches	17
NANO-DRUG DELIVERY	25
Nano- <i>drug delivery</i> in cancer.....	26
Functionalized nanoparticles	29
Drug resistance and nanoparticles	30
Toxicity of nanoparticles	30
Types of nanoparticles	33
Liposomes.....	33
Gold NPs.....	34
Quantum dots (QD).....	35
Superparamagnetic nanoparticles	36
Dendrimers.....	37
Solid lipid nanoparticles (SLNs).....	37
CD-NSs.....	39
Solid lipid nanoparticles carrying temozolomide for melanoma treatment...	43
Enhanced cytotoxic effect of camptothecin nanosponges in anaplastic thyroid cancer cells in vitro and in vivo on orthotopic xenograft tumors	43
CD-NSs and improvement of paclitaxel solubility.....	45
Introduction.....	47
Methods and results	48
Conclusion	49
CD-NSs and reduction of doxorubicin toxicity	54
Introduction.....	54
Methods and results	54
Conclusion	57
CD-NSs and responsiveness to GSH and pH	62
Introduction.....	62
Methods and results	62
Conclusion	64

Discussion	69
STUDY OF NEW TUMOR BIOMARKERS	75
Biomarkers and target therapy	76
Detection of Biomarkers for pancreatic cancer in extracellular vesicles.....	79
Pancreatic cancer	79
General features	79
Causes	80
Incidence and diagnosis	82
Therapy	84
Extracellular vesicles	86
Exosomes	89
Methods and results	93
Isolation of EVs	93
Internalization in HUVECs.....	94
Western blotting for the identification of exosomes.....	98
Analysis of exosomal protein content.....	99
Mouse strains and plasma EVs	102
Discussion.....	107
Osteopontin as tumor biomarker.....	110
General features	110
Role in inflammation	112
Role in angiogenesis	113
New insights on OPN activity.....	115
Thrombin cleavage of OPN in multiple sclerosis.....	115
Proteasome cleavage of OPN.....	121
Additional results	126
CD44 as key mediator of OPN effect	126
Discussion	132
OPN and cancer	135
Introduction.....	135
Methods and results	137
Discussion.....	145
Bibliography	147

AIM

My thesis had the aim to develop and investigate new therapeutic strategies for the treatment of cancer. In particular, two different approaches were carried out: the improvement of conventional anticancer drugs by nano-drug delivery and the study of new potential tumor biomarkers.

Part 1:

Concerning the first approach, we evaluated the effects of specific nanoparticles as systems for drug-delivery on different cancer models. Our study started from the assertion that to date, even if many new anticancer agents, such as immunotherapeutic drugs and inhibitors of tumor targets, were developed and continue to be studied, chemotherapeutic drugs still remain important for cancer treatment. However, most of these treatments present limitations because of the high toxicity towards healthy organs and tissues, and the acquisition of drug resistance. Therefore, an interesting goal for cancer therapy is to improve the characteristics of these 'old' anticancer drugs of already known pharmacokinetic and pharmacodynamic properties. Nano-drug delivery has been achieving lots of interest in cancer therapy, and nanoparticles able to incorporate hydrophilic and lipophilic drugs are being largely characterized in their different form. Resulting formulations permit a prolonged and controlled drug release directly into the tumor tissue in a specific way, allowing to employ lower drug doses, thereby reducing toxicity.

We focused our study on solid lipid nanoparticles (SLN) and β -cyclodextrin nanosponges (CD-NS) for the delivery of potent chemotherapeutic drugs, such as temozolomide, paclitaxel, camptothecin and doxorubicin, on *in vitro* and *in vivo* models of melanoma, thyroid and breast cancers.

Part 2:

The second approach of my PhD project was to identify and analyze new cancer biomarkers. Biomarkers' identification can give evidence of the presence of early stages cancers in patients without symptoms at the diagnosis. Biomarkers can also give important information about the individual's risk of developing cancer, prognosis or response to therapy. Moreover, some biomarkers can become targets for a specific therapy in order to prevent the development of the disease.

Starting from these considerations, we investigated the role played by extracellular vesicles (EVs) in pancreatic cancer. EVs are known to be involved in cancer intercellular communication, through the function of their cargo on cell signaling. Therefore, an analysis of EVs protein content was performed at the University of East Paris (CRRET laboratory), in order to identify new possible biomarkers that may allow to improve diagnosis and therapy for this highly lethal tumor.

Furthermore, the last study was performed to investigate the involvement of osteopontin (OPN), an ubiquitary protein acting among others as pro-inflammatory cytokine, in cancer. For this evaluation, we started from the analysis of OPN function in multiple sclerosis (MS), since OPN role in autoimmune diseases is well documented. Moreover, the inflammatory background that characterizes MS allowed us to investigate either the specific role played by the two (C- and N-terminal) OPN forms generated by thrombin cleavage during inflammation, and the role of another protease, that is the immune-proteasome, in generating OPN fragments which are able to exert different functions in the development of the disease.

The results obtained from the study of OPN in MS were extended to the subsequent analysis of its function in cancer. Indeed, the assessment of the different roles played by the cleavage generated forms of OPN allow to investigate the involvement of this important cytokine in the processes at the base of cancer pathogenesis.

BACKGROUND

Cancer

Cancer incidence

Cancer is the second leading cause of death globally, and was responsible for 8.8 million deaths in 2015 (“Cancer, Fact Sheet” 2017). The number of cancer cases and related deaths is expected to grow rapidly in line with population growth, age and adoption of lifestyles that increase the risk to develop the disease. Approximately 70% of deaths from cancer occur in low- and middle-income countries. Many of the lifestyle risk factors include tobacco and alcohol use, physical inactivity, excess body weight due to low fruit and vegetable intake. Cancer causing infections, such as hepatitis and human papilloma virus (HPV), are responsible for up to 25% of cancer cases in low- and middle-income countries (Plummer et al. 2016).

In order to report a statistical analysis of cancer incidence, in 2012, an estimated 14.1 million new cancer cases and 8.2 million cancer deaths occurred worldwide (Ferlay et al. 2013). Incidence rates in the 50 selected registries range from over 400 per 100,000 males and 300 per 100,000 females to less than 100 per 100,000 in both males and females. Mortality rates in the 50 selected countries range from over 200 deaths per 100,000 males and over 100 deaths per 100,000 females to less than 50 deaths per 100,000 in both males and females. For both sexes, the highest rates are generally in North America, Oceania, and Europe. Although there are many cancer types, only a few of them occur frequently. More than a million cases of cancer are diagnosed annually in the United States, and more than 500,000 Americans die of cancer each year. Cancers of 10 different body sites account for more than 75% of this total cancer incidence.

The four most common cancers, accounting for more than half of all cancer cases, are those of the breast, prostate, lung, and colon/rectum.

According to GLOBOCAN 2012, prostate cancer is the most commonly diagnosed cancer among males in 87 countries, especially in North and South America; Northern, Western, and Southern Europe; and Oceania. Lung cancer is the most commonly diagnosed cancer among males in Eastern Europe. In contrast with the consistency in the leading cancer within most regions, there is considerable heterogeneity in leading cancers among males in Africa and Asia. Among females, breast is the most common cancer in North America, Europe, and Oceania. Breast and cervical cancers are the most frequently diagnosed cancers in Latin America and the Caribbean, Africa, and most of Asia. However, the most common female cancers in Asia also include lung (China, North Korea), liver (Lao People's Democratic Republic, Mongolia), and thyroid (South Korea). These cancers account for more than 60% of total global cases and deaths (Ferlay et al. 2013).

In 2015, only 35% of low-income countries reported having pathology services generally available in the public sector. More than 90% of high-income countries reported treatment services are available compared to less than 30% of low-income countries. The economic impact of cancer is significant and is increasing. The total annual economic cost of cancer in 2010 was estimated at approximately US\$ 1.16 trillion (Stewart and Wild 2014).

Cancer causes

Cancer is caused by internal factors (mutations, hormones, and immune conditions) and environmental factors. Substances that can cause cancer are called carcinogens and have been identified by studies in experimental animals

and by epidemiological analysis of cancer frequencies in human populations. Since the development of malignancy is a complex multistep process, many factors may affect the likelihood that cancer will develop, and it is overly simplistic to speak of single causes of most cancers. Radiation and many chemical carcinogens act by damaging DNA and inducing mutations. These carcinogens are generally referred to as initiating agents, since the induction of mutations in key target genes is thought to be the initial event leading to tumour development (Cooper 2000). Tobacco and alcohol constitute two important factors to be considered. Tobacco use increases the risk of developing at least 14 types of cancer. In addition, it accounts for about 25–30% of all deaths from cancer and 87% of deaths from lung cancer and it is implicated in cancers of the oral cavity, pharynx, larynx, esophagus (Anand et al. 2008). The carcinogens in tobacco smoke (including benzo(a)pyrene, dimethylnitrosamine, and nickel compounds) are the major identified causes of human cancer. In total, it is estimated that smoking is responsible for nearly one-third of all cancer deaths—an impressive toll for a single carcinogenic agent. Several studies have revealed that chronic alcohol consumption is a high risk factor for cancer of the upper aerodigestive tract, including cancer of the oral cavity, pharynx, hypopharynx, larynx, and esophagus, but also cancer of liver, pancreas, mouth, and breast. Also diet is linked to cancer deaths, such in 70% of colorectal cancer cases. How diet contributes to cancer is not fully understood. Most carcinogens are ingested, such as nitrates, nitrosamines, pesticides, and dioxins, and they come from food additives or from cooking. According to an American Cancer Society study (ACS) (Calle et al. 2003), obesity has been associated with increased mortality from cancers of the colon, breast, endometrium, kidneys, esophagus, gastric, pancreas, prostate, gallbladder, and liver. Increased modernization and

a Westernized diet and lifestyle have been associated with an increased prevalence of overweight people in many developing countries (Drewnowski and Popkin 1997). Findings from this ACS study suggest that of all deaths from cancer in the United States, 14% in men and 20% in women are attributable to excess weight or obesity. For instance, hyperglycemia, has been shown to activate NF- κ B (Nareika et al. 2008), which could link obesity with cancer. Moreover, several cytokines produced by adipocytes, such as leptin, tumor necrosis factor (TNF), and interleukin-1 (IL-1) are known to activate NF- κ B. Hormones, particularly estrogens, are important as tumor promoters in the development of some human cancers. The proliferation of cells of the uterine endometrium, for example, is stimulated by estrogen, and exposure to excess estrogen significantly increases the likelihood that a woman will develop endometrial cancer (Cooper 2000).

Moreover, there is evidence that in the world, an estimated 17.8% of neoplasms are associated with infections; this percentage ranges from less than 10% in high-income countries to 25% in African countries (Pisani et al. 1997; Parkin 2006). Human papillomavirus, Epstein Barr virus, Kaposi's sarcoma-associated herpes virus, human T-lymphotropic virus 1, HIV, HBV, and HCV are associated with risks for cervical cancer, anogenital cancer, skin cancer, nasopharyngeal cancer, Burkitt's lymphoma, Hodgkin's lymphoma, Kaposi's sarcoma, adult T-cell leukemia, B-cell lymphoma, and liver cancer. These viruses are important not only as causes of human cancer, but also studies on tumor viruses have played a key role in elucidating the molecular events responsible for the development of cancers induced by both viral and nonviral carcinogens. Another factor that is responsible for the growing risk of developing cancer is environmental pollution. It includes outdoor air pollution by carbon particles

associated with polycyclic aromatic hydrocarbons (PAHs); indoor air pollution by environmental tobacco smoke, formaldehyde, and volatile organic compounds such as benzene and 1,3-butadiene (which may particularly affect children); food pollution by food additives and by carcinogenic contaminants; carcinogenic metals and metalloids; pharmaceutical medicines; and cosmetics. Finally, a physical factor that induces cancer in a stochastic way is radiation. Up to 10% of total cancer cases may be induced by radiation (Belpomme et al. 2007), both ionizing and nonionizing, typically from radioactive substances, ultraviolet (UV) and pulsed electromagnetic fields. Cancers induced by radiation include some types of leukemia, lymphoma, thyroid cancers, skin cancers, sarcomas, lung and breast carcinomas.

Cancer features

Cancer is a pathological process that derives from abnormal proliferation of any of the different cell types in the body, so there are more than a hundred distinct types of cancer, which substantially vary also in behavior and response to treatment. The most important issue in cancer pathology is the distinction between benign and malignant tumors. While benign tumours remain confined to their original location, not invading surrounding normal tissue or spreading to distant sites, malignant tumour are able of both invading surrounding normal tissue and spreading throughout the body via the circulatory or lymphatic systems, giving life to metastasis. The ability of cancer to invade and metastasize makes it so dangerous. Both benign and malignant tumors are classified according to the type of cell from which they derive. Most cancers fall into one of three main groups: carcinomas, sarcomas, and leukemias or lymphomas. Carcinomas include approximately 90% of human cancers and

regard epithelial cells. Sarcomas are rare in humans and they are solid tumors of connective tissues, such as muscle, bone, cartilage, and fibrous tissue. Leukemias and lymphomas account for approximately 8% of human malignancies and involve blood-forming cells and immunitary cells, respectively. A classification of tumours is also based on their tissue of origin and on the cell type involved. For example, fibrosarcomas arise from fibroblasts, and erythroid leukemias from precursors of erythrocytes.

One of the fundamental features of cancer is tumour clonality, the development of tumors from single cells that start an abnormal proliferation. The clonal origin of tumors does not, however, mean that the original progenitor cell that gives rise to a tumour has initially acquired all of the characteristics of a cancer cell. On the contrary, the development of cancer is a multistep process in which cells gradually become malignant through progressive alterations. One indication of the multistep development of cancer is that most cancers develop late in life. Such a dramatic increase of cancer incidence with age suggests that most cancers develop as a consequence of multiple abnormalities, which accumulate over periods of many years. At the cellular level, the development of cancer involving mutation and selection for cells with progressively increasing capacity for proliferation, survival, invasion, and metastasis. This is due to the fact that the new mutations confer a selective advantage, such as more rapid growth, and the descendants of a cell bearing such a mutation will consequently become dominant within the tumor population. This process is called “clonal selection”, and it continues throughout tumor development, so tumors continuously become more rapid-growing and increasingly malignant. The uncontrolled proliferation of tumour cells *in vivo* is mimicked by their behavior in cell culture. A primary distinction between cancer cells and normal cells in culture is that

normal cells proliferate until they reach a finite cell density, which is determined in part by the availability of growth factors added to the culture medium. On the contrary, many cancer cells have reduced requirements for extracellular growth factors and so, in some cases, tumour cells produce growth factors that stimulate their own proliferation. This process is called “autocrine growth stimulation”. Another characteristic of many cancer cells is the loss of cell-cell and cell-matrix adhesion, often as a result of reduced expression of cell surface adhesion molecules. Therefore, cancer cells are unrestrained by interactions with other cells and tissue components, contributing to the ability of malignant cells to invade and metastasize. The reduced adhesiveness of cancer cells also leads to morphological and cytoskeletal alterations. Moreover, tumor cells are not affected by the phenomenon of contact inhibition and they continue moving after contact with their neighbors, migrating over adjacent cells, and growing in disordered patterns. Two additional properties of cancer cells play important roles in invasion and metastasis. First, malignant cells generally secrete proteases that digest extracellular matrix components, allowing cancer cells to invade adjacent tissues. Second, cancer cells secrete growth factors that promote the formation of new blood vessels in order to support their growth. The formation of such new blood vessels is important not only in supporting tumor growth, but also in providing a ready opportunity for cancer cells to enter the circulatory system and metastasize. Finally, cancer cells do not differentiate normally. Indeed, they are usually blocked at an early stage of differentiation, consistent with their continued active proliferation (Cooper 2000).

Metastasis is the first cause of cancer morbidity and mortality (90% of cancer related deaths). The term metastasis generally indicates the spread of cancer

cells from a primary tumour to adjacent or distant organs (Tarin 2011; Chambers, Groom, and MacDonald 2002). Some cancer types predominantly spread to one organ or show sequential organ specific colonization (for example, colorectal cancer frequently metastasizes first to the liver, later to lungs and brain). Other cancer types, such as breast cancer, lung cancer, or melanoma, are able to colonize many different organ sites, either sequentially or synchronously (Nguyen, Bos, and Massagué 2009; Budczies et al. 2014; Urosevic et al. 2014). While defined organ tropisms are not rigid phenomena, the organ-specific patterns of metastasis are clear. Beyond lymph node spread, the liver, lung, bone and brain are frequently colonized by a variety of cancer types. The skin, ovaries and spleen are less common sites of metastasis. Skin metastases generally occur in melanoma and breast cancer, ovarian metastases in breast and gastric cancers, and spleen metastases almost exclusively in melanoma (Budczies et al. 2014). Although some general mechanisms of dissemination enable cancer cells to leave the primary tumour and reach distal organs, more specialized mechanisms might be necessary for the infiltration of specific organs. Infiltration into these organs is influenced in part by circulation process (Obenauf and Massagué 2015). In colorectal carcinoma, the mesenteric circulation from the bowels and the permissiveness of the liver capillary sinusoids are thought to favour liver metastasis (Paku et al. 2000; Lalor et al. 2006). The second most frequent sites of metastasis are the lungs (K. R. Hess et al. 2006). However, in addition to the influence of haematogenous dynamics, colon carcinoma cells preferentially adhere to the liver and lung endothelium, suggesting the existence of specific molecular interactions that promote the retention of tumour cells in these organs (Schlüter et al. 2006). The role of unique endothelial surface molecules as target sites for compatible

disseminating cancer cells has been shown in breast cancer cell lines overexpressing the cell adhesion molecule metadherin. Indeed, in a mouse model, Brown et al. demonstrated that metadherin specifically bound to the pulmonary vasculature and enhanced lung metastasis (D. M. Brown and Ruoslahti 2004).

Metastasis involves a series of sequential passages that include detachment of cancer cells from the original tissue, intravasation into circulatory and lymphatic systems, extravasation at distant capillary vessels, and invasion of distant organs (Bacac and Stamenkovic 2008; Duffy, McGowan, and Gallagher 2008). Metastatic cells also establish a microenvironment that facilitates angiogenesis and proliferation, resulting in macroscopic, malignant secondary tumors. Invasion of cancer cells into surrounding tissues and vasculature is one of the first steps. For this process, a chemotactic migration of cancer cells involves protrusive activity of the cell membrane and its attachment to the extracellular matrix (H. Yamaguchi, Wyckoff, and Condeelis 2005). The loss of cell-cell adhesion capacity allows malignant tumor cells to dissociate from the primary tumor mass and changes in cell-matrix interaction enable the cells to invade the surrounding stroma. This involves the secretion of substances to degrade the basement membrane and extracellular matrix and also the expression/suppression of proteins involved in the control of motility and migration. Moreover, cancer cells adhesion to endothelium and subsequent blood intravasation are key processes that precede cell migration in the circulatory system (Martin et al. 2013). Recent advances in *in vitro*, including migration and adhesion assays, and *in vivo* studies have provided new insights into the molecular mechanisms of cell protrusive activity and chemotactic migration (H. Yamaguchi, Wyckoff, and Condeelis 2005). Various mechanisms

that confer invasiveness, such as cellular motility and basement membrane degradation, have been proposed to mediate cancer cell entry into the circulation (Kedrin et al. 2007; G. F. Weber 2008). Also deregulated cytoskeletal modifiers such as RHOC can specifically enhance metastatic dissemination (Clark et al. 2000). Another example can be the aberrant expression of developmental transcription factors that might trigger EMT, which can be associated with cellular plasticity and invasion (Yang and Weinberg 2008).

For the metastatic invasion of cancer cells, the processes of angiogenesis and lymphangiogenesis are essential in order to supply nutrients, oxygen, and also to remove waste products (Folkman 1971). The basement membrane is firstly injured, therefore destruction and hypoxia occur. In a second moment, endothelial cells activated by angiogenic factors migrate, and then endothelial cells proliferate and stabilize. Finally, angiogenic factors contribute at influencing the formation of new vessels. There are activator and inhibitor molecules that regulate this process (Nishida et al. 2006). The new formed vessels are not completely defined but present fenestrations that enhance vasculature permeability, and moreover, the lymphatic tumour system is poorly operational and macromolecules leaking from the blood vessels can accumulate into the tumour site. This phenomenon is known as “enhanced permeability and retention (EPR) effect” (Davis, Chen, and Shin 2008), and will be exploited in nanomedicine in order to use nano-size particles for the delivery of drugs directly into the tumour tissue.

Therapeutic approaches

Surgery is the first and the most effective treatment of localized primary tumor. Surgery operates by zero-order kinetics, in which 100% of excised cells are killed.

With the advent of radiation therapy in the 1920s and chemotherapy after the 1940s, cancer surgery has become conservative. In contrast to surgery, chemotherapy and radiation therapy are only capable of killing a fraction of tumor cells by each treatment. Both processes are complementary (Delaney et al. 2005). Radiotherapy is responsible for 40% of cancer cure providing an excellent cost-effectiveness ratio since it is responsible of only a 5% of the total budget dedicated to cancer control in industrialized countries. The most common use of radiotherapy is in combination with surgery and/or chemotherapy. Preoperative radiotherapy is used in a limited number of tumour locations such as rectal and oesophageal carcinomas while postoperative radiotherapy is used in many tumor sites including breast and central nervous system tumors among others (Urruticoechea et al. 2010).

Chemoradiotherapy approaches have been shown to improve local control and also micrometastatic disease. For almost a century, systemic therapy of cancer has been dominated by the use of cytotoxic chemotherapeutics. Most of these drugs are DNA-damaging agents that are designed to kill or inhibit rapidly dividing cells. They are often administered in single doses or short courses of therapy at the highest doses possible without no life-threatening levels of toxicity (Kerbel and Kamen 2004; Hanahan, Bergers, and Bergsland 2000). The high doses of chemotherapics require an extended treatment-free period to permit recovery of normal host cells, for example through the administration of growth factors (Bailar and Gornik 1997).

In the last years, a lot of studies gave life to the era of 'targeted therapy'. Indeed, several new biotechnological drugs have been developed, directed to many cancer targets in a selective and specific manner. Even if each cancer is expected to have its own spectrum of mutations, some aberrations in signalling are

present in many cancers. The new targets include growth factors, signalling molecules, cell-cycle proteins, modulators of apoptosis and molecules that promoted angiogenesis. Two main approaches have been proposed for use in clinical practice of specific molecular targeting: therapeutic monoclonal antibodies (mAbs) - that deplete the tumour of growth factors or block growth factor- receptor interactions - and small agents that target various mechanisms of transduction of the growth signal and its execution. These agents should be metabolically stable, with a long half-life in model systems and in humans, well-absorbed after oral administration, and should show a favourable toxicity profile at biologically effective doses, with limited effects on bone marrow and intestinal epithelium (Urruticoechea et al. 2010).

Among all developed mAbs, trastuzumab is a therapeutic mAb having received regulatory approval for the treatment of breast cancer. It demonstrates high affinity for the extracellular domain of ErbB2 and is a potent inhibitor of the proliferation of breast cancer cells overexpressing ErbB2. HER-2/neu is a receptor belonging to a family of four transmembrane receptor tyrosine kinases that mediate cell growth, differentiation, and survival (Yarden and Sliwkowski 2001). HER- 2/neu-positive breast cancer is an aggressive type that has a high rate of recurrence and short disease- free intervals after adjuvant chemotherapy. The ErbB2 receptor is also an accessible extracellular target for specific anticancer treatment. Trastuzumab promotes accelerated ErbB2 internalization and degradation, induces antibody-dependent cytotoxic responses depending on the level of ErbB2 expression and inhibits the growth of ErbB2- positive human tumor xenografts.

Among target inhibitors, imatinib is a moderately potent inhibitor of the kinase BCR- ABL, the fusion protein product of a chromosomal translocation that is

involved in the pathogenesis of chronic myeloid leukaemia (CML), a clonal hematopoietic stem cell disorder that accounts for 15–20% of all cases of leukemia. Imatinib also inhibits the KIT tyrosine kinase and platelet derived growth factor receptor- (PDGFR) tyrosine kinase. These latter effects have been successfully exploited for therapy of gastrointestinal stromal tumours and the hypereosinophilic syndrome, respectively. Another strategy is to inhibit tumour angiogenesis, that is regulated by numerous pro-angiogenic factors such as vascular endothelial growth factor (VEGF), angiopoietin, basic fibroblast growth factor (bFGF), placenta-like growth factor (PlGF), platelet-derived growth factor (PDGF), and IL-8, as well as the anti-angiogenic factors angiostatin, endostatin, thrombospondin or a tissue inhibitor of metalloproteinase (TIMP). So far, VEGF- α and its receptors are the best-characterized signalling pathways in developmental angiogenesis (Folkman 1971; Holash et al. 1999; Hurwitz et al. 2004). VEGF- α binds to two receptor tyrosine kinases (RTK), VEGFR-1 (Flt-1) and VEGFR-2 (KDR, Flk-1). It is now generally agreed that VEGFR-2 is the major mediator of the mitogenic, angiogenic and permeability-enhancing effects of VEGF- α . Different pharmacological inhibitors have been designed to specifically block angiogenesis, such as bevacizumab (a specific blocking VEGF- α antibody), but they must be used in association with other anticancer drugs, since in monotherapy they reported to be inefficient in the majority of cases.

Moreover, in the last years, another emerging strategy in the treatment of cancer is constituted by gene therapy, that implies procedures intended to treat or alleviate a disease by genetically modifying the cell of a patient (Strachan 1999). The material to be transferred into patient cells may be genes, gene segments, or oligonucleotides. Once the transgene enters a cancer cell, it can then assist in its death or restore normal cellular functions, whereas for normal

cells, the transgene can protect them from drug-induced toxicities, or activate an immune cell to get rid of the cancer cell. Gene and vector-based molecular therapies for cancer comprise a wide range of treatment modalities to modify cancer cells, normal cells, and/or a tumor microenvironment (Weichselbaum and Kufe 1997; Amer 2014).

However, the spread of malignant tumors to distant body sites frequently makes them resistant to such localized treatment. Relapse following systemic treatments might be due to cell-intrinsic mechanisms such as genetic alterations that confer drug resistance following a period of therapeutic response. For example, lung adenocarcinomas with epidermal growth factor receptor (EGFR) mutations respond to EGFR kinase inhibitors but frequently relapse owing to secondary EGFR mutations that confer resistance (Sharma et al. 2007). Certain mechanisms of drug resistance might simultaneously render the tumour more competent for metastasis.

Although several therapies might select for specific metastatic traits, however aggressive metastatic cells could also emerge independently of intervention and be intrinsically resistant to subsequent treatment. This might be particularly relevant in rapidly progressing tumour types, such as lung cancer and metastatic melanoma.

Another approach for finding a different way to reach and destroy the tumour can be achieved by investigating new messengers that can be present not only in cancer cells but also in the tumour microenvironment and which may play important functions in cancer progression. For example, panitumumab is a fully humanized IgG2 mAb that binds to extracellular domain of the EGFR of tumor and normal cells with high affinity. By competing with endogenous ligand binding, this mAb inhibits receptor phosphorylation and activation of EGFR

associated cell signaling, with antitumor effects of inhibition of tumor growth, induction of apoptosis and inhibition of angiogenesis in colorectal cancer (Hocking and Price 2014).

Other promising and active areas for the realization of new therapeutic strategies is the modulation of the immune response with biologics, an approach called “immunotherapy”. In fact, the immunitary system is perturbed in cancer and its activation to target and eliminate malignancies is recognized as one of the most promising directions for cancer therapy. For example, ipilimumab is the first-in-class immunotherapeutic drug (targeting CTLA-4) that received FDA approval for the treatment of metastatic melanoma in 2011 (Ramagopal et al. 2017).

Although great strides have been made in antibody engineering and target cancer therapy, there are some limitations on the use of these new drugs. The major challenge is that among cancer patients there is a wide variability in terms of some expressed proteins and targets. Even if many cancers may look the same, not all patients express the same antigen against which a specific mAb or cancer vaccine is targeted. In general, response rates to targeted therapy appear to be around 25% (Coulson, Levy, and Gossell-Williams 2014). Moreover, tumour cells can accumulate mutations during the course of the disease, and thereby their antigens at which the therapy is directed can change becoming no longer recognized. In order to optimize this type of therapy, it will be necessary to identify each subgroup of patients with a specific cancer and develop therapies targeted to, or directed specifically at, their individual cancers (Cel-Sci, n.d.).

Concerning side effects related to the use of new biological drugs, they result to be milder compared with conventional chemotherapy, while conjugated mAbs

precipitate severe adverse effects (Hansel et al. 2010). These adverse effects are commonly related to the antigens they target and the intravenous route of administration. Other common adverse effects are chills, weakness, headache, nausea, vomiting, diarrhoea, hypotension and rashes.

Finally, although great strides have been made in antibody engineering and target cancer therapy, production cost is estimated at twice that required for conventional drugs (Craik et al. 2013). Production requires the use of very large cultures of cells, which are expensive to maintain, primarily as a consequence of high turnover of disposables, such as media, and the continuous requirement for sophisticated purification steps to ensure clinical quality (Farid 2007). Thereby, the cost to the users is restrictive. Moreover, while the introduction of substitutes (generics) for innovator brands of drug molecules provides cost savings of 80% to USA medical expense, no such benefit occurs with the biological substitutes (biosimilars), where the savings amounts to 30% at best (Walsh 2014; Chow 2013).

To date, conventional chemotherapeutic drugs still remain important for cancer treatment, eventually for second line therapy, since their major limitations, such as acquisition of drug resistance and patient relapse, still exist with currently marketed biological drugs, such as mAbs and TKIs. As a consequence, the future success of targeted cancer therapeutics will be also dependent on overcoming these obstacles.

In the last years, a strategy emerging as a goal for cancer therapy, is to improve the characteristics of 'old' drugs of well known efficacy but related high toxicity. Several many chemotherapeutic drugs present problems due to some intrinsic characteristics of the molecule, such as low instability and insolubility, and lack of specificity towards cancer cells. Moreover, as before reported, cancer cells

develop a high resistance against most potent anticancer drugs during the course of the disease. Therefore, an increasing dose of the drug is required to obtain a therapeutic effect, but it can lead to a high cytotoxicity towards normal cells. The problem of toxicity considerably limits the usage of many chemotherapeutic agents. Among several approaches developed with the aim to overcome these limitations, nano-drug delivery has been achieving lots of interest. Nanoparticles able to incorporate hydrophilic and lipophilic drugs are being largely characterized in their different form. These formulations allow a prolonged and controlled drug release directly into the tumour tissue in a specific way, thanks to enhanced permeability retention (EPR) effect, and thus lower doses of drugs can be employed (Davis, Chen, and Shin 2008). As a consequence, toxicity can be strongly reduced by using these systems.

In conclusion, many approaches can be used for overcoming major limitations of conventional therapies, and however also target therapy used alone can present some problems. As a consequence, the goal in cancer treatment is to develop multiple strategies to block cancer progression by acting on different ways and pathways.

NANO-DRUG DELIVERY

Nano-drug delivery in cancer

Since last century, nanotechnology is an explored field of research that deals with interactions between molecules, cells and engineered substances such as molecular fragments, atoms and molecules (Khan, Saeed, and Khan 2017).

Nanotechnology has given rise to nanomedicine, among other applications including those associated with physics, biochemistry, and biotechnology, in order to create molecular devices that can facilitate therapeutic and diagnostic procedures on the nanoscale. Thereby, applications of nanotechnology have achieved lots of interest in various fields for different approaches. In terms of size details, the National Nanotechnology Initiative (NNI) defines nanotechnology in dimensions of roughly 1 to 100 nanometers (nm) and particles that fall within this range appear to be optimal nano-carriers, able to exert functions such as alter drug's reactivity, strength, electrical properties, and its behavior *in vivo* (Bharali et al. 2009).

The vasculature in tumors is known to be leaky to macromolecules. Moreover, as reported before, entities in the order of hundreds of nanometer in size can leak out of the blood vessels and accumulate within tumours, thanks to EPR effect (Davis, Chen, and Shin 2008). Long circulating macromolecular carriers can take advantage of this phenomenon for preferential extravasation from tumor vessels. Therefore, well designed NP in the 50-350nm size range and with a surface charge either slightly positive or negative should have accessibility to disseminated tumours when dosed into the circulatory system (Hu-Lieskovan et al. 2005). As a consequence, NPs have been proposed as carriers for the delivery of many drugs. Indeed, conventional preparations like solutions, suspensions or emulsions suffer from certain limitations like high dose and low availability,

intolerance, instability, and they exhibit fluctuations in plasma drug levels not providing sustained effect, therefore nanoparticles can constitute an optimal system for overcoming these problems. The key advantages for nanoparticles use are: (1) improved bioavailability by enhancing aqueous solubility, (2) increasing time action profile in the body and (3) targeting drug to specific sites (Mudshinge et al. 2011). This results in concomitant reduction in quantity of the drug required and thereby toxicity, enabling the safe delivery of toxic therapeutic drugs and protection of non target tissues and cells from severe side effects (Irving 2007).

Rising research and development costs, alternative investment opportunities for drug firms, fewer firms conducting pharmaceutical research, and erosion of effective patent life have resulted in a decline in the introduction of new chemical drugs since the late 1950s (Tiwari et al. 2012). So, there is great interest in developing new nanodelivery systems for drugs that are already on the market, especially for cancer therapy. Indeed, the pharmacokinetic and pharmacodynamic properties of chemotherapeutic drugs are already known, and this will lower the research costs.

By using nanotechnology in drug design and delivery, researchers are trying to make nanomedicine able to deliver the drug to the target tissue, release the drug at a controlled rate, being a safe and biodegradable system able to escape from degradation processes of the body (Bharali et al. 2009).

Among all developed and characterized nanoparticles carrying drugs, Doxil[®] and Abraxane[®] are two well known US Food and Drug Administration (FDA)-approved nanoformulations currently available on market for cancer treatment. Doxil[®] is a long circulating liposomal formulation of doxorubicin (DOX), which

has shown to be significantly more efficient than free DOX (MARTIN 1998; Nishiyama and Kataoka 2006; J. W. Park 2002). Liposomal anthracyclines constitute an efficient system able to exert a significant anticancer activity with reduced cardiotoxicity. After extravasation into tumor tissue, liposomes remain within tumor stroma as a drug-loaded depot, releasing the drug into the tumor cells. However, they present some limitations such as fixed functionality after synthesis and lack of colloidal stability (Adair et al. 2010). Therefore, some strategies were proposed for improving liposome formulations. In the case of DOX, pegylated DOX was developed as a version with greatly prolonged circulation. Pegylated DOX showed substantial efficacy in breast cancer treatment as monotherapy, but also in combination with other chemotherapeutics. Additional liposome constructs have been developed for the delivery of other drugs. The next generation of delivery systems will include other ligand-directed constructs directed against the tumor tissue in a very specific way (Krishna and Pandit 1996).

Abraxane[®] is used in the treatment for metastatic breast cancer, is an albumin-bound nanoparticle formulation of paclitaxel (Sparreboom et al. 2005; Gradishar et al. 2005; Moreno-Aspitia and Perez 2005). Abraxane[®] for injectable suspension overcomes the limits associated with Cremophor EL, the traditionally used solvent to reduce the low aqueous solubility of paclitaxel, but its use causes adverse effects, such hypersensitivity reaction. Abraxane[®] is able to convert insoluble or poorly soluble drugs, avoiding the need for toxic organic solvents. However, some adverse effects, such as alopecia, neurotoxicity and granulocytopenia, even if at low grade if compared to free paclitaxel, can occur also with Abraxane[®] treatment (M. R. Green et al. 2006). In order to overcome

these limits and also high costs of these drugs, new systems can be developed and studied.

Functionalized nanoparticles

The ideal nanoparticle-based system should be able to specifically target pathologic tissues, in order to minimize off-target effects of the active therapeutic agents on healthy tissues. Nanoparticles can be targeted to cancer cells surfaces that overexpress small molecules, peptides, proteins or antibodies. A lot of studies have developed for conjugating ligands, which recognize cell surface components typical of dysplastic and pathologic tissues, to nanoparticle surfaces. These ligands are constituted by: small molecules, polypeptide-based peptides, protein domains, antibodies, and nucleic acid-based aptamer (Tiwari et al. 2012). Each ligand class displays particular advantages, disadvantages, unique attributes, and conjugation strategies (Friedman, Claypool, and Liu 2013).

The addition of ligands can also play a vital role in the ultimate location of the nanoparticle. These molecules enable nanoparticles to bind to cell-surface receptors and enter cells by receptor-mediated endocytosis. Moreover, recent works comparing non-targeted and targeted nanoparticles have demonstrated that the primary role of the targeting ligands is to enhance cellular uptake into cancer cells rather than increasing the accumulation in the tumour (Kirpotin et al. 2006).

Early clinical results have also reported that functionalization of nanoparticles with specific recognition chemical entities not only enhances their efficacy, but also simultaneously reduces side effects, due to the targeted localization in the tumors and the active cellular uptake (Subbiah, Veerapandian, and S. Yun 2010).

Drug resistance and nanoparticles

One of the main problems of chemotherapy is the frequent development of cancer chemoresistance. A number of mechanisms were studied to be responsible for chemoresistance or poor response to chemotherapeutic drugs. The best investigated mechanism of resistance is mediated by alteration in the drug efflux proteins responsible for the removal of many commonly used anticancer drugs and it is called “multidrug resistance” (MDR) (Tiwari et al. 2012). Physiological barriers or alterations in the biological and biochemical characteristics of cancer cells are responsible for MDR. In the first case, the poorly vascularized tumor regions greatly reduce drug access to the tumor tissues and so protect tumour cells from drug-induced cytotoxicity. In the second case, resistance can be caused by cellular mechanisms, such as alteration of specific enzyme system for drug metabolism, reduction of apoptotic activity, induction of the cellular repair system, mutation of the drug target, or increasing drug efflux in tumour cells (Davis, Chen, and Shin 2008). Nanoparticles can overcome chemoresistance prolonging drug systemic circulation lifetime, inducing an accumulation in tumour tissue and allowing a stimuli-responsive drug release. Furthermore, they induce an endocytic uptake of drugs, escaping the drug efflux proteins, and also permit the co-delivery of chemo-sensitizing agents (Jack Hu and Zhang 2009).

Toxicity of nanoparticles

When evaluating the potential of nanoparticles for *in vivo* applications, toxicity of these systems is a crucial factor to be considered. Size, concentration, geometry and surface composition can be responsible for nanoparticles toxicity. Moreover, they can contain toxic elements, such as cadmium and selenium, that

can lead to unpredictable damage.

The greater surface area to volume ratio of nanoparticles can cause their higher chemical reactivity resulting in increased production of reactive oxygen species (ROS). Indeed, the nanoparticles surface area is a key factor in their intrinsic toxicity because of the interaction of their surfaces with biological system (Fard et al. 2015).

ROS formation is one of the mechanisms of nanoparticles toxicity which could cause oxidative stress, inflammation and consequent damage to proteins, cell membrane and DNA. Therefore, *in vitro* and *in vivo* assessment of nanoparticles toxicity is necessary during the study of nano-drug delivery.

Cytotoxicity assays of nanoparticles

Cytotoxicity assays are classified as *in vivo* and *in vitro* tests. *In vivo* toxicity assays (cell-based assay) are time-consuming and expensive and involve ethical issues, while *in vitro* toxicity tests (cell cultured-based assay) are faster, convenient, less expensive and free of any ethical issues. Due to these advantages, *in vitro* assays are the first choice for toxicity assessment of most nanomaterials (Mahmoudi et al. 2012).

In vitro methods include approaches for assessment of integrity of the cell membrane and the metabolic activity of viable cells. Evaluation of cell membrane integrity is one of the most common approaches to measure cell viability. It is based on the leakage of substances such as lactate dehydrogenase (LDH) that normally reside inside cells to the external environment and the measurement of LDH activity in the extracellular media. Alternatively, membrane integrity can be determined by penetration of dyes such as trypan blue and neutral red into the damaged cells and staining intracellular components. These dyes cannot enter living cells. Metabolic activity of viable

cells could be determined through colorimetric assays, such as the MTT and MTS assays (Fischer et al. 2010; Rabolli et al. 2010; Kumbıçak et al. 2014; Fotakis and Timbrell 2006).

Bioluminescent methods including methods using luciferase, which catalyzes the formation of light from adenosine triphosphate (ATP), are also commonly used as cell viability assays in which the number of surviving cells is determined by measuring the uptake and accumulation of neutral red dye and trypan blue after exposure to the toxic (Crouch et al. 1993; Schiewe and et Al. 1985; Benton et al. 1995). Among *in vitro* methods, LDH, MTT and MTS assay are most widely used for assessment of nanoparticles cytotoxicity. Another evaluation that needs to be performed *in vitro* is the *hemolytic activity assession on erythrocytes*.

Furthermore, it is always necessary to evaluate *in vivo* if NPs accumulate into healthy organs and tissues generating degradation products that may damage the involved sites.

Types of nanoparticles

Several types of nanoparticles, characterized by different sizes, shapes and materials, and with various chemical and surface properties, were developed. The field of nanotechnology is under constant and rapid growth and among new formulations, the classes of most used nanoparticles are listed below.

Liposomes

Liposomes are phospholipid vesicles (dimension of 50-100nm and even larger) that have a bilayered membrane structure, similar to that of biological membranes, together with an internal aqueous phase (Pizzimenti et al. 2016). Phospholipids are GRAS (Generally Recognised As Safe) ingredients, therefore minimizing the potential for adverse effects. Solutes, such as drugs, in the core cannot pass through the hydrophobic bilayer however hydrophobic molecules can be absorbed into the bilayer, enabling the liposome to carry both hydrophilic and hydrophobic molecules. The lipid bilayer of liposomes can fuse with other bilayers such as the cell membrane, which promotes release of its contents, making them useful for drug delivery and cosmetic delivery applications. Liposomes that have vesicles in the range of nanometers are also called nanoliposomes (Liangfang Zhang and Granick 2006; Cevc 1996). Liposomes can have either a single layer (unilamellar) or multiple phospholipid bilayer membranes (multilamellar) structure. Unilamellar vesicles (ULVs) are further classified into small unilamellar vesicles (SUVs) and large unilamellar vesicles (LUVs) depending on their size range (Vemuri and Rhodes 1995). To escape from reticuloendothelial system (RES) uptake after IV injection, PEGylated liposomes, “stealth liposomes”, were developed for reducing

clearance and prolonging circulation half-life (Li Zhang and Zhang 2013). Liposomes show excellent circulation, penetration, and diffusion properties. The possibility to link the liposomes surface with ligands and/or polymers increases significantly the drug delivery specificity (Torchilin 2005). The next generation of drug carriers under development features direct molecular targeting of cancer cells via antibody or other ligand mediated interactions. Currently, several liposomal formulations in the clinical practice contain several drugs for the treating of ovarian cancer, AIDS-related Kaposi's sarcoma, multiple myeloma, lymphoma, etc (Slingerland, Guchelaar, and Gelderblom 2012; Pizzimenti et al. 2016).

Gold NPs

Gold NPs (1-150nm) represent another kind of inorganic metal particle used in targeting tumours. They can be prepared with different geometries, such as nanospheres, nanoshells, nanorods, or nanocages. The advantages of these particles are their ease of preparation in a range of sizes, good biocompatibility, ease of functionality, and ability to conjugate with other biomolecules, without altering their biological properties (Sonavane, Tomoda, and Makino 2008). Gold NPs with diameters ≤ 50 nm have been shown to cross the BBB. They can be used to sensitize cells and tissue for treatment regimens (Nazir et al. 2014), and to monitor and guide surgical procedures (Jokerst and Gambhir 2011). Different types of drugs, including proteins and DNA as well as smaller drug molecules, have been linked to the surface chemistry of gold NPs, inducing a therapeutic effect in several types of tumors, including melanoma. They are also excellent labels for biosensors, because they can be detected by numerous techniques, such as optical absorption, fluorescence and electric conductivity (Huang et al.

2007). The use of the confocal reflectance microscope with antibody-conjugated gold NPs has made the development of highly sensitive cancer imaging possible (Kimling et al. 2006). Furthermore, they are not toxic and biocompatible. In fact, they do not elicit any allergic or immune response (Pan et al. 2007; Pizzimenti et al. 2016).

Quantum dots (QD)

The quantum dots are semiconductor nanocrystals and core-shell nanocrystals containing interface between different semiconductor materials. The size of quantum dots can be continuously tuned from 2 to 10nm, which, after polymer encapsulation, generally increases to 5–20nm in diameter. Particles smaller than 5nm are quickly cleared by renal filtration (Choi et al. 2007). Semiconductor nanocrystals have unique and fascinating optical properties, become an indispensable tool in biomedical research, especially for multiplexed, quantitative and long-term fluorescence imaging and detection (Michalet et al. 2005; Medintz et al. 2005; Alivisatos 2004; Smith et al. 2006). QD core can serve as the structural scaffold, and the imaging contrast agent and small molecule hydrophobic drugs can be embedded between the inorganic core and the amphiphilic polymer coating layer. Hydrophilic therapeutic agents including small interfering RNA (siRNA) and antisense oligodeoxynucleotide (ODN) and targeting biomolecules such as antibodies, peptides and aptamers can be immobilized onto the hydrophilic side of the amphiphilic polymer via either covalent or non-covalent bonds. This fully integrated nanostructure will not only identify, but bind to diseased cells and treat it. It will also emit detectable signals for real-time monitoring of its trajectory (Qi and Gao 2008).

These benefits enable applications of QDs in medical imaging and disease detection.

Superparamagnetic nanoparticles

Various multistimuli-responsive polymeric matrix system loaded with magnetic NPs have been developed to control the behaviour of nanosystems. In particular, it is possible to trigger drug release in complex luminescent/magnetic nanosystems under magnetic guidance and near-infrared irradiation *in vivo* (Baldi et al. 2014). Nanoparticles of iron oxide with diameters in the 5–100nm range have been used for selective magnetic bioseparations. Typical techniques involve the coating of particles with antibodies to cell-specific antigens, for separation from the surrounding matrix. The main advantages of superparamagnetic nanoparticles are that they can be visualized in magnetic resonance imaging (MRI) due to their paramagnetic properties (Irving 2007). Superparamagnetic nanoparticles belong to the class of inorganic based particles having an iron oxide core coated by either inorganic (silica, gold) and organic (phospholipids, fatty acids, polysaccharides, peptides or other surfactants and polymers) materials (Gupta and Curtis 2004; Babic et al. 2008; Euliss et al. 2003). In contrast to other nanoparticles, superparamagnetic nanoparticles based on their inducible magnetization, and their magnetic properties allow them to be directed to a defined location or heated in the presence of an externally applied magnetic field. These characteristics make them attractive for many applications, ranging from agents for MRI drug delivery systems, magnetic hyperthermia (local heat source in the case of tumor therapy), and magnetically assisted transfection of cells (Horák et al. 2005; Gupta and Gupta 2005; Jordan et al. 2001; Neuberger et al. 2005)

Dendrimers

Dendrimers are a unique class of repeatedly branched polymeric macromolecules with a nearly perfect 3D geometric pattern. The structure of dendrimers consists of three distinct architectural regions: 1) a core; 2) layers of branched repeat units emerging from the core; 3) functional end groups on the outer layer of repeat units. They are known to be robust three dimensional structures possessing both a solvent-filled interior core (nanoscale container) as well as a homogenous, mathematically defined, exterior surface functionality (Grayson and Fréchet 2001; Svenson and Tomalia 2012). Dendrimeric vectors are most commonly used as parenteral injections, either directly into the tumor tissue or intravenously for systemic delivery (Tomalia, Reyna, and Svenson 2007). There are several potential applications of dendrimers in the field of imaging, drug delivery, gene transfection and non-viral gene transfer. They have been extensively studied in the area of therapeutics and diagnostics for cancer as well as photodynamic therapy (Wolinsky and Grinstaff 2008), boron neutron capture therapy (Barth et al. 2005), and hyperthermia therapies using gold NPs (Shi et al. 2007). Their surface can be engineered with a variety of functionalities, enhancing their biocompatibility and biodegradability for widespread biomedical applications (Kievit and Zhang 2011; Pizzimenti et al. 2016).

Solid lipid nanoparticles (SLNs)

SLNs mainly comprise lipids that are in solid phase at the room temperature and surfactants for emulsification, the mean diameters of which range from 50nm

to 1000nm for colloid drug delivery applications (zur Mühlen, Schwarz, and Mehnert 1998). SLNs offer unique properties such as small size, large surface area, high drug loading, the interaction of phases at the interfaces, and are attractive for their potential to improve performance of pharmaceuticals, nutraceuticals and other materials (Roberta Cavalli et al. 2002). SLNs present a high physical stability, they can protect the drugs against degradation, and they allow an easy control of the drug release. The preparation of SLNs does not require the use of organic solvents. They are biodegradable, biocompatible, and have low toxicity. In addition, the production and sterilization on a large scale are rather easy (Yano et al. 2004). Solid lipids utilized in SLN formulations include fatty acids (e.g. palmitic acid, decanoic acid, and behenic acid), triglycerides (e.g. trilaurin, trimyristin, and tripalmitin), steroids (e.g. cholesterol), partial glycerides (e.g. glyceryl monostearate and glyceryl behenate) and waxes (e.g. acetyl palmitate). Several types of surfactants are commonly used as emulsifiers to stabilize lipid dispersion, including soybean lecithin, phosphatidylcholine, poloxamer 188, sodium cholate, and sodium glycocholate (L Zhang et al. 2010). Advantages of these solid lipid nanoparticles (SLN) are the use of physiological lipids, the avoidance of organic solvents in the preparation process, and a wide potential application spectrum (dermal, oral, intravenous). Additionally, they improve bioavailability, protect sensitive drug molecules from the environment (water, light) and induce a controlled and/or targeted drug release (Mäder and Mehnert 2001; Müller, Radtke, and Wissing 2002; Müller, Mäder, and Gohla 2000). Moreover, SLNs improve stability of pharmaceuticals, and are able to carry both lipophilic and hydrophilic drugs and most lipids being biodegradable (Müller, Radtke, and Wissing 2002; Jennings et al. 2000). Among many examples of formulations, SLNs containing docetaxel showed to improve the efficacy of

this chemotherapeutic agent in colorectal (C-26) and malignant melanoma (A375) cell lines in *in vitro* and *in vivo* experiments (Mosallaei et al. 2013). Cholesteryl butyrate SLNs have shown to inhibit tumour cell migration, human umbelical vein endothelial cells' adhesiveness to cancer cell lines derived from human colon-rectum, breast, prostate cancers, and melanoma (R Minelli et al. 2012). Furthermore, this formulation demonstrated a complete inhibition of lung metastasis formation in an *in vivo* model of prostate cancer (R Minelli et al. 2013).

CD-NSs

Cyclodextrins (CDs) are truncated cone-shaped cyclic oligosaccharides composed of glucopyranose units arranged around a slightly hydrophobic cavity, which can incorporate guest molecules through the formation of inclusion complexes. These nano-sized cavities make CDs suitable building blocks for organic nanosystems (Duchêne 2011). Reactive hydroxyl groups oriented towards the exterior side of CDs allow them to act as polyfunctional monomers, able to be cross-linked using a wide variety of bi- or polyfunctional chemicals, such as dianhydrides, diisocyanates, active carbonyl compounds, epoxides, carboxylic acids, etc. CDs, owing to its typical toroidal structure of inner hydrophobic and outer hydrophilic orientation, present a unique opportunity for the drug molecules to interact and complex. They are widely used in the pharmaceutical, food, textile, and home-based consumer products. However, native CDs typically do not form viable complexes with hydrophilic molecules, or macromolecules, and most commonly used CD form, β -CD, has poor water solubility which limits their complexation ability. Moreover, β -CD cannot be injected intravenously as they are known to complex with cholesterol, thereby

leading to nephrotoxicity (Swaminathan, Cavalli, and Trotta 2016).

To overcome these potential problems of native CDs, they have been cross-linked in three-dimensional structures to form nanosponges (NSs) (Trotta, Zanetti, and Cavalli 2012). Trotta and collaborators first published proof of concept NSs results with model drug (Roberta Cavalli, Trotta, and Tumiatti 2006). Final characteristic properties of CD-NSs are strongly influenced by the nature of the cross-linker used and degree of cross-linking taking place (Trotta 2011). In general, CD-NSs are able to form complexes with a wider series of molecules. This is due to the presence of interstitial spaces among CDs, which can host more hydrophilic guests. Moreover, the polymer network that surrounds the cavities hampers the diffusion of entrapped guest molecules, thereby promoting slower release kinetics. No less important is the fact that NSs are insoluble, hence they can be easily recovered from aqueous media and recycled (Caldera et al. 2017).

NS-based systems have emerged as one of the leading polymeric carriers based on CDs to be explored recently as seen from the explosion in the number of research and review articles (Trotta, Zanetti, and Cavalli 2012; Ahmed, Patil, and Zaheer 2013; Trotta et al. 2014). Indeed, a recent EU report highlighted the use of CD NSs as a promising innovative system for drug delivery applications (“Nanotechnology in Therapeutics,” n.d.).

Figure 1 presents a schematic structure of NS.

The application of CD-NSs in several scientific and technological fields, including chemistry, agriculture, environment, food, cosmetics, has been widely explored. Moreover, CDs are widely recognized and used in several pharmaceutical products, and enjoy a ‘generally regarded as safe (GRAS)’ status, therefore, NSs presents a promising carrier also in terms of future regulatory approvals of drug

products.

NSs are thermally stable up to 300 °C and autoclave-compliant, thereby allowing a feasible sterilization of the product. X-ray powder diffraction (XRD) coupled with high resolution transmission electron microscopy (TEM) confirmed the presence of the hexagonal geometry of CD in NSs, which was also used to tease apart the crystalline and paracrystalline forms of NSs. In most studies, the particle sizes obtained range between 200 and 500nm, with a low polydispersity index (PI). The conventional NS has a negative surface charge, in the order of -20 to -40 mV zeta potential, thereby lending stability to the nanosuspension. NSs were found to be stable releasing a small amount of free CD molecules at 60 °C after 2 h in acidic conditions. However, it remained intact in basic conditions. Dynamic vapor absorption studies demonstrated that NSs retained their crystal structure after several programmed cycles of absorption and desorption (Trotta 2011). Further, the elastic properties of NSs were demonstrated by analysis of the spectral modification of the Boson peak and Brillouin frequency (Rossi et al. 2012).

Extensive in vitro cell line toxicity (evaluated on MCF-7, HT-29, Vero, HCPC-I cell lines), hemolytic activity assessment, and preclinical safety/toxicity assessments were performed on NSs (Trotta, Zanetti, and Cavalli 2012; Swaminathan et al. 2010; Trotta et al. 2014; Shende et al. 2015). Hemolytic activity revealed the nonhemolytic/blood compatible nature of NSs. Also in their preliminary in vivo studies, Swaminatha and Vavia (Vavia PR, Swaminathan S., Trotta F 2006) showed that NSs did not display any apparent sign of toxicity in mice via oral administration. Subsequently, Shende et al. (Shende et al. 2015) carried out acute and repeated dose toxicity studies on rats, that reported a lack of toxicity with NSs.

In vivo studies also pointed out that NSs did not accumulate into healthy organs, further demonstrating the safe nature of NSs.

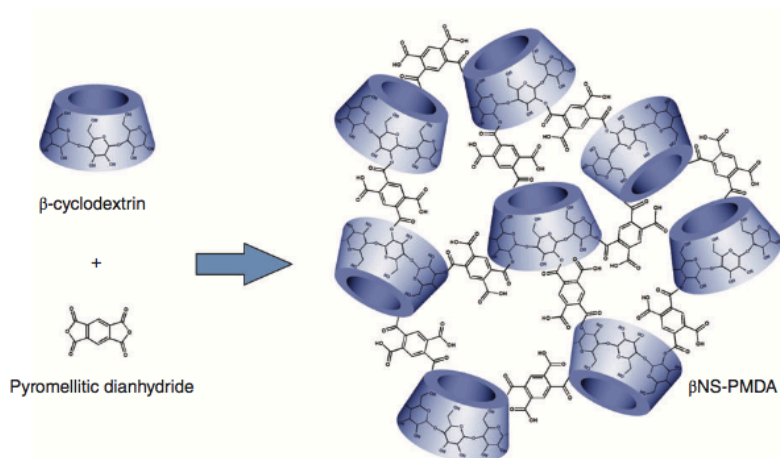


Figure 1: Schematic structure of cyclodextrin nanosponge.

Solid lipid nanoparticles carrying temozolomide for melanoma treatment

Background: Temozolomide (TMZ) is an alkylating agent used as anticancer drug, used for the treatment of glioblastoma and malignant melanoma in order to prevent brain metastasis. At neutral pH, TMZ is hydrolyzed spontaneously to its active metabolite (MTIC), which quickly turns into its reactive form able to generate the DNA damage. This activation of TMZ leads to drug instability and rapid clearance, thereby causing accumulation of MTIC in non target tissues. Therefore, an increase in TMZ dosage must be necessary to achieve therapeutic effect, but the derived side effects limit its use in clinical application and lead to the development of new therapeutic approaches.

Aim: The aim of this work was to study a new system for the delivery of TMZ, based on solid lipid nanoparticles (SLN) that are biocompatible and able to incorporate drugs.

Methods: TMZ-C12 loaded SLN were obtained through fatty acid coacervation, an approach used to allow a more controlled hydrolysis of TMZ that occurs at neutral pH. The effects of TMZ-C12 loaded SLN were evaluated on the progression of melanoma *in vitro*, using MTT and clonogenic assay to assess cell proliferation and using tubuly-forming test for evaluating angiogenesis. For the *in vivo* evaluation, C57BL6/J mice were injected with B16F10 cells and ten days after melanoma induction they were i.v. treated for two weeks with empty SLN, free TMZ or TMZ-C12 loaded SLN.

Results: SLN showed to be safe and biocompatible, since they did not display a cytotoxic effect on human lymphocytes. Results obtained on human (A2058 and M14) and mouse (B16F10) melanoma cell viability, revealed that TMZ-C12

loaded SLN were able to exert a significant higher inhibition of proliferation (50% at 50 and 25 μ g/ml; 30% at 10 μ g/ml; 15% at 5 μ g/ml) than free TMZ (30%, 15% and 5%, respectively). Moreover, results obtained on angiogenesis reported an inhibition of tube formation exerted by TMZ-C12 loaded SLN at concentration 25, 10 and 1 μ g/ml, while free TMZ evinced an inhibition only at the concentration 25 μ g/ml. Concerning *in vivo* evaluation, TMZ-C12 loaded SLN reported great evidence of efficacy, since they were able to reduce tumor growth and neo-angiogenesis, compared to free TMZ (57% of tumour volume reduction vs 17%; 45% vs 23% of tumour weight reduction), as afterwards demonstrated by histological and immunohistochemical evaluation.

Conclusion: Promising obtained results allow to hypothesize that an innovative system based on SLN could be a great strategy for the delivery of TMZ, allowing an increased stability of the drug and thereby its employment for the second line treatment of aggressive melanoma.



Article

Solid Lipid Nanoparticles Carrying Temozolomide for Melanoma Treatment. Preliminary In Vitro and In Vivo Studies

Nausicaa Clemente ¹ , Benedetta Ferrara ², Casimiro Luca Gigliotti ¹ , Elena Boggio ¹ ,
Maria Teresa Capucchio ³ , Elena Biasibetti ³, Davide Schiffer ⁴, Marta Mellai ⁴,
Laura Annovazzi ⁴, Luigi Cangemi ², Elisabetta Muntoni ², Gianluca Miglio ² ,
Umberto Dianzani ¹, Luigi Battaglia ^{2,*} and Chiara Dianzani ²

¹ Dipartimento di Scienze della Salute, Università del Piemonte Orientale, Via Solaroli, 17, 28100 Novara, Italy; nausicaa.clemente@med.uniupo.it (N.C.); luca.gigliotti@med.uniupo.it (C.L.G.); elena.boggio@med.uniupo.it (E.B.); umberto.dianzani@med.uniupo.it (U.D.)

² Dipartimento di Scienza e Tecnologia del Farmaco, Università degli Studi di Torino, Via Pietro Giuria 9, 10124 Torino, Italy; benedetta.ferrara@unito.it (B.F.); luigi.cangemi@unito.it (L.C.); elisabetta.muntoni@unito.it (E.M.); gianluca.miglio@unito.it (G.M.); chiara.dianzani@unito.it (C.D.)

³ Dipartimento di Scienze Veterinarie, Università degli Studi di Torino, Largo Paolo Braccini 2, 10095 Grugliasco (TO), Italy; mariateresa.capucchio@unito.it (M.T.C.); elena.biasibetti@unito.it (E.B.)

⁴ Centro di Neuro Bio Oncologia, Policlinico di Monza, Via Pietro Micca 5, 13100 Vercelli, Italy; davide.schiffer@unito.it (D.S.); marta.mellai@cnbo.it (M.M.); laura.annovazzi@cnbo.it (L.A.)

* Correspondence: luigi.battaglia@unito.it; Tel.: +39-011-670-7142

Received: 20 December 2017; Accepted: 18 January 2018; Published: 24 January 2018

Abstract: Aim: To develop an innovative delivery system for temozolomide (TMZ) in solid lipid nanoparticles (SLN), which has been preliminarily investigated for the treatment of melanoma. Materials and Methods: SLN-TMZ was obtained through fatty acid coacervation. Its pharmacological effects were assessed and compared with free TMZ in in vitro and in vivo models of melanoma and glioblastoma. Results: Compared to the standard free TMZ, SLN-TMZ exerted larger effects, when cell proliferation of melanoma cells, and neoangiogenesis were evaluated. SLN-TMZ also inhibited growth and vascularization of B16-F10 melanoma in C57/BL6 mice, without apparent toxic effects. Conclusion: SLN could be a promising strategy for the delivery of TMZ, allowing an increased stability of the drug and thereby its employment in the treatment of aggressive malignancies.

Keywords: SLN; melanoma; temozolomide

1. Introduction

Temozolomide (TMZ) is an imidazotetrazine anticancer drug (194 MW) endowed with an interesting profile. The presence of three adjacent nitrogen atoms in the heterocyclic ring, confers to this compound unique physical-chemical properties, as well as a remarkable antitumour activity [1].

TMZ is not affected by the acid pH of the stomach and is rapidly absorbed by the gastro-intestinal tract. However, in the blood and other tissues, it is first hydrolyzed to 5-(3-dimethyl-1-triazenyl) imidazole-4-carboxamide (MTIC), which is then quickly converted into its reactive form, the methyl-diazonium ion [2]. The methyl-diazonium ion formed by the breakdown of MTIC primarily methylates guanine residues in the DNA molecule, resulting in the formation of O6- and N7-methylguanines (Figure 1). Initially, it was speculated that the first step of this activation process could be promoted by the specific local microenvironment conditions found in the major loop of the DNA helix. However, this hypothesis was difficult to be confirmed, and now it is believed that TMZ turns into MTIC even in the absence of DNA [3–5]. Furthermore, the similarity between the half-life

of TMZ in phosphate buffer pH 7.4 and in plasma from patients undergoing i.v. or oral administration indicates that the transformation TMZ \rightarrow MTIC is a spontaneous and pH-dependent reaction, which occurs without the involvement of any catalysis by enzymes or other macromolecules [6]. The absence of any hepatic involvement in the activation process of TMZ may contribute to its high reproducibility pharmacokinetics, regardless of interpersonal variations in hepatic conversion rate [7].

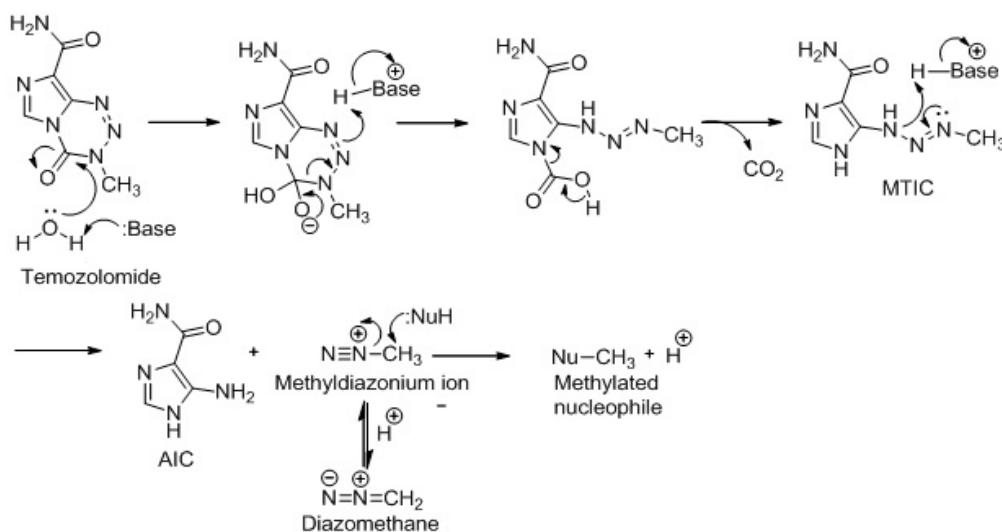


Figure 1. Scheme of TMZ ring opening, methyldiazonium ion

The spontaneous and rapid activation, is however an unwanted change of this drug, with relevant consequences. Indeed, an intense dosage is required to gain therapeutic efficacy of TMZ. Moreover, it has been associated to the accumulation of MTIC in off-target tissues, and the occurrence of several side effects, such as myelosuppression, liver, heart and pulmonary toxicity [8].

The development of resistance to TMZ, that can decrease its efficacy towards tumour cells, can also affect the therapeutic potential of this agent. The O6-alkylguanine-trasferase (AGT) repairing enzyme and the mismatch repair system (MMR) are involved in the molecular processes underlying resistance to TMZ. Moreover, it is well known that patients with hyper-methylated AGT promoter are more sensitive to TMZ chemotherapy; it is also reported, however, that TMZ is able to deplete the levels of AGT in various cell types, thus reducing the potential for drug resistance [9]. The ability of TMZ to cross the blood-brain barrier (BBB) allows its use as an agent for the adjuvant chemotherapy of glioblastoma (GB). Moreover, despite the fact that melanoma often tends to be resistant to TMZ and consequently a poor response rate is chemotherapy, due to its ease of use and high bioavailability, it can be employed in place of dacarbazine as the second line chemotherapy for this type of malignancies [10,11].

In a previous study, TMZ esters with short chain alcohols were synthesized, aiming to topical melanoma treatment. The median inhibitory concentration (IC₅₀) of the esters was comparable to that of the standard TMZ, but the esters showed increased activity, because of improved skin penetration [12]. However, owing to the stage of the disease, treatment of advanced/metastatic melanoma often needs systemic administration of chemotherapeutic compounds [13]. Therefore, the aim of this study was to develop novel nanoparticulate delivery system for TMZ suitable for i.v. administration, in order to overcome its intrinsic drawbacks, and improve its therapeutic efficacy. Among nanoparticles, solid lipid nanoparticles (SLN) proved to be safe, biocompatible and effective to encapsulate drugs in order to ameliorate their ability to cross biological barriers, increase their stability in the biological environment, and overcome drug resistance [14].

In this experimental study an optimized formulation was obtained, through the fatty acid coacervation method [15], in order to encapsulate TMZ in SLN, as a dodecyl (long chain) ester derivative (TMZ-C12) [16]. This approach should allow protecting TMZ from the aqueous environment, slowing down the drug release and the following spontaneous activation, that occurs in the bloodstream at neutral pH. The therapeutic potential of the new formulation was then assessed on human and mouse melanoma cells in in vitro. Finally, the efficacy of TMZ-C12 loaded SLN (SLN-TMZ) was assessed in the mouse B16-F10 melanoma model.

2. Results

Blank SLN and SLN-TMZ were obtained through the coacervation technique. Precipitation of sodium behenate from hot micellar solution was obtained by two alternative methods (Table 1). Method 1 was the classic method employed in previous experimental works, and involves the drop-wise addition of sodium phosphate followed by hydrochloric acid [15,16]. In method 2, sodium hydroxide is added to the starting micellar solution, because in hot aqueous solution sodium behenate partially undergoes protonation to insoluble behenic acid, leading to a slight turbidity. After sodium hydroxide addition, a complete and regular precipitation of behenic acid nanoparticles was obtained by substituting sodium phosphate with ammonium chloride.

Table 1. SLN composition.

	Method 1	Method 2
80% Hydrolyzed polyvinyl alcohol of 9000–10,000 MW (PVA9000)	200 mg	200 mg
Sodium behenate	100 mg	100 mg
NaOH 1 M		120 µL
Na ₂ HPO ₄ 1 M	200 µL	
NH ₄ Cl 5 M		260 µL
HCl 1 M	400 µL	400 µL
TMZ-C12		4 mg in 400 µL dimethylformamide (DMF)
Deionized Water		10 mL

Through optical microscopy (Figure 2a,b), we noticed that method 2 leads to a more homogeneous nanosuspension, being free from microparticle impurities. This was confirmed by particle size and polydispersity reduction observed in dynamic light scattering (DLS) analysis (Table 2).

Table 2. SLN particle size and encapsulation efficiency (EE%).

	Particle Size	Polydispersity	EE% Efficiency (Centrifugation)	EE% Efficiency (Gel Filtration)
Blank SLN method 1	400.1 ± 65 nm	0.269 ± 0.83	-	-
Blank SLN method 2	278.6 ± 4 nm	0.066 ± 0.01	-	-
Concentrated blank SLN	278.8 ± 28 nm	0.052 ± 0.02	-	-
SLN-TMZ	279.0 ± 50 nm	0.038 ± 0.01	93.10 ± 3.29	57.91 ± 21.70
Concentrated SLN-TMZ	273.15 ± 5 nm	0.084 ± 0.01	91.10 ± 0.22	N.D.

Particle shape was investigated through transmission electron microscopy (TEM) analysis (Figure 2c–e). Microparticle impurities were detectable only in SLN obtained with method 1, while mean particle size was comprised between 200–400 nm with method 2. Indeed, SLN by method 2 were deeper investigated. In fact, PVA9000 removal, obtained by SLN centrifugation and resuspension in distilled water, led to a less contrasted image, and the nanoparticle surface seemed rougher and less regular, compared to non-centrifuged SLN. Thus, an interaction between SLN and PVA9000 at the surface can be hypothesized. This was confirmed by scanning electron microscopy (SEM) (Figure 2f). Here the polymer seems to act as a coating shell around the groups of nanoparticles. However, both

TEM and SEM allow to assess a rough, but spherical shape of SLN by method 2, with approximately the same particle size detected by DLS.

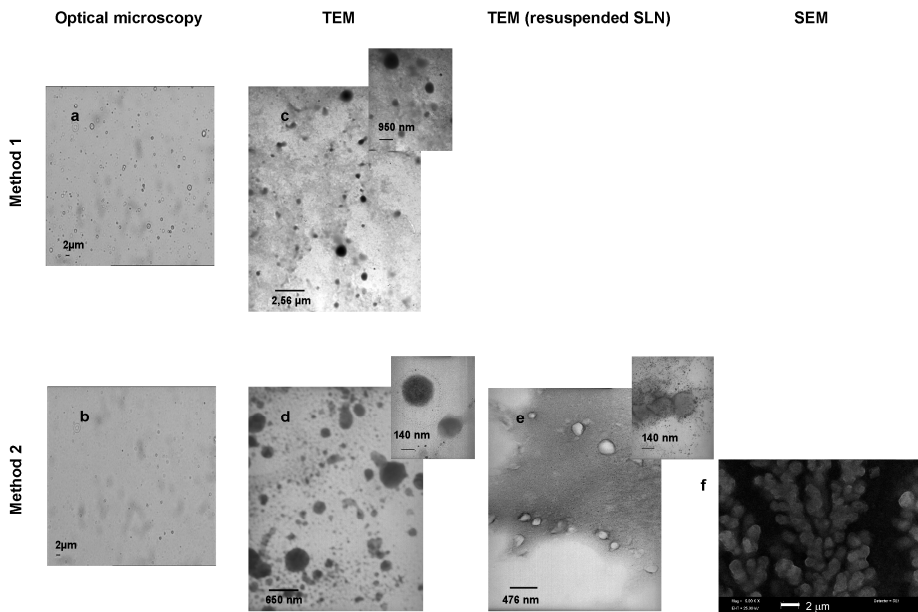


Figure 2. Microscopy of blank SLN. (a) optical microscopy of SLN obtained by method 1; (b) optical microscopy of SLN obtained by method 2; (c) TEM of SLN obtained by method 1; (d) TEM of SLN obtained by method 2; (e) TEM of SLN, centrifuged and resuspended, obtained by method 2; (f) SEM of SLN obtained by method 2.

Figure 3 shows differential scanning calorimetry (DSC) patterns of raw behenic acid and SLN obtained with method 1 and 2: the nanoparticles showed the endothermic peak of behenic acid, with a reduction of crystallization degree compared to raw material, regardless of the precipitation method employed.

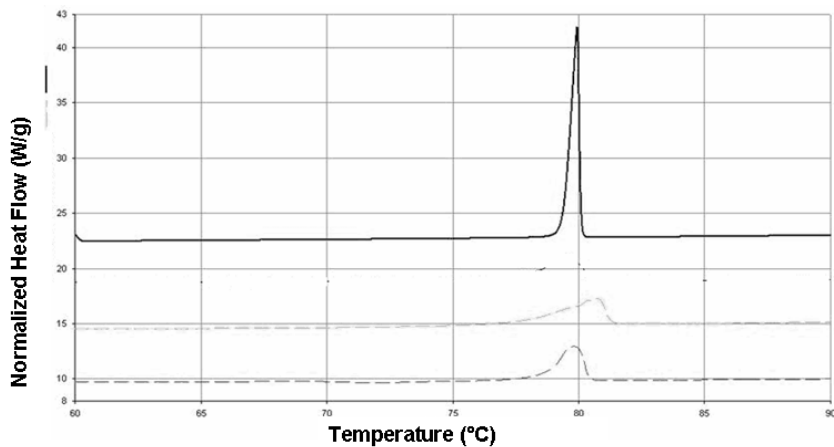


Figure 3. DSC of raw behenic acid (upper curve), blank SLN obtained with method 1 (intermediate curve) and method 2 (lower curve).

Since SLN obtained with method 2 showed a more reduced and homogeneous particle size, they were employed for the following parts of the study.

TMZ-C12 was loaded in SLN after melting of blank nanoparticles, owing to a method employed in previous works [16,17]. In fact, operating at acid pH does not hamper the stability of the alkylating drug. In order to reach the therapeutic dose, SLN-TMZ were concentrated through ultracentrifugation and resuspension in a small amount of PVA9000/citrate buffer. The pH of the final suspension was kept acid through diluted citrate buffer. In this condition TMZ-C12 was stable during storage. The resuspension process did not compromise either the particle size or the TMZ EE% of the nanoparticles (Table 2). EE% was measured either by centrifugation or by gel filtration, and a lower EE% was obtained by the latter. This could be attributed to the fact that size exclusion requires rather long time and it is performed by employing pH = 7.4 PBS buffer as eluent. In these conditions partial cleavage of TMZ ring can occur.

The stability of TMZ and its prodrug loaded in SLN was investigated both in Roswell Park Memorial Institute 1640 medium (RPMI 1640) and in plasma (Figure 4). Both media caused drug degradation, even if this phenomenon was quicker in plasma. In RPMI 1640 the lipophilic prodrug (TMZ-C12) was cleaved more slowly than the parent drug (TMZ), probably because of the influence of its low solubility, and the loading in SLN increased its stability. In the plasma the pure prodrug stability was not investigated because of its low solubility, but important differences were detected between free TMZ and SLN-TMZ, which resulted more stable.

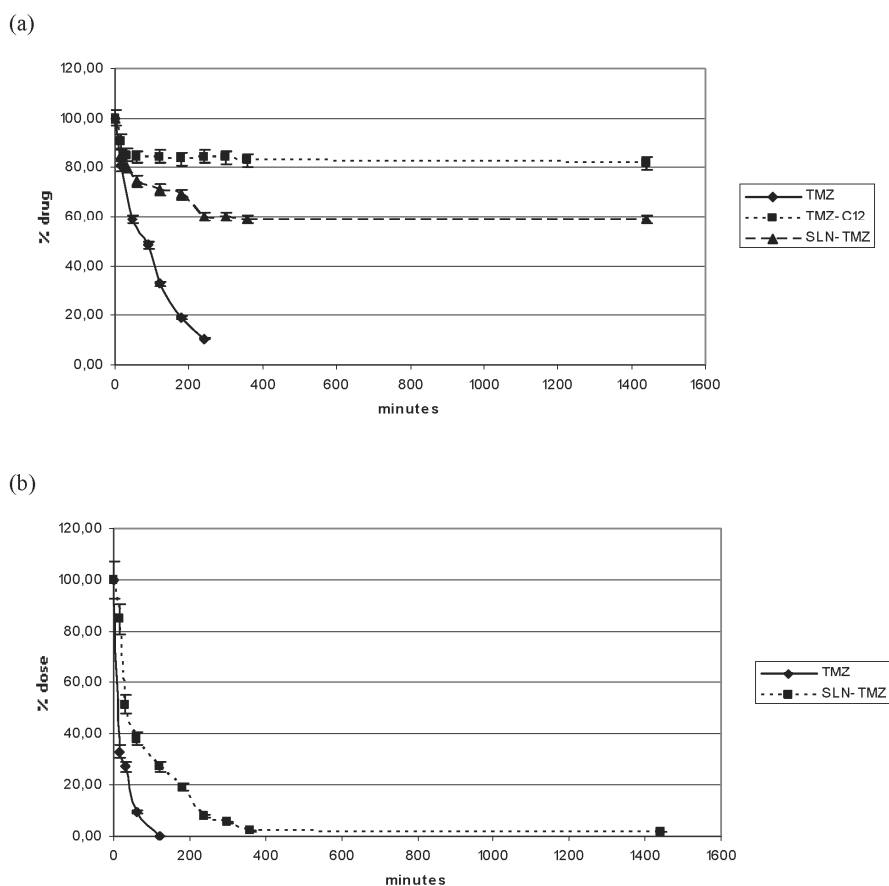


Figure 4. Stability of formulations in RPMI 1640 and in plasma. (a) Stability in RPMI 1640 of free TMZ, TMZ-C12 and SLN-TMZ; (b) Stability in plasma of free TMZ and SLN-TMZ. Error bar means SEM.

Cytotoxicity studies were performed on different cell lines, employing blank SLN, free TMZ and SLN-TMZ, while pure TMZ-C12 was excluded, because of its reduced solubility, that would make these experiments troublesome. The treatment was performed on human and mouse melanoma cells lines (A2058, JR8 and B16-F10) as potential chemotherapy targets.

Figure 5 shows that SLN-TMZ displayed higher toxicity than free TMZ in all melanoma cell lines. Indeed, on B16-F10 cell line, SLN-TMZ induce $70 \pm 6\%$ of viability inhibition at $50 \mu\text{M}$, while free TMZ only $34 \pm 2\%$. The inhibitory effect was concentration dependent. Thus, at the concentration of $10 \mu\text{M}$, while SLN-TMZ caused a $35 \pm 4\%$ viability inhibition, free TMZ was ineffective.

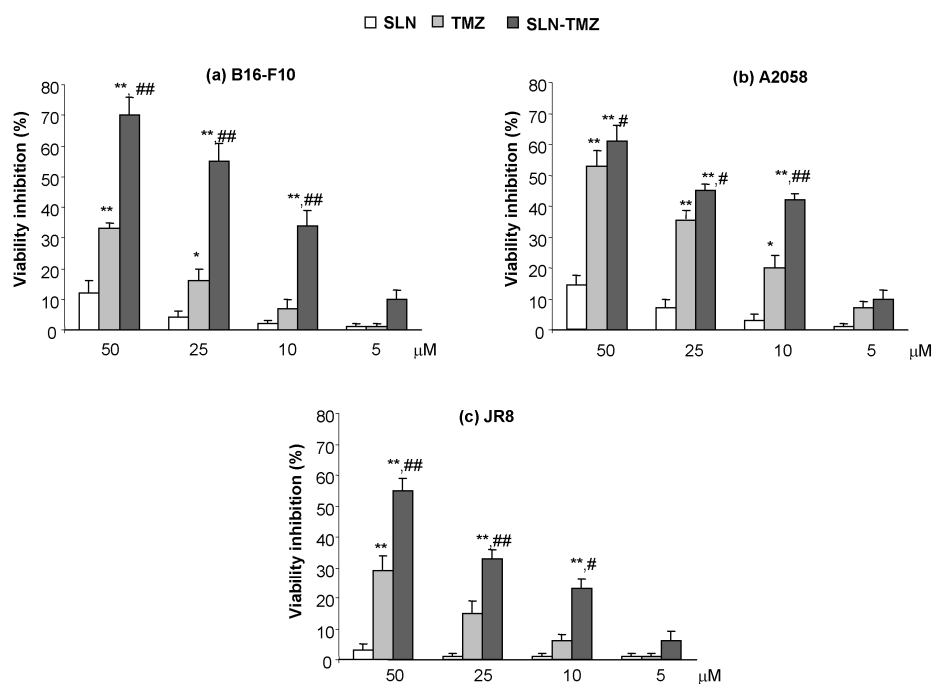


Figure 5. Cytotoxicity on melanoma cells: (a) B16-F10; (b) A2058; (c) JR8. Cells were treated with free TMZ and SLN-TMZ at 50–5 μM concentration for 72 h. Then, the cell proliferation reagent WST-1 is used for 2 h. Cells that had received no drug, as control, were normalized to 100%, and the readings from treated cells were expressed as % of viability inhibition. Eight replicates were used to determine each data point and five different experiments were performed. Data are shown as mean \pm SEM. Statistical analyses were performed using one-way ANOVA and the Dunnett test. ** $p < 0.01$ compared to the PBS-treated group. * $p < 0.05$ compared to the PBS-treated group. ## $p < 0.01$ compared to the TMZ-treated group. # $p < 0.05$ compared to the TMZ-treated group.

In order to validate these findings, clonogenic survival assays were performed. In fact, while 2-(4-iodophenyl)-3-(4-nitrophenyl)-5-(2,4-disulfophenyl)-2H-tetrazolium (WST-1) assay reveals cell viability after drug treatment, clonogenic assay shows only the viable cells that are still able to proliferate, after drug removal by the culture medium. Indeed, cells were treated with the drugs for 72 h, then after the removal of the drug, the cultures were prolonged in drug free medium for the following 7 days, when only a fraction of the seeded cells retained the ability to produce colonies [18]. Results confirmed those obtained with the WST-1 assay (Figure 6).

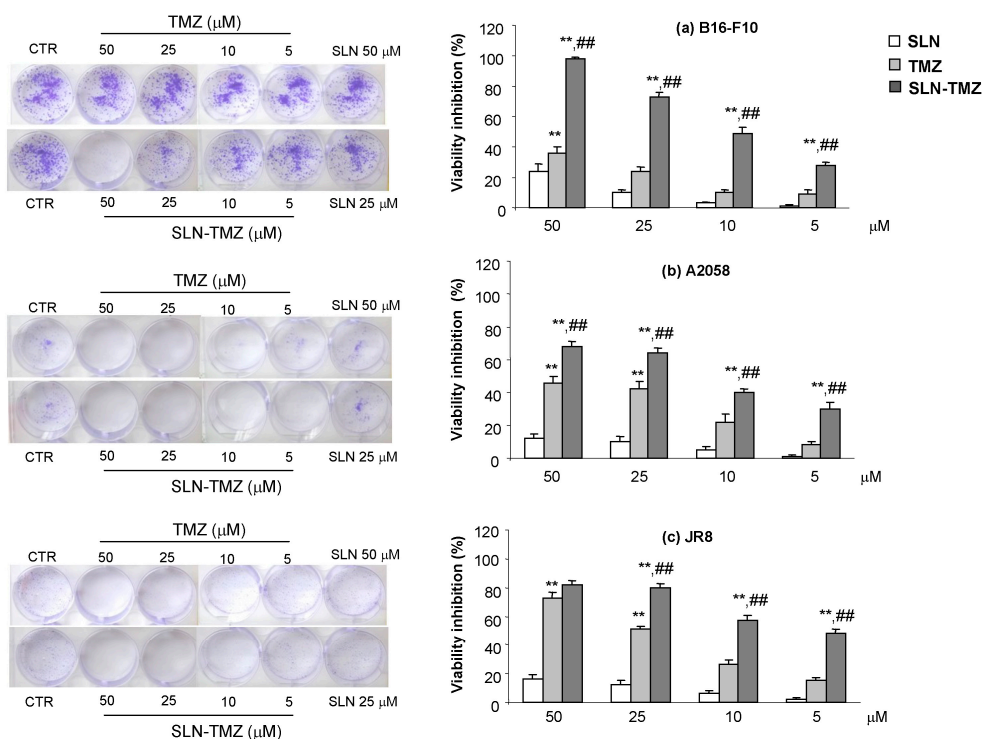


Figure 6. Clonogenic assay: (a) B16-F10; (b) A2058; (c) JR8. Cells were treated with free TMZ and SLN-TMZ at 50–5 μM concentration for 72 h. Then, the cells medium was changed and cells were cultured for additional 7 days in a drug-free medium. Colonies were then photographed. Then, the cells were treated with acetic acid to induce a completely dissolution of the crystal violet and absorbance was evaluated. Five different experiments were performed. Data are shown as mean \pm SEM. Statistical analyses were performed using one-way ANOVA and the Dunnett test. ** $p < 0.01$ compared to the PBS-treated group. ### $p < 0.01$ compared to the TMZ-treated group.

Angiogenesis is essential for tumour growth and metastasization. Kurzen H. et al. (2003) [19] demonstrated that TMZ inhibits angiogenesis when used at low and non-toxic doses. Therefore we compared the anti-angiogenetic effect of SLN-TMZ and TMZ on human umbilical vein endothelial cells (HUVEC) cells. In preliminary experiments, we selected drug concentrations that were not cytotoxic on HUVEC cells after 24 h treatment. Then, we assessed their effects on the tubuli-formation assay in the presence or absence of titrated amounts of each drug formulation. The morphology of capillary-like structures formed by HUVEC was analyzed after 15 h of culture. Results showed that SLN-TMZ significantly inhibited tubuli-formation in a concentration-dependent manner. At 25 μM, the structure and organization of the tubuli were strongly disrupted and at 1–10 μM, only few cells were able to form basic tubuli. By contrast, free TMZ was less effective and significant effect was measured only at the highest 25 μM concentration (Figure 7). The inhibition of capillary network formation was $60 \pm 5\%$ and $48 \pm 2\%$ for SLN-TMZ 25 and 10 μM, respectively; $30 \pm 4\%$ and $15 \pm 5\%$ for free TMZ 25 and 10 μM, respectively.

To assess the in vivo effect of our formulations, we compared development of melanoma in C57BL6/J mice using the transplanted B16-F10 model. Tumor measurements, performed after animal sacrifice, showed that SLN-TMZ significantly decreased tumor growth, since tumor weight was inhibited by 50% (Figure 8a). Moreover, all mice treated with SLN-TMZ survived to the end of the experiments, compared to about 50% of control mice (Figure 8b). By contrast, blank SLN did not show

any effect on mouse survival and tumor growth, and free TMZ displayed lower or not significant effects. Improved survival rate, compared to controls, could be related to a lower tumor Ki-67 expression in the SLN-TMZ group (Figure 8c). An additional positive effect on SLN-TMZ treatment efficacy, compared to controls, could be ascribed to the anti-angiogenic action of SLM-TMZ (Figure 8d).

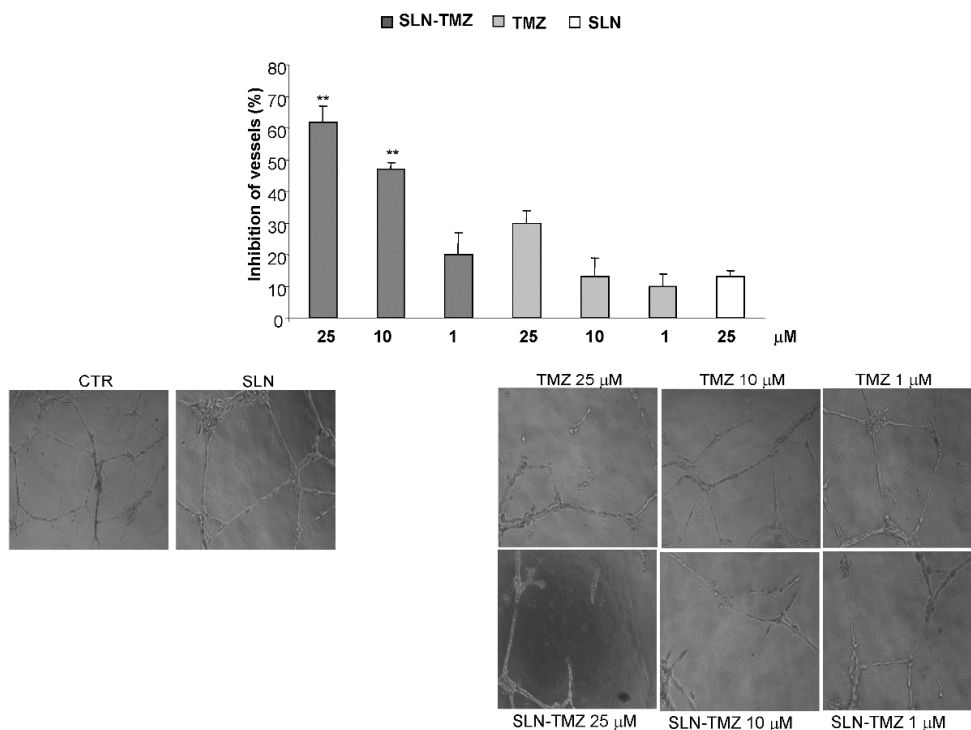


Figure 7. Tube formation assay on HUVEC. Cells were seeded onto 48-well plates (5×10^4 /well) previously coated with 75 μ L of growth factor-reduced Matrigel, in the presence and in the absence of different concentrations of each drug formulation. Tube formation was then photographed (10 \times magnification) and evaluated by counting the total number of tubes in three wells; five different experiments were performed. Data are shown as mean \pm SEM. Statistical analyses were performed using one-way ANOVA and the Dunnett test. ** $p < 0.01$ compared to the PBS-treated group.

To assess the effect of the therapies on the anti-tumor-immune response, we assessed expression of IFN- γ and IL-17A marking pro-inflammatory T helper type 1 (TH1) and T helper type 17 (TH17) cells, respectively, and IL-10 marking anti-inflammatory regulatory T cells (Treg) in the tumor mass by real time PCR (Figure 9). Results showed that treatment with SLN-TMZ strikingly increased expression of IL-17A (9.06 ± 1.62) compared to mice treated with PBS (1.04 ± 0.11 , $p < 0.01$), or empty SLN (0.29 ± 0.12 , $p < 0.01$), or free TMZ (0.59 ± 0.23 , $p < 0.01$). By contrast, expression of IL-10 was increased in mice treated with empty SLN (9.14 ± 1.16) compared to mice treated with PBS (1.30 ± 0.35 , $p < 0.01$) or free TMZ (3.79 ± 0.35 , $p < 0.01$) or SLN-TMZ (1.70 ± 0.08 , $p < 0.01$), and in mice treated with free TMZ compared to mice treated with PBS ($p < 0.05$). By contrast, expression of IFN- γ was not substantially modulated by any treatment.

SLN-TMZ did not display any apparent toxic effect on mice since it did not affect their weight, feeding behavior and motor activity (data not shown). In line with absence of toxic effects, histological analysis of explanted liver and kidney tissues did not detect any morphological alteration (Figure 10).

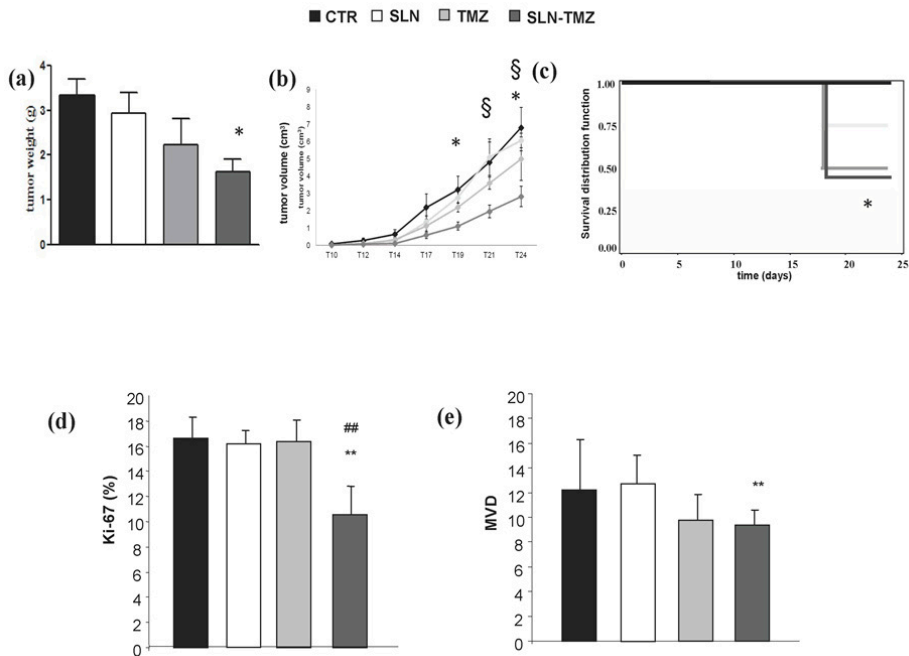


Figure 8. In vivo experiments on mouse melanoma model. C57BL6/J mice were injected subcutaneously with B16-F10 cells (1×10^5 in $100 \mu\text{L}$ /mouse). Ten days after the tumor injection, mice were treated three times a week for two weeks by i.v. injection of free TMZ, SLN-TMZ or empty SLN ($100 \mu\text{L}$ each— $0.5 \mu\text{M}/\text{g}$) or the same volume of PBS as control. Mice were sacrificed at the end of the experiment. Then, tumors, organs and blood were collected and kept for histological analysis. Graphs show: (a) tumor weight (grams—mean \pm SEM), (b) tumor volume curves (cm^3 —mean \pm SEM), (c) survival distribution function, (d) % of Ki-67-positive cells among tumor cells (e) MVD determined by counting the individual CD31+ microvessels. Ten randomly selected areas from three tumors from each group were analyzed; data are expressed as media and interquartile ranges. Statistical analyses were performed using one-way ANOVA and the Dunnett test. * $p < 0.05$; ** $p < 0.01$ compared to the PBS-treated group. § $p < 0.05$ compared to the empty SLN group. ## $p < 0.001$ compared to the TMZ-treated group.

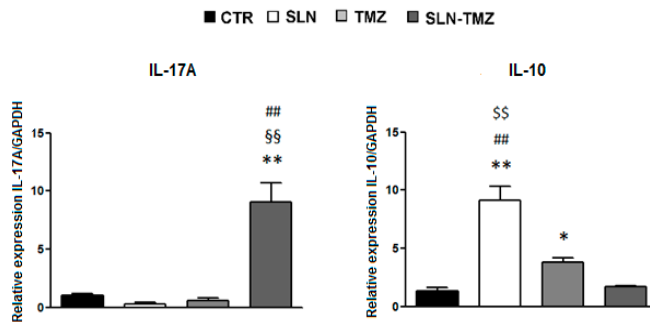


Figure 9. Effect of the different in vivo treatments on IL-17A and IL-10 expression in the tumor mass. IL-17A and IL-10 expression was evaluated in the tumor mass by Real Time PCR analysis. Data are expressed as mean \pm SEM of fold increase versus GAPDH expression ($n = 5$). Statistical analyses were performed using one-way ANOVA and the Dunnett test. * $p < 0.05$; ** $p < 0.01$ compared to the PBS-treated group. §§ $p < 0.01$ compared to the empty SLN group. ## $p < 0.01$ compared to the free TMZ-treated group. \$ $p < 0.01$ compared to the SLN-TMZ-treated group.

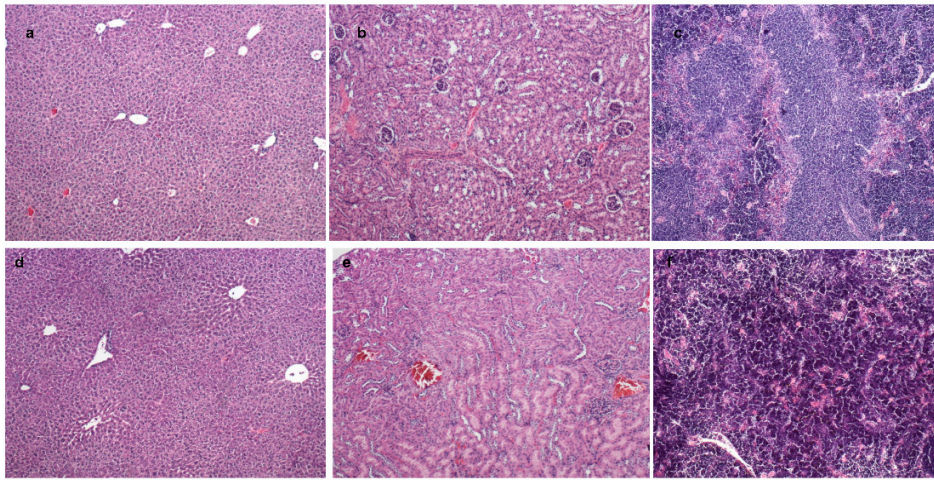


Figure 10. Histopathology of liver (a), kidney (b) and spleen (c) in SLN-TMZ group mice; liver (d), kidney (e) and spleen (f) in control group mice (haematoxylin and eosin, 100 \times).

Immunohistochemical (IHC) analysis of the tumors showed higher Ki-67 staining (marking proliferating cells) in control mice and TMZ-treated mice, compared to SLN-TMZ treated mice (Figures 8d and 11b,d,f). Moreover, to confirm *in vitro* new vascularization inhibition, tumor angiogenesis was evaluated by tumor microvessel density (MVD) [20] in tumor sections stained for CD31. A decreased CD31 expression was revealed in treated mice (Figure 11c,e) compared to controls (Figure 11a), even if differences between free TMZ and SLN-TMZ groups were not significant (Figure 11e).

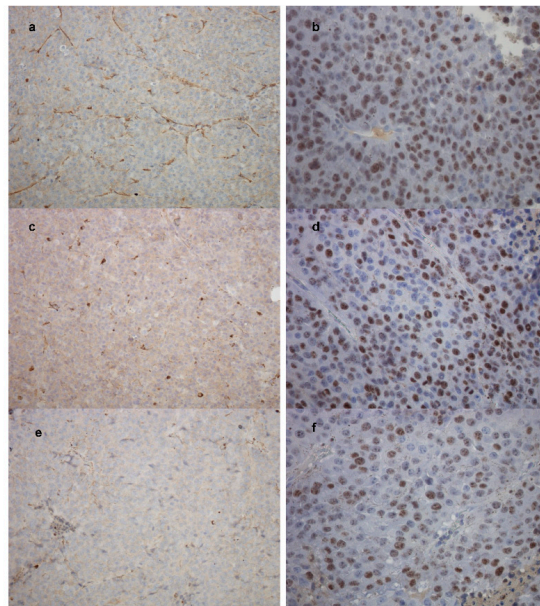


Figure 11. Immunohistochemical staining of CD31 (200 \times) and Ki-67 (400 \times) in tumor sections. (a,b) CD31 and Ki-67 in control group; (c,d) CD31 and Ki-67 in free TMZ group; (e,f) CD31 and Ki-67 in SLN-TMZ group.

3. Discussion

TMZ is an alkylating chemotherapeutic drug commonly employed for GB treatment by oral route. Moreover, it has been proposed for the treatment of melanoma via topical application [12]. Its low stability at physiologic pH limits the administration of TMZ via parenteral routes. Delivery and sustained release of TMZ via a nanomedicine formulation could provide a tool both to enhance its therapeutic index. The efficient encapsulation of TMZ in nanoparticle-based systems that can protect the drug from rapid degradation in physiological solutions is a challenge and several carriers of TMZ, including functionalized liposomes, lactoferrin nanoparticles, poly[lactic-co-glycolic acid] (PLGA) nanoparticles, etc. have been tested for their efficacy [21–24]. The success of these formulations was, however, limited due to: the lack of specific delivery to tumor cells, the poor drug cell uptake, the excessive drug efflux from cells, and the inability to maintain the cytotoxic efficacy.

Our approach is based on lipophilization of the parent molecule and following encapsulation in a nanoparticulate lipid matrix, in order to increase its stability after i.v. administration, which should lead to an improved pharmacokinetic profile with regard to its therapeutic potential.

To this aim, we chose a feasible technique to produce SLN-TMZ that is fatty acid coacervation. Compared to previous works [15,16], the formulation technique was changed. By employing method 2 a more homogeneous sized of the behenic acid nanosuspension was obtained, as assessed by DLS analysis (Table 2), optical microscopy and TEM (Figure 2a–e). This is likely due to the addition of sodium hydroxide to the starting micellar solution, which inhibits the spontaneous protonation of sodium behenate in hot water. In method 1, this unwanted phenomenon could drive the nucleation of crystals during sodium monohydrogen phosphate/hydrochloric acid addition, leading to a less homogeneous particle size distribution and to the presence of microparticle impurities. When starting pH is set to alkaline conditions with sodium hydroxide, the micellar solution is completely clear, but we have to shift to ammonium chloride/hydrochloric acid to observe the complete precipitation of behenic acid. Regardless of the precipitation method, employed and of the particle size obtained, DSC confirmed that nanoparticles were constituted from solid behenic acid (Figure 3). From SEM and TEM analyses (Figure 2d–f) we can hypothesize that PVA9000, which is employed as a water soluble polymeric stabilizer, effectively interacts with nanoparticles surface, forming a hydrophilic coating on their surface. Encapsulation of TMZ-C12 in the lipid matrix was obtained after melting of blank SLN in order to avoid the risk of TMZ ring cleavage at alkaline pH of the micellar solution. Then SLN were concentrated by ultracentrifugation and resuspension in acid buffer, in order to preserve TMZ ring stability. Sometimes resuspension of SLN can be troublesome, because of particle irreversible aggregation after ultracentrifugation; in our case this process was feasible, because of PVA9000 employed in resuspending medium. Just before in vivo administration, pH of the suspension was adjusted to neutral with sodium carbonate, in order to avoid pain during injection.

Instability of TMZ, both in cell medium and in plasma, can be ascribed to the non-enzymatic ring opening. The collected data on SLN-TMZ level in RPMI 1640 and in plasma allow to predict a changed pharmacokinetic profile for SLN-TMZ compared to free parent drug. This hypothesis was also suggested by results obtained on both tumour cell cultures and animal models, which in addition provided the first evidence on the improved therapeutic potential of the new formulation. In fact, while blank nanoparticles did not exert not toxic effects (Figure 5), SLN-TMZ were more effective against tumor cells, compared to free TMZ. Cytotoxicity was tested on two human melanoma cell lines, as well as on a mouse melanoma cell line, in perspective of employment on an in vivo melanoma mouse models (Figures 5 and 6). The superiority of SLN-TMZ vs. TMZ was shown in vitro. The anti-angiogenic activity of TMZ, which is described in the literature as an important factor to inhibit the tumor growth [19], was also improved with SLN-TMZ (Figure 7). The increased efficacy of the nanoformulation may be related to its improved stability in culture medium (Figure 4a). However, it cannot be ruled out that a different mechanism of cell internalization between SLN-TMZ and TMZ may also play a role.

The *in vitro* results indicate that the nanoformulated TMZ-C12 is suitable for *i.v.* administration, because of its increased stability in cell culture medium and plasma, and enhanced activity against tumor cells. Moreover, the improved efficacy shown *in vitro* allows predicting a reduction of the therapeutic dose *in vivo*, with decrease of side effects. In fact, in our preliminary *in vivo* experiments, we used a dosage regime less aggressive than those employed in literature [25–28]. Results showed that, at these sub-therapeutic doses, free TMZ did not show significant effects on tumor growth and weight compared to control; SLN-TMZ, instead, displayed significant effects on these parameters, and also on mouse survival, which was increased from 50 to 100%. The superiority of SLN-TMZ vs. TMZ was also shown by Ki67 expression in tumor cells, which was significantly decreased only in mice treated with SLN-TMZ. By contrast, despite *in vitro* tumor angiogenesis was highly inhibited by SLN-TMZ, *in vivo* similar effects on MVD were obtained by treatment with SLN-TMZ and free TMZ.

The observation that treatment with SLN-TMZ increases expression of IL-17A without affecting expression of IL-10 suggests that this treatment may also exert positive effects on the anti-tumor immune response by increasing the TH17/Treg cell ratio. This marks a difference with treatment with free TMZ that increased expression of IL-10 without affecting expression of IL-17, which suggests that it induced a decrease of the TH17/Treg ratio. The striking effect of empty SLN in increasing expression of IL-10 is in line with previous data obtained in rat cells *in vitro* [29].

The landscape of current treatment for advanced melanoma has changed rapidly in the last few years, and there are now several different classes of therapy that can be offered to patients depending on their mutational status and disease burden. TMZ is not adopted as a first line therapy for melanoma, especially after the approval of immunotherapeutic drugs, such as ipilimumab and nivolumab [30–33]. However, only 25% of patients respond to these agents and several of them became resistant. Therefore, investigation of novel strategies for the delivery of new and old drugs could allow achievement of further innovations [34]. Nanotechnology allows to potentially improve the effectiveness of traditional cytotoxic chemotherapeutics, overcoming their drawbacks and side effects. The employment of nanoparticulate TMZ has been recently reported for melanoma treatment. Targeting and uptake of TMZ loaded polyamide-amine dendrimer was demonstrated in A375 metastatic melanoma cell line, with an increase of sensitivity to the drug [35]. Likewise, this work shows that TMZ delivery using SLN may be an effective manner to increase the anti-cancer effect of the drug, allowing for decreasing dosage and, possibly, the side effects. However, further studies are needed to deeply investigate the fate of SLN-TMZ after *i.v.* administration, with regards to the nanoparticles half-life in the bloodstream and their accumulation in the tumor site, as well as to determine the optimal drug dosage and frequency of administration to increase the therapeutic efficacy *in vivo*.

4. Experimental Section

4.1. Materials

4.1.1. Chemicals

Sodium behenate was from Nu-Chek Prep, Inc. (Elysian, MN, USA); acetic acid, triethylamine, sodium nitrite, anhydrous dimethylformamide (DMF), TMZ, 80% hydrolyzed polyvinyl alcohol of 9000–10,000 MW (PVA9000), penicillin–streptomycin, Hepes, M199 medium, Dulbecco's Modified Eagle Medium (DMEM), Roswell Park Memorial Institute 1640 medium (RPMI 1640), heparin, and crystal violet were from Sigma-Aldrich (St. Louis, MO, USA); sodium monohydrogen phosphate, citric acid, ammonium chloride, sodium hydroxide from Azienda Chimica e Farmaceutica—ACEF (Fiorenzuola d'Arda, Italy); sulphuric acid, hydrochloric acid from Merck (Darmstadt, Germany); Br-dodecane, dichloromethane, chloroform, methanol and acetonitrile from Carlo Erba (Val De Reuil, France); EBM-2 basal medium was from Lonza (Basel, Switzerland); fetal bovine serum (FBS) Gold from PAA The Cell Culture Company (Pasching, Austria); rat collagen-I was from Trevigen (Gaithersburg, MD, USA); chemically defined lipid concentrate was from Invitrogen Life technologies (Carlsbad, CA, USA); fetal calf serum (FCS) was from Invitrogen (Burlington, ON, Canada); Matrigel, were from BD

Biosciences; 2-(4-iodophenyl)-3-(4-nitrophenyl)-5-(2,4-disulfophenyl)-2H-tetrazolium, monosodium salt (WST-1) and 1-methoxy-5-methylphenazinium methylsulfate (1-methoxy-PMS) were from Dojindo Molecular Technologies (Kumamoto, Japan).

Deionized water was obtained by a MilliQ system (Millipore, MO, USA). All other chemicals were analytical grade and used without any further purification.

4.1.2. TMZ-C12 Synthesis

TMZ-C12 synthesis was performed according to the literature (Figure 12) [12,16].

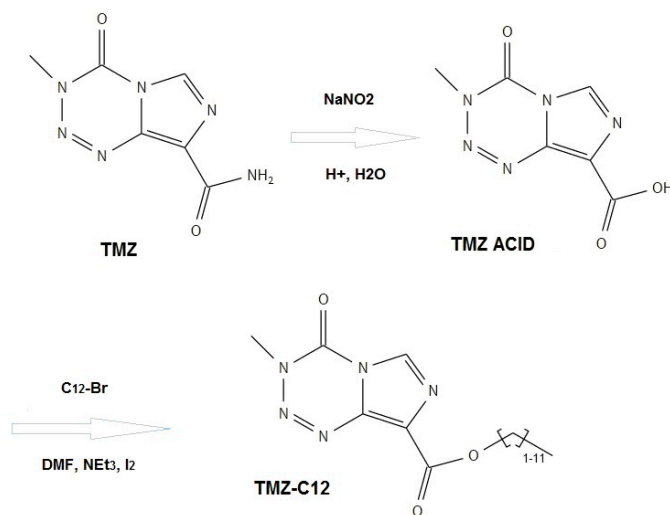


Figure 12. Scheme of TMZ-C12 synthesis.

4.1.3. SLN Preparation

Blank SLN were prepared according to the coacervation method [15], as reported in Table 1. Briefly, sodium behenate was dispersed in water with PVA9000 and the mixture was then heated under stirring (300 rpm), to obtain a clear solution. Two acidifying (coacervating) conditions were compared: sodium monohydrogen phosphate, followed by hydrochloric acid; and ammonium chloride followed by hydrochloric acid; they were added drop-wise to the mixture until complete behenic acid precipitation. The obtained suspension was then cooled under stirring at 300 rpm until 15 °C temperature was reached.

For drug loaded SLN, TMZ-C12 was dissolved in a small amount of DMF, and this solution was added to the blank SLN, led to their melting point; the drug was allowed to partition in the melted lipid for 5 min under stirring and then cooled to room temperature.

For in vitro and in vivo experiments, SLN were concentrated 10-fold under sterile hood, in order to reach a drug therapeutic concentration/dose. 10 mL of suspension were centrifuged at 62,000 × *g* (Allegra 64R centrifuge, Beckman Coulter, Brea, CA, USA) for 15 min, followed by re-suspension of the precipitate in 1 mL of 0.01 M citrate buffer pH = 3.0 containing 100 mg/mL PVA9000, with the help of an ultrasonic bath (Transsonic, Elma Schmidbauer GmbH, Singen, Germany).

4.1.4. SLN Characterization

SLN particle sizes and polydispersity indexes (PDI) were determined one hour after preparation using dynamic light scattering technique-DLS (Brookhaven, NY, USA). Size measurements were obtained at an angle of 90° at 25 °C. All data were determined in triplicate.

The homogeneity of the suspension was checked with optical microscopy (DM2500, Leica Microsystems, Wetzlar, Germany). Particle shape was determined through Transmission Electronic Microscopy (TEM-CH10, Philips, Amsterdam, The Netherlands) and Scanning Electronic Microscopy (SEM-Stereoscan 410, Leica Microsystems, Wetzlar, Germany). For TEM analysis, SLN were employed as such, or after centrifugation and resuspension in water, in order to discriminate for the effect of PVA9000. Instead, SLN were properly diluted (1:25) in order to be analyzed with SEM; then samples were placed on the stub and left to dry under vacuum for one night. The sample obtained, not being conductive, has been subjected to gold metallization by sputtering.

Differential Scanning Calorimetry (DSC) was performed through a DSC7 (Perkin Elmer, Waltham, MS, USA) on SLN centrifuged and dried under vacuum, in order to assess their solid state and the absence of supercooled melts.

Entrapment efficiency (EE%) determination was performed as follows: 0.5 mL SLN suspension was diluted with 0.5 mL water and centrifuged for 15 min at $62,000 \times g$; the precipitate was washed with 1 mL acetonitrile/0.1 M pH = 3.0 citrate buffer to eliminate adsorbed drug; the lipophilic prodrug was extracted from the solid residue by dissolution in 0.3 mL dimethylsulfoxide (DMSO) and 0.2 mL acetonitrile, then 0.25 mL 0.1 M citrate buffer pH = 3.0 was added to precipitate the lipid matrix and the supernatant was injected in a Reversed Phase High Performance Liquid Chromatography (RP-HPLC) system (Shimadzu LC-10, Kyoto, Japan). EE% was calculated as the ratio between drug amount in the residue and the weighted one.

EE% was also determined by size exclusion. 1 mL SLN underwent gel filtration using a matrix of cross-linked of agarose (Sephacrose CL 4B) as stationary phase. The opalescent fractions containing the purified SLN were concentrated under nitrogen up to 1 mL final volume. The prodrug in the resultant suspension was determined solubilizing 0.05 mL SLN into 0.95 mL acetonitrile and analyzing it by HPLC. In this case, EE% was calculated as the ratio between the drug recovery after and before gel filtration.

4.1.5. Stability Studies in Plasma and Cell Medium

A suitable method for the determination of stability of free TMZ, free TMZ-C12, and SLN-TMZ, both in cell culture medium (RPMI 1640, Sigma-Aldrich, St. Louis, MO, USA) and in rat plasma has been developed. Briefly, stability was assessed by dissolving/suspending under stirring at 37 °C 0.5 mM of TMZ, or TMZ-C12, or SLN-TMZ, alternatively in RPMI 1640, or in rat plasma, in separate experiments. At scheduled times 100 μ L were withdrawn and centrifuged at $16,000 \times g$ for 1 min, and the supernatant was injected in the HPLC system, while the precipitate, was dissolved in 100 μ L acetonitrile before injection. Stability of drugs was evaluated by considering the cumulative amount in the supernatant and in the precipitate, compared to the starting.

4.1.6. High Performance Liquid Chromatography (HPLC)

TMZ: a reversed-phase column (Mediterranea Sea, 18 5 μ m 25 \times 0.46 mm) was used. Linear gradient (10 min) from 100% acetic acid to 50% acetonitrile, followed by 5 min at 50% acetonitrile was performed at a flow rate of 1 mL/min. UV-Vis detector was set at 329 nm. Retention time was 9 min.

TMZ-C12: a reversed-phase column (Allsphere™ ODS, 2.5 μ m 250 \times 4.6 mm) was used. HPLC grade acetonitrile/water (70/30 *v/v*) was used as a mobile phase with a flow rate of 1 mL/min. UV-Vis detector was set at 329 nm. Retention time was 8.5 min.

4.1.7. Cytotoxicity Assays

JR8 human melanoma cells were a kind gift of Dr. Pistoia (Gaslini Institute, Genoa, Italy), A2058 human melanoma cells and B16-F10 mouse melanoma cells were from the American Type Culture Collection (ATCC; Manassas, VA, USA). A2058 was chosen as a tumorigenic and metastatic model cell line [36], while JR8 was chosen as a tumorigenic model cell line [37]. Both are derived from human lymph nodes metastasis. A2058 and JR8 cell lines were cultured in RPMI 1640 and B16-F10 cell

lines in DMEM with 10% FBS, 2 mmol/L L-glutamine and penicillin/streptomycin (100 units/mL), at 37 °C in 5% CO₂ humidified atmosphere. Cells (1×10^3 /well) were seeded in 96-well plates and incubated for 24 h. Then, they were treated with at 5–50 µM concentrations of the studied drugs for 72 h. The cell proliferation reagent WST-1 was used, as described by the manufacturer's protocol. Cells that had received no drug, as control, were normalized to 100%, and the readings from treated cells were expressed as % of viability inhibition. Eight replicates were used to determine each data point and five different experiments were performed.

4.1.8. Clonogenic Assay

Melanoma cells (8×10^2 /well) were seeded into six-well plates. The day after they were treated with different concentrations of the studied drugs for 72 h. Then the medium was changed and cells were cultured for additional 7 days in a drug-free medium. Subsequently, cells were fixed and stained with a solution of 80% crystal violet and 20% methanol. Colonies were then photographed. Then the cells were perfectly washed and 30% *v/v* acetic acid was added to induce a completely dissolution of the crystal violet. Absorbance was recorded at 595 nm by a 96-well-plate ELISA reader. Five different experiments were performed.

4.1.9. Tubule-Formation Assay on Human Umbilical Vein Endothelial Cells (HUVEC)

HUVEC were isolated from human umbilical veins by trypsin treatment (1%) and cultured in M199 medium with the addition of 20% FCS, 100 U/mL penicillin, 100 µg/mL streptomycin, 5 UI/mL heparin, 12 µg/mL bovine brain extract, and 200 mM glutamine. The HUVEC were grown to confluence in flasks and used at the 2nd–5th passages. The use of HUVEC was approved by the Ethics Committee of the "Presidio Ospedaliero Martini" of Turin and conducted in accordance with the Declaration of Helsinki. Written informed consent was obtained from all donors. HUVEC were seeded in 96-well plates and treated at 37 °C, 5% CO₂, for 24 h with different concentrations of the studied drugs. The cell proliferation reagent WST-1 was used. Drug concentrations that were not cytotoxic were used for the tubule-formation assay. Then, HUVEC were seeded onto 48-well plates (5×10^4 /well) previously coated with 75 µL of growth factor-reduced Matrigel, in the absence or presence of free TMZ and SLN-TMZ (1–25 µg/mL), or empty SLN at the concentration corresponding to that used with entrapped drugs. The morphology of the capillary-like structures formed by the HUVECs was analyzed by an inverted microscope after 15 h of culture, and photographed with a digital camera. Tube formation was analyzed with an imaging system (Image Pro Plus Software for microimaging, Media Cybernetics, version 5.0, Bethesda, MD, USA). Tubule-formation was evaluated by counting the total number of tubes in three wells and five different experiments were performed, as previously described [18]. Cells that had received no drug, as control, were normalized to 100% of new formed vessels and the readings from treated cells were expressed as % of vessel inhibition.

4.2. Animal Studies

Female 6- to 9-week-old C57BL6/J (The Jackson Laboratory, Bar Harbor, ME, USA) mice were bred under pathogen-free conditions in the animal facility of the University of Eastern Piedmont, and treated in accordance with the University Ethical Committee and European guidelines. The mice were injected subcutaneously with B16-F10 cells (1×10^5 in 100 µL/mouse) and the tumour growth was monitored every two days. Ten days after the tumor induction, the mice were treated via the i.v. injection of TMZ, SLN-TMZ or empty SLN (100 µL each—0.5 µmol TMZ/g) or the same volume of PBS as control. Since all the formulations were obtained in diluted acid buffers, in order to preserve TMZ ring stability, prior to animal administration pH of the suspension was neutralized with 10 µL of 0.2 M Na₂CO₃. The treatment had be carried out three times a week for two weeks (6 i.v./mouse) and the mice were sacrificed after three days after the last injection, or when they displayed sufferance. Six animals for groups were employed for each group.

4.2.1. Histology and Immunohistochemistry on Animal Specimens

After euthanasia, all animals underwent complete necropsy. Lung, liver, kidney and spleen were collected and stored in 10% neutral buffered formalin for histological evaluation. Samples were trimmed into cassettes, paraffinized, sectioned (5 μm thick), stained with haematoxylin and eosin, and evaluated by light microscopy.

Immunohistochemical staining was performed on sections of selected tumors. Primary antibodies included a monoclonal antibody Ki-67 (1:100 dilution; code M7248; Dako, Santa Clara, CA, USA) and a polyclonal anti-CD31 (1:100 dilution; code ab28364; Abcam, Cambridge, UK). Antibodies were detected using the avidin–biotin–peroxidase complex technique with the Vectastain ABC-AP Kit (Universal; Vector Laboratories, Burlingame, CA, USA). Antigen retrieval was done by heating the sections in citrate buffer (0.01 M, pH 6.0) at 98 °C for 25 min. Endogenous peroxidase activity was quenched. The slides were then incubated overnight in a humidified chamber at 4 °C with the primary antibodies, followed by sequential 10 min incubation with biotinylated link antibody and peroxidase labelled streptavidin. The reaction was visualized using 3,3'-diaminobenzidine tetrahydrochloride (Sigma-Aldrich). The nuclei were counterstained with haematoxylin and eosin stain. Positive and negative immunohistochemistry controls were routinely used. The reproducibility of the staining was confirmed by reimmunostaining via the same method in multiple, randomly selected specimens.

All reactions were visualized by light microscopy and assessed blinded by two observers and the discordant cases were reviewed at a multi-head microscope until a consensus was reached. Each slide for histological staining was captured with a Nikon DS-Fi1 digital camera (Nikon, Shinjuku, Japan) coupled to a Zeiss Axiophot microscope (Zeiss, Oberkochen, Germany) using a 40 \times objective lens. NIS-Elements F software (V4.30.01, Nikon, Shinjuku, Japan) was used for image capturing. Each immunohistochemical marker was evaluated in at least ten different fields, and particularly measuring the numbers of positive cells for cleaved Ki-67 (Image Pro Plus analysis system—Media Cybernetics, version 5.0, Bethesda, MD, USA) and of microvessels for anti-CD31.

4.2.2. Real Time PCR on Tumors

Total RNA was isolated from tumors, using TRIzol reagent (Sigma-Aldrich). RNA (1 μg) was retrotranscribed using the QuantiTect Reverse Transcription Kit (Qiagen, Hilden, Germany). IFN- γ , IL-17A and IL-10 expression were evaluated with a gene expression assay (Assay-on Demand; Applied Biosystems, Foster City, CA, USA). The GAPDH gene was used to normalize the cDNA amounts. Real-time PCR was performed using the CFX96 System (Bio-Rad Laboratories, Hercules, CA, USA) in duplicate for each sample in a 10 μL final volume containing 1 μL of diluted cDNA, 5 μL of TaqMan Universal PCR Master Mix (Applied Biosystems, Foster City, CA, USA), and 0.5 μL of Assay-on Demand mix. The results were analyzed with a $\Delta\Delta$ threshold cycle method.

4.2.3. Statistical Analysis

Data are shown as mean \pm SEM. Statistical analyses were performed with Prism 3.0 software (GraphPad Software, La Jolla, CA, USA) using one-way ANOVA and the Dunn test. Kaplan-Mayer survival curves were evaluated with the Chi-Square test.

Acknowledgments: We thank the Pathology Unit and the Obstetrics and Gynecology Unit, Martini Hospital, Torino, for providing human umbilical cords. This work was supported by the University of Turin 2015 (Ricerca Locale quota A), by Fondazione Amici di Jean, and Associazione Italiana Ricerca sul Cancro (IG 14430, AIRC, Milan).

Author Contributions: Luigi Battaglia, Chiara Dianzani, Davide Schiffer and Umberto Dianzani conceived and designed the experiments; Nausicaa Clemente, Benedetta Ferrara, Luigi Cangemi, Elena Biasibetti, Laura Annovazzi, Elena Boggio performed the experiments; Casimiro Luca Gigliotti, Marta Mellai, Maria Teresa Capucchio performed data analysis; Gianluca Miglio, Elisabetta Muntoni wrote the paper.

Conflicts of Interest: The authors declare no conflict of interest.

References

1. Stevens, M.F.; Hickman, J.A.; Stone, R.; Gibson, N.W.; Baig, G.U.; Lunt, E.; Newton, C.G. Antitumor imidazotetrazines. 1. Synthesis and chemistry of 8-carbamoyl-3-(2-chloroethyl)imidazo[5,1-*d*]-1,2,3,5-tetrazin-4(3*H*)-one, a novel broad-spectrum antitumor agent. *J. Med. Chem.* **1984**, *27*, 196–201. [[CrossRef](#)] [[PubMed](#)]
2. Stupp, R.; Hegi, M.E.; Mason, W.P.; van den Bent, M.J.; Taphoorn, M.J.; Janzer, R.C.; Ludwin, S.K.; Allgeier, A.; Fisher, B.; Belanger, K.; et al. Effects of radiotherapy with concomitant and adjuvant temozolomide versus radiotherapy alone on survival in glioblastoma in a randomised phase III study: 5-year analysis of the EORTC-NCIC trial. *Lancet Oncol.* **2009**, *10*, 459–466. [[PubMed](#)]
3. Clark, A.S.; Stevens, M.F.G.; Sansom, C.E.; Schwalbe, C.H. Anti-tumour imidazotetrazines. Part XXI. Mitozolomide and temozolomide: Probes for the major groove of DNA. *Anticancer Drug Des.* **1990**, *5*, 63–68. [[PubMed](#)]
4. Lowe, P.R.; Sansom, C.E.; Schwalbe, C.H.; Stevens, M.F.; Clark, A.S. Antitumor imidazotetrazines. 25. Crystal structure of 8-carbamoyl-3-methylimidazo[5,1-*d*]-1,2,3,5-tetrazin-4(3*H*)-one (temozolomide) and structural comparisons with the related drugs mitozolomide and DTIC. *J. Med. Chem.* **1992**, *35*, 3377–3382. [[CrossRef](#)] [[PubMed](#)]
5. Clark, A.S.; Deans, B.; Stevens, M.F.; Tisdale, M.J.; Wheelhouse, R.T.; Denny, B.J.; Hartley, J.A. Antitumor imidazotetrazines. 32. Synthesis of novel imidazotetrazinones and related bicyclic heterocycles to probe the mode of action of the antitumor drug temozolomide. *J. Med. Chem.* **1995**, *38*, 1493–1504. [[CrossRef](#)] [[PubMed](#)]
6. Denny, B.J.; Wheelhouse, R.T.; Stevens, M.F.G.; Tsang, L.L.H.; Slack, J.A. NMR and molecular modeling investigation of the mechanism of activation of the antitumor drug temozolomide and its interaction with DNA. *Biochemistry* **1994**, *33*, 9045–9051. [[CrossRef](#)] [[PubMed](#)]
7. Patel, M.; McCully, C.; Godwin, K.; Balis, F.M. Plasma and cerebrospinal fluid pharmacokinetics of temozolomide. *Proc. Am. Soc. Clin. Oncol.* **1995**, *14*, 461a. [[CrossRef](#)] [[PubMed](#)]
8. Ekeblad, S.; Sundin, A.; Janson, E.T.; Welin, S.; Granberg, D.; Kindmark, H.; Dunder, K.; Kozlovacki, G.; Orlefors, H.; Sigurd, M.; et al. Temozolomide as Monotherapy Is Effective in Treatment of Advanced Malignant Neuroendocrine Tumors. *Clin. Cancer Res.* **2007**, *13*, 2986–2991. [[CrossRef](#)] [[PubMed](#)]
9. Pegg, A.E.; Dolan, M.E.; Moschel, R.C. Structure, function, and inhibition of O6-alkylguanine-DNA alkyltransferase. *Prog. Nucleic Acid Res. Mol. Biol.* **1995**, *51*, 167–223. [[PubMed](#)]
10. Reuland, S.N.; Goldstein, N.B.; Partyka, K.A.; Cooper, D.A.; Fujita, M.; Norris, D.A.; Shellman, Y.G. The combination of BH3-mimetic ABT-737 with the alkylating agent temozolomide induces strong synergistic killing of melanoma cells independent of p53. *PLoS ONE* **2011**, *6*, e24294. [[CrossRef](#)] [[PubMed](#)]
11. Patel, P.M.; Suci, S.; Mortie, L.; Kruit, W.H.; Robert, C.; Schadendorf, D.; Trefzer, U.; Punt, C.J.; Dummer, R.; EORTC Melanoma Group. Extended schedule, escalated dose temozolomide versus dacarbazine in stage IV melanoma: Final results of a randomised phase III study (EORTC 18032). *Eur. J. Cancer* **2011**, *47*, 1476–1483. [[CrossRef](#)] [[PubMed](#)]
12. Suppasansatorn, P.; Wang, G.; Conway, B.R.; Wang, W.; Wang, Y. Skin delivery potency and antitumor activities of temozolomide ester prodrugs. *Cancer Lett.* **2006**, *244*, 42–52. [[CrossRef](#)] [[PubMed](#)]
13. Agarwal, S.S.; Kirkwood, J.M. Temozolomide, a Novel Alkylating Agent with Activity in the Central Nervous System, May Improve the Treatment of Advanced Metastatic Melanoma. *Oncologist* **2000**, *5*, 144–151. [[CrossRef](#)]
14. Battaglia, L.; Gallarate, M. Lipid nanoparticles: State of the art, new preparation methods and challenges in drug delivery. *Exp. Opin. Drug Deliv.* **2012**, *9*, 497–508. [[CrossRef](#)] [[PubMed](#)]
15. Battaglia, L.; Gallarate, M.; Cavalli, R.; Trotta, M. Solid lipid nanoparticles produced through a coacervation method. *J. Microencaps.* **2010**, *27*, 78–85. [[CrossRef](#)] [[PubMed](#)]
16. Annovazzi, L.; Schiffer, D.; Mellai, M.; Marina, G.; Luigi, B.; Daniela, C.; Elena, P.; Elisabetta, M.; Konstantin, C.; Alessandro, B.; et al. Solid Lipid Nanoparticles Loaded with Antitumor Lipophilic Prodrugs Aimed to Glioblastoma Treatment: Preliminary Studies on Cultured Cells. *J. Nanosci. Nanotechnol.* **2017**, *17*, 3606–3614. [[CrossRef](#)]

17. Peira, E.; Chirio, D.; Battaglia, L.; Barge, A.; Chegaev, K.; Gigliotti, C.L.; Ferrara, B.; Dianzani, C.; Gallarate, M. Solid lipid nanoparticles carrying lipophilic derivatives of doxorubicin: Preparation, characterization, and in vitro cytotoxicity studies. *J. Microencapsul.* **2016**, *33*, 381–390. [[CrossRef](#)] [[PubMed](#)]
18. Boggio, E.; Dianzani, C.; Gigliotti, C.L.; Soluri, M.F.; Clemente, N.; Cappellano, G.; Toth, E.; Raineri, D.; Ferrara, B.; Comi, C.; et al. Thrombin Cleavage of Osteopontin Modulates Its Activities in Human Cells In Vitro and Mouse Experimental Autoimmune Encephalomyelitis In Vivo. *J. Immunol. Res.* **2016**, *2016*, 9345495. [[CrossRef](#)] [[PubMed](#)]
19. Kurzen, H.; Schmitt, S.; Näher, H.; Möhler, T. Inhibition of angiogenesis by non-toxic doses of temozolomide. *Anticancer Drugs* **2003**, *14*, 515–522. [[CrossRef](#)] [[PubMed](#)]
20. Sabo, E.; Boltenko, A.; Sova, Y.; Stein, A.; Kleinhaus, S.; Resnick, M.B. Microscopic analysis and significance of vascular architectural complexity in renal cell carcinoma. *Clin. Cancer Res.* **2011**, *7*, 533–537.
21. Kumari, S.; Ahsan, S.M.; Kumar, J.M.; Kondapi, A.K.; Rao, N.M. Overcoming blood brain barrier with a dual purpose Temozolomide loaded Lactoferrin nanoparticles for combating glioma (SERP-17-12433). *Sci. Rep.* **2017**, *7*, 6602. [[CrossRef](#)] [[PubMed](#)]
22. Kim, S.S.; Rait, A.; Kim, E.; DeMarco, J.; Pirollo, K.F.; Chang, E.H. Encapsulation of temozolomide in a tumor-targeting nanocomplex enhances anti-cancer efficacy and reduces toxicity in a mouse model of glioblastoma. *Cancer Lett.* **2015**, *369*, 250–258. [[CrossRef](#)] [[PubMed](#)]
23. Fang, C.; Wang, K.; Stephen, Z.R.; Mu, Q.; Kievit, F.M.; Chiu, D.T.; Press, O.W.; Zhang, M. Temozolomide nanoparticles for targeted glioblastoma therapy. *ACS Appl. Mater. Interfaces.* **2015**, *7*, 6674–6682. [[CrossRef](#)] [[PubMed](#)]
24. Ananta, J.S.; Paulmurugan, R.; Massoud, T.F. Temozolomide-loaded PLGA nanoparticles to treat glioblastoma cells: A biophysical and cell culture evaluation. *Neurol. Res.* **2016**, *38*, 51–59. [[CrossRef](#)] [[PubMed](#)]
25. Jiang, G.; Sun, C.; Li, R.; Wei, Z.P.; Zheng, J.N.; Liu, Y.Q. Enhanced antitumor efficacy of a novel oncolytic adenovirus combined with temozolomide in the treatment of melanoma in vivo. *J. Cancer Res. Clin. Oncol.* **2015**, *141*, 75–85. [[CrossRef](#)] [[PubMed](#)]
26. Mathieu, V.; le Mercier, M.; de Neve, N.; Sauvage, S.; Gras, T.; Roland, I.; Lefranc, F.; Kiss, R. Galectin-1 Knockdown Increases Sensitivity to Temozolomide in a B16F10 Mouse Metastatic Melanoma Model. *J. Invest. Dermatol.* **2007**, *127*, 2399–2410. [[CrossRef](#)] [[PubMed](#)]
27. Middleton, M.R.; Kelly, J.; Thatcher, N.; Donnelly, D.J.; McElhinney, R.S.; McMurry, T.B.H.; McCormick, J.E.; Margison, G.P. O6-(4-bromothienyl)guanine improves the therapeutic index of temozolomide against A375M melanoma xenografts. *Int. J. Cancer* **2000**, *85*, 248–252. [[CrossRef](#)]
28. Karmali, R.A.; Maxuitenko, Y.Y.; Gorman, G.S.; Qu, Z. Combinatorial treatment with carboxyamidotriazoleorotate and temozolomide in sc-implanted human LOX IMVI melanoma xenografts. *J. Solid Tumors* **2012**, *2*, 13–28. [[CrossRef](#)]
29. Gallarate, M.; Serpe, L.; Foglietta, F.; Zara, G.P.; Giordano, S.; Peira, E.; Chirio, D.; Battaglia, L. Solid lipid nanoparticles loaded with fluorescent-labelled Cyclosporine A: Anti-inflammatory activity in vitro. *Protein Pept. Lett.* **2014**, *21*, 1157–1162. [[CrossRef](#)] [[PubMed](#)]
30. Robert, C.; Thomas, L.; Bondarenko, I.; O'Day, S.; Weber, J.; Garbe, C.; Lebbe, C.; Baurain, J.F.; Testori, A.; Grob, J.J.; et al. Ipilimumab plus dacarbazine for previously untreated metastatic melanoma. *N. Engl. J. Med.* **2011**, *364*, 2517–2526. [[CrossRef](#)] [[PubMed](#)]
31. Barrera, G.; Daga, M.; Ferrara, B.; Dianzani, C.; Pizzimenti, S.; Argenziano, M.; Cavalli, R.; Trotta, F. Drug delivery nanoparticles in treating chemoresistant tumor cells. *Curr. Med. Chem.* **2017**, *24*, 4800–4815. [[CrossRef](#)]
32. Pizzimenti, S.; Dianzani, C.; Zara, G.P.; Barrera, G. Challenges and Opportunities of Nanoparticle-based Theranostics in Skin Cancer. In *Nanoscience in Dermatology*; Hamblin, M.R., Avci, P., Prow, T.W., Eds.; Elsevier: London, UK, 2016; pp. 177–188.
33. Daga, M.; Dianzani, C.; Ferrara, B.; Nardoza, V.; Cavalli, R.; Barrera, G.; Pizzimenti, S. Latest News on Nanotechnology for Melanoma Therapy and Diagnosis. *SM J. Neurol. Neurosci.* **2016**, *2*, 1005.
34. Atkinson, V. Recent advances in malignant melanoma. *Intern. Med. J.* **2017**, *47*, 1114–1121. [[CrossRef](#)] [[PubMed](#)]

35. Jiang, G.; Li, R.; Tang, J.; Ma, Y.; Hou, X.; Yang, C.; Guo, W.; Xin, Y.; Liu, Y. Formulation of temozolomide-loaded nanoparticles and their targeting potential to melanoma cells. *Oncol. Rep.* **2017**, *37*, 995–1001. [[CrossRef](#)] [[PubMed](#)]
36. Gehrke, S.; Otsuka, A.; Huber, R.; Meier, B.; Kistowska, M.; Fenini, G.; Cheng, P.; Dummer, R.; Kerl, K.; Contassot, E.; et al. Metastatic melanoma cell lines do not secrete IL-1beta but promote IL-1beta production from macrophages. *J. Dermatol. Sci.* **2014**, *74*, 167–169. [[CrossRef](#)] [[PubMed](#)]
37. Malori, W.; Formisano, G.; Molinari, A. In vitro effects of 2,5 hexanedione on a melanoma cell line: A morphological study. *Toxicology* **1987**, *43*, 269–282. [[CrossRef](#)]



© 2018 by the authors. Licensee MDPI, Basel, Switzerland. This article is an open access article distributed under the terms and conditions of the Creative Commons Attribution (CC BY) license (<http://creativecommons.org/licenses/by/4.0/>).

Enhanced cytotoxic effect of camptothecin nanosponges in anaplastic thyroid cancer cells *in vitro* and *in vivo* on orthotopic xenograft tumors

Background: Anaplastic carcinoma of the thyroid (ATC) is one of the most lethal human malignant cancer with median survival of 6 months from the diagnosis. To date there is no treatment that can successfully change the course of the ATC. Camptothecin (CPT) is an inhibitor of DNA Topoisomerase-I with a wide spectrum of anticancer activities. The use of CPT has been hampered by a poor aqueous solubility and a high degradation rate. Previously, we have reported that CPT encapsulated in β -cyclodextrin-nanosponges (CN-CPT) has an increased solubility, is protected from degradation and displays an enhanced inhibitory effect on prostate tumor cells *in vitro* and *in vivo*.

Aim: The aim of this study was to evaluate whether β -cyclodextrin nanosponges carriers display their antitumoral efficacy on two ATC cell lines (Cal-62 and BTH-101) and on an orthotopic thyroid cancer model *in vivo*.

Methods: The effects of CN-CPT on cell proliferation, adhesion and migration were evaluated *in vitro*. Moreover, effects on cell cycle and cell apoptosis were investigated. For determining mechanisms underlying CN-CPT-mediated inhibition of cell proliferation, adhesion and migration, CN-CPT effects on expression of β -PIX, involved in rearrangement of the cytoskeleton and cell migration, and on phosphorylation of Erk1.2, involved in signaling of multiple surface receptors, were evaluated by western blotting. Finally, the *in vivo* study was carried out on orthotopic ATC xenografts in SCID/beige mice.

Results: CN-CPT reported a significant inhibition of both cell lines viability, in the concentration range $2 \times 10^{-10} \text{M}$ – $6 \times 10^{-8} \text{M}$, showing a faster and enhanced

effect compared to free CPT. The inhibition of clonogenic capacity and cell cycle progression validated previous obtained data. CN-CPT demonstrated its anti-metastatic potential by inhibiting tumor cell adhesion to endothelial cells (10^{-11}M – 10^{-8}M) and tumor cell migration ($6 \times 10^{-8}\text{M}$ – $6 \times 10^{-9}\text{M}$). The effects on intracellular signalling, assessed by western blot analysis, revealed an inhibition of the Rho family activator β -PIX expression and of the MAPK Erk1,2 phosphorylation. Finally, *in vivo* obtained data reported that CN-CPT, in comparison with the unencapsulated drug, significantly inhibited the growth and the volume of the tumor in ATC mice, without apparent toxic effects.

Conclusion: This work extends previous observations showing that β -cyclodextrin nanosponges, in association to conventional approaches such as surgery or radiotherapy, appear to be a promising tool for the treatment of anaplastic thyroid cancers.



Enhanced cytotoxic effect of camptothecin nanosponges in anaplastic thyroid cancer cells in vitro and in vivo on orthotopic xenograft tumors

Casimiro Luca Gigliotti, Benedetta Ferrara, Sergio Occhipinti, Elena Boggio, Giuseppina Barrera, Stefania Pizzimenti, Mirella Giovarelli, Roberto Fantozzi, Annalisa Chiocchetti, Monica Argenziano, Nausicaa Clemente, Francesco Trotta, Caterina Marchiò, Laura Annaratone, Renzo Boldorini, Umberto Dianzani, Roberta Cavalli & Chiara Dianzani

To cite this article: Casimiro Luca Gigliotti, Benedetta Ferrara, Sergio Occhipinti, Elena Boggio, Giuseppina Barrera, Stefania Pizzimenti, Mirella Giovarelli, Roberto Fantozzi, Annalisa Chiocchetti, Monica Argenziano, Nausicaa Clemente, Francesco Trotta, Caterina Marchiò, Laura Annaratone, Renzo Boldorini, Umberto Dianzani, Roberta Cavalli & Chiara Dianzani (2017) Enhanced cytotoxic effect of camptothecin nanosponges in anaplastic thyroid cancer cells in vitro and in vivo on orthotopic xenograft tumors, *Drug Delivery*, 24:1, 670-680, DOI: [10.1080/10717544.2017.1303856](https://doi.org/10.1080/10717544.2017.1303856)

To link to this article: <http://dx.doi.org/10.1080/10717544.2017.1303856>



© 2017 The Author(s). Published by Informa UK Limited, trading as Taylor & Francis Group.



[View supplementary material](#)



Published online: 03 Apr 2017.



[Submit your article to this journal](#)



Article views: 29






[View related articles](#)



[View Crossmark data](#)

RESEARCH ARTICLE

Enhanced cytotoxic effect of camptothecin nanosponges in anaplastic thyroid cancer cells *in vitro* and *in vivo* on orthotopic xenograft tumors

Casimiro Luca Gigliotti^{1*}, Benedetta Ferrara^{2*} , Sergio Occhipinti^{3*}, Elena Boggio¹, Giuseppina Barrera⁴, Stefania Pizzimenti⁴, Mirella Giovarelli³ , Roberto Fantozzi², Annalisa Chiocchetti¹, Monica Argenziano², Nausicaa Clemente¹, Francesco Trotta⁵, Caterina Marchiò⁶, Laura Annaratone⁶, Renzo Boldorini¹, Umberto Dianzani¹, Roberta Cavalli², and Chiara Dianzani² 

¹Department of Health Sciences, Interdisciplinary Research Center of Autoimmune Diseases, UPO, Novara, Italy, ²Department of Drug Science and Technology, University of Torino, Torino, Italy, ³Department of Molecular Biotechnology and Health Sciences, University of Torino, Torino, Italy, ⁴Department of Clinical and Biological Sciences, University of Torino, Torino, Italy, ⁵Department of Chemistry, University of Torino, Torino, Italy, and ⁶Department of Medical Sciences, University of Torino, Torino, Italy

Abstract

Anaplastic carcinoma of the thyroid (ATC) is a lethal human malignant cancer with median survival of 6 months. To date, no treatment has substantially changed its course, which makes urgent need for the development of novel drugs or novel formulations for drug delivery. Nanomedicine has enormous potential to improve the accuracy of cancer therapy by enhancing availability and stability, decreasing effective doses and reducing side effects of drugs.

Camptothecin (CPT) is an inhibitor of DNA topoisomerase-I with several anticancer properties but has poor solubility and a high degradation rate. Previously, we reported that CPT encapsulated in β -cyclodextrin-nanosponges (CN-CPT) increased solubility, was protected from degradation and inhibited the growth of prostate tumor cells both *in vitro* and *in vivo*. The aim of this study was to extend that work by assessing the CN-CPT effectiveness on ATC both *in vitro* and *in vivo*.

Results showed that CN-CPT significantly inhibited viability, clonogenic capacity and cell-cycle progression of ATC cell lines showing a faster and enhanced effect compared to free CPT. Moreover, CN-CPT inhibited tumor cell adhesion to vascular endothelial cells, migration, secretion of pro-angiogenic factors (IL-8 and VEGF- α), expression of β -PIX, belonging to the Rho family activators, and phosphorylation of the Erk1/2 MAPK.

Finally, CN-CPT significantly inhibited the growth, the metastatization and the vascularization of orthotopic ATC xenografts in SCID/beige mice without apparent toxic effects *in vivo*. This work extends the previous insight showing that β -cyclodextrin-nanosponges are a promising tool for the treatment of ATC.

Introduction

Thyroid cancers are the most common tumors of endocrine origin and their incidence has increased globally over the past 10 years (Jemal et al., 2011). They derive from follicular and para-follicular cells and most of them are differentiated papillary and follicular carcinomas, while 1% of cases are

partly differentiated or undifferentiated and classified as anaplastic thyroid carcinoma (ATC). Most differentiated carcinomas display slow progression and are effectively treated with thyroidectomy and radioiodine ablation (Broecker-Preuss et al., 2015). By contrast, ATC progression is extremely rapid and no effective systemic therapy has been established so that the overall survival level is only 13% (Gilliland et al., 1997). At the time of diagnosis, ATC often display an advanced stage of development, local invasion of the trachea, esophagus, blood vessels and muscles and development of distant metastases to the mediastinum, lung, liver, bone and brain (Phay & Ringel, 2013; Chen et al., 2014; Mirrieles et al., 2014; Varinot et al., 2014). Risk factors for thyroid cancers include environmental and genetic factors, exposure to ionizing radiation and preexisting thyroid neoplasia (Campanella et al., 2014). Genetic alterations that contribute to thyroid carcinoma include point mutations

*These authors have contributed equally to this work.

Address for correspondence: Umberto Dianzani, Department of Health Sciences, Interdisciplinary Research Center of Autoimmune Diseases, University of Piemonte Orientale, 28100 Novara, Italy. Email: umberto.dianzani@med.uniupo.it

This is an Open Access article distributed under the terms of the Creative Commons Attribution-NonCommercial-NoDerivatives License (<http://creativecommons.org/licenses/by-nc-nd/4.0/>), which permits non-commercial re-use, distribution, and reproduction in any medium, provided the original work is properly cited, and is not altered, transformed, or built upon in any way.

Keywords

Camptothecin, β -cyclodextrin-nanosponges, anaplastic thyroid carcinoma, cell migration, cell adhesion

History

Received 16 January 2017

Revised 2 March 2017

Accepted 5 March 2017

of BRAF and RAS (Fukushima & Takenoshita, 2005; Marotta et al., 2011); translocations involving RET/PTC1, RET/PTC3 and PAX8/PPAR- γ (Romei & Elisei, 2012; Raman & Koenig, 2014) and alterations of the DNA methylation pattern (Ragazzi et al., 2014; Faam et al., 2015).

To date, no effective therapies are available for ATC, which are currently treated with trivalent therapies including surgery, chemotherapy and radiotherapy resulting in an increased median survival of only 5 months (Wein & Weber, 2011; Parenti et al., 2014).

Camptothecin (CPT) is a pentacyclic alkaloid isolated from the bark of *Camptotheca acuminata*, (Wall et al., 1996). It quickly enters into cells and exerts antitumor activity by blocking topoisomerase-1 (TOP-1) in a specific and reversible manner. Unfortunately, it is weakly soluble in water and undergoes spontaneous and rapid inactivation at neutral pH by the opening of its six-member lactone E ring. Therefore, it requires a prolonged infusion, so that the complex TOP-1 is kept in place long enough to allow the induction of DNA damage (Fassberg & Stella, 1992; Chourpa et al., 1998). Moreover, its dosage and antitumor efficacy are limited by severe side effects, such as severe myelosuppression accompanied by prolonged diarrhea, fever, nausea and vomiting (Basili & Moro, 2009). The main water-soluble derivatives of CPT are the irinotecan (Compostar[®]) and topotecan (Hycamtin[®]).

To overcome problems in administering the drug, we previously investigated the antineoplastic effects of CPT loaded into nanosponges of β -cyclodextrin (CN-CPT) (Gigliotti et al., 2016a). Results showed that CN-CPT increased solubility was protected from degradation and inhibited the growth of prostate tumor cells both *in vitro* and *in vivo* to a higher extent than free CPT. Cyclodextrin nanosponges are novel biocompatible polymer nanoparticles obtained by cross linking of cyclodextrins (Subramanian et al., 2012), which are cyclic oligosaccharides consisting of multiple α -D-glucopyranose units linked together by an α -1,4 bond and include α -, β - and γ -cyclodextrins carrying six, seven or eight glucopyranose units, respectively. β -Cyclodextrin is the most widely used for nanosponge production because of its high capability to encapsulate drugs (Torre et al., 2013; Trotta et al., 2014).

The aim of this study was to extend that work by assessing the CN-CPT effectiveness on ATC both *in vitro* and *in vivo*. Results showed that CN-CPT inhibited the growth of ATC cell lines both *in vitro* and *in vivo* to a higher extent than free CPT. Moreover, it inhibited tumor cell adhesion to endothelial cells and migration which suggest that it may be effective also to inhibit tumor metastatic dissemination.

Methods

Materials

CPT was purchased from Sigma-Aldrich (Sigma-Aldrich, St Louis, MO). β -Cyclodextrins (β -CDs) were a gift from Roquette (France). CD nanosponges (CNs) cross linked at 1:4 molar ratio with carbonyldiimidazole were prepared as described previously (Swaminathan et al., 2010). All reagents were of analytical grade. Laboratory reagents were from Sigma-Aldrich unless otherwise specified. Cell culture

reagents were purchased from Gibco/Invitrogen (Life Technologies, Paisley, UK) except where otherwise indicated.

Preparation of CPT in solution and camptothecin-loaded nanosponges (CN-CPT)

To prepare the CPT solution, about 1 mg of CPT was dissolved in 1 mL of dimethylsulfoxide (DMSO):water mixture (1:1, w/w) at pH = 5.5. A further dilution was carried out using 0.9% NaCl solution at pH = 5.5 containing 30% of DMSO.

To load CPT in CNs, 4 mg of CPT were added to an aqueous suspension of CNs in a ratio of 1:4 (drug to CN by weight) at pH 5.5 and stirred for 24 h in the dark. The aqueous suspension was then centrifuged at 8000 rpm for 10 min to separate the free drug, not incorporated, as a solid residue below the colloidal supernatant. The colloidal supernatant was freeze-dried to obtain drug-loaded nanosponges as a powder. This powder can be stored at 4 °C until use.

A weighed amount of freeze-dried CN-CPT was dispersed in a sterile aqueous solution at pH 6.0 containing 0.9% NaCl and 3% polyethylene glycol (PEG)-400 w/v under stirring to obtain an isotonic aqueous nanosuspension containing 100 $\mu\text{g mL}^{-1}$ of CPT for the *in vivo* administration. For the free CPT formulation, a weighed amount of CPT was dissolved in a DMSO:water mixture (1:1, w/w) at pH = 5.5 and then diluted to a sterile aqueous solution at pH 6.0 containing 0.9% NaCl and 3% PEG-400 w/v to obtain a 100 $\mu\text{g mL}^{-1}$ concentration. The quantitative determination of CPT concentration in the formulations was evaluated by HPLC (Swaminathan et al., 2010).

CN-CPT sizes and polydispersity indices were measured by dynamic light scattering using a 90 Plus particle sizer (Brookhaven Instruments Corporation, Holtsville, NY) equipped with MAS OPTION (Brookhaven Instruments Corporation, Holtsville, NY) particle sizing software. The measurements were made at a fixed angle of 90° for all samples. The samples were suitably diluted with filtered distilled water for every measurement. Zeta potential measurement was then carried out using an additional electrode in the same instrument. For zeta potential determination, samples were diluted with 0.1 mM KCl and placed in the electrophoretic cell, where an electric field of about 15 V/cm was applied.

The *in vitro* release was carried out using multicompartiment rotating cells with a dialysis membrane (Sartorius, cutoff 12 000 Da). The donor phase consisted of CPT-nanosponge formulation in phosphate buffer at pH 7.4 (1 mL). The receiving phase consisted of phosphate buffer, pH 7.4. The receiving phase was completely withdrawn and replaced with fresh medium after fixed time intervals, suitably diluted and analyzed using the HPLC method described before.

CN-CPT showed an average diameter of about 350 nm, a polydispersity index of 0.11 and a negative surface charge with a zeta potential value of -27.4 mV. The *in vitro* release kinetics of CPT from nanosponge formulation was slow and prolonged over time, reaching 15.5% after 24 h.

Cells

Human umbilical vein endothelial cells (HUVEC) were isolated from human umbilical veins by collagenase treatment

(1%) and cultured in M199 medium with the addition of 20% fetal calf serum (FCS) 100 U/mL⁻¹ penicillin, 100 µg/mL⁻¹ streptomycin, 5 U/mL⁻¹ heparin, 12 µg/mL⁻¹ bovine brain extract and 200 mM glutamine. HUVEC were grown to confluence in flasks and used from the second to the fifth passage. Use of HUVEC was approved by the Ethics Committee of the ‘‘Presidio Ospedaliero Martini’’ of Turin and conducted in accordance to the Declaration of Helsinki. Written informed consent was obtained from all donors.

The study was performed on two ATC cell lines, BHT-101 and CAL-62. Cells were purchased from Deutsche Sammlung von Mikroorganismen und Zellculturen (Braunschweig, Germany), which certifies the origin and identity of the cells. The cell lines were grown in culture dishes as a monolayer in RPMI 1640 medium plus 10% FCS, 100 U/mL⁻¹ penicillin, and 100 µg/mL⁻¹ streptomycin at 37 °C in a 5% CO₂ humidified atmosphere (Schweppe et al., 2008).

Cell viability assay

CAL-62 and BHT-101 cells (1 × 10³/well) were seeded in 96-well plates and incubated at 37 °C, 5% CO₂, for 24 h. Then, cells were treated with different concentrations of CN-CPT or CPT (2 × 10⁻¹⁰–2 × 10⁻⁸ M). After 24–48 h of incubation, viable cells were evaluated by 2,3-bis[2-methoxy-4-nitro-5sulfophenyl]-2 H-tetrazolium-5-carboxanilide (MTT) inner salt reagent at 570 nm, as described by the manufacturer’s protocol. The controls (i.e. cells that had received no drug) were normalized to 100%, and the readings from treated cells were expressed as % of viability inhibition. Eight replicates were used to determine each data point and five different experiments were performed.

Colony-forming assay

CAL-62 and BHT-101 cells (800/well) were seeded into six-well plates and treated with the compounds (10⁻¹⁰–10⁻⁸ M). The medium was changed after 72 h and cells were cultured for additional 10 days. Subsequently, cells were fixed and stained with a solution of 80% crystal violet and 20% methanol. Colonies were then photographed and counted with a Gel Doc equipment (Bio-Rad Laboratories, Hercules, CA). Then, cells were washed and 30% acetic acid were added to induce a complete dissolution of the crystal violet. Absorbance was recorded at 595 nm by a 96-well-plate ELISA reader. Five different experiments were performed.

Cell adhesion assay

HUVEC were grown to confluence in 24-well plates. Then, they were pretreated with increasing concentrations of CPT or CN-CPT (10⁻¹¹–10⁻⁸ M) for 24 h and washed twice with fresh medium. The tumor cells (1 × 10⁵ cells/well) were seeded and left to adhere with HUVEC for 1 h, as previously reported (Minelli et al., 2012a, 2012b). Unattached tumor cells were washed away and the number of adherent cells was evaluated by the Image Pro Plus Software for micro-imaging (Media Cybernetics, version 5.0, Bethesda, MD). Viability of the unattached cells was evaluated by the Trypan Blue test. Data are shown as percentage of the inhibition of treated cells versus the control adhesion measured on untreated cells; the

control adhesion was 48 ± 4 cells per microscope field (n = 6) for BHT-101 cells and in a similar range (44 ± 5 cells) for CAL-62 (mean ± SEM) (Dianzani et al., 2010).

Cell motility assay

In the wound-healing assay, after starvation for 18–24 h in serum-free medium, cells were plated onto six-well plates (10⁶ cell/well) and grown to confluence. Cell monolayers were wounded by scratching with a pipette tip along the diameter of the well, and they were washed twice with serum-free medium before their incubation with culture medium in the absence or presence of CPT or CN-CPT (10⁻⁸ M) and mitomycin C (50 µg/mL⁻¹, Sigma-Aldrich, St Louis, MO). In order to monitor cell movement into the wounded area, five fields of each wound were photographed immediately after the scratch (0 h) and after 24 h (Dianzani et al., 2014; Gigliotti et al., 2016a).

In the Boyden chamber (BD Biosciences, San Jose, CA) invasion assay, cells (8000) were plated onto the apical side of 50 µg/mL⁻¹ Matrigel-coated filters (8.2 mm diameter and 0.5 µm pore size; Neuro Probe, Inc.; BIOMAP snc, Milan, Italy) in serum-free medium with or without increasing concentration of the drugs (2 × 10⁻⁹–2 × 10⁻⁸ M). Medium containing 20% FCS was placed in the basolateral chamber as a chemo attractant. After 24 h, cells on the apical side were wiped off with Q-tips. Cells on the bottom of the filter were stained with crystal violet and counted (five fields of each triplicate filter) with an inverted microscope. Data are shown as percentages of the inhibition of treated cells versus the control migration measured on untreated cells. Control migration was 52 ± 4 cells per microscope field (n = 5) for BHT-101 cells and 66 ± 5 for CAL-62 (Occhipinti et al., 2013).

ELISA assay

CAL-62 or BHT-101 cells (1 × 10⁵/well) were plated in 24-well plates and treated with CPT or CN-CPT (10⁻¹¹–10⁻⁸ M) for 48 h. CPT and CN-CPT were replenished every 24 h (48 h culture: 24 + 24 h) without changing the culture medium. Cell-free supernatants were collected and concentrations of Interleukin-8 (IL-8), vascular endothelial growth factor α (VEGF-α) and angiopoietin 2 were measured by ELISA according to the instructions of the manufacturers (IL-8, eBioscience, San Diego, CA; VEGF-α and angiopoietin 2, R&D Systems, Minneapolis, MN). Absorbance was detected with a microplate reader (Bio-Rad Laboratories, Hercules, CA), and the Excel program was used to calculate the standard curve.

Protein extraction and western blot analysis

Cells were seeded into six-well plates and treated for 48 h with CPT or CN-CPT (10⁻⁸–10⁻⁹ M). CPT and CN-CPT were replenished every 24 h (48 h culture: 24 + 24 h) without changing the culture medium. Cells were then lysed in a buffer composed of 50 mM Tris-HCl pH 7.4, 150 mM NaCl, 5 mM EDTA, 1% sodium deoxycholate, 1% Nonidet P-40, 0.1% SDS, phosphatase and protease inhibitor cocktail. Cell lysates were cleared from insoluble fractions by high-speed

centrifugation, and protein concentration was determined with a commercially available kit (Bio Rad Laboratories, Hercules, CA) and measured with a spectrophotometer (Jasco Analytical Instruments, Easton, MD). Proteins (40 µg) were loaded on 10% SDS-PAGE gels and transferred onto nitrocellulose membranes after electrophoresis. These were blocked by incubation for 1 h at room temperature with 5% nonfat milk dissolved in TBS-Tween 20. The membranes were then probed overnight with antibodies to β-PIX (AdipoGen International, San Diego, CA), phospho-Erk1,2 (Santa Cruz Biotechnology, Dallas, TX), or β-actin (Sigma-Aldrich, St Louis, MO) and, after three washes, incubated for 1 h with the HRP-conjugated secondary antibody antibody antibody (Sigma-Aldrich, St Louis, MO). Bands were detected by chemiluminescence, and densitometric analysis was performed with the Multi-Analyst software (version 1.1, Bio-Rad Laboratories, Hercules, CA).

Cell-cycle analysis

Cells (1.5×10^5) were treated with CPT or CN-CPT as reported earlier. After 48 h, adherent and nonadherent cells were collected, washed in PBS and fixed in 75% ice-cold ethanol and subsequently resuspended in a buffer containing 0.02 mgmL⁻¹ RNase A (Worthington Biochemical Corporation, Lakewood, NJ), 0.05 mgmL⁻¹ propidium iodide (BD Biosciences, San Jose, CA), 0.2% v/v Nonidet P-40, 0.1% w/v sodium citrate. Samples were analyzed with a FACSCalibur cytometer (BD Biosciences, San Jose, CA).

Annexin V staining and caspase-3 activity

Cells (1.5×10^5) were treated with CPT or CN-CPT as reported earlier. After 48 h, they were stained with annexin V using the Annexin V Fluos kit (BD Biosciences, San Jose, CA) and analyzed by flow cytometry. Live cells were those not displaying shrunken/hypergranular morphology and unstained by AnnexinV. Caspase-3 activity was assessed in cell lysates using a fluorimetric assay (MBL, Watertown, MA) following the manufacturer instructions.

In vivo animal models and tumor growth

Animal studies were performed in accordance with EU and institutional guidelines approved by the Bioethics Committee for Animal Experimentation of the University of Turin, Italy (Prot. No. 4.2/2012) using NOD-SCID IL2Rγ^{null} (NSG; 10/11-week-old female) mice, bred under sterile conditions in our animal facilities. Animals were anesthetized with intramuscular injection of Zoletil® (Zolaxepan and Tiletamina) and Rompun® (Xylazina). CAL-62 cells were harvested from subconfluent cultures by trypsinization and washed in PBS. Then, cells (10^6 cells in 10 µL) were injected into the right thyroid lobe under surgical sterile conditions and tumors were allowed to grow during the following 10 days. Mice were then randomized into three groups receiving twice weekly intravenous injection of PBS (control group, $n = 5$) or 1 mgkg⁻¹ CPT ($n = 7$) or 1 mgkg⁻¹ CN-CPT ($n = 7$).

Mice were weighed twice weekly and sacrificed when the animals appeared moribund. Tumor growth velocity (T_v) was determined using the formula: $T_v = V/\text{days}$ from cells injection to excision.

Tumors and lungs were fixed in 10% formalin and paraffin embedded. Four serial sections/tumor were obtained and processed for immunohistochemistry using an automated slide processing platform (Ventana BenchMark XT AutoStainer, Roche) and a mouse monoclonal anti-human Ki-67 (Clone MIB-1) or a rabbit polyclonal anti-mouse CD31 (Abcam, Cambridge, UK) antibodies. Sections of lungs were stained with hematoxylin and eosin (H&E).

Ki-67-positive cells were heterogeneously distributed throughout the tumor. The Ki67-labeled nuclei were evaluated in the tumor areas where these markers were predominant (hot spots) using a digital camera (Olympus Q-colour 3, Tokyo, Japan) with area-based image analysis software (Dot-Slide 1.2 version, Tokyo, Japan). Ki-67 expression was calculated as the ratio between the labeled and the total nuclear areas. Only nuclei with a strongly positive label were counted. The 10 fields with the highest density of positive nuclei were captured. A mean of 3000 tumor cells per case (range 2000–3800) was counted. Tumor microvessel density (TMD) was measured by evaluating the CD31-positive area and total tumor area per field upon slide after scan (Panoramic midi II, 3D Histech, Budapest, Hungary) of the immunostaining, as previously described (Gigliotti et al., 2016a; Passaro et al., 2016).

Data analysis

Data are shown as mean ± standard error of the mean (SEM). Statistical analyses were performed with GraphPad Prism 5.0 software (San Diego, CA). For the *in vivo* experiments, the results are expressed as the median with interquartile range. One-way ANOVA was performed, followed by Tukey's multiple comparison post-test when needed. Kaplan–Meier survival curves were evaluated with the log rank Mantel-Cox test. Only p values <0.05 were considered to be significant.

Results

CN-CPT inhibits cell proliferation *in vitro*

We compared the ability of CN-CPT and free CPT to inhibit the growth of BHT-101 and CAL-62 *in vitro*. Cells were cultured in the presence and absence of titrated amounts (2×10^{-10} – 2×10^{-8} M) of each compound for 24–48 h and the amount of viable cells was then assessed by the MTT assay. Figure 1 shows that CN-CPT inhibited the growth of both cell lines to a higher extent than CPT. The effect was concentration- and time-dependent with small differences between the two cell lines. The different effect of the two compounds was detectable in terms of timing, maximal inhibition, and effective doses.

To validate these findings, we performed clonogenic survival assays. Cells were seeded onto six-well plates and treated with titrated doses (10^{-10} – 10^{-8}) of each compound. The culture medium was changed after 72 h, and cells were cultured for 10 additional days in the absence of the compounds. Results showed that treatment with CN-CPT inhibited the ability to form colonies of both cell lines to a higher extent than CPT (supporting information, Figure S1).

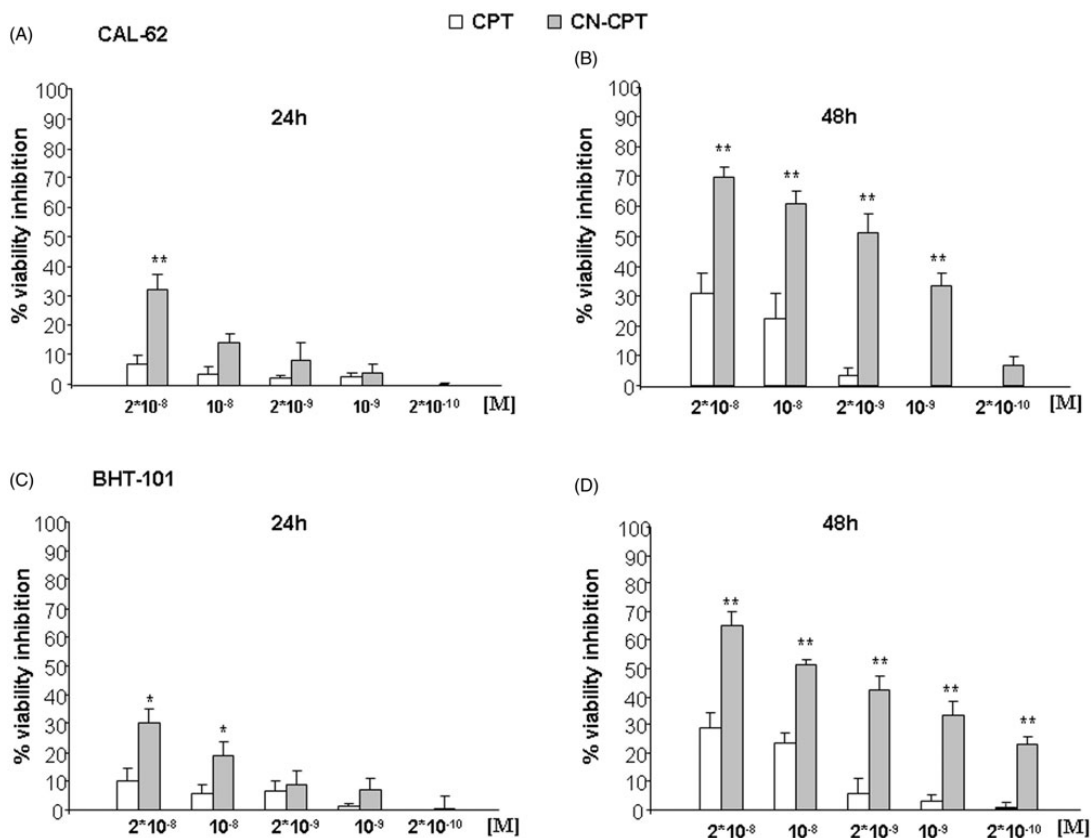


Figure 1. Inhibition of cell viability following CPT or CN-CPT treatments. CAL-62 (A, B) or BHT-101 (C, D) cells (1×10^3 /well) were treated with the indicated concentrations of drug for 24–48 h. Results are expressed as % of viability inhibition of control and shown as mean \pm SEM ($n = 5$). * $p < 0.05$, ** $p < 0.01$ significantly different from the same concentration of CPT.

The effect was concentration dependent with small differences between the two cell lines. The different effect of the two compounds was detectable in terms of effective doses but not in terms of maximal inhibition that was similar at the highest dose.

To assess whether inhibition of cell proliferation induced by CN-CPT-affected cell-cycle progression, we analyzed the cell cycle in CAL-62 and BHT-101 cells cultured in the presence and absence of titrated amounts of CN-CPT or CPT (10^{-9} and 10^{-8} M) for 48 h. Results showed that both doses of CN-CPT induced a substantial accumulation of cells in S phase compared to the untreated control in both cell lines. This effect was exerted also by CPT but only at the highest dose (Figure 2).

To assess whether inhibition of cell proliferation induced by CN-CPT involved cell death, we analyzed Annexin V staining, detecting both apoptotic and necrotic cells, and caspase 3 activation, detecting apoptosis, in CAL-62 and BHT-101 cells cultured in the presence and absence of titrated amounts (10^{-9} and 10^{-8} M) of CN-CPT or CPT for 48 h. Results showed that CN-CPT induced higher Annexin V staining and caspase 3 activation than CPT in both cell lines (Figure 3).

CN-CPT inhibits cell adhesion and migration *in vitro*

Adhesion of tumor cells to the vascular endothelium and their release into the bloodstream is a key step for metastasis formation (Ma & Waxman, 2008). Therefore, we performed *in vitro* experiments comparing the effect of CN-CPT and CPT on adhesion to HUVEC and motility of tumor cells.

In the adhesion experiments, HUVEC were pretreated for 24 h with titrated doses (10^{-11} and 10^{-8} M) of CN-CPT and CPT, washed, and used for adhesion assays with CAL-62 and BHT-101 cells. Results showed that CN-CPT inhibited adhesion of both cell lines at higher levels than CPT. The effect was concentration dependent with small differences between the two cell lines. The different effect of the two compounds was detectable in terms of both effective doses and maximal inhibition (Figure 4A–B). The difference was not due to an effect on cell viability since cells were still alive after the 24-h incubation with the drug.

Cell motility was initially assessed using a wound healing assay evaluating cell random migration. A linear scratch was done in confluent monolayers of CAL-62 and BHT-101 cells, which were then cultured in FCS-free medium to minimize cell proliferation in the presence or absence of CN-CPT and CPT (10^{-8} M). Analysis of the cell ability to migrate into the

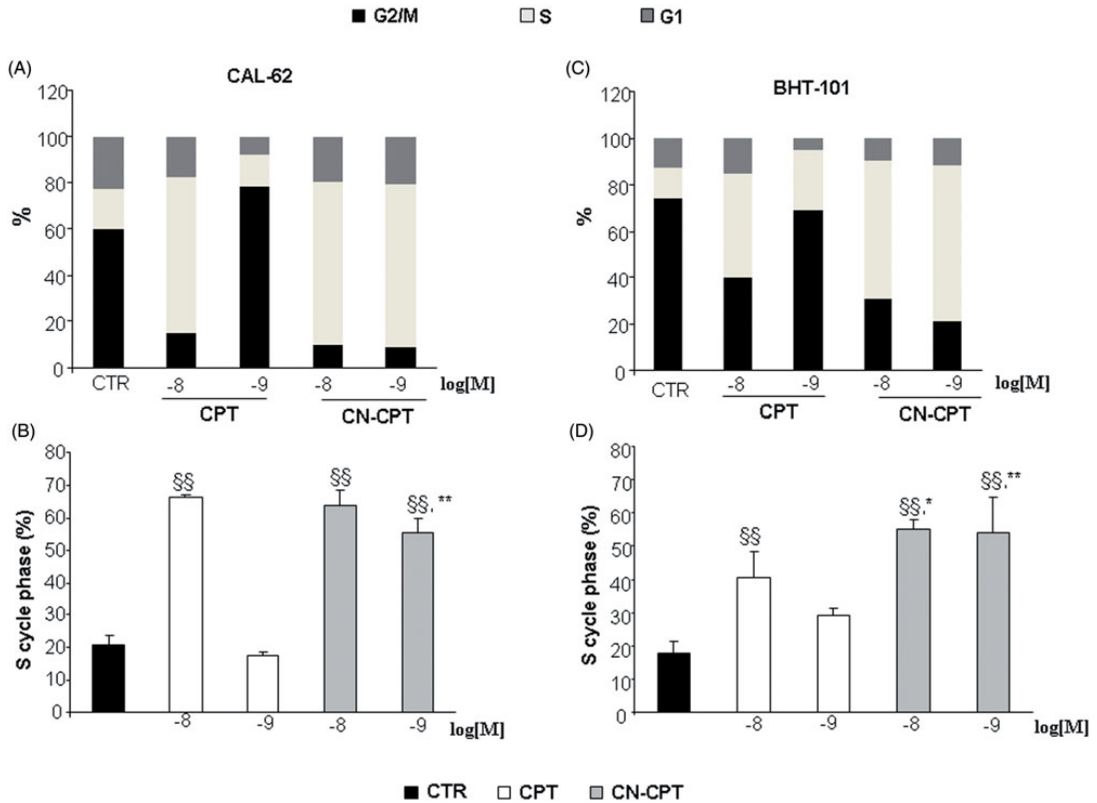


Figure 2. Induction of cell-cycle arrest by CPT or CN-CPT treatment. CAL-62 (A, B) and BHT-101 (C, D) cells (1.5×10^5) were treated or not with CPT or CN-CPT (10^{-8} and 10^{-9} M) for 48 h and cell cycle was then assessed by flow cytometry. CPT and CN-CPT were replenished every 24 h (48 h culture: 24 + 24 h) without changing the culture medium. Graphs show: (A, C) the % of cells in each cycle phase detected in one representative experiment, (B, D) the % of cells in S phase cycle expressed as means \pm SEM ($n=3$). Each experiment was performed in triplicate. §§ $p < 0.01$, significantly different from untreated cells; * $p < 0.05$, ** $p < 0.01$, significantly different from treated cells at the same drug concentration.

scratch after 24 h showed that CN-CPT inhibited adhesion of both cell lines at higher levels than CPT (supporting information, Figure S2). Then, cell motility was assessed using a Boyden chamber assay assessing directional migration of cells. CAL-62 and BHT-101 cells were seeded in the upper chamber of a Boyden chamber in serum-free medium in the presence or absence of titrated doses (2×10^{-9} and 2×10^{-8} M) of CN-CPT and CPT and allowed to migrate for 24 h toward the lower chamber containing medium with and without 20% FCS, used as a chemoattractant. Results showed that CN-CPT inhibited cell migration at higher levels than CPT in both cell lines (Figure 4C–D). The CN-CPT effect was concentration dependent with small differences between the two cell lines, whereas CPT displayed some effect on CAL-62 cells but it was almost ineffective on BHT-101 cells.

In both migration assays, doses and timing of treatments minimized the possible confounding effects due to the drug effect on cell growth.

CN-CPT inhibits VEGF- α and IL-8 secretion *in vitro*

Since ATC cells express high levels of pro-angiogenic molecules (Jayasooriya et al., 2011; Passaro et al., 2016),

we evaluated the effect of the drugs on secretion of VEGF- α , IL-8 and angiopoietin 2. CAL-62 and BHT-101 cells were incubated with titrated doses (10^{-11} – 10^{-8} M) of CN-CPT or CPT for 48 h. Then, secretion of VEGF- α , IL-8 and angiopoietin 2 was evaluated by ELISA in the culture supernatants. Results showed that the ATC cells produced a substantial amount of these factors and CN-CPT inhibited the secretion of VEGF- α and IL-8 compared to the free drug at the same concentrations (supporting information, Figure S3). No differences were found for angiopoietin 2 secretion (data not shown).

CN-CPT inhibits β -PIX expression and ERK_{1,2} phosphorylation *in vitro*

In order to investigate the mechanisms underlying CN-CPT-mediated inhibition of cell proliferation, adhesion and migration, we evaluated the effect of the drug on expression of β -PIX, involved in rearrangement of the cytoskeleton and cell migration and on Erk1,2 phosphorylation involved in signaling of multiple surface receptors (Kim et al., 2013; Occhipinti et al., 2013; Dianzani et al., 2014; Stevens et al., 2014; Gigliotti et al., 2016b). CAL-62 and BHT-101 cells were incubated with titrated doses (10^{-9} and 10^{-8} M) of CN-

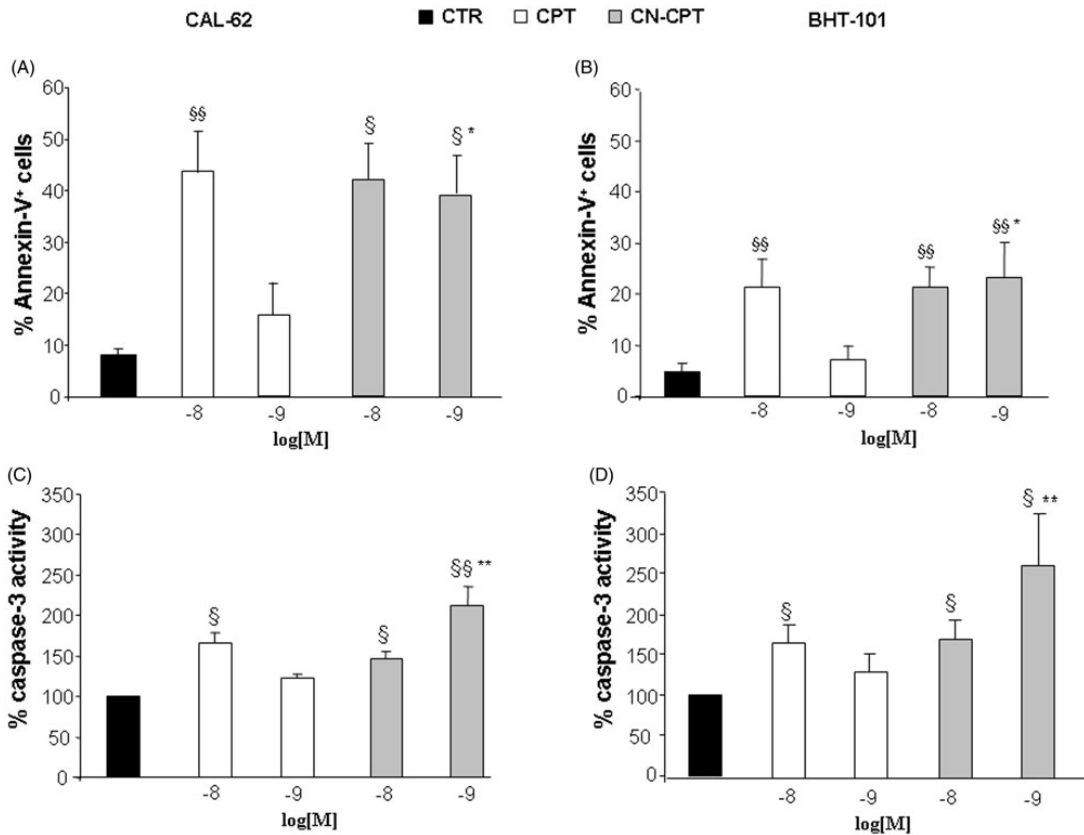


Figure 3. Proportions of Annexin-V-positive cells and levels of caspase-3 activity after CPT or CN-CPT treatment. Annexin-V-positive cells (A, B) and caspase-3 activity (C, D) was evaluated in CAL-62 (A, C) and BHT-101 (B, D) cells cultured for 48 h in the presence or absence of CPT or CN-CPT. CPT and CN-CPT were replenished every 24 h (48 h culture: 24 + 24 h) without changing the culture medium. Results are expressed as % of Annexin-V-positive cells and relative caspase activity %, calculated as result displayed by each treatment/the results displayed by untreated cells ($n = 5$). §§ $p < 0.01$, significantly different from untreated cells; § $p < 0.05$; §§* $p < 0.01$, significantly different from treated cells at the same drug concentration.

CPT or CPT for 48 h, lysed and analyzed for β -PIX expression and Erk1,2 phosphorylation by Western blot. Results showed that CN-CPT inhibited β -PIX expression and Erk1,2 phosphorylation at higher levels than CPT in both cell lines (Figure 5).

In vivo studies

We compared the effect of CN-CPT and CPT tumor growth and metastatic dissemination in NSG mice injected orthotopically in the thyroid lobe with CAL-62 cells and treated 10 days later with twice weekly injections of PBS, CPT or CN-CPT in the tail vein. Results showed that the overall survival of mice treated with CN-CPT was higher than that displayed by mice injected with either PBS or CPT (Figure 6A). In particular, median survivals of mice treated with PBS, CPT and CN-CPT were 28, 25 and 38 days, respectively. The difference of survival between the CN-CPT group and the control group was significant ($p = 0.0422$, log-rank test).

Analysis of tumor growth velocity showed that CN-CPT significantly inhibited the growth velocity of orthotopic anaplastic thyroid carcinoma xenografts compared to the control group, whereas CPT had no effect (Figure 6B).

Analysis of lung metastases showed that CN-CPT significantly inhibited development metastases compared to the control group, whereas CPT had no effect (Figure 6C).

Histologic analysis of the primary tumor showed that, in control mice, the tumors displayed diffuse necrosis whereas, in CN-CPT-treated mice, tumors displayed decreased necrosis, and in CPT-treated mice an intermediate picture. Immunohistochemical staining, performed 34 days after tumor challenge showed that Ki-67⁺ cells were homogeneously distributed in the tumor mass in PBS- and CPT-treated mice, whereas, they were concentrated at the invasive edge in the peripheral area of the tumor, but rare in the center of the tumor, in CN-CPT-treated mice (Figure 6D). This enrichment of Ki67⁺ cells was detected also at 51 days after tumor challenge (Figure 6E). To assess the effects on tumor angiogenesis, we stained the tumor sections for CD31 and evaluated the TMD. Results showed that treatment with CN-CPT substantially decreased the TMD compared with untreated mice and CPT-treated mice, whereas CPT had no effect (Figure 6F).

All treatments were well tolerated by the animals without significant weight loss in any group.

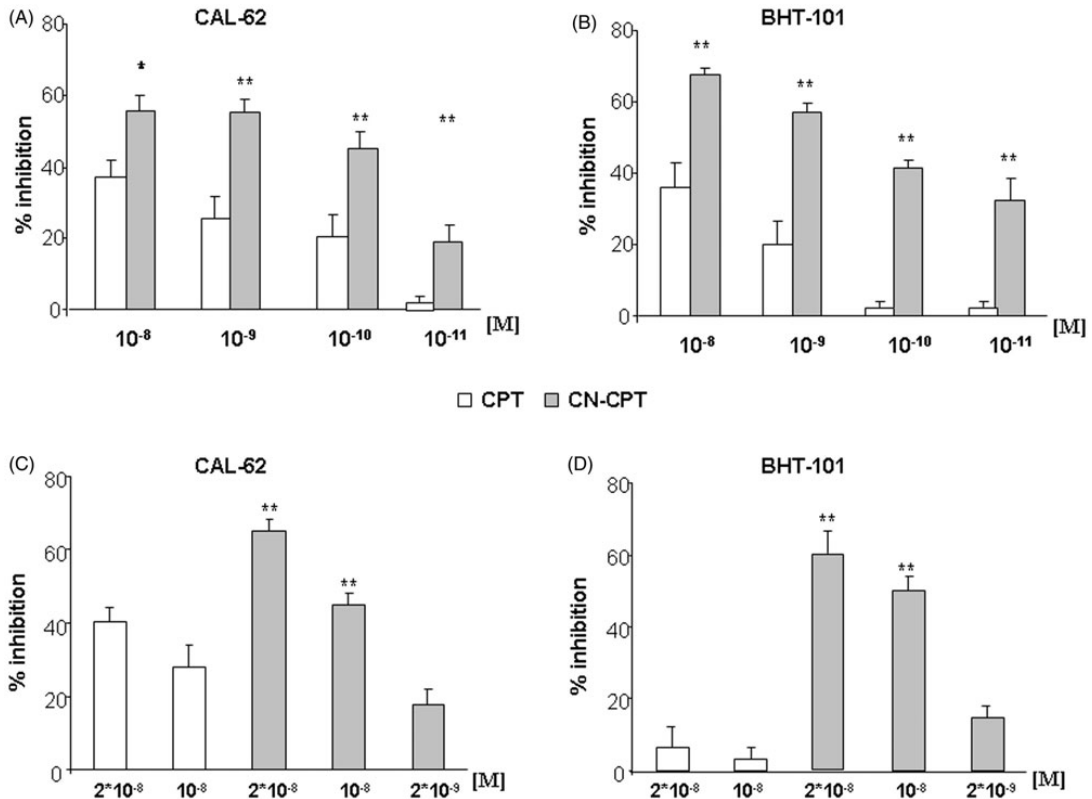


Figure 4. Effect of CPT and CN-CPT on cells adhesion and cell migration of CAL-62 and BHT-101 cell lines. (A,B) HUVEC were treated or not treated with CPT or CN-CPT for 24 h, washed and used in the adhesion assay with untreated CAL-62 (A) and BHT-101 (B) cells (1×10^5 /well). The data are presented as percentage of inhibition of the adhesion of treated cells compared to control (untreated cells). Each experiment was performed in triplicate. Data shown are means \pm SEM ($n = 5$). * $p < 0.05$; ** $p < 0.01$ significantly different from the same concentration of CPT. (C,D) In the Boyden chamber assay, CAL-62 (C) and BHT-101 (D) cells were plated onto the apical side of Matrigel-coated filters in the presence and absence of either CPT or CN-CPT, and FCS 20% was loaded in the basolateral chamber as a chemotactic stimulus. Data are expressed as mean \pm SEM ($n = 5$) of the percentage of inhibition versus control migration ** $p < 0.01$ significantly different from the same concentrations of CPT.

Discussion

ATC is a highly aggressive tumor with a poor prognosis and the long-term survival is extremely rare. To date, available therapies do not significantly improve the survival of patients and have only a palliative effect (Patel & Shaha, 2006; Cornett et al., 2007).

CPT belongs to the drug category of inhibitors of DNA TOP-1 by specifically blocking TOP-1 during the cleavage reaction of DNA and preventing repair of the single-strand breaks. This effect produces blocking of cells in the S phase of the cell cycle, conversion of DNA breaks from single to double helix and death of cells by apoptosis (Huang et al., 2000; Desai et al., 2001; Minelli et al., 2012a). Several studies demonstrated CPT activity in tumors of various origins, but CPT did not reach clinical use because of its numerous side effects. Moreover, its use is restricted by poor solubility and stability at physiological pH, at which CPT undergoes spontaneous inactivation due to opening of the E ring, decreased bioavailability and enhanced side effects. Several strategies have been described to improve the CPT activity and to decrease the side effects in several type of cancers

(Acevedo-Morantes et al., 2013; Xie et al., 2016; Yang et al., 2016).

Previously, we have reported that CN-CPT displays increased solubility, is protected from degradation and displays an enhanced inhibitory effect on prostate tumor cells both *in vitro* and *in vivo* (Fassberg & Stella, 1992; Chourpa et al., 1998; Minelli et al., 2012a, 2012b; Gigliotti et al., 2016a).

This work extends those observations to ATC showing that CN-CPT displays increased inhibitory effects *in vitro* on cell proliferation, as assessed by the MTT and clonogenic assay and increased ability to block the cell cycle into the S phase and to induce apoptosis. These effects may be ascribable to the inhibitory activity of CPT on TOP-1. Moreover, a role may be played also by inhibition of Erk 1,2 phosphorylation since constitutive activation of MAPK signaling is involved in cell survival and proliferation in several cancers, including thyroid cancer (Lim & Cha, 2011; Perri et al., 2015). It is noteworthy that inhibitors of the MAPK pathway may increase the efficacy of radioiodine therapy in cancer with BRAF mutations (Knauf et al., 2009).

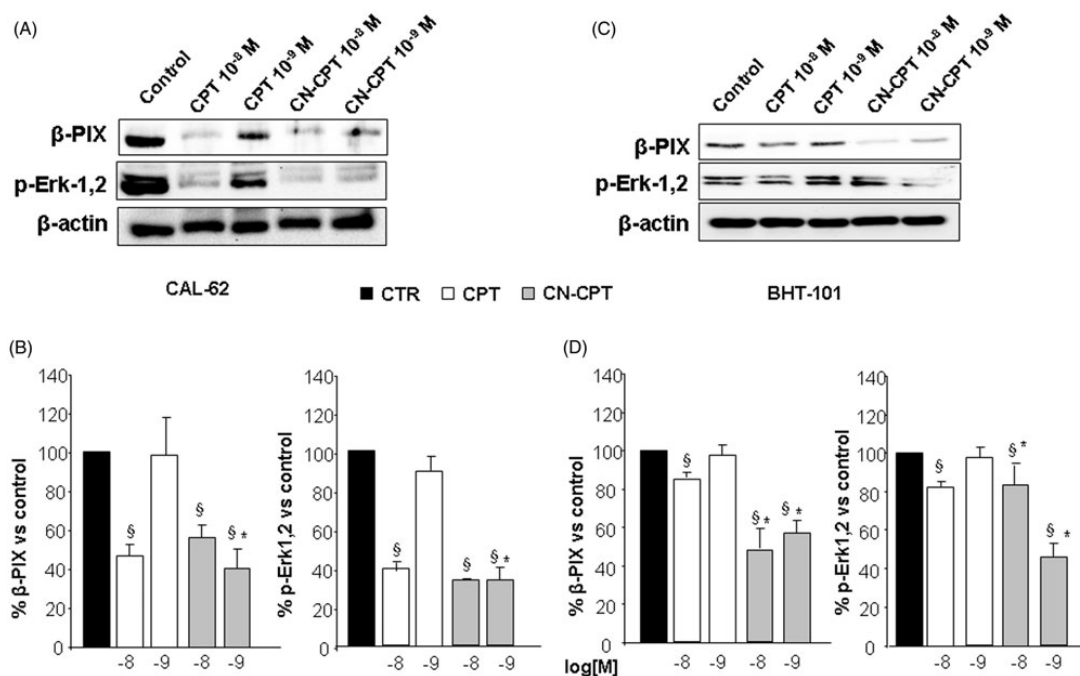


Figure 5. Effect of CPT and CN-CPT on β -PIX expression and Erk1,2 phosphorylation in CAL-62 (A), and BHT-101 (C). Cells were treated with CPT or CN-CPT (10^{-8} and 10^{-9} M) for 48 h. CPT and CN-CPT were replenished every 24 h (48 h culture: 24 + 24 h) without changing the culture medium. The same blots were probed with anti β -actin antibody as a control. (A, C): Western blot analysis from a representative experiment. (B, D): Densitometric analysis of β -PIX expression and Erk1,2 phosphorylation expressed in arbitrary units; data are expressed as means \pm SEM ($n = 3$) and shown as % of the controls. § $p < 0.05$ significantly different from untreated cells; * $p < 0.05$ significantly different from treated cells at the same concentration.

The *in vitro* experiments demonstrated that CN-CPT also shows increased ability to inhibit endothelial cells adhesiveness to ATC cells and migration of ATC cells, similarly to what we previously showed for prostate cancer cells. This activity might be related to the ability of CN-CPT to downmodulate expression of β -Pix involved in negative regulation of formation of focal adhesions, which may enhance formation of lamellipodia and cell motility (Kim et al., 2013; Occhipinti et al., 2013; Dianzani et al., 2014; Stevens et al., 2014).

The *in vivo* experiments using the SCID xenograft orthotopic model implanted with CAL-62 cells substantially supported these findings since treatment with CN-CPT was more effective than the free drug in improving mice survival and decreasing tumor growth and metastatization at a dose (1 mg kg^{-1}) that did not display any substantial side effects.

Beside the effect on cell proliferation, apoptosis, adhesion and migration, the antitumor CN-CPT activity may also involve inhibition of tumor neoangiogenesis as suggested by the CN-CTP ability to inhibit VEGF- α and IL-8 secretion in ATC cells lines *in vitro* and tumor vascularization *in vivo*. We previously showed that CN-CPT, but not free CPT, inhibits proliferation and migration of endothelial cells, proteolytic degradation of the extracellular matrix, and in several *in vitro* models of angiogenesis, inhibited tumor neoangiogenesis in mouse models of prostate cancer (Gigliotti et al., 2016a). Solid tumors cannot grow beyond a certain size, generally

$1\text{--}2 \text{ mm}^3$, without being supported by tumor neoangiogenesis (Li et al., 2012), that plays a key role also for metastatic dissemination of cancer cells. Another point is that the higher *in vivo* activity of CN-CPT compared to free CPT may be partly due to its ability, displayed by most nanoparticles, to accumulate in tumors because of the enhanced permeation and retention effect across the atypical highly fenestrated blood vessels of the tumor (Wang & Thanou, 2010).

The greater size of the necrotic core detected in the tumors of the control group compared to those of the CN-CPT-treated group may be ascribed to the faster growth of the former that may prevent adequate nutrition of the tumor core. The finding that the tumors of CN-CPT-treated mice contained a high density of Ki67⁺ cells at the invasive edge suggests that the antiproliferative activity of the drug has limited effects in this area of the tumor. However, the CN-CPT effect might be potentiated by combination of CN-CPT with surgery and radiation, since the multimodality approach represents the standard treatment of choice in ATC (Denaro et al., 2013) and the striking CN-CPT effect on tumor metastatization may be crucial to implement the effect of those therapies. The safety (Gigliotti et al., 2016a) and the cheap cost of CN-CPT are also to be considered.

Conclusions

In conclusion, the antineoplastic activity of CN-CPT may result from the combination of the antiproliferative effect

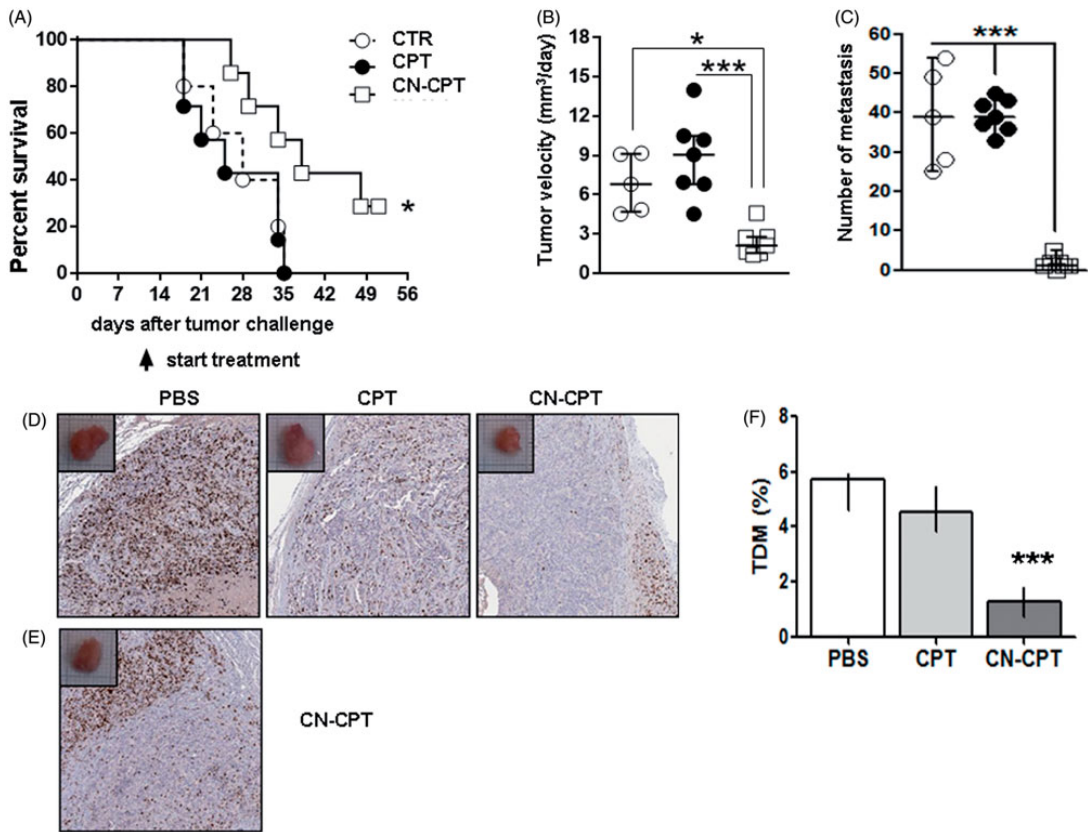


Figure 6. Treatment with CN-CPT delays the growth of orthotopic anaplastic thyroid carcinoma xenografts *in vivo*. CAL-62 cells (1×10^6) were injected into the right thyroid lobe of NSG mice. Mice were injected with PBS (\circ , $n = 5$), CPT (\bullet , $n = 7$) or CN-CPT (\square , $n = 7$) at day 10 after tumor challenge. (A) Kaplan–Meier survival analysis of untreated and treated mice. $*p < 0.05$ compared to the PBS-treated group. Graphs show: (B) tumor velocity and (C) the number of metastasis in the lung for each group, expressed as median and interquartile range. $*p < 0.05$; $**p < 0.001$ compared to the PBS-treated group and CPT-treated group. (D) Representative immunohistochemical staining for Ki-67 of tumor sections from mice treated with PBS, CPT or CN-CPT sacrificed at day 34 after tumor challenge. (E) Ki-67 staining of tumor section from a mouse treated with CN-CPT and sacrificed at day 51 after tumor challenge. (F) Graph shows the tumor microvessel density (TMD) determined as the percentage of CD31-positive area on the tumor sections. Three randomly selected areas from three tumors from each group were analyzed; data are expressed as median and interquartile ranges. $***p < 0.001$ compared to the PBS-treated group and CPT-treated group.

associated with the increase in apoptosis in the tumor cells, the inhibition of migration, invasion and metastatization, and the inhibition of the neoplastic neovascularization. Therefore, the anticancer activity of CN-CPT, without evident toxicity, opens up therapeutic perspectives for the ATC, which does not respond to conventional therapy. Translational and clinical studies will ultimately determine the clinical utility and safety of CN-CPT, used alone or in combination with other chemotherapies, as an option for the treatment of this kind of tumor.

Declaration of interest

The authors report no conflicts of interest. The authors alone are responsible for the content and writing of this article. This work was supported by the University of Turin 2014 (ex 60% by G.B., R.C., and C.D.), by Fondazione Amici di Jean, and Associazione Italiana Ricerca sul Cancro (IG 14430, AIRC, Milan).

ORCID

Benedetta Ferrara <http://orcid.org/0000-0002-2569-5115>
Mirella Giovarelli <http://orcid.org/0000-0002-7397-3466>
Chiara Dianzani <http://orcid.org/0000-0002-2246-3183>

References

- Acevedo-Morantes CY, Acevedo-Morantes MT, Suleiman-Rosado D, Ramirez-Vick JE. (2013). Evaluation of the cytotoxic effect of camptothecin solid lipid nanoparticles on MCF7 cells. *Drug Deliv* 20: 338–48.
- Basili S, Moro S. (2009). Novel camptothecin derivatives as topoisomerase I inhibitors. *Expert Opin Ther Pat* 19:555–74.
- Broecker-Preuss M, Müller S, Britten M, et al. (2015). Sorafenib inhibits intracellular signaling pathways and induces cell cycle arrest and cell death in thyroid carcinoma cells irrespective of histological origin or BRAF mutational status. *BMC Cancer* 15:184.
- Campanella P, Ianni F, Rota CA, et al. (2014). Quantification of cancer risk of each clinical and ultrasonographic suspicious feature of thyroid nodules: a systematic review and meta-analysis. *Eur J Endocrinol* 170: R203–11.

- Chen ED, Cheng P, Yan XQ, et al. (2014). Metastasis of distal esophageal carcinoma to the thyroid with presentation simulating primary thyroid carcinoma: a case report and review of the literature. *World J Surg Oncol* 12:106.
- Chourpa I, Riou JF, Millot JM, et al. (1998). Modulation in kinetics of lactone ring hydrolysis of camptothecins upon interaction with topoisomerase I cleavage sites on DNA. *Biochemistry* 37:7284–91.
- Cornett WR, Sharma AK, Day TA, et al. (2007). Anaplastic thyroid carcinoma: an overview. *Curr Oncol Rep* 9:152–58.
- Denaro N, Nigro CL, Russi EG, Merlano MC. (2013). The role of chemotherapy and latest emerging target therapies in anaplastic thyroid cancer. *Onco Targets Ther* 6:1231–41.
- Desai SD, Li TK, Rodriguez-Bauman A, et al. (2001). Ubiquitin/26S proteasome-mediated degradation of topoisomerase I as a resistance mechanism to camptothecin in tumor cells. *Cancer Res* 61:5926–32.
- Dianzani C, Minelli R, Mesturini R, et al. (2010). B7h triggering inhibits umbilical vascular endothelial cell adhesiveness to tumor cell lines and polymorphonuclear cells. *J Immunol* 185:3970–9.
- Dianzani C, Minelli R, Gigliotti CL, et al. (2014). B7h triggering inhibits the migration of tumor cell lines. *J Immunol* 192:4921–31.
- Faam B, Ghaffari MA, Ghadiri A, Azizi F. (2015). Epigenetic modifications in human thyroid cancer. *Biomed Rep* 3:3–8.
- Fassberg J, Stella VJ. (1992). A kinetic and mechanistic study of the hydrolysis of camptothecin and some analogues. *J Pharm Sci* 81: 676–84.
- Fukushima T, Takenoshita S. (2005). Roles of RAS and BRAF mutations in thyroid carcinogenesis. *Fukushima J Med Sci* 51:67–75.
- Gigliotti CL, Minelli R, Cavalli R, et al. (2016a). In vitro and in vivo therapeutic evaluation of camptothecin-encapsulated β -cyclodextrin nanosponges in prostate cancer. *J Biomed Nanotechnol* 12:114–27.
- Gigliotti CL, Boggio E, Clemente N, et al. (2016b). ICOS-ligand triggering impairs osteoclast differentiation and function in vitro and in vivo. *J Immunol* 197:3905–16.
- Gilliland FD, Hunt WC, Morris DM, Key CR. (1997). Prognostic factors for thyroid carcinoma. A population-based study of 15,698 cases from the Surveillance, Epidemiology and End Results (SEER) program 1973–1991. *Cancer* 79:564–73.
- Huang TT, Wuerzberger-Davis SM, Seufzer BJ, et al. (2000). NF- κ B activation by camptothecin. A linkage between nuclear DNA damage and cytoplasmic signaling events. *J Biol Chem* 275:9501–9.
- Jayasooriya RG, Park SR, Choi YH, et al. (2011). Camptothecin suppresses expression of matrix metalloproteinase-9 and vascular endothelial growth factor in DU145 cells through PI3K/Akt-mediated inhibition of NF- κ B activity and Nrf2-dependent induction of HO-1 expression. *Environ Toxicol Pharmacol* 39:1189–98.
- Jemal A, Bray F, Center MM, et al. (2011). Global cancer statistics. *CA Cancer J Clin* 61:134.
- Kim YS, Noh MY, Kim JY, et al. (2013). Direct GSK-3 β inhibition enhances mesenchymal stromal cell migration by increasing expression of β -PIX and CXCR4. *Mol Neurobiol* 47:811–20.
- Knauf JA, Fagin JA. (2009). Role of MAPK pathway oncoproteins in thyroid cancer pathogenesis and as drug targets. *Curr Opin Cell Biol* 21:296–303.
- Li J, Chen F, Cona MM, et al. (2012). A review on various targeted anticancer therapies. *Target Oncol* 7:69–85.
- Lim YC, Cha YY. (2011). Epigallocatechin-3-gallate induces growth inhibition and apoptosis of human anaplastic thyroid carcinoma cells through suppression of EGFR/ERK pathway and cyclin B1/CDK1 complex. *J Surg Oncol* 104:776–80.
- Ma J, Waxman DJ. (2008). Combination of antiangiogenesis with chemotherapy for more effective cancer treatment. *Mol Cancer Ther* 7:3670–84.
- Marotta V, Guerra A, Sapio MR, Vitale M. (2011). RET/PTC rearrangement in benign and malignant thyroid diseases: a clinical standpoint. *Eur J Endocrinol* 165:499–507.
- Minelli R, Cavalli R, Ellis L, et al. (2012a). Nanosponge-encapsulated camptothecin exerts anti-tumor activity in human prostate cancer cells. *Eur J Pharm Sci* 47:686–94.
- Minelli R, Serpe L, Pettazzoni P, et al. (2012b). Cholesteryl butyrate solid lipid nanoparticles inhibit the adhesion and migration of colon cancer cells. *Br J Pharmacol* 166:587–601.
- Mirrieles JA, Kapur JH, Szalkucki LM, et al. (2014). Metastasis of primary lung carcinoma to the breast: a systematic review of the literature. *J Surg Res* 188:419–31.
- Occhipinti S, Dianzani C, Chiochetti A, et al. (2013). Triggering of B7h by the ICOS modulates maturation and migration of monocyte-derived dendritic cells. *J Immunol* 190:1125–34.
- Parenti R, Salvatorelli L, Magro G. (2014). Anaplastic thyroid carcinoma: current treatments and potential new therapeutic options with emphasis on TFR1/CD71. *Int J Endocrinol* 2014:685396.
- Passaro C, Borriello F, Vastolo V, et al. (2016). The oncolytic virus d1922-947 reduces IL-8/CXCL8 and MCP-1/CCL2 expression and impairs angiogenesis and macrophage infiltration in anaplastic thyroid carcinoma. *Oncotarget* 7:1500–15.
- Patel KN, Shaha AR. (2006). Poorly differentiated and anaplastic thyroid cancer. *Cancer Control* 13:119–28.
- Perri F, Pezzullo L, Chiofalo MG, et al. (2015). Targeted therapy: a new hope for thyroid carcinomas. *Crit Rev Oncol/Hematol* 94:55–63.
- Phay JE, Ringel MD. (2013). Metastatic mechanisms in follicular cell-derived thyroid cancer. *Endocr Relat Cancer* 20:R307–19.
- Ragazzi M, Ciarrocchi A, Sancisi V, et al. (2014). Update on anaplastic thyroid carcinoma: morphological, molecular, and genetic features of the most aggressive thyroid cancer. *Int J Endocrinol* 2014:790834.
- Raman P, Koenig RJ. (2014). Pax-8-PPAR- γ fusion protein in thyroid carcinoma. *Nat Rev Endocrinol* 10:616–23.
- Romei C, Elisei R. (2012). RET/PTC translocations and clinicopathological features in human papillary thyroid carcinoma. *Front Endocrinol (Lausanne)* 3:54.
- Schweppe RE, Klopper JP, Korch C, et al. (2008). Deoxyribonucleic acid profiling analysis of 40 human thyroid cancer cell lines reveals cross-contamination resulting in cell line redundancy and misidentification. *J Clin Endocrinol Metab* 93:4331–41.
- Stevens BM, Folts CJ, Cui W, et al. (2014). Cool-1-mediated inhibition of c-Cbl modulates multiple critical properties of glioblastomas, including the ability to generate tumors in vivo. *Stem Cells* 32: 1124–35.
- Subramanian S, Singireddy A, Krishnamoorthy K, Rajappan M. (2012). Nanosponges: a novel class of drug delivery system-review. *J Pharm Pharm Sci* 15:103–11.
- Swaminathan S, Pastero L, Serpe L, et al. (2010). Cyclodextrin-based nanosponges encapsulating camptothecin: physicochemical characterization, stability and cytotoxicity. *Eur J Pharm Biopharm* 74:193–201.
- Torne S, Darandale S, Vavia P, et al. (2013). Cyclodextrin-based nanosponges: effective nanocarrier for tamoxifen delivery. *Pharm Dev Technol* 18:619–25.
- Trotta F, Dianzani C, Caldera F, et al. (2014). The application of nanosponges to cancer drug delivery. *Expert Opin Drug Deliv* 11: 931–41.
- Varinot J, Ménégau F, Bitker MO, Compérat E. (2014). Renal metastasis from thyroid carcinoma: a case report. *Anal Quant Cytopathol Histopathol* 36:46–50.
- Wall ME, Wani MC, Cook CE, et al. (1966). Plant antitumor agent I: the isolation and structure of camptothecin, a novel alkaloidal leukemia and tumor inhibitor from *Camptotheca acuminata*. *J Am Chem* 88: 3888–90.
- Wang M, Thanou M. (2010). Targeting nanoparticles to cancer. *Pharmacol Res* 62:90–9.
- Wein RO, Weber RS. (2011). Anaplastic thyroid carcinoma: palliation or treatment?. *Curr Opin Otolaryngol Head Neck Surg* 19:113–8.
- Xie X, Lin W, Liu H, et al. (2016). Ultrasound-responsive nanobubbles contained with peptide-camptothecin conjugates for targeted drug delivery. *Drug Deliv* 23:2756–64.
- Yang A, Liu Z, Yan B, et al. (2016). Preparation of camptothecin-loaded targeting nanoparticles and their antitumor effects on hepatocellular carcinoma cell line H22. *Drug Deliv* 23:1699–706.

CD-NSs and improvement of paclitaxel solubility

Introduction

Paclitaxel is a versatile small molecule anticancer diterpenoid originally isolated from the tree bark *Taxus brevifolia*. Paclitaxel has reported to possess strong anticancer activity against ovarian, breast, nonsmall cell lung cancer, Kaposi's sarcoma, pancreatic cancer, and head and neck tumors (Surapaneni, Das, and Das 2012). Paclitaxel acts via its activity on microtubules, during the mitotic phase of the cell division wherein it promotes polymerization of the tubulin proteins and stabilizes the microtubules making them dysfunctional. Paclitaxel is a highly lipophilic molecule with very poor aqueous solubility (<0.5 mg/L), dissolution and oral bioavailability (Bilensoy et al. 2008). Paclitaxel also undergoes first pass metabolism in liver and intestine via the cytochrome P450 pathway. As discussed before, Cremophor EL, used for the delivery of paclitaxel, is reported to be associated with severe side effects and hypersensitivity reactions such as bronchospasms, hyperlipidemia, neurotoxicity, hypotension, vasodilatation, and labored breathing (Trotta et al. 2014; Surapaneni, Das, and Das 2012). As before reported, Abraxane[®] is better tolerated than cremophor EL in the delivery of paclitaxel. However, also Abraxane[®] presents limitations, such as neurotoxicity, increased risk of infections or anemia (American Pharmaceutical Partners, n.d.). Thereby, novel systems for the delivery of paclitaxel can be developed and investigated.

In our study, we decided to evaluate the effects of paclitaxel included in nanosponges of β -cyclodextrin (paclitaxel-CDNS) on melanoma. The paclitaxel form available on the market (Taxol[®]), which displays a high efficacy, was used

for our study.

Methods and results

CDNS were produced by the group of Prof. Trotta, (department of Chemistry, UniTO) and drugs were incorporated in CDNS by the group of Prof. Cavalli (DSTF, UniTO). Concerning *in vitro* study, we compared the ability of paclitaxel-CDNS and free paclitaxel to inhibit the growth of human (A2058, JR8, A375, M14, PCF2) and murine (B16-F10) melanoma cell lines. As previously described (Gigliotti et al. 2017), cells were cultured in the presence and absence of titrated amounts (10^{-7} - 10^{-13} M) of each formulation for 72h and the amount of viable cells was then assessed by the MTT assay. Figure 2 shows that paclitaxel-CDNS inhibited the growth of all cell lines to a higher extent than the free drug. Indeed, paclitaxel-CDNS were effective in the picomolar range concentration, while free paclitaxel was effective only in the nanomolar range. In order to validate these findings in cell types which are closer to the real model, we also evaluated the effect of our formulation (10^{-5} - 10^{-13} M) on two primary melanoma human cells (6874-14 and 8363-13) obtained from a melanoma explant (S. Lazzaro hospital, Turin). Even using these *ex vivo* models, paclitaxel-CDNS exerted a higher inhibition of cell viability after 72 h, being significant even at 10^{-9} - 10^{-13} M for both the cell lines. Figure 3 reports data obtained on 6874-14 cells; similar results were obtained for 8363-13.

Since it is well known that paclitaxel displays the ability to inhibit tumor angiogenesis (Bocci, Di Paolo, and Danesi 2013), a tubuly-formation assay was carried out to evaluate the effect of paclitaxel-CDNS on HUVECs. Drug concentrations that were not cytotoxic (evaluated by MTT assay on HUVECs) were used for the tubuly-formation assay. Then, HUVECs were seeded onto 48-well plates (5×10^4 /well) previously coated with 75 μ l of growth factor-reduced

Matrigel, in the absence or presence of free paclitaxel and paclitaxel-CDNS (10^{-7} - 10^{-14} M), or empty CDNS. The morphology of the capillary-like structures formed by the HUVECs was analyzed by an inverted microscope after 15h of culture, and photographed with a digital camera. Results showed that paclitaxel-CDNS significantly inhibited tubule-formation in a concentration-dependent manner. At 10^{-10} and 10^{-11} M, the structure and organization of the tubuli were strongly disrupted and at 10^{-14} M only few cells were able to form basic tubuli. By contrast, free paclitaxel did not display any anti-angiogenic effect in the used range of concentration. The inhibition of capillary network formation was $98\pm3\%$, $90\pm2\%$ and $60\pm5\%$ for paclitaxel-CDNS 10^{-10} , 10^{-11} and 10^{-12} M, respectively (Fig. 4). We decided to translate our findings also *in vivo*, by comparing the effect of paclitaxel-CDNS and free paclitaxel on tumor growth. 8 weeks old C57/BL6 mice were subcutaneously injected with B16-F10 cells and 10 days later treated i.v. with 2,5mg/kg of paclitaxel-CDNS, free paclitaxel or empty CDNS three times a week for three weeks. Mice were sacrificed at the end of the experiment, and tumor weight and volume were measured at that time. Volume was calculated with this formula: $V=l*w*h$. Obtained data showed that paclitaxel-CDNS significantly decreased tumor growth, since tumor weight and volume were inhibited by 80% with respect to the control group, and by 60% when compared with the paclitaxel group (Fig. 5). Moreover, no signs of animal suffering and toxicity were reported. Indeed, the fur and the weight of the mice were not affected by the treatment with paclitaxel-CDNS.

Conclusion

In conclusion, this preliminary study showed that paclitaxel delivery using CDNS may be an effective manner to increase the anti-cancer effect of paclitaxel, allowing an improvement of its efficacy even at concentrations definitely lower.

Thereby, obtained results give a further confirmation of the efficacy of CDNS in delivering an instable drug, such as paclitaxel, ameliorating its activity both *in vitro* and *in vivo*.

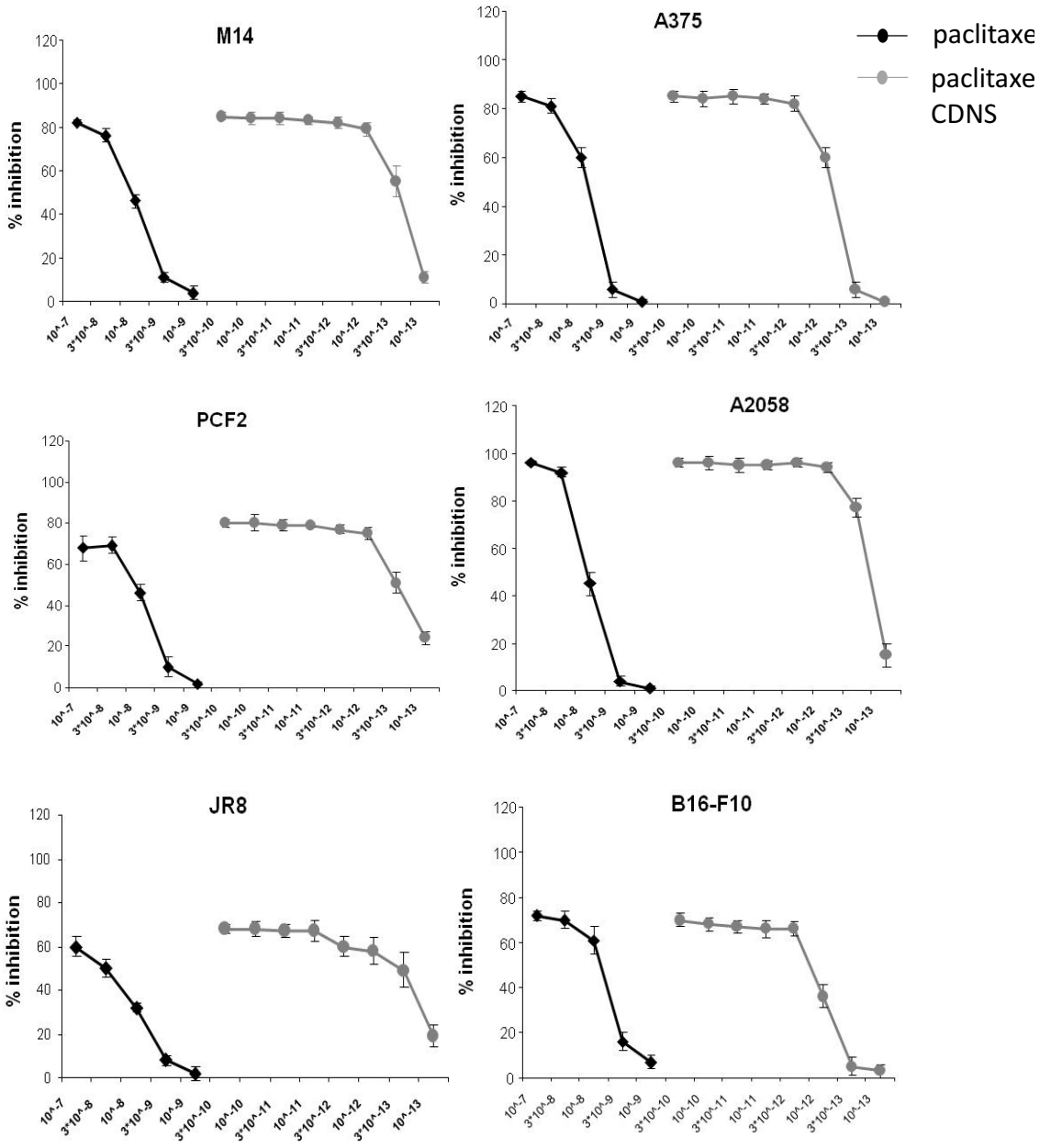


Figure 2: Percentage of cell survival following paclitaxel and paclitaxel-CDNS treatment. The results are expressed as % of cell viability inhibition and shown as mean \pm SEM ($n = 5$). Eight replicate wells were used to determine each data point, and five different experiments were performed. Statistical analysis was performed using one-way ANOVA and Dunnett’s test.

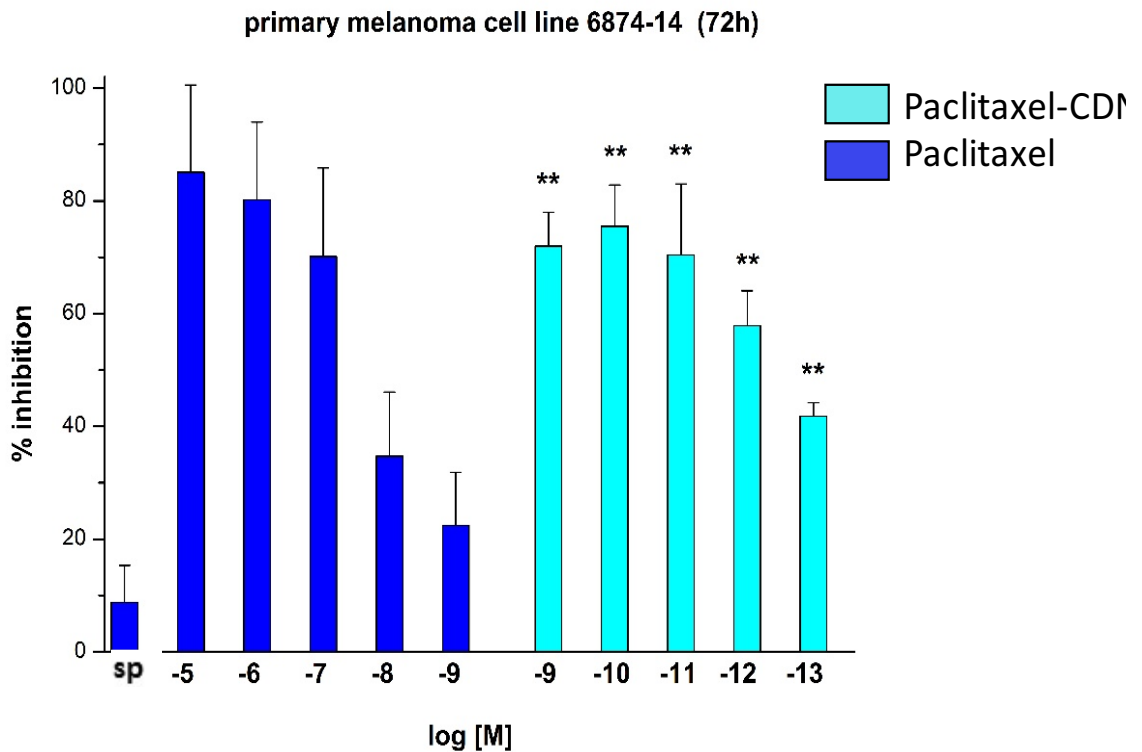


Figure 2: Percentage of cell survival following paclitaxel and paclitaxel-CDNS treatment. The results are expressed as % of cell viability inhibition and shown as mean \pm SEM ($n = 3$). Eight replicate wells were used to determine each data point, and three different experiments were performed. Statistical analysis was performed using one-way ANOVA and Dunnett’s test. ** $p < 0.01$; * $p < 0.05$ compared to the paclitaxel group at the same concentration.

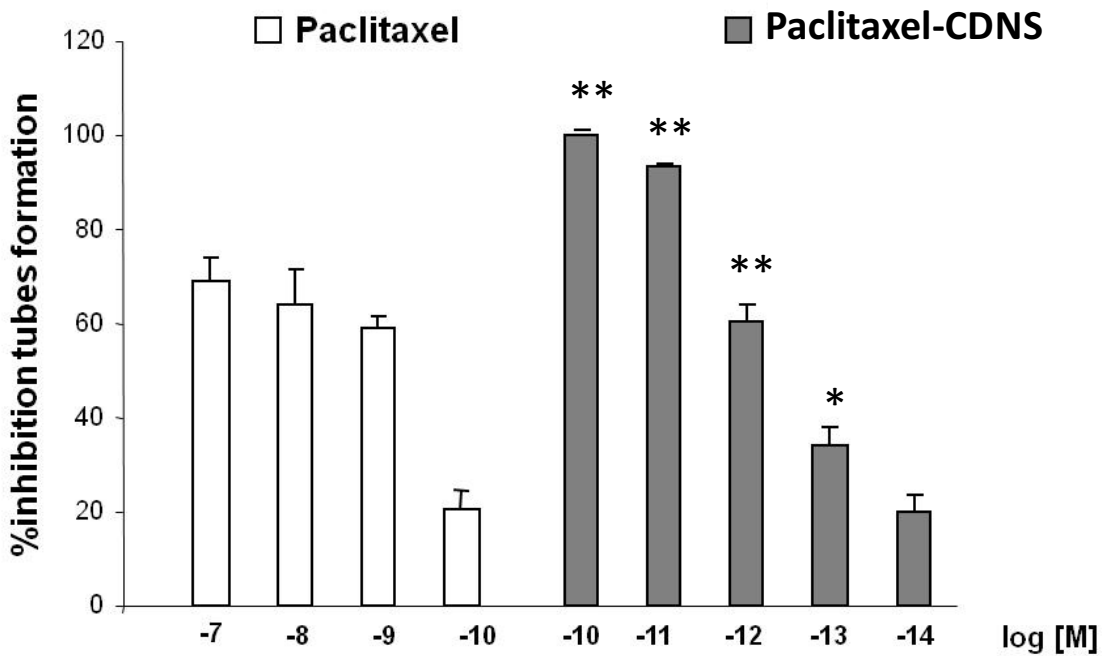
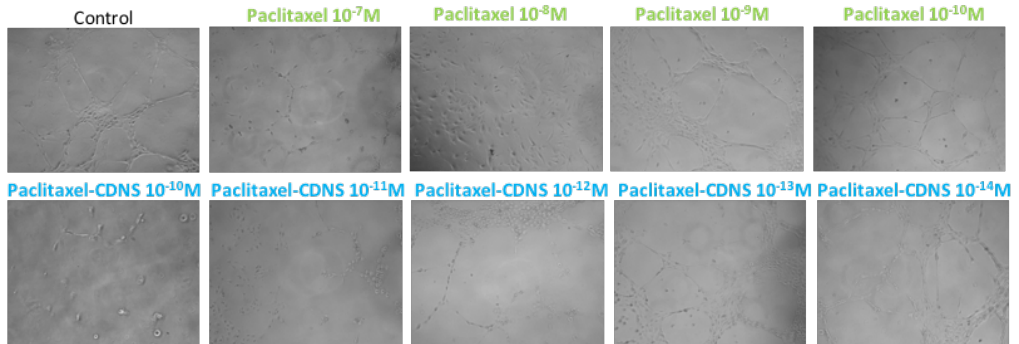


Figure 4: Tube formation assay on HUVECs. After treatment with paclitaxel or paclitaxel-CDNS, tube formation was photographed and evaluated by counting the total number of tubes in three wells; five different experiments were performed. Data are shown as mean \pm SEM. Statistical analyses were performed using one-way ANOVA and the Dunnett test. **p<0.01; *p<0.05 compared to the paclitaxel group at the same concentration.

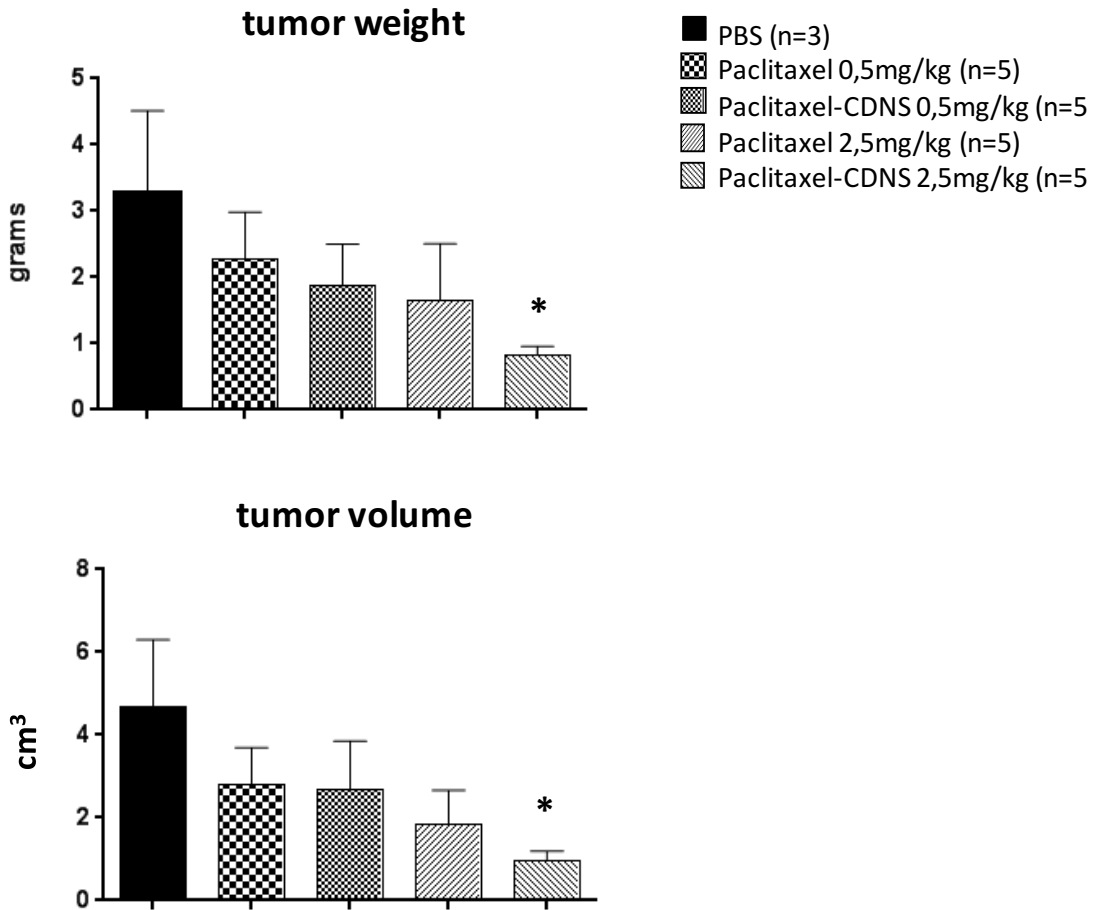


Figure 5: Effect of paclitaxel and paclitaxel-CDNS on tumor growth *in vivo*. The graph shows an average of the tumor mass weight and volume, expressed as % compared to the control group. *p<0.05 vs PBS group.

CD-NSs and reduction of doxorubicin toxicity

Introduction

Doxorubicin (DOX) is one of the most important anticancer drugs used against solid tumors of different origin and in particular for the treatment of breast cancer. However, its application is associated with several adverse effects and cardiotoxicity is the most severe one, leading to a very narrow therapeutic dose (Humber et al. 2007). Moreover, its anticancer efficacy is limited by some conditions of the tumor environment, such as hypoxia, acidity, and defect in vasculature and lymphatic vessels, as well as multidrug resistance (MDR) of cancer cells (Prasad et al. 2013).

As before reported, Doxil[®] (liposomal DOX formulation) achieved the FDA approval of in 1995. However, this formulation presents some limitations such as fixed functionality after synthesis, some leakage of encapsulated agent and lack of colloidal stability, without forgetting the high cost of manufacturing (Adair et al. 2010).

Therefore, the research for developing an efficient system able to reduce DOX toxicity is still ongoing, and it is within this context that our study collocates.

We decided to evaluate the effects of DOX included in nanosponges of β -cyclodextrins (BNS-DOX).

Methods and results

In a first moment, we analyzed the cytotoxicity of doxorubicin (DOX) and of doxorubicin-loaded nanosponges (BNS-DOX) on several cell lines derived from a panel of solid tumors. As reported by MTT assay, BNS-DOX displayed a higher efficacy than free DOX in all tested cell lines. Figure 6 reports the inhibition of proliferation on human (MDA-MB231) and murine (4T1) mammary cancer cell

lines (Fig. 6). Then, we evaluated BNS-DOX effect on cell cycle: we performed a cell cycle analysis 72 hours after treatment with different concentrations of DOX or BNS-DOX on MDA-MB231 and 4T1 cells. Different patterns of cell cycle distribution were found in these two cell lines: 4T1 control cells expressed a high proportion of G1phase cells (about by 70%), whereas, in MDA-MB231 cells, the proportion of S plus G2 cells reached about 50% of the cell population. However, in both cell lines the treatment with DOX and BNS-DOX greatly reduced the proportion of G1, S and G2 cells by increasing the cells withdrawn from cell cycle (G0 cells). The differences between DOX and BNS-DOX treatments were observed at the concentration of 10^{-6} M in 4T1 cells and at the concentration of 10^{-8} M and 10^{-7} M in MDA-MB231 cells (Fig. 7). Since the most important side effect of DOX is cardiotoxicity we decided to evaluate the effect of the drug on the viability of murine cardiomyocytes and no differences were observed between the two DOX formulations (data not shown). After having demonstrated the higher efficacy of BNS-DOX in comparison with free DOX in all tested cell lines, included breast cancer ones, we selected NeuT mouse model for this study because BALB-neuT tumors are highly homologous to human HER-2 positive breast cancer and so an ideal model to evaluate the effect of new antitumor drugs (Conti et al. 2014). BALB-neuT mice are transgenic for the rat neu oncogene (Her-2/neu, ErbB-2), with a point mutation in the transmembrane region of the gene that makes it highly tumorigenic, compared with wild-type neu (WT-neu) or human EGFR 2 (Quaglino et al. 2008). At 21–28 d of age, the neuT protein is overexpressed in mammary glands in BALB-neuT mice (Di Carlo et al. 1999), which progress to *in situ* carcinomas at about day 60, to invasive cancers by day 120–150, and by about day 230 all 10 mammary glands contain palpable tumors (Calogero et al. 2007). Because this model mimics some of the

most critical features of human disease, it was successfully used to investigate the efficacy of several therapeutic agents (Iezzi et al. 2012).

The *in vivo* experiments strictly strengthened the higher effectiveness of BNS-DOX in comparison with free DOX treatments. Tumor weights, after 7 weeks from the beginning of treatments with 2 mg/kg of BNS-DOX, were reduced by about 60% with respect to the control, while the same treatments, performed by using DOX and empty BNS, were completely ineffective (Fig. 8A). This is particularly relevant since we employed a dose that is five times lower than the therapeutic one.

To assess if BNS-DOX were less cardiotoxic than free DOX *in vivo*, we decided to evaluate the effect of our treatment on the heart of NeuT mice by H&E staining. The histological analysis showed that BNS-DOX did not affect the integrity and histology of the heart tissue in NeuT mice, underlining that the treatment is safe and not toxic to the heart (Fig. 8B).

To further explore the tumor neoangiogenesis and lymphangiogenesis on treated NeuT mice, we analyzed the vascular density, as determined by CD31-positive area, and the lymphatic vessel density/lymphatic area, as determined by Lyve-1. Immunofluorescence analysis was performed with anti-CD31 and with anti-Lyve-1 primary antibodies. The staining was performed on cryostat sections cut in OCT, because these retain the structural micro-architecture better than those stored in nitrogen. The results showed multiple areas of active angiogenesis and growth of lymphatic vasculature in the tissues of the mice treated with free DOX, while very few of these areas were detected in tissues of mice treated with BNS-DOX (Fig. 8C).

Biodistribution has been evaluated on mice organs at the moment of explantation. In order to assess the possible toxicity of BNS-DOX and free DOX

also on healthy mice, we used BALB WT mice as negative control. As a demonstration of the higher antitumour effect of BNS-DOX *in vivo*, they displayed a significant higher distribution in the tumor site compared to free DOX in NeuT mice. In addition, a very strong reduction in the accumulation of BNS-DOX in the heart tissue has been revealed (Fig. 8D). Nevertheless, results obtained after analysis of lungs, liver, kidneys, spleen and brain revealed that the distribution of BNS-DOX was similar to the one of free DOX in the examined organs of NeuT and WT mice.

Conclusion

In conclusion BNS-DOX proved to be an effective formulation in the treatment of breast cancer. The increased effectiveness, with respect to DOX, may be due to an increased stability of the drug, a higher accumulation inside the tumor tissue due to the EPR effect, and a poor lymphatic drainage of the tumor microenvironment. Moreover, at the cellular level, BNS-DOX is internalized into the cells by endocytosis, and thereafter, is not flushed out by the MDR-associated protein pumps (Gigliotti et al. 2016; Garcia-Carbonero and Supko 2002).

Our data suggest that BNS are crucial to increase the therapeutic effect of DOX and reduce the cardiotoxicity. A related article on this work is ready to be submitted to *Journal of controlled release*.

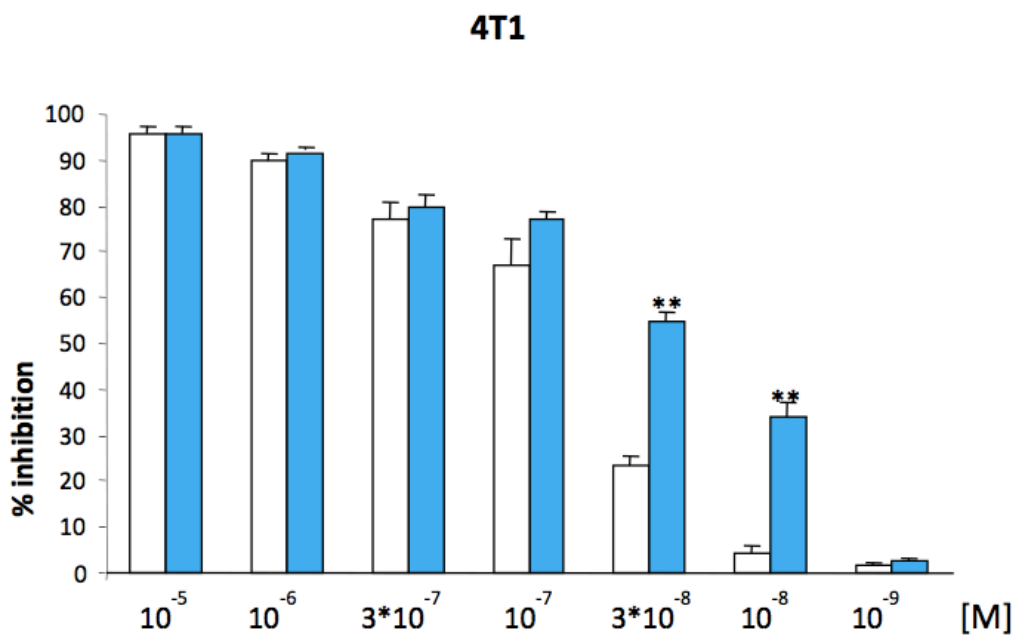
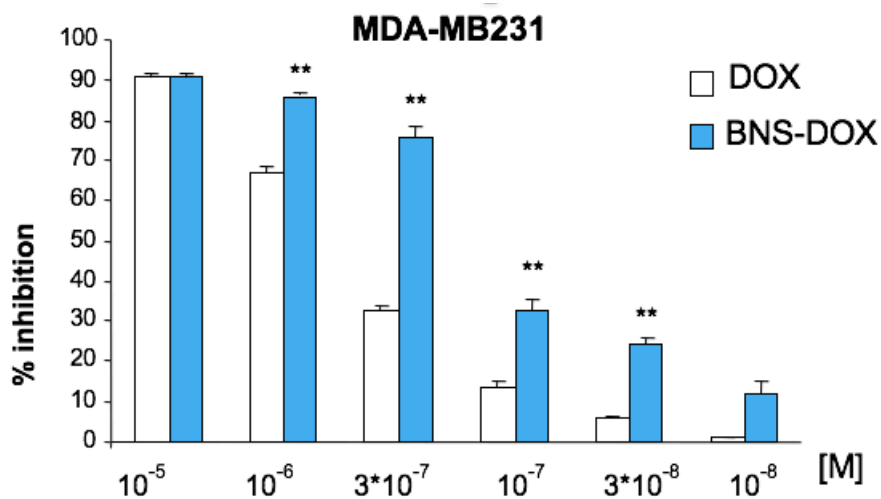


Figure 6: Percentage of MDA-MB231 and 4T1 cell survival following DOX and BNS-DOX treatment. The results are expressed as % of cell viability inhibition and shown as mean \pm SEM ($n = 5$). Eight replicate wells were used to determine each data point, and five different experiments were performed. ** $p < 0.01$, significantly different from free DOX; one-way ANOVA and Dunnett's test.

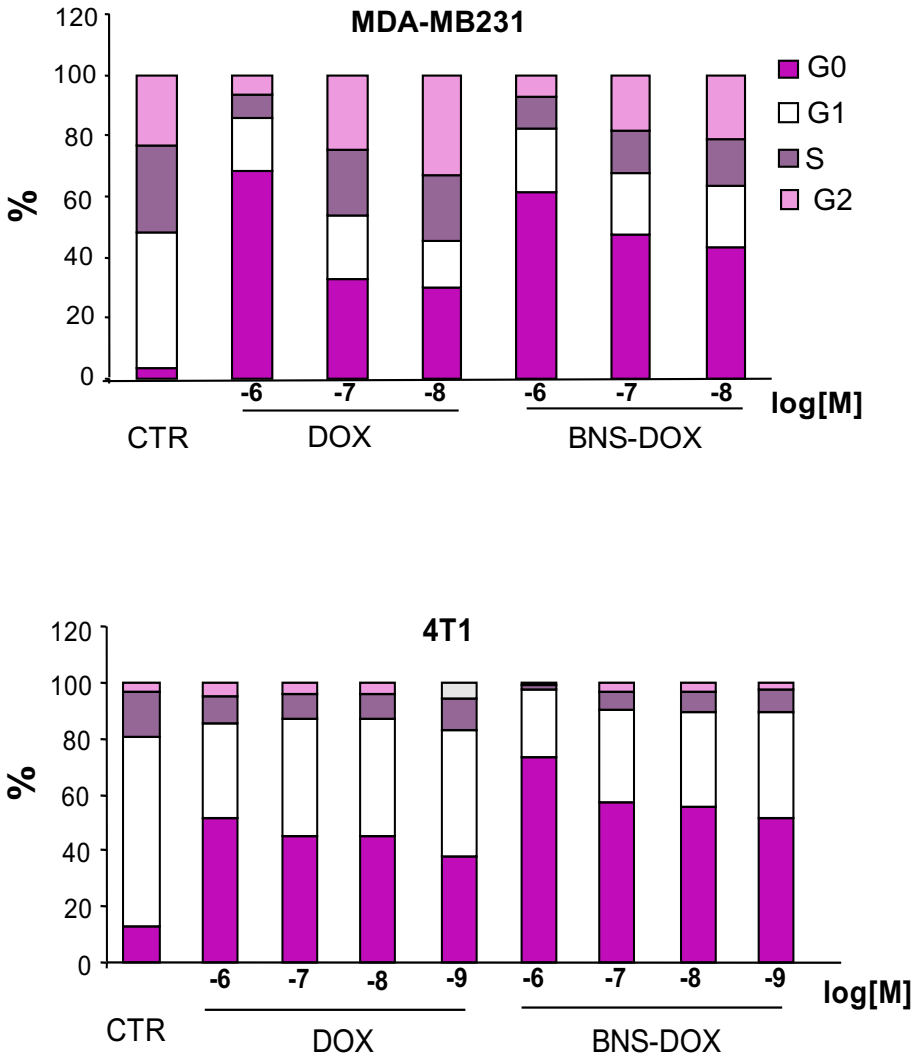
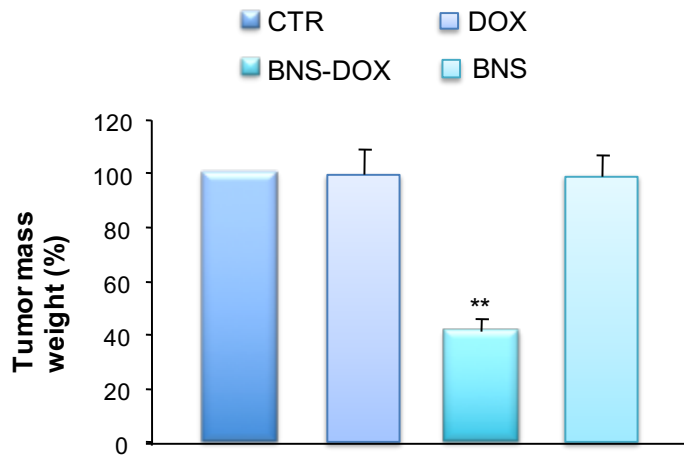
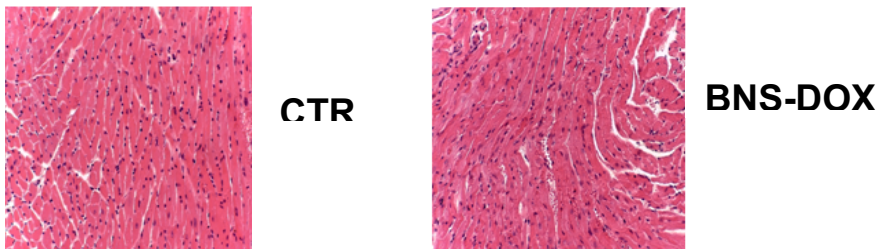


Figure 7: Effects of DOX and BNS-DOX treatment on cell cycle. MDA-MB231 and 4T1 cells were treated or not with DOX and BNS-DOX for 72 h and the cell cycle was then assessed by flow cytometry. Graphs represented the % of the quantification of cell cycle phases from 3 independent experiments.

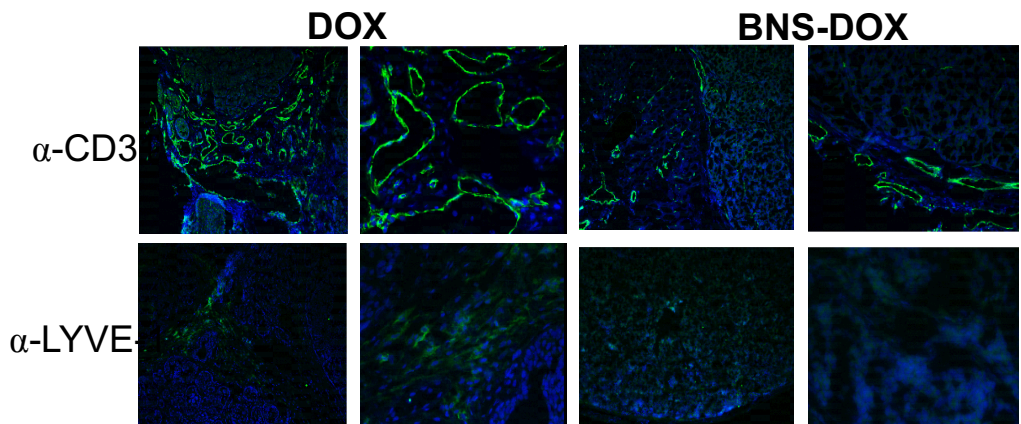
A



B



C



D

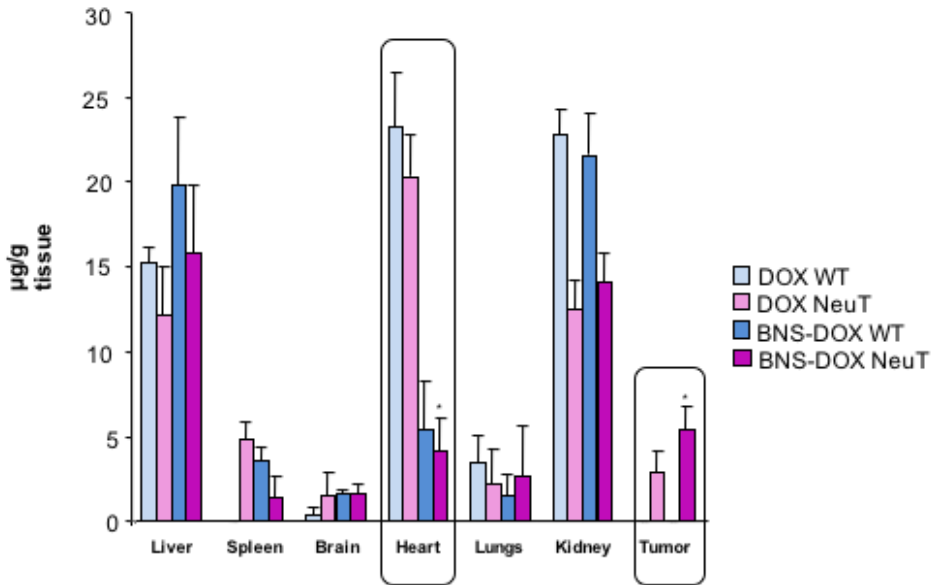


Figure 8: Effect of DOX and BNS-DOX on tumor growth in vivo. **(A)** The graph shows an average of the tumor mass weight, expressed as % compared to the control group. ** $p < 0.01$ vs CTR, DOX, BNS.

(B) Histopathologic analysis of the heart. H&E stained were observed with 20X magnification. Representative image of heart tissue from Neu-T mice treated with PBS or BNS-DOX. Similar pictures were observed in mice treated with BNS or DOX. Representative images of 3 independent experiments are shown. **(C)** Immunofluorescence staining of CD-31 and LYVE-1 of tumour tissue sections from of Neu-T mice treated with DOX or BNS-DOX. The slides were stained with either pAb rabbit α -mouse CD31 or pAb rabbit α -mouse LYVE-1 plus a secondary antibody α -rabbit conjugated with Alexa Fluor[®] 488. Representative images of 3 independent experiments are shown. **(D)** Biodistribution analysis of DOX and BSN-DOX accumulation in tissues.

CD-NSs and responsiveness to GSH and pH

Introduction

There is strong evidence that tumour cells can achieve resistance to oxidative stress, thus by-passing the action of several anticancer drugs. Glutathion (GSH) is a tripeptide that exerts a potent anti-oxidative activity, by reacting with ROS and thus preventing DNA damage and cell death (Lemire et al. 2017). Therefore, cells that present high intracellular levels of GSH develop high resistance to most potent drugs used for cancer. As a consequence, a system able to recognize and target high GSH-tumor cells may present an important strategy for the delivery of potent drugs that in the free form do not obtain a response from these cell types.

Basing on these findings, CD-NSs GSH- and pH-responsive were developed by Prof. Trotta (Department of Chemistry, UniTo), in order to permit a specific and quantitative controlled release of drugs. Indeed, a further difference between normal and cancer cells is pH; while systemic pH value is 7.4, in the tumour tissue it is more acid (Daga et al. 2016). A low pH value destabilizes GSH-NSs enhancing drug release (Daga et al. 2016; Yu, Yao, and Yang 2016).

Methods and results

These NSs have dimensions of $\approx 200\text{nm}$ and Z-potential -30mV (Trotta et al. 2016) and were generated using an one-step procedure in which 2-hydroxyethyl disulphide bonds and β -CD reacted with pyromellitic dianhydride at room temperature for few minutes. The disulphide bonds allow GSH-NSs to release drugs in response to GSH and pH variations. Previous studies showed that GSH-NSs improved DOX efficacy in high GSH-tumor cells, where DOX GSH-NSs were more internalized than free DOX (Daga et al. 2016). Indeed, DOX-internalization

was directly correlated to the anti-proliferative effect (Takemura and Fujiwara, n.d.).

In our work, GSH-NSs were studied in the delivery of strigolactones (SLs), phytohormones of natural origin released from plants in the soil, acting on plant growth and in regulation of biological functions in the rizosphere (Gomez-Roldan et al. 2008; Koltai et al. 2010). Recently, a role of SLs as anticancer molecules was pointed out, since they inhibit cell cycle, induce oxidative stress and apoptosis of several solid tumour cell types, as prostate, colon, lung and melanoma; on the contrary, they do not exert cytotoxicity against normal cells (C B Pollock et al. 2012). In vegetals, SLs regulate cyclin- β expression via ubiquitine-proteasome system, suggesting that a similar mechanism can be at the base of their antitumour activity in mammals (Rasmussen et al. 2012).

However, since SLs are released in the soil at very low concentrations and they are rapidly decomposed because of their instability, two analogs of SLs, MEB55 and ST362, were synthesized by Prof. Prandi (Department of Chemistry, UniTo). The problem of these two compounds is the low water solubility, and thus they must be solved in a solvent, such as DMSO. However, DMSO cannot be employed *in vivo*, therefore a safe system for their delivery is required.

GSH-NSs have been proposed for the delivery of MEB55 and ST362 in order to assess their effect on prostate cancer and the two analogs were incorporated in GSH-NSs by the group of Prof. Cavalli (DSTF, UniTO).

The *in vitro* kinetics release profile of GSH-NSs was evaluated in the presence of different GSH concentrations (Fig. 9) and the effects of this formulation were evaluated on tumour cells.

We chosed two cell lines, that are DU-145 and PC-3, since they display different intracellular GSH levels. Indeed, DU-145 GHS levels are high, 12 $\mu\text{g}/\text{mg}$ of

protein, while PC-3 GSH levels are low, 7 µg/mg of protein (Claire B Pollock et al. 2014). *In vitro* obtained results showed that SLs-GSH-NSs are able to inhibit cell viability on DU-145, in a dose-dependent way and significantly more than the free drug, with MEB55 three times more efficient than ST362. On the contrary, no significant differences were reported on PC-3 cells (Fig. 10).

The levels of internalization were determined by FACS in PC-3 or DU-145 after treatment with labelled GSH-NSs at 4 °C or 37 °C. While PC-3 did not show a significant increase in fluorescence at 37 °C, DU-145 displayed high levels of fluorescence. No internalization was observed neither for PC-3 and DU-145 at 4 °C, demonstrating that an active transport into the cells is needed (Fig. 11 and 12).

Moreover, an induction of apoptosis was observed in DU-145 after treatment with SLs-GSH-NSs, while this effect was not observed in PC-3, suggesting that this cell line probably undergoes oxidative stress death (Fig. 13). Indeed, in a previous work, the authors demonstrated that the intracellular level of reactive oxygen species (ROS) was inversely related to GSH content (Daga et al. 2016). This observation suggested that the antioxidant potential of PC-3 was lower than that of DU-145, and for this reason they may die for oxidative stress. Cell-uptake experiments confirmed obtained results, demonstrating that SLs-GSH-NSs are rapidly internalized in DU-145, inducing apoptosis by exploiting high GSH levels and low pH that accelerate SLs release (Fig. 14).

Conclusion

In conclusion, GSH-NSs revealed to be efficient nanocarriers for the intracellular controlled release of SLs, by-passing its problems of insolubility and allowing a GSH and pH mediated cell-specific effect. A related article on this work is ready to be submitted to *Oncotarget*.

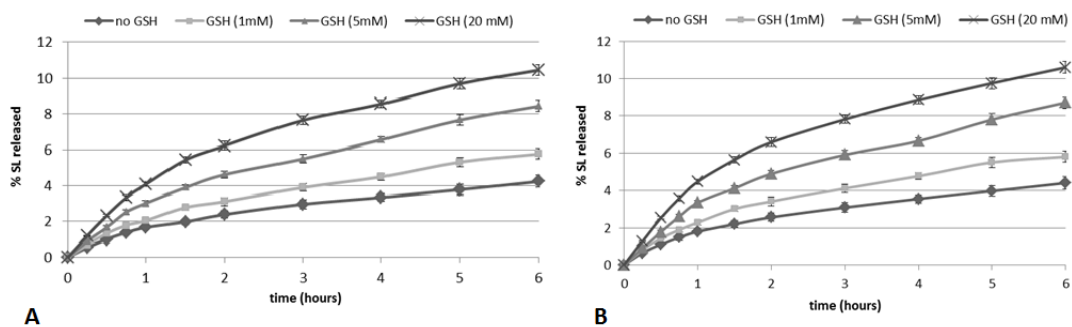


Figure 9. *In vitro* release kinetics of ST362 (A) and MEB55 (B) from GSH-responsive NS formulations in the presence of different GSH concentration (1, 5, 20 mM).

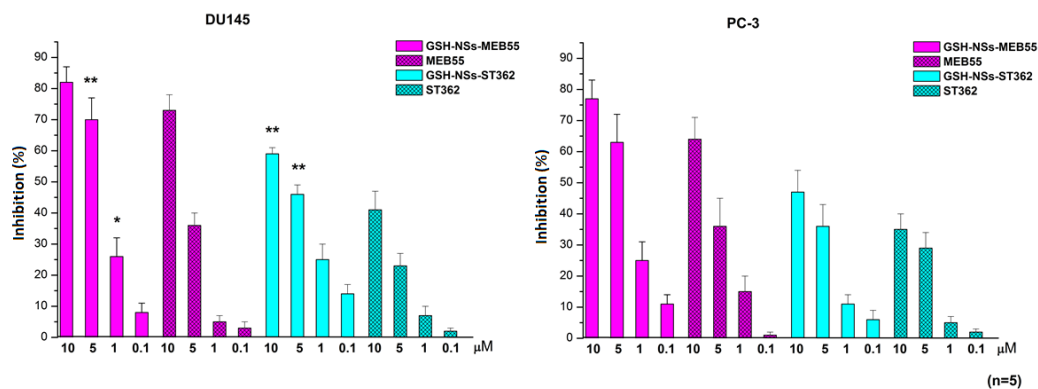


Figure 10. Cell viability after free SL or SL-loaded GSH-NS treatment. Results are expressed as percent of inhibition of control values, obtained after 24 h of treatment in the presence or absence of free ST362, ST362 GSH-NS, free MEB55, MEB55 GSH-NS. * $p < 0.05$, significantly different from free-drug treated cells at the same concentration.

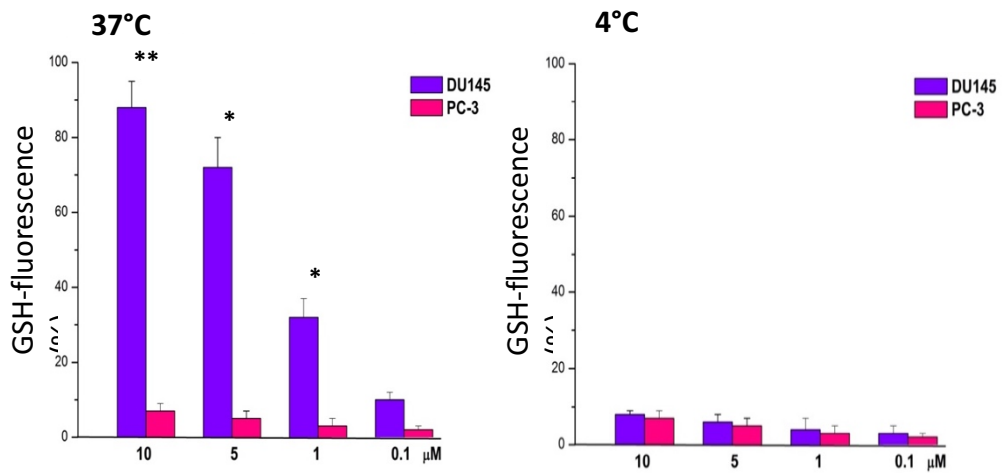


Figure 11. Cellular uptake of GSH-NS: DU-145 or PC-3 cell lines were treated with or without different doses of GSH-NS and then analyzed by flow cytometry. Results are expressed as mean±SEM of the percentage of fluorescent positive cells from four independent experiments (** p<0.01, *p<0.05 compared to the control, paired T-test).

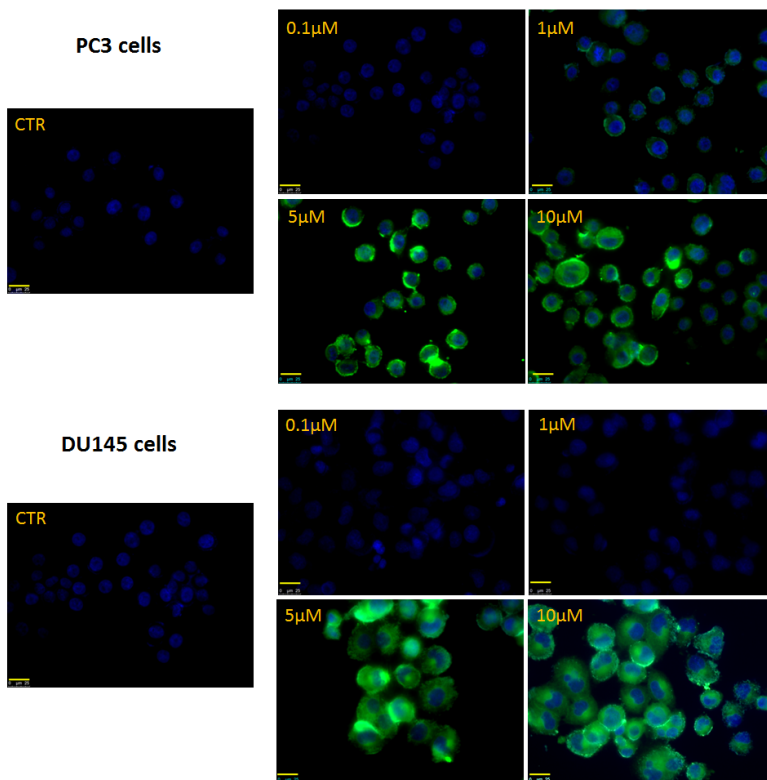


Figure 12. Fluorescence microscope images (400X magnification) of GSH-NS (green) in PC-3 and DU-145 cells. Untreated cells (CTR) and 10, 5, 1, 0.1 μM GSH-NS observed after 4 h of treatment.

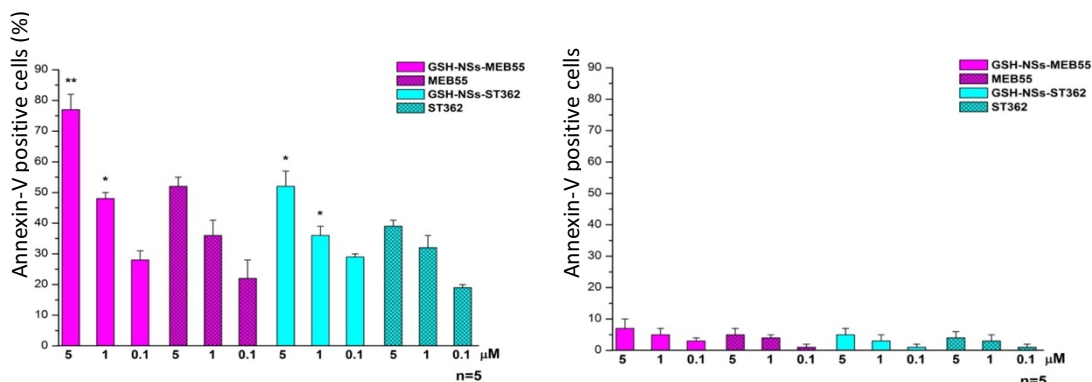


Figure 13. Levels of Annexin-V positive cells after free SL or SL-loaded GSH-NS treatment. Annexin-V positive cells was evaluated in DU-145 (left panel) and PC-3 (right panel) cells cultured for 24 h in the presence or absence of free ST362, ST362 GSH-NS, free MEB55, MEB55 GSH-NS. Results are expressed as % of positive cells * $p < 0.05$; ** $p < 0.01$, significantly different from free-drug treated cells at the same concentration.

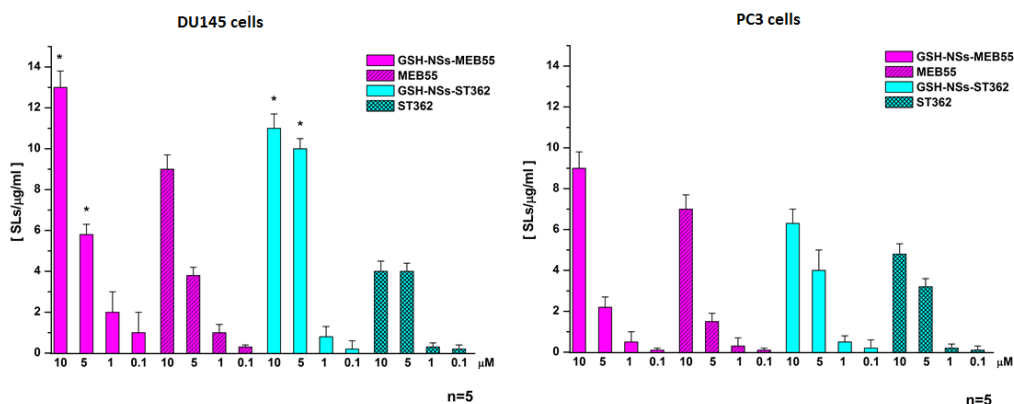


Figure 14. SL intracellular content in PC-3 and DU-145 cells after 24 h treatment with 10, 5, 1, 0.1 μM free SL or SL-loaded GSH-NS.

Discussion

Nanotherapeutics research has been at the center stage of the cancer therapeutic drug design and discovery for over three decades. High publication volumes and significant government spending on nanomedicine have made nanotechnology achieving lots of interest, and further investigations are now ongoing in order to define the future of nanomedicine and the bench to bedside transition of promising technologies (Juliano 2013). A vast majority of the chemotherapeutic agents have poor aqueous solubility owing to their multistep synthetic routes that aim toward a higher selectivity and specificity, making the formulation development difficult. Many molecules also suffer from degradation in the gastrointestinal tract, poor physicochemical stability, and low half-lives necessitating frequent dosing and severe dose-dependent side effects.

Leaving from this background, our research started from an investigation of new systems for the delivery of instable chemotherapeutic drugs, such as temozolomide (TMZ), camptothecin (CPT) and paclitaxel, in order to assess if our formulations were able to improve the intrinsic drug characteristics.

In the first study, we focused on TMZ, an alkylating chemotherapeutic drug that is used, among others, for topical melanoma treatment (Suppasansatorn et al. 2006), but whose low stability at physiologic pH constitutes the main limitation for i.v. delivery. Our approach was based on lipophilization of the parent molecule and following encapsulation in solid lipid nanoparticles (SLNs; produced by Dr. Battaglia, DSTF, UniTO), in order to increase its stability after i.v. administration, which should lead to a longer duration of action and a higher efficacy. SLNs are a safe and biocompatible system, characterized by high

stability in *in vitro* and *in vivo* systems (Pizzimenti et al. 2016). In our models, SLN-TMZ showed a significant higher effect on inhibition of cell viability, proliferation and angiogenesis *in vitro*, when compared to the free drug. Moreover, our formulation significantly improved the ability of TMZ to reduce tumour growth and angiogenesis also *in vivo*, on a B16-F10 subcutaneous model of melanoma.

It is known that TMZ does not constitute the first line therapy for melanoma, since it is based on immunotherapeutic drugs, such as ipilimumab and nivolumab (J. S. Weber et al. 2015; Robert et al. 2015; Force and Salama 2017). However, only a low percentage of patients respond to these immunotherapies (Postow et al. 2013) and several of them become resistant. Therefore, there is always a strong necessity to investigate novel methods for the delivery of new or old drugs.

The promising obtained results allow to consider SLN as an efficient system for the delivery of TMZ, increasing its stability and thereby its activity, reducing the use of high doses of this drug.

Another nano-delivery system that has been largely studied in this work, was based on β -cyclodextrin nanosponges (β CD-NS). We investigated the effects of β CD-NS in the delivery of CPT (CN-CPT) on anaplastic thyroid cancer (ATC) models, since there are not efficient drugs for the treatment of this highly lethal cancer (Gigliotti et al. 2017).

CPT in its native form is not employed in clinics because of its numerous side effects. Moreover, its use is restricted by poor solubility and stability at physiological pH, at which CPT undergoes spontaneous inactivation due to opening of the E-ring, decreasing its bioavailability and enhancing side effects. CN-CPT displayed higher inhibitory effects on cell proliferation and increased

ability to block the cell cycle into the S-phase, to inhibit new vascularization and to induce apoptosis *in vitro* (Gigliotti et al. 2016). Furthermore, this formulation more strongly inhibited ATC cells adhesiveness to endothelial cells and ATC cells migration, two mechanisms at the base of metastatic process that is responsible for the high lethality of this tumour. The *in vivo* experiments using a xenograft orthotopic model of ATC substantially supported these findings, since treatment with CN-CPT was more effective than the free drug in improving mice survival and decreasing tumor growth and metastatization at a dose that did not display any substantial side effect.

The anticancer activity of CN-CPT, without evident toxicity, opens up therapeutic perspectives for the ATC, which does not respond to conventional therapy. Indeed, even if on *in vivo* ATC model CN-CPT reported a lower effect than the one displayed in prostate cancer (Gigliotti et al. 2016), it is necessary to consider a possible employment of this novel formulation in combination with other common approaches for the treatment of ATC, such as preventive surgery and radiotherapy, resulting in a final successful strategy with high therapeutic potential.

A further study was carried out on paclitaxel, an anticancer drug with high insolubility. The old systems used for the delivery of paclitaxel, such as Cremophor EL, are known to be toxic for the organism, therefore several formulations were developed, such as liposomes and Abraxane[®] (M. R. Green et al. 2006). However, as previously reported, they present some limitations and high production costs. Several studies have been carried out in order to ameliorate paclitaxel efficacy, and in our work we decided to investigate the effects of β CD-NS in the delivery of paclitaxel on melanoma models. *In vitro* results showed an efficacy of this system that was three orders of magnitude

higher than the one of free paclitaxel, in the inhibition of melanoma cells proliferation and migration. Also effects on angiogenesis were evaluated, because paclitaxel is known to inhibit this process. Paclitaxel- β CD-NS reported a greater inhibition of angiogenesis when compared to the free drug, even at very lower concentrations. *In vivo* obtained results gave a further confirmation of the best activity of paclitaxel- β CD-NS on tumour growth, in B16-F10 melanoma cells subcutaneously injected mice. These findings demonstrated that β CD-NSs not only allow a safe delivery of paclitaxel, but also enable to employ very low doses of this potent anticancer drug. Indeed, β CD-NS are able to solubilize this drug allowing a high protection from the external environment. A further evaluation may be carried out to strengthen the efficacy of our formulation, by comparing its effects with the ones of Abraxane[®].

Another limitation for the use of many chemotherapeutic drugs is their high toxicity. This is due to the fact that their effect is not selectively directed to cancer cells, but they can reach healthy organs and cause cell death, perturbing the organ structure and function. Doxorubicin (DOX) is an anthracycline that was widely used against solid tumors of different origins and in particular for the treatment of breast cancer. However, several limitations to the use of DOX were related to its severe side effects, and in particular cardiotoxicity (Humber et al. 2007). Also in this case, we decided to investigate β CD-NS for the delivery of DOX, in order to see if this formulation could specifically enhance its activity, thereby reducing its toxicity. DOX β CD-NS showed to be able to inhibit cell proliferation and induce cell cycle block on breast cancer cell lines in a dose-dependent way. *In vivo* data, obtained on a spontaneous model of breast cancer (Balb Neu-T mice), reported a greater inhibition of tumor weight and angiogenesis exerted from DOX- β CD-NS, compared to Dox. However, the most

interesting result was obtained by biodistribution study, which showed that DOX- β CD-NS accumulated to a high extent into the tumour tissue and not into the heart tissue. On the contrary, a high accumulation of free DOX was found in heart tissue and less in the tumour site. Histological analysis further confirms that β CD-NS did not induce cardiotoxicity. Basing on these findings, β CD-NS revealed to be an important strategy for allowing DOX use without reporting cardiotoxicity.

The higher antitumour effect observed *in vivo* with all these NP systems is also ascribable to the fact that tumor environment provides a very unique opportunity for the molecules to be delivered specifically to the tumour site. A tumor exhibits increased vasculature permeability, leakiness, and decreased lymphatic function. Nanoparticles (100–500nm) can utilize the EPR effect through extravasation via gaps in hyper permeable tumor vasculature. This characteristic can be exploited in order to make chemotherapeutic drugs more selective, reducing their systemic effect and increasing their bioavailability, by taking advantage of endocytosis and efflux pumps escape.

Besides increased vasculature permeability, other characteristics of tumour cells are their lower intracellular pH in comparison with the normal cell types. Moreover, chemoresistant cells often display high intracellular concentration of glutathione (GSH), that is about threefolds higher than the extracellular levels. Stimuli-sensitive drug delivery using nanoparticles helps in targeting of nanoparticles to the tumor site. Therefore, we evaluated the effect of GSH and pH disulfide-responsive NS (GSH-NS), in which GSH/GSH-disulfide switches can be easily turned on after the intracellular delivery thereby leading to cleavage of the disulfide bond and subsequent targeted release of the encapsulated drugs (R Cavalli, Argenziano, and Dianzani 2014). These NSs showed good

swelling capacity without causing any cytotoxic effects on several tested cancer cell lines (Trotta et al. 2014). In particular, we studied GSH-NSs in the delivery of strigolactones (SLs), natural compounds with anticancer properties. SLs are released in the soil at very low concentrations and they are rapidly decomposed because of their instability. Two analogs of SLs have been synthesized, but they displayed a very low solubility and thereby needed to be delivered. We tested SLs-GSH-NSs on two prostate cancer cell lines, DU-145 with high GSH content and PC-3, with low GSH content. Obtained results showed a higher accumulation of the formulation, and a consequent higher inhibition of cell viability, in DU-145 cells, when compared to free SLs and to PC-3 cells. Therefore, GSH-NSs represent an efficient nanocarrier system for a controlled intracellular release of SLs, since they can be specifically directed against chemoresistant cells which display high intracellular GSH cancer cells.

In conclusion, SLNs and β CD-NSs showed remarkable encapsulation efficiency and reported to be able to increase stability, solubility and controlled release of several molecules. By taking advantage of EPR effect, they specifically reach the tumour site, allowing a lower administered dose and preventing the damage to healthy tissues. All together, these findings suggest the importance of nano-drug delivery as a strategy for overcoming limitations of most important anticancer drugs, by improving drug efficacy and reducing related adverse reactions, often allowing a reduction of manufacturing and market costs.

STUDY OF NEW TUMOR BIOMARKERS

Biomarkers and target therapy

The National Cancer Institute defines a biomarker as “a biological molecule found in blood, other body fluids, or tissues that is a sign of a normal or abnormal process, or of a condition of disease”. Biomarkers give evidence of the presence of several diseases, including cancer.

There are numerous biological components among the large variety of cancer biomarkers, including antibodies and inflammatory molecules, nucleic acids and peptides.

Biomarkers are used for patient assessment in multiple clinical settings, including estimating risk of disease, screening for occult primary cancers, and distinguishing benign from malignant forms. Biomarkers’ identification can give important information about an individual’s risk of developing cancer. Several cancers are difficult to diagnose at early stages, since they do not present symptoms before the disease has progressed and become metastatic.

Effective risk reduction strategies (such as lifestyle changes, prophylactic surgery, or chemoprevention) and screening are helpful in determining a patient’s risk of developing a malignancy. In a patient with an abnormality, biomarkers can also be used to distinguish between different possibilities for a differential diagnosis (N. L. Henry and Hayes 2012).

Moreover, biomarkers are useful for determining prognosis and prediction for patients who have been diagnosed with cancer and monitoring status of the disease. Finding molecules characteristic of a particular disease is important in detecting recurrence or determining response to therapy. Biomarkers can be used as response modifiers, or “predictive factors,” for a specific therapy, or for determining which therapy is likely to be most effective.

Potential somatic markers for prediction of response to therapy are detected with chemotherapy sensitivity and resistance assays. Numerous clinical studies have been published and these assays are commercially available.

Circulating soluble protein tumor markers are known for monitoring therapy response in metastatic colorectal, prostate, ovarian, breast, and pancreatic cancers (Harris et al. 2007; Locker et al. 2006). Biomarkers can be used to detect early recurrence of disease in patients who have completed adjuvant therapy before the patients become symptomatic. For example, CEA is monitored serially following adjuvant treatment for colon cancer with the goal of detecting liver metastases when they are still resectable and potentially curable (Locker et al. 2006). Similarly, alpha fetoprotein, beta-HCG, and lactate dehydrogenase are monitored serially in nonseminomatous germ cell tumors in order to detect early disease recurrence (Gilligan et al. 2010).

In conclusion, the detection of tumour biomarkers is vital for allowing an early diagnosis of cancer, prognosis, and response to therapy. In the majority of cases, there is a correlation between biomarkers and molecular targets, that can be useful for a better, specific and personalized therapy.

Target therapy aims at delivering drugs to particular genes or proteins that are specific to cancer cells or the tissue environment that promotes cancer growth. Effectiveness of the therapy lies in targeted release of therapeutics at the disease site while minimizing the off-target side effects caused to normal tissues. It is often used in conjunction with chemotherapy and other cancer treatments (Padma 2015). Target therapy involves developing drugs that block cancer cell proliferation, promote cell cycle regulation or induce apoptosis or autophagy and targeted delivery of toxic substances specifically to cancer cells to destroy them. This approach involves the use of monoclonal antibodies or

oral small drugs (Gerber 2008).

Therefore, our work further aimed at investigating the role of specific biomarkers which can be predictive for an early diagnosis or can become targets for a specific cancer therapy.

Detection of Biomarkers for pancreatic cancer in extracellular vesicles

Pancreatic cancer

General features

Pancreas is an organ of endodermal derivation that is a key regulator of protein and carbohydrate digestion and glucose homeostasis. The exocrine pancreas (80% of the tissue mass of the organ) is composed of acinar and duct cells. The acinar cells, are organized in functional units along the duct and synthesize and secrete zymogens into the ductal lumen in response to stomach- and duodenum-stimuli. The endocrine pancreas regulates metabolism and glucose homeostasis through the secretion of hormones into the blood-stream. It is composed of four specialized endocrine cell types grouped together into clusters called “Islets of Langerhans” (Hezel et al. 2006).

Distinct pancreatic malignancies possess histological and molecular features that recall the characteristics of the various normal cellular constituents. Pancreatic ductal adenocarcinoma (PDAC), whose nomenclature derives from its histological resemblance to ductal cells, is the most common pancreatic neoplasm (Warshaw and Fernández-del Castillo 1992; Li et al. 2004).

PDAC normally develops in the head of the pancreas with infiltration into surrounding tissues including lymphonodes, spleen, and peritoneal cavity. The disease is characterized by the presence of a dense stroma of fibroblasts and inflammatory cells, called desmoplasia. PDAC primarily exhibits a glandular pattern with duct-like structures and varying degrees of cellular atypia and

differentiation. Less common subtypes of PDAC include colloid, adenosquamous, or sarcomatoid histology. Often within an individual tumor, there are regional differences in histology, tumor grade, and degree of differentiation. Even the smallest primary lesions commonly exhibit perineural and lymphovascular invasion, suggesting a propensity for early distant spread (Hezel et al. 2006). Different clinical staging systems were developed to categorize pancreatic cancer according to surgical resectability, and these clinical staging systems help treatment planning for patients. *Resectable disease* is characterized by: 1) the absence of extrapancreatic disease; 2) a patent superior mesenteric vein-portal vein (SMV-PV) confluence; 3) clear tissue planes between the celiac axis (CA), superior mesenteric artery (SMA), and the common hepatic artery (Bose, Katz, and Fleming 2012). *Borderline resectable disease* is characterized by: 1) the absence of extrapancreatic disease and the presence of tumor involvement or occlusion of the SMV-PV confluence that is favourable to resection and reconstruction; 2) tumor abutment of the SMA for less than 180° of its circumference; 3) short segment encasement of the hepatic artery. *Locally advanced disease* is characterized by the presence of tumor encasement of the SMA for more than 180° of its circumference in the absence of extrapancreatic disease (Bose, Katz, and Fleming 2012). In addition to these three, there is the category of *metastatic disease*, which is characterized by radiographic or clinical evidence of pancreatic cancer that has spread to distant organs or the peritoneum.

Causes

Among the environmental causes of pancreatic cancer, tobacco smoking is recognized as a strong risk factor (Lochan et al. 2011). Alcohol consumption,

chronic pancreatitis, and diabetes mellitus are also postulated to be causes of this cancer but further epidemiologic studies and clinical research are required. Multiple studies have established that advanced age and long-standing chronic pancreatitis as clear risk factors; diabetes and obesity also appear to confer increased risk (Everhart and Wright, n.d.; Fuchs et al. 1996; Gapstur et al. 2000; Michaud et al., n.d.; Berrington de Gonzalez, Sweetland, and Spencer 2003; Stolzenberg-Solomon et al. 2005). However, PDAC is associated with a handful of autosomal dominant genetic conditions. Genetics and a family history of disease are recognized risk factors for developing pancreatic cancer as well. Indeed, approximately 5% to 10% of patients with pancreatic cancer have a family history of the disease (Hidalgo 2010). Patients that present the *BRCA2* mutation, which are known to have an increased risk for developing breast and ovarian cancers, are now recognized to have an increased risk for developing PDAC (Moran et al. 2012). Other genes with variants associated with increased pancreatic cancer risk include *BRCA1*, *PALB2*, *ATM*, *CDKN2A*, *APC*, *MLH1*, *MSH2*, *MSH6*, *PMS2*, *PRSS1*, and *STK11* (Solomon et al., n.d.). Among the germline mutations linked to familial PDAC, those targeting the tumor suppressor genes *INK4A*, *BRCA2*, and *LKB1*, the DNA mismatch repair gene *MLH1*, are included (Whitcomb et al. 1996; Jaffee et al. 2002). While the question to how these separate genetic conditions lead to PDAC remains to be fully understood, the clinical observation of exocrine insufficiency and pancreatitis as a common patho-physiologic process leading to PDAC is object of interest. Exocrine organ dysfunction and pancreatitis could promote tumorigenesis in part by promoting the local release of growth factors, cytokines, and reactive oxygen species (ROS), thereby inducing cell proliferation, disrupting cell differentiation states, and selecting for oncogenic

mutations. Consistently with this hypothesis, activating *K-RAS* mutations are detectable in up to a third of patients with chronic pancreatitis (Löhr, Maisonneuve, and Lowenfels 2000). In states of pancreatic inflammation or damage, an expanded “stem cell”-like compartment could represent a subpopulation of cells susceptible to oncogenic transformation upon somatic mutation of key proto-oncogenes and tumor suppressor genes (Beachy, Karhadkar, and Berman 2004).

Incidence and diagnosis

Pancreatic cancer is the fourth leading cause of cancer death in the USA (Becker et al. 2014). In 2014, the American Cancer Society (ACS) estimated 46,420 new cases of pancreatic cancer with 39,590 deaths in the United States. Unfortunately, 80% of patients diagnosed with pancreatic cancer present metastatic or local disease at initial diagnosis (Karmazanovsky et al., n.d.). While the 5-year survival rates for many oncologic diseases have improved, for pancreatic cancer it remains dismal at 6% (ACS, 2014). Even at high-volume specialty centers, where the 5-year survival rate for patients is higher than in the general population, disease recurrence is still a major problem. As before reported, PDAC is the most common pancreatic cancer type (90% of cases) and the most malignant. PDAC has a poor outcome and an increasing incidence during the last years. Several factors contribute to the poor prognosis of PDAC, such as late tumor diagnosis, early invasion of blood vessels, high ability to metastasize, low immunogenicity and poor response to cytotoxic agents. However, the high mortality rate is mainly caused by the lack of highly sensitive and specific tools to detect the disease in an early stage (Greenhalf et al. 2009), and therefore most of the patients are diagnosed in advanced tumor stages. The

only treatment for pancreatic cancer with curative potential is resection of the involved portion of the pancreas. Since metastatic and locally advanced disease is an exclusion criterion for surgical treatment, only a small number of patients (15%) presenting a resectable tumor at the time of diagnosis, can be surgically treated (Distler et al. 2014). In the majority of PDAC patients, symptoms do not manifest at early stages of the disease and diagnosis occurs when the tumor is locally advanced or metastatic, with liver, lungs and peritoneum as most common metastatic sites. However, when surgery is possible, often patients additionally receive an adjuvant therapy, in order to avoid relapse (Kleeff et al. 2016; Distler et al. 2014). The only screening programs that are currently available are in research settings and are narrowly focused on detecting potentially precancerous lesions among high-risk individuals. Current knowledge about pancreatic carcinogenesis points out a stepwise progression from intraepithelial neoplasia to invasive cancer (Conroy et al. 2011). Resected pancreas obtained from a patient with family history of pancreatic cancer or with PDAC showed multifocal, microscopic pancreatic intraepithelial neoplasms (PanINs) (Burris et al. 1994; Von Hoff et al. 2013). Moreover, two precursor lesions for this cancer are represented by intraductal papillary mucinous neoplasms (IPMNs) and mucinous cystic neoplasms (MCNs) (Moore et al. 2007; Kindler et al. 2010; Philip et al. 2010; Gourgou-Bourgade et al. 2013). An early detection of these precursor lesions could prevent a disease progression. Up to 50% of pancreatic cancer patients present with jaundice, which is more common in patients whose cancers are located in the head of the pancreas where tumors can cause obstruction of the adjacent biliary system (Bose, Katz, and Fleming 2012). Other common manifestations include vague abdominal discomfort, nausea, and weight loss. Steatorrhea can result from obstruction of

the pancreatic duct, whereas hyperglycemia and diabetes have been associated with early manifestation of disease. Patients with advanced disease can also present with pain, ascites, and depression.

Therapy

For resectable pancreatic cancer, the primary treatment from the National Comprehensive Cancer Network (NCCN) is surgery, followed by adjuvant chemotherapy. However, there are also phase II clinical trials data that support the delivery of neoadjuvant therapy (i.e., chemotherapy and radiation administered prior to surgical resection) in selected patients with biopsy confirmation of adenocarcinoma (Halperin and Varadhachary 2014). The primary chemotherapeutic agents that have shown benefit in patients with pancreatic cancer are gemcitabine and fluorouracil (5-FU). The use of gemcitabine showed to increase the median disease-free survival to 13.4 months compared with 6.7 months in an observation group (Oettle et al. 2007). A 5-year survival of 21% was observed in patients treated with adjuvant 5-FU compared with 9% in patients selected to receive nonadjuvant treatment in a random way (Halperin and Varadhachary 2014). Folfirinox (made up of: folinic acid, 5-FU, irinotecan and oxaliplatin) was shown to offer a survival advantage but increased toxicity compared with gemcitabine in patients with advanced disease (Conroy et al. 2011). As such, Folfirinox has become an option for patients with metastatic disease, providing an otherwise good performance status. In unresectable tumour patients, treatment usually consists of systemic chemotherapy and in some cases chemoradiation. The role of radiation in combination with chemotherapy for locally advanced disease was studied: chemoradiation has shown benefit but a noted increase in toxicity has been

reported. Nonetheless, the effects achieved by both approaches are mainly a mildly increased survival rate and lowered cancer-related symptoms. Also multidrug regimens, such as Abraxane[®] and Folfirinox, have been recently developed moderately improving patients' outcomes; however, their efficacy still remains low and their use leads to several adverse effects (Adamska, Domenichini, and Falasca 2017). Further studies were carried out focusing on the high variety of miRNAs aberrantly expressed in PDAC and their role in the control of cell proliferation, invasion and apoptosis. The strategy of altering their expression and activity in order to prevent cancer development and progression seems to be promising. Synthetic nanoparticles for the delivery of miRNAs, which are downregulated in cancer tissues, as well as inhibition of overexpressed miRNA, were explored. Both approaches showed promising *in vitro* and *in vivo* results. However, considering that each miRNA has multiple targets, their alteration might cause unpredictable modifications in many pathways, contributing to fatal consequences. Therefore, more advanced pre-clinical and clinical studies are needed to fully elucidate the potential of miRNAs modulation in PDAC therapy. Huge heterogeneity and complexity of PDAC is regarded to be a major clinical obstacle in the development of successful therapies. Indeed, PDAC displays a high resistance to conventional therapies. Targeting individual molecules is not a sufficient approach, as it is counteracted by upregulation of members of adjacent pathways, contributing to therapy failure. Therefore, strategies combining chemotherapy with targeting multiple targets and nano-drug delivery could considerably reduce this risk. In the last years, the strategy of combining targeted agents with chemotherapy has been widely explored; however, in pancreatic cancer, the only drug that reported an effect was erlotinib (Traceva[®]).

Further research and clinical studies should be also focused on the role of pancreatic cancer stem-like cells, a subpopulation of slow-cycling highly metastatic cells showing increased chemoresistance. The ability to control this subpopulation of cancer cells, responsible for enhanced aggressiveness and invasion potential, could be of great clinical value. Nevertheless, in all therapeutic regimens, some general side effects are expected, including complications associated with a reduction in blood cell counts, vomiting and nausea, diarrhoea, constipation, mouth ulcers, poor appetite, hair loss, nervous system changes, and infertility. It has been considered that some of these adverse effects, especially blood clotting and weight loss, may be one of the reasons for the ineffectiveness of current therapies, forcing their early termination. Thereby, learning how to manage these adverse symptoms could significantly improve patients' outcomes (Adamska, Domenichini, and Falasca 2017).

In conclusion, pancreatic cancer is a complex disease that need to be managed with an integrative approach, and therefore, there is an urgent clinical need to develop best therapeutic strategies aimed at specific subpopulations of patients.

Extracellular vesicles

Among emerging key players in the study of new potential cancer targets, extracellular vesicles (EVs) have reported to promote several tumour processes, and therefore we focused our project on evaluating their involvement in pancreatic cancer. EVs are small membrane vesicles that constitute critical components of intercellular communication (Lobb et al. 2015).

Although the release of apoptotic bodies during apoptosis has been long known

(Hristov 2004), the fact that also perfectly healthy cells shed vesicles from their plasma membrane has only recently become appreciated. These vesicles are generally referred to as exosomes, microvesicles, ectosomes, shedding vesicles, or microparticles among others (Holme et al. 1994; C. Hess et al. 1999; Cocucci, Racchetti, and Meldolesi 2009; György et al. 2011). They are capable of inducing local and systemic changes, thereby promoting disease progression in a number of settings (EL Andaloussi et al. 2013). The functional impact of EVs is imparted by the molecular components (e.g. protein and RNA cargo) they carry, prompting the increased interest in EVs as potential novel biomarkers for the diagnosis and prognosis of disease progression (Théry, Ostrowski, and Segura 2009).

EVs were shown to convey molecular information within the tumour microenvironment and beyond, as they efficiently travel throughout the organism and can be detected in various organic fluids and secretions (H. Shao et al. 2012; Treps et al. 2016).

The machineries involved in scission/release of EVs from the plasma membrane and those implicated in the mobilization of secretory EVs to the cell periphery, their docking and fusion with the cell surface are still at an early stage of comprehension. These processes require the cytoskeleton (actin and microtubules), associated molecular motors (kinesins and myosins), molecular switches (small GTPases), and the fusion machinery (SNAREs and tethering factors) (Cai, Reinisch, and Ferro-Novick 2007). The first indications for the involvement of Rab GTPases in exosome secretion were from studies on reticulocyte cell lines, which required the function of Rab 11 for exosome secretion (Savina, Vidal, and Colombo 2002). More recently, in an RNAi screen in HeLa cells targeting 59 members of the Rab GTPase family, knockdown of

Rab27a or Rab27b significantly reduced the amount of secreted exosomes (Ostrowski et al. 2010). Rab27 could be involved directly or indirectly in the transport and tethering at the cell periphery of the secretory EVs. Release of EVs was found to be regulated in several cellular model systems. For example, it can be stimulated through activation of purinergic receptors with ATP (Wilson et al. 2004). Platelets are stimulated to shed vesicles from the plasma membrane and to release exosomes in response to thrombin receptor activation (Heijnen et al. 1999). Dendritic cells increase the release of MVs and change the protein composition in response to activation by lipopolysaccharides (Obregon et al. 2006; Nolte-'t Hoen et al. 2013), whereas peptide-loaded immature dendritic cells were stimulated to release exosomes in response to their interaction with T cells recognizing peptide-loaded MHC class II (Buschow et al. 2009). Similarly, plasma membrane depolarization increases the rapid secretion of exosomes by neuronal cells (Fauré et al. 2006; Lachenal et al. 2011), and cross-linking of CD3 in T cells stimulates exosome release by T cells (Blanchard et al. 2002). In a recent study, it was demonstrated that secretion of exosomes carrying the morphogen Wnt is dependent on the R-SNARE Ykt6 (Gross et al. 2012). Functions of EVs in physiological and pathological processes depend on the ability of EVs to interact with recipient cells to deliver their contents. EVs released by a human intestinal epithelial cell line have found to interact preferentially with dendritic cells rather than with B or T lymphocytes (Mallegol et al. 2007). The cellular and molecular basis for EVs targeting is still undetermined, but several target cell-dependent and -conditional aspects are beginning to emerge. Target cell specificity is likely to be determined by adhesion molecules, such as integrins, that are present in EVs. After binding to recipient cells, EVs may remain stably associated with the plasma membrane or

dissociate, directly fuse with the plasma membrane, or are internalized through distinct endocytic pathways. When endocytosed, EVs may subsequently fuse with the endosomal delimiting membrane or be targeted to lysosomes for degradation. Stable and persistent cell surface exposure can be expected, particularly on cells that display little if any endocytic activity (Denzer et al. 2000). Detection of fusion of small EVs with the plasma membrane by fluorescence microscopy in live cells is limited by resolution and the fast dynamics of fusion events. Several studies provided evidence for the accumulation of captured EVs in endocytic or phagocytic compartments, with uptake depending on the actin cytoskeleton, phosphatidylinositol 3-kinase activity, and dynamin-2 function (Morelli 2006; Tian et al. 2010; Graça Raposo and Stoorvogel 2013)

A current problem impeding the advancement in EVs research is the lack of characterization of current methodologies evaluating their usability, vesicle purity and yield from cell culture conditioned media (CCM) and complex biological fluids such as plasma. High-throughput methods that minimize the co-isolation of protein aggregates are essential to develop accurate biomarker signatures for disease and assess the downstream biological impacts of EVs in recipient cells (Lobb et al. 2015).

Exosomes

The term exosome was initially used for membrane vesicles ranging from 40 to 1,000nm that are released by a variety of cultured cells (Trams et al. 1981), but the subcellular origin of these vesicles remained unclear. Later, this nomenclature was adopted for 40–150nm vesicles released during reticulocyte differentiation as a consequence of multivesicular endosome (MVE) fusion with

the plasma membrane (Harding, Heuser, and Stahl 1984). One decade later, exosomes were found to be released by B lymphocytes and dendritic cells through a similar route (G. Raposo 1996). Several additional cell types of both hematopoietic and non-hematopoietic origin were also shown to release exosomes through MVE fusion with the cell surface (Simons and Raposo 2009). Vesicles with hallmarks of exosomes have been isolated from diverse body fluids, including semen (Aalberts et al. 2012; K.-H. Park et al. 2011), blood (Caby et al. 2005), urine (Pisitkun, Shen, and Knepper 2004), saliva (Ogawa et al. 2011), breast milk, amniotic fluid (Asea et al. 2008), ascites fluid (Andre et al. 2002), cerebrospinal fluid (Vella et al. 2007), and bile (Masyuk et al. 2010). Most of these studies attributed the isolated vesicles to exosomes because of their exosome-like protein contents. However, circulating vesicles are likely composed of both exosomes and microvesicles (MVs) and a single cell type releases both exosomes and MVs has, for example, either been demonstrated or suggested for platelets (Heijnen et al. 1999), endothelial cells (Deregibus et al. 2007), and breast cancer cells (Muralidharan-Chari et al. 2009). Currently available purification methods do not always allow one to fully discriminate between exosomes and MVs.

Exosomes are formed from multivesicular bodies (MVBs), which are intracellular endosomal organelles, characterized by multiple intraluminal vesicles within a single outer membrane. MVBs are formed from early endosomes, which as prelysosomal structures belong to the degradative endosomal pathway of internalized proteins. It is known now that they are involved in numerous endocytic and trafficking functions, including protein sorting, recycling, transport, storage, and release. Early endosomes can interact with the Golgi apparatus and the endoplasmic reticulum. Exosomes can be formed by

endocytosis of the early endosome membrane having a unique orientation of the involuted cytoplasmic side (Palay 1960). Generation of MVBs as well as secretion of exosomes are mediated through the action of endosomal protein complexes required for transport. They are involved in the recognition of ubiquitinated cargo by MVBs, as well as the invagination of the MVB outer membrane (Babst et al. 2002; Wollert and Hurley 2010). The origin of exosomes suggests that their production is stimulated in response to alterations in the microenvironment. The formation of early endosomes and MVBs has been shown to increase upon signaling through growth factor receptors, suggesting that the cell adjusts exosome production according to its need (Borges, Reis, and Schor 2013; Pisitkun, Shen, and Knepper 2004). Exosomes are now emerging as key players involved in several pathological processes, including cancer. Indeed, exosomes are also released by cancer cells and are considered messengers in tumour intercellular communication (Taverna et al. 2012). Biochemical and proteomic analysis of exosomes revealed that these vesicles contain cell-type specific proteins that characterize their functional activity (Mathivanan, Ji, and Simpson 2010). The exact function of exosomes in malignant cells has yet to be elucidated, but investigation has suggested roles in cell-to-cell communication, tumor-stroma interaction and antigen presentation, thereby potentially affecting cancer progression at different steps (Iero et al. 2008). Exosomes have been shown to interact with endothelial cells (Dutta et al. 2015; Putz et al. 2012). Tumour-derived exosomes can increase tumour invasiveness and proliferation in an autocrine fashion (Skog et al. 2008), in addition to interactions with host stromal cells, such as the conversion of fibroblasts to a myofibroblast phenotype resulting in extracellular matrix (ECM) remodelling that is conducive to tumour growth (Webber et al. 2015). The

presence of matrix metalloproteinases allows for direct modulation of the ECM by tumour-derived exosomes in the primary tumour microenvironment and metastatic spread (Mu, Rana, and Zöller 2013). Exosome secretion may also facilitate advantageous exocytosis and cellular removal of tumour suppressors, showing the complex role of exosomes within tumour progression (Chairoungdua et al. 2010; Ostefeld et al. 2014). The release of exosomes into the interstitial space and subsequent dissemination throughout the body highlights a potential role for tumour-derived exosomes in formation of a pre-metastatic niche (Costa-Silva et al. 2015; Hood, San, and Wickline 2011) beyond that of an auto/paracrine action at the primary tumour site. This potential is further supported by increased vascular leakiness and concomitant increased metastatic lesion formation in the lungs of mice after systemic administration of malignant cell-derived exosomes (Peinado et al. 2012).

The current “gold standard” for the purification of exosomes is differential centrifugation, which typically consists of low-speed centrifugation to remove cells and large vesicles, and high-speed ultra-centrifugation to pellet exosomes (Théry et al. 2006). Density gradients can then be utilized to remove contaminating impurities such as non-specific argonaute proteins (Van Deun et al. 2014). Ultracentrifugation of large volumes of CCM can result in sample loss depending on the skill of the operator. It has also been suggested in the literature that repeated ultracentrifugation steps can damage vesicles and reduce yields, thereby potentially impacting proteomic and RNA analysis of exosome content (Lamparski et al. 2002). An alternative to ultracentrifugation is concentration of large volumes of CCM using ultrafiltration devices.

Methods and results

Isolation of EVs

Basing on previous reported findings, an approach with the aim to identify new molecular markers for the early diagnosis and for a specific therapy of pancreatic cancer needs to be developed. In this study, we investigated and characterized exosomes released by different pancreatic cancer cell types, focusing on a detailed proteomic analysis of their content. Exosomes have shown to contain a large number of proteins that can be responsible of their activity and their pro-tumoral function. This analysis will lead to the detection of potential biomarkers that can be isolated and studied for their role in pancreatic cancer progression.

To perform this evaluation, we cultured PDAC, PANC2, KPC (mouse) and PANC1, miaPACA2 (human) pancreatic cancer cell lines in their recommended conditions. After 72h in which cells were maintained in culture with a cell conditioned medium, we proceeded with exosome isolation from cell supernatant. We used a conditioned medium in which exosomes were removed from the serum, in order to avoid contaminations in our final product. At the moment of exosome extraction, cell supernatant was collected, since EVs are normally released in the extracellular space. A procedure of differential centrifugation was developed: supernatant was centrifuged at 200g for 10min at 4 °C to remove cell debris; then a centrifugation at 16,500g for 30min at 4 °C followed; finally supernatant was ultracentrifuged at 100,000g for 90min at 4 °C. EVs were obtained from this last centrifugation and thus the pellets were resuspended in a large volume of ultrapure water, washed and collected by a further ultracentrifugation at 100,000g for 90min at 4 °C. The preparation was stored at 4 °C, to prevent degradation.

Once obtained, the EVs preparation was verified by electron microscopy, to assess purity and dimension. Moreover, EVs size and particle number were analysed using the dynamic light scattering (DLS) and transmission electronic microscope (TEM) nanoparticle characterization system. Performed analysis showed the presence of EVs with a very small size (50-150nm) which is attributable to exosomes (Fig. 25).

We concentrated this study on the analysis of proteins which are contained in exosomes. The concentration of exosome proteins was determined by BCA Protein Assay Kit (Thermo).

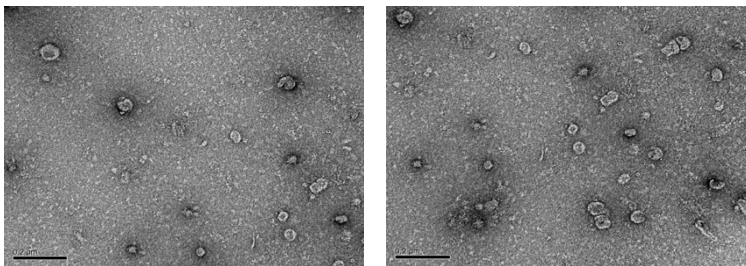


Figure 25: TEM image of PDAC isolated EVs.

Internalization in HUVECs

Since exosomes are known to be involved in intercellular communication, they transport their material from some cells to other. Thereby, we decided to investigate the internalization of exosomes isolated from PDAC cells in HUVECs. Indeed, this assessment will allow future investigations on exosomes influence on tumour processes, such as cell migration and angiogenesis. First, exosomes

derived from PDAC cell line were fluorescently labelled using PKH67 membrane dye (Sigma) and then HUVECs were incubated with labelled exosomes. Unlabelled exosomes were used as controls of signal specificity. The analysis of cells which incorporated exosomes was performed by flow cytometry and confocal evaluation.

For the flow cytometry analysis, HUVECs (1×10^4 /well) were seeded in 24-well plates and treated with $50 \mu\text{g/ml}$ of labelled exosomes for 30min, 1h or 2h. The samples were analyzed and obtained results showed that exosomes internalization in HUVECs followed a time-dependent trend. Indeed, the obtained peaks indicated a growing increment of exosomes⁺ cells from 30min to 2h (Fig. 26).

In order to observe exosomes internalization, HUVECs treated with $50 \mu\text{g}$ of labelled exosomes for 30min, 1h or 2h were observed by a confocal microscope (Olympus with DSU spinning disk). Images at each time were acquired, captured and observed. Previous findings were validated, since also in this case the amount of cells with internalized exosomes increased over time. At 2h, most of all exosomes showed to be present into the exposed cells (Fig. 27).

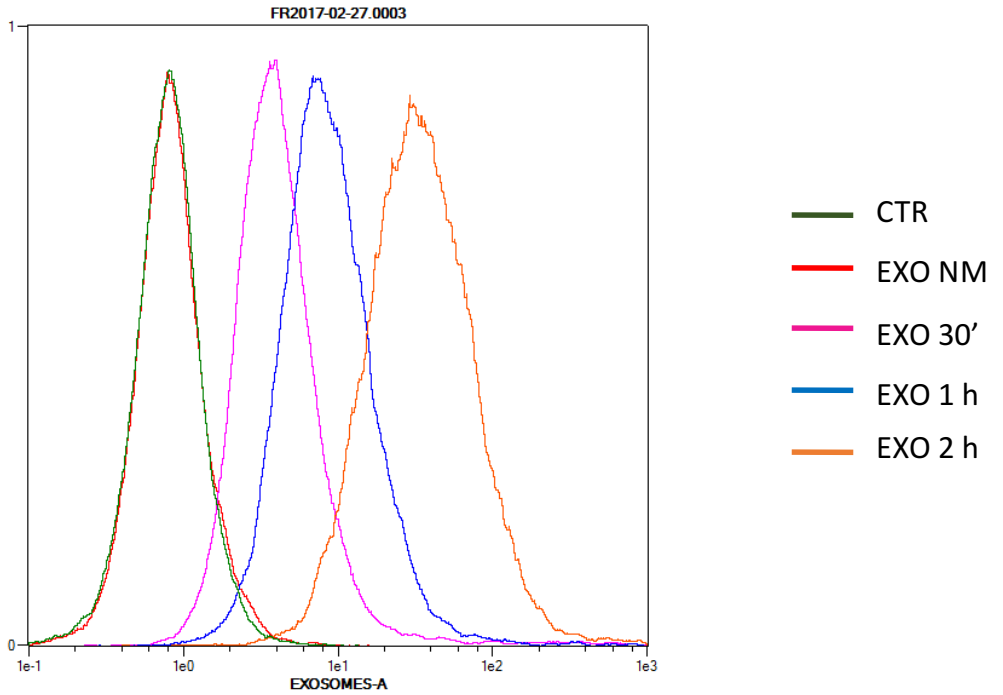


Figure 26: Exosomes⁺ HUVECs after 30', 1h or 2h of incubation. Samples were analyzed with a MACSQuant Analyzer (Miltenyi Biotec) for flow cytometry experiments (CYBIO Plateform, Institut Cochin, Paris, France). Files were processed and analysed using CFlow plus software (BD Biosciences). PKH-67-positive events were recorded and analyzed. Not marked exosomes (EXO NM) was used as a negative control.

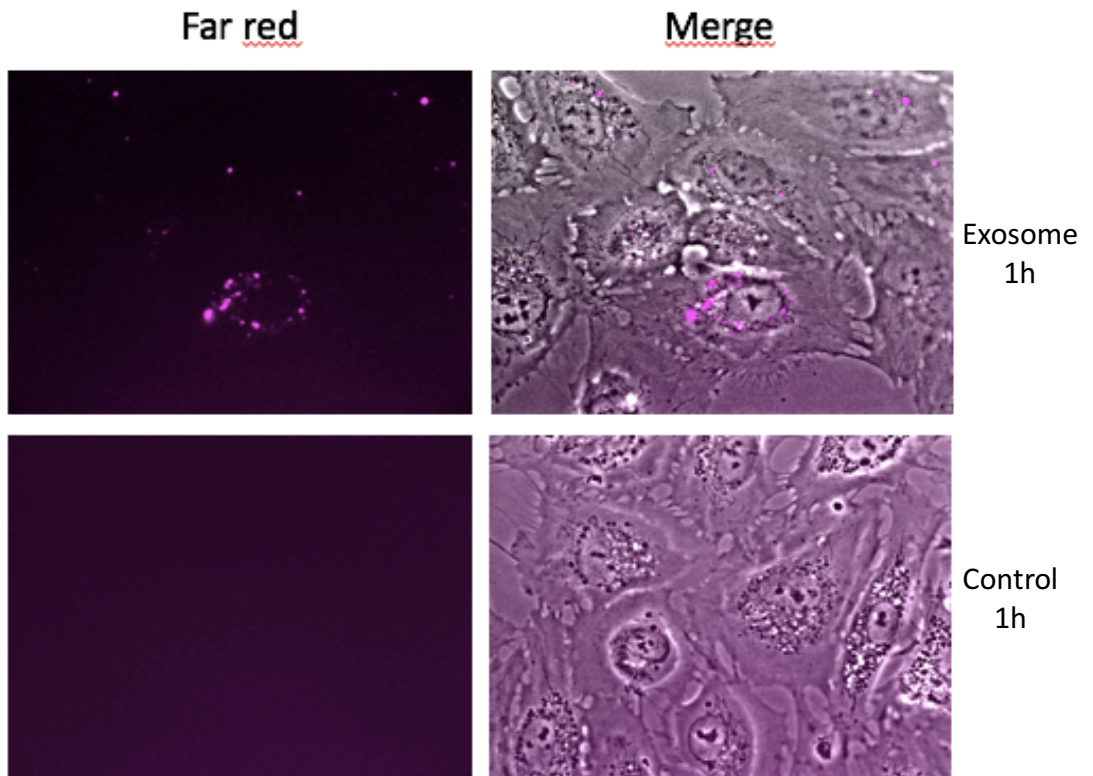


Figure 27: Exosomes internalization in HUVECs after 30', 1h or 2h of treatment. Images at each time were acquired with a IX81 Olympus equipped with a DSU spinning disk confocal system, coupled to an OrcaR2 Hamamatsu CCD camera. Axial z-stacks were acquired in order to observe cells at each level from the base to the top with a 60 x ph3 NA 1.25 Oil Objective.

Western blotting for the identification of exosomes

Exosomal protein content was detected by western blot, using antibodies directed to known exosomal markers, such as CD-9 and tetraspanin-8 (Rana et al. 2012). For this evaluation, 50µg of PDAC exosomal proteins were loaded on a polyacrilamide gel and SDS-PAGE was performed. Samples were then transferred onto a PVDF membrane (Millipore). After transfer, membranes' aspecific binding sites were blocked in 3% BSA. Subsequently, they were incubated with primary anti-TSPAN8 antibody (TA339425, 1:1,000, Origene) and anti-CD9 (ab92726, 1:2,000, Abcam) diluted in 3% BSA. A HRP-goat anti-rabbit IgG (jackson, 1:10,000) diluted in 3% BSA was used as secondary antibody. Once the incubation was ultimated, membranes were rinsed in ECL western blot substrate (Thermo) before scanning. Finally, membranes were scanned and analysed using an OdysseyH IR scanner using OdysseyH imaging software 3.0. The two antibodies detected binded proteins in our samples, demonstrating that exosomes were present in our preparation. Figure 28 reports CD-9 detection on the membrane.

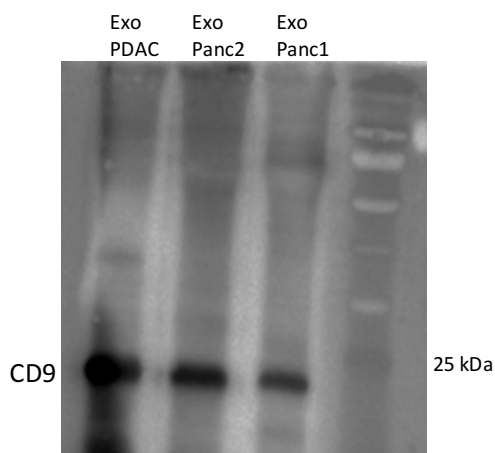


Figure 28: Western blotting image reporting CD-9 detection on exosomal samples obtained from PDAC, PANC2 or PANC1 cell lines.

Analysis of exosomal protein content

In order to define the proteomic profile of isolated pancreatic cancer exosomes, a proteomic-LC/MS analysis of all obtained exosomes was carried out. For this analysis, 50µg of exosomal proteins were loaded on a polyacrilamide gel and SDS-PAGE was performed. Then, after gel staining with colloidal coomassie blue and destaining in double-distilled H₂O, each band on the gel was cut, and protein digestion was performed, by using a nano-LC-MS/SynaptG2-S, a UPLC/HDMS^E method and, for data extraction, Uniprot complete Human or Mouse proteome databases concatenated with common contaminants using ProteinLynx Global SERVER (PLGS; Waters).

Therefore, the protein content of exosomes derived from all examined pancreatic cancer cell lines was analyzed, and a list of revealed proteins for each of them was obtained. Table 1 shows a list of the proteins obtained from PDAC cell line derived exosomes.

We decided to group common proteins among different analyzed exosomes for each cell line. For example, four PDAC derived exosomal contents were analyzed and common proteins were grouped. The common proteins were analyzed by using bioinformatic softwares (string-db.org and FunRich.org) and some of them were found to be common exosomal markers, such as Tetraspanin-8, Heat shock cognate 71 kDa protein and Tubulin beta-1 chain (Fig. 29).

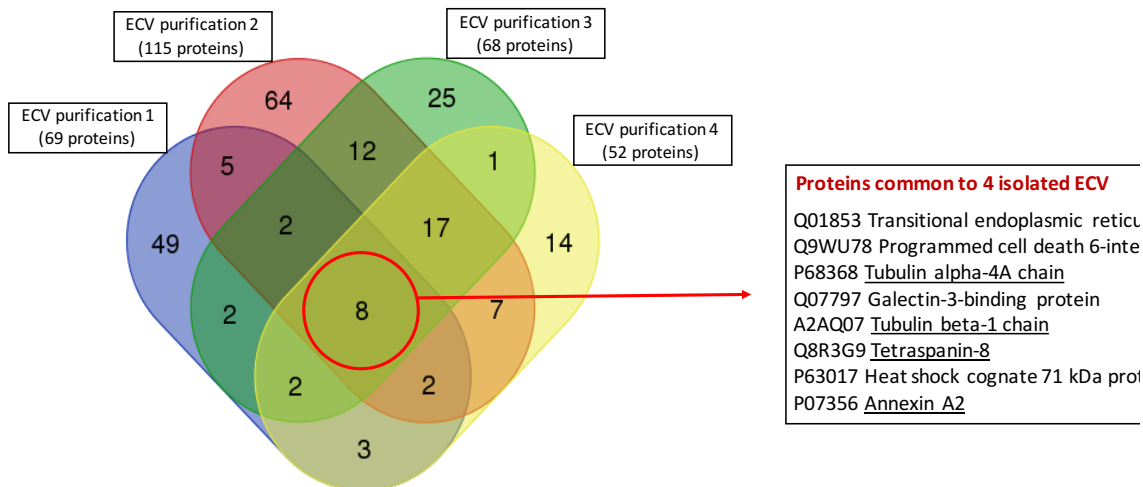
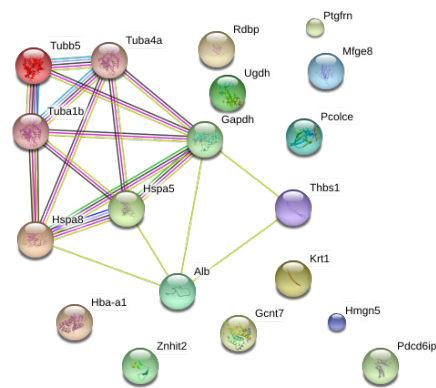
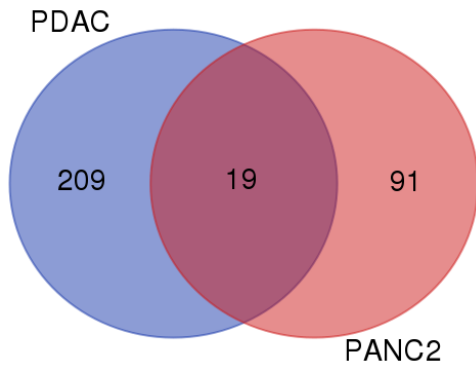


Figure 29: Identification of proteins common to four different exosome extracts belonging to four PDAC cell lines. 8 common proteins were found and then analyzed through the use of bioinformatic softwares.

Moreover, a preliminary analysis of proteins common to PDAC exosomes and PANC2 exosomes was performed, in order to see if some proteins were present in both exosomes derived from the two different pancreatic cancer cell types (Fig. 30). Among common proteins, lactadherin has been found; this protein is known to promote the process of neo-angiogenesis and therefore its presence among two different pancreatic cancer exosomes may underlie an exosomal involvement in this process. However, a deeper study on a larger number of exosomal contents needs to be performed. Further analyses have been started and are now ongoing for comparing exosomal lists of proteins even for the other studied murine and human cancer cell types. The evaluation of common proteins will be useful to identify possible pancreatic cancer biomarkers.



P99024	<u>Tubulin beta-5 chain</u>
O70475	UDP-glucose 6-dehydrogenase
Q9WV91	Prostaglandin F2 receptor negative regulator
Q3V3K7	Beta-1,3-galactosyl-O-glycosyl-glycoprotein beta-1,6-N-acetylglucosaminyltransferase 7
P68368	<u>Tubulin alpha-4A chain</u>
Q61398	Procollagen C-endopeptidase enhancer 1
P05213	<u>Tubulin alpha-1B chain</u>
P07724	Serum albumin
P01942	Hemoglobin subunit alpha
P21956	<u>Lactadherin</u>
Q9JL35	High mobility group nucleosome-binding domain-containing protein 5
Q9WU78	Programmed cell death 6-interacting protein
P19426	Negative elongation factor E
P16858	Glyceraldehyde-3-phosphate dehydrogenase
P20029	78 kDa glucose-regulated protein
P63017	<u>Heat shock cognate 71 kDa protein</u>
Q9QY66	Zinc finger HIT domain-containing protein 2
P35441	Thrombospondin-1

Figure 30: Identification of proteins common to exosome extracts belonging to PDAC and PANC2 cell lines. 19 common proteins were found and then analyzed through the use of string-db.org.

Mouse strains and plasma EVs

All mouse work was performed in accordance with institutional french guidelines. For the exosome-isolation from PDAC mice, 10week-old FVB female mice were used for all animal experiments. For the exosome-isolation from PANC2 and KPC injected mice, 10week-old C57/Bl6 female mice were used. Animals were anesthetized and injected into the head of the pancreas with 1,000 PDAC cells in 50µl, or 300,000 PANC2 cells in 100µl, or 10,000 KPC cells in 50µl. Tumors were allowed to grow during the following 3 weeks. After 3 weeks, mice were sacrificed and plasma was collected and processed for exosome isolation.

The procedure of exosome isolation from plasma was similar to the one used for isolation from cell supernatant. Plasma was centrifuged at 200g for 10min at 4 °C to remove cell debris; then a centrifugation at 16,500g for 30min at 4 °C followed; finally supernatant was ultracentrifuged at 100,000g for 90min at 4 °C. EVs were obtained from this last centrifugation and thus the pellets were resuspended in a large volume of ultrapure water, washed and collected by a further ultracentrifugation at 100,000g for 90min at 4 °C. The preparation was stored at 4 °C, to prevent degradation.

Afterwards, proteomic-LC/MS analysis of all obtained exosomes was carried out to analyze their protein content, using the previously shown procedure. The protein content of exosomes derived from all examined mice plasma was analyzed, and a list of revealed proteins for each of them was obtained. An interesting point was to analyze the different exosomal protein content between tumour and healthy mice plasma, both in qualitative and in quantitative terms (Fig. 31). Among PDAC mice and their healthy control, 107 common proteins were identified and their quantity reported to be different in

the two examined groups. The % fold change tumour/healthy > or < 20% (fmol) was taken into consideration, and proteins with higher differences between the groups showed to be involved in processes such as negative regulation of protein metabolic process, acute-phase response and regulation of blood coagulation (Fig. 32).

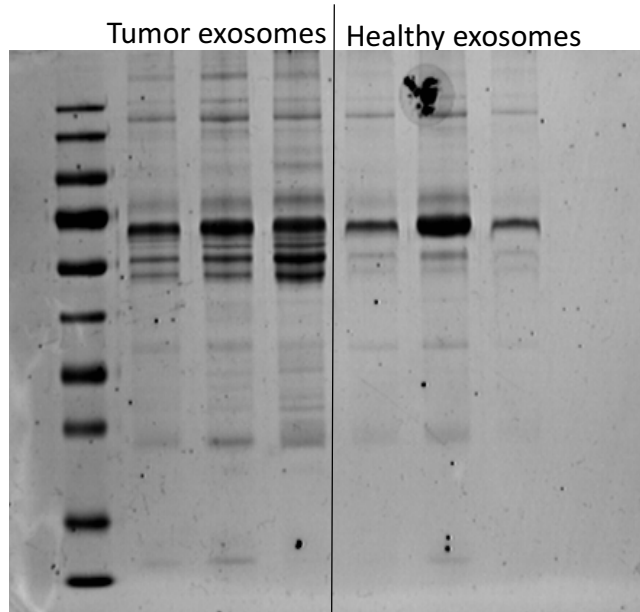
Further analyses are in progress for comparing exosomal lists of proteins even between plasma exosomes derived by other studied mouse models and their healthy counterpart.

Finally, the detection of proteins common to exosomes derived from a pancreatic cancer cell line and the respective mouse model may result important for identifying potential biomarkers for that specific pancreatic cancer type. Figure 33 shows a comparison between the protein content of exosomes deriving from PDAC cell line and from PDAC mice plasma.

Results obtained from the analysis of plasma exosomes are being implemented with the study of biological processes and pathways in which these proteins are involved, and more represented proteins can represent biomarkers for this tumour.

Mass-spectrometry analysis

A



B

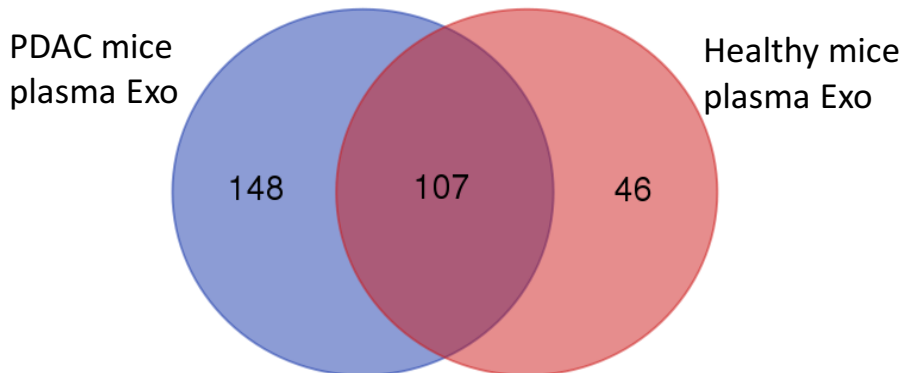


Figure 31: (A) Polyacrilamide gel after SDS-PAGE, reporting plasma exosomes of three PDAC mice and the respective healthy controls. **(B)** Exosomal proteins common to three PDAC and healthy mice plasmas analyzed through the use of bioinformatic softwares.

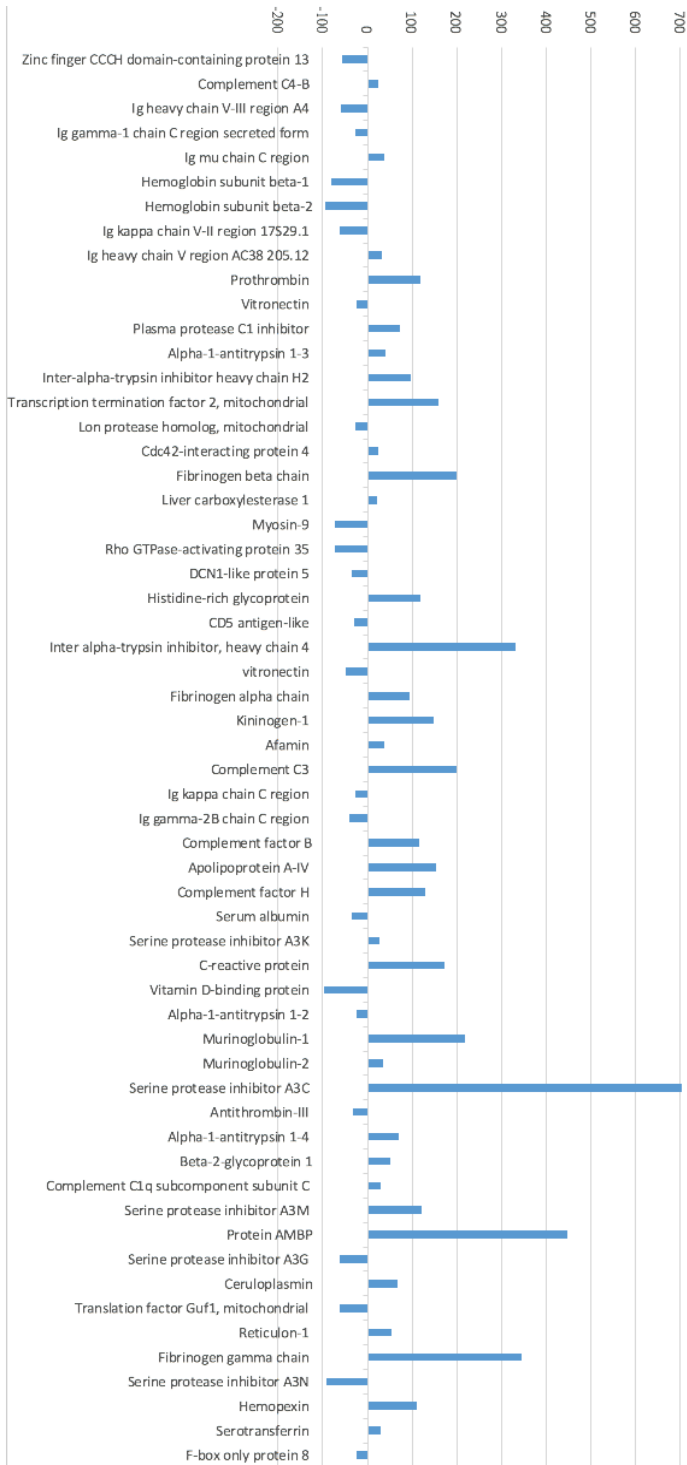
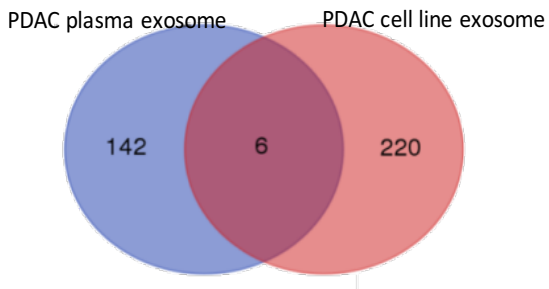


Figure 32: % fold change between exosome proteins from plasma of PDAC and healthy mice.



6 common proteins:
Pigment epithelium-derived factor
Clusterin
Actin, cytoplasmic 1
High mobility group nucleosome-binding domain-containing protein 5
FERM domain-containing protein 5
Thrombospondin-1

Figure 33: Analysis of proteins common to exosomes deriving from PDAC cell line and respective PDAC mice plasma.

Table 1: List of PDAC exosomal proteins.

Accession	Entry	Description
P39061	COIA1_MOUSE	Collagen alpha-1(XVIII) chain OS=Mus musculus GN=Col18a1 PE=1 SV=4
P62204	CALM_MOUSE	Calmodulin OS=Mus musculus GN=Calm1 PE=1 SV=2
Q9JL35	HMG5_MOUSE	High mobility group nucleosome-binding domain-containing protein 5 OS=Mus musculus GN=Hmgn5 PE=1 SV=2
Q9CQM5	TXD17_MOUSE	Thioredoxin domain-containing protein 17 OS=Mus musculus GN=Txndc17 PE=1 SV=1
P62204	CALM_MOUSE	Calmodulin OS=Mus musculus GN=Calm1 PE=1 SV=2
P39061	COIA1_MOUSE	Collagen alpha-1(XVIII) chain OS=Mus musculus GN=Col18a1 PE=1 SV=4
Q9JL35	HMG5_MOUSE	High mobility group nucleosome-binding domain-containing protein 5 OS=Mus musculus GN=Hmgn5 PE=1 SV=2
P01942	HBA_MOUSE	Hemoglobin subunit alpha OS=Mus musculus GN=Hba PE=1 SV=2
Q6P5H6	FRMD5_MOUSE	FERM domain-containing protein 5 OS=Mus musculus GN=Frmd5 PE=1 SV=1
P01942	HBA_MOUSE	Hemoglobin subunit alpha OS=Mus musculus GN=Hba PE=1 SV=2
Q6P5H6	FRMD5_MOUSE	FERM domain-containing protein 5 OS=Mus musculus GN=Frmd5 PE=1 SV=1
Q8CBY8	DCTN4_MOUSE	Dynactin subunit 4 OS=Mus musculus GN=Dctn4 PE=1 SV=1
Q8BHL4	RAI3_MOUSE	Retinoic acid-induced protein 3 OS=Mus musculus GN=Gprc5a PE=1 SV=1
O54879	HMGB3_MOUSE	High mobility group protein B3 OS=Mus musculus GN=Hmgb3 PE=1 SV=3
Q68FD5	CLH1_MOUSE	Clathrin heavy chain 1 OS=Mus musculus GN=Cltc PE=1 SV=3
Q8BHN5	RBM45_MOUSE	RNA-binding protein 45 OS=Mus musculus GN=Rbm45 PE=1 SV=1
Q8CGB3	UACA_MOUSE	Uveal autoantigen with coiled-coil domains and ankyrin repeats OS=Mus musculus GN=Uaca PE=1 SV=2
Q9R0B6	LAMC3_MOUSE	Laminin subunit gamma-3 OS=Mus musculus GN=Lamc3 PE=1 SV=2
Q9WV91	FPRP_MOUSE	Prostaglandin F2 receptor negative regulator OS=Mus musculus GN=Ptgfrn PE=1 SV=2
Q9R100	CAD17_MOUSE	Cadherin-17 OS=Mus musculus GN=Cdh17 PE=1 SV=1
Q9JLQ0	CD2AP_MOUSE	CD2-associated protein OS=Mus musculus GN=Cd2ap PE=1 SV=3
P09055	ITB1_MOUSE	Integrin beta-1 OS=Mus musculus GN=Itgb1 PE=1 SV=1
Q8VDM1	ZGPAT_MOUSE	Zinc finger CCCH-type with G patch domain-containing protein OS=Mus musculus GN=Zgpat PE=1 SV=1
Q9WU78	PDC6I_MOUSE	Programmed cell death 6-interacting protein OS=Mus musculus GN=Pdc6ip PE=1 SV=3
O35450	FKBPL_MOUSE	FK506-binding protein-like OS=Mus musculus GN=Fkbp1 PE=2 SV=1
Q3UJK4	GTPB2_MOUSE	GTP-binding protein 2 OS=Mus musculus GN=Gtbbp2 PE=1 SV=1
Q8VDN2	AT1A1_MOUSE	Sodium/potassium-transporting ATPase subunit alpha-1 OS=Mus musculus GN=Atp1a1 PE=1 SV=1
Q91V92	ACLY_MOUSE	ATP-citrate synthase OS=Mus musculus GN=Acly PE=1 SV=1
Q9WV91	FPRP_MOUSE	Prostaglandin F2 receptor negative regulator OS=Mus musculus GN=Ptgfrn PE=1 SV=2
Q9R100	CAD17_MOUSE	Cadherin-17 OS=Mus musculus GN=Cdh17 PE=1 SV=1
Q62470	ITA3_MOUSE	Integrin alpha-3 OS=Mus musculus GN=Itga3 PE=1 SV=1
A2AGH6	MED12_MOUSE	Mediator of RNA polymerase II transcription subunit 12 OS=Mus musculus GN=Med12 PE=1 SV=1

Q8VDM1	ZGPAT_MOUSE	Zinc finger CCCH-type with G patch domain-containing protein OS=Mus musculus GN=Zgpat PE=1 SV=1
P09055	ITB1_MOUSE	Integrin beta-1 OS=Mus musculus GN=Itgb1 PE=1 SV=1
Q60823	AKT2_MOUSE	RAC-beta serine/threonine-protein kinase OS=Mus musculus GN=Akt2 PE=1 SV=1
Q8VDN2	AT1A1_MOUSE	Sodium/potassium-transporting ATPase subunit alpha-1 OS=Mus musculus GN=Atp1a1 PE=1 SV=1
Q9WU78	PDC6I_MOUSE	Programmed cell death 6-interacting protein OS=Mus musculus GN=Pdcd6ip PE=1 SV=3
Q7TNC6	KI26B_MOUSE	Kinesin-like protein KIF26B OS=Mus musculus GN=Kif26b PE=1 SV=3
Q4VAC9	PKHG3_MOUSE	Pleckstrin homology domain-containing family G member 3 OS=Mus musculus GN=Plekhg3 PE=1 SV=2
Q922J3	CLIP1_MOUSE	CAP-Gly domain-containing linker protein 1 OS=Mus musculus GN=Clip1 PE=1 SV=1
E9Q784	ZC3HD_MOUSE	Zinc finger CCCH domain-containing protein 13 OS=Mus musculus GN=Zc3h13 PE=1 SV=1
Q8CIH5	PLCG2_MOUSE	1-phosphatidylinositol 4,5-bisphosphate phosphodiesterase gamma-2 OS=Mus musculus GN=Plcg2 PE=1 SV=1
O35450	FKBPL_MOUSE	FK506-binding protein-like OS=Mus musculus GN=Fkbp1 PE=2 SV=1
Q61739	ITA6_MOUSE	Integrin alpha-6 OS=Mus musculus GN=Itga6 PE=1 SV=3
P30999	CTND1_MOUSE	Catenin delta-1 OS=Mus musculus GN=Ctnnd1 PE=1 SV=2
Q9R100	CAD17_MOUSE	Cadherin-17 OS=Mus musculus GN=Cdh17 PE=1 SV=1
Q62470	ITA3_MOUSE	Integrin alpha-3 OS=Mus musculus GN=Itga3 PE=1 SV=1
Q9JLQ0	CD2AP_MOUSE	CD2-associated protein OS=Mus musculus GN=Cd2ap PE=1 SV=3
Q9WV91	FPRP_MOUSE	Prostaglandin F2 receptor negative regulator OS=Mus musculus GN=Ptgfrn PE=1 SV=2
Q8VDM1	ZGPAT_MOUSE	Zinc finger CCCH-type with G patch domain-containing protein OS=Mus musculus GN=Zgpat PE=1 SV=1
O35450	FKBPL_MOUSE	FK506-binding protein-like OS=Mus musculus GN=Fkbp1 PE=2 SV=1
Q9WU78	PDC6I_MOUSE	Programmed cell death 6-interacting protein OS=Mus musculus GN=Pdcd6ip PE=1 SV=3
Q9WU78	PDC6I_MOUSE	Programmed cell death 6-interacting protein OS=Mus musculus GN=Pdcd6ip PE=1 SV=3
Q01853	TERA_MOUSE	Transitional endoplasmic reticulum ATPase OS=Mus musculus GN=Vcp PE=1 SV=4
P26231	CTNA1_MOUSE	Catenin alpha-1 OS=Mus musculus GN=Ctnna1 PE=1 SV=1
Q9EQK5	MVP_MOUSE	Major vault protein OS=Mus musculus GN=Mvp PE=1 SV=4
O54890	ITB3_MOUSE	Integrin beta-3 OS=Mus musculus GN=Itgb3 PE=1 SV=2
O88398	AVIL_MOUSE	Advillin OS=Mus musculus GN=Avil PE=1 SV=2
Q9WV91	FPRP_MOUSE	Prostaglandin F2 receptor negative regulator OS=Mus musculus GN=Ptgfrn PE=1 SV=2
Q7TPR4	ACTN1_MOUSE	Alpha-actinin-1 OS=Mus musculus GN=Actn1 PE=1 SV=1
Q9R100	CAD17_MOUSE	Cadherin-17 OS=Mus musculus GN=Cdh17 PE=1 SV=1
P56203	CATW_MOUSE	Cathepsin W OS=Mus musculus GN=Ctsw PE=2 SV=2
Q9Z0G0	GIPC1_MOUSE	PDZ domain-containing protein GIPC1 OS=Mus musculus GN=Gipc1 PE=1 SV=1
Q9WU78	PDC6I_MOUSE	Programmed cell death 6-interacting protein OS=Mus musculus GN=Pdcd6ip PE=1 SV=3

Q01853	TERA_MOUSE	Transitional endoplasmic reticulum ATPase OS=Mus musculus GN=Vcp PE=1 SV=4
Q9EQK5	MVP_MOUSE	Major vault protein OS=Mus musculus GN=Mvp PE=1 SV=4
O54890	ITB3_MOUSE	Integrin beta-3 OS=Mus musculus GN=Itgb3 PE=1 SV=2
P26231	CTNA1_MOUSE	Catenin alpha-1 OS=Mus musculus GN=Ctnna1 PE=1 SV=1
Q9WV91	FPRP_MOUSE	Prostaglandin F2 receptor negative regulator OS=Mus musculus GN=Ptgfrn PE=1 SV=2
Q9WU78	PDC6I_MOUSE	Programmed cell death 6-interacting protein OS=Mus musculus GN=Pdcd6ip PE=1 SV=3
Q01853	TERA_MOUSE	Transitional endoplasmic reticulum ATPase OS=Mus musculus GN=Vcp PE=1 SV=4
Q9EQK5	MVP_MOUSE	Major vault protein OS=Mus musculus GN=Mvp PE=1 SV=4
O54890	ITB3_MOUSE	Integrin beta-3 OS=Mus musculus GN=Itgb3 PE=1 SV=2
O88398	AVIL_MOUSE	Advillin OS=Mus musculus GN=Avil PE=1 SV=2
Q9R100	CAD17_MOUSE	Cadherin-17 OS=Mus musculus GN=Cdh17 PE=1 SV=1
P26231	CTNA1_MOUSE	Catenin alpha-1 OS=Mus musculus GN=Ctnna1 PE=1 SV=1
P63017	HSP7C_MOUSE	Heat shock cognate 71 kDa protein OS=Mus musculus GN=Hspa8 PE=1 SV=1
P17156	HSP72_MOUSE	Heat shock-related 70 kDa protein 2 OS=Mus musculus GN=Hspa2 PE=1 SV=2
O08688	CAN5_MOUSE	Calpain-5 OS=Mus musculus GN=Capn5 PE=1 SV=1
Q61696	HS71A_MOUSE	Heat shock 70 kDa protein 1A OS=Mus musculus GN=Hspa1a PE=1 SV=2
P10852	4F2_MOUSE	4F2 cell-surface antigen heavy chain OS=Mus musculus GN=Slc3a2 PE=1 SV=1
Q8BG17	NOL12_MOUSE	Nucleolar protein 12 OS=Mus musculus GN=Nol12 PE=1 SV=1
Q61503	5NTD_MOUSE	5'-nucleotidase OS=Mus musculus GN=Nt5e PE=1 SV=2
P19426	NELFE_MOUSE	Negative elongation factor E OS=Mus musculus GN=Nelfe PE=1 SV=2
P63017	HSP7C_MOUSE	Heat shock cognate 71 kDa protein OS=Mus musculus GN=Hspa8 PE=1 SV=1
O08688	CAN5_MOUSE	Calpain-5 OS=Mus musculus GN=Capn5 PE=1 SV=1
Q6PAJ1	BCR_MOUSE	Breakpoint cluster region protein OS=Mus musculus GN=Bcr PE=1 SV=3
Q7TPQ3	SHPRH_MOUSE	E3 ubiquitin-protein ligase SHPRH OS=Mus musculus GN=Shprh PE=1 SV=1
A2AGT5	CKAP5_MOUSE	Cytoskeleton-associated protein 5 OS=Mus musculus GN=Ckap5 PE=1 SV=1
P63017	HSP7C_MOUSE	Heat shock cognate 71 kDa protein OS=Mus musculus GN=Hspa8 PE=1 SV=1
Q61696	HS71A_MOUSE	Heat shock 70 kDa protein 1A OS=Mus musculus GN=Hspa1a PE=1 SV=2
O08688	CAN5_MOUSE	Calpain-5 OS=Mus musculus GN=Capn5 PE=1 SV=1
P10852	4F2_MOUSE	4F2 cell-surface antigen heavy chain OS=Mus musculus GN=Slc3a2 PE=1 SV=1
Q8BG17	NOL12_MOUSE	Nucleolar protein 12 OS=Mus musculus GN=Nol12 PE=1 SV=1
Q9CXP8	GBG10_MOUSE	Guanine nucleotide-binding protein G(I)/G(S)/G(O) subunit gamma-10 OS=Mus musculus GN=Gng10 PE=3 SV=1
P19426	NELFE_MOUSE	Negative elongation factor E OS=Mus musculus GN=Nelfe PE=1 SV=2
P0CG49	UBB_MOUSE	Polyubiquitin-B OS=Mus musculus GN=Ubb PE=2 SV=1

P63017	HSP7C_MOUSE	Heat shock cognate 71 kDa protein OS=Mus musculus GN=Hspa8 PE=1 SV=1
Q8C1C8	PNMA1_MOUSE	Paraneoplastic antigen Ma1 homolog OS=Mus musculus GN=Pnma1 PE=1 SV=2
Q61696	HS71A_MOUSE	Heat shock 70 kDa protein 1A OS=Mus musculus GN=Hspa1a PE=1 SV=2
P63017	HSP7C_MOUSE	Heat shock cognate 71 kDa protein OS=Mus musculus GN=Hspa8 PE=1 SV=1
P0CG49	UBB_MOUSE	Polyubiquitin-B OS=Mus musculus GN=Ubb PE=2 SV=1
P63017	HSP7C_MOUSE	Heat shock cognate 71 kDa protein OS=Mus musculus GN=Hspa8 PE=1 SV=1
Q61696	HS71A_MOUSE	Heat shock 70 kDa protein 1A OS=Mus musculus GN=Hspa1a PE=1 SV=2
Q8C1C8	PNMA1_MOUSE	Paraneoplastic antigen Ma1 homolog OS=Mus musculus GN=Pnma1 PE=1 SV=2
Q07797	LG3BP_MOUSE	Galectin-3-binding protein OS=Mus musculus GN=Lgals3bp PE=1 SV=1
Q9DC53	CPNE8_MOUSE	Copine-8 OS=Mus musculus GN=Cpne8 PE=2 SV=3
P21956	MFGM_MOUSE	Lactadherin OS=Mus musculus GN=Mfge8 PE=1 SV=3
Q61398	PCOC1_MOUSE	Procollagen C-endopeptidase enhancer 1 OS=Mus musculus GN=Pcolce PE=1 SV=2
P16627	HS71L_MOUSE	Heat shock 70 kDa protein 1-like OS=Mus musculus GN=Hspa1l PE=1 SV=4
P63017	HSP7C_MOUSE	Heat shock cognate 71 kDa protein OS=Mus musculus GN=Hspa8 PE=1 SV=1
P58242	ASM3B_MOUSE	Acid sphingomyelinase-like phosphodiesterase 3b OS=Mus musculus GN=Smpdl3b PE=1 SV=1
P52480	KPYM_MOUSE	Pyruvate kinase PKM OS=Mus musculus GN=Pkm PE=1 SV=4
Q9WU78	PDC6I_MOUSE	Programmed cell death 6-interacting protein OS=Mus musculus GN=Pcd6ip PE=1 SV=3
Q8VCI7	SWAP1_MOUSE	ATPase SWSAP1 OS=Mus musculus GN=Swsap1 PE=2 SV=2
Q9D824	FIP1_MOUSE	Pre-mRNA 3'-end-processing factor FIP1 OS=Mus musculus GN=Fip111 PE=1 SV=1
P08553	NFM_MOUSE	Neurofilament medium polypeptide OS=Mus musculus GN=Nefm PE=1 SV=4
Q07797	LG3BP_MOUSE	Galectin-3-binding protein OS=Mus musculus GN=Lgals3bp PE=1 SV=1
Q9DC53	CPNE8_MOUSE	Copine-8 OS=Mus musculus GN=Cpne8 PE=2 SV=3
P63017	HSP7C_MOUSE	Heat shock cognate 71 kDa protein OS=Mus musculus GN=Hspa8 PE=1 SV=1
P16627	HS71L_MOUSE	Heat shock 70 kDa protein 1-like OS=Mus musculus GN=Hspa1l PE=1 SV=4
P52480	KPYM_MOUSE	Pyruvate kinase PKM OS=Mus musculus GN=Pkm PE=1 SV=4
P21956	MFGM_MOUSE	Lactadherin OS=Mus musculus GN=Mfge8 PE=1 SV=3
Q9EQJ9	MAGI3_MOUSE	Membrane-associated guanylate kinase, WW and PDZ domain-containing protein 3 OS=Mus musculus GN=Magi3 PE=1 SV=2
Q61398	PCOC1_MOUSE	Procollagen C-endopeptidase enhancer 1 OS=Mus musculus GN=Pcolce PE=1 SV=2
P58242	ASM3B_MOUSE	Acid sphingomyelinase-like phosphodiesterase 3b OS=Mus musculus GN=Smpdl3b PE=1 SV=1
Q9DC53	CPNE8_MOUSE	Copine-8 OS=Mus musculus GN=Cpne8 PE=2 SV=3
P21956	MFGM_MOUSE	Lactadherin OS=Mus musculus GN=Mfge8 PE=1 SV=3

Q07797	LG3BP_MOUSE	Galectin-3-binding protein OS=Mus musculus GN=Lgals3bp PE=1 SV=1
P16627	HS71L_MOUSE	Heat shock 70 kDa protein 1-like OS=Mus musculus GN=Hspa1l PE=1 SV=4
P63017	HSP7C_MOUSE	Heat shock cognate 71 kDa protein OS=Mus musculus GN=Hspa8 PE=1 SV=1
P58242	ASM3B_MOUSE	Acid sphingomyelinase-like phosphodiesterase 3b OS=Mus musculus GN=Smpdl3b PE=1 SV=1
P52480	KPYM_MOUSE	Pyruvate kinase PKM OS=Mus musculus GN=Pkm PE=1 SV=4
P68368	TBA4A_MOUSE	Tubulin alpha-4A chain OS=Mus musculus GN=Tuba4a PE=1 SV=1
Q61398	PCOC1_MOUSE	Procollagen C-endopeptidase enhancer 1 OS=Mus musculus GN=Pcolce PE=1 SV=2
P0C7N9	PSMG4_MOUSE	Proteasome assembly chaperone 4 OS=Mus musculus GN=Psmg4 PE=1 SV=1
Q8R3G9	TSN8_MOUSE	Tetraspanin-8 OS=Mus musculus GN=Tspan8 PE=1 SV=1
Q99JR5	TINAL_MOUSE	Tubulointerstitial nephritis antigen-like OS=Mus musculus GN=Tinag1 PE=1 SV=1
O70475	UGDH_MOUSE	UDP-glucose 6-dehydrogenase OS=Mus musculus GN=Ugdh PE=1 SV=1
P68368	TBA4A_MOUSE	Tubulin alpha-4A chain OS=Mus musculus GN=Tuba4a PE=1 SV=1
P63017	HSP7C_MOUSE	Heat shock cognate 71 kDa protein OS=Mus musculus GN=Hspa8 PE=1 SV=1
P68372	TBB4B_MOUSE	Tubulin beta-4B chain OS=Mus musculus GN=Tubb4b PE=1 SV=1
O08688	CAN5_MOUSE	Calpain-5 OS=Mus musculus GN=Capn5 PE=1 SV=1
Q3TTY5	K22E_MOUSE	Keratin, type II cytoskeletal 2 epidermal OS=Mus musculus GN=Krt2 PE=1 SV=1
Q99JR5	TINAL_MOUSE	Tubulointerstitial nephritis antigen-like OS=Mus musculus GN=Tinag1 PE=1 SV=1
Q3TZ89	SC31B_MOUSE	Protein transport protein Sec31B OS=Mus musculus GN=Sec31b PE=1 SV=2
O70475	UGDH_MOUSE	UDP-glucose 6-dehydrogenase OS=Mus musculus GN=Ugdh PE=1 SV=1
Q9CS72	FLIP1_MOUSE	Filamin-A-interacting protein 1 OS=Mus musculus GN=Filip1 PE=1 SV=2
Q9DCV7	K2C7_MOUSE	Keratin, type II cytoskeletal 7 OS=Mus musculus GN=Krt7 PE=1 SV=1
P04104	K2C1_MOUSE	Keratin, type II cytoskeletal 1 OS=Mus musculus GN=Krt1 PE=1 SV=4
P68368	TBA4A_MOUSE	Tubulin alpha-4A chain OS=Mus musculus GN=Tuba4a PE=1 SV=1
Q61398	PCOC1_MOUSE	Procollagen C-endopeptidase enhancer 1 OS=Mus musculus GN=Pcolce PE=1 SV=2
P0C7N9	PSMG4_MOUSE	Proteasome assembly chaperone 4 OS=Mus musculus GN=Psmg4 PE=1 SV=1
P17182	ENOA_MOUSE	Alpha-enolase OS=Mus musculus GN=Eno1 PE=1 SV=3
A2AQ07	TBB1_MOUSE	Tubulin beta-1 chain OS=Mus musculus GN=Tubb1 PE=1 SV=1
P21956	MFGM_MOUSE	Lactadherin OS=Mus musculus GN=Mfge8 PE=1 SV=3
Q99JY9	ARP3_MOUSE	Actin-related protein 3 OS=Mus musculus GN=Actr3 PE=1 SV=3
Q9D8E6	RL4_MOUSE	60S ribosomal protein L4 OS=Mus musculus GN=Rpl4 PE=1 SV=3
P63005	LIS1_MOUSE	Platelet-activating factor acetylhydrolase IB subunit alpha OS=Mus musculus GN=Pafah1b1 PE=1 SV=2
P97298	PEDF_MOUSE	Pigment epithelium-derived factor OS=Mus musculus GN=Serpinf1 PE=1 SV=2
A2AQ07	TBB1_MOUSE	Tubulin beta-1 chain OS=Mus musculus GN=Tubb1 PE=1 SV=1
P17182	ENOA_MOUSE	Alpha-enolase OS=Mus musculus GN=Eno1 PE=1 SV=3

P21956	MFGM_MOUSE	Lactadherin OS=Mus musculus GN=Mfge8 PE=1 SV=3
Q9D8E6	RL4_MOUSE	60S ribosomal protein L4 OS=Mus musculus GN=Rpl4 PE=1 SV=3
P63005	LIS1_MOUSE	Platelet-activating factor acetylhydrolase IB subunit alpha OS=Mus musculus GN=Pafah1b1 PE=1 SV=2
P63260	ACTG_MOUSE	Actin, cytoplasmic 2 OS=Mus musculus GN=Actg1 PE=1 SV=1
Q8BFZ3	ACTBL_MOUSE	Beta-actin-like protein 2 OS=Mus musculus GN=Actbl2 PE=1 SV=1
P63260	ACTG_MOUSE	Actin, cytoplasmic 2 OS=Mus musculus GN=Actg1 PE=1 SV=1
Q8BFZ3	ACTBL_MOUSE	Beta-actin-like protein 2 OS=Mus musculus GN=Actbl2 PE=1 SV=1
P07356	ANXA2_MOUSE	Annexin A2 OS=Mus musculus GN=Anxa2 PE=1 SV=2
O35639	ANXA3_MOUSE	Annexin A3 OS=Mus musculus GN=Anxa3 PE=1 SV=4
P16858	G3P_MOUSE	Glyceraldehyde-3-phosphate dehydrogenase OS=Mus musculus GN=Gapdh PE=1 SV=2
Q9D8B3	CHM4B_MOUSE	Charged multivesicular body protein 4b OS=Mus musculus GN=Chmp4b PE=1 SV=2
P07356	ANXA2_MOUSE	Annexin A2 OS=Mus musculus GN=Anxa2 PE=1 SV=2
O35639	ANXA3_MOUSE	Annexin A3 OS=Mus musculus GN=Anxa3 PE=1 SV=4
Q9D8B3	CHM4B_MOUSE	Charged multivesicular body protein 4b OS=Mus musculus GN=Chmp4b PE=1 SV=2
P97429	ANXA4_MOUSE	Annexin A4 OS=Mus musculus GN=Anxa4 PE=1 SV=4
Q9R0P3	ESTD_MOUSE	S-formylglutathione hydrolase OS=Mus musculus GN=Esd PE=1 SV=1
P19221	THRB_MOUSE	Prothrombin OS=Mus musculus GN=F2 PE=1 SV=1
P40240	CD9_MOUSE	CD9 antigen OS=Mus musculus GN=Cd9 PE=1 SV=2
P97429	ANXA4_MOUSE	Annexin A4 OS=Mus musculus GN=Anxa4 PE=1 SV=4
Q9R0P3	ESTD_MOUSE	S-formylglutathione hydrolase OS=Mus musculus GN=Esd PE=1 SV=1
P40240	CD9_MOUSE	CD9 antigen OS=Mus musculus GN=Cd9 PE=1 SV=2
P10107	ANXA1_MOUSE	Annexin A1 OS=Mus musculus GN=Anxa1 PE=1 SV=2
P12970	RL7A_MOUSE	60S ribosomal protein L7a OS=Mus musculus GN=Rpl7a PE=1 SV=2
P62754	RS6_MOUSE	40S ribosomal protein S6 OS=Mus musculus GN=Rps6 PE=1 SV=1
P14148	RL7_MOUSE	60S ribosomal protein L7 OS=Mus musculus GN=Rpl7 PE=1 SV=2
Q9CQL5	RM18_MOUSE	39S ribosomal protein L18, mitochondrial OS=Mus musculus GN=Mrpl18 PE=1 SV=1
P10107	ANXA1_MOUSE	Annexin A1 OS=Mus musculus GN=Anxa1 PE=1 SV=2
P12970	RL7A_MOUSE	60S ribosomal protein L7a OS=Mus musculus GN=Rpl7a PE=1 SV=2
P62754	RS6_MOUSE	40S ribosomal protein S6 OS=Mus musculus GN=Rps6 PE=1 SV=1
P14148	RL7_MOUSE	60S ribosomal protein L7 OS=Mus musculus GN=Rpl7 PE=1 SV=2
Q9R0P3	ESTD_MOUSE	S-formylglutathione hydrolase OS=Mus musculus GN=Esd PE=1 SV=1
P62242	RS8_MOUSE	40S ribosomal protein S8 OS=Mus musculus GN=Rps8 PE=1 SV=2
P63101	1433Z_MOUSE	14-3-3 protein zeta/delta OS=Mus musculus GN=Ywhaz PE=1 SV=1
Q9DBJ1	PGAM1_MOUSE	Phosphoglycerate mutase 1 OS=Mus musculus GN=Pgam1 PE=1 SV=3
P01942	HBA_MOUSE	Hemoglobin subunit alpha OS=Mus musculus GN=Hba PE=1 SV=2
P68510	1433F_MOUSE	14-3-3 protein eta OS=Mus musculus GN=Ywhah PE=1 SV=2
P63101	1433Z_MOUSE	14-3-3 protein zeta/delta OS=Mus musculus GN=Ywhaz PE=1 SV=1
P62242	RS8_MOUSE	40S ribosomal protein S8 OS=Mus musculus GN=Rps8 PE=1 SV=2
P01942	HBA_MOUSE	Hemoglobin subunit alpha OS=Mus musculus GN=Hba PE=1 SV=2
P68510	1433F_MOUSE	14-3-3 protein eta OS=Mus musculus GN=Ywhah PE=1 SV=2

P17751	TPIS_MOUSE	Triosephosphate isomerase OS=Mus musculus GN=Tpi1 PE=1 SV=4
Q8R3G9	TSN8_MOUSE	Tetraspanin-8 OS=Mus musculus GN=Tspan8 PE=1 SV=1
P01942	HBA_MOUSE	Hemoglobin subunit alpha OS=Mus musculus GN=Hba PE=1 SV=2
P17751	TPIS_MOUSE	Triosephosphate isomerase OS=Mus musculus GN=Tpi1 PE=1 SV=4
P01942	HBA_MOUSE	Hemoglobin subunit alpha OS=Mus musculus GN=Hba PE=1 SV=2
Q8R3G9	TSN8_MOUSE	Tetraspanin-8 OS=Mus musculus GN=Tspan8 PE=1 SV=1
Q91V41	RAB14_MOUSE	Ras-related protein Rab-14 OS=Mus musculus GN=Rab14 PE=1 SV=3
P62821	RAB1A_MOUSE	Ras-related protein Rab-1A OS=Mus musculus GN=Rab1A PE=1 SV=3
P51150	RAB7A_MOUSE	Ras-related protein Rab-7a OS=Mus musculus GN=Rab7a PE=1 SV=2
P29391	FRIL1_MOUSE	Ferritin light chain 1 OS=Mus musculus GN=Ftl1 PE=1 SV=2
O08992	SDCB1_MOUSE	Syntenin-1 OS=Mus musculus GN=Sdcbp PE=1 SV=1
Q91V41	RAB14_MOUSE	Ras-related protein Rab-14 OS=Mus musculus GN=Rab14 PE=1 SV=3
P51150	RAB7A_MOUSE	Ras-related protein Rab-7a OS=Mus musculus GN=Rab7a PE=1 SV=2
P62821	RAB1A_MOUSE	Ras-related protein Rab-1A OS=Mus musculus GN=Rab1A PE=1 SV=3
O08992	SDCB1_MOUSE	Syntenin-1 OS=Mus musculus GN=Sdcbp PE=1 SV=1
P29391	FRIL1_MOUSE	Ferritin light chain 1 OS=Mus musculus GN=Ftl1 PE=1 SV=2
Q99JI6	RAP1B_MOUSE	Ras-related protein Rap-1b OS=Mus musculus GN=Rap1b PE=1 SV=2
P35762	CD81_MOUSE	CD81 antigen OS=Mus musculus GN=Cd81 PE=1 SV=2
P29391	FRIL1_MOUSE	Ferritin light chain 1 OS=Mus musculus GN=Ftl1 PE=1 SV=2
Q9WVA4	TAGL2_MOUSE	Transgelin-2 OS=Mus musculus GN=Tagln2 PE=1 SV=4
Q3V3K7	GCNT7_MOUSE	Beta-1,3-galactosyl-O-glycosyl-glycoprotein beta-1,6-N-acetylglucosaminyltransferase 7 OS=Mus musculus GN=Gcnt7 PE=2 SV=1
Q8BM54	MYLIP_MOUSE	E3 ubiquitin-protein ligase MYLIP OS=Mus musculus GN=Mylip PE=1 SV=1
P29391	FRIL1_MOUSE	Ferritin light chain 1 OS=Mus musculus GN=Ftl1 PE=1 SV=2
Q9WVA4	TAGL2_MOUSE	Transgelin-2 OS=Mus musculus GN=Tagln2 PE=1 SV=4
P35762	CD81_MOUSE	CD81 antigen OS=Mus musculus GN=Cd81 PE=1 SV=2
Q3V3K7	GCNT7_MOUSE	Beta-1,3-galactosyl-O-glycosyl-glycoprotein beta-1,6-N-acetylglucosaminyltransferase 7 OS=Mus musculus GN=Gcnt7 PE=2 SV=1
Q62132	PTPRR_MOUSE	Receptor-type tyrosine-protein phosphatase R OS=Mus musculus GN=Ptprr PE=1 SV=1
B2RY56	RBM25_MOUSE	RNA-binding protein 25 OS=Mus musculus GN=Rbm25 PE=1 SV=2
Q91Y11	PCDA9_MOUSE	Protocadherin alpha-9 OS=Mus musculus GN=Pcdha9 PE=2 SV=1
E9Q784	ZC3HD_MOUSE	Zinc finger CCCH domain-containing protein 13 OS=Mus musculus GN=Zc3h13 PE=1 SV=1

Discussion

Pancreatic cancer is the fourth leading cause of cancer death in the USA, with a 5-year survival rate of 6%. Pancreatic ductal adenocarcinoma (PDAC) is the most common pancreatic cancer type (90% of cases) and the most malignant. In the majority of PDAC patients, symptoms do not manifest at the early stages of the disease and diagnosis occurs when the tumor is locally advanced or metastatic, with liver, lungs and peritoneum as most common metastatic sites. Therefore, surgery, that constitutes the most successful treatment for resectable tumors, is possible in only 15% of patients, who manifest the disease at early stages. In the other cases, systemic therapy based on the use of chemotherapeutic agents represents the most efficient option with the aim to prevent disease progression and prolong life (Distler et al. 2014). However, PDAC displays a high resistance to conventional therapies, thereby leading to the study of new therapeutic strategies able to overcome these limits. Consequently, there is an urgent need to identify molecular markers used in the diagnosis and therapeutic monitoring of this tumour.

Extracellular vesicles (EVs) play a critical role in the intercellular communication and can induce modifications in target cells. EVs ability to transfer molecular information through cells is supported by the molecules that they carry that include proteins, mRNA, miRNA and lipids (Lobb et al. 2015). Among EVs, exosomes (30-150nm) are membrane vesicles deriving from late endosome; their size is around 30-150nm and they can be detected in biological fluids and secretions. Exosomes are now emerging as key players involved in several pathological processes, including cancer. As a matter of fact, their content can be crucial for the interaction with other cells in the tumour microenvironment, and tumour-derived exosomes can interact with extracellular matrix inducing a

remodeling that promotes cancer progression. Furthermore, exosomes have shown to be implicated in the metastatic process and in particular in the formation of pre-metastatic niches, that prepare future metastatic sites for the arrival and survival of tumour cells (Taverna et al. 2012; Costa-Silva et al. 2015). The aim of our study was to investigate and characterize exosomes released by different pancreatic cancer cell types, focusing on a detailed proteomic analysis of their content. Indeed, exosomes have shown to contain proteins that can be responsible of their activity and their pro-tumoral function.

Initially, EVs were isolated from the supernatant of PDAC, PANC2, KPC (mouse) and PANC1, miaPACA2 (human) pancreatic cancer cell lines, using a protocol of differential centrifugation. Once EVs were obtained, the product was analyzed by TEM and DLS, demonstrating the presence of exosomes (50-150nm) in our preparation.

In a second moment, since exosomes play a role in the intercellular communication, we decided to evaluate the internalization of PDAC exosomes in HUVECs. Results obtained by FACS and confocal analysis reported that exosomes are internalized in a time-dependent manner, starting from 30 min and achieving a maximal internalization at 2 h. These findings are particularly relevant in order to facilitate future studies on exosomal influence on endothelial mediated tumour processes, such as cell migration and angiogenesis.

Concerning the evaluation of exosomal protein contents, a proteomic-LC/MS analysis of all obtained exosomes was carried out. Therefore, a list of revealed proteins for exosomes isolated from each pancreatic cancer cell line was obtained. We grouped common proteins among different examined exosomes for each cell line and we analyzed them with bioinformatic softwares. Some

detected proteins revealed to be common exosomal markers, such as Tetraspanin-8, Heat shock cognate 71 kDa protein and Tubulin beta-1 chain. Moreover, proteins common to exosomes from different cell types were figured out, and lactadherin, which is involved in the process of neo-angiogenesis, was detected among PDAC and PANC2 exosomes, indicating a potential exosomal involvement in this process.

Afterwards, a similar proteomic-LC/MS analysis was performed on the exosomal content derived from plasma of PDAC mice and their healthy counterpart. Among them, 107 common proteins were identified but their quantity reported to be different in the two examined groups. In particular, proteins with higher differences between the groups showed to be involved in processes such as negative regulation of protein metabolic process, acute-phase response and regulation of blood coagulation. Furthermore, the detection of proteins common to exosomes derived from a pancreatic cancer cell line and its respective mouse model may result important for identifying possible biomarkers for a specific pancreatic cancer type. Thereby, this assessment started from comparing the protein content of exosomes derived from PDAC cell line and PDAC mice plasma, and it is now proceeding also for other studied models. In conclusion, data obtained from this preliminary study allowed to determine the proteomic profile of exosomes from different pancreatic cancer cell lines, giving information about more represented proteins. Moreover, the *in vivo* study was useful to point out quantitative differences in exosomal proteins of PDAC mice with respect to healthy mice, and to compare the protein content of both exosomes derived from a cell line and the respective mouse model. This evaluation may lead to the discovery of new potential biomarkers that can be isolated and studied for their role in pancreatic cancer progression.

Osteopontin as tumor biomarker

General features

Osteopontin (OPN) is an extracellular matrix protein involved in multiple physiological and pathological processes (Castello et al. 2017; Vaschetto et al. 2008; Clemente et al. 2016). In particular, OPN plays a key role in cancer progression by enhancing proliferation, survival, motility, and invasion of tumor cells in breast cancer, hepatic carcinoma, prostate cancer, colorectal cancer, lung cancer and melanoma (Cook et al. 2005; Bandopadhyay et al. 2014; Irby, McCarthy, and Yeatman 2004; Zhou et al. 2005; Chambers, Groom, and MacDonald 2002; Thalmann et al. 1999; Gotoh et al. 2002). Overexpression of OPN has been detected at the tumor sites and in the blood of patients, and its levels correlate with tumor stage and aggressiveness, suggesting that OPN can be a diagnostic and prognostic biomarker for several cancers (Irby, McCarthy, and Yeatman 2004).

OPN is expressed by many cell types such as bone cells (e.g., osteoblasts, osteoclasts, and osteocytes), immune cells (e.g., T cells, B cells, natural killer cells, and macrophages), neural cells, epithelial cells, fibroblasts, smooth muscle cells, and endothelial cells (Murry et al. 1994; Kunii et al. 2009; Kruger et al. 2014) and in several tumor-derived cell lines. It is distributed in a variety of tissues and secreted in body fluids including blood, urine, bile, and milk. OPN consists of 314 amino acid residues, which confer a predicted molecular weight of 35 kDa. However, because of splicing and post-translational modifications (PTMs), such as phosphorylation, glycosylation, and protein cleavage mediated by thrombin and other proteases, the actual molecular weight ranges from 41 to 75kDa (Christensen, Petersen, and Sørensen 2008). The protein exists in a

myriad of different soluble isoforms due to alternative splicing and a large number of PTMs. The expression patterns and functions of OPN-splicing isoforms appear to be tumour-specific and clinically relevant in some cases.

OPN mediates several biological functions such as bone remodeling, macrophage response, cell migration and adhesion, and it is involved in the pathogenesis of several diseases including atherosclerosis, cancer, chronic inflammatory diseases, and several autoimmune diseases (Grassinger et al. 2009; Cho, Cho, and Kim 2009; Liu et al. 2014; A. Brown 2012). OPN is a member of the SIBLING (Small Integrin Binding Ligand N-linked Glycoprotein) protein family. It has two calcium binding sites, two heparin binding domains, and multiple adhesion motifs which allow interaction with several receptors and cell types (Kon et al. 2002). OPN has RGD (arginine-glycine-aspartate) integrin binding domain, through which it mediates interactions with several integrins (Liaw et al. 1998; Hu et al. 1995; Yokosaki et al. 1995). $\alpha 9\beta 1$, $\alpha 4\beta 1$, and $\alpha 4\beta 7$ integrins bind to a cryptic SVVYGLR sequence which is exposed upon thrombin cleavage occurring at the Arg168-Ser169 site near to the RGD motif (Yokosaki et al. 1995; P. M. Green et al. 2001; Ito, Obata, and Saito 2009). This cleavage generates two fragments, the N- and C-terminal, displaying functional differences from the full length protein (Morimoto et al. 2010). The N-terminal fragment (OPN-N, approx. 35kDa) binds to integrins through the RGD or the cryptic binding site, promotes IFN- γ secretion in T cells, and stimulates cell migration by binding to $\alpha 9\beta 1$ and $\alpha 4\beta 1$ integrins (Grassinger et al. 2009; Yokosaki and Sheppard 2000). The C-terminal fragment (OPN-C, approx. 25 kDa) inhibits IL-10 secretion and stimulates cell-cell adhesion by interacting with CD44 isoforms containing the v6 and v7 domains (Desai, Rogers, and Chellaiah 2007; Iczkowski 2010).

Besides its secreted form, OPN can be found in its intracellular form (iOPN), which is a truncated version of the full-length protein lacking the signal sequence due to initiation of translation from a downstream noncanonical start codon (Shinohara, Kim, Kim, et al. 2008). The biological functions of iOPN are related mainly to the regulation of cytoskeletal rearrangement and signal transduction pathways [50]. iOPN was found in dendritic cells (Shinohara, Kim, Kim, et al. 2008; Inoue and Shinohara 2011; Zhu et al. 2004; Shinohara et al. 2006), macrophages (Zhu et al. 2004), and nervous cells (Wung et al. 2007). Indeed, iOPN localizes to the nucleus of cells where it mediates cell duplication through association with polo-like kinase 1, whereas in fibroblasts, iOPN plays a role in cell migration (Zohar et al. 2000).

Role in inflammation

Among the many functions of OPN, it can act as pro-inflammatory cytokine in the progression of several inflammatory and immunitary processes. The main role of OPN during inflammation is to trigger different leucocytes eliciting a functional response and inducing cytokine secretion, in order to shape the entire immune response. As an integrin-binding protein, OPN not only stimulates migration, accumulation, and retention of macrophages at sites of injury but can also modulate their cytokine production by promoting Th1 cell-mediated immunity and stimulating their differentiation from monocytes. OPN also controls several immune cells functions including monocyte adhesion, migration, differentiation, and phagocytosis (Liaw et al. 1998). Nevertheless, OPN is also able to enhance Th1 and Th17 differentiation and inhibit Th2 cytokine expression. By interacting with CD44 in Th cells, OPN induces the production of IFN- γ and IL-17A (Desai, Rogers, and Chellaiah 2007). Finally, OPN

even acts on neutrophil recruitment but has no influence on their phagocytic activity and superoxide, cytokine, and MMP-9 production (Iczkowski 2010).

Role in angiogenesis

OPN is highly expressed in several tumors, where it can be cleaved by thrombin and can act as a proangiogenic factor. Proliferation, migration, and tissue infiltration of pericytes, vascular smooth muscle, and endothelial cells from preexisting blood vessels are needed for tumor angiogenesis, and OPN may participate in all these processes (Lu et al. 2007; Castello et al. 2017). The role of OPN in tumor angiogenesis is associated with VEGF- α as both are frequently and simultaneously upregulated during angiogenesis (Takahashi et al. 2002). In the preclinical model, OPN stimulates angiogenesis by inducing VEGF- α expression in endothelial cells (Dai et al. 2009). OPN itself can be upregulated by fibroblast growth factor- (FGF-) 2 in endothelial cells *in vitro* and *in vivo*, leading to the recruitment of proangiogenic monocytes to the tumor microenvironment (Leali et al. 2003). OPN-N and OPN-C have shown to display a stronger angiogenic potential *in vitro*, compared to full-length OPN. These results are in line with the reports from Senger et al. (Senger et al. 2002) showing that VEGF- α induces OPN and $\alpha v\beta 3$ expression in endothelial cells and stimulates cleavage of OPN by thrombin and that the resulting OPN fragments are strongly chemotactic for endothelial cells promoting angiogenesis (Orimo and Weinberg 2006). However, these authors used a mixture of the two OPN fragments obtained by thrombin-mediated cleavage of OPN-full length (OPN-FL) *in vitro*. Therefore, they could not distinguish the specific contributions of OPN-N versus OPN-C. Moreover, other studies have shown that, in vascular endothelial cells, OPN enhances VEGF- α expression, which, in turn, mediates a

positive feedback on OPN expression; the blocking of this feedback signal by anti-VEGF- α antibodies partially inhibited OPN-induced HUVECs motility, proliferation, and tube formation (Dai et al. 2009).

New insights on OPN activity

Thrombin cleavage of OPN in multiple sclerosis

Before investigating OPN involvement in cancer, we decided to investigate the role played by OPN-C and OPN-N on human cells, with a particular focus on multiple sclerosis (MS) processes, where the inflammatory background allowed us to investigate the specific role played by the two OPN forms generated by thrombin cleavage during inflammation.

Indeed, several studies reported that the two fragments deriving from thrombin cleavage may play different functions in the development of autoimmune diseases. For example, full length OPN (OPN-FL) is expressed at similar levels in the synovial fluid of patients with rheumatoid arthritis (RA) and in those with osteoarthritis, but OPN-N levels in RA synovial fluid samples are around 30-fold higher than in those from osteoarthritis and correlate with the disease status (Hasegawa et al. 2011).

A considerable body of evidence suggests that OPN exerts an important function in MS and its animal model, experimental autoimmune encephalomyelitis (EAE) (Chiocchetti et al. 2005; Comi et al. 2012; Chabas et al. 2001). In MS lesions, high OPN levels are present in the perivascular cuff that surrounds inflamed blood vessels, contains inflammatory lymphocytes and is delimited by the endothelium and the basement membrane. Studies in MS tissue and in models of relapsing-remitting (RR) and progressive EAE showed that OPN might have a role in the progression from RR disease to the more chronic form (Chabas et al. 2001). As reported before, OPN serves as a ligand for CD44 and various integrin (Ashkar et al. 2000), including $\alpha 4\beta 1$ integrin. These

adhesion molecules are crucial in modulating disease in mice with EAE, and $\alpha 4\beta 1$ integrin is the main adhesion molecule involved in MS relapse (Yednock et al. 1992; Brocke et al. 1999; Steinman 2005; Polman et al. 2006; Rudick et al. 2006; Hur et al. 2007; Stromnes and Goverman 2007; Vogt et al. 2003).

OPN plays a role in lymphocyte recruitment into the MS lesion, which involves $\alpha 4\beta 1$ integrin that is the target of the anti-MS drug natalizumab, a humanized monoclonal antibody that has had beneficial effects for relapses prevention in RR-MS (Steinman 2005). In fact, after discovering the importance of $\alpha 4\beta 1$ integrin in lymphocyte homing to the inflamed brain, investigators searched for its binding partners. The first binding partner discovered for $\alpha 4\beta 1$ integrin was vascular cell adhesion molecule 1 (VCAM1) (Cannella and Raine 1995), and the second binding partner was OPN. In a model of RR-EAE induced by peptide 139–151 from proteolipid protein (PIP_{139–151}) in Sjl/j mice, administration of recombinant OPN after the first remission induced a rapid relapse and increased neurological defects. In this model there were indications that animals receiving a control injection of saline went into remission after relapse, but mice treated with recombinant OPN developed a more progressive disease and never returned to a state of remission. This suggested that OPN could be crucial during the transition from RR disease to secondary progressive disease (Hur et al. 2007).

OPN binds to $\alpha 4\beta 1$ integrin only upon cleavage by thrombin which unmasks two $\alpha 4\beta 1$ integrin binding sites located into the N-terminal fragment. Recent studies showed that the administration of recombinant OPN-FL exacerbates EAE, but the relative role of OPN-N and OPN-C is not known (Hur et al. 2007). However, thrombin-mediated cleavage may play a role, since thrombin activity increases with the progression of neuroinflammation, and is detectable in the

demyelinating lesions where also OPN is present at high levels (Beilin et al. 2005; Davalos et al. 2012).

Administration of OPN to mice with established EAE quickly triggers neurological relapse by two mechanisms. First, OPN stimulates the expression of pro-inflammatory mediators, including T helper 1 (Th1)- and 17 (Th17)-type cytokines (Chabas et al. 2001; Jansson et al. 2002) in myelin-specific T cells, the expression of which is regulated by nuclear factor- κ B (NF- κ B) (Shinohara et al. 2008; Murugaiyan, Mittal, and Weiner 2008). Simultaneously, OPN inhibits forkhead box O3A (FOxO3A)-dependent apoptosis of autoreactive immune cells (Hur et al. 2007). The transcription factors FOxO3A and NF- κ B have inverse effects on the apoptotic death of activated T cells and, as expected, OPN displays reciprocal effects on these opposing transcription factors. The sum of effects on these key factors after OPN-mediated signaling promotes the survival of autoreactive T cells. In a detailed series of experiments, we showed that following stimulation with OPN, phosphorylated FOxO3A was excluded from the nucleus and was inactivated. When FOxO3A translocated to the nucleus, it promoted apoptosis, whereas its exclusion from the nucleus led to cell survival. By contrast, OPN increased the degradation of I κ B α (an inhibitor of NF- κ B α -subunit; also known as NF- κ BIA), thereby triggering the transcriptional activation and nuclear translocation of NF- κ B. Furthermore, OPN activated I κ B kinase- β (IKK β), which leads to increased nuclear translocation of NF- κ B. OPN therefore cooperatively regulated the function of both FOxO3A and NF- κ B, thus controlling the death and survival of activated T cells (Hur et al. 2007). The fact that OPN not only increases the production of Th1- (Chabas et al. 2001; Jansson et al. 2002) and Th17-type cytokines, but also increases the survival of activated Th1 cells and Th17 cells, drives the relapses that follow the administration of

recombinant OPN.

It has been demonstrated that patients with RRMS display high levels of anti-OPN autoAbs and these levels are more elevated in remission than in relapse phase. Indeed, vaccination with OPN before developing EAE, induces production of anti-OPN autoAbs, ameliorating the course of the disease. Concerning MS, anti-OPN autoAbs levels were evaluated in a cohort of RR patients (Leone et al. 2008; Clemente et al. 2017). The anti-OPN autoAbs presence marks the inflammatory phase of MS. In fact, these Abs levels were inversely correlated with disease duration and higher during remission, since they are increased by the OPN peak that occurs during relapse. Intriguingly, the anti-OPN response recognized OPN-C better than OPN-N in all patients, which may mark both quantitative and qualitative differences of the auto-Abs produced against the two fragments. The focus on OPN-C was further noted by EAE-experiments because vaccination with OPN-C resulted in the greatest induction of anti-OPN autoAbs, ameliorating disease progression, particularly in terms of inducing disease remission and decreasing the autoantigen-driven production of IFN- γ and IL-17 (Clemente et al. 2017). These data suggest that production of anti-OPN autoAbs may favor remission in both MS and EAE. Discriminating the role of each fragment in MS and EAE is crucial for developing a specific therapy directed against the most pathogenic fragment, preserving the physiological activity of the others.

PAPER 1

Background: In MS, OPN plays a pathogenetic role by recruiting autoreactive T cells into the central nervous system. During inflammation, OPN is cleaved by thrombin in an N-terminal (OPN-N) and a C-terminal (OPN-C) fragment. The OPN cleavage unmasks a cryptic domain of interaction with $\alpha 4\beta 1$ integrin that is the main adhesion molecule involved in lymphocyte transmigration to the brain and is the target for natalizumab, the most potent drug preventing relapses observed during the disease course.

Aim: The aim of this work was to investigate the involvement of the two fragments in the disease. **Methods:** OPN-N and OPN-C were produced in an eukaryotic system and their effect was evaluated *in vitro* on human peripheral blood mononuclear cells (PBMCs) by studying cell migration, adhesion, angiogenesis and cytokine production, and *in vivo* on experimental autoimmune encephalomyelitis (EAE), the MS animal model.

Results: *In vitro* obtained results show that OPN-N up-regulates the secretion of IL-17 (70% positive cells), that is involved in breaking the blood brain barrier, and cell migration (65%), whereas OPN-C is able to increase cell adhesion (70%), thus suggesting a role of the two fragments in the homing of autoreactive lymphocytes in the central nervous system lesions. On the other hand, they play a role in local inflammation, since OPN-N induces secretion of IL-6 in monocytes (75% positive cells), OPN-C inhibits production of IL-10 (14% positive cells), and both increase secretion of IFN- γ . These effects are exerted at higher levels by the appropriate OPN fragment than by OPN-FL, and it suggests that thrombin-mediated cleavage plays a key role in OPN activity. Moreover, OPN-N and OPN-C were much more active than OPN-FL in inducing tubulogenesis (70% vs 30%).

The *in vivo* experiments showed that OPN-FL was much more effective in inducing EAE relapses than OPN-FL_{mut}, which is resistant to thrombin cleavage. Therefore, the effect of OPN-FL must be ascribed to fragments produced by thrombin cleavage *in vivo*. Results obtained after administration of the recombinant OPN-C and OPN-N revealed that OPN-C was more responsible of this induction, while OPN-N displayed only a weak effect.

Conclusion: These findings suggest that drugs targeting each fragment may be used to fine tune pathological effects of OPN in MS.

Research Article

Thrombin Cleavage of Osteopontin Modulates Its Activities in Human Cells *In Vitro* and Mouse Experimental Autoimmune Encephalomyelitis *In Vivo*

Elena Boggio,¹ Chiara Dianzani,² Casimiro Luca Gigliotti,¹ Maria Felicia Soluri,¹ Nausicaa Clemente,¹ Giuseppe Cappellano,³ Erika Toth,¹ Davide Raineri,¹ Benedetta Ferrara,² Cristoforo Comi,⁴ Umberto Dianzani,¹ and Annalisa Chiocchetti¹

¹Department of Health Sciences and Interdisciplinary Research Center of Autoimmune Diseases (IRCAD), "A. Avogadro" University of Piemonte Orientale (UPO), 28100 Novara, Italy

²Department of Drug Science and Technology, University of Torino, 10125 Torino, Italy

³Biocenter, Division for Experimental Pathophysiology and Immunology, Laboratory of Autoimmunity, Medical University of Innsbruck, 6020 Innsbruck, Austria

⁴Department of Translational Medicine, Neurology Unit, "A. Avogadro" UPO, 28100 Novara, Italy

Correspondence should be addressed to Umberto Dianzani; umberto.dianzani@med.uniupo.it

Received 20 May 2016; Accepted 8 June 2016

Academic Editor: Yao Yao

Copyright © 2016 Elena Boggio et al. This is an open access article distributed under the Creative Commons Attribution License, which permits unrestricted use, distribution, and reproduction in any medium, provided the original work is properly cited.

Osteopontin is a proinflammatory cytokine and plays a pathogenetic role in multiple sclerosis and its animal model, experimental autoimmune encephalomyelitis (EAE), by recruiting autoreactive T cells into the central nervous system. Osteopontin functions are modulated by thrombin cleavage generating N- and C-terminal fragment, whose individual roles are only partly known. Published data are difficult to compare since they have been obtained with heterogeneous approaches. Interestingly, thrombin cleavage of osteopontin unmasks a cryptic domain of interaction with $\alpha_4\beta_1$ integrin that is the main adhesion molecule involved in lymphocyte transmigration to the brain and is the target for natalizumab, the most potent drug preventing relapses. We produced recombinant osteopontin and its N- and C-terminal fragments in an eukaryotic system in order to allow their posttranslational modifications. We investigated, *in vitro*, their effect on human cells and *in vivo* in EAE. We found that the osteopontin cleavage plays a key role in the function of this cytokine and that the two fragments exert distinct effects both *in vitro* and *in vivo*. These findings suggest that drugs targeting each fragment may be used to fine-tune the pathological effects of osteopontin in several diseases.

1. Introduction

Osteopontin (OPN) is a matricellular protein originally isolated from the bone, expressed by various cell types including macrophages, dendritic cells, and activated T cells. OPN mediates several biological functions such as bone remodeling, macrophage response, cell migration, and adhesion, and it is involved in the pathogenesis of several diseases including atherosclerosis, cancer, chronic inflammatory diseases, and several autoimmune diseases [1–3]. OPN costimulates T cell activation and supports differentiation of proinflammatory T helper 1 (Th1) and Th17 cells [4, 5].

OPN is a member of the SIBLING (Small Integrin Binding Ligand N-linked Glycoprotein) protein family. It has two calcium binding sites, two putative heparin binding domains, and multiple adhesion motifs which allow interaction with several receptors and cell types [6]. OPN biological functions are influenced by posttranslational modifications, such as phosphorylation, glycosylation, and protein cleavage mediated by thrombin and metalloproteinases [7–9]. OPN has RGD (arginine-glycine-aspartate) integrin binding domain, through which it mediates interactions with $\alpha\nu\beta_1$, $\alpha\nu\beta_3$, $\alpha\nu\beta_5$, $\alpha\nu\beta_6$, $\alpha 8\beta_1$, and $\alpha 5\beta_1$ integrins [10–13]. Moreover, $\alpha 9\beta_1$, $\alpha 4\beta_1$, and $\alpha 4\beta_7$ integrins bind to a cryptic SVVYGLR

(SLAYGLR in mice) sequence which is exposed upon thrombin cleavage occurring at the Arg168-Ser169 site near to the RGD motif [14–16]. This cleavage generates two fragments, the N- and C-terminal, displaying functional differences from the full length protein [17]. The N-terminal fragment (OPN-N, approx. 35 kDa) binds to integrins through the RGD or the cryptic binding site, promotes IFN- γ secretion in T cells, and stimulates cell migration by binding to $\alpha 9\beta 1$ and $\alpha 4\beta 1$ [18, 19]. The C-terminal fragment (OPN-C, approx. 25 kDa) inhibits IL-10 secretion and stimulates cell-cell adhesion by interacting with CD44 isoforms containing the v6 and v7 domains [20, 21].

OPN is highly expressed in several tumors, where it can be cleaved by thrombin and acts as a proangiogenic factor [22–25]. Moreover, the OPN:CD44 interaction promotes metastasis dissemination in a variety of malignancies [26]. The individual role of OPN-N and OPN-C has been investigated mainly in cancer cells because of the expression of both OPN and activated thrombin in the microenvironment of several tumors [22, 27, 28]. On the contrary, little information is available on their role in autoimmune diseases. Full length OPN (OPN-FL) is expressed at similar levels in the synovial fluid of patients with rheumatoid arthritis (RA) and in those with osteoarthritis, but OPN-N levels in RA synovial fluid samples are around 30-fold higher than in those from osteoarthritis and correlate with the disease status [29].

A considerable body of evidence suggests that OPN plays a detrimental role in multiple sclerosis (MS) and its animal model, experimental autoimmune encephalomyelitis (EAE) [30–32]. In MS lesions, high OPN levels are present in the perivascular cuff that surrounds inflamed blood vessels, contains inflammatory lymphocytes, and is delimited by the endothelium and the basement membrane. At this site, OPN plays a role in lymphocyte recruitment into the MS lesion, which involves $\alpha 4\beta 1$ integrin that is the target of the anti-MS drug natalizumab, a humanized monoclonal antibody that has had benefic effects for relapses prevention in RR-MS [33]. OPN binds to $\alpha 4\beta 1$ integrin only upon cleavage by thrombin which unmasks two $\alpha 4\beta 1$ integrin binding sites located into the N-terminal fragment. Hur et al. showed that the administration of recombinant OPN-FL exacerbates EAE, but the relative role of OPN-N and OPN-C is not known [34]. However, thrombin-mediated cleavage may play a role, since thrombin activity increases with the progression of neuroinflammation, and it is detectable in the demyelinating lesions where also OPN is present at high levels [35, 36]. Moreover, *in vivo* administration of hirudin, a thrombin inhibitor, decreases clinical severity, demyelination, and secretion of Th1- and Th17-type cytokines in EAE [37, 38].

OPN modulates several cell activities *in vitro*, but the role of OPN cleavage and the relative role of OPN-C and OPN-N are only partly known. Moreover, several available data are difficult to compare because they have been obtained with heterogeneous approaches, such as antibody-mediated blockage of the OPN receptors, use of OPNs produced in bacteria and eukaryotic cells, which influence the posttranslational modifications involved in OPN function, or use of

a mixture of OPN fragments obtained by *in vitro* treatment with thrombin.

The aim of our research was to recapitulate, *in vitro*, the OPN effects on human cells with a particular focus on processes involved in MS relapse, that is, T cell and monocyte activation, T cell apoptosis, lymphocytes, and endothelial cell migration and adhesion, by using recombinant forms of OPN-FL, OPN-N, and OPN-C produced in an eukaryotic system in order to ensure their posttranslation modifications.

Moreover, we investigated the activity of these OPNs and a point-mutated form of OPN resistant to thrombin cleavage (OPN-FL^{mut}) on the EAE course *in vivo* in mice, since the functional *in vivo* role of the OPN cleavage and OPN fragments is far from being elucidated.

2. Materials and Methods

2.1. Production of Human and Murine Recombinant Proteins. Both human and mouse OPN cDNAs were purchased from imaGenes GmbH, Germany. The coding sequences lacking the signal sequence, of the OPN full length (OPN-FL) and the two thrombin-cleaved fragments (OPN-N and OPN-C), were amplified by PCR with specific oligonucleotides and cloned into pMB-SV5 vector [39] downstream from the immunoglobulin leader sequence. The thrombin-uncleavable OPN constructs (OPN-FL^{mut}) was generated by mutating the mouse OPN sequence from AGGTCA coding for amino acids R₁₅₃ and S₁₅₄ to the AGCTTT coding for S₁₅₃ and F₁₅₄. This substitution has been described as yielding a thrombin cleavage resistant OPN [23]. In order to introduce the mutation, we performed site-directed mutagenesis using a mutagenic oligonucleotide specific for each sequence in combination with the reverse oligonucleotide mapping on the C-terminal end of the molecule. After amplification and restriction digestion, each mutated fragment was ligated with the wild-type upstream fragment obtained by restriction digestion to reconstitute the full length sequence. All these OPN constructs were subsequently amplified with specific oligonucleotides and cloned as six histidine- (6xHis-) tagged molecules into pUCOE vector [40]. For this cloning, we used a common forward oligonucleotide annealing on the Kozak sequence of the pMB-SV5 vector and a specific reverse oligonucleotide carrying 6xHis sequence. Recombinant OPN molecules were produced in Chinese Hamster Ovary Suspension Cells (CHOs; Invitrogen, Burlington, ON, Canada, USA). Cells were cultured in CHOS-SFMII medium (Invitrogen) and transfected with the pUCOE-OPN6xHis plasmids using FreeStyle MAX Reagent (Invitrogen) according to the manufacturer's instructions. To maintain stable transgene expression, transfected cells were cultured under selective pressure using 200 μ g/mL of hygromycin B (Invitrogen). The presence of each recombinant OPN construct in the cell supernatant was verified by western blotting using either an antibody directed against the His tag (Tetra-His Antibody, Qiagen, Valencia, CA, USA) or an anti-OPN antibody directed against an epitope located in the N- or C-terminal half of the molecule: SPP1 Polyclonal Antibody (Invitrogen) and Polyclonal Anti-Osteopontin Antibody (Millipore, Billerica, MA, USA), respectively. These antibodies

were detected using the appropriate horseradish peroxidase-conjugated secondary antibody (Sigma-Aldrich, St. Louis, MO, USA). The reactive proteins were visualized by the ECL (Perkin Elmer, Waltham, MA, USA). All recombinant proteins were correctly recognized, and they displayed the expected size (i.e., 60 kDa for OPN-FL and OPN-FL^{mut}, 35 kDa for OPN-N, and 25 kDa for OPN-C). Cells were grown at high density using CELLline™ devices (BD Biosciences, San Diego, CA, USA) and collected twice a week. After centrifugation at 400 ×g for 10 minutes, cell supernatants were collected and each recombinant protein was purified on HIS Trap Excel Ni-Sepharose resin (GE Healthcare, Uppsala, Sweden), dialyzed overnight against PBS, and analyzed by western blotting and coomassie gel staining (Sigma-Aldrich).

2.2. Cells. Peripheral blood mononuclear cells (PBMCs) were separated from human blood samples obtained from healthy donors, who signed their written informed consent, by density gradient centrifugation using the Ficoll-Hypaque reagent (Lympholyte-H, Cedarlane Laboratories, Burlington, ON, Canada). The use of PBMCs was approved by the ethics committee of the “Azienda Ospedaliera Universitaria Maggiore della Carità” of Novara (Prot. 962/CE). CD4⁺ T cells and monocytes were negatively purified from PBMCs using the EasySep™ Human CD4 Negative Selection Kit and EasySep Human CD14 Negative Selection Kit, respectively (Stem Cells Technologies, Vancouver, BC, USA). Cell purity was checked by immunophenotypic analyses and was higher than 95%. Peripheral blood lymphocytes (PBL) were obtained from PBMC after 2 h adhesion to remove monocytes. Cultures were performed in RPMI 1640 supplemented with 10% fetal bovine serum (FBS), and 100 U/mL penicillin, 100 µg/mL streptomycin (Invitrogen). For interferon- (IFN-) γ, interleukin- (IL-) 17A, and IL-10 secretion and intracellular staining, 0.1 × 10⁶ CD4⁺ T cells were activated with anti-CD3 (1 µg/mL, clone: OKT3) and anti-CD28 (2 µg/mL, Ancell, Bayport, MN, USA) in the presence or absence of OPN-FL 1 µg/mL, OPN-N, or OPN-C 0.5 µg/mL for 5 days. For Tissue Inhibitor Metalloproteinase-1 (TIMP-1) and IL-6 secretion, 0.1 × 10⁶ monocytes were cultured in the presence or absence of OPN-FL 1 µg/mL, OPN-N, or OPN-C 0.5 µg/mL for 2 days. The effects of OPN-FL were compared to that of a commercial OPN-FL purchased from R&D System, and we obtained the same results.

Human umbilical vein endothelial cells (HUVECs) were isolated from human umbilical veins via trypsin treatment (1%) and cultured in M199 medium (Sigma-Aldrich) with the addition of 20% FCS (Invitrogen) and 100 U/mL penicillin, 100 µg/mL streptomycin, 5 U/ml heparin, 12 µg/mL bovine brain extract, and 200 mM glutamine (HyClone Laboratories, South Logan, USA). Cells were grown to confluence in flasks and used at the 2nd–5th passage. The purity of the EC preparation was evaluated using morphologic criteria and positive immunofluorescence for factor VIII. Contamination with blood leukocytes was assessed via immunofluorescence with an anti-CD45 antibody. The use of HUVECs was approved by the institutional review board of the “Presidio Ospedaliero Martini” of Turin (Prot. 263-07/NF) that waived the need for

consent; the data were analyzed anonymously and conducted in accordance with the Declaration of Helsinki.

2.3. ELISA. Concentrations of IL-17A, IFN-γ, IL-10, IL-6, and TIMP-1 were measured in culture supernatants by ELISA according to the instructions of the manufacturers (R&D System, Minneapolis, MN, USA; eBioscience San Diego, CA, USA and BioLegend, San Diego, CA, USA). Absorbance was detected with a microplate reader (Bio-Rad, Hercules, CA, USA), and the I-smart program was used to calculate the standard curve.

2.4. Intracellular Staining. CD4⁺ T cells (1 × 10⁵) were cultured for 5 days in round-bottomed 96-well plates in the presence of anti-CD3 (1 µg/mL) plus anti-CD28 (1 µg/mL) mAb and in the presence of recombinant OPN-FL 1 µg/mL, OPN-N, or OPN-C 0.5 µg/mL. After 5 days of culture, the cells were restimulated with phorbol 12-myristate 13-acetate (PMA, 50 ng/mL; Sigma-Aldrich) plus ionomycin (500 ng/mL; Sigma-Aldrich) for 5 hours in the presence of BFA (10 µg/mL; Sigma-Aldrich). Then, cells were permeabilized, stained with a PE-conjugated anti-IL-10 mAb (Miltenyi Biotec GmbH, Bergisch Gladbach, Germany) and APC-conjugated anti-IL-17A mAb (eBioscience, San Diego, CA, USA), and analyzed by flow cytometry.

2.5. Cell Death Assay. Activation induced cell death (AICD) was evaluated on T cell lines obtained by activating PBMC with phytohemagglutinin (PHA, Sigma-Aldrich; 1 µg/mL) and cultured in RPMI 1640 medium + 10% FBS + IL-2 (2 U/mL; Sigma-Aldrich) for 6 days. In the AICD assay, cells (5 × 10⁴/well) were cultured in wells coated with anti-CD3 mAb (OKT3, 1 µg/mL) with RPMI + 5% FBS + 1 U/mL IL-2 in the presence or absence of OPN-FL (1 µg/mL), OPN-N, or OPN-C (0.5 µg/mL). Live cells were then counted in each well using the trypan blue exclusion test. Assays were performed in triplicate and results were expressed as relative cell survival % calculated as follows: (total live cell count in the assay well/total live cell count in the respective control well) × 100.

2.6. Cell Migration Assay. In the Boyden chamber (BD Biosciences) migration assay, resting PBL or HUVECs (5 × 10⁴ or 2 × 10³, resp.) were plated onto the apical side of 50 µg/mL matrigel-coated filters (8.2 mm diameter and 0.3 µm or 0.5 µm pore size; Neuro Probe, Inc.; BIOMAP snc, Milan, Italy) in RPMI or M200 serum-free medium, with or without OPN-FL (10 µg/mL), OPN-N (5 µg/mL), or OPN-C (5 µg/mL). Mediums containing 1 ng/mL RANTES (R&D System) or 10 ng/mL vascular endothelial growth factor (VEGF-α, R&D System) were placed in the basolateral chamber as a positive chemoattractant stimuli for PBL and HUVECs, respectively. The chamber was incubated at 37°C under 5% CO₂. After 20 h, the cells on the apical side were wiped off with Q-tips. The cells on the bottom of the filter were stained with crystal violet, and all were counted (four-fold filter) with an inverted microscope (magnification 40x). Data are shown as percentages of the treated cells migration *versus* the control migration measured for untreated cells.

Control migration is (mean \pm SEM) 263 ± 45 cells for HUVECs ($n = 5$) and 155 ± 25 for lymphocytes ($n = 5$).

2.7. Cells Adhesion Assay. HUVECs were grown to confluence in 24-well plates in complete M200 medium (PromoCell GmbH, Heidelberg, Germany) and then treated or not with OPN-FL (10 $\mu\text{g}/\text{mL}$), OPN-N (5 $\mu\text{g}/\text{mL}$), or OPN-C (5 $\mu\text{g}/\text{mL}$) for 30 min, washed with fresh medium twice, and incubated for 1 h with resting PBL (5×10^4 cell/well). The 1 h incubation time was chosen to allow full sedimentation of the adhering cells, but similar results were obtained with a shorter incubation time (30 min). After incubation in the adhesion assay, nonadherent cells were removed by washing three times with M200. The center of each well was analyzed by fluorescence image analysis. Adherent cells were counted by the Image-Pro Plus Software for microimaging (Media Cybernetics, Bethesda, MD, version 5.0). Data are shown as percentages of the treated cells adhesion *versus* the control adhesion measured for untreated cells. This control adhesion was (mean \pm SEM) 35 ± 4 cells per microscope field ($n = 5$).

2.8. Angiogenesis Assay. In the tube formation assay, HUVECs were cultured in M200 serum-free medium and seeded onto 48-well plates (2.5×10^4 /well) previously coated with 150 μL of growth factor-reduced matrigel (BD Biosciences) in the presence of OPN-FL (10 $\mu\text{g}/\text{mL}$), OPN-N (5 $\mu\text{g}/\text{mL}$), OPN-C (5 $\mu\text{g}/\text{mL}$), or control medium with VEGF- α (10 ng/mL, R&D System).

The morphology of the capillary-like structures formed by the HUVECs was analyzed after 6 h of culture using an inverted microscope (Leica Microsystem; magnification 10x) and was photographed with a digital camera (Leica Microsystem). Tube formation was analyzed and the number of tubes (with branching at both ends) was counted with an imaging system (Image-Pro Plus software for microimaging, Media Cybernetics, version 5.0, Bethesda, MD, USA). Tube formation was evaluated by counting the total number of tubes in three wells ($n = 5$) as previously described [41].

2.9. EAE Induction and OPN Treatment. Specific pathogen-free female C57BL/6 mice were purchased from Harlan (Harlan Laboratories, Indianapolis, IN, USA). The experimental protocol and animal handling were approved by CESAPO, the ethical committee of the University of Piemonte Orientale (Permit Number: 10/2013). To induce EAE, eight-week-old mice ($n = 48$) were immunized with 200 μg of MOG₃₅₋₅₅ peptide (Espikem, Firenze, Italy) emulsified in complete Freund adjuvant (Sigma-Aldrich) containing 4 mg/mL heat-killed *Mycobacterium tuberculosis* (Difco laboratories, Detroit, MI, USA). On the day of MOG₃₅₋₅₅ immunization and 48 h later, the mice were injected intraperitoneally (i.p.) with pertussis toxin (Sigma-Aldrich, 500 μg in 0.1 mL of PBS). The mice were examined daily for clinical signs of EAE and scored as reported [42]. Twenty days after the remission, mice were divided into different experimental groups receiving daily injection of 5 μg of different OPN variants (OPN-FL, OPN-N, OPN-C, or a mixture of OPN-C + OPN-N). Moreover, since OPN-FL is cleaved by thrombin *in vivo*, we also injected OPN-FL^{mut}, lacking the thrombin cleavage site.

Animal health was evaluated daily, throughout the duration of the experiment. Since the applied EAE protocol and the treatments with recombinant OPNs do not cause a long and intense suffering, we never administered an analgesic therapy. To prevent malnutrition in palsy mice, starting from EAE score 3.5 on, we put food and water directly into the cage, where they could easily reach. No unexpected death was recorded. Euthanasia was performed by cervical dislocation after a light inhalational anesthesia with isoflurane (2-chloro-2-(difluoromethoxy)-1,1,1-trifluoro-ethane) (ISOFLURANE VET FL VT, Merial Italia SpA, PD, Italy) using a precision out-of-circuit vaporizer (ISOTEC 4 series 1789, 2Biological Instruments SNC, VA, Italy) in a rodent induction chamber (2Biological Instruments SNC).

2.10. Data Analysis. The data are shown as the % of mean \pm SEM. The statistical analyses were performed with Graph-Pad Prism 3.0 software (San Diego, CA, USA) using the Wilcoxon's signed rank test. The Friedman ANOVA test for repeated measures followed by Dunn's multiple comparison was used to analyze the daily clinical EAE score. p values < 0.05 were considered significant.

3. Results

3.1. Production of Human and Murine Recombinant Proteins. Both the human and murine leaderless OPN sequences, lacking the signal sequence, were cloned into pUCOE vector (OPN-FL). In order to assess the role of thrombin cleavage on OPN activity, we also cloned the following mouse and human OPN variants: OPN-N including aa 17–168 (human) or 17–153 (mouse) of OPN; OPN-C including aa 169–314 (human) or 154–294 of OPN; OPN-FL^{mut} carrying a mutated thrombin cleavage site (from R₁₅₃-S₁₅₄ to S₁₅₃-F₁₅₄) (Figure 1(a)) [23]. The cDNA coding for all these variants was cloned as fusion proteins with the 6xHis Tag and stably transfected into CHO cells. The presence of the recombinant proteins was verified in the culture supernatants by coomassie staining and by western blotting using antibodies designed against different epitopes of OPN or the His Tag (Figure 1(b)). All recombinant proteins displayed the expected sizes, that is, 60 kDa for OPN-FL and OPN-FL^{mut}, 35 kDa for OPN-N, and 25 kDa for OPN-C, without presence of degradation products and/or contamination by other proteins. As expected, OPN-FL^{mut} was not cleaved by thrombin (Figure 1(c)).

3.2. Effects of OPN on Human Immune Cells In Vitro. We evaluated the effect of the human OPN-FL, OPN-N, and OPN-C on secretion of IFN- γ , IL-17, and IL-10 by T cells, since OPN is known to stimulate secretion of IFN- γ and IL-17 and to inhibit secretion of IL-10 [43, 44]. CD4⁺ T cells from healthy donors were activated by triggering CD3 and CD28 and cultured in the presence and absence of OPN-FL, OPN-N, and OPN-C for 5 days. Then, secretion of IL-17A, IFN- γ , and IL-10 was evaluated by ELISA in the culture supernatants. The results showed that all OPN preparations were similarly active in increasing secretion of IFN- γ (Figure 2(a)), whereas secretion of IL-17A was significantly increased by OPN-FL and OPN-N but not OPN-C (Figure 2(b)), and secretion of

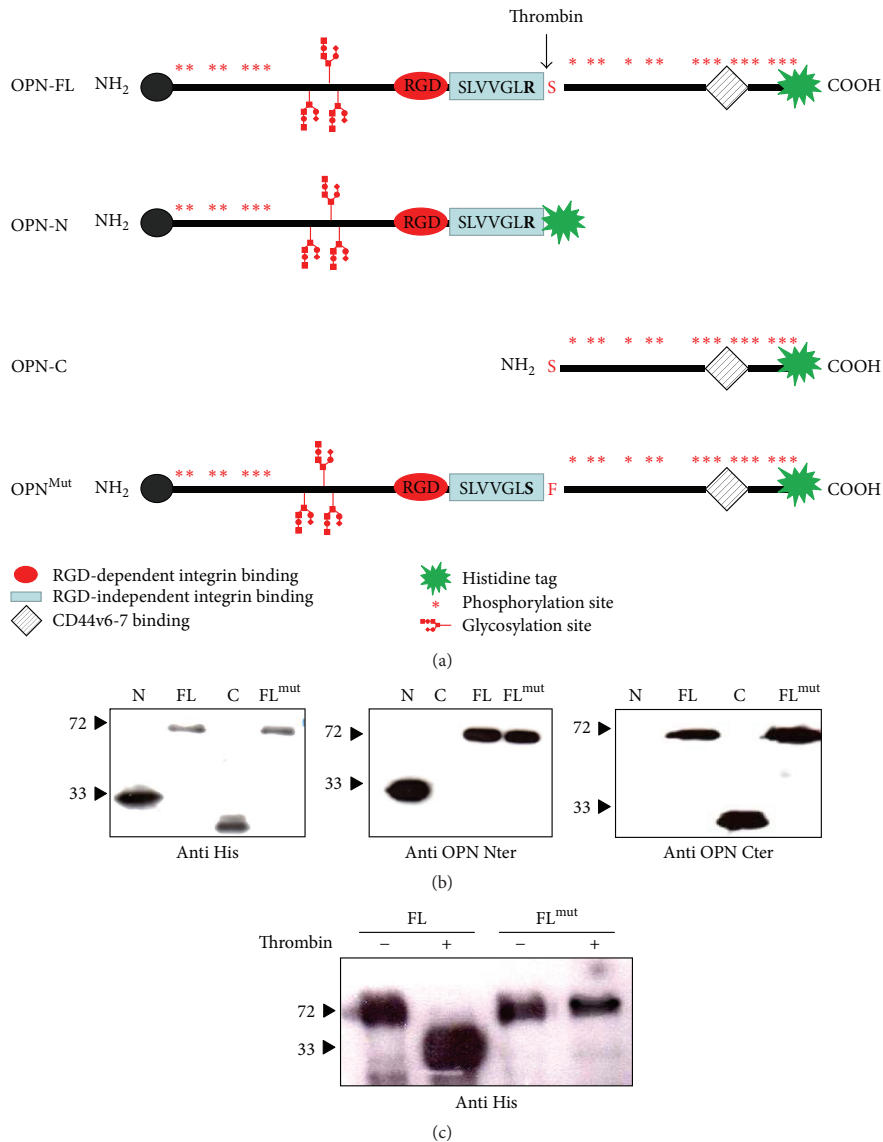


FIGURE 1: Recombinant OPN variants. (a) The figure depicts the recombinant OPN variants: OPN-FL (aa 17–314 human and aa 17–294 mouse), OPN-N including aa 17–168 (human) or 17–153 (mouse) of OPN; OPN-C including aa 169–314 (human) or 154–294 of OPN; mouse OPN-FL^{mut} carrying a mutated thrombin cleavage site (from R₁₅₃-S₁₅₄ to S₁₅₃-F₁₅₄). (b) Western blotting showing the recombinant proteins after purification probed with the anti-His-tag (left panel) or antibodies specific for the N (middle panel) or C-terminal portion (right panel). (c) OPN-FL but not OPN-FL^{mut} is cleaved by thrombin.

IL-10 was significantly decreased by OPN-FL and OPN-C but not OPN-N (Figure 2(c)). IL-10 and IL-17 expression was evaluated also by intracellular staining of cells restimulated for 5 h with PMA and ionomycin after the 5-day cultures. Cytofluorimetric analysis showed that the proportion of IL-17A single positive cells was significantly increased by OPN-FL and OPN-N but not OPN-C, whereas the proportions of IL-10 single positive cells and IL-17A/IL-10 dual positive

cells were significantly decreased by all OPN preparations (Figure 2(d)).

We evaluated the effect of the human OPN-FL, OPN-N, and OPN-C on secretion of IL-6 and TIMP-1 in monocytes, since OPN is known to stimulate secretion of both molecules which play a key role in inflammation and several pathological conditions [45, 46]. Monocytes from healthy donors were cultured in the presence and absence of OPN-FL, OPN-N,

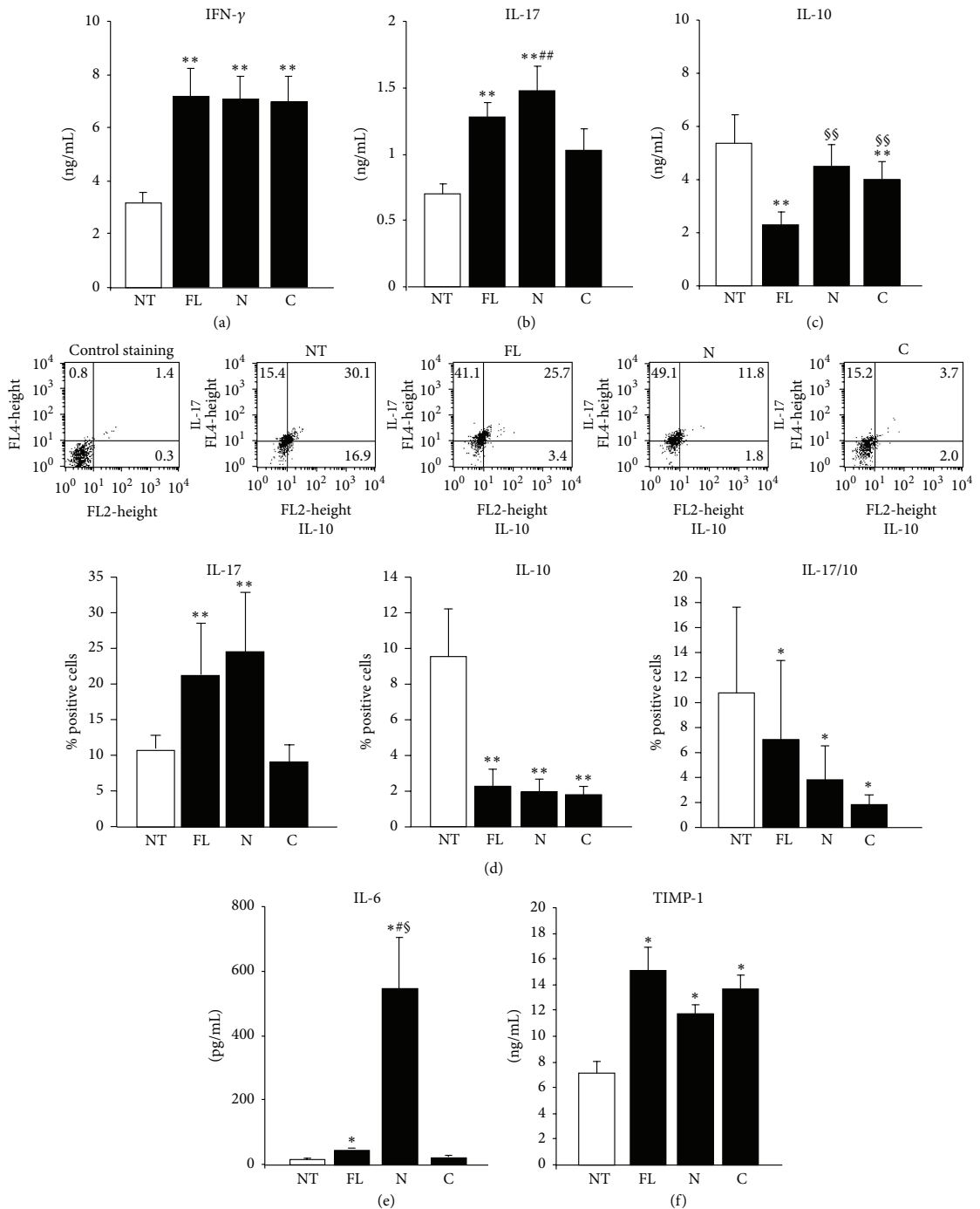


FIGURE 2: Effect of OPN fragments on cytokine secretion. (a) IFN- γ , (b) IL-17A, and (c) IL-10 protein evaluated in the culture supernatants from CD4⁺ T cells by ELISA or (d) by intracellular staining with anti-IL-17A and anti-IL-10 after 5 days of treatment with OPN variants. (e) IL-6 and (f) TIMP-1 protein secreted by monocytes after 2 days of treatment with OPN variants. Data are expressed as the mean \pm SE from 6 independent experiments (* p < 0.05; ** p \leq 0.01 versus the control; § p < 0.05; §§ p \leq 0.01 versus OPN-FL; # p < 0.05; ## p \leq 0.01 versus OPN-C; Wilcoxon's signed rank test).

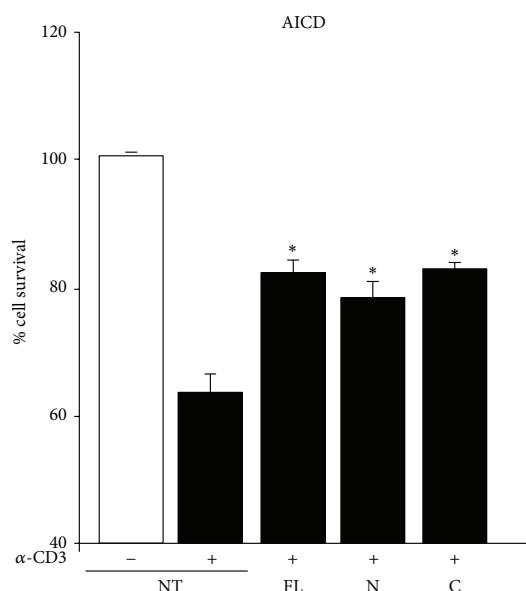


FIGURE 3: Effect of OPN variants on AICD of T cells. AICD was induced in PHA-derived T cell lines from healthy controls in the presence/absence of anti-CD3 and OPN variants. Results are expressed as relative cell survival % and are the mean \pm SEM from 6 experiments. (* $p < 0.05$ versus the control; Wilcoxon's signed rank test).

and OPN-C for 2 days. Then, secretion of IL-6 and TIMP-1 was evaluated by ELISA in the culture supernatants. The results showed that secretion of IL-6 was induced mildly by OPN-FL and strikingly by OPN-N, whereas OPN-C had no significant effect (Figure 2(e)). By contrast, secretion of TIMP-1 was similarly induced by OPN-FL, OPN-N, and OPN-C (Figure 2(f)).

We evaluated the effect of the human OPN-FL, OPN-N, and OPN-C in AICD of T cells, since OPN is known to inhibit T cell AICD, which is a key mechanism of peripheral tolerance [47]. PHA-activated T cells obtained from healthy donors were treated with anti-CD3 mAb to induce AICD in the presence and absence of OPN-FL, OPN-N, and OPN-C, and cell survival was evaluated after 16 h. The results showed that AICD was inhibited to the same extent by OPN-FL, OPN-N, and OPN-C (Figure 3).

We evaluated the effect of the human OPN-FL, OPN-N, and OPN-C on lymphocyte migration and adhesion to vascular endothelial cells, since OPN is known to induce both cell adhesiveness and migration. In the migration experiments, PBL were seeded in the upper side of a Boyden chamber in serum-free medium; OPN-FL, OPN-N, and OPN-C and RANTES, used as positive controls for chemoattraction of lymphocytes, were loaded in the lower side of the Boyden chamber. The results showed that migration of lymphocytes was induced by OPN-FL and, to a greater extent, OPN-N, but not OPN-C (Figure 4(a)). In the adhesion experiments, HUVECs were treated with OPN-FL, OPN-N, and OPN-C

for 30 min, washed, and then used in the adhesion assay with PBL. The results showed that adhesion was induced by both OPN-FL and, to a greater extent, OPN-N but not OPN-C (Figure 4(b)).

We evaluated the effect of the human OPN-FL, OPN-N, and OPN-C in angiogenesis *in vitro* by assessing migration and tube formation on HUVECs, since OPN is known to induce angiogenesis [48]. The migration assay was performed as with PBL using VEGF- α as a positive control. The results overlapped those obtained with PBL, since migration was induced by OPN-FL and, to a greater extent, OPN-N, but not OPN-C (Figure 5(a)). In the tubulogenesis assay, HUVECs were seeded onto growth factor-reduced matrigel in the presence or absence of OPN-FL, OPN-N, and OPN-C, and the morphology of capillary-like structures formed by HUVECs was analyzed after 6 h. The results showed that OPN-N and OPN-C induced high levels of tube formation, whereas OPN-FL had a mild, although significant, effect (Figure 5(b)).

3.3. Effect of OPN in Mouse EAE *In Vivo*. The first part of this work has been performed on human cells which are the therapeutic targets in human diseases. To assess whether the OPN forms exert different effects also *in vivo*, we moved to mouse EAE, a model of MS [32]. EAE is a T cell-mediated autoimmune disease characterized by perivascular CD4⁺ T cell and mononuclear cell infiltration, causing demyelination areas in the central nervous system, leading to progressive hind-limb paralysis.

Several works showed that, in the mouse, OPN displays similar effects than in human cells in terms of cytokine secretion [49], cell migration [50, 51], and angiogenesis [52]. Moreover, we performed pilot experiments using T cells and OPN variants from mice, which confirmed the pattern of OPN-FL, OPN-C, and OPN-N effects detected in the human model in terms of secretion of IFN- γ , IL-17, and IL-10, migration, and adhesion, which are key factors in EAE pathogenesis (data not shown).

EAE can be induced by immunization with myelin proteins, such as proteolipid protein (PLP) or myelin basic protein (MBP) or myelin oligodendrocyte glycoprotein (MOG) in complete Freund's adjuvant (CFA). In C57BL/6 mice, the disease can be induced by immunization with the MOG immunodominant epitope corresponding to amino acids from 35 to 55 (MOG₃₅₋₅₅). In this model, mice develop progressive paralysis (relapse) followed by a stable remission. However, administration of OPN in the remission phase induces a prompt relapse [34]. Therefore, we induced EAE in C57BL/6 mice and waited for the remission and, 20 days later, we started daily injections with the OPN variants and monitored relapse development. We compared the effect of the mouse OPN-FL, OPN-N, OPN-C, or OPN-C + OPN-N. Since OPN-FL *in vivo* is cleaved by thrombin, we also injected OPN-FL^{mut}, lacking the thrombin cleavage site. The results showed that OPN-FL, OPN-C, and OPN-C + OPN-N induced a similar strong relapse of the disease ($p < 0.001$) (Figure 6), whereas OPN-N induced a mild relapse ($p < 0.05$) and OPN-FL^{mut} had no significant effect.

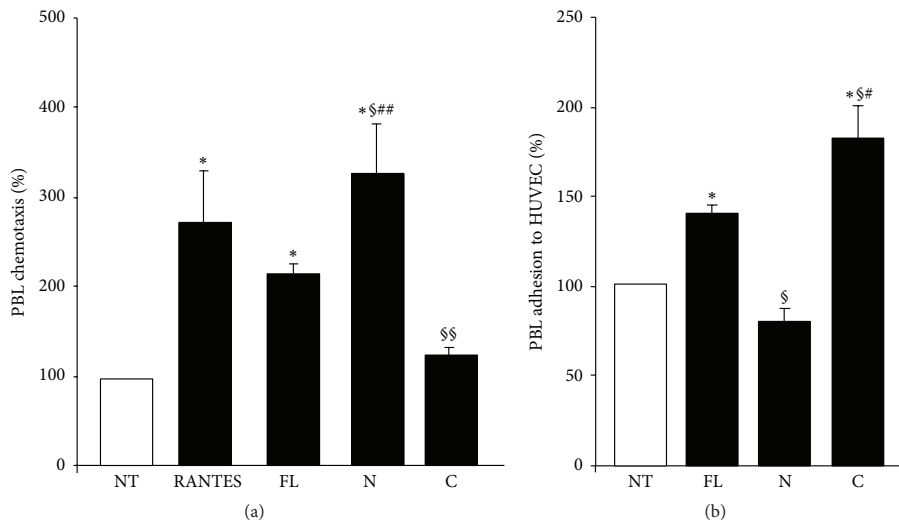


FIGURE 4: Effect of OPN variants on PBL migration and adhesion. (a) PBL were plated onto the apical side of matrigel-coated filters in 50 μ L of medium in the presence or absence of either 10 μ g/mL OPN-FL, 5 μ g/mL OPN-N, or OPN-C; RANTES (10 ng/mL) was loaded in the basolateral chamber as a positive control for migration. The cells that migrated to the bottom of the filters were stained using crystal violet and counted (5 fields for each triplicate filter) using an inverted microscope. (b) PBL were pretreated or not with OPN-FL, OPN-N, or OPN-C (10 μ g/mL) for 30 min, washed, and then incubated together for 1 h in the adhesion assay. Data are expressed as the mean \pm SEM of the percentage of migration or adhesion versus the control obtained from untreated cells set at 100% from 5 independent experiments. (* $p < 0.05$; versus the control; § $p < 0.05$; §§ $p \leq 0.01$ versus OPN-FL; # $p < 0.05$; ## $p \leq 0.01$ versus OPN-C or OPN-N; Wilcoxon's signed rank test).

4. Discussion

In this study, we produced recombinant proteins corresponding to the human OPN-FL, OPN-N, and OPN-C. These proteins were produced in an eukaryotic system in order to ensure the posttranslational modifications influencing OPN functions, and they were used to investigate their individual activity on key players in the immune response, such as lymphocytes, monocytes, and endothelial cells. We also used the same approach to produce the mouse OPN-FL, OPN-N, and OPN-C, together with a thrombin-resistant form of OPN-FL in which the thrombin cleavage site was mutated (OPN-FL^{mut}) and assessed their individual effect *in vivo* on mouse during EAE relapse.

In T cells, OPN cleavage seems not to influence the effect on IFN- γ secretion, which marks activation of Th1 cells since secretion of this cytokine is similarly costimulated by OPN-FL, OPN-N, and OPN-C. This suggests that production of IFN- γ is similarly costimulated by the triggering of either integrins or CD44, and no incremental effect is ascribable to the integrin cryptic site exposed in OPN-N. A similar reasoning may be applied to inhibition of AICD, which plays a key role in switching off the immune response and was similarly inhibited by OPN-FL, OPN-N, and OPN-C. This was not surprising, since both the RGD-dependent triggering of integrins and the triggering of CD44 v6-7 have been shown to protect cells from apoptosis [53, 54].

By contrast, secretion of IL-17 and IL-10, respectively, upmodulated and downmodulated by OPN-FL, differentially involves the two OPN fragments, since IL-17 upmodulation is

mainly ascribable to OPN-N, whereas IL-10 downmodulation is mainly ascribable to OPN-C. These results are in line with reports showing that the OPN effects on IL-17 and IL-10 are selectively inhibited by anti-integrin and anti-CD44 antibodies, respectively [43].

The IL-17A secretion data were confirmed by intracytoplasmic expression of IL-17A. By contrast, the different effects of the OPN preparations on IL-10 secretion were not confirmed by intracytoplasmic staining of IL-10 since all OPNs similarly decreased the proportion of IL-10⁺ cells. Since cell staining was performed at day 5, whereas supernatant analysis evaluated the overall secretion during the whole culture time, it is possible that the supernatant differences were ascribable to initial phases of the culture. Another point is that all OPN preparations decreased the proportions of IL-10/IL-17A double positive cells, which suggest that they can work in pushing these cells toward a frankly proinflammatory Th17 effector function [55, 56].

A similar coordinated effect of OPN fragments can be envisaged on lymphocyte adhesion to endothelial cells and migration, which are two key steps of lymphocyte extravasation and homing into tissues. Our results, indeed, showed that both adhesion and migration are supported by OPN-FL, but adhesion is ascribable to OPN-C, whereas migration is ascribable to OPN-N, and each fragment displays its effect at higher levels than OPN-FL.

The experiment on HUVECs showed that also the OPN effect on migration of endothelial cells was ascribable to OPN-N and not to OPN-C. By contrast, both OPN-N and OPN-C displayed a strikingly higher effect than OPN-FL

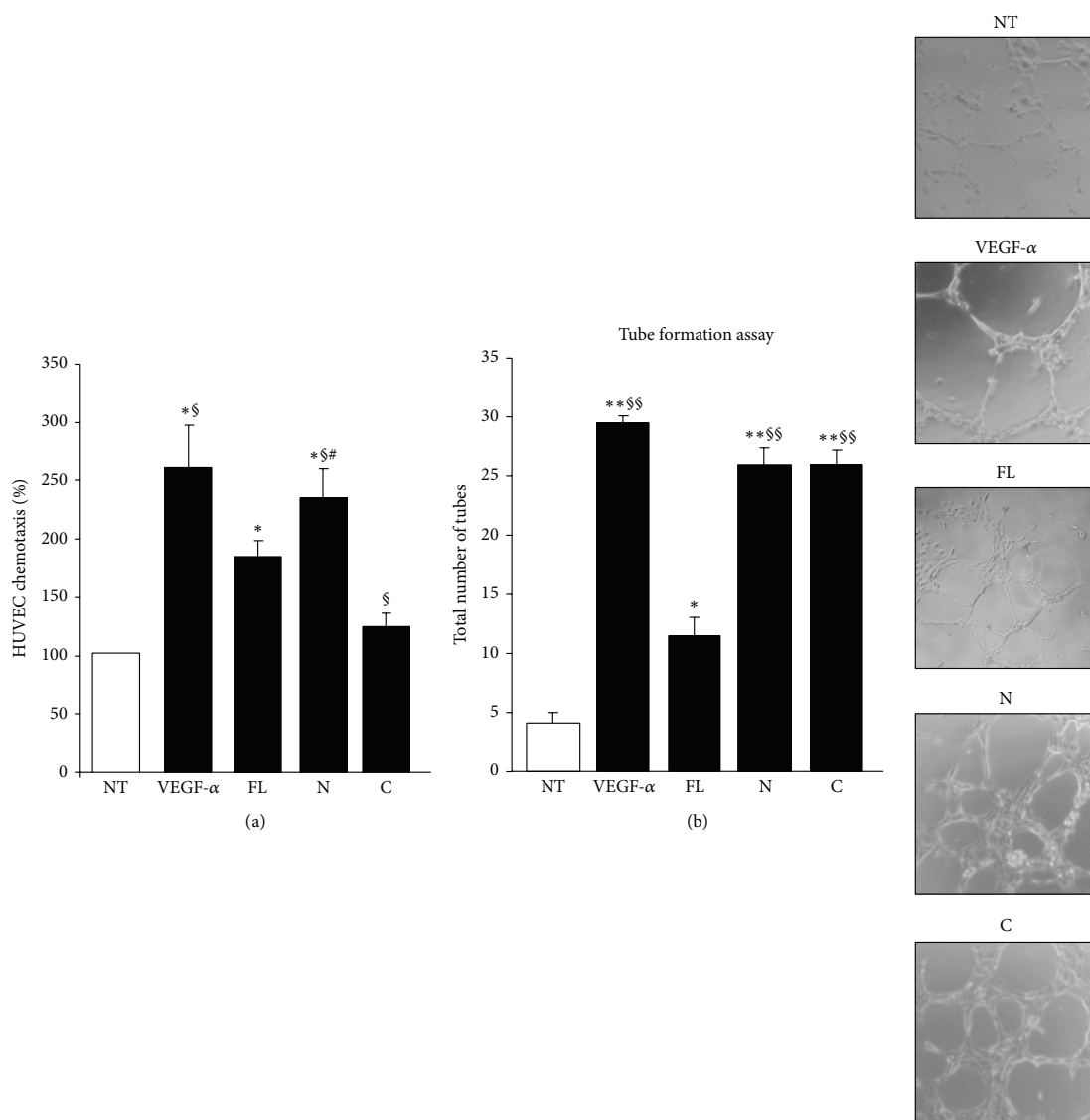


FIGURE 5: Effect of OPN variants on angiogenesis. (a) HUVECs were plated onto the apical side of matrigel-coated filters in 50 μ L of medium in the presence or absence of either 10 μ g/mL OPN-FL, 5 μ g/mL OPN-N, or OPN-C; VEGF- α (10 ng/mL) was loaded in the basolateral chamber as a positive control for migration. The cells that migrated to the bottom of the filters were stained using crystal violet and counted (5 fields for each triplicate filter) using an inverted microscope. Results are expressed as in Figure 4. (b) In the tube formation assay, HUVECs were plated in the presence and absence of OPN-FL (10 μ g/mL), OPN-N (5 μ g/mL), OPN-C (5 μ g/mL), or VEGF- α (10 ng/mL), as a control. The morphology of capillary-like structures formed by HUVECs was analyzed 6 h after culturing. Results are expressed as means \pm SEM from 3 experiments (* p < 0.05; ** p \leq 0.01 versus the control; \S p < 0.05; $\S\S$ p \leq 0.01 versus OPN-FL; * p < 0.05; versus OPN-C; Wilcoxon's signed rank test). Right panels show a representative tubulogenesis experiment.

in inducing tubulogenesis, which is an *in vitro* assay of neoangiogenesis. These results are in line with the reports from Senger and colleagues [48] showing that VEGF induces OPN and α v β ₃ expression in endothelial cells and stimulates cleavage of OPN by thrombin and that the resulting OPN fragments are strongly chemotactic for endothelial cells and

promote angiogenesis [57]. However, these authors used a mixture of the two OPN fragments obtained by *in vitro* thrombin-mediated cleavage of OPN-FL, and they could not distinguish the individual role of OPN-N and OPN-C. Moreover, other studies have shown that, in vascular endothelial cells, OPN enhances VEGF- α expression, which,

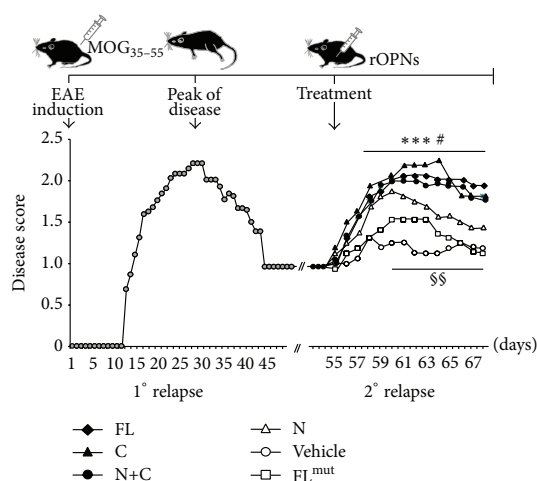


FIGURE 6: Effect of different forms of OPN on the EAE remission phase. The upper schema depicts the timing of the experiment: $n = 48$ mice were immunized at day 0 with MOG₃₅₋₅₅ peptide to induce EAE. The mice were examined daily for clinical signs of EAE and scored as reported in the lower panel (grey circles). Twenty days after the remission, at day 55 after EAE induction, mice were randomized into different experimental groups and received daily injection of either OPN-FL (black diamonds), OPN-FL^{mut} (white squares), OPN-N (white triangles), OPN-C (black triangles), OPN-C + OPN-N (black circles), or vehicle (white circles). A nonparametric ANOVA test was used for clinical score comparisons (^{***} $p < 0.001$ PBS versus OPN-FL, OPN-C, and OPN-N + OPN-C; [#] $p < 0.05$ PBS versus OPN-N; ^{§§} $p < 0.01$ OPN-C versus OPN-N and versus OPN-FL^{mut}).

in turn, mediates a positive feedback on OPN expression; the blocking of this feedback signal by anti-VEGF- α antibodies partially inhibits the OPN-induced HUVECs motility, proliferation, and tube formation [58].

In monocytes, the main finding was a marked putative effect of thrombin cleavage on IL-6 secretion, which was induced moderately by OPN-FL and strikingly by OPN-N, whereas OPN-C displayed no effect. This differential effect was detected on IL-6 but not on TIMP-1 whose secretion was similarly induced by all OPN preparations, and this suggests that OPN-N fine-tunes monocyte activation [32, 49, 59, 60].

Altogether our *in vitro* experiments show not only that the OPN effects on IL-17 and IL-6 secretion and cell migration are mainly ascribable to OPN-N, whereas those on IL-10 secretion and cell adhesion are mainly ascribable to OPN-C, but also that these effects are exerted at higher levels by the appropriate OPN fragment than by OPN-FL, which suggests that thrombin-mediated cleavage plays a key role in OPN activity. A striking gain of function was also detected in the tubulogenesis assay in which both OPN-N and OPN-C were much more active than OPN-FL. In the case of OPN-N, this gain of function may be ascribed to exposure of the cryptic integrin binding site that allows binding to integrins unbound by OPN-FL. By contrast, it is difficult to explain it for OPN-C, whose only known binding site is that for CD44, which

is present also in OPN-FL. Besides the possibility that OPN-C exposes unknown cryptic binding site(s) for unknown ligand(s), the gain of function of OPN-C might be ascribed to removal of the N-terminal portion of OPN-FL, which may exert a partial steric or functional interference on CD44 triggering.

Also the *in vivo* experiments showed that thrombin-mediated cleavage of OPN plays a key role in OPN function, since OPN-FL was much more effective in inducing EAE relapses than OPN-FL^{mut}, which is resistant to thrombin-mediated cleavage. Therefore, the effect of OPN-FL must be ascribed to the fragments produced by thrombin cleavage *in vivo*. Use of the recombinant OPN-C and OPN-N showed that the effect was ascribable to OPN-C, whereas OPN-N was active only weakly. The critical role of OPN-C was surprising, since the presence of the cryptic binding sites for $\alpha 4\beta 1$ would instead draw the attention to OPN-N because $\alpha 4\beta 1$ is involved in the homing of T cells into the central nervous system, and it is the target of the anti-MS drug natalizumab.

Substantial evidence indicates that OPN-FL plays a detrimental role in MS and EAE [32, 46, 61]. OPN-FL has been found to be the most abundantly expressed cytokine in the lesions of MS patients and EAE mice. Moreover, OPN deficient mice and mice injected with anti-OPN antibodies develop a mild EAE, whereas administration of OPN-FL triggers relapses in several EAE models [34]. Recently, proteomic analysis of MS lesions has unraveled a potential link between the coagulation cascade and MS pathology, which is supported by EAE data showing that administration of the thrombin inhibitor hirudin decreases clinical severity, demyelination, and Th1 and Th17 cytokines secretion [36, 38]. Intriguingly, thrombin activity is increased in the demyelinating lesions [37] where OPN is expressed at high levels. Our data confirm that thrombin-mediated cleavage of OPN plays a key role in MS relapse by exerting a dual effect. On the one hand, they may play a key role in the homing of autoreactive lymphocytes in the central nervous system lesions, since OPN-N increases production of IL-17 involved in breaking the blood brain barrier and stimulates lymphocyte migration, whereas OPN-C increases lymphocyte adhesion to vascular endothelial cells. On the other hand, they may support local inflammation, since OPN-N induces secretion of IL-6 in monocytes, OPN-C inhibits production of IL-10, and both increase secretion of IFN- γ .

5. Conclusion

In conclusion, this study shows that the OPN fragments generated by thrombin exert distinct effects on cells involved in the immune and inflammatory response, and it suggests that drugs targeting each fragment may be used to fine-tune the wide effects of this cytokine.

Disclosure

The funding sources had no involvement in the study design or in its performance.

Competing Interests

The authors declare that they have no competing interests regarding the publication of this paper.

Authors' Contributions

Elena Boggio, Chiara Dianzani, Casimiro Luca Gigliotti, Maria Felicia Soluri, Nausicaa Clemente, and Giuseppe Cappellano performed the functional experiments and analyzed the data, Erika Toth, Davide Raineri, and Benedetta Ferrara produced recombinant proteins, Cristoforo Comi contributed to write the paper, and Umberto Dianzani and Annalisa Chiocchetti designed the study, supervised the research, and wrote the paper. The authors are grateful to the Obstetrics and Gynecology Unit, Martini Hospital, Torino, for providing human umbilical cords. Elena Boggio and Chiara Dianzani contributed equally to this work.

Acknowledgments

This research was supported by the Fondazione Italiana Sclerosi Multipla (FISM, Genova 2010/R/12-2011/R/11), the Associazione Italiana Ricerca sul Cancro (IG 14430, AIRC, Milan), Fondazione Amici di Jean (Torino), and Fondazione Cassa di Risparmio di Cuneo (Cuneo).

References

- [1] H.-J. Cho, H.-J. Cho, and H.-S. Kim, "Osteopontin: a multifunctional protein at the crossroads of inflammation, atherosclerosis, and vascular calcification," *Current Atherosclerosis Reports*, vol. 11, no. 3, pp. 206–213, 2009.
- [2] J. Liu, Q. Liu, Y. Wan et al., "Osteopontin promotes the progression of gastric cancer through the NF- κ B pathway regulated by the MAPK and PI3K," *International Journal of Oncology*, vol. 45, no. 1, pp. 282–290, 2014.
- [3] A. Brown, "Osteopontin: a key link between immunity, inflammation and the central nervous system," *Translational Neuroscience*, vol. 3, no. 3, pp. 288–293, 2012.
- [4] G. Chen, X. Zhang, R. Li et al., "Role of osteopontin in synovial Th17 differentiation in rheumatoid arthritis," *Arthritis and Rheumatism*, vol. 62, no. 10, pp. 2900–2908, 2010.
- [5] M. H. Santamaría and R. S. Corral, "Osteopontin-dependent regulation of Th1 and Th17 cytokine responses in *Trypanosoma cruzi*-infected C57BL/6 mice," *Cytokine*, vol. 61, no. 2, pp. 491–498, 2013.
- [6] S. Kon, Y. Yokosaki, M. Maeda et al., "Mapping of functional epitopes of osteopontin by monoclonal antibodies raised against defined internal sequences," *Journal of Cellular Biochemistry*, vol. 84, no. 2, pp. 420–432, 2002.
- [7] E. S. Sorensen, P. Hojrup, and T. E. Petersen, "Posttranslational modifications of bovine osteopontin: identification of twenty-eight phosphorylation and three O-glycosylation sites," *Protein Science*, vol. 4, no. 10, pp. 2040–2049, 1995.
- [8] R. Agnihotri, H. C. Crawford, H. Haro, L. M. Matrisian, M. C. Havrda, and L. Liaw, "Osteopontin, a novel substrate for matrix metalloproteinase-3 (stromelysin-1) and matrix metalloproteinase-7 (matrilysin)," *Journal of Biological Chemistry*, vol. 276, no. 30, pp. 28261–28267, 2001.
- [9] L. L. Smith and C. M. Giachelli, "Structural requirements for $\alpha 9\beta 1$ -mediated adhesion and migration to thrombin-cleaved osteopontin," *Experimental Cell Research*, vol. 242, no. 1, pp. 351–360, 1998.
- [10] L. Liaw, D. E. Birk, C. B. Ballas, J. S. Whitsitt, J. M. Davidson, and B. L. Hogan, "Altered wound healing in mice lacking a functional osteopontin gene (spp1)," *The Journal of Clinical Investigation*, vol. 101, no. 7, pp. 1468–1478, 1998.
- [11] D. D. Hu, E. C. K. Lin, N. L. Kovach, J. R. Hoyer, and J. W. Smith, "A biochemical characterization of the binding of osteopontin to integrins $\alpha v\beta 1$ and $\alpha v\beta 5$," *The Journal of Biological Chemistry*, vol. 270, no. 44, pp. 26232–26238, 1995.
- [12] S. Denda, L. F. Reichardt, and U. Müller, "Identification of osteopontin as a novel ligand for the integrin $\alpha 8\beta 1$ and potential roles for this integrin-ligand interaction in kidney morphogenesis," *Molecular Biology of the Cell*, vol. 9, no. 6, pp. 1425–1435, 1998.
- [13] Y. Yokosaki and F. Higashikawa, "Osteopontin receptors and signal transduction," *Nippon Rinsho. Japanese Journal of Clinical Medicine*, vol. 63, supplement 10, pp. 613–617, 2005.
- [14] Y. Yokosaki, M. Kido, N. Nagata et al., "Hypoglycemia associated with localized fibrous mesothelioma of the pleura," *Journal of UOEH*, vol. 17, no. 3, pp. 191–197, 1995.
- [15] P. M. Green, S. B. Ludbrook, D. D. Miller, C. M. T. Horgan, and S. T. Barry, "Structural elements of the osteopontin SVVYGLR motif important for the interaction with $\alpha 4$ integrins," *FEBS Letters*, vol. 503, no. 1, pp. 75–79, 2001.
- [16] N. Ito, H. Obata, and S. Saito, "Spinal microglial expression and mechanical hypersensitivity in a postoperative pain model: comparison with a neuropathic pain model," *Anesthesiology*, vol. 111, no. 3, pp. 640–648, 2009.
- [17] J. Morimoto, S. Kon, Y. Matsui, and T. Uede, "Osteopontin; as a target molecule for the treatment of inflammatory diseases," *Current Drug Targets*, vol. 11, no. 4, pp. 494–505, 2010.
- [18] J. Grassinger, D. N. Haylock, M. J. Storan et al., "Thrombin-cleaved osteopontin regulates hemopoietic stem and progenitor cell functions through interactions with $\alpha 9\beta 1$ and $\alpha 4\beta 1$ integrins," *Blood*, vol. 114, no. 1, pp. 49–59, 2009.
- [19] Y. Yokosaki and D. Sheppard, "Mapping of the cryptic integrin-binding site in osteopontin suggests a new mechanism by which thrombin can regulate inflammation and tissue repair," *Trends in Cardiovascular Medicine*, vol. 10, no. 4, pp. 155–159, 2000.
- [20] B. Desai, M. J. Rogers, and M. A. Chellaiyah, "Mechanisms of osteopontin and CD44 as metastatic principles in prostate cancer cells," *Molecular Cancer*, vol. 6, article 18, pp. 1–16, 2007.
- [21] K. A. Iczkowski, "Cell adhesion molecule CD44: its functional roles in prostate cancer," *American Journal of Translational Research*, vol. 3, no. 1, pp. 1–7, 2010.
- [22] M. Franchini and P. M. Mannucci, "Thrombin and cancer: from molecular basis to therapeutic implications," *Seminars in Thrombosis and Hemostasis*, vol. 38, no. 1, pp. 95–101, 2012.
- [23] Z. Mi, T. Oliver, H. Guo, C. Gao, and P. C. Kuo, "Thrombin-cleaved COOH-terminal osteopontin peptide binds with cyclophilin C to CD147 in murine breast cancer cells," *Cancer Research*, vol. 67, no. 9, pp. 4088–4097, 2007.
- [24] P. Y. Wai and P. C. Kuo, "Osteopontin: regulation in tumor metastasis," *Cancer and Metastasis Reviews*, vol. 27, no. 1, pp. 103–118, 2008.
- [25] D. R. Senger and C. A. Perruzzi, "Cell migration promoted by a potent GRGDS-containing thrombin-cleavage fragment of osteopontin," *Biochimica et Biophysica Acta (BBA)—Molecular Cell Research*, vol. 1314, no. 1-2, pp. 13–24, 1996.

- [26] T. C. Fok, H. Lapointe, A. B. Tuck et al., "Expression and localization of osteopontin, homing cell adhesion molecule/CD44, and integrin $\alpha_5\beta_1$ in mucoepidermoid carcinoma and acinic cell adenocarcinoma of salivary gland origin," *Oral Surgery, Oral Medicine, Oral Pathology and Oral Radiology*, vol. 118, no. 3, pp. 320–329, 2014.
- [27] Y. Yamaguchi, Z. Shao, S. Sharif et al., "Thrombin-cleaved fragments of osteopontin are overexpressed in malignant glial tumors and provide a molecular niche with survival advantage," *Journal of Biological Chemistry*, vol. 288, no. 5, pp. 3097–3111, 2013.
- [28] M. S. Beausoleil, E. B. Schulze, D. Goodale, C. O. Postenka, and A. L. Allan, "Deletion of the thrombin cleavage domain of osteopontin mediates breast cancer cell adhesion, proteolytic activity, tumorigenicity, and metastasis," *BMC Cancer*, vol. 11, article 25, pp. 1–12, 2011.
- [29] M. Hasegawa, T. Segawa, M. Maeda, T. Yoshida, and A. Sudo, "Thrombin-cleaved osteopontin levels in synovial fluid correlate with disease severity of knee osteoarthritis," *The Journal of Rheumatology*, vol. 38, no. 1, pp. 129–134, 2011.
- [30] A. Chiochetti, C. Comi, M. Indelicato et al., "Osteopontin gene haplotypes correlate with multiple sclerosis development and progression," *Journal of Neuroimmunology*, vol. 163, no. 1–2, pp. 172–178, 2005.
- [31] C. Comi, G. Cappellano, A. Chiochetti et al., "The impact of osteopontin gene variations on multiple sclerosis development and progression," *Clinical and Developmental Immunology*, vol. 2012, Article ID 212893, 6 pages, 2012.
- [32] D. Chabas, S. E. Baranzini, D. Mitchell et al., "The influence of the proinflammatory cytokine, osteopontin, on autoimmune demyelinating disease," *Science*, vol. 294, no. 5547, pp. 1731–1735, 2001.
- [33] L. Steinman, "Blocking adhesion molecules as therapy for multiple sclerosis: natalizumab," *Nature Reviews Drug Discovery*, vol. 4, no. 6, pp. 510–518, 2005.
- [34] E. M. Hur, S. Youssef, M. E. Haws, S. Y. Zhang, R. A. Sobel, and L. Steinman, "Osteopontin-induced relapse and progression of autoimmune brain disease through enhanced survival of activated T cells," *Nature Immunology*, vol. 8, no. 1, pp. 74–83, 2007.
- [35] O. Beilin, D. M. Karussis, A. D. Korczyn et al., "Increased thrombin inhibition in experimental autoimmune encephalomyelitis," *Journal of Neuroscience Research*, vol. 79, no. 3, pp. 351–359, 2005.
- [36] D. Davalos, J. K. Ryu, M. Merlino et al., "Fibrinogen-induced perivascular microglial clustering is required for the development of axonal damage in neuroinflammation," *Nature Communications*, vol. 3, article 1227, 15 pages, 2012.
- [37] D. Davalos, K. M. Baeten, M. A. Whitney et al., "Early detection of thrombin activity in neuroinflammatory disease," *Annals of Neurology*, vol. 75, no. 2, pp. 303–308, 2014.
- [38] M. H. Han, S.-I. Hwang, D. B. Roy et al., "Proteomic analysis of active multiple sclerosis lesions reveals therapeutic targets," *Nature*, vol. 451, no. 7182, pp. 1076–1081, 2008.
- [39] R. Di Niro, F. Ziller, F. Florian et al., "Construction of miniantibodies for the in vivo study of human autoimmune diseases in animal models," *BMC Biotechnology*, vol. 7, article 46, pp. 1–10, 2007.
- [40] S. Boscolo, F. Mion, M. Licciulli et al., "Simple scale-up of recombinant antibody production using an UCOE containing vector," *New Biotechnology*, vol. 29, no. 4, pp. 477–484, 2012.
- [41] K. L. DeCicco-Skinner, G. H. Henry, C. Cataisson et al., "Endothelial cell tube formation assay for the in vitro study of angiogenesis," *Journal of Visualized Experiments*, no. 91, Article ID e51312, pp. 1–8, 2014.
- [42] G. Cappellano, A. D. Woldetsadik, E. Orilieri et al., "Subcutaneous inverse vaccination with PLGA particles loaded with a MOG peptide and IL-10 decreases the severity of experimental autoimmune encephalomyelitis," *Vaccine*, vol. 32, no. 43, pp. 5681–5689, 2014.
- [43] S. Ashkar, G. F. Weber, V. Panoutsakopoulou et al., "Eta-1 (osteopontin): an early component of type-1 (cell-mediated) immunity," *Science*, vol. 287, no. 5454, pp. 860–864, 2000.
- [44] H. Cantor and M. L. Shinohara, "Regulation of T-helper-cell lineage development by osteopontin: the inside story," *Nature Reviews Immunology*, vol. 9, no. 2, pp. 137–141, 2009.
- [45] R. Vaschetto, S. Nicola, C. Olivieri et al., "Serum levels of osteopontin are increased in SIRS and sepsis," *Intensive Care Medicine*, vol. 34, no. 12, pp. 2176–2184, 2008.
- [46] E. Boggio, M. Indelicato, E. Orilieri et al., "Role of tissue inhibitor of metalloproteinases-1 in the development of autoimmune lymphoproliferation," *Haematologica*, vol. 95, no. 11, pp. 1897–1904, 2010.
- [47] A. Chiochetti, M. Indelicato, T. Bensi et al., "High levels of osteopontin associated with polymorphisms in its gene are a risk factor for development of autoimmunity/lymphoproliferation," *Blood*, vol. 103, no. 4, pp. 1376–1382, 2004.
- [48] D. R. Senger, S. R. Ledbetter, K. P. Claffey, A. Papadopoulos-Sergiou, C. A. Perruzzi, and M. Detmar, "Stimulation of endothelial cell migration by vascular permeability factor/vascular endothelial growth factor through cooperative mechanisms involving the $\alpha_5\beta_1$ integrin, osteopontin, and thrombin," *The American Journal of Pathology*, vol. 149, no. 1, pp. 293–305, 1996.
- [49] G. Murugaiyan, A. Mittal, and H. L. Weiner, "Increased osteopontin expression in dendritic cells amplifies IL-17 production by CD4+ T cells in experimental autoimmune encephalomyelitis and in multiple sclerosis," *Journal of Immunology*, vol. 181, no. 11, pp. 7480–7488, 2008.
- [50] F. Zhao, Y. Zhang, H. Wang et al., "Blockade of osteopontin reduces alloreactive CD8+ T cell-mediated graft-versus-host disease," *Blood*, vol. 117, no. 5, pp. 1723–1733, 2011.
- [51] N. Yamamoto, F. Sakai, S. Kon et al., "Essential role of the cryptic epitope SLAYGLR within osteopontin in a murine model of rheumatoid arthritis," *The Journal of Clinical Investigation*, vol. 112, no. 2, pp. 181–188, 2003.
- [52] D. Leali, P. Dell'Era, H. Stabile et al., "Osteopontin (Eta-1) and fibroblast growth factor-2 cross-talk in angiogenesis," *The Journal of Immunology*, vol. 171, no. 2, pp. 1085–1093, 2003.
- [53] Y.-H. Lin and H.-F. Yang-Yen, "The osteopontin-CD44 survival signal involves activation of the phosphatidylinositol 3-kinase/Akt signaling pathway," *The Journal of Biological Chemistry*, vol. 276, no. 49, pp. 46024–46030, 2001.
- [54] M. Scatena, M. Almeida, M. L. Chaisson, N. Fausto, R. F. Nicosia, and C. M. Giachelli, "NF- κ B mediates $\alpha v\beta 3$ integrin-induced endothelial cell survival," *Journal of Cell Biology*, vol. 141, no. 4, pp. 1083–1093, 1998.
- [55] M. J. McGeachy, K. S. Bak-Jensen, Y. Chen et al., "TGF- β and IL-6 drive the production of IL-17 and IL-10 by T cells and restrain T_H-17 cell-mediated pathology," *Nature Immunology*, vol. 8, no. 12, pp. 1390–1397, 2007.
- [56] R. Mesturini, C. L. Gigliotti, E. Orilieri et al., "Differential induction of IL-17, IL-10, and IL-9 in human T helper cells by B7h and B7.1," *Cytokine*, vol. 64, no. 1, pp. 322–330, 2013.

- [57] D. R. Senger, C. A. Perruzzi, M. Streit, V. E. Kotliansky, A. R. De Fougères, and M. Detmar, "The $\alpha_1\beta_1$ and $\alpha_2\beta_1$ integrins provide critical support for vascular endothelial growth factor signaling, endothelial cell migration, and tumor angiogenesis," *The American Journal of Pathology*, vol. 160, no. 1, pp. 195–204, 2002.
- [58] J. Dai, L. Peng, K. Fan et al., "Osteopontin induces angiogenesis through activation of PI3K/AKT and ERK1/2 in endothelial cells," *Oncogene*, vol. 28, no. 38, pp. 3412–3422, 2009.
- [59] M. H. J. Vogt, L. Lopatinskaya, M. Smits, C. H. Polman, and L. Nagelkerken, "Elevated osteopontin levels in active relapsing-remitting multiple sclerosis," *Annals of Neurology*, vol. 53, no. 6, pp. 819–822, 2003.
- [60] C. Sinclair, M. Mirakhur, J. Kirk, M. Farrell, and S. McQuaid, "Up-regulation of osteopontin and α B-crystallin in the normal-appearing white matter of multiple sclerosis: an immunohistochemical study utilizing tissue microarrays," *Neuropathology and Applied Neurobiology*, vol. 31, no. 3, pp. 292–303, 2005.
- [61] M. Carecchio and C. Comi, "The role of osteopontin in neurodegenerative diseases," *Journal of Alzheimer's Disease*, vol. 25, no. 2, pp. 179–185, 2011.

Proteasome cleavage of OPN

After investigating the role of thrombin cleavage on OPN and demonstrating *in vitro* and *in vivo* that OPN-N and OPN-C exert different functions on MS pathological processes, we decided to take into account another protease that may act on OPN, that is proteasome.

The study of proteasome-cleavage of OPN is important for the investigation on the products of proteasome-digestion. Indeed, the generated OPN peptides may play different roles and some of them may display a gain of function, compared to the whole protein, because of the exposure of particular binding sites that become unmasked.

The ubiquitin-proteasome system is responsible for destruction of the majority of cytoplasmic proteins, exerting housekeeping functions and maintaining cellular homeostasis (Bellavista et al. 2014). Proteins are usually targeted by enzyme-mediated poly-ubiquitination, carried into the proteasome proteolytic chamber, fragmented and expelled (Schwartz and Ciechanover 2009). Poly-ubiquitin tagging (when it occurs), transport and peptide-bond hydrolysis regulate protein half-life and thereby affect the majority of metabolic processes in the cell. Proteins that reflect particular stress conditions, proteins involved in cell cycle progression, cellular growth control, and oncogenesis, are some of the many proteins regulated by the complex of 20S proteasome (Ben-Nissan and Sharon 2014). The 20S (700-kDa) standard proteasome (s-proteasome) is a dynamic enzyme with an activity that varies over time because of interactions between substrates and products and the proteolytic and regulatory sites. It is a cylinder-shaped complex, composed of four stacked rings, each consisting of seven protein subunits. Among them the $\beta 1$, $\beta 2$, and $\beta 5$ subunits harbour the proteolytic active sites (Voges, Zwickl, and Baumeister 1999). The 26S (2000-

kDa) complex contains in addition to the 20S proteasome a 19S regulatory complex composed of multiple ATPases and components necessary for binding protein substrates (Structure and functions of the 20S and 26S proteasomes (Coux, Tanaka, and Goldberg 1996).

Mathematical modelling approaches have been proposed for a mechanistic analysis of proteasome, in order to point out its activity. Obtained results show that proteasome digestion velocity is dependent on mechanisms of transport inside and outside the proteolytic chamber. Moreover, proteasome activity is mediated by regulatory sites (Liepe et al. 2015).

The immunoproteasome (i-proteasome) is an isoform of the 20S proteasome. When a cell experiences inflammation, proteasomes can change some of their subunits and form an i-proteasome. It carries specific catalytic subunits, $\beta 1i$, $\beta 2i$, and $\beta 5i$, which confer to the i-proteasome quicker proteins digestion and differences in cleavage preferences and substrate degradation rates, compared to the s-proteasome. I-proteasome is generally synthesized upon interferon- γ (IFN- γ) stimuli, but tumor necrosis factor- α (TNF- α) or lipopolysaccharide has also been found to be involved in its inducible expression (Pintado et al. 2012; Ferrington and Gregerson 2012). The vast majority of endogenous peptides presented by the MHC class I molecules at the cell surface and recognised by CD8⁺ T cells are generated by proteasomes. I-proteasome is generally highly efficient in generating MHC class I-restricted epitopes. In support to this, i-proteasomes are predominantly expressed by professional antigen presenting cells (APCs), such as dendritic cells (DCs) and B cells, or by other cell types during inflammation (Ebstein et al. 2012; Qureshi, Morrison, and Reis 2012). Previous studies demonstrated an accumulation of i-proteasome and its regulator PA28 $\alpha\beta$ in different cell types of MS patients, such as oligodendrocytes,

macrophages/microglia, infiltrating lymphocytes, and weakly neurons (Mishto et al. 2010). Such disease-related expression of i-proteasome is in agreement with recent observations in EAE. In this model, the cerebral expression of i-proteasome and PA28 $\alpha\beta$ was increased as compared with baseline levels during the acute phase of EAE (Zheng, Dasgupta, and Bizzozero 2012). The expression of i-proteasome in MS lesions or in cells involved in MS mechanisms is important because this isoform was recently linked to different inflammatory processes. Indeed, i-proteasomes are specifically implicated in cytokine-mediated inflammation, cell growth, and differentiation in mice (Ebstein et al. 2012). I-proteasome depletion alters the T cell antigen receptor (TCR) repertoire formation, the number and differentiation of CD8⁺ T cells, and the production of proinflammatory cytokines (Groettrup, Kirk, and Basler 2010). Also the activity of Th-17 cells could be regulated by gut microbiota and i-proteasome, in EAE. Moreover, it may influence onset and progression of MS by affecting the response of different cell types to the inflammatory aggression in the CNS. The i-proteasome exists also in an extracellular form, that is proteolytically active, but whose role as well as its cellular origin and mechanisms of release remain elusive (Sixt and Dahlmann 2008; Zoeger et al. 2006). In patients with solid tumors, extracellular proteasome levels increase and correlate with occurrence, severity, as well as clinical outcome of the diseases (L Henry et al. 2009; Laurent Henry et al. 2013; de Martino et al. 2012). In some autoimmune diseases, including MS, the levels of extracellular proteasome are increased and mark cell damage and immunological activity (Egerer et al. 2002; Minagar et al. 2012). Therefore, proteasome is largely involved in MS development and the study of proteasome-related biomarkers, such as proteasome antibodies and circulating proteasome, may represent a field of interest in MS.

PAPER 2

Background: OPN is involved in several diseases including MS. Secreted OPN is cleaved by few known proteases, modulating its pro-inflammatory activities. The proteasome, involved in processes aimed at eliminating cellular waste products, may cleave OPN. Moreover, high levels of extracellular proteasome were detected in MS patients, thereby the function of OPN and proteasome may be related.

Aim: The aim of this work was to investigate whether secreted OPN can be processed by extracellular proteasome, thereby producing fragments with novel chemotactic activity.

Methods: Proteasome digestion products of OPN-C were obtained and analyzed by mass spectrometry. The effect of proteasome digestion-derived peptides was assessed *in vitro* on migration of HUVECs, lymphocytes and monocytes.


Results: In HUVECs and monocytes, the treatment with 20S proteasome significantly hampered the chemotactic activity of OPN-N, whereas it increased the chemotactic activity of OPN-FL and, especially, OPN-C on HUVEC and lymphocytes. This suggests that proteasome-mediated degradation of OPN-FL and OPN-C generates novel OPN chemotactic fragments. The analysis of proteasome digestion of OPN-C detected 6 main fragments, which were then synthesized and analyzed for their chemotactic activity. Four of these peptides exerted a strong chemotactic activity towards HUVEC and lymphocytes in a dose-dependent manner. Since the levels of both the extracellular proteasome and OPN are increased in MS patients, these data suggest that these peptides may play a role in MS.

Furthermore, OPN reduced the release of proteasomes in the extracellular space. The latter phenomenon seems to occur *in vivo* in multiple sclerosis,

where it reflects the remission/relapse alternation.

Conclusion: The extracellular proteasome-mediated inflammatory pathway may represent a general mechanism to control inflammation in inflammatory diseases.

SCIENTIFIC REPORTS



OPEN

Extracellular proteasome-osteopontin circuit regulates cell migration with implications in multiple sclerosis

Received: 11 October 2016

Accepted: 27 January 2017

Published: 09 March 2017

Chiara Dianzani^{1,*}, Elena Bellavista^{2,*}, Juliane Liepe³, Claudia Verderio^{4,5}, Morena Martucci², Aurelia Santoro², Annalisa Chiocchetti⁶, Casimiro Luca Gigliotti⁶, Elena Boggio⁶, Benedetta Ferrara¹, Loredana Riganti⁶, Christin Keller^{7,8}, Katharina Janek⁷, Agathe Niewianda⁷, Chiara Fenoglio⁹, Melissa Sorosina¹⁰, Roberto Cantello¹¹, Peter M. Kloetzel^{7,8}, Michael P. H. Stumpf³, Friedemann Paul^{12,13,14}, Klemens Ruprecht^{13,15}, Daniela Galimberti⁹, Filippo Martinelli Boneschi¹⁰, Cristoforo Comi^{6,11}, Umberto Dianzani⁶ & Michele Mishto^{7,8,16}

Osteopontin is a pleiotropic cytokine that is involved in several diseases including multiple sclerosis. Secreted osteopontin is cleaved by few known proteases, modulating its pro-inflammatory activities. Here we show by *in vitro* experiments that secreted osteopontin can be processed by extracellular proteasomes, thereby producing fragments with novel chemotactic activity. Furthermore, osteopontin reduces the release of proteasomes in the extracellular space. The latter phenomenon seems to occur *in vivo* in multiple sclerosis, where it reflects the remission/relapse alternation. The extracellular proteasome-mediated inflammatory pathway may represent a general mechanism to control inflammation in inflammatory diseases.

Osteopontin (OPN), a component of bone matrix and a soluble pleiotropic cytokine, plays a pivotal role in several diseases such as tumors, myocardial and kidney dysfunctions, and autoimmune diseases. OPN has a particular relevance in multiple sclerosis (MS), a disease in which the autoimmune response targets the myelin sheaths of the central nervous system (CNS)¹. Indeed, in MS secreted OPN stimulates the expression of Th1 and Th17 cytokines, inhibits apoptosis of autoreactive T cells, and regulates leukocyte adhesion, migration, and trafficking into the CNS by binding to CD44 and various integrins². Increased concentrations of OPN occur in peripheral

¹Department of Drug Science and Technology, University of Turin, 10126 Torino, Italy. ²Department of Experimental, Diagnostic and Specialty Medicine (DIMES), University of Bologna, 40126 Bologna, Italy. ³Centre for Integrative Systems Biology and Bioinformatics, Department of Life Sciences, Imperial College London, SW7 2AZ London, UK. ⁴Institute of Neuroscience, Centro Nazionale delle Ricerche (CNR), 20129 Milano, Italy. ⁵IRCCS Humanitas, 20089 Rozzano, Italy. ⁶Interdisciplinary Research Centre of Autoimmune Diseases (IRCAD), University of Piemonte Orientale, Amedeo Avogadro, 28100 Novara, Italy. ⁷Institut für Biochemie, Charité - Universitätsmedizin Berlin, 10117 Berlin, Germany. ⁸Berlin Institute of Health, 10117 Berlin, Germany. ⁹Neurology Unit, Department of Pathophysiology and Transplantation, University of Milan, "Dino Ferrari" Centre, Fondazione IRCCS Cà Granda, Ospedale Maggiore Policlinico, 20100 Milano, Italy. ¹⁰Department of Neuro-rehabilitation and Laboratory of genetics of Neurological complex disorders, Institute of Experimental Neurology (INSPE) Scientific Institute San Raffaele, 20132 Milano, Italy. ¹¹Department of Translational Medicine, Section of Neurology, University of Piemonte Orientale, 28100 Novara, Italy. ¹²AG Klinische Neuroimmunologie des Neurocure Clinical Research Center, Charité - Universitätsmedizin Berlin, 10117 Berlin, Germany. ¹³Clinical and Experimental Multiple Sclerosis Research Centre - Universitätsmedizin Berlin, 10117 Berlin, Germany. ¹⁴Experimental and Clinical Research Center, Max Delbrueck Center for Molecular Medicine and Charité - Universitätsmedizin Berlin, Berlin, Germany. ¹⁵Department of Neurology, Charité - Universitätsmedizin Berlin, 10117 Berlin, Germany. ¹⁶Department of Health Science, University of Piemonte Orientale, 28100 Novara, Italy. *These authors contributed equally to this work. Correspondence and requests for materials should be addressed to M.M. (email: michele.mishto@charite.de)

blood and cerebrospinal fluid during the relapse phase in MS patients^{3–5}. Moreover, OPN is strongly expressed in MS lesions. A similar phenomenon occurs also in the experimental autoimmune encephalomyelitis (EAE), an MS mouse model in which the administration of the OPN results in rapid induction of relapse, increased level of neurological defects and progression of the disease⁶.

Secreted OPN molecules are cleaved by matrix metalloproteinases and thrombin¹. Thrombin cleaves the full length OPN (OPN-FL) into N-terminal (OPN-N) and C-terminal (OPN-C) fragments, which exert different biological activities^{1,7,8}. Another protease present in different types of biological fluids, including blood, is the 20S proteasome. Depending on its incorporated catalytic subunit pattern proteasome is named as either standard proteasome, intermediate-type proteasome or immunoproteasome. Standard proteasome is the most common proteasome isoform, whereas intermediate-type proteasome and immunoproteasome are expressed during inflammation or in immune cells⁹. The proteasome isoforms possess different proteolytic dynamics^{10–12}. The difference in protein turnover results in preferential tasks carried out by either standard proteasome or immunoproteasome. For instance, immunoproteasome specifically regulates some aspects of the cytokine-mediated inflammation and cell-mediated immunity⁹. It is generally believed that these immunological tasks are carried out by the proteasome only as intracellular protease; indeed, the role of extracellular proteasomes as well as their cellular origin and the mechanisms of release remain elusive¹³. However, it is known that extracellular proteasome purified from plasma is proteolytically active¹⁴. Active release rather than passive leakage from injured/apoptotic cells was suggested to cause the early increase of extracellular proteasome levels in sepsis and severe injury¹⁵. Active mechanisms of proteasome release have been proposed through various types of extracellular vesicles (EVs), *i.e.* microparticle/ectosomes shedding from the surface of T lymphocytes¹⁶, or exosomes derived from endocytic compartments of mesenchymal stem cells¹⁷. In patients with solid tumors and hematological malignancies, extracellular proteasome levels increase and correlate with occurrence, severity, as well as clinical outcome of the diseases^{18–20}. In some autoimmune diseases, such as rheumatoid arthritis, MS and systemic lupus erythematosus, extracellular proteasome levels are increased and are markers of cell damage and immunological activity^{21,22}.

No function of proteasome in the extracellular space has been demonstrated so far.

Results and Discussion

20S proteasome processes OPN molecules and modulates their chemotactic activities. To investigate whether extracellular proteasome could be involved in the OPN-mediated inflammatory events, we first investigate whether 20S proteasome can fragment OPN molecules in an ubiquitin-independent manner. We use purified 20S proteasome because there is no evidence that the entire ubiquitin-proteasome system is present and functional in the extracellular space. Furthermore, 20S proteasome is the only active proteasome form that has been identified in extracellular microparticles¹⁶. Therefore, we perform *in vitro* degradation of different portions of recombinant OPNs, *i.e.* OPN-FL (OPN-FL_{17–314}-6His), OPN-N (OPN-FL_{17–168}-6His) and OPN-C (OPN-FL_{169–314}-6His) by purified erythrocyte 20S standard proteasomes. Testing different ratios of proteasome/OPNs, we observe a concentration-dependent degradation of OPN substrates, thereby showing that 20S standard proteasome can cleave OPNs outside the cell in an ubiquitin-independent manner (Fig. 1a and Supplementary Fig. 1). Furthermore, we investigate the degradation rate of the three OPNs by using 20S standard proteasome derived from a different cell source, *i.e.* derived from T2 cells. Thereby we verify that the OPN processing is not a singularity of erythrocyte 20S standard proteasome (Fig. 1b and Supplementary Fig. 1).

Since a key function of OPNs during inflammation is the regulation of cell chemotaxis, we study whether proteasome-mediated processing of OPNs affects the *in vitro* chemotaxis of different cell types, *i.e.* human umbilical vein endothelial cells (HUVEC), peripheral blood lymphocytes (PBLs) and monocytes (PBM). These cells are recruited through OPN-mediated chemotaxis to the inflammation site in different physiological and pathological conditions. HUVECs are a standardized model for investigating the behavior of vascular endothelial cells, which are key players in inflammation by regulating inflammatory cell trafficking. Furthermore, the migration of PBLs and PBMs in the CNS is considered to be an important pathological inflammatory factor for the MS development.

HUVECs, PBLs and PBMs are treated with OPNs pre-incubated or not with 20S proteasomes. The chemotaxis is measured in a Boyden chamber migration assay after 20 h (Fig. 2a). We use as positive control the well-known chemotactic factors VEGF- α for the HUVECs and RANTES for PBLs and PBMs.

In HUVECs, the presence of 20S proteasome significantly hampers the chemotactic stimulus by OPN-N whereas OPN-FL and OPN-C gain chemotactic activity upon proteasome digestion. Proteasome has only marginal effects *per se* on spontaneous migration or in the chemotaxis induced by VEGF- α (Fig. 2a). 20S proteasome also significantly hampers the chemotaxis of PBLs induced by OPN-N, whereas it boosts the chemotaxis upon processing of OPN-FL and OPN-C. The proteasome has neither effects *per se* on chemotaxis nor on the RANTES-induced chemotaxis (Fig. 2b). Similar effects of proteasome-catalyzed OPN cleavage are observed in PBMs; indeed, proteasome-mediated digestion of OPN-N significantly reduces its chemotactic activity, whereas it significantly enhances the PBMs' chemotaxis induced by OPN-FL and OPN-C. Proteasome has no effect in absence of OPNs but it reduces, mildly although significantly, the chemotactic activity of RANTES in PBMs (Fig. 2c).

Specific proteasome-generated fragments of the OPN-C stimulate HUVEC and PBL chemotaxis. The fact that 20S proteasome can cleave OPN-FL and OPN-C thereby increasing their chemotactic activity suggests that 20S proteasome-catalyzed degradation of OPN-FL and OPN-C might unmask cryptic OPN chemotactic fragments. Such fragments would then be able to activate chemotaxis better than when they were included and folded in the OPN-FL. Similar mechanism has been proposed for the activation of other cryptic sites of OPN-FL upon processing by thrombin^{2,7}.

To identify these active fragments, we digest recombinant OPN-C by 20S proteasome and analyze the products by mass spectrometry. Among more than hundred identified fragments (data not shown), we select 6 fragments,

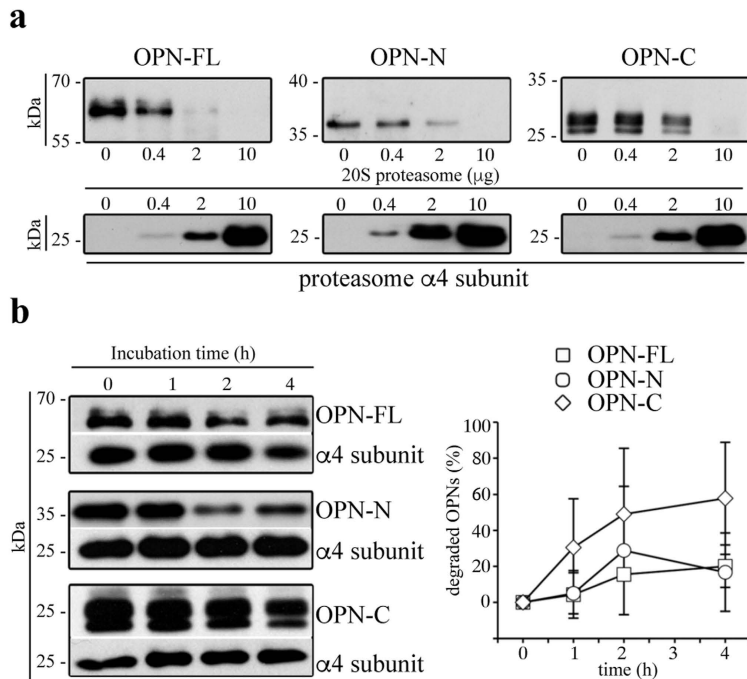


Figure 1. Extracellular 20S standard proteasomes cleave OPN molecules. (a) Representative *in vitro* digestion ($n = 3$) of recombinant OPN-FL, OPN-N, OPN-C by different amount of human erythrocyte 20S standard proteasomes. (b) Degradation kinetics of OPN-FL, OPN-N and OPN-C by T2 20S standard proteasomes are shown by representative Western Blot assay (left panel; the proteasome $\alpha 4$ subunit is used as control marker since it is incorporated in each proteasome). The density of the Western Blot bands is measured and the corresponding relative OPNs' degradation computed (right panel; mean and SD of 4–5 independent experiments measured in duplicate). The relevant bands of the Western Blot assays shown here are cropped from the full blots shown in Supplementary Fig. 1. No significant differences between the degradation rate of the three OPNs are observed by Kruskal-Wallis test. In (b) we use a ratio OPNs/proteasome that roughly resembles that observed in the peripheral blood of healthy and MS donors (Fig. 5) and that used in the cell migration experiments (Fig. 2).

i.e. OPN-FL₂₁₇₋₂₃₀, OPN-FL₂₄₉₋₂₆₆, OPN-FL₂₆₇₋₂₇₈, OPN-FL₂₆₈₋₂₇₈, OPN-FL₂₈₆₋₃₀₆ and OPN-FL₂₉₂₋₃₀₆ (Fig. 3a), showing dominant mass spectrometry ion peak areas in a 20h degradation of OPN-C by 20S proteasome from erythrocytes (Supplementary Fig. 2). These peptides are synthesized and analyzed for their ability to induce HUVEC chemotaxis. Among them, four peptides – *i.e.* OPN-FL₂₁₇₋₂₃₀, OPN-FL₂₄₉₋₂₆₆, OPN-FL₂₆₇₋₂₇₈ and OPN-FL₂₉₂₋₃₀₆ – exert their chemotactic activity towards HUVECs in a dose-dependent manner (Supplementary Fig. 3). In particular, they are effective at the dose of 100 nM (Fig. 3b), which is likely the maximal OPN fragment concentration generated by extracellular 20S proteasome during our chemotaxis experiments (Fig. 2). Their activity is sequence-dependent, and not only related to chemical properties of the peptides, since control peptides with inverted sequences compared to the functional peptides have no chemotactic activity towards HUVECs (Fig. 3c).

The same response towards the 6 OPN-derived peptides is observed for the cell migration of PBLs. Indeed, the four peptides OPN-FL₂₁₇₋₂₃₀, OPN-FL₂₄₉₋₂₆₆, OPN-FL₂₆₇₋₂₇₈ and OPN-FL₂₉₂₋₃₀₆ are chemoattractant also towards PBLs, whereas the peptides OPN-FL₂₆₈₋₂₇₈, OPN-FL₂₈₆₋₃₀₆ exert no effect (Fig. 3d).

According to the prediction of the OPN-FL 3D structure (Fig. 3e) the four active OPN fragments are either buried in the OPN-FL structure, or part of loops and strongly secondary structured alpha-helices.

OPNs reduce the release of proteasome by endothelial cells in the extracellular space. In biological systems, negative feedback loops exist to control the activity of mediators. Thus, we investigate whether a reciprocal regulation could exist between OPN and extracellular proteasome, whereby OPNs regulate proteasome release in the extracellular space. To this end, we measure the concentration of extracellular proteasome in cultures of HUVECs, PBLs or PBMs upon treatment with the three OPNs, and either VEGF- α or RANTES, respectively. We observe a significant decrease in the extracellular proteasome concentration in the medium of HUVEC cultures upon stimulation with either each of the three OPNs or with VEGF- α compared to untreated cells (Fig. 4). On the contrary, these cytokines do not have any effect on proteasome released by PBLs (Fig. 4); a similar lack of effect is also detected with PBMs (data not shown).

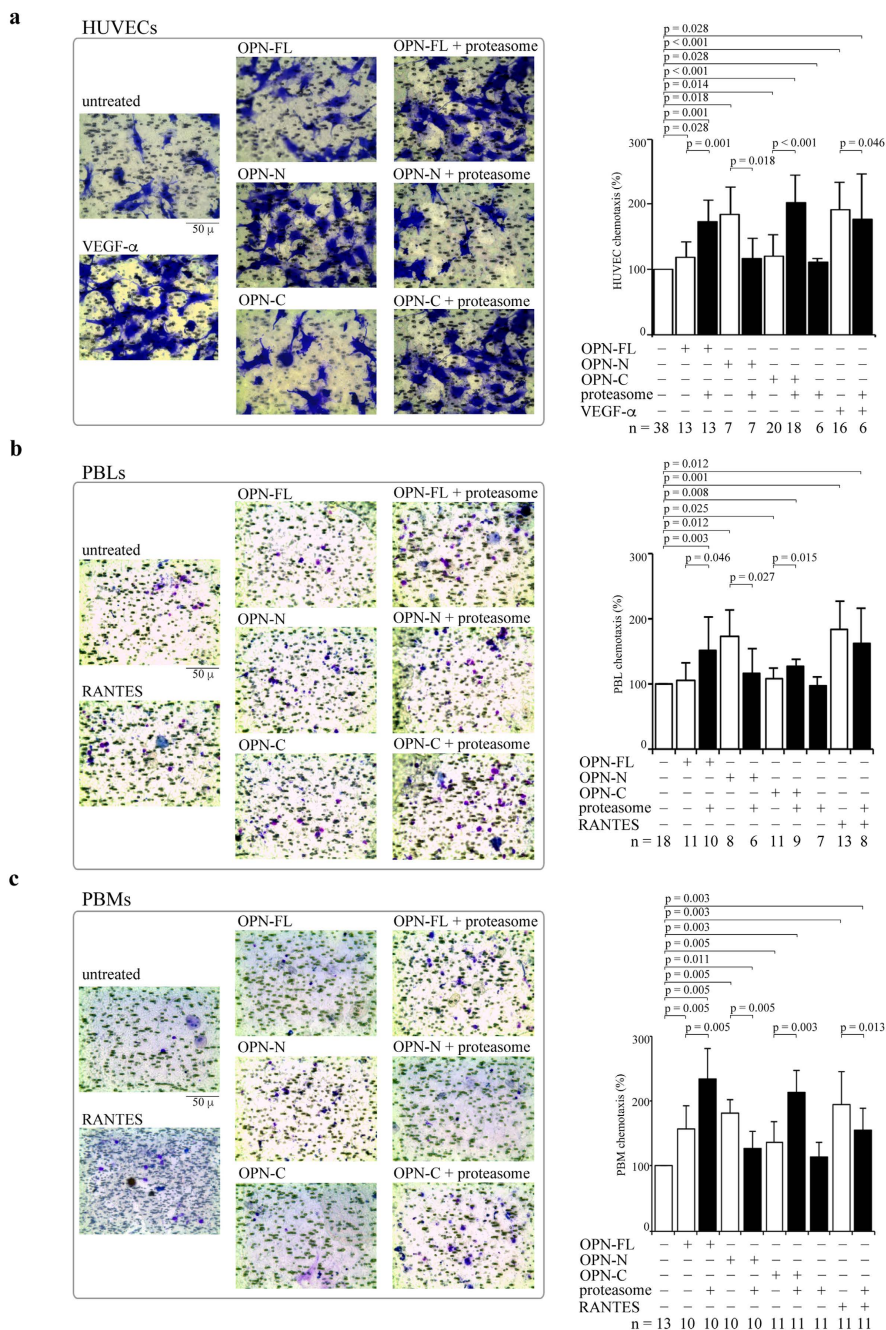


Figure 2. Extracellular proteasome modulates chemotactic activity of OPN molecules. (a) Representative pictures of migrated HUVECs (stained by crystal violet) treated with OPNs \pm 20S proteasome and VEGF- α as positive control on the HUVEC chemotaxis (n = 6–38) is shown. (b) Representative pictures of migrated PBLs treated with OPNs \pm 20S proteasome (and RANTES as positive control) on the chemotaxis of PBLs (n = 6–18) is shown. (c) Representative pictures of migrated PBMs treated with OPNs \pm 20S proteasome (and RANTES as positive control) on the chemotaxis of PBMs (n = 11–13) is shown. In (a–c) cell migration is measured by applying the Boyden chamber migration assay; values are percentage of treated vs untreated cells that migrated after 20 h and are the mean and the SD of independent experiments. Wilcoxon test for paired samples $p < 0.05$ are shown.

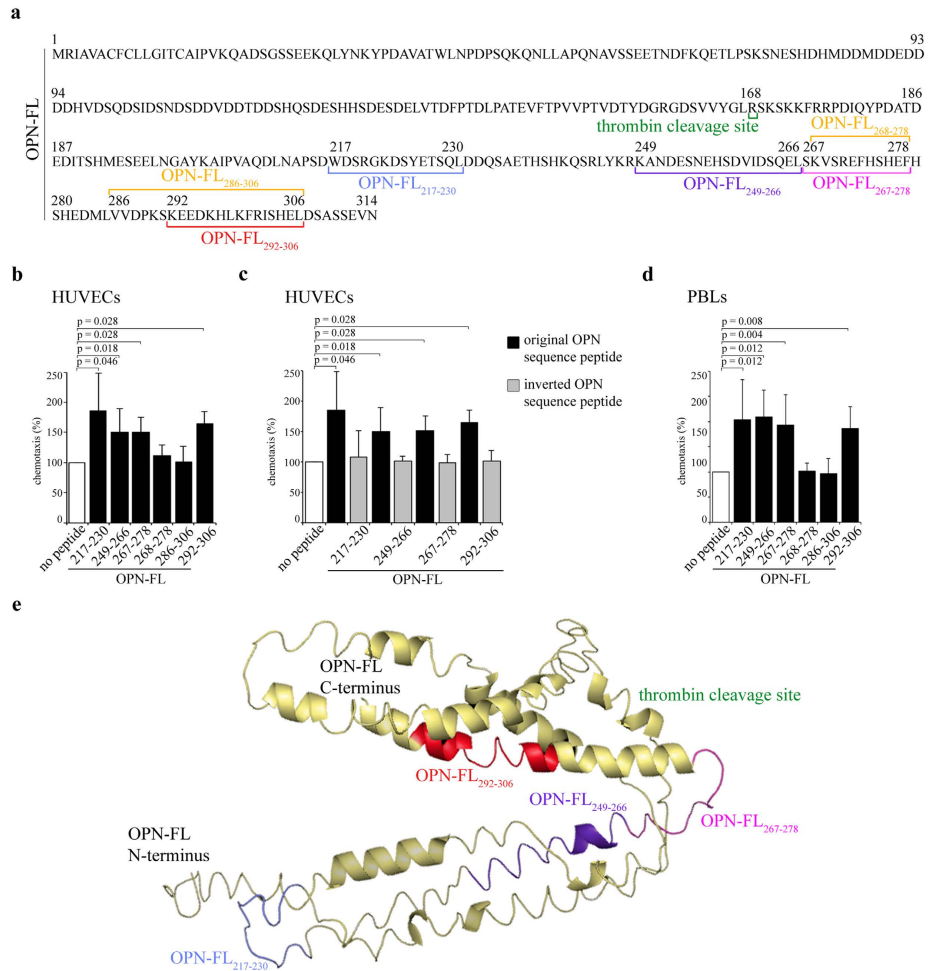


Figure 3. Location and chemotactic effect of proteasome-generated OPN fragments towards HUVECs and PBLs. (a) The sequence of the OPN-FL (P10451.1) and of the studied proteasome-generated OPN fragments is here disclosed. (b) The effect of different OPN fragments (100 nM) on the HUVEC chemotaxis is shown. (c) The comparison between the efficacy of the proteasome-generated OPN fragments and of the corresponding peptides with inverted sequence in inducing chemotaxis in HUVECs is shown. (d) The effect of the studied OPN fragments (50 nM) on the PBL chemotaxis is shown. (b–d) Values are reported as percentage of treated vs untreated cells that have migrated after 20 h and are expressed as the mean and the SD of independent experiments ($n = 4–14$). Cell migration is measured by the Boyden chamber migration assay. Wilcoxon test for paired samples $p < 0.05$ are shown. (e) Tertiary structure prediction of OPN-FL. The predicted structure is shown as a cartoon representation indicating disordered regions and α -helices. Highlighted are the sequences produced by proteasome that show strong chemotactic activity and the thrombin cleavage site; colors correspond to (a). The structure is predicted with I-TASSER server.

An inverse correlation between extracellular OPN and proteasome is confirmed in peripheral blood of RRMS patients. We then verify whether this negative feedback loop between extracellular OPN and proteasome concentration is detectable also *in vivo*. This could be detected through an inverse correlation of extracellular OPN and proteasome concentration. We would expect that the proteasome release is regulated by different factors in non-inflamed and inflamed subjects. In the latter, when OPN function and concentration raises, the impact of OPNs in the release of proteasome might become evident and an inverse correlation between OPN and proteasome concentration should be detectable in bodily fluids. This should be the case in the relapsing-remitting multiple sclerosis (RRMS), which is the most prevalent form of MS, and it is anticipated in 85% of people by an acute onset named clinically isolated syndrome (CIS). RRMS is characterized by disability episodes (relapses) followed by a complete or partial recovery (remission). During (or right before) the relapse

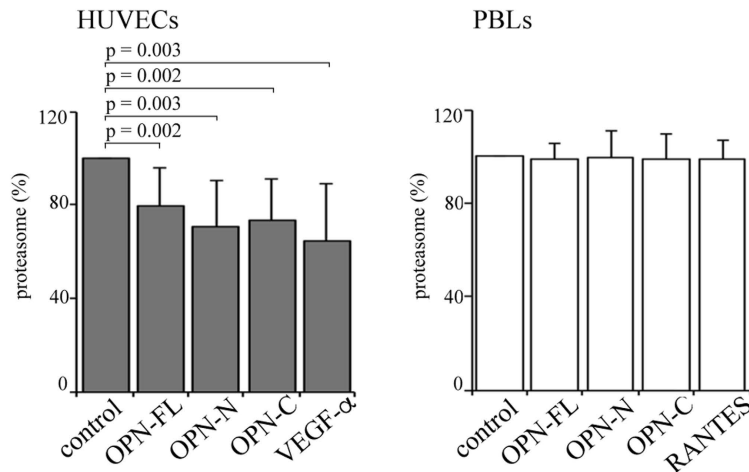


Figure 4. OPNs and VEGF- α partially inhibit the release of proteasome by HUVECs. The proteasome release by HUVECs (left panel) and PBLs (right panel) in serum-free medium with OPN-FL, OPN-N, OPN-C and VEGF- α (with HUVECs) or RANTES (with PBLs) is shown. Values are reported as proteasome concentration ratio of treated vs untreated cells and they correspond to the mean and the SD of independent experiments (HUVECs, $n = 14$; PBLs, $n = 10$) measured by ELISA. Statistically significant variations from the control are detected by Wilcoxon test for paired samples and $p < 0.05$ are annotated.

of RRMS patients, the levels of OPN rise together with the exacerbation of the CNS inflammation, while they decrease in the following remission¹.

In line with our hypothesis, in the sera of a first Italian cohort (Supplementary table 1), we observe a significantly higher concentration of OPNs in RRMS patients in relapse compared to those in remission and healthy donors (Fig. 5a), and a significant inverse non-linear correlation between extracellular proteasome and OPN concentrations by pooling together relapses and remissions (Fig. 5b). To further assess the robustness of this correlation, we perform a bootstrap analysis to obtain confidence intervals. All bootstrap samples show a significant correlation coefficient between 0.25 and 0.55, which assures that the observed correlation is stable to potential outliers (Fig. 5b). This inverse correlation within the RRMS cohort suggests that the dramatic increase of OPN levels in the relapse leads to a corresponding decrease of serum proteasome concentration. According to our hypothesis, such effect should disappear during the remission when the secreted OPN concentration drops. This is indeed what we observe in the serum of the RRMS cohort: the extracellular proteasome levels are significantly higher in Italian RRMS patients in remission compared to those in relapse (Fig. 5c). They are also higher than those measured in healthy controls in agreement with the study of Minagar and colleagues²². This latter observation is confirmed in a second German cohort of RRMS patients in remission compared to healthy donors as well as of CIS patients compared to healthy donors (Fig. 5d).

EVs-free extracellular proteasome varies amongst disease groups. Extracellular vesicles (EVs) have been hypothesized to be one of the mechanisms for the proteasome release in the extracellular space. EVs have been also suggested as the active delivery mechanism of biological mediators in peripheral blood and other bodily fluids of several diseases including MS^{16,23,24}. Hence, we investigate whether serum EVs might be responsible for the differences in extracellular proteasome concentration we observed in RRMS and CIS cohorts compared to healthy donor cohort.

Different factors might affect EV stability in extracellular fluids and lead to difference when plasma and serum are considered²⁵. Therefore, we initially analyze the proteasome content in large vesicles (p2p3, > 100 nm), small vesicle/exosomes (p4 < 100 nm) or all vesicles (p2p4), as well as the corresponding supernatants centrifuged from freshly isolated healthy donor plasma and serum by western blotting. Proteasomes are present in both large and small vesicle fractions and at a similar extent comparing plasma and serum samples (Fig. 6a). By ELISA on healthy donor plasma and serum supernatants, we find that a large portion of extracellular proteasomes is not associated with EVs, both in frozen and fresh samples (Fig. 6b). Accordingly, extracellular proteasomes are mainly present in the EVs-depleted serum in a sub-cohort of both German healthy donors ($n = 11$; mean = $74.4 \pm 14.8\%$) and German CIS patients ($n = 14$; mean = $74.9 \pm 12.0\%$). In the same sub-cohorts, the amount of extracellular proteasomes measured in non-fractionated serum correlates with that of the supernatant after p2p4 separation (Fig. 6c) but not with vesicular proteasomes (p2p4 fraction) (Fig. 6d), thereby suggesting that the variation of extracellular proteasome we detect in the CIS and RRMS patient sera is not due to the EVs' content.

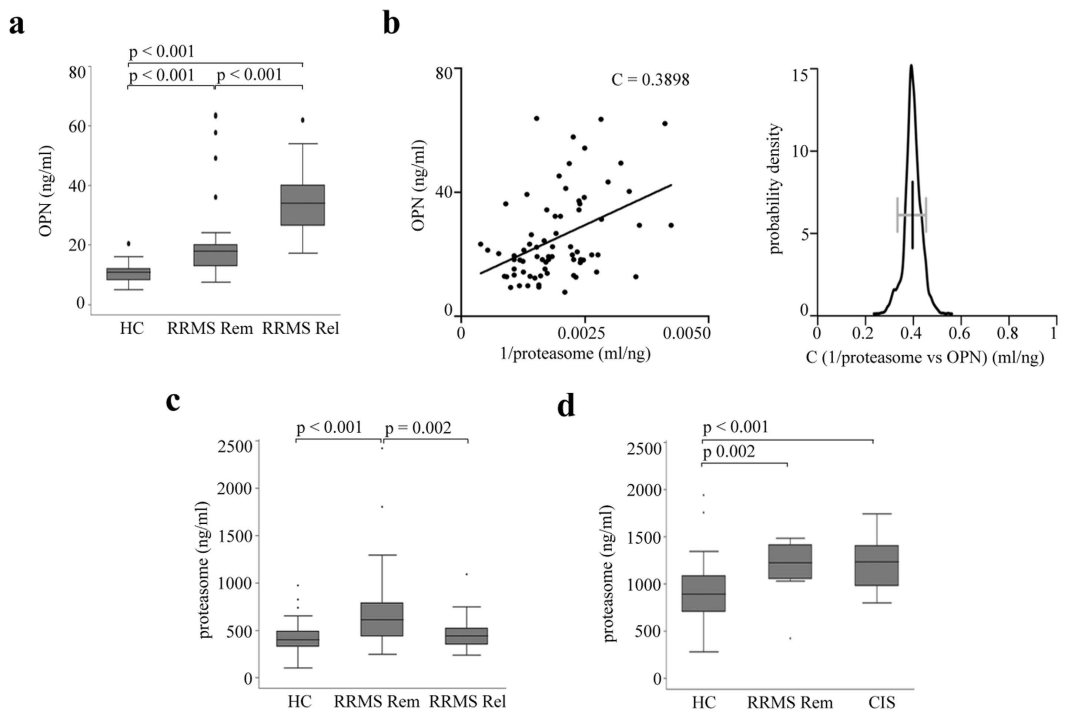


Figure 5. Serum OPN and proteasome levels inversely correlate in RRMS patients. (a) Serum OPN concentration is significantly increased in an Italian cohort of RRMS patients in remission (RRMS Rem, $n = 48$) and relapse (RRMS Rel, $n = 24$) compared to healthy controls (HC; $n = 28$), as well as in RRMS Rel vs RRMS Rem. The Kruskal-Wallis test is applied with a Bonferroni correction for multiple comparisons, and $p < 0.05$ are reported. (b) Serum OPN and proteasome concentration in Italian RRMS patient cohort ($n = 72$) are nonlinearly and inversely correlated as shown by plotting OPN vs $1/\text{extracellular proteasome concentrations}$ (Pearson's test, $p < 0.001$; C value is shown in the chart). Bootstrap test using 1000 samples with 100% of the data shows a significant correlation coefficient between 0.25 and 0.55 (right panel). (c) Serum proteasome concentration in Italian healthy donors ($n = 62$), RRMS patients in remission (RRMS Rem, $n = 50$) or in relapse (RRMS Rel, $n = 25$). (d) Serum proteasome concentration in German healthy controls ($n = 50$), RRMS patients in remission (RRMS Rem, $n = 12$) and CIS patients ($n = 35$). 3–6 technical ELISA replicates for each samples are used in the analysis. Kruskal-Wallis test is applied for multiple comparison with Bonferroni correction and $p < 0.05$ are reported. In (a,c,d) the median, the 25–75 quartiles (the grey box), the 0–100 quartiles (the error bars) and the outliers are shown.

Conclusions

Extracellular proteasome has been proposed as a suitable biomarker in some cancers and autoimmune diseases, potentially allowing for better diagnosis, patient stratification, and prediction of the response to therapy^{18–21}, even though its function is not yet understood. Here, we elucidate one of its potential functions in the extracellular space. The OPN chemotactic activity toward three cell types is indeed enhanced by extracellular proteasome through the release of active OPN fragments during OPN processing. These peptide fragments are buried in the C-terminal portion of OPN-FL. When they are removed from the original protein they have likely lost their secondary conformation and the absence of surrounding bulky structures might facilitate an enhanced binding to chemotactic receptors. This could enhance their chemotactic activity towards migrating cells, such as HUVECs, PBLs and PBMs. Similar mechanism has been proposed for the activation of other cryptic sites of OPN-FL upon processing by thrombin^{2,7}. The action of these novel OPN peptides seems to be sequence-specific since peptides with inverted sequences do not have chemotactic activity and small variations of the sequence alter the peptide efficacy. Indeed, the removal of a single residue from the peptide OPN_{267–278} remarkably reduces its chemotactic activity, whereas the removal of six residues from the peptide OPN_{286–306} confers a stronger chemotactic efficacy to the peptide (Fig. 3 and Supplementary Fig. 3). It is noteworthy that peptide hydrolysis might not be the only mechanism whereby extracellular proteasome modulates OPN activities. Indeed, proteasome is also able to ligate peptide fragments thereby generating novel peptides with sequences that are not present in the parental protein. This process, named proteasome-catalyzed peptide splicing, is much more frequent than expected^{26–28} and it has been already hypothesized to be involved in generating autoimmune epitopes in diseases such as MS^{29,30}. Although proteasome-generated spliced peptides have been investigated so far only as target of T cell response, they might have other functions and cells might use them to multiply the variety of functional peptides derivable from a parental protein.

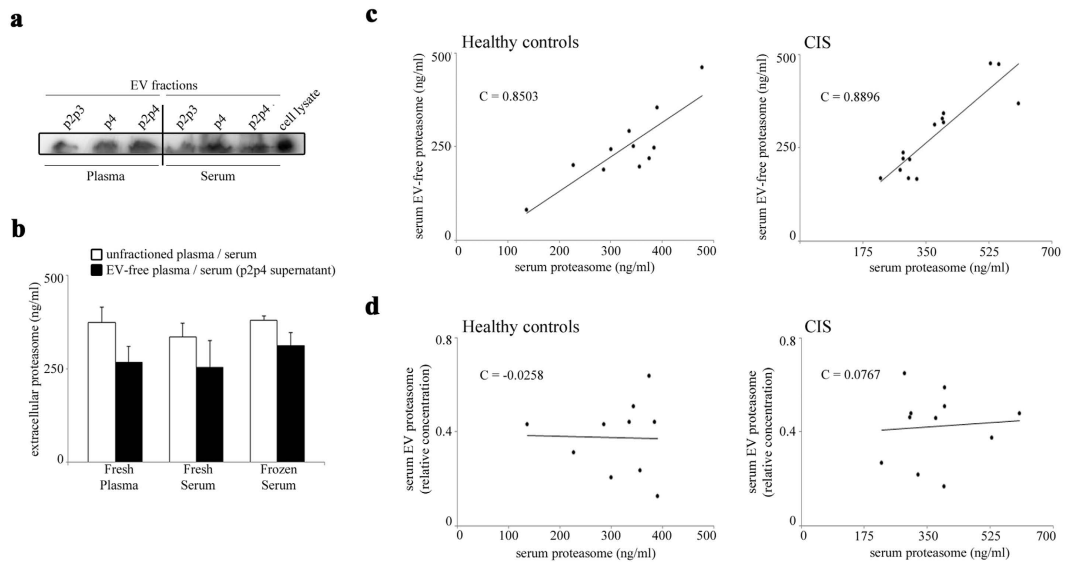


Figure 6. The main portion of serum extracellular proteasome is not stored in isolated EVs. (a) Representative Western blot analysis ($n = 3$) of p2p3 (large vesicles), p4 (small vesicles) and p2p4 (all vesicles) protein extracts are shown. They derive from healthy donor's freshly-isolated plasma and serum samples. Cell lysate from lymphoblastoid cell lines is used as control. (b) The quantitative evaluation of extracellular proteasome concentration is here shown and is obtained by applying ELISA on the fresh plasma ($n = 5$) and serum ($n = 3$) or frozen serum ($n = 3$) of healthy donors, or on their corresponding EV-free supernatants, which are obtained by removing the p2p4 vesicles upon ultra-centrifugations. (c) The correlation between the proteasome concentration in the total serum and the EV-free (p2p4-free) serum supernatant of a subset of German healthy donor ($n = 11$) and CIS patient ($n = 14$) cohorts (measured by ELISA) is shown. A statistically significant positive correlation is observed between the extracellular proteasome concentration in the EV-free (p2p4-free) serum supernatant and in the unfractionated serum (Pearson's test; in healthy donors, $p = 0.001$; in CIS patients, $p < 0.001$). (d) The proteasome concentration in p2p4 vesicles of a subset of healthy donors ($n = 10$) and CIS patients ($n = 11$) is shown. It is measured by Western blotting and by using anti- $\alpha 6$ proteasome subunit antibody. It is expressed as proteasome concentration relative to that of the cell lysate of lymphoblastoid cell lines. No correlation between the extracellular proteasome concentration measured in serum p2p4 vesicles or in whole serum is observed. Pearson's test C values are reported in each chart.

The cellular origins of the serum proteasome remain unknown, and we can only refer to the extensive study of Zoeger *et al.*¹⁴, who have shown how proteasome subtype profiles cannot be assigned to any of the investigated blood cells. Here, we demonstrate that although EVs contain proteasomes, only a minor portion of extracellular proteasome that we measure in sera is stored by EVs. This portion does correlate neither with total extracellular proteasome concentration nor with the variations we observe in CIS sera. We cannot exclude the possibility that extracellular proteasome is initially released in short-lived EVs, whose content is rapidly liberated into the extracellular space after the release from the cells. Indeed, the content of these short-lived EVs would be detected as free extracellular proteasome in our assays. However, multiple mechanisms of release are a common feature for both secretory molecules (ATP), or proteins lacking a conventional leader sequence (IL1- β or tau protein); these could be used also by proteasome.

It is noteworthy that, in this study, we investigate only the chemotactic effect of OPNs; however, OPNs also mediate other pro-inflammatory mechanisms involved in MS. Indeed, in EAE it has been demonstrated that OPN is able to trigger the neurological relapse by supporting the recruitment of autoimmune T cells into the CNS, by stimulating the expression of Th1 and Th17 cytokines, and by inhibiting T cell apoptosis through the regulation of Foxo3 and NF- κ B transcription factors expression⁶. Additionally, activated T cells can secrete OPN, thus enhancing the Th1 and inhibiting the Th2 responses². Recently, it has been demonstrated that the immunoproteasome is also involved in the regulation of Th1 and Th17 cytokine production and T cell differentiation^{9,31,32}. Moreover, the administration of a selective immunoproteasome inhibitor prevents EAE progression and ameliorates a relapse when the treatment is started in the recovery phase. These effects depend on the reduction of immune cell infiltration into the brain and spinal cord, as well as the inhibition of Th17 cell differentiation³³. Thus, based on our *in vitro* results, we might speculate that the role of immunoproteasome in promoting EAE could be, at least in part, the direct outcome of an altered activation of OPN pro-inflammatory mechanisms by extracellular immunoproteasome.

Materials and Methods

***In vitro* processing of cytokines by purified 20S proteasome.** 20S proteasomes are purified from human erythrocytes or T2 cell line, which contain only standard proteasome. The purity of 20S proteasome preparation has been previously shown¹².

For the *in vitro* degradation assays, 0.4 µg recombinant OPN-FL (OPN₁₇₋₃₁₄-6His), OPN-N (OPN₁₇₋₁₆₈-6His) and OPN-C (OPN₁₆₉₋₃₁₄-6His) are incubated in 20 µl solution at 37 °C with different concentration of erythrocyte 20S proteasome for 4 h (Fig. 1a), or 4 µg erythrocyte 20S proteasome for 20 h at 37 °C (Supplementary Fig. 2), or by 3.5 µg 20S proteasomes from the T2 cell line for 1–4 h (Fig. 1b). The ratio of OPNs/proteasomes used in the kinetics assays mimics that observed in serum of healthy controls and MS patients (Fig. 5), and that used in the cell migration assays (Fig. 2). Substrate degradation is detected by immunoblotting using antibodies for human OPN-N, or -C (1: 250 Maine Biotechnology Services), or OPN-FL (1: 400 Enzo Life science) as previously described³⁴. A secondary anti-mouse or anti-rabbit horseradish peroxidase-conjugated antibody (1:5000; Calbiochem) is used for 1.5 h at room temperature followed by ECL detection (Amersham). The samples described in Supplementary Fig. 2 are analyzed by mass spectrometry (see below).

OPN fragment identification and peptide synthesis. Liquid chromatography tandem mass spectrometry analyses are performed as previously described³⁵ on a 4700 proteomics Analyzer (ABSCIEX, Framingham, MS) off-line coupled with a Dionex UltiMate 3000 RSLC system and Probot fractionation device (Thermo Scientific, Idstein, Germany). Mass spectrometry spectra are recorded in the range of *m/z* 600–4000 and with the accumulation of 1200 sub-spectra. Fragmentation spectra are measured from the five most intensive precursor ions (*S/N* > 40). 5000–10.000 laser shots are accumulated. The peak lists are generated by the “Peak to Mascot” tool of the 4000er Series Explorer v3.6. For data analysis the MASCOT server (version 2.3, Matrixscience, London, UK) is used. Database searches are performed using SwissProt (2014_08; 546238 protein sequences) and the following parameters: no enzyme, mass tolerances for precursor ions 100 ppm and for fragment ions 0.5 Da. Peptides of OPN-C produced by 20S proteasome *in vitro* are accepted as identified if they provide a MASCOT score for identity with *p* < 0.01. MALDI/TOF/TOF fragmentation spectrum of OPN-FL₂₁₇₋₂₃₀ does not fulfill this criterion. However, its identity is verified by comparison with the fragment pattern of the synthetic analog. The reference peptide is synthesized in-house using Fmoc solid phase chemistry as previously described³⁵, and have the following sequences: WDSRGKDSYETSQQL (OPN₂₁₇₋₂₃₀), KANDESNEHSDVIDSQEL (OPN₂₄₉₋₂₆₆), SKVSRFHSHEF (OPN₂₆₇₋₂₇₈), KVSREFHSHEF (OPN₂₆₈₋₂₇₈), VVDPKSKEEDKHLKFRISHL (OPN₂₈₆₋₃₀₆), and KEEDKHLKFRISHL (OPN₂₉₂₋₃₀₆). Inverted peptides are designed by inverting the sequence of the related peptides identified in the proteasome-mediated digestion of the OPN-C have the following sequences: LQSTEYSDKGRSDW (inverted OPN₂₁₇₋₂₃₀), LEQSDIVDSHENSEDNAK (inverted OPN₂₄₉₋₂₆₆), FEHSHFERSVKS (inverted OPN₂₆₇₋₂₇₈), and LEHSIRFKLHKDEEK (inverted OPN₂₉₂₋₃₀₆).

Spatial localization of OPN fragments within OPN-FL 3D structure. I-Tasser³⁶ is used to predict the tertiary protein structure of OPN-FL. The *c*-score (value between -5 and 2, where higher *c*-scores indicate higher confidence in the predicted structure) of the best model predicted by I-TASSER is -3.33, which is comparable to the confidence obtained by predicting the structure of OPN-C³⁷. Pymol is used for graphic visualization (The PyMOL Molecular Graphics System, Version 1.7.4 Schrödinger, LLC).

Cell culture. HUVECs are isolated from human umbilical veins via trypsin treatment (1%) and cultured in M199 medium (Sigma-Aldrich) with the addition of 20% FCS (Invitrogen, Burlington, ON, Canada) and 100 U/ml penicillin, 100 mg/ml streptomycin (Invitrogen), 5 UI/ml heparin (Sigma-Aldrich), 12 mg/ml bovine brain extract, and 200 mM glutamine (Hyclone Laboratories). HUVECs are grown to confluence in flasks and used at the second to fifth passage. The use of HUVECs is approved by the Ethics Committee of the “Presidio Ospedaliero Martini” of Torino and conducted in accordance with the Declaration of Helsinki. Written informed consent is obtained from all donors. 2 × 10³ HUVEC are used for migration assay and cultured in M200 medium (GIBCO) with 100 U/ml penicillin, 100 mg/ml streptomycin and 200 mM glutamine.

Peripheral blood mononuclear cells are separated from buffy coat, provided by the local Blood Transfusion Service of Novara, Italy, with the Ficoll-Hypaque reagent (Limpholyte-H, Cedarlane Laboratories) by density-gradient centrifugation. PBLs are obtained from peripheral blood mononuclear cells cultured in RPMI 1640 (Euroclone) supplemented with 10% FBS, L-glutamine, penicillin-streptomycin, and let 2 h on plate to remove the adherent monocytes; PBMs (CD14⁺) are isolated with the EasySep™ Human CD14 Negative Selection Kit (StemCells Technologies, Vancouver, BC, USA). For both cell types the cell purity is checked by immunophenotypic analysis and is higher than 98%. 5 × 10⁴ PBLs or 2 × 10⁴ PBMs are used for migration assay and cultured in medium X-vivo 20 or X-vivo 15 (Lonza), respectively, with 100 U/ml penicillin, 100 mg/ml streptomycin and 200 mM glutamine.

Cell migration assay. In the Boyden chamber (BD Biosciences) migration assay, cells are plated onto the apical side of 50 µg/ml Matrigel-coated filters (0.5 µm pore size, Neuro Probe, BIOMAP snc) in M200 serum-free medium for HUVECs or X-vivo serum-free medium for PBLs or PBMs.

10 µg/ml OPN-FL, OPN-C and OPN-N (Fig. 2) or 10–500 nM OPN-C peptides (Fig. 3 and Supplementary Fig. 3), are placed in the basolateral chamber; 10 ng/ml vascular endothelial growth factor-α (VEGF-α; Sigma-Aldrich) or 1 ng/ml recombinant human RANTES (rh RANTES/CCL5; ImmunoTools GmbH) are placed as reference chemoattractant for the HUVECs or the PBLs and the PBMs, respectively.

20S proteasome is pre-incubated with OPN-FL, OPN-C and OPN-N (with ratio ng proteasome: ng OPNs = 20:1) for 2 h at 37 °C under 5% CO₂ and subsequently placed in the basolateral chamber.

The chamber is incubated at 37 °C (5% CO₂). After 20 h, the cells on the apical side are wiped off with Q-tips. The cells on the bottom of the filter are stained with crystal violet (HUVECs), or eosin Y and thiazine (PBLs and PBMs), and all counted with an inverted microscope (magnification x40). Data are shown as percentage of the treated cells migration vs the control migration measured for untreated cells. Control migration of the experiments shown in Fig. 2 is (mean ± SEM) 287 ± 39 cells for HUVECs (n = 38), 175 ± 28 for PBLs (n = 18), and 250 ± 32 for PBLs (n = 13).

Proteasome release in cell cultures. 7 × 10⁴ HUVECs are seeded in 48 well plates with M199 20% FCS medium. After 20 h HUVECs are twice washed with M200 medium and refilled with M200 medium. Then, HUVECs are treated with 10 µg/ml OPN-FL, OPN-C, OPN-N or 10 ng/ml VEGF-α. After 6 h culture the supernatant is collected. Four replicate wells are used for each donor (n = 14).

1 × 10⁵ lymphocytes are seeded in 96 well plates with RPMI 1640 medium + supplements. After 20 h lymphocytes are washed and refilled with X-Vivo 20 medium. Then, lymphocytes are treated with 10 µg/ml OPN-FL, OPN-C, OPN-N or 1 ng/ml RANTES. After 20 h culture the supernatant is collected. Four replicate wells are used for each donor (n = 10).

Medium supernatant is processed by ELISA assay to measure the proteasome concentration (see below).

Trypan blu assay is assessed in order to evaluate cell viability. Viable cells are measured, by 2,3-bis(2-methoxy-4-nitro-5sulphophenyl)-2H-tetrazolium-5-carboxanilide (Sigma-Aldrich) inner salt reagent, at UV 570 nm, as described by the manufacturer's protocol.

Donor enrolment, blood drawing, serum separation. The blood samples of the Italian cohorts are obtained after informed consent and ethical approval by the University of Piemonte Orientale "Amedeo Avogadro" (Novara; ethical committee approval: CE 18/04), IRCCS Fondazione Ospedale Maggiore Policlinico and Ospedale San Raffaele (Milano; ethical committee approval: Banca-INSPE and MSGENE02). The blood samples of the German cohort are obtained after informed consent and ethical approval by the Clinical and Experimental MS Research Centre, Charité – Universitätsmedizin Berlin (Berlin; ethical committee approval: EA1/182/10). All methods and procedures are performed in accordance with the relevant guidelines and regulations of the ethical committee approvals. RRMS and CIS patients as well as age-, gender-, and ethnicity-matched healthy controls without a history of any neurological or other chronic disease are recruited (Supplementary Table 1). All participants are older than 18 years; an information sheet related to the study is provided and an informed consent is undersigned by each participant. Diagnosis of MS is made according to the McDonald 2010 criteria³⁸. The clinical workup and examinations of MS patients at the visit include: detailed medical and demographic history, neurological examination, determination of the expanded disability status scale score, brain Magnetic Resonance Imaging, type of therapy (Glatiramer acetate or IFN-β). Inclusion criteria are the following: age > 18 years, a first clinical event suggestive of central nervous system demyelination within 6 months before inclusion into the study for CIS patients or a diagnosis of RRMS according to the McDonald 2010 criteria³⁸ within 24 months before inclusion into the study. Exclusion criteria are the inability or unwillingness to provide informed consent, a history of alcohol or drug abuse, any ocular diseases precluding performance of optical coherence tomography, and any conditions (e.g. allergies) or devices (e.g. cardiac pacemaker) precluding MRI examinations. Serum samples of RRMS patients are obtained from 10 ml of peripheral blood, which are drawn either at the time of relapse (2–7 days from its onset) or in remission (after 1–12 months from the last relapse) as previously reported³⁹. The RRMS patients receive a corticosteroid treatment after the blood withdrawal during the relapse.

Extracellular proteasome and OPN quantification in serum. The concentration of the extracellular proteasomes is measured in serum by enzyme-linked immunosorbent assay (ELISA), as previously described with minor modifications⁴⁰. Plates (FA9439454, Nunc Immuno MaxiSorp Surfaces, Thermo Fisher Scientific Inc.) are coated overnight with mouse monoclonal antibodies towards 20S proteasome subunit α6 (PW 8100, Enzo Life Sciences Inc.) 1:1500 in 100 µL PBS at pH 7.4. The plates are washed 5 times in PBS-Tween20 (PBST) 0.1% and incubated 6 h at room temperature with a blocking solution of PBST-BSA 1% to prevent non-specific bindings of the samples. Samples are diluted in PBST-BSA 1% (serum 1:15–1:30; plasma/serum supernatant 1:15; medium of *in vitro* experiments 1:2.5–1:10) and 100 µl are applied to each well overnight at 4 °C. Standard curves are established for every plate using purified 20S proteasomes with concentrations ranging from 0 to 100 ng/ml (8 linear dilution steps). The plates are washed 3 times and 100 µl of anti-proteasome rabbit polyclonal antibody 1:750 (K42, in house) in PBST solution are added for 3 h at 4 °C. After additional washing steps, 100 µl of 1:15000 peroxidase-conjugated mouse anti-rabbit IgG (11-035-003, Jackson ImmunoResearch Laboratories Inc.) in PBST solution are used for antigen detection (1 h at 4 °C). Finally, plates are washed five times and 100 µl of TMB substrate added (T0440, Sigma-Aldrich). The reaction is stopped with sulphuric acid and OD-values are determined at 450 nm. Serum from a young healthy control is added in each plate as internal control.

Serum OPN concentration is evaluated by ELISA according to the protocol provided by the manufacturer (Calbiochem) as previously described³⁹. The optical density is measured with a microplate reader (Bio-Rad).

All assays are performed in duplicate in three independent measurements, and the observer is blinded to the diagnosis.

Analysis of EVs. 100–200 µl of human serum and plasma are diluted 1:5 in PBS and processed by serial centrifugations to collect EVs⁴¹ into p2p3, p4 or p2p4 fractions. The supernatants are recovered and analyzed for extracellular proteasome content by ELISA, as above described, thereby reckoning the proportion of extracellular proteasomes in the supernatant vs unfractionated sample. The pellets are lysed in 20 µl of RIPA buffer supplemented with Protease Inhibitor Cocktail (P2714, Sigma Aldrich) and the protein content is analyzed by SDS-PAGE and western blotting, as previously described⁴². Anti-α6 proteasome subunit antibody (PW 8100,

Enzo Life Sciences Inc.) is used to measure total proteasomes content within isolated EVs. Crude protein extract from lymphoblastoid cell line is used as control and for normalizing data of samples loaded in different gels. Equal loading of EVs proteins is assessed by SDS-PAGE and Coomassie Blue gel staining.

Statistical analysis. For the statistical analysis, peripheral blood samples are analyzed separately in the following categories: RRMS in relapse, RRMS in remission and healthy controls for Italian samples, and CIS, RRMS in remission and healthy control cohorts for German samples. For each sample, serum levels of extracellular proteasome and OPN contents are measured in triplicate and the mean value is calculated. Each cohort is tested to assess whether extracellular proteasome correlated to gender or age of the donors, as well as to the clinical history and parameters measured at the withdrawal (data not shown). Data are tested for normality distribution and homoscedasticity by Shapiro-Francia, Shapiro-Wilk and Skewness-Kurtosis tests. To identify significant difference between groups, One-way ANOVA, Mann-Whitney or Kruskal-Wallis tests are applied depending on the underlying distributions. To identify significant variation in proteasome release or chemotaxis in cell culture upon different stimuli we apply Wilcoxon test for paired samples. Pearson's correlation coefficients are computed for correlation analyses. Descriptive statistics are carried out with STATA v.9.0 (Stata Corp.), SPSS (version 17) and R; a p -value < 0.05 is considered statistically significant. After applying Bonferroni correction method for multiple comparisons, the p value threshold for significance is set at $p = 0.0083$. A bootstrap test (1000 samples using 100% of the data) is performed to obtain confidence intervals for the correlation coefficient between OPN and 1/extracellular proteasome. We extract the bootstrap distribution of the correlation coefficient as well as the 5% and 95% quantiles for the confidence intervals.

References

- Steinman, L. Immunology of relapse and remission in multiple sclerosis. *Annu Rev Immunol* **32**, 257–281 (2014).
- Steinman, L. A molecular trio in relapse and remission in multiple sclerosis. *Nat Rev Immunol* **9**, 440–447 (2009).
- Chowdhury, S. A., Lin, J. & Sadiq, S. A. Specificity and correlation with disease activity of cerebrospinal fluid osteopontin levels in patients with multiple sclerosis. *Arch Neurol* **65**, 232–235 (2008).
- Chiocchetti, A. *et al.* Osteopontin gene haplotypes correlate with multiple sclerosis development and progression. *J Neuroimmunol* **163**, 172–178 (2005).
- Comabella, M. *et al.* Plasma osteopontin levels in multiple sclerosis. *J Neuroimmunol* **158**, 231–239 (2005).
- Hur, E. M. *et al.* Osteopontin-induced relapse and progression of autoimmune brain disease through enhanced survival of activated T cells. *Nat Immunol* **8**, 74–83 (2007).
- Shao, Z., Morser, J. & Leung, L. L. Thrombin cleavage of osteopontin disrupts a pro-chemotactic sequence for dendritic cells, which is compensated by the release of its pro-chemotactic C-terminal fragment. *J Biol Chem* **289**, 27146–27158 (2014).
- Boggio, E. *et al.* Thrombin Cleavage of Osteopontin Modulates Its Activities in Human Cells *In Vitro* and Mouse Experimental Autoimmune Encephalomyelitis *In Vivo*. *J Immunol Res* **2016**, 9345495, doi: 10.1155/2016/9345495 (2016).
- Groettrup, M., Kirk, C. J. & Basler, M. Proteasomes in immune cells: more than peptide producers? *Nat Rev Immunol* **10**, 73–78 (2010).
- Liepe, J. *et al.* Quantitative time-resolved analysis reveals intricate, differential regulation of standard- and immuno-proteasomes. *Elife* **4** (2015).
- Arciniega, M., Beck, P., Lange, O. F., Groll, M. & Huber, R. Differential global structural changes in the core particle of yeast and mouse proteasome induced by ligand binding. *Proc Natl Acad Sci USA* **111**, 9479–9484 (2014).
- Mishto, M. *et al.* Proteasome isoforms exhibit only quantitative differences in cleavage and epitope generation. *Eur J Immunol* **44**, 3508–3521 (2014).
- Sixt, S. U. & Dahlmann, B. Extracellular, circulating proteasomes and ubiquitin - incidence and relevance. *Biochim Biophys Acta* **1782**, 817–823 (2008).
- Zoeger, A., Blau, M., Egerer, K., Feist, E. & Dahlmann, B. Circulating proteasomes are functional and have a subtype pattern distinct from 20S proteasomes in major blood cells. *Clin Chem* **52**, 2079–2086 (2006).
- Roth, G. A. *et al.* Heightened levels of circulating 20S proteasome in critically ill patients. *Eur J Clin Invest* **35**, 399–403 (2005).
- Bochmann, I. *et al.* T lymphocytes export proteasomes by way of microparticles: a possible mechanism for generation of extracellular proteasomes. *J Cell Mol Med* **18**, 59–68 (2014).
- Lai, R. C. *et al.* Proteolytic Potential of the MSC Exosome Proteome: Implications for an Exosome-Mediated Delivery of Therapeutic Proteasome. *Int J Proteomics* **2012**, 971907 (2012).
- Henry, L. *et al.* Plasma proteasome level is a reliable early marker of malignant transformation of liver cirrhosis. *Gut* **58**, 833–838 (2009).
- Henry, L. *et al.* Clinical use of p-proteasome in discriminating metastatic melanoma patients: comparative study with LDH, MIA and S100B protein. *Int J Cancer* **133**, 142–148 (2013).
- de Martino, M. *et al.* Serum 20S proteasome is elevated in patients with renal cell carcinoma and associated with poor prognosis. *Br J Cancer* **106**, 904–908 (2012).
- Egerer, K. *et al.* Circulating proteasomes are markers of cell damage and immunologic activity in autoimmune diseases. *J Rheumatol* **29**, 2045–2052 (2002).
- Minagar, A. *et al.* Plasma ubiquitin-proteasome system profile in patients with multiple sclerosis: correlation with clinical features, neuroimaging, and treatment with interferon-beta-1b. *Neurol Res* **34**, 611–618 (2012).
- Colombo, E., Borgiani, B., Verderio, C. & Furlan, R. Microvesicles: novel biomarkers for neurological disorders. *Front Physiol* **3**, 63 (2012).
- Mueller, O. *et al.* Circulating extracellular proteasome in the cerebrospinal fluid: a study on concentration and proteolytic activity. *J Mol Neurosci* **46**, 509–515 (2011).
- Witwer, K. W. *et al.* Standardization of sample collection, isolation and analysis methods in extracellular vesicle research. *J Extracell Vesicles* **2** (2013).
- Liepe, J. *et al.* A large fraction of HLA class I ligands are proteasome-generated spliced peptides. *Science* **354**, 354–358 (2016).
- Ebstein, F. *et al.* Proteasomes generate spliced epitopes by two different mechanisms and as efficiently as non-spliced epitopes. *Sci Rep* **6**, 24032 (2016).
- Mishto, M. *et al.* Driving Forces of Proteasome-catalyzed Peptide Splicing in Yeast and Humans. *Mol Cell Proteomics* **11**, 1008–1023 (2012).
- Bellavista, E. *et al.* Current understanding on the role of standard and immunoproteasomes in inflammatory/immunological pathways of multiple sclerosis. *Autoimmune Dis* **2014**, 739705 (2014).
- Bellavista, E. *et al.* Immunoproteasome in cancer and neuropathologies: a new therapeutic target? *Curr Pharm Des* **19**, 702–718 (2013).

31. Kalim, K. W., Basler, M., Kirk, C. J. & Groettrup, M. Immunoproteasome subunit LMP7 deficiency and inhibition suppresses Th1 and Th17 but enhances regulatory T cell differentiation. *J Immunol* **189**, 4182–4193 (2012).
32. Muchamuel, T. *et al.* A selective inhibitor of the immunoproteasome subunit LMP7 blocks cytokine production and attenuates progression of experimental arthritis. *Nat Med* **15**, 781–787 (2009).
33. Basler, M. *et al.* Inhibition of the immunoproteasome ameliorates experimental autoimmune encephalomyelitis. *EMBO Mol Med* **6**, 226–238 (2014).
34. Mishto, M. *et al.* Proteasome isoforms exhibit only quantitative differences in cleavage and epitope generation. *Eur J Immunol* (2014).
35. Liepe, J. *et al.* The 20S Proteasome Splicing Activity Discovered by SpliceMet. *PLOS Computational Biology* **6**, e1000830 (2010).
36. Yang, J. *et al.* The I-TASSER Suite: protein structure and function prediction. *Nat Methods* **12**, 7–8 (2015).
37. Sivakumar, S. & Niranjali Devaraj, S. Tertiary structure prediction and identification of druggable pocket in the cancer biomarker - Osteopontin-c. *J Diabetes Metab Disord* **13**, 13 (2014).
38. Polman, C. H. *et al.* Diagnostic criteria for multiple sclerosis: 2010 revisions to the McDonald criteria. *Ann Neurol* **69**, 292–302 (2011).
39. Quaglia, M. *et al.* Osteopontin circulating levels correlate with renal involvement in systemic lupus erythematosus and are lower in ACE inhibitor-treated patients. *Clin Rheumatol* **33**, 1263–1271 (2014).
40. Heubner, M. *et al.* The prognostic impact of circulating proteasome concentrations in patients with epithelial ovarian cancer. *Gynecol Oncol* **120**, 233–238 (2011).
41. Bianco, F. *et al.* Acid sphingomyelinase activity triggers microparticle release from glial cells. *Embo J* **28**, 1043–1054 (2009).
42. Mishto, M. *et al.* A structural model of 20S immunoproteasomes: effect of LMP2 codon 60 polymorphism on expression, activity, intracellular localisation and insight into the regulatory mechanisms. *Biol Chem* **387**, 417–429 (2006).

Acknowledgements

We thank for intellectual or technical assistance: E. Pini, B. Petrovic and L. Zamboni (Unibo); D. Vecchio, N. Clemente, G. Cappellano and E. Toth (UPO); U. Kuckelkorn, B. Dahlmann, P. Henklein, P. Kunert, B. Brecht-Jachan, N. Albrecht-Köpke and L. Rasche (Charité Berlin). This work was financed in part by the grant Giovani Ricercatori 2007 from Italian Ministry of Health to M.M., D.G., C.C. and F.M.B., by Berlin Institute of Health (BIH, CRG1-TP1) and Einstein Stiftung to P.M.K., by Associazione Italiana Ricerca sul Cancro (AIRC, IG 14430) to U.D., by Fondazione Italiana Sclerosi Multipla (FISM, grant 2012/R/17) to C.V. J.L. was supported by National Centre for the Replacement Refinement and Reduction of Animals in Research (NC3Rs) through a David Sainsbury Fellowship. M.P.H.S. was supported by BBSRC, The Leverhulme Trust and the Royal Society through a Wolfson Research Merit Award. M. Martucci was supported by Fondazione Italiana Sclerosi Multipla (2011/B/5). F.P. is supported by the Deutsche Forschungsgemeinschaft (DFG Exc 257).

Author Contributions

E.B., C.D., U.D. and Mic.Mis. designed the study, performed part of the experiment and/or analyzed the data, and wrote the manuscript. J.L., C.V., F.P., K.R., D.G., F.M.B. and C.C. analyzed the data, and wrote the manuscript. Mor.Mar., A.C., C.L.G., E.B., B.F., L.R., C.K., K.J., A.N., C.F. and M.S., performed part of the experiments, A.S. performed part of the statistical analysis, R.C., P.M.K. and M.P.H.S. wrote the manuscript and supervised the study.

Additional Information

Supplementary information accompanies this paper at <http://www.nature.com/srep>

Competing Interests: The authors declare no competing financial interests.

How to cite this article: Dianzani, C. *et al.* Extracellular proteasome-osteopontin circuit regulates cell migration with implications in multiple sclerosis. *Sci. Rep.* **7**, 43718; doi: 10.1038/srep43718 (2017).

Publisher's note: Springer Nature remains neutral with regard to jurisdictional claims in published maps and institutional affiliations.



This work is licensed under a Creative Commons Attribution 4.0 International License. The images or other third party material in this article are included in the article's Creative Commons license, unless indicated otherwise in the credit line; if the material is not included under the Creative Commons license, users will need to obtain permission from the license holder to reproduce the material. To view a copy of this license, visit <http://creativecommons.org/licenses/by/4.0/>

© The Author(s) 2017

Additional results

CD44 as key mediator of OPN effect

There is strong evidence that CD44 interacts with the C-terminal fragment of OPN (Z. Shao, Morser, and Leung 2014; Steinman 2009). Therefore, after having demonstrated that OPN-C digestion allows the exposure of binding sites for important mediators, which are responsible for OPN activity on cell migration and adhesion, we investigated if CD44 could be the receptor bound by the OPN-C fragments whereby triggering these processes.

We evaluated whether an anti-CD44 antagonist (Ancell) could affect OPN function on HUVECs chemotaxis, and obtained results showed that the blocking of CD44 did not allow OPN-N current stimulation on cell migration (Fig. 15). Moreover, since the previous article reported that 4 peptides produced by OPN-C proteasome digestion exerted a chemotactic activity toward HUVECs and other cell types (Dianzani et al. 2017), we tested whether or not the presence of anti-CD44 could influence their activity on HUVECs chemotaxis, using OPN-C peptides (50 or 500 nM) and anti-CD44. For all the 4 peptides, the use of anti-

CD44 antibody suppressed their chemotactic activity (Fig. 16). A mathematical modelling (Liepe et al. 2015) was explored to perform peptide docking, in order to simulate their binding to CD44. In accordance with this model, two residues in the OPN₂₁₇₋₂₃₀ peptide, OPN-E₂₂₆ and OPN-S₂₂₈, were found to be responsible for the binding to CD44, inducing the conformational change that activates the receptor. To confirm these data, three different modifications were performed on the three residues, generating peptides that were no longer active. Indeed, they were not able to report the chemotaxis induction mediated by the wild type OPN₂₁₇₋₂₃₀ peptide on HUVECs (Fig. 17). The same result was reported on lymphocytes (PBLs) migration. As a matter of fact, the interaction between these specific residues on the peptide and CD44 is crucial for the activation of the receptor and the promotion of chemotaxis.

Moreover, lymphocytes need to adhere to endothelium in order to extravasate in inflamed tissue. Since there is evidence that the lymphocytes capturing-rolling-arrest steps are mediated, among the other molecules, by CD44, which recognizes the hyaluronic acid (HA) on the endothelium cell membrane (Baaten et al. 2012), we tested the six peptides (at the concentration 50 nM) derived from OPN-C proteasome digestion (Dianzani et al. 2017) to determine their ability to stimulate the HA-CD44-mediated adhesion of PBLs (PMA was used as positive control). OPN₂₄₉₋₂₆₆, OPN₂₆₇₋₂₇₈, OPN₂₆₈₋₂₇₈, and less intensely also OPN₂₄₉₋₂₆₆ peptides showed an ability to induce PBL adhesion to HA. The enhancement of the HA-mediated adhesion revealed to be sequence-specific because the treatment of the PBLs with peptides having a reverse sequence as compared to the four latter peptides fails to exert the same effect (Fig. 18A).

While OPN-C binds CD44 that interacts with HA in the process of cell adhesion, OPN-N binds to $\alpha 4\beta 1$ integrin which is an interactor for fibronectin. In order to

further demonstrate that the process of adhesion was induced by OPN-C activated CD44 which binds to HA, we tested cells ability to adhere to fibronectin in presence of the three stimulating peptides. As expected, in this condition no enhancement of cell adhesion was observed (Fig. 18B). Moreover, we tested if the presence of anti-CD44 could influence their activity on PBL adhesion to HA. The use of anti-CD44 antibody suppressed the chemotactic activity of peptides (Fig. 19).

In conclusion, CD44 demonstrated to be responsible even for PBLs-adhesion to the vascular endothelium, thereby becoming the molecular interactor for OPN peptides in the promotion of this process.

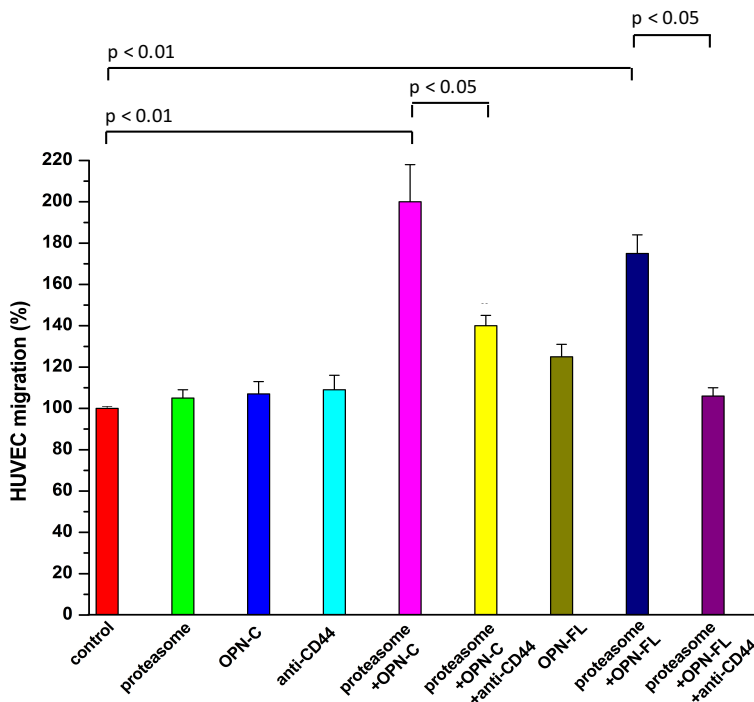


Figure 15: Influence of anti-CD44 on OPN/proteasome induced cell migration on HUVECs. Data are expressed as the mean \pm SEM of the percentage of migration versus the control obtained from untreated cells set at 100% from 5 independent experiments. Statistical analysis was performed using Wilcoxon test for paired samples

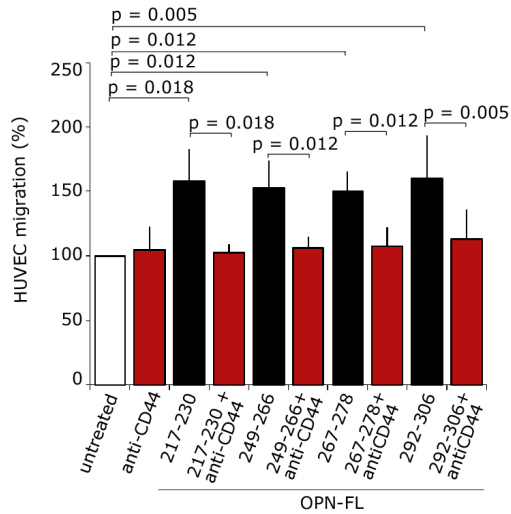


Figure 16: Influence of anti-CD44 on HUVECs migration after treatment with peptides derived from OPN proteasome digestion. Data are expressed as the mean \pm SEM of the percentage of migration versus the control obtained from untreated cells set at 100% from 5 independent experiments. Statistical analysis was performed using Wilcoxon test for paired samples.

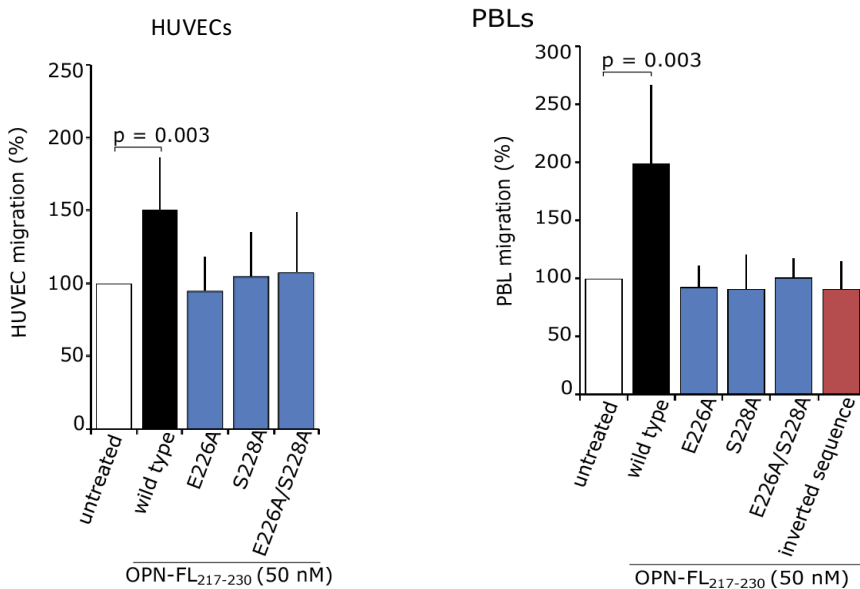


Figure 17: Influence of anti-CD44 on HUVECs and PBL migration after treatment with mutated peptides derived from OPN proteasome digestion. Data are expressed as the mean \pm SEM of the percentage of migration versus the control obtained from untreated cells set at 100% from 5 independent experiments. Statistical analysis was performed using Wilcoxon test for paired samples.

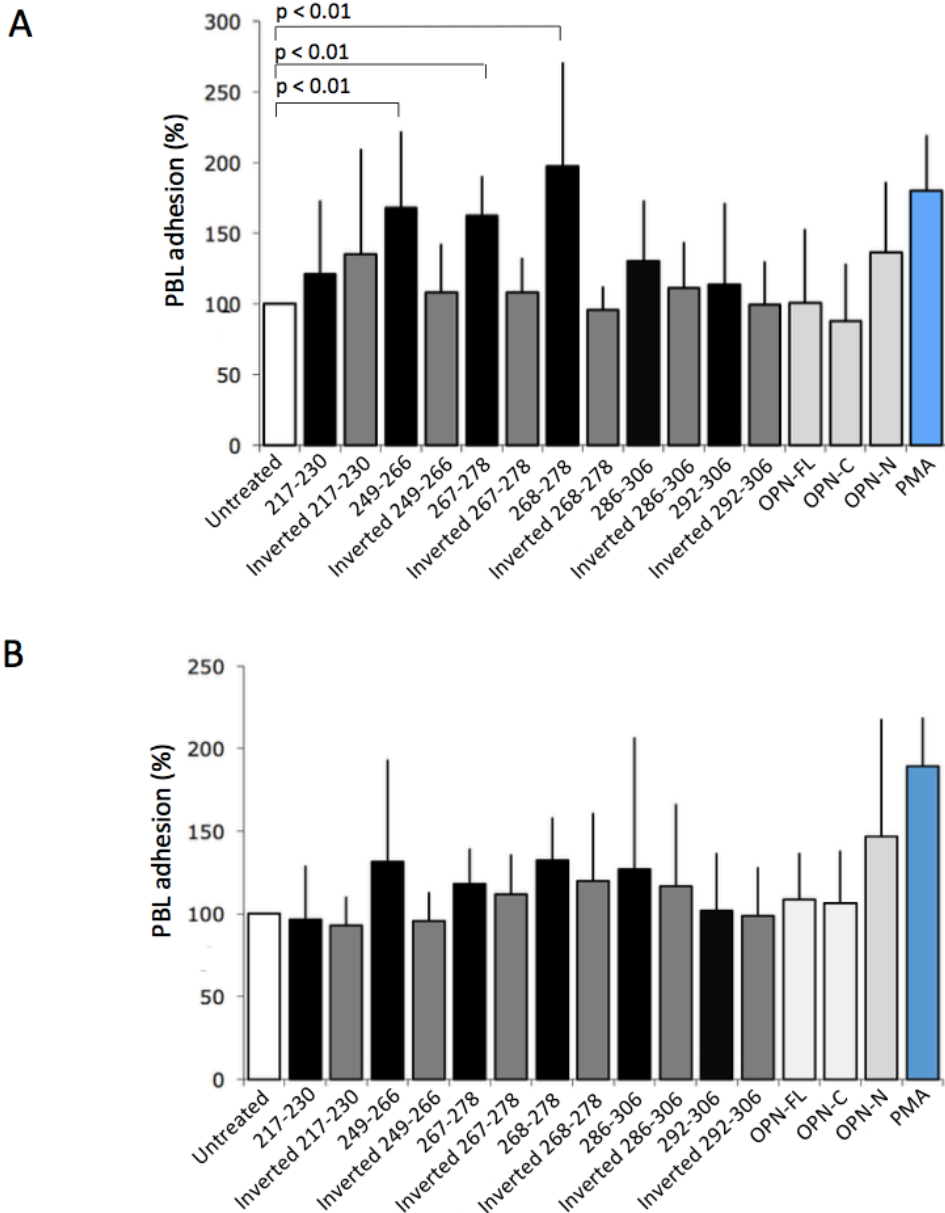


Figure 18: (A) Effect of WT and inverted peptides derived from OPN proteasome digestion on PBL adhesion to HA. **(B)** Effect of peptides derived from OPN proteasome digestion on PBL adhesion to fibronectin. Data are expressed as the mean \pm SEM of the percentage of adhesion versus the control obtained from untreated cells set at 100% from 5 independent experiments. Statistical analysis was performed using Wilcoxon test for paired samples.

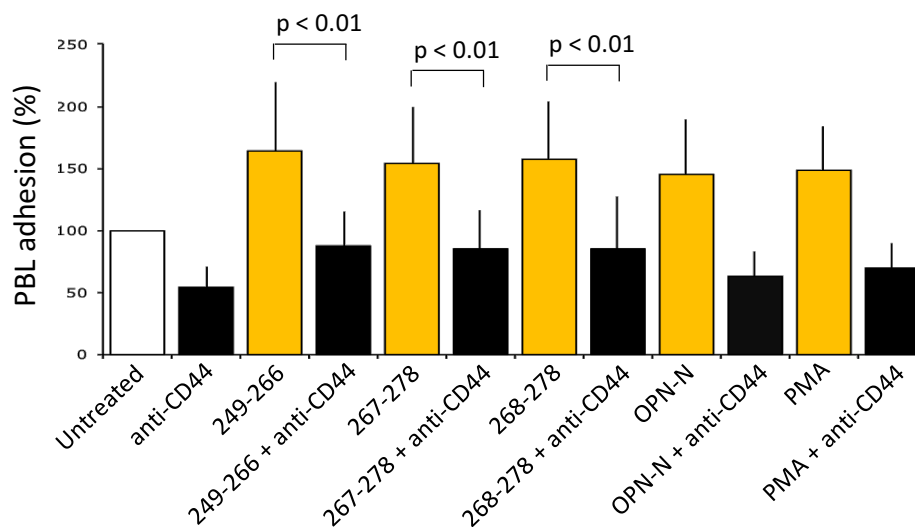


Figure 19: Influence of anti-CD44 on PBL adhesion to HA after treatment with peptides derived from OPN proteasome digestion. Data are expressed as the mean \pm SEM of the percentage of adhesion versus the control obtained from untreated cells set at 100% from 5 independent experiments. Statistical analysis was performed using Wilcoxon test for paired samples.

Discussion

OPN is an ubiquitous protein distributed in a variety of tissues and secreted in biological fluids. It is produced by several cell types, such as bone cells, immune cells, endothelial cells, and also tumour-derived cell lines. OPN is involved in many physiological processes, such as bone remodelling, macrophage response, cell migration and adhesion, but it can also take part in the pathogenesis of several diseases including cancer, atherosclerosis, chronic inflammatory diseases and several autoimmune diseases (Cho, Cho, and Kim 2009; Liu et al. 2014; A. Brown 2012). OPN acts as pro-inflammatory cytokine in the progression of several inflammatory and immunitary processes and thereby its role has been largely investigated in several autoimmune diseases, such as RA and LES. Furthermore, OPN is involved in multiple sclerosis (MS); indeed high levels of this cytokine were detected in patients lesions and plasma, and in its animal model - experimental autoimmune encephalomyelitis (EAE) (Chiocchetti et al. 2005; Comi et al. 2012; Chabas et al. 2001). Previous studies demonstrated that OPN plays a role in lymphocyte recruitment into the MS lesions, in the inhibition of autoreactive T cells apoptosis and in the induction of pro-inflammatory cytokines production. However, the molecular mechanisms by which OPN can exert these functions are only partly known. During inflammation, OPN cleavage by thrombin generates an N-terminal fragment, which binds several integrins, and a C-terminal fragment which is known to interact with CD44 (Steinman 2009). Before evaluating OPN function in cancer progression, the initial aim of this project was to characterize the role of the two distinct OPN fragments in the pathogenesis of MS, since it is well known the cytokine involvement in this pathology and the inflammatory background allows us to investigate the separate function of the two OPN forms.

OPN-N and OPN-C effect was evaluated on lymphocyte adhesion to endothelial cells and migration, which constitute two key steps of lymphocyte extravasation and homing into tissues. Obtained results revealed a coordinated effect of the two fragments, since cell migration was supported by OPN-N, while cell adhesion was ascribable to OPN-C. The effect of OPN-FL was weaker in both the processes. Also *in vivo* experiments revealed the importance of thrombin cleavage of OPN, since the administration of OPN-FL could induce rapid EAE relapse, while OPN-FL^{mut}, which is resistant to thrombin-mediated cleavage, was not able to do that. Moreover, OPN-C was more effective in inducing EAE relapses than OPN-N.

Taken together, these data allow us to deduce that thrombin cleavage of OPN is fundamental for the exposure of particular sites that are unmasked and thus can bind to their ligands. Indeed, the two generated fragments revealed to exert different but synergic functions.

Another protease which has recently proposed as a suitable biomarker in some cancers and autoimmune diseases, such as MS, is the 20S proteasome. In particular i-proteasome, that is an isoform expressed during inflammation or in immune cells, can be present in an extracellular form that is even proteolytically active (Zoeger et al. 2006). We decided to investigate whether extracellular proteasome is involved in the OPN-mediated inflammatory events, and thereby we evaluated its activity on OPN. Purified 20S proteasome was incubated with OPN and its effect was determined on HUVECs, lymphocytes and monocytes migration. Reported results revealed that the presence of 20S proteasome significantly hampered the chemotactic stimulus by OPN-N whereas OPN-FL and OPN-C gained chemotactic activity only upon proteasome digestion. The fact that proteasome can cleave OPN-FL and OPN-C thereby increasing or inducing,

respectively, their chemotactic activity suggests that 20S proteasome degradation might unmask cryptic OPN chemotactic fragments. Such fragments would then be able to activate chemotaxis better than when they were included and folded in the OPN-FL. For this reason, six peptides derived from OPN-C digestion by proteasome were chosen and considered for our analysis.

The effect of these peptides was tested on cell migration and only four of them resulted as being responsible for the induction of this process, either on HUVECs and on lymphocytes. It means that proteasome cleavage of OPN is necessary for achieving its stimulatory effect on cell migration. Indeed, when the single peptides are removed from the original protein they have likely lost their secondary conformation and the absence of surrounding bulky structures might facilitate an enhanced binding to chemotactic receptors.

Since OPN-C is known to bind CD44 (Steinman 2009), the subsequent step was to assess if this receptor could be the molecular interactor for OPN to exert its pro-chemotactic activity. The treatment with anti-CD44 of cells inhibited the stimulatory effect of proteasome/OPN on cell migration. Cells were then treated with anti-CD44 in the presence of the four chemotactic peptides, and an inhibition of their effect was also observed in this case. Docking studies performed on CD44 binding to the most active peptide showed that two residues on the peptide were essential for the binding to CD44. This interaction is required to induce a conformational change which activates CD44 and is necessary for inducing the chemotactic activity.

Even on cell adhesion to endothelium, CD44 resulted a key interactor that binds HA through the action of three OPN peptides generated by proteasome digestion, suggesting their involvement in MS pathogenetical processes.

OPN and cancer

Introduction

After investigating the role played by OPN in MS processes, we extended our research to the study of its function even on cancer cell types.

As previously reported, there is strong evidence of OPN involvement in cancer processes, such as cell growth, angiogenesis, and metastasis (Cook et al. 2005; Bandopadhyay et al. 2014; Irby, McCarthy, and Yeatman 2004; Zhou et al. 2005; Chambers, Groom, and MacDonald 2002; Thalmann et al. 1999; Gotoh et al. 2002).

OPN is produced by many cell types present in the tumor microenvironment, including the tumor itself. Several functions of OPN have yet been elucidated, but elevated levels of OPN in the tumor site and in plasma have been associated with poor prognosis and with reduced survival in patients with breast cancer (Patani et al., n.d.). OPN is also one of the highest expressed genes in a large percentage of patients with glioblastoma (Atai et al. 2011), and the depletion of OPN in glioblastoma-initiating cells leads to the loss of their tumorigenic potential (Lamour et al. 2015). Within a tumor mass, the functional activities of OPN are complex, since OPN is generally expressed by both tumor and stroma cells in its secreted form. It has been detected in a growing number of human tumour types, including lung, breast, prostate, gastric, oesophageal, ovarian and glioma, by immunohistochemistry on tumour tissue sections (Furger et al. 2001; A B Tuck and Chambers 2001). In addition to being present in tumours and some normal tissues, OPN was also found in biological fluids. OPN plasma levels were significantly elevated in women with metastatic breast cancer. Indeed, elevated OPN levels were significantly associated with increased

numbers of metastatic sites.

Taken together, this growing list of studies suggests that OPN blood levels have a potential as a prognostic or diagnostic marker in prostate, breast, head and neck, and likely other cancers.

The mechanisms by which OPN may enhance malignancy are still unclear, but OPN participates in pathways regulating migration of several cell types, including tumour cells (A B Tuck et al. 2000). Invasiveness is clearly related to migration, but not only cells need to be motile in order to invade as they also need to degrade the extracellular matrix. Several studies suggest that OPN increases invasiveness by inducing proteinases, particularly uPA (Alan B Tuck et al. 1999; Das, Mahabeleshwar, and Kundu 2003). Recent experiments suggest that OPN acts in concert with several growth factors, including hepatocyte growth factor (HGF) (Medico et al. 2001) and EGF (Alan B Tuck et al. 2003), to induce malignant properties.

Finally, as previously reported, OPN was found implicated in the process of angiogenesis, particularly as it is a high-affinity ligand for the $\alpha v\beta 3$ integrin, which is highly expressed on some endothelial cells. Signalling through the $\alpha v\beta 3$ is necessary for endothelial cell survival and indeed OPN enhances survival of endothelial cells (Scatena et al. 1998). However, recent data demonstrating that OPN accelerates blood vessel formation in matrigel assays in the presence of FGF-2, however, suggest that OPN may act in concert with other proangiogenic molecules to enhance angiogenesis (Leali et al. 2003). Moreover, the OPN:CD44 interaction promotes metastasis dissemination in a variety of malignancies (Fok et al. 2014) and the individual role of OPN-N and OPN-C has been achieving interest in cancer cells because of the higher expression of both OPN and activated thrombin in the microenvironment of several tumors (Franchini and

Mannucci 2012; Y. Yamaguchi et al. 2013; Beausoleil et al. 2011).

Again, these results underscore the idea that the exact function of OPN in any given situation may be determined by interactions with other factors in the microenvironment (Rittling and Chambers 2004).

Methods and results

In order to evaluate the mechanisms underlying OPN effects in cancer, we performed an *in vitro* evaluation of tumour cells processes, including cell migration and adhesion to the endothelium, after treatment with the different OPN forms.

First, the effect of OPN-FL, OPN-N and OPN-C was evaluated on several human cancer cell lines migration using a Boyden chamber assay with a previously described protocol (Boggio et al. 2016), plating 2000 cells/well, using 5µg/ml OPN-C and OPN-N and 10µg/ml OPN-FL, with 20% FBS as positive control. Interestingly, obtained results showed that OPN-N was able to strongly increase migration of PC-3, M14 and JR8 cell lines, while A2058, RPMI-7932 and PCF-2 were not affected, pointing out the role of the OPN N-terminal fragment in selectively mediating this process. Indeed, OPN-FL exerted a weaker but still high effect on cell migration, while OPN-C did not influence this process. A representative image of OPN induced cell migration on PC-3 cell line is shown in figure 20A. A similar result was obtained for other tested cell lines.

Another essential process for tumour cells to extravasate and reach a new tissue to colonize and give life to metastases is the adhesion to endothelium. Consequently, we assayed how the ability of PC-3, M14 and JR8 human cancer cell lines to adhere to endothelial cells (HUVECs) was affected by the different OPN forms, using a protocol previously described (Boggio et al. 2016). Fig. 20B

shows that OPN-C is the fragment responsible for cell adhesion to endothelium, since it was the only OPN form able to highly induce this process, while OPN-FL displayed a weaker effect and OPN-N did not report any effect. The same effect was reported either treating tumour cells for 24h and then using them for cell adhesion, and treating HUVECs for 24h and then using PC-3 for cell adhesion. Therefore, OPN was able to activate both HUVECs and tumour cells.

These results are in line with previous findings obtained on OPN study in MS (Boggio et al. 2016), in which we demonstrated that OPN-C and OPN-N played a different role in regulating cell processes, such as migration and adhesion. Therefore, even in tumours, OPN cleavage by thrombin is essential since it allows the exposure of binding sites for integrins and receptors that are important mediators for these processes.

Further experiments were carried out in order to evaluate the role of proteasome in influencing activity of OPN even on cancer cells. The six peptides previously generated from the proteasome-mediated digestion of OPN-C were tested to assess their effect on cancer cells migration. HeLa, A2780res, PC3 and A2058 tumour cell lines were treated with the six peptides (50-100nM) and cell migration was evaluated with a Boyden chamber assay. Obtained results revealed that only two peptides (OPN₂₁₇₋₂₃₀ and OPN₂₄₉₋₂₆₆) were responsible of enhanced migration of HeLa, A2780res and PC-3 cell lines (Fig. 21). No effect was observed using an inverted sequence form of each peptide, demonstrating that the effect is sequence-specific (Fig. 22). However, an interesting finding was figured out as we noticed that cell lines influenced by the two peptides displayed a common characteristic, which is the presence of a particular surface receptor. This was in line with previous findings on OPN induction of tumour cell migration, where its effect was selectively directed only to some cell lines. In

our research group, several studies on this receptor (which cannot be denominated for patent protection reasons) have been carried out, revealing its role as a key interactor in cancer pathogenetical process. We decided to deeper investigate the involvement of this receptor in tumour cell migration, by inducing genetical modifications in A2058 cell line, which does not express the receptor. These cells were engineered by transfection with the whole form of the receptor, the tail-less receptor or the only-tail receptor, by the group of prof U. Dianzani (Department of Health Science, UniUPO) and three A2058 cell lines were generated with these genomic modifications. In line with previous findings, cell migration was induced by OPN-N only in whole receptor transfected cells (Fig. 23). Finally, to confirm the involvement of this receptor in cell migration, HUVECs, which constitutively express the receptor at the surface, were silenced by using a siRNA. As expected, OPN-N was not able to report its pro-chemotactic effect on receptor-silenced HUVECs (Fig. 24). Therefore, obtained data enable considering this receptor as an important mediator of OPN-influenced chemotaxis process.

PC-3

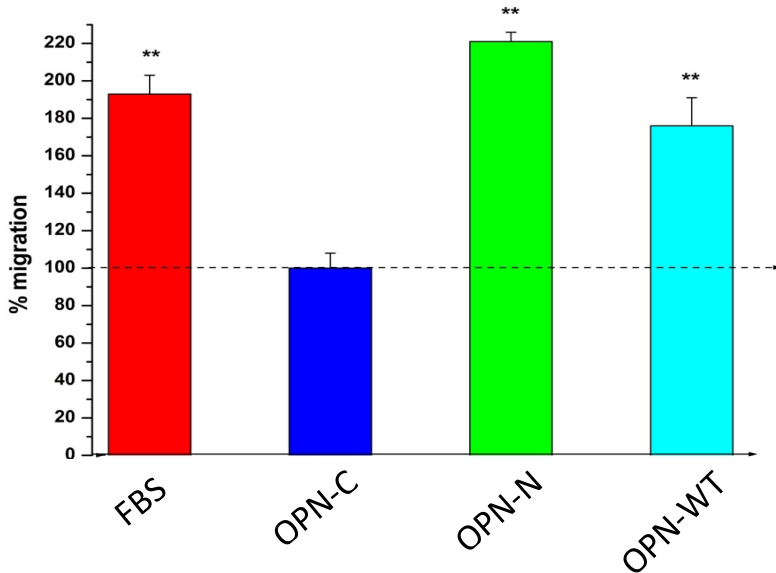
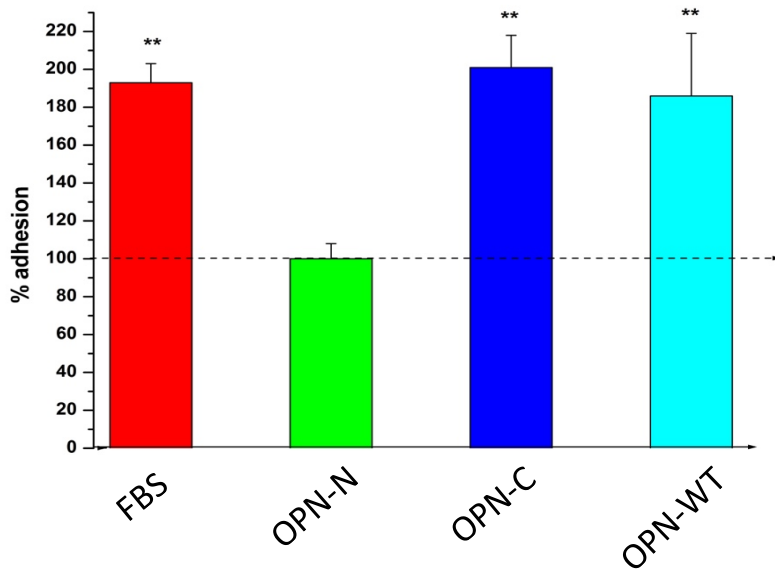


Figure 20: Effect of OPN variants on PC-3 migration and adhesion. Data are expressed as the mean \pm SEM of the percentage of migration or adhesion versus the control obtained from untreated cells set at 100% from 5 independent experiments. (** $p < 0.01$ vs control; Wilcoxon's signed rank test).

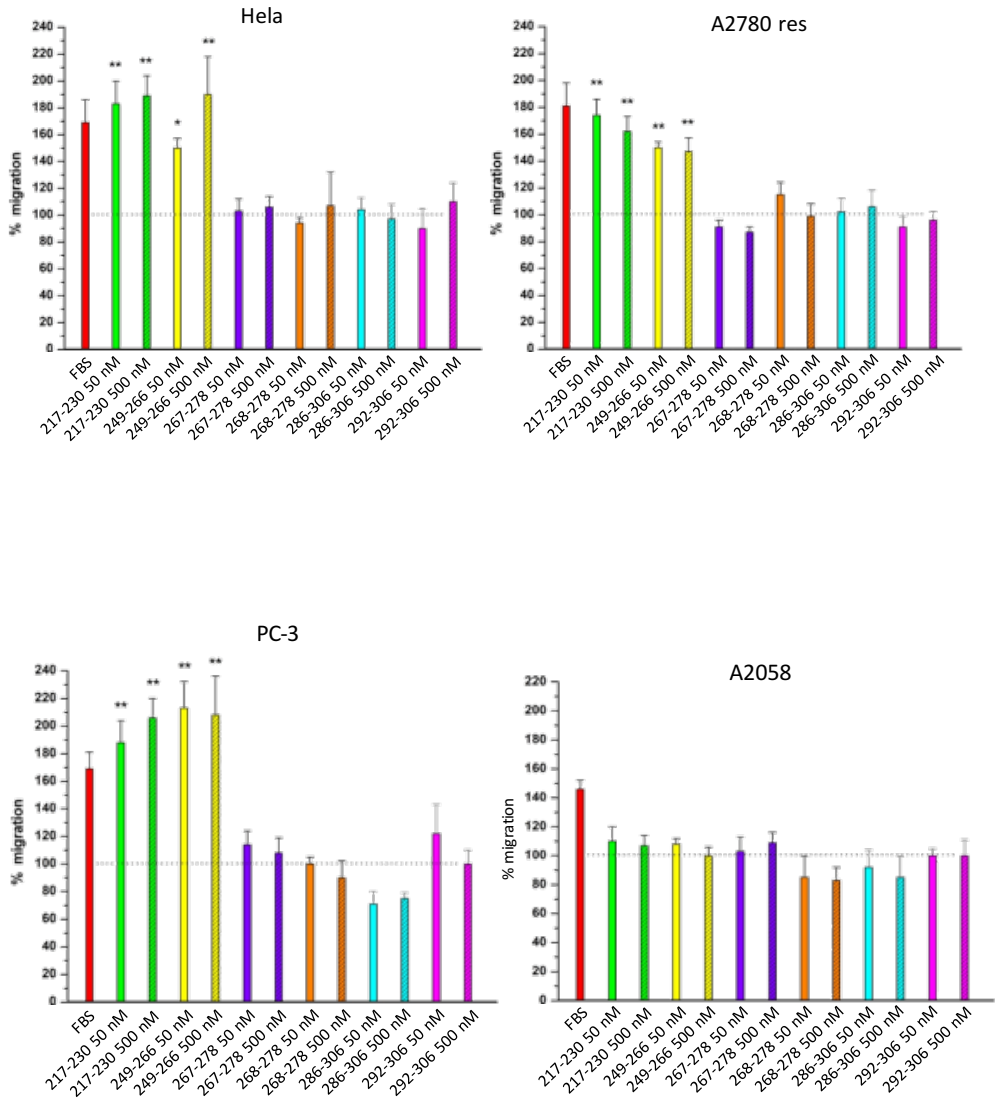


Figure 21: Effect of the six peptides derived from OPN proteasome digestion on migration of different tumour cell lines. Data are expressed as the mean \pm SEM of the percentage of migration versus the control obtained from untreated cells set at 100% from 5 independent experiments. (* $p < 0.05$; ** $p < 0.01$ vs control; Wilcoxon's signed rank test).

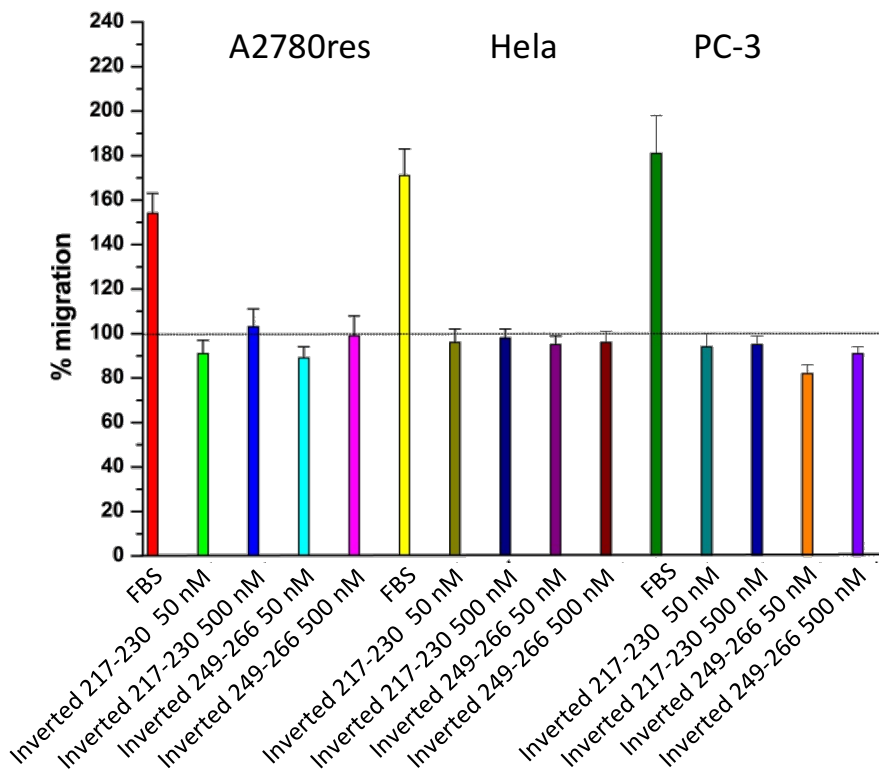


Figure 22: Effect of the inverted six peptides derived from OPN proteasome digestion on migration of A2780res, HeLa and PC-3 cell lines.

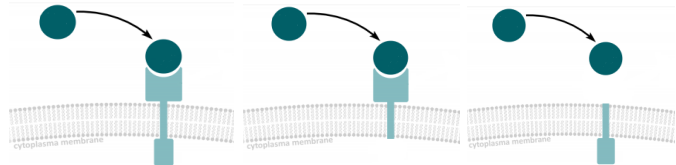
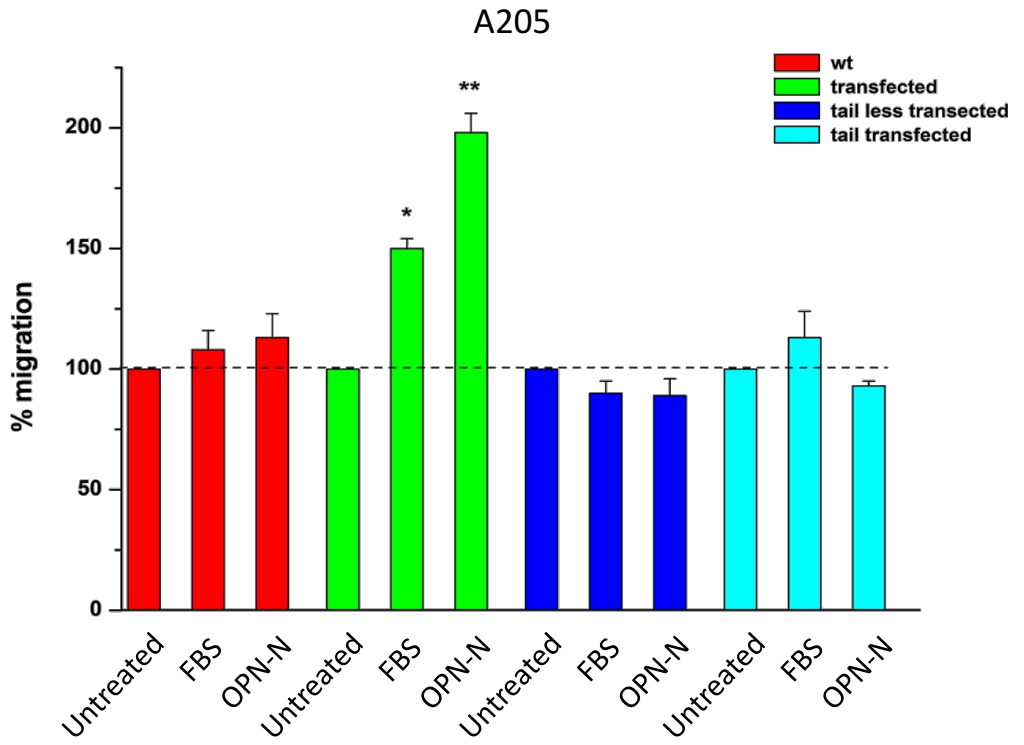


Figure 23: Effect of OPN-N on A2058 transfected with the receptor in the whole form, tail less or only tail. Data are expressed as the mean \pm SEM of the percentage of migration. (* $p < 0.05$; ** $p < 0.01$ vs control; Wilcoxon's signed rank test).

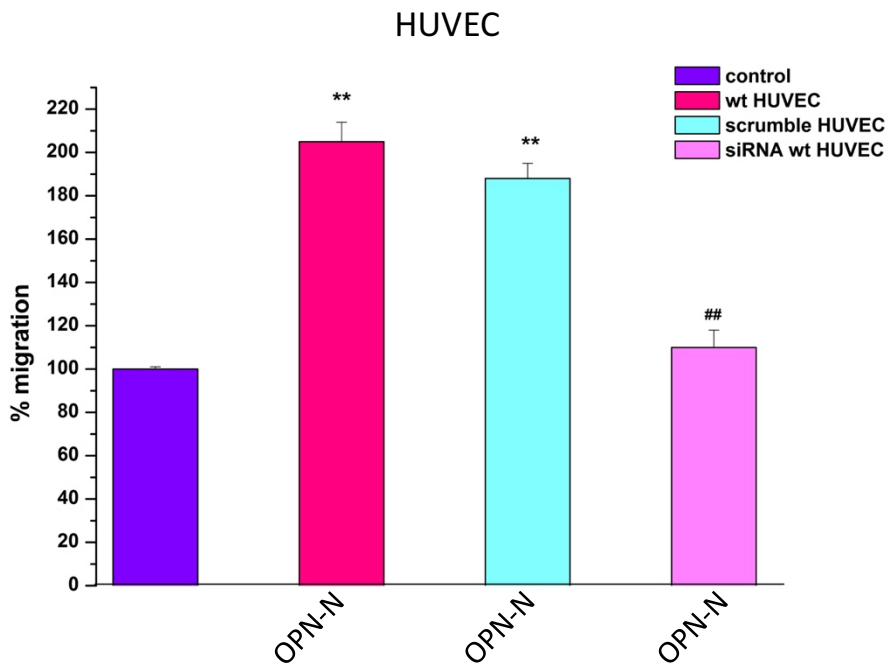


Figure 24: Effect of OPN-N on HUVECs silenced with a siRNA against the receptor. Data are expressed as the mean \pm SEM of the percentage of migration. (## $p < 0.05$ vs WT HUVEC; ** $p < 0.01$ vs control; Wilcoxon's signed rank test).

Discussion

The study on OPN involvement in MS allowed us to determine the different role played by OPN-N and OPN-C in pathological processes, such as cell migration and adhesion. This is a key point for deeper understanding the function of this protein and its derived forms. Indeed, the cleavage of OPN revealed to be fundamental for the gain of function of the two deriving fragments, since it allows the exposure of sites for the binding of specific molecules, such as CD44 and integrins. As a result, the effect of the two OPN forms reported to be higher than the one displayed by the whole OPN. After investigating the role played by OPN-FL, OPN-N and OPN-C in MS, our study addressed the evaluation of the function of the different OPN forms even in cancer. Indeed, OPN is overexpressed in a variety of human carcinomas, being implicated in inflammation, tumor progression, and metastasis (Thalmann et al. 1999; Chambers, Groom, and MacDonald 2002; Gotoh et al. 2002; Irby, McCarthy, and Yeatman 2004; Cook et al. 2005; Zhou et al. 2005; Bandopadhyay et al. 2014). Within the tumor microenvironment, OPN is produced by many cell types including the tumor itself and stromal or immune cells. For all these reasons, OPN is regarded by many as one of the most attracting targets for cancer therapy. Nevertheless, targeting OPN for therapeutic purposes needs to take into account the heterogeneous functions of the multiple OPN forms with regard to cancer formation and progression.

We decided to study how the two different OPN forms, OPN-N and OPN-C, triggered some of cancer processes, such as tumor cell migration and adhesion to endothelium. Therefore, OPN-N and OPN-C effects on tumour proliferation were tested on several tumour cell lines *in vitro*, and the obtained results were in line with those obtained on HUVECs and lymphocytes: OPN-N reported a

stimulatory effect on cell migration, whereas the induction of cell adhesion was ascribable to OPN-C. Also in this case, OPN cleavage by thrombin is responsible for the exposure of binding sites for an improved binding to its ligands.

Another evaluation was carried out on the fragments derived from the proteasome digestion of OPN, since also the levels of proteasome reported to be high in MS patients and the proteasome cleavage of OPN generates peptides which exert different functions in MS processes (Dianzani et al. 2017).

We tested the effect of the six generated peptides on tumor cells migration, in order to define if OPN proteasome digestion could be implicated even in cancer. Two of these six peptides revealed to be able to induce the migration of several cancer cell lines. Therefore, also in this case, OPN cleavage allows a binding sites exposure and thereby an improved interaction with its ligands, thus enhancing OPN effect on cell migration.

An important finding was figured out, since either OPN-N or the two peptides induced migration only on tumour cell lines that shared a particular feature: the presence of a specific receptor (which cannot be denominated for patent protection reasons) on their surface.

When this receptor in its whole form was transfected in a tumour cell line not expressing it, the stimulatory effect of OPN peptides on cell migration was reached. On the other hand, HUVECs silenced with a siRNA depleting the receptor, were no longer able to migrate after the peptides chemotactic stimulation. Obtained findings allow us to assert that this receptor is involved in OPN-triggered cancer cell migration. At present, further experiments and evaluations are ongoing to better understand the mechanisms underlying the activities of different OPN forms, with the aim of investigating novel approaches targeting distinct OPN forms and activities in distinct cells and tissues.

PUBLICATIONS

Article

Cyclodextrin-Based Nanohydrogels Containing Polyamidoamine Units: A New Dexamethasone Delivery System for Inflammatory Diseases

Monica Argenziano ¹, Chiara Dianzani ¹, Benedetta Ferrara ¹, Shankar Swaminathan ², Amedea Manfredi ³, Elisabetta Ranucci ³, Roberta Cavalli ^{1,*} and Paolo Ferruti ³

¹ Department of Drug Science and Technology, University of Torino, via P. Giuria 9, 10125 Torino, Italy; monica.argenziano@unito.it (M.A.); chiara.dianzani@unito.it (C.D.); benedetta.ferrara@unito.it (B.F.)

² Department of Ophthalmology, University of Tennessee Health Science Center, Memphis, TN 38163, USA; sswamin4@uthsc.edu

³ Dipartimento di Chimica, Università degli Studi di Milano, via C. Golgi 19, 20133 Milano, Italy; amedeamanfredi@unimi.it (A.M.); elisabetta.ranucci@unimi.it (E.R.); paolo.ferruti@unimi.it (P.F.)

* Correspondence: roberta.cavalli@unito.it; Tel.: +39-011-6707825

Academic Editor: Gaio Paradossi

Received: 10 March 2017; Accepted: 1 June 2017; Published: 8 June 2017

Abstract: Glucocorticoids are widely prescribed in treatment of rheumatoid arthritis, asthma, systemic lupus erythematosus, lymphoid neoplasia, skin and eye inflammations. However, well-documented adverse effects offset their therapeutic advantages. In this work, novel nano-hydrogels for the sustained delivery of dexamethasone were designed to increase both bioavailability and duration of the administered drug and reducing the therapeutic dose. Hydrogels are soft materials consisting of water-swollen cross-linked polymers to which the insertion of cyclodextrin (CD) moieties adds hydrophobic drug-complexing sites. Polyamidoamines (PAAs) are biocompatible and biodegradable polymers apt to create CD moieties in hydrogels. In this work, β or γ -CD/PAA nanogels have been developed. In vitro studies showed that a pretreatment for 24–48 h with dexamethasone-loaded, β -CD/PAA nanogel (nanodexa) inhibits adhesion of Jurkat cells to human umbilical vein endothelial cells (HUVEC) in conditions mimicking inflammation. This inhibitory effect was faster and higher than that displayed by free dexamethasone. Moreover, nanodexa inhibited COX-2 expression induced by PMA+A23187 in Jurkat cells after 24–48 h incubation in the 10^{-8} – 10^{-5} M concentration range, while dexamethasone was effective only at 10^{-5} M after 48 h treatment. Hence, the novel nanogel-dexamethasone formulation combines faster action with lower doses, suggesting the potential for being more manageable than the free drug, reducing its adverse side effects.

Keywords: dexamethasone; cyclodextrin/polyamidoamine nanohydrogels; topical delivery; β - and γ -Cyclodextrins; COX-2 expression

1. Introduction

Glucocorticoids (GCs) are anti-inflammatory and immunosuppressive agents widely used to treat systemic autoimmune diseases and a number of different conditions, such as asthma, skin diseases, eyes inflammations, allergic reactions, and cancers. They are also common medications in palliative care [1,2]. Despite their clinical efficacy, GCs cause several adverse reactions limiting their clinical usefulness. These adverse effects are mostly dependent on the duration and dosage of the therapy and are, therefore, particularly relevant in chronic diseases that require long-lasting treatments [3,4].

Dexamethasone is a potent glucocorticoid with a high effectiveness in downregulating the expression of anti-inflammatory cytokines. It is used to treat many ocular diseases and it is mainly administered as eye-drops. Unfortunately, high drug concentrations can lead to severe local and systemic side-effects. Moreover, eye-drops are rapidly cleared and consequently frequent instillations of high doses of dexamethasone are required [5].

To enhance the efficacy of dexamethasone and control the release kinetics to the target site in the meantime, decreasing doses and minimizing toxicity, efficient biodegradable and biocompatible nanodelivery systems have been studied. Nanoparticles present a number of advantages for the ocular delivery of drugs, comprising controlled drug release, drug targeting, increased surface adhesion, and drug penetration through mucus membranes. Various nanocarriers with different characteristics and architectures have been studied for the topical delivery of dexamethasone. A number of liposomes have been proposed as dexamethasone delivery systems. The effects of formulation parameters on the liposome physico-chemical properties were deeply investigated, showing that dexamethasone incorporation and release from liposomes was dependent on the type of lipid used and their sizes [6,7]. Previously, β -cyclodextrin-based nanosponges were developed for dexamethasone ocular delivery. Nanosponge formulations showed prolonged drug release kinetics and an increase of dexamethasone corneal permeability compared to marketed formulations [8]. Moreover, "smart" polymer nanoparticles responsive to external stimuli, such as temperature and pH values, or with mucoadhesion properties, received much attention to improve the therapeutic effects and minimize side effects. Polymer nanoparticles able to swell with the pH values can be exploited for the design of nanoformulations with controlled and targeted release kinetics suitable for ocular administration.

Very recently, dexamethasone-loaded Eudragit[®] RS (an anionic acrylate polymer) and ethyl cellulose nanoparticles exhibited the capability to adhere to the corneal surface and release the drug slowly and in a controlled manner over time [9]. Particularly, dexamethasone showed slower release kinetics in pH 4.5 acetic buffer than in pH 7.5 phosphate buffer. These results are in line with the swelling behavior of the acrylate polymer.

In addition, pH-sensitive polymeric nanoparticles showed a great potential for dermal and transfollicular dexamethasone delivery [10].

In this context, recent advances in drug nanotechnology underline the role played by nanogels for the delivery of dexamethasone [11]. Nanogels are nanostructures consisting of hydrophilic polymer networks and are promising vehicles for the delivery of a variety of different therapeutic agents [12]. Swelling and shrinkage of nanogels can be induced by changes in pH or temperature providing a triggered drug release [13]. Nanogels of methylcellulose hydrophobized with *N*-tert-butylacrylamide and containing dexamethasone were formulated in order to improve the topical ocular therapy by reducing the dosage and frequency of administration. Interestingly, cyclodextrins (CDs) could be integrated as functional units of nanogels in polymer networks acting as carriers of molecules with poor water solubility. Moreover, CD-based nanogels provide useful functionalities, such as effective bioconjugation, good adhesion to surfaces, controlled drug complexation, and drug release [14]. Moya-Ortega and colleagues showed that dexamethasone γ -cyclodextrin-based nanogel eye drops increased ocular bioavailability and gave high drug concentrations in the aqueous humor for at least 3 h after ocular administration in rabbits [15].

Polyamidoamines (PAAs) are biocompatible and biodegradable synthetic polymers apt to create hydrogels, and previously exploited for nanomedicine formulations [16].

Combining PAAs and cyclodextrins, a new nanogel platform was designed aimed at improving the topical administration of dexamethasone.

Here, we report on the development and in vitro characterization of a new ocular nanoformulation of dexamethasone, i.e., dexamethasone nanogel, attempting to ameliorate its therapeutic index by increasing the efficacy and decreasing the side effects.

2. Results

2.1. Characterization of Blank and Dexamethasone-Loaded Nanogels

The synthetic procedure tuned for preparing cyclodextrin-based nanogels allowed to obtain either β - or γ -cyclodextrin moieties in the hydrogel network. Two hydrogels were prepared as previously described [17] with modifications and were named β -CD/PAA and γ -CD/PAA, respectively.

The Fourier transformed infrared (FTIR) spectra of β -CD/PAA compared to β -CD are reported in Figure 1.

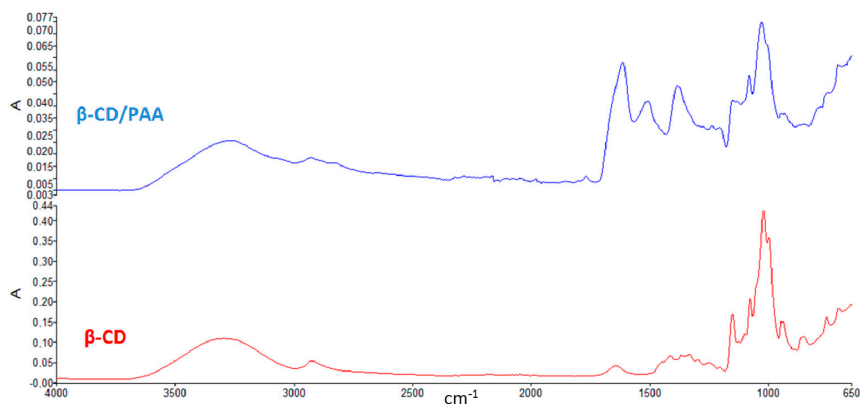


Figure 1. FTIR spectra of β -CD and β -CD/PAA.

The presence of peaks around 1500 cm^{-1} detectable only in the spectrum of β -CD/PAA confirmed the interaction of β -CD with the cross-linked units.

The two hydrogels were then reduced to nanometric size by the High Pressure Homogenization (HPH) technique, a top-down technology currently used as a pharmaceutical process for producing colloidal systems [18]. The procedure consisted of forcing a coarse hydrogel suspension in water with a piston having an applied pressure between 100 and 1500 bar through a tiny gap (5–10 μm). The mechanical stresses caused fragmentation of hydrogel matrices, thus producing nanosized particles with the same swelling capability of the parent hydrogels. Interestingly, β -CD/PAA and γ -CD/PAA nanohydrogels were pH sensitive due to the amphoteric nature of their PAA portion. In particular, the swelling degree of both types of nanogels increased regularly from pH 4.0 to 7.4.

Figure 2 reports the swelling degree of the two nanogels as a function of the pH value of the external medium. It may be observed that β -CD/PAA nanogel always exhibited a higher water uptake capability than γ -CD/PAA.

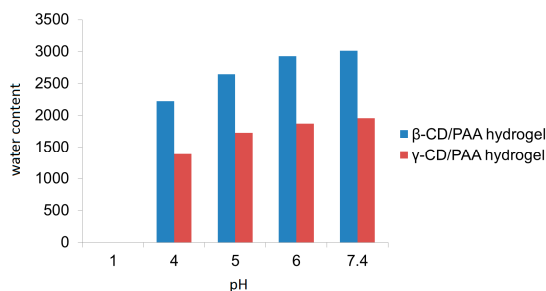


Figure 2. pH Dependence of β -CD/PAA and γ -CD/PAA nanogel swelling in aqueous media.

The β -CD/PAA nanogel showed a higher swelling degree compared to γ -CD/PAA nanogel; in particular at pH 7.4 an increase of 46% on the nanogel water uptake capability was observed.

Both unloaded nanogels showed average sizes of about 300 nm with a narrow size distribution and negative surface charge. The incorporation of dexamethasone was easily achieved without organic solvents. β -CD/PAA and γ -CD/PAA nanogels were able to incorporate dexamethasone with a loading capacity of 5.15% and 3.61%, respectively.

The physico-chemical characteristics of dexamethasone-loaded β -CD/PAA and γ -CD/PAA nanogels are reported in Table 1. Dynamic light scattering (DLS) analyses showed average diameters of about 310 nm and 370 nm for dexamethasone-loaded β -CD/PAA and γ -CD/PAA nanogels, respectively. The low polydispersity indices indicated a rather uniform population distribution due to the HPH step performed during the nanogel preparation. The zeta potential determination evidenced highly negative surface charges, with a ζ potential of about -30 mV, values essential for the physical stability of nanosuspensions, the electrostatic repulsions avoiding nanogel aggregation. Moreover, the negative charge can favor the interaction with mucin, which is positively charged. Indeed, a large amount of mucin was absorbed on the two nanogel surfaces, reaching a mucin binding efficiency of about 85%.

Table 1. Sizes and ζ potential values of dexamethasone-loaded β -CD/PAA and γ -CD/PAA nanogels.

Loaded Nanogels	Average Diameter (nm)	Polydispersity Index	ζ -Potential (mV)
β -CD/PAA	314 ± 3.5	0.10	-29.85 ± 1.5
γ -CD/PAA	372 ± 5.1	0.11	-33.30 ± 1.8

Transmission electron microscope image of blank and dexamethasone-loaded nanogels show the spherical shape of the system and confirmed the small sizes (Figure 3).

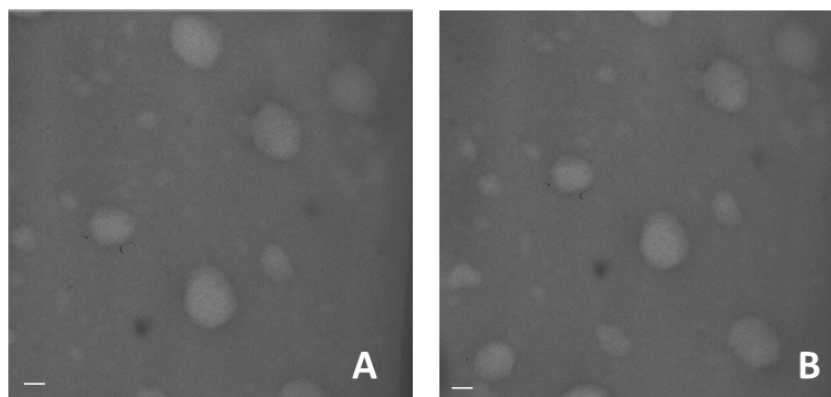


Figure 3. TEM image of blank (A) and dexamethasone-loaded nanogels (B) (scale bar 150 nm).

Figure 4 reports SEM images of the blank and dexamethasone-loaded nanogels.

Differential scanning calorimetry (DSC) analysis showed the incorporation of dexamethasone in the two types of nanogels. The absence of the drug endothermic peak (262 – 264 °C) in the thermograms of the loaded nanogels confirmed the occurrence of dexamethasone molecular interactions with the polymer matrices (Figure 5).

The in vitro release kinetics of dexamethasone from β -CD/PAA and γ -CD/PAA nanogels are reported in Figure 6.

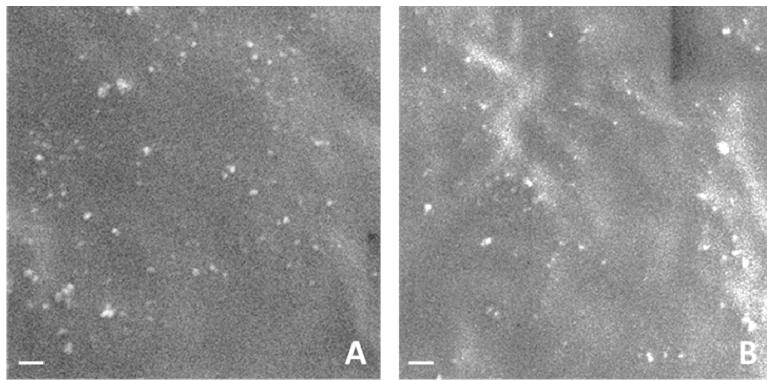


Figure 4. SEM image of blank (A) and dexamethasone-loaded nanogels (B) (scale bar 1 μm).

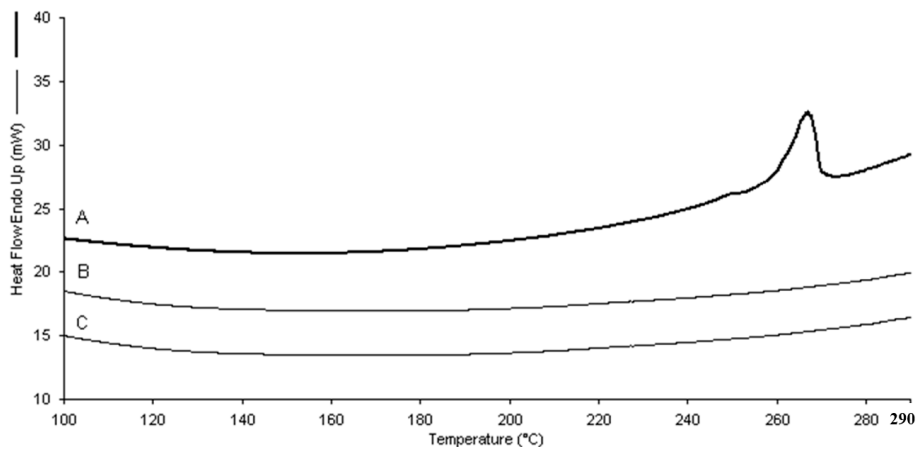


Figure 5. DSC thermograms of dexamethasone (A) and dexamethasone-loaded β -CD/PAA (B) and γ -CD/PAA (C) nanogels.

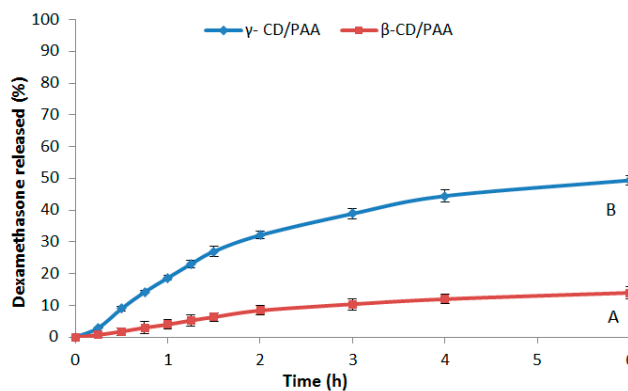


Figure 6. In vitro release kinetics of dexamethasone from β -CD/PAA (A) and γ -CD/PAA (B) nanogels at pH 7.4. Results are shown as means \pm SEM from three independent experiments ($n = 3$).

Both nanogels showed a slow and prolonged release profile over time at pH 7.4 and no initial burst effect was observed. In particular, only 14% of dexamethasone was released from the β -CD/PAA

nanogel after 6 h. On the contrary, after 6 h the percentage of dexamethasone recovered in the receiving phase from γ -CD-PAA was about 50%.

Concerning nanogel safety, no significant hemolysis caused by β -CD/PAA and γ -CD/PAA nanogels, either blank or dexamethasone-loaded, was observed, confirming their good biocompatibility and the presence of tonicity values suitable for ocular administration.

Based on their smaller size values, higher loading capability and on the slower release kinetics, β -CD/PAA nanogel was selected for the cell experiments and was named as nanodexa.

2.2. Effect of Dexamethasone or Nanodexa on Jurkat Cell Adhesion to IL-1 β -Stimulated HUVEC

GCs act on endothelial cells by decreasing vascular permeability, adhesion molecule expression, and production of IL-1 and prostaglandins (PGs). However, Kerachian et al. [19] also showed that high doses of GCs could sensitize HUVEC to the effect of inflammatory mediators favoring their development of pro-adhesive features. Therefore, we performed our adhesion assays using HUVEC treated or not with the pro-inflammatory cytokine IL-1 β to mimic pro-inflammatory conditions. HUVEC were treated for 24–48 h with increasing concentration of either dexamethasone (dexa) or nanodexa (10^{-9} – 10^{-5} M), then stimulated or not with IL-1 β for further 18 h and, finally, incubated with Jurkat cells in the adhesion assay for 45 min. Figure 7 shows the effect of dexa or nanodexa on Jurkat cell adhesion to IL-1 β -stimulated HUVEC after 24 h of treatment.

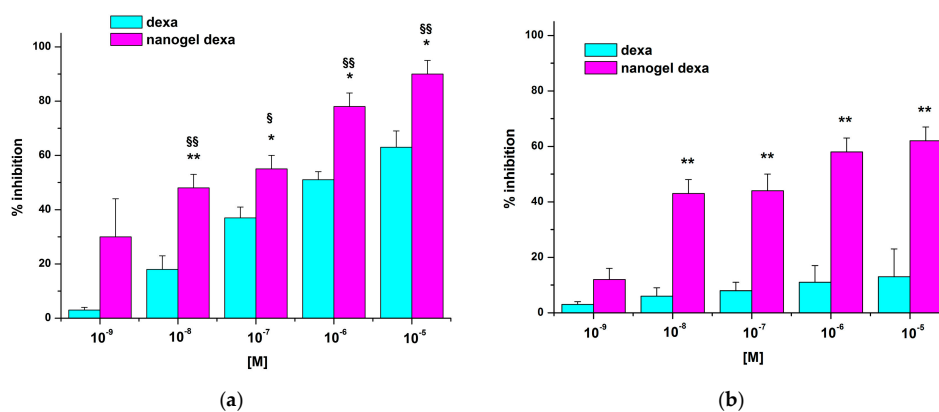


Figure 7. Effect of HUVEC treatment with dexa and nanodexa on adhesiveness to Jurkat cells. HUVEC were pretreated or not with titrated amounts of dexa and nanodexa (10^{-9} – 10^{-5} M) for 24 h (a) and 48 h (b), stimulated with IL-1 β for 18 h, then incubated with Jurkat cells for 45 min. Data are expressed as mean \pm SEM ($n = 5$) of the percentage of inhibition versus the control. * $p \leq 0.05$ and ** $p \leq 0.01$ nanodexa versus dexa (significance was assessed with Student's t -test for paired varieties). § $p < 0.05$; §§ $p < 0.01$, significantly different from untreated cells.

Nanodexa inhibited Jurkat cell adhesion in a concentration-dependent manner; the effect was already significant at 10^{-7} M (about 40% inhibition), with maximal inhibition (about 60%) obtained at 10^{-6} – 10^{-5} M. By contrast, no significant inhibition was detected with any concentration of free dexa at this time. Extending the duration of the treatment to 48 h, adhesion inhibition was detectable also for dexa, but only in the 10^{-7} – 10^{-5} M range of concentrations. By contrast, nanodexa was already effective at the 10^{-8} M dose and its concentration-response curve was substantially different from that of dexa ($p \leq 0.01$).

Figure 8 shows micrographs of the Jurkat adhesion assay on IL-1 β -stimulated HUVEC untreated (a) or treated with 10^{-7} M of either dexa (b: 36% of inhibition) or nanodexa (c: 55% of inhibition) for 48 h.

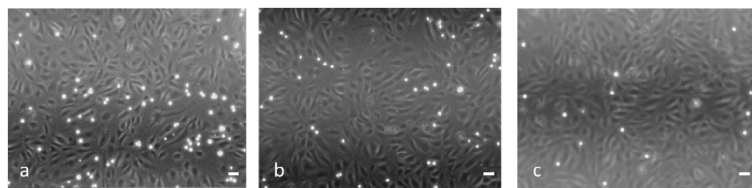


Figure 8. Fluorescent microscopy of Jurkat cells adherent to HUVECs that were not treated (a) or treated with dexa and nanodexa (b,c, respectively) (scale bar 10 μ m; magnification 100 \times).

2.3. Effect of Dexamethasone or Nanodexa on COX-2 Expression in Stimulated Jurkat Cells

COX-2 is upregulated during pathological conditions, such as inflammation and cancer, and glucocorticoids inhibit induction of COX-2 expression in a variety of cell lines and in response to different stimuli [20,21]. Since COX-2 is upregulated in T cells upon activation, we compared the activity on this induction exerted by dexa and nanodexa in Jurkat cell activated by the phorbol ester PMA (15 ng/mL) and calcium ionophore A23187 (1 μ M) [22]. Jurkat cells were treated for 24–48 h with increasing concentration of dexa and nanodexa (10^{-8} – 10^{-5} M) and COX-2 expression was then stimulated with PMA+A23187. Figure 9 shows the effect of dexa and nanodexa after 24 h (panel A,C) and 48 h (panel B,D) of treatment. While dexa inhibited COX-2 expression only by 35% at 10^{-7} M after 48 h incubation, nanodexa was already maximally active after 24 h in the 10^{-8} – 10^{-5} M concentration range.

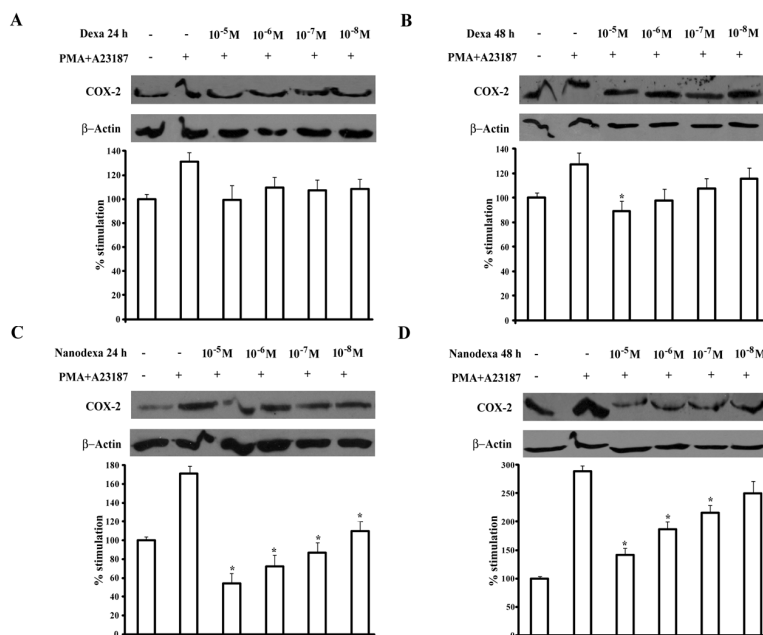


Figure 9. Effect of dexa or nanodexa on COX-2 expression in stimulated Jurkat. Jurkat were pretreated or not with titrated amounts of dexa or nanodexa (10^{-8} – 10^{-5} M) for 24 h (A,C, respectively) and 48 h (B,D, respectively) and then stimulated with PMA+A23187 for 18 h. Then, cells were lysed, and COX-2 expression was analyzed by Western blot. The bar graphs show data (mean \pm SEM) normalized to β -actin, expressed as the percentage of inhibition versus the control. * $p \leq 0.05$ (significance was assessed with one-way ANOVA and the Dunnett test). Top: Western blot analysis from a representative experiment. Bottom: Densitometric analysis of COX-2 expression expressed in arbitrary units of three independent experiments.

3. Discussion

Two cyclodextrin-based nanogels were obtained with attractive and promising properties as new biomaterial for dexamethasone ocular delivery. A polymer architecture comprising cross-linked cyclodextrin units was purposely tuned to load lipophilic molecules in a hydrophilic matrix. Indeed, the two nanogels were able to incorporate dexamethasone in good amounts due to the interaction with the hydrophobic cyclodextrin cavities and polymer networks. It is worth noticing that dexamethasone-CD complexes have been previously described in the literature [23–25]. Dexamethasone has a poor water solubility (about 0.1 mg/mL) and CDs showed the capability to improve the solubility and the topical bioavailability of the drug [5]. Previous studies suggested that the A-ring of the steroid molecule was predominantly included in the cavity of CDs. The inclusion complexation of dexamethasone with a number of CDs were determined, showing that the stability constant values of β -CD and γ -CD complexes were 9560 and 37,300 M^{-1} , respectively [26]. Here, the nanogel formulations were designed to increase the apparent water solubility of the drug and to enhance the contact time with the eye surface, key factors for improving the ocular drug delivery.

The β -CD/PAA nanogel provided a more stable complexation of dexamethasone than γ -CD/PAA, as the drug loading capacity and the *in vitro* release kinetics demonstrated. This behavior appeared in contrast with the stability constant values of the dexamethasone with the two parent CDs, as previously reported [26]. Indeed, we speculated that the bonding of CDs with the cross-linking agents in the nanogels may distort the CD cavity, so modifying the complexation capability with a guest molecule, as previously observed with alkylcarbonates derivatives of γ -cyclodextrins [27].

Intriguingly, the insertion of cyclodextrin moieties did not affect the high hydration properties of nanogels and the pH sensitive swelling capacity. β -CD/PAA showed a greater water content in comparison to the one of γ -CD/PAA. Different cross-linking degree and dimensions of network nanochannels might be present in the polymer matrix of β -CD/PAA and γ -CD/PAA, due to the different sizes of the two cyclodextrins, i.e., 262 and 427 \AA^3 for β -CD and γ -CD, respectively. The differences in the polymer nanostructure might affect the water uptake capability of the two nanohydrogels.

The *in vitro* release study showed prolonged release profiles of dexamethasone without a burst effect, but the drug kinetics varied according to the type of nanogels. The observed differences might be related to the presence of different nanochannel network in the polymer matrices, besides different interactions with the CD cavities. The slow and constant dexamethasone release might be useful to achieve a sustained drug concentration in the tear fluid on the eye surface.

For effective topical drug delivery into the eye, various polymer nanodelivery systems have been described in the literature showing a great potential to control the release kinetics and the penetration of corticosteroid [9,23].

Considering a possible future clinical application of the new dexamethasone delivery system the pharmacology activity was evaluated.

Dexamethasone is widely used for its ocular anti-inflammatory effect [1,28–30] but can also treat lymphoid neoplasia [31], and it has been used in solid cancer therapies in combination with antitumor drugs, such as 5-fluorouracil and cisplatin [32]. It exerts its anti-inflammatory and immunosuppressive effects by reducing the expression of cytokines and adhesion molecules, inhibiting leukocyte trafficking and access to inflammation sites and interfering with leukocyte, fibroblast and endothelial cell function. In this work, to evaluate the nanodexa activity, Jurkat cells were used to assess the inhibitory effect on adhesion to human umbilical vein endothelial cells (HUVEC) and COX-2 expression. Interestingly, we found that nanodexa inhibited Jurkat cell adhesion to HUVEC and COX-2 expression with earlier effects and at lower doses than free dexamethasone.

The anti-inflammatory and immunosuppressive actions of GCs are exerted by two different mechanisms. In the classic genomic pathway, dexamethasone modulates the expression of proteins via their interactions with the cytosolic GC receptor (GR). However, GCs can also act by non-genomic mechanisms [33]. The genomic pathway is considered responsible for many adverse effects of

GCs, most of which are time- and dose-dependent, such as osteoporosis, osteonecrosis, cataracts, hyperglycemia, coronary heart disease, and cognitive impairment, among others [34]. Consequently, the dose decrease is a key factor to control side effects of dexamethasone.

The marked anti-inflammatory effect obtained with nanodexa at lower concentration of the drug may play an important role in decreasing the administered dose and the adverse side effects.

Inflammation involves adhesive interactions between circulating leukocytes and endothelial cells lining the vascular wall. In response to various stimuli, such as the pro-inflammatory cytokines TNF- α , IL-1 β , INF- γ , and endothelial cells undergo inflammatory activation, producing an increased surface expression of cell adhesion molecules (CAMs), such as ICAM-1, VCAM-1, and E-selectin [35]. These endothelial CAMs play a fundamental role in leukocyte recruitment from the blood for tissue infiltration. Chronic induction of these CAMs leads to abnormal leukocyte recruitment, as seen in chronic inflammatory diseases [36]. Therefore, the effective inhibitory activity displayed by nanodexa on CAM expression by "inflamed" endothelial cells may be beneficial in blunting detrimental inflammatory reactions [37,38].

Even the potent inhibitory effect of nanodexa on COX-2 expression is intriguing. Prostaglandins (PGs) are known to be an important mediators of acute inflammation. They are synthesized by cyclooxygenase, comprising the constitutively expressed isoform COX-1 and the inducible isoform COX-2. COX-1 is expressed in most tissues that generate PGs during their normal physiological functions, and its expression does not fluctuate in response to stimuli. In contrast, COX-2 induction has critical roles in the response to tissue injury and infection and is an essential component of the inflammatory response and tissue repair [39]. Although the physiological activity of COX-2 may provide a definite benefit to the organism, its aberrant or excessive expression has been implicated in the pathogenesis of many diseases, such as chronic inflammations [40]. Taking into account that the positive effects of dexamethasone-loaded nanogels are exerted through earlier effectiveness and at lower doses than those of free dexamethasone, it may be hypothesized that this innovative nanogel formulation may increase the therapeutic efficacy with less adverse reactions. Finally, the small sizes and the mucoadhesive property of nanodexa can favor the ocular retention of the nanoformulation, contributing to the sustained release of the drug at the target site [41]. This might provide a long-lasting pharmacological activity with less frequent dexamethasone instillations.

4. Conclusions

Two promising cyclodextrin-based pH-sensitive nanogels were obtained. Morphological and physico-chemical properties of the dexamethasone-loaded nanogels made them suitable as prolonged release delivery systems for ocular administration.

Taken together, the *in vitro* results demonstrated that the β -CD/PAA dexamethasone nanoformulation is effective at lower doses and with faster onset compared to the free drug.

Therefore, dexamethasone in CD-PAA nanogels may represent a potential novel strategy to formulate eye drops able to overcome the shortcomings of this drug.

5. Materials and Methods

5.1. Materials

All materials were from Sigma-Aldrich (St. Louis, MO, USA). All reagents were of analytical grade.

5.2. PAA Hydrogel Synthesis

Two hydrogels were prepared as previously described [16] with modifications. Briefly, the polyaddition reaction between *prim*- or *bis-sec*-amines and bisacrylamides leads to polyamidoamines (PAAs). At pH \geq 11.5 the hydroxyl groups of cyclodextrins react with bisacrylamides in the same way and cyclodextrins behave as multifunctional monomers and give cross-linked polymer named nanosponges. With bisacrylamides, mixtures of cyclodextrins and amines give copolymeric hydrogels.

The CD-containing hydrogels used in this work were prepared from 2,2-bisacrylamido acetic acid (BAC) as bisacrylamide, 2-methyl piperazine (2-MP) as amine and β - or γ -cyclodextrin. The resultant hydrogels were named β -CD/PAA and γ -CD/PAA, respectively. In them, the PAA short chains connecting the CD moieties contained carboxyl- and amine groups and, in principle, had amphoteric properties. In a typical procedure, β -CD/PAA was prepared dissolving β -CD (734.84 mg, 0.62 mmol) and LiOH·H₂O (77.7 g, 1.83 mmol) in H₂O (0.4 mL) in a test tube. BAC (188.7 mg, 0.935 mmol) and LiOH·H₂O (39.6 mg, 0.935 mmol) were dissolved in H₂O (0.3 mL) in a second test tube, then 2-methylpiperazine (93.7 mg, 0.935 mmol) was added. The two solutions were thoroughly mixed and allowed to react at 25 °C for 48 h. The final product appeared as a homogeneous, transparent, and soft gel, which was triturated under water, and purified by repeated water/ethanol extraction cycles. The nanosponge sample was first soaked in deionized H₂O (50 mL) and allowed swelling for 2 h, the pH was lowered to 5 with HCl 37% *w/w* then the nanosponge was soaked in ethanol (50 mL) for 2 h. This procedure was repeated three times. The product was dried to a constant weight. Yield: 76%.

γ -CD/PAA was prepared following the same procedure described for β -CD/PAA. The monomers used and their amounts are reported below. The γ -CD was dissolved at about 95 °C.

γ -CD/PAA: γ -CD (1030.52 mg, 0.77 mmol), LiOH·H₂O (158.4 mg, 3.74 mmol), H₂O (0.7 mL), BAC (192.4 mg, 0.96 mmol), LiOH·H₂O (40.8 mg, 0.96 mmol), H₂O (0.3 mL), 2-methylpiperazine (96.3 mg, 0.96 mmol). Yield: 45%.

5.3. FTIR Analysis

Fourier transformed infrared (FTIR) spectra of β -CD and β -CD/PAA were obtained using a Perkin Elmer Spectrum 100 FT-IR in the region of 4000–650 cm⁻¹. Data acquisition was done by Spectrum software version 10.03.05 (Perkin Elmer Corporation, Waltham, MA, USA).

5.4. Swelling Capacity Evaluation

The swelling capacity of nanogels was evaluated by gravimetric analysis. A weighted amount of dry β -CD/PAA or γ -CD/PAA (W_d) was dispersed in 5.0 mL of PBS buffer at different pH values (i.e., 1, 4, 5, 6, 7.4). The mixture was stirred at 25 and 37 °C overnight. The supernatant was removed and then the wet weight (W_w) of the nanogels was measured. The swelling capacity (S_c) was calculated as the following equation: $S_c = (W_w - W_d)/W_d$.

5.5. Nanogel Preparation by HPH

Nanogels were obtained using a top down method. To this purpose, β -CD/PAA or γ -CD/PAA were suspended in saline solution (NaCl 0.9% *w/v*) at a concentration of 10 mg/mL and homogenized using a high shear homogenizer (Ultraturrax) for 10 min at 24,000 rpm. To further reduce the size of the nanogels and obtain an almost homogenous nanoparticle distribution, the sample underwent to high pressure homogenization for 90 min at a back-pressure of 500 bar, using an EmulsiFlex C5 instrument (Avastin, Ottawa, ON, Canada). The nanogels were then purified by dialysis (membrane cutoff of 12,000 Da) to eliminate potential synthesis residues.

5.6. Preparation of Dexamethasone-Loaded Nanogel

Dexamethasone was incorporated in the pre-formed nanogels, by the addition of dexamethasone (1 mg/mL) to the aqueous nanosuspension of β -CD/PAA or γ -CD/PAA. Then, the mixture was stirred at room temperature in dark conditions over night. A purification step by dialysis (Spectrapore, Rancho Dominguez, CA, USA, cellulose membrane, cutoff of 12,000 Da) was carried out to eliminate the unbound drug.

5.7. Physico-Chemical Characterization of Nanogels

The average diameters and polydispersity indices of nanogels were determined, after their dispersion in water, by photon correlation spectroscopy (PCS) using a 90 Plus Instrument (Brookhaven, NY, USA) at a fixed angle of 90° and at a temperature of 25 °C. Each sample was analyzed in triplicate. The nanogel zeta potentials were measured by electrophoretic mobility (90 Plus Instrument, Brookhaven, NY, USA). For zeta potential determination, the samples were diluted in water and placed in the electrophoretic cell, where an electric field of approximately 15 V/cm was applied. The morphology of nanogels was evaluated by scanning electron microscopy and transmission electron microscopy. For TEM analysis a Philips CM 10 transmission electron microscope was used. The samples were sprayed on Formvar-coated copper and air-dried before observation.

5.8. Thermal Analysis

Differential scanning calorimetry (DSC) was carried out by means of a Perkin Elmer DSC/7 differential scanning calorimeter (Perkin-Elmer, Waltham, MA, USA) equipped with a TAC 7/DX instrument controller. The instrument was calibrated with indium for melting point and heat of fusion. A heating rate of 10 °C/min was employed in the 25–250 °C temperature range. Standard aluminum sample pans (Perkin-Elmer) were used; an empty pan was used as a reference standard. Analyses were performed in triplicate on 3 mg freeze-dried samples under a nitrogen purge.

5.9. In Vitro Release Kinetics of Dexamethasone from Nanogels

In vitro drug release experiments were conducted in a multi-compartment rotating cell, comprising a donor chamber separated by a cellulose membrane (Spectrapore, cut-off = 12,000 Da) from a receiving chamber. One milliliter of dexamethasone-loaded nanogels was placed in the donor chamber. The receiving compartment contained 1 mL of phosphate-buffered saline (PBS) at pH 7.4 with 0.1% sodium dodecyl sulfate (SDS) to assure drug solubility. The receiving phase was withdrawn at regular intervals and completely replaced with the same amount of fresh solution, to maintain sink conditions. The concentration of dexamethasone in the withdrawn samples was detected by HPLC.

For the dexamethasone quantitative determination an HPLC analysis was performed using a Perkin Elmer pump (Perkin Elmer PUMP 250B, Waltham, MA, USA) equipped with a spectrophotometer detector (Flexar UV/Vis LC spectrophotometer detector, Perkin Elmer, Waltham, MA, USA). A reversed phase Agilent TC C18 column (150 cm × 4.6 mm, pore size 5 µm; Agilent Technologies, Santa Clara, CA, USA) was used. A mixture of acetonitrile – 25 mM phosphate buffer pH 3 (27:73, v/v) was used as the mobile phase at a flow rate of 1.0 mL/min and the effluent monitored by measuring absorbance at 246 nm. HPLC chromatograms of dexamethasone are reported in Supplementary Material (Figure S1).

5.10. Mucoadhesion Test

The in vitro evaluation of the mucoadhesive properties of nanogels was carried out. To this purpose, the interaction between mucin and nanogels was determined by turbidimetric assay.

Stock solutions of mucin (from porcine stomach) were prepared in water in the concentration range from 0.1 to 1 mg/mL. The transmittance of mucin solutions was measured at 500 nm with an UV spectrophotometer and a calibration curve was obtained. 1 mL of β-CD/PAA suspension was mixed with mucin stock solution and incubated under magnetic stirring for 30 min. Then, the samples were centrifuged for 5 min at 10,000 rpm and the transmittance of the supernatant, which contains the mucin non-adhesive to the β-CD/PAA hydrogel, was measured at 500 nm.

5.11. Determination of the Hemolytic Activity

For hemolytic activity determination, 100 µL of nanogels were incubated at 37 °C for 90 min with diluted blood (1:4 v/v) obtained by adding freshly-prepared PBS at pH = 7.4. After incubation,

nanogels-containing blood was centrifuged at 1000 rpm for 5 min to separate plasma. The amount of hemoglobin released due to hemolysis was determined spectrophotometrically (absorbance readout at 543 nm using a Duo spectrophotometer, Beckman, Brea, CA, USA). The hemolytic activity was calculated to reference with nanogel-free diluted blood. Complete hemolysis was induced by the addition of ammonium sulfate (20% *w/v*).

Optical microscopy was used to evaluate changes in red blood cell morphology after incubation with the formulations.

5.12. Cell Culture

HUVEC were isolated from human umbilical veins by trypsin treatment (1%) and cultured at 37 °C (5% CO₂, 85–95% humidity) in M199 medium with the addition of 20% fetal calf serum (FCS) and 100 U/mL penicillin, 100 µg/mL streptomycin, 5 UI/mL heparin, 12 µg/mL bovine brain extract, and 200 mM glutamine. HUVEC were grown to confluence in flasks and used at the 2nd–5th passage. Informed consent was obtained from all donors. All subjects gave their informed consent for inclusion before they participated in the study. The study was conducted in accordance with the Declaration of Helsinki, and the protocol was approved by the Ethics Committee of Turin University (Project DIAC_RLO1601). HUVEC viability was not affected by the treatment with the drug.

Leukemic human T cells (Jurkat, clone E6-1) were obtained from the American Type Culture Collection (ATCC; Manassas, VA, USA), and were cultured in RPMI 1640 medium supplemented with 10% FCS, 100 U/mL penicillin, and 100 µg/mL streptomycin at 37 °C in a 5% CO₂ humidified atmosphere.

5.13. Cells Adhesion Assay

HUVEC were grown to confluence in 24-well plates, washed, and rested for one day in M199 plus 10% FCS. The cells were incubated or otherwise with increasing concentrations of dexa or nanodexa (10⁻⁹–10⁻⁵ M) for 24–48 h, washed with fresh medium twice, stimulated for 24 h with IL-1β 1 ng/mL, and incubated with the Jurkat cells (1 × 10⁵ cell/well) for 45 min; this incubation time was chosen to allow full sedimentation of the adhering cells. After incubation, non-adherent cells were removed by being washed three times with M199. The centre of each well was analysed by fluorescence image analysis [33]. Adherent cells were counted by the Image Pro Plus Software for micro-imaging (version 5.0, Media Cybernetics, Rockville, MD, USA). Single experimental points were assayed in triplicate, and the standard error of the three replicates was always below 10%. Percentage inhibition of adhesion was calculated as follows: $(100 - (a)/(b)) \times 100$, where *a* is adhesion measured in the presence of the compound plus stimulus minus basal adhesion and *b* is adhesion elicited by stimulus minus basal adhesion. The adhesion measured on untreated cells was 25 ± 2 cells/microscope fields, and on IL-1β-stimulated cells was 58 ± 6 cells/microscope fields (*n* = 19).

5.14. Protein Extraction and Western Blot Analysis

In order to compare dexa with nanodexa effects on COX-2 expression, Jurkat cells were pre-treated with increasing concentrations of the drugs (10⁻⁸–10⁻⁵ M) for 24–48 h, and then stimulated with Phorbol 12-myristate 13-acetate (PMA) 15 ng/mL + A23187 1 µM for 18 h.

Cells were lysed in a buffer composed of 50 mM Tris-HCl pH 7.4, 150 mM NaCl, 5 mM EDTA, 1% NP40, phosphatase, and protease inhibitor cocktails. Cell lysates were cleared from insoluble fractions through high-speed centrifugation, and protein concentrations were determined with a commercially available kit (Bio Rad Laboratories, Hercules, CA, USA). Then, 10–40 µg proteins were separated on 10% SDS PAGE gels and transferred onto nitrocellulose membranes. These were blocked by incubation for 1 h at room temperature with 5% nonfat milk dissolved in TBS Tween 20. The membranes were probed overnight with the primary antibodies (Cell Signaling, Danvers, MA, USA, dilution 1/1000) and, after three washes, incubated for 1 h with horseradish peroxidase (HRP)-conjugated secondary

antibodies. Bands were detected by chemiluminescence, and densitometric analysis was performed with the Multi-Analyst software (version 1.1, Bio-Rad Laboratories, Hercules, CA, USA).

5.15. Statistical Analysis

If not differently stated, data are expressed as means \pm SEM. ($n = 3$). Statistical analysis was performed with GraphPad Prism 4.0 software (Graphpad Software Inc, San Diego, CA, USA). Significance was assessed with Student's *t*-test for paired varieties or with the one-way ANOVA and the Dunnett test with $p \leq 0.05$ as the cut-off.

Supplementary Materials: The following are available online at www.mdpi.com/2310-2861/3/2/22/s1.

Acknowledgments: We are grateful to the Obstetrics and Gynecology Unit, Martini Hospital, Torino, for providing human umbilical cords. This work was supported by the University of Turin Progetti di Ricerca di Ateneo Anno 2015.

Author Contributions: Monica Argenziano and Shankar Swaminathan formulated and in vitro characterized the nanoformulations, Benedetta Ferrara and Chiara Dianzani performed cell culture experiments, Amedea Manfredi synthesized PAA hydrogel, Paolo Ferruti designed the two PAA hydrogel structure and the synthetic route, Elisabetta Ranucci and Roberta Cavalli conceived the experiments and gave the intellectual rationale to the work.

Conflicts of Interest: The authors declare no conflict of interest.

Abbreviations

The following abbreviations are used in this manuscript:

HUVEC	human umbilical vein endothelial cells
Polyamidoamines	(PAAs)
Cyclodextrins	(CD)
2,2-bisacrylamidoacetic acid	(BAC)
2-methylpiperazine	(2-MeP)
High Pressure Homogenization	(HPH)
Glucocorticoids	(GCs)
Phorbol 12-myristate 13-acetate	(PMA)
GC receptor	(GR)
Prostaglandins	(PGs)

References

1. Barnes, P.J.; Adcock, I.; Spedding, M.; Vanhoutte, P.M. Anti-inflammatory actions of steroids: Molecular mechanisms. *Trends Pharmacol. Sci.* **1993**, *14*, 436–441. [[CrossRef](#)]
2. Thiem, A.; Rolke, R.; Radbruch, L. Glucocorticoids and androgens for treatment of tiredness and weakness in palliative care patients: A systematic review. *Schmerz* **2012**, *26*, 550–567. [[CrossRef](#)] [[PubMed](#)]
3. Harris, E.; Tigancescu, A.; Tubeuf, S.; Mackie, S.L. The prediction and monitoring of toxicity associated with long-term systemic glucocorticoid therapy. *Curr. Rheumatol. Rep.* **2015**, *17*, 513–523. [[CrossRef](#)] [[PubMed](#)]
4. Minneci, P.C.; Deans, K.J.; Banks, S.M.; Eichacker, P.Q.; Natanson, C. Meta-analysis: The effect of steroids on survival and shock during sepsis depends on the dose. *Ann. Intern. Med.* **2004**, *141*, 47–56. [[CrossRef](#)] [[PubMed](#)]
5. Villanueva, J.R.; Villanueva, L.R.; Navarro, M.G. Pharmaceutical technology can turn a traditional drug, dexamethasone into a first-line ocular medicine. A global perspective and future trends. *Int. J. Pharm.* **2017**, *516*, 342–351. [[CrossRef](#)] [[PubMed](#)]
6. Bhardwaj, U.; Burgess, D.J. Physicochemical properties of extruded and non-extruded liposomes containing the hydrophobic drug dexamethasone. *Int. J. Pharm.* **2010**, *388*, 181–189. [[CrossRef](#)] [[PubMed](#)]
7. Choksi, A.; Sarojini, K.V.; Vadnal, P.; Dias, C.; Suresh, P.K.; Khandare, J. Comparative anti-inflammatory activity of poly(amidoamine) (PAMAM) dendrimer-dexamethasone conjugates with dexamethasone-liposomes. *Int. J. Pharm.* **2013**, *449*, 28–36. [[CrossRef](#)] [[PubMed](#)]

8. Swaminathan, S.; Vavia, P.R.; Trotta, F.; Cavalli, R. Nanosponges encapsulating dexamethasone for ocular delivery: Formulation design, physicochemical characterization, safety and corneal permeability assessment. *J. Biomed. Nanotechnol.* **2013**, *9*, 998–1007. [[CrossRef](#)] [[PubMed](#)]
9. Balzus, B.; Sahle, F.F.; Hönzke, S.; Gerecke, C.; Schumacher, F.; Hedtrich, S.; Kleuser, B.; Bodmeier, R. Formulation and ex vivo evaluation of polymeric nanoparticles for controlled delivery of corticosteroids to the skin and the corneal epithelium. *Eur. J. Pharm. Biopharm.* **2017**, *115*, 122–130. [[CrossRef](#)] [[PubMed](#)]
10. Sahle, F.F.; Gerecke, C.; Kleuser, B.; Bodmeier, R. Formulation and comparative in vitro evaluation of various dexamethasone-loaded pH-sensitive polymeric nanoparticles intended for dermal applications. *Int. J. Pharm.* **2017**, *516*, 21–31. [[CrossRef](#)] [[PubMed](#)]
11. Jamard, M.; Hoare, T.; Sheardown, H. Nanogels of methylcellulose hydrophobized with N-tert-butylacrylamide for ocular drug delivery. *Drug Deliv. Transl. Res.* **2016**, *6*, 648–659. [[CrossRef](#)] [[PubMed](#)]
12. Kabanov, A.V.; Vinogradov, S.V. Nanogels as pharmaceutical carriers: Finite networks of infinite capabilities. *Angew. Chem. Int. Ed. Engl.* **2009**, *48*, 5418–5429. [[CrossRef](#)] [[PubMed](#)]
13. Urban, M.W.; Motornov, M.; Roiter, Y.; Tokarev, I.; Minko, S. Stimuli-responsive nanoparticles, nanogels and capsules for integrated multifunctional intelligent systems. *Prog. Polym. Sci.* **2010**, *35*, 174–211.
14. Moya-Ortega, M.D.; Alvarez-Lorenzo, C.; Concheiro, A.; Loftsson, T. Cyclodextrin-based nanogels for pharmaceutical and biomedical applications. *Int. J. Pharm.* **2012**, *428*, 152–163. [[CrossRef](#)] [[PubMed](#)]
15. Moya-Ortega, M.D.; Alves, T.F.G.; Alvarez-Lorenzo, C.; Concheiro, A.; Stefánsson, E.; Thorsteinsdóttira, M.; Loftsson, T. Dexamethasone eye drops containing-cyclodextrin-based nanogels. *Int. J. Pharm.* **2013**, *441*, 507–515. [[CrossRef](#)] [[PubMed](#)]
16. Ekkelenkamp, A.E.; Jansman, M.M.T.; Roelofs, K.; Engbersen, J.F.J.; Paulusse, J.M.J. Surfactant-free preparation of highly stable zwitterionic poly(amido amine) nanogels with minimal cytotoxicity. *Acta Biomater.* **2016**, *30*, 126–134. [[CrossRef](#)] [[PubMed](#)]
17. Ferruti, P.; Ranucci, E.; Cavalli, R. Nanogeli di Poliammidoammine. U.S. Patent MI2012A001407, 7 August 2012.
18. Leone, F.; Cavalli, R. Drug nanosuspensions: A ZIP tool between traditional and innovative pharmaceutical formulations. *Expert Opin. Drug Deliv.* **2015**, *12*, 1607–1625. [[CrossRef](#)] [[PubMed](#)]
19. Kerachian, M.A.; Cournoyer, D.; Harvey, E.J.; Chow, T.Y.; Neagoe, P.E.; Sirois, M.G.; Séguin, C. Effect of high-dose dexamethasone on endothelial haemostatic gene expression and neutrophil adhesion. *J. Steroid Biochem. Mol. Biol.* **2009**, *116*, 127–133. [[CrossRef](#)] [[PubMed](#)]
20. Iñiguez, M.A.; Punzón, C.; Fresno, M. Induction of cyclooxygenase-2 on activated T lymphocytes: Regulation of T cell activation by cyclooxygenase-2 inhibitors. *J. Immunol.* **1999**, *163*, 111–119. [[PubMed](#)]
21. Zarghi, A.; Arfaei, S. Selective COX-2 Inhibitors: A Review of Their Structure-Activity Relationships. *Iran. J. Pharm. Res.* **2011**, *10*, 655–683. [[PubMed](#)]
22. De Gregorio, R.; Iñiguez, M.A.; Fresno, M.; Alemany, S. Cot kinase induces cyclooxygenase-2 expression in T cells through activation of the nuclear factor of activated T cells. *J. Biol. Chem.* **2011**, *276*, 27003–27009. [[CrossRef](#)] [[PubMed](#)]
23. Loftsson, T.; Stefánsson, E. Cyclodextrins and topical drug delivery to the anterior and posterior segments of the eye. *Int. J. Pharm.* **2017**, in press. [[CrossRef](#)] [[PubMed](#)]
24. Jansook, P.; Ritthidej, G.C.; Ueda, H.; Stefánsson, E.; Loftsson, T. γ CD/HP γ CD mixtures as solubilizer: Solid-state characterization and sample dexamethasone eye drop suspension. *J. Pharm. Pharm. Sci.* **2010**, *13*, 336–350. [[CrossRef](#)] [[PubMed](#)]
25. Doile, M.M.; Fortunato, K.A.; Schmücker, I.C.; Schucko, S.K.; Silva, M.A.; Rodrigues, P.O. Physicochemical properties and dissolution studies of dexamethasone acetate- β -cyclodextrin inclusion complexes produced by different methods. *AAPS PharmSciTech* **2008**, *9*, 314–321. [[CrossRef](#)] [[PubMed](#)]
26. Uekama, K.; Fujinaga, T.; Hirayama, F.; Otagiri, M.; Yamasaki, M. Inclusion complexations of steroid hormones with cyclodextrins in water and in solid phase. *Int. J. Pharm.* **1982**, *10*, 1–15.
27. Cavalli, R.; Trotta, F.; Trotta, M.; Pastero, L.; Aquilano, D. Effect of alkylcarbonates of γ -cyclodextrins with different chain lengths on drug complexation and release characteristics. *Int. J. Pharm.* **2007**, *339*, 197–204. [[CrossRef](#)] [[PubMed](#)]
28. Giuliano, C.; Smalligan, R.D.; Mitchon, G.; Chua, M. Role of dexamethasone in the prevention of migraine recurrence in the acute care setting: A review. *Postgrad. Med.* **2012**, *124*, 110–115. [[CrossRef](#)] [[PubMed](#)]

29. Abadia, B.; Calvo, P.; Ferreras, A.; Bartol, F.; Verdes, G.; Pablo, L. Clinical Applications of Dexamethasone for Aged Eyes. *Drugs Aging* **2016**, *33*, 639–646. [[CrossRef](#)] [[PubMed](#)]
30. Rafie, F.; Javadzadeh, Y.; Javadzadeh, A.R.; Ghavidel, L.A.; Jafari, B.; Moogooee, M.; Davaran, S. In vivo evaluation of novel nanoparticles containing dexamethasone for ocular drug delivery on rabbit eye. *Curr. Eye Res.* **2010**, *35*, 1081–1089. [[CrossRef](#)] [[PubMed](#)]
31. De Bosscher, K.; van den Berghe, W.; Haegeman, G. The interplay between the glucocorticoid receptor and nuclear factor-kappaB or activator protein-1: Molecular mechanisms for gene repression. *Endocr. Rev.* **2003**, *24*, 488–522. [[CrossRef](#)] [[PubMed](#)]
32. Li, M.; Chen, F.; Liu, C.P.; Li, D.M.; Li, X.; Wang, C.; Li, J.C. Dexamethasone enhances trichosanthin-induced apoptosis in the HepG2 hepatoma cell line. *Life Sci.* **2010**, *86*, 10–16. [[CrossRef](#)] [[PubMed](#)]
33. Ruiz-Irastorza, G.; Danza, A.; Khamashta, M. Glucocorticoid use and abuse in SLE. *Rheumatology* **2012**, *51*, 1145–1153. [[CrossRef](#)] [[PubMed](#)]
34. Zhang, D.; Marconi, A.; Xu, L.-M.; Yang, C.; Sun, G.; Feng, X.; Ling, C.; Qin, W.; Uzan, G.; D'Alessio, P. Tripterine inhibits the expression of adhesion molecules in activated endothelial cells. *J. Leukoc. Biol.* **2006**, *80*, 309–319. [[CrossRef](#)] [[PubMed](#)]
35. Szmítok, P.E.; Wang, C.; Weisel, R.D.; Jeffries, G.A.; Anderson, T.J.; Verma, S. Biomarkers of vascular disease linking inflammation to endothelial activation Part II. *Circulation* **2003**, *108*, 1917–1923. [[CrossRef](#)] [[PubMed](#)]
36. Meager, A. Cytokine regulation of cellular adhesion molecule expression in inflammation. *Cytokine Growth Factor Res.* **1999**, *10*, 27–39. [[CrossRef](#)]
37. D'Alessio, P. Endothelium as a pharmacological target. *Curr. Opin. Investig. Drugs* **2001**, *2*, 1720–1724. [[PubMed](#)]
38. Vane, J.R.; Botting, R.M. Anti-inflammatory drugs and their mechanism of action. *Inflamm. Res.* **1998**, *47* (Suppl. 2), S78–S87. [[CrossRef](#)] [[PubMed](#)]
39. Schottenfeld, D.; Beebe-Dimmer, J. Chronic Inflammation: A Common and Important Factor in the Pathogenesis of Neoplasia. *CA Cancer J. Clin.* **2006**, *56*, 69–83. [[CrossRef](#)] [[PubMed](#)]
40. Dianzani, C.; Minelli, R.; Mesturini, R.; Chiochetti, A.; Barrera, G.; Boscolo, S.; Sarasso, C.; Gigliotti, C.L.; Sblattero, D.; Yagi, J.; et al. B7h triggering inhibits umbilical vascular endothelial cell adhesiveness to tumor cell lines and polymorphonuclear cells. *J. Immunol.* **2010**, *185*, 3970–3979. [[CrossRef](#)] [[PubMed](#)]
41. Chetoni, P.; Burgalassi, S.; Monti, D.; Tampucci, S.; Tullio, V.; Cuffini, A.M.; Muntoni, E.; Spagnolo, R.; Zara, G.P.; Cavalli, R. Solid lipid nanoparticles as promising tool for intraocular tobramycin delivery: Pharmacokinetic studies on rabbits. *Eur. J. Pharm. Biopharm.* **2016**, *109*, 214–223. [[CrossRef](#)] [[PubMed](#)]



Basic Study

Solid lipid nanoparticles delivering anti-inflammatory drugs to treat inflammatory bowel disease: Effects in an *in vivo* model

Chiara Dianzani, Federica Foglietta, Benedetta Ferrara, Arianna Carolina Rosa, Elisabetta Muntoni, Paolo Gasco, Carlo Della Pepa, Roberto Canaparo, Loredana Serpe

Chiara Dianzani, Federica Foglietta, Benedetta Ferrara, Arianna Carolina Rosa, Elisabetta Muntoni, Carlo Della Pepa, Roberto Canaparo, Loredana Serpe, Department of Drug Science and Technology, University of Torino, 10125 Torino, Italy

Paolo Gasco, Nanovector s.r.l, 10144 Torino, Italy

Author contributions: Dianzani C, Foglietta F, Ferrara B and Rosa AC performed the *in vitro* and *in vivo* experiments; Muntoni E was responsible for animal handling and performed the *in vivo* disease activity evaluation; Gasco P synthesized and characterized the anti-inflammatory drug nanoformulation; Della Pepa C analyzed the data and contributed to the discussion; Canaparo R analyzed the data, contributed to the discussion and reviewed the manuscript; Serpe L designed the study, analyzed the data and wrote the manuscript. All the authors have read and approved the final manuscript.

Supported by Regione Piemonte (grant “Converging Technologies”, NanoIGT) and University of Torino (grant “Ricerca Locale”, Linea A).

Institutional review board statement: The study was reviewed and approved by the Institutional Review Board of the University of Torino (Torino, Italy).

Conflict-of-interest statement: The authors declare that they have no competing interests.

Data sharing statement: The technical appendix, statistical code, and dataset are available from the corresponding author at email address loredana.serpe@unito.it.

Open-Access: This article is an open-access article which was selected by an in-house editor and fully peer-reviewed by external reviewers. It is distributed in accordance with the Creative Commons Attribution Non Commercial (CC BY-NC 4.0) license, which permits others to distribute, remix, adapt, build upon this work non-commercially, and license their derivative works on different terms, provided the original work is properly cited and the use is non-commercial. See: <http://creativecommons.org/licenses/by-nc/4.0/>

[licenses/by-nc/4.0/](http://creativecommons.org/licenses/by-nc/4.0/)

Manuscript source: Invited manuscript

Correspondence to: Loredana Serpe, MD, PhD, Department of Drug Science and Technology, University of Torino, Via Pietro Giuria 13, 10125 Torino, Italy. loredana.serpe@unito.it
Telephone: +39-11-6706235
Fax: +39-11-6706230

Received: February 7, 2017

Peer-review started: February 10, 2017

First decision: March 21, 2017

Revised: April 3, 2017

Accepted: May 4, 2017

Article in press: May 4, 2017

Published online: June 21, 2017

Abstract**AIM**

To improve anti-inflammatory activity while reducing drug doses, we developed a nanoformulation carrying dexamethasone and butyrate.

METHODS

Dexamethasone cholesteryl butyrate-solid lipid nanoparticles (DxCb-SLN) were obtained with the warm microemulsion method. The anti-inflammatory activity of this novel nanoformulation has been investigated *in vitro* (cell adhesion to human vascular endothelial cells and pro-inflammatory cytokine release by lipopolysaccharide-induced polymorphonuclear cells) and *in vivo* (disease activity index and cytokine plasma concentrations in a dextran sulfate sodium-induced mouse colitis) models. Each drug was also administered separately to compare its effects with those induced by their co-administration in SLN at the same concentrations.

RESULTS

DxCb-SLN at the lowest concentration tested (Dx 2.5 nmol/L and Cb 0.1 μ mol/L) were able to exert a more than additive effect compared to the sum of the individual effects of each drug, inducing a significant *in vitro* inhibition of cell adhesion and a significant decrease of pro-inflammatory cytokine (IL-1 β and TNF- α) in both *in vitro* and *in vivo* models. Notably, only the DxCb nanoformulation administration was able to achieve a significant cytokine decrease compared to the cytokine plasma concentration of the untreated mice with dextran sulfate sodium-induced colitis. Specifically, DxCb-SLN induced a IL-1 β plasma concentration of 61.77% \pm 3.19%, whereas Dx or Cb used separately induced a concentration of 90.0% \pm 2.8% and 91.40% \pm 7.5%, respectively; DxCb-SLN induced a TNF- α plasma concentration of 30.8% \pm 8.9%, whereas Dx or Cb used separately induced ones of 99.5% \pm 4.9% and 71.1% \pm 10.9%, respectively.

CONCLUSION

Our results indicate that the co-administration of dexamethasone and butyrate by nanoparticles may be beneficial for inflammatory bowel disease treatment.

Key words: Nanoparticles; Dexamethasone; Butyrate; Inflammatory bowel disease; Drug delivery systems

© The Author(s) 2017. Published by Baishideng Publishing Group Inc. All rights reserved.

Core tip: The oral treatment with dexamethasone and butyrate co-loaded into nanoparticles was effective in achieving strong anti-inflammatory effects at doses significantly lower than those required for each single drug. This nanoformulation may open a new window on the treatment of chronic inflammatory conditions such as inflammatory bowel disease, where dose- and time-dependent side effects can limit the drug's therapeutic usefulness. Notably, dexamethasone cholesteryl butyrate-solid lipid nanoparticles significantly relieved and repaired colon inflammation in a colitis mouse model thanks to the nanoformulation, which displayed an additive synergism among the corticosteroid, dexamethasone, and the short-chain fatty acid, butyrate.

Dianzani C, Foglietta F, Ferrara B, Rosa AC, Muntoni E, Gasco P, Della Pepa C, Canaparo R, Serpe L. Solid lipid nanoparticles delivering anti-inflammatory drugs to treat inflammatory bowel disease: Effects in an *in vivo* model. *World J Gastroenterol* 2017; 23(23): 4200-4210 Available from: URL: <http://www.wjgnet.com/1007-9327/full/v23/i23/4200.htm> DOI: <http://dx.doi.org/10.3748/wjg.v23.i23.4200>

INTRODUCTION

Inflammation is a physiological process that involves different cells, such as leukocytes and endothelial cells that establish adhesive interactions in order

to transverse the vascular wall and migrate to the damaged tissue. Inflammatory bowel diseases (IBDs), including ulcerative colitis and Crohn's disease, are comprised of chronic and deregulated inflammation of the intestinal mucosa characterized by active inflammation, tissue destruction and repeated attempts at tissue repair that lead to a waxing-waning course. This persistent inflammation is triggered by neutrophil and macrophage infiltration, with activated macrophages producing a potent mixture of broadly active inflammatory cytokines, including interleukin (IL)-1 β and tumor necrosis factor (TNF)- α ^[1,2]. In response to such pro-inflammatory cytokines, endothelial cells undergo inflammatory activation, resulting in an increased surface expression of cell adhesion molecules (CAMs), such as ICAM-1, VCAM-1 and E-selectin^[3]. These endothelial CAMs play a fundamental role in leukocyte recruitment from the blood for tissue infiltration. Chronic induction of these CAMs leads to abnormal leukocyte recruitment, like that observed in chronic inflammatory diseases characterized by profound tissue remodeling and loss of function^[4].

Recently, the traditional therapeutic approach of IBD, with the introduction of biologic agents, has moved away from non-specific immunomodulators, including corticosteroids, thiopurines, and methotrexate toward a pathway-based anti-inflammatory approach. Even though the introduction of TNF inhibitors such as infliximab, as well as anti-integrins, has initiated a new therapeutic era, these biologics are clinically effective only in a subgroup of IBD patients^[5,6]. Therefore, IBD treatment is still a difficult challenge, and efforts to facilitate effective drug treatment are still necessary. Corticosteroids exert their anti-inflammatory and immunosuppressive effects by reducing the expression of cytokines and adhesion molecules, inhibiting leukocyte traffic and access to the inflammation site. In particular, dexamethasone (Dx) has been used for decades in the treatment of IBD flares, even if a such life-long treatment might produce several adverse reactions that are mostly time- and dose-dependent, limiting its clinical usefulness^[1,7,8]. Hence, attempts to maintain the IBD therapeutic effects of corticosteroids while minimizing their systemic side effects might provide a major therapeutic improvement.

With regard to corticosteroids and pharmaceutical technology, to date only the novel oral formulation of budesonide using multi-matrix (MMX) drug delivery technology has been introduced as a treatment option for patients with ulcerative colitis, allowing a wider colonic targeting with low systemic bioavailability. The MMX strategy is an extension of the pH-responsive polymer technique that allows the sustained release of a drug enclosed within a gastro-resistant, pH-dependent coating^[9]. However, it seems likely that all such systems relying on pH-responsive polymers will not be truly colon site-specific^[10].

Recent advances in nanotechnology have enabled the development of new corticosteroid formulations with a nanometric approach to ameliorate

pharmacological properties, resulting in increased efficacy and reduction of side effects^[11]. Different from the MMX strategy, the nanoparticle drug delivery strategy relies on the nanosize as the cardinal property for interaction with biological systems. Indeed, the nanosize determines the ability to penetrate cell membranes, thus facilitating the passage across biological barriers, interaction with the immune system, uptake, absorption and distribution^[12]. For instance, the size of orally assumed nanoparticles may somehow determine their fate, addressing the kind of cell with which to interact (*i.e.*, epithelial or phagocytic cells), or the depth level in the intestinal mucosa. Moreover, nanoparticles can directly enter into phagocytic cells populating the inflamed tissue, thus providing a wider distribution and an additional mechanism for drug targeting^[13].

Furthermore, the potential inhibitory effect of nanoparticle formulations of Dx on cyclooxygenase-2 (COX-2) expression is interesting. Although the physiological activity of COX-2 may provide a benefit to the organism, its aberrant expression has been implicated in the pathogenesis of many diseases, such as chronic inflammation and carcinogenesis^[14]. Moreover, the effective inhibitory activity displayed by nanoparticle formulations of Dx on CAM expression by "inflamed" endothelial cells may be beneficial in blunting detrimental inflammatory reactions^[15,16]. In particular, the incorporation of Dx into solid lipid nanoparticles (SLN) showed a significant improvement of its anti-inflammatory activity in a human IBD whole-blood model. SLN loaded with Dx exerted earlier anti-inflammatory effects and at lower doses than free Dx, highlighting how this nanoparticle formulation may be of therapeutic interest^[17]. It is well-known that nanoparticles are efficiently taken up by immunocompetent cells, so that nanoparticulate drug carriers may be useful in targeting the inflamed regions. Indeed, in the presence of IBD there is a strong cellular immunoresponse from the inflamed regions, and the nanoparticle passive targeting may allow for the accumulation of the drug loaded into the nanoparticulate carrier in the inflamed area^[11].

Furthermore, our group investigated whether the association between Dx and another anti-inflammatory agent such as butyrate might be of therapeutic interest in IBD. Butyrate is a short-chain fatty acid (SCFA) normally released by intestinal epithelial cells, which exhibit several physiological and immunological functions^[18]. Like other SCFA, such as acetate and propionate, butyrate has regulatory effects on the proliferation, differentiation, gene expression and immune regulation of colon epithelial and immune cells. In particular, in experimental models, butyrate has been demonstrated to stimulate mucus production by colon epithelial cells, to inhibit colon inflammation and oxidative stress, and to improve the colon defense barriers, inhibiting colon carcinogenesis as well^[19-21]. Butyrate has emerged as a modulator of adaptive responses, owing to its multiple biofunctions, *i.e.*,

restoring transforming growth factor- β (TGF- β) and IL-10 production in the colonic mucosa, inducing T cell apoptosis and dampening interferon- γ (IFN- γ) secretion^[22,23]. Clinical trials have shown the effectiveness of butyrate monotherapy and/or in combination with conventional treatment in patients with diversion colitis, acute radiation proctitis, as well as ulcerative colitis^[24-27]. In this regard, in the 1990s non-controlled pilot clinical trials using oral administration or enemas of butyrate yielded promising results in ulcerative colitis patients^[28]. However, extended confirmatory studies have not yet been performed. On the other hand, in a randomized, double-blind, placebo-controlled study on ulcerative colitis patients, the combined treatment of oral sodium butyrate tablets in combination with mesalazine significantly decreased the disease activity index score and improved disease outcomes with respect to mesalazine alone^[26].

Therefore, owing to partial patient compliance or restricted indications, these treatments were not established as a standard of care. Recent studies have renewed the expectations in regard to strategies related to intestinal SCFA. The administration of probiotic bacteria with the capacity to produce butyrate has been shown to improve the symptoms in IBD models *in vivo*^[29]. Moreover, the treatment with butyrate has been shown to increase apoptosis and differentiation, and to inhibit proliferation in colon, breast, gastric, lung, brain and pancreas cancer cells^[30,31]. Butyrate is characterized by a short half-life, due to its rapid metabolism and excretion through the liver. Therefore, continuous administration of the drug is required in order to maintain therapeutic concentrations^[32]. In addition, the use of butyrate in therapy is limited by its dose-dependent side effects, such as anemia, headache, nausea, diarrhea and abdominal cramps.

In order to overcome these limitations, SLN have been proposed for improving butyrate therapy, in that they constitute a drug delivery system able to ensure high drug loading, enhanced drug pharmacokinetic profile, good biocompatibility and scale-up feasibility^[33-35]. The use of SLN has been under investigation in various preclinical and clinical trials, especially in cancer therapy, and their employment has been approved for clinical use in some cases^[36]. Cholesteryl butyrate (Cb) as a butyrate SLN formulation has been evaluated in several *in vitro* and *in vivo* studies as an anticancer agent^[37-41] and only in *in vitro* studies as anti-inflammatory agent^[17,42].

Thus, our group sought to develop a new SLN formulation carrying dexamethasone and cholesteryl butyrate (DxCb) and investigated the efficacy of this strategy in strengthening the effect of each single drug in the treatment of inflammation. Specifically, investigations of this new anti-inflammatory SLN formulation were carried out in the following IBD models: (1) *in vitro*, evaluating the effects on cell adhesion to human vascular endothelial cells and on pro-inflammatory cytokine release by lipopolysaccharide

Table 1 Composition of warm microemulsion for cholesteryl butyrate and dexamethasone cholesteryl butyrate-solid lipid nanoparticles formulations

Molar composition of warm microemulsion	Cb, mmol/L	DxCb-SLN, mmol/L
Dexamethasone 21-acetate	-	8.1
Cholesteryl butyrate	273.7	273.7
Epikuron™ 200 (purified phosphatidylcholine 92%)	335.5	335.5
Sodium glycocholate	194.8	194.8

Cb: Cholesteryl butyrate; DxCb-SLN: Dexamethasone cholesteryl butyrate-solid lipid nanoparticles.

Table 2 Concentration of main components of water dispersion of cholesteryl butyrate and dexamethasone cholesteryl butyrate-solid lipid nanoparticles formulations after 4 washing steps (HPLC method determination)

Molar composition of final dispersion after washing	Cb, mmol/L	DxCb-SLN, mmol/L
Dexamethasone 21-acetate	-	1.1
Cholesteryl butyrate	36.0	38.5
Phosphatidylcholine	48.4	49.2
Sodium glycocholate	12.5	11.2

Cb: Cholesteryl butyrate; DxCb-SLN: Dexamethasone cholesteryl butyrate-solid lipid nanoparticles.

Table 3 Average value of hydrodynamic diameter (*Zave*) and polydispersity index of cholesteryl butyrate and dexamethasone cholesteryl butyrate-solid lipid nanoparticles formulations

Physical characterization DLS analysis	Cb	DxCb-SLN
<i>Zave</i> in nm	79.6	72.9
Polydispersity index	0.25	0.28

Cb: Cholesteryl butyrate; DxCb-SLN: Dexamethasone cholesteryl butyrate-solid lipid nanoparticles.

(LPS)-induced polymorphonuclear cells; and (2) *in vivo*, evaluating the effects in dextran sulfate sodium-induced mouse colitis.

MATERIALS AND METHODS

Preparation and characterization of DxCb-SLN

Cb and DxCb-SLN were obtained with the warm microemulsion method (patent WO0030620). This process is based on mixing, in precise ratio, the melted lipid matrix loaded with hydrophobic drug with water phase (maintained at the same melting temperature as the lipid matrix) which contains surfactants, mainly phospholipids, and other co-surfactants, like SCFA, bile salts or short-chain fatty alcohols. When a clear warm microemulsion is obtained, it is dispersed in cold water (2 °C) to generate nanoparticles by solidifying the lipid matrix. The SLN dispersion obtained is then washed

by tangential flow filtration (cut-off 30-100 kDa) to remove components and drug not incorporated into SLN, and the final product can then be filtered at 0.2 µm for sterility or can be subjected to freeze drying.

The Cb was prepared from cholesteryl butyrate (Asia Talent Chemical, Shenzhen China), Epikuron 200 (Cargill, Milano, Italy) and sodium glycocholate (PCA, Basaluzzo, Italy). In this formulation, cholesteryl butyrate lipid matrix acts as a prodrug of butyrate. For preparation of the DxCb-SLN, Dx 21-acetate (hereafter referred to as Dx; Sigma-Aldrich, Milano, Italy) was previously added and dissolved into melted cholesteryl butyrate matrix before adding other excipients as by the preparation protocol of Cb. The full compositions of warm microemulsions used to prepare Cb and DxCb-SLN are reported in Table 1. The temperature of these warm microemulsions was 85 °C for both. After clear microemulsions had been obtained, they were dispersed in cold water (2 °C) under stirring, at a 1:5 volume ratio. The dispersions obtained were then washed by tangential flow filtration (Vivaflow50 membrane with cut-off of 100 kDa; Sartorius Stedim Biotech GmbH, Goettingen, Germany) by adding and removing the same volume of water 4 times (4 washings); the final concentrations of the main components are reported in Table 2. In both formulations, 2-phenylethanol was added to aid in microemulsion formation. In particular, it works mainly to reduce viscosity and further helps in the formation of an interface between the oil phase and the lipid phase. Due to the multiple washings applied to purify the final products - four washings in this case - the concentration of 2-phenylethanol was strongly reduced in the final dispersion, where it finally acted as a preservative. Dx (water:ethanol 9:1, 1 mmol/L) was also prepared as a free drug reference.

Physical characterization was performed by dynamic light scattering (DLS) (Malvern Zetasizer - Nano ZS; Malvern Instruments, Malvern, United Kingdom). The data are reported in Table 3. Finally, electron microscopy analysis by ZEISS Supra 40 Field Emission Scanning Electron Microscopy confirmed the regular shape and nanosize of the particles (Figure 1) (courtesy of Prof. Pirri, Laboratory FESEM Microscopy, DISAT, Politecnico di Torino).

Cell lines

Leukemic human T cells (Jurkat, clone E6-1) were obtained from American Type Culture Collection (ATCC) (Manassas, VA, United States), and were cultured in RPMI 1640 medium supplemented with 10% fetal calf serum (FCS) (v/v), 2 mmol/L L-glutamine and antibiotics (100 U/mL streptomycin and 200 U/mL penicillin) (Sigma-Aldrich).

Human vascular endothelial cells (HUVECs) were isolated from human umbilical veins from healthy parturients aged between 18-35 years undergoing a natural birth (informed consent was obtained from all donors). The umbilical cord was collected at birth

and stored at 4 °C until the isolation procedure by trypsin treatment (1%). HUVECs were cultured in M199 medium with the addition of 20% FCS (v/v) and 100 U/mL penicillin, 100 mg/mL streptomycin, 5 UI/mL heparin, 12 mg/mL bovine brain extract and 200 mmol/L glutamine (Sigma-Aldrich). HUVECs were grown to confluence in flasks and used between the second and fifth passages; HUVEC viability was not affected by the drug treatment.

Peripheral blood mononuclear cells (PBMCs) were isolated from heparinized peripheral rat blood samples by density-gradient centrifugation over Ficoll-Paque (Pharmacia Biotech, Uppsala, Sweden) according to the method of Liu *et al.*^[43] (the study was approved by the Ethics Committee of the University of Torino). PBMCs were cultured in RPMI 1640 medium supplemented with 10% FCS (v/v), 2 mmol/L L-glutamine and antibiotics (100 U/mL streptomycin and 200 U/mL penicillin). All the cell lines were cultured at 37 °C in a humidified 5% CO₂-95% air incubator.

In vitro cell adhesion assay

HUVECs were grown to confluence in 24-well culture plates, washed and rested for 1 d in M199 medium plus 10% FCS (v/v). Cells were pre-activated with IL-1 β (0.01 μ mol/L) for 1 h and then exposed or not exposed to increasing concentrations of Dx (2.5, 25 and 250 nmol/L), Cb (0.1, 1 and 10 μ mol/L) and DxCb-SLN (2.5 nmol/L:0.1 μ mol/L, 25 nmol/L:1 μ mol/L and 250 nmol/L:10 μ mol/L) for 24 h, washed with fresh medium twice and incubated for 1 h with Jurkat cells (1 \times 10⁵ per well). The 1 h incubation time was chosen to allow full sedimentation of the adhering cells, but similar results were obtained with shorter incubation times (10 and 20 min). After incubation, non-adherent cells were removed by being washed three times with M199 medium. The center of each well was analyzed by fluorescence imaging^[42]. Adherent cells were counted by the ImagePro Plus Software for micro-imaging (version 5.0; Media Cybernetics, Bethesda, MD, United States). Single experimental points were assayed in triplicate, and the standard error of three replicates was always below 10%. Data are shown as the percentage of inhibition of treated cells vs the control adhesion measured on untreated cells (control adhesion was 65 \pm 5 cells per microscope field; *n* = 5).

In vitro PBMC assay

PBMC viability was assayed by trypan blue dye exclusion, and 5 \times 10⁵/mL viable cells were cultured in 24-well culture plates with culture medium containing 1 μ g/mL LPS (Sigma-Aldrich) for 24 h. PBMCs were then incubated with increasing concentration of Dx (2.5, 25 and 250 nmol/L), Cb (0.1, 1 and 10 μ mol/L) and DxCb-SLN (2.5 nmol/L:0.1 μ mol/L, 25 nmol/L:1 μ mol/L and 250 nmol/L:10 μ mol/L) for 24 h. In order to exclude the possibility that the drugs might affect cell viability, 24 h after drug incubation a trypan blue dye exclusion assay was performed for each condition.

The IL-1 β and TNF- α protein concentrations in culture supernatants of PBMCs were determined at 24 h incubation by specific enzyme-linked immunosorbent assay (ELISA) (eBioscience, Thermo Fisher Scientific, Milano, Italy) according to the manufacturer's instructions. Data are shown as the percentage of the cytokine secretion of LPS-treated PBMCs after each drug treatment vs the cytokine secretion of control cells, *i.e.*, LPS-stimulated PBMCs.

Animals

Male, 8 wk-old BALB/c mice, with an average weight of 18 g, were obtained from Charles River (Milano, Italy). The mice were housed in a specific pathogen-free environment, and a 12 h light/dark cycle was maintained. The mice had access to water and rodent laboratory chow *ad libitum*; the weights of the mice as well as diarrhea were recorded daily. The procedures for the care and handling of the animals used in the study were approved by the local "Animal Use and Care Committee" (protocol number 12201), and they were in accordance with the European Directive 2010/63/EU on the protection of animals used for scientific purposes.

In vivo model of colitis

Colitis was induced in mice by adding 4% (w/v) dextran sulfate sodium salt (DSS, molecular weight 40000) (Sigma-Aldrich) to the drinking water and allowing *ad libitum* access, starting from day 0 for 5 d. Groups of mice (at least 5 mice per group) were then orally treated (by gavage) daily with Dx (0.0001 mg/g bw), Cb (0.004 mg/g bw) or DxCb-SLN (0.0001 mg/g bw:0.004 mg/g bw) starting from day 6 for 3 d. Moreover, in a group in which colitis was induced, as a sham treatment mice were administered orally with sterile phosphate-buffered saline solution (150 μ L/mouse per day) starting from day 6 for 3 d (DSS group), whereas in another group colitis was not induced (control group). All groups were sacrificed on day 10. There were at least 5 mice per group, and two separate experiments were carried out. There was no significant difference in the water consumption and food intake of each group during all experimental periods.

Assessment of in vivo inflammation

The mice were weighed and inspected for diarrhea and rectal bleeding every day. The disease activity index (DAI) (*i.e.*, the combined score of weight loss and bleeding) was determined according to a standard scoring system, as previously described by Rachmilewitz *et al.*^[44]. Specifically, the scores were defined as follows: (1) bodyweight (bw) loss (0: no bw loss; 1: 5%-10% bw loss; 2: 10%-15% bw loss; 3: 15%-20% bw loss; 4: > 20% bw loss); (2) fecal occult blood (0: no blood; 2: positive; 4: gross blood); and (3) diarrhea (0: no diarrhea; 1: mild diarrhea, 2: severe diarrhea). All groups were sacrificed on day 10.

The IL-1 β and TNF- α plasma concentrations were determined on day 9, *i.e.*, 24 h after the different

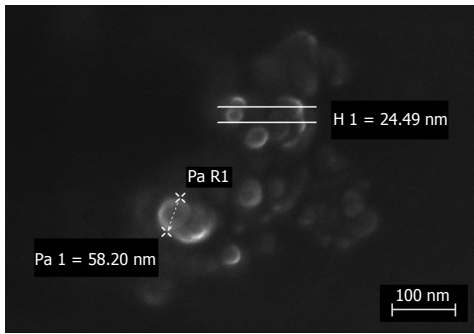


Figure 1 FeSEM micrograph of dexamethasone cholesteryl butyrate-solid lipid nanoparticles. Electron microscopy analysis showed regular shape and nanosize of particles by height (H) or radius (R) measurements.

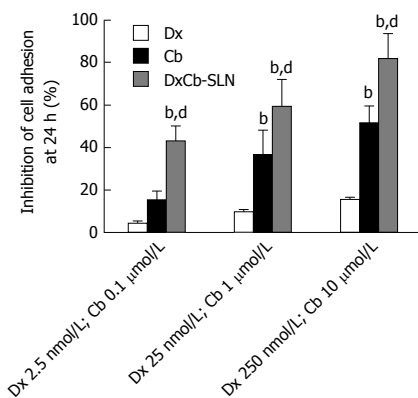


Figure 2 Effect of dexamethasone, cholesteryl butyrate and dexamethasone cholesteryl butyrate-solid lipid nanoparticles on human vascular endothelial cell adhesiveness to Jurkat cells. Human vascular endothelial cells were pre-activated with IL-1 β (0.01 μ mol/L) for 1 h and then exposed or not exposed to increasing concentrations of Dx (2.5, 25 and 250 nmol/L), Cb (0.1, 1 and 10 μ mol/L) and DxCb-SLN (2.5 nmol/L:0.1 μ mol/L, 25 nmol/L:1 μ mol/L and 250 nmol/L:10 μ mol/L) for 24 h and then incubated with Jurkat for 1 h. ^b $P < 0.01$, vs Dx; ^d $P < 0.01$, vs Cb. Dx: Dexamethasone; Cb: Cholesteryl butyrate; DxCb-SLN: Dexamethasone cholesteryl butyrate-solid lipid nanoparticles.

treatments by specific sandwich enzyme immunoassay (eBioscience, Thermo Fisher Scientific) according to the manufacturer's instructions. Data are shown as the percentage of the cytokine secretion of DSS-treated mice after each drug treatment vs the cytokine secretion of DSS-treated mice.

Statistical analysis

Results are expressed throughout as mean \pm SD of three independent experiments for *in vitro* studies and of two independent experiments for *in vivo* studies. Statistical analyses were performed on GraphPad Prism 6.0 software (La Jolla, CA, United States). The two-way or one-way analysis of variance and Bonferroni's test were used to determine statistical significance in the different treatment groups. The statistical significance threshold was set at $P < 0.05$.

RESULTS

Effects of DxCb-SLN on *in vitro* cell adhesion

First, we analyzed the effect of DxCb-SLN on the adhesion of Jurkat cells, a widely used continuous model of human T lymphocytes, to HUVECs comparing it with the effect of the drug separately, *i.e.*, Dx and Cb. In order to reproduce an inflammatory environment, we pre-activated HUVECs with 0.01 μ mol/L IL-1 β for 1 h. The treatment with IL-1 β increased Jurkat adhesion by 180%, and this value was used as control. The concentration used for each drug had been found not to be toxic for HUVECs.

HUVECs were treated with increasing concentrations of each single drug, *i.e.*, Dx (2.5, 25 and 250 nmol/L) and Cb (0.1, 1 and 10 μ mol/L), and of the DxCb nanoformulation (DxCb-SLN with a Dx:Cb concentration of 2.5 nmol/L:0.1 μ mol/L, 25 nmol/L:1 μ mol/L and 250 nmol/L:10 μ mol/L) for 24 h, washed and used in the adhesion assay with Jurkat cells. Figure 2 shows that DxCb SLN inhibited cell adhesion to HUVEC in a concentration-dependent manner. A significant 43.1% \pm 7.3% inhibition of cell adhesion was already determined at the lowest concentration tested of the DxCb nanoformulation (DxCb-SLN with a Dx:Cb concentration of 2.5 nmol/L M:0.1 μ mol/L), reaching an 81.8% \pm 11.7% inhibition of cell adhesion at the highest concentration tested (DxCb-SLN with a Dx:Cb concentration of 250 nmol/L:10 μ mol/L). Considering the inhibition of cell adhesion determined by the single drugs, Dx produced a 4.2% \pm 0.8% inhibition at the lowest concentration tested (2.5 nmol/L), reaching a 15.4% \pm 0.9% inhibition at the highest concentration tested (250 nmol/L) and Cb determined a 14.9% \pm 4.3% inhibition at the lowest concentration tested (0.1 μ mol/L), reaching a 51.6% \pm 7.8% inhibition at the highest concentration tested (10 μ mol/L). Therefore, taking all the data together, the nanoformulation containing Dx 2.5 nmol/L and Cb 0.1 μ mol/L was able to exert an inhibition of cell adhesion in a more than additive manner with respect to the sum of the individual effects of each drug if they had been used separately (Figure 2).

Effects of DxCb-SLN on *in vitro* cytokine production

With respect to the effects on IL-1 β production in PBMC culture supernatant, 24 h after the incubation a statistically significant ($P < 0.05$) higher decrease of IL-1 β compared to the effect induced by each single drug was observed only with the nanoformulation containing the lowest concentrations tested (DxCb-SLN with a Dx:Cb concentration of 2.5 nmol/L:0.1 μ mol/L; Figure 3A). Assuming as 100% the IL-1 β production of untreated PBMCs, an IL-1 β production of 74.3% \pm 8.7% was observed with the nanoformulation, in contrast to a 98.7% \pm 9.8% and a 89.1% \pm 8.2% production with Dx (2.5 nmol/L) and with Cb (0.1 μ mol/L), respectively. On increasing the concentrations, no significant differences on the IL-1 β production were

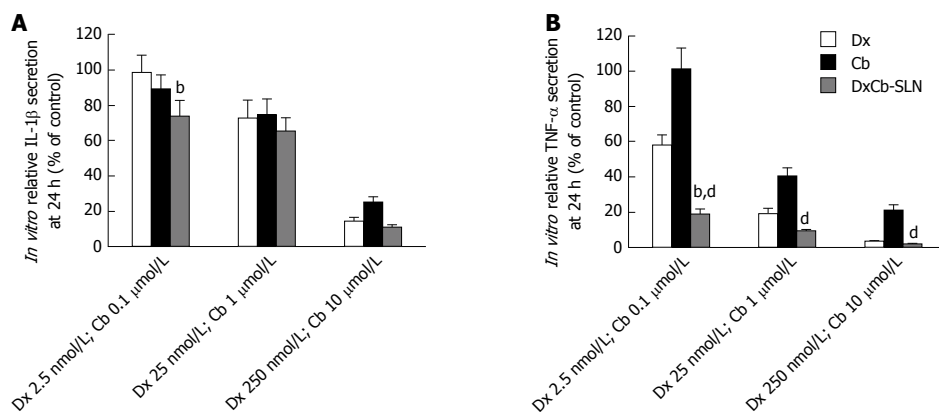


Figure 3 *In vitro* effect of dexamethasone, cholesteryl butyrate and dexamethasone cholesteryl butyrate-solid lipid nanoparticles on interleukin-1 β and tumor necrosis factor- α secretion. Cells were treated with increasing concentrations of Dx (2.5, 25 and 250 nmol/L), Cb (0.1, 1 and 10 μ mol/L) and DxCb-SLN (2.5 nmol/L:0.1 μ mol/L, 25 nmol/L:1 μ mol/L and 250 nmol/L:10 μ mol/L) for 24 h. IL-1 β (A) and TNF- α (B) secretion in culture supernatant of PBMCs stimulated with lipopolysaccharide (LPS; 1 μ g/mL for 24 h) were analyzed by ELISA. ^b $P < 0.01$, vs Dx; ^d $P < 0.01$, vs Cb. Dx: Dexamethasone; Cb: Cholesteryl butyrate; DxCb-SLN: Dexamethasone cholesteryl butyrate-solid lipid nanoparticles; IL: Interleukin; TNF: Tumor necrosis factor.

observed using either the DxCb nanoformulation or each single drug (Figure 3A).

Regarding the effects on TNF- α production in the PBMC culture supernatant, 24 h after incubation a statistically significant ($P < 0.001$) higher decrease of TNF- α compared to the effect induced by single Dx was observed only with the nanoformulation at the lowest concentrations tested (DxCb-SLN with a Dx: Cb concentration of 2.5 nmol/L:0.1 μ mol/L; Figure 3B). Assuming as 100% the TNF- α production of untreated PBMCs, a TNF- α production of $19.2\% \pm 2.8\%$ was observed with the nanoformulation, compared to a $58.4\% \pm 5.3\%$ and a $101.3\% \pm 11.3\%$ production with Dx (2.5 nmol/L) and with Cb (0.1 μ mol/L), respectively. On increasing the concentrations, no significant differences on TNF- α production were observed using either the DxCb nanoformulation or Dx single drug (Figure 3B). Therefore, in regard to all the data, the nanoformulation containing Dx 2.5 nmol/L and Cb 0.1 μ mol/L was able to exert a strong decrease of TNF- α production in a more than additive manner with respect to the sum of the individual effects of each drug if they had been used separately (Figure 3B).

Effects of DxCb-SLN on *in vivo* mice colitis

In order to evaluate the effect of the DxCb nanoformulation on a mouse colitis model, the mice were divided into groups, and each was given drugs separately or as DxCb-SLN at the same concentrations. Specifically, doses of Dx (0.0001 mg/g bw), Cb (0.004 mg/g bw) or DxCb-SLN (0.0001 mg/g bw:0.004 mg/g bw) per day were administered orally from day 6 to day 8 after the colitis induction from day 0 to day 5. In addition, another group was composed of untreated mice (DSS group), and another of mice in which colitis was not induced (control group). Changes in mice bw were significantly different between the control group

and the DSS group starting from day 7 and between groups treated with Dx or Cb and the control group starting from day 9 (Figure 4A). Instead, a slight but significant change in mice bw between DxCb-SLN treated-group and control group was recorded only at the last day of observation, *i.e.*, day 10 ($P < 0.05$; Figure 4A). According to the DAI score determined for each treatment group, we observed that Dx alone was able to induce a significant decrease of the score compared to untreated mice (DSS group), with a 25% reduction of the disease symptoms (*i.e.*, 6.0 vs 4.5, $P < 0.05$; Figure 4B). Notably, DxCb-SLN was able to induce a higher significant decrease of the disease score compared to untreated mice, with a 42% reduction of the disease symptoms (*i.e.*, 6.0 vs 3.5, $P < 0.01$; Figure 4B).

Considering the cytokine plasma concentration on day 9, *i.e.*, 24 h after drug treatment, only the DxCb nanoformulation administration was able to achieve a significant cytokine decrease compared to the cytokine plasma concentration of the DSS group. Assuming as 100% the IL-1 β or TNF- α production of mice with DSS-induced colitis on day 9, 24 h after the 3 d of oral treatments, only DxCb-SLN (0.0001 mg/g bw:0.004 mg/g bw) were able to induce a significant decrease (Figure 5). Specifically, DxCb-SLN induced a IL-1 β plasma concentration of $61.77\% \pm 3.19\%$, whereas Dx or Cb used separately induced a concentration of $90.0\% \pm 2.8\%$ and $91.40\% \pm 7.5\%$, respectively (Figure 5A); DxCb-SLN induced a TNF- α plasma concentration of $30.8\% \pm 8.9\%$, whereas Dx or Cb used separately induced ones of $99.5\% \pm 4.9\%$ and $71.1\% \pm 10.9\%$, respectively (Figure 5B). Thus, DxCb-SLN significantly ameliorated DSS-induced colitis in the mice compared to the treatments with each drug separately, given that the observed anti-inflammatory effect was higher than what would be expected from a

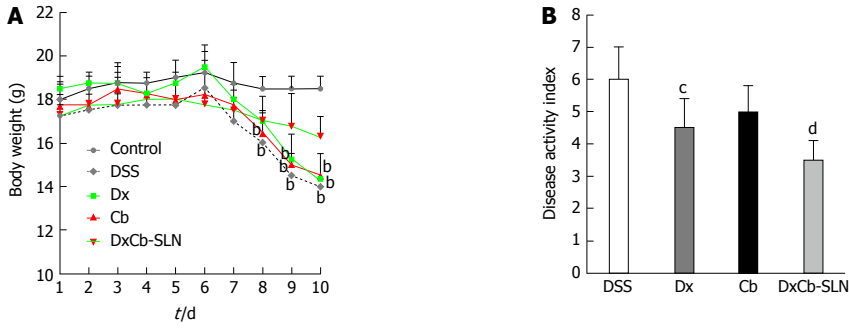


Figure 4 *In vivo* effect of dexamethasone, cholesteryl butyrate and dexamethasone cholesteryl butyrate-solid lipid nanoparticles on bodyweight and disease activity index. Animals received no treatment (control), DSS alone (DSS), or a combination of DSS and Dx (Dx, 0.0001 mg/g bw for 3 d), DSS and Cb (Cb, 0.004 mg/g bw for 3 d) and DSS and DxCb-SLN (DxCb-SLN, 0.0001 mg/g bw:0.004 mg/g bw for 3 d). After 7 d, DSS was replaced with a water cycle (*ad libitum*) for another 7 d. Body weight of the mice was recorded daily (A) and the disease activity rate at day 9 (B). ^b*P* < 0.01, vs control; ^c*P* < 0.05, vs DSS. Dx: Dexamethasone; Cb: Cholesteryl butyrate; DxCb-SLN: Dexamethasone cholesteryl butyrate-solid lipid nanoparticles; DSS: Dextran sulfate sodium.

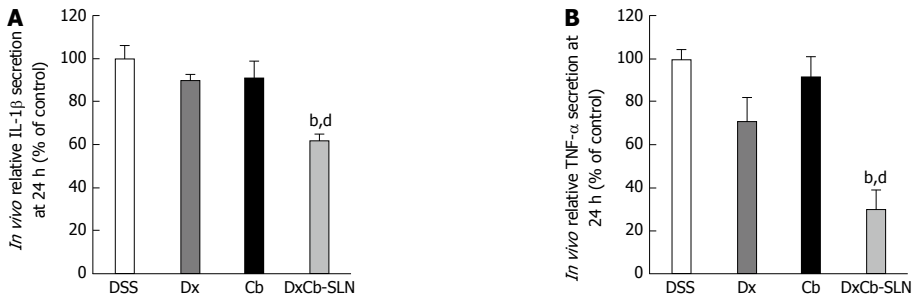


Figure 5 *In vivo* effect of dexamethasone, cholesteryl butyrate and dexamethasone cholesteryl butyrate-solid lipid nanoparticles on interleukin-1β and tumor necrosis factor-α secretion. Animals were treated with DSS alone (DSS), or a combination of DSS and Dx (Dx, 0.0001 mg/g bw for 3 d), DSS and Cb (Cb, 0.004 mg/g bw for 3 d) and DSS and DxCb-SLN (DxCb-SLN, 0.0001 mg/g bw:0.004 mg/g bw for 3 d). IL-1β and TNF-α secretion in mice plasma were analyzed by ELISA at day 9, 24 h after drug treatment. ^b*P* < 0.01, vs Dx; ^d*P* < 0.01, vs Cb. Dx: Dexamethasone; Cb: Cholesteryl butyrate; DxCb-SLN: Dexamethasone cholesteryl butyrate-solid lipid nanoparticles; DSS: Dextran sulfate sodium; IL: Interleukin; TNF: Tumor necrosis factor.

simple additive effect (Figures 4 and 5).

DISCUSSION

In a previous work, we observed that the incorporation of butyrate and Dx separately into SLN was effective in enhancing the anti-inflammatory activity of the drugs on PBMCs of IBD patients^[17]. In the research presented herein, we observed that the combination therapy of Dx and butyrate co-loaded into an oral nanoformulation, namely DxCb-SLN, was effective in reducing the disease activity in a mouse model of DSS-induced colitis, as verified by its effect on macroscopic and biochemical parameters.

Before moving to an *in vivo* IBD model, we first tested DxCb-SLN on *in vitro* inflammation models. In a IL-1β-stimulated leukocyte-endothelial cell adhesion model, where the use of the cytokine allowed us to reproduce the initiation phase of IBD, the combination treatment with DxCb-SLN was able to significantly inhibit cell adhesion already at the lowest concentration tested, showing a significant inhibition at doses 10-fold lower than the dose required to achieve the same effects with each single drug. In a LPS-stimulated

PBMC model, DxCb-SLN demonstrated a significant decrease of cytokine release that was higher for TNF-α rather than IL-1β secretion. Once again, the combination treatment was more effective at doses 10-fold lower than the dose required to achieve the same effects with the single drug treatment, *i.e.*, 2.5 nmol/L:0.1 μmol/L Cb for DxCb-SLN with respect to 25 nmol/L for Dx and 1 μmol/L for Cb. We did not observe significant further decreases of both cytokine release at the highest concentration tested of DxCb-SLN because the free drugs, especially Dx, had a strong anti-inflammatory activity by themselves.

We then investigated this novel oral nanoformulation on a DSS-induced colitis *in vivo* model, which is one of the experimental models most frequently used in investigation of novel treatments for IBD^[45]. Confirming the data observed *in vitro*, the *in vivo* pro-inflammatory cytokine release was significantly decreased by the DxCb-SLN oral administration, the decrease for TNF-α being more pronounced than IL-1β plasma concentration, 24 h after a daily treatment for 3 d. It is interesting that, on comparing the *in vitro* cytokine release at the lowest concentration of DxCb-SLN, we observed the same more pronounced decrease for

TNF- α than IL-1 β secretion.

This anti-inflammatory activity was consistent with the decreased DAI determined by the oral treatment with DxCb-SLN compared to the effects induced by the treatment with each drug separately. Notably, the bw loss induced by DSS was recovered significantly only after the oral treatment with DxCb-SLN. Therefore, thanks to this novel oral formulation, the combination therapy of Dx and butyrate had better effects than any other single treatment, as specifically revealed by the significant decrease of plasma pro-inflammatory cytokines, *i.e.*, IL-1 β and TNF- α , and of the DAI. The efficacy of DxCb-SLN demonstrated in these *in vitro* and *in vivo* models may be explained by various mechanisms, such as particular abilities of nanoparticulate drug delivery systems and positive interaction mechanisms between Dx and butyrate.

However, further research is necessary to examine in depth the mechanism underpinning the enhanced anti-inflammatory effect determined by the simultaneous oral administration of Dx and butyrate as SLN formulation rather than as free drugs. For instance, a pharmacokinetic study comparing the simultaneous administration of the two drugs as free or loaded into the same SLN will be necessary to evaluate if the drug delivery system is effective in improving the bioavailability and inflamed tissue targeting. Also, molecular investigations will be necessary to evaluate differences in modulating inflammatory pathways by administering, at the same time, the two drugs as free or SLN formulation.

Thanks to pharmaceutical technology, we had the opportunity to develop an efficient drug delivery system able to improve the treatment of such a disease mediated by inflammation^[11,46]. The use of a nanoparticulate drug carrier is useful to prevent early drug biological environmental degradation, to modulate drug pharmacokinetics, but also to enhance the treatment selectivity by targeting. Indeed, nanoparticles depending on their physico-chemical properties can preferentially accumulate in areas of intestinal inflammation when delivered orally^[11,12]. They are particularly well-suited to the treatment of IBD through the local delivery of drugs to areas of inflammation, allowing site-specific delivery and minimizing side effects in other organs.

Targeting IBD sites is a challenging task to ensure the release of an intact and quantitatively clear amount of the administered drugs. Since drugs encounter a harmful environment after oral administration, high doses and/or frequent administration are usual to counter the degradation by stomach acidic pH or small intestine digestive enzymes; on the other hand, the occurrence of side effects are more likely^[11,47]. In particular, SLN have been one of most studied carriers worldwide for drug delivery, since this nanosystem is mainly composed of solid lipid core and lecithin, has very low toxicity profile, good affinity for biological membrane, ability to facilitate up-taking/overcoming, and capacity to improve drug pharmacokinetics^[48,49].

Therefore, the therapeutic potential of this novel anti-inflammatory drug nanoformulation in IBD is due to: (1) time protection of the loaded drug, especially for butyrate; (2) controlled release of the loaded drug, allowing a prolonged drug exposure; and (3) passive targeting of IBD sites, as a result of the abnormal permeability of inflamed colonic mucosa and the nanoparticle preferential uptake by immunocompetent cells.

Moreover, because some studies have reported the ability of butyrate to enhance the anti-inflammatory activity of corticosteroids or non-steroidal drugs^[50,51], we decided to evaluate the effect of a combination therapy of Dx and butyrate. It is well-known that butyrate may play an important role in regulating intestinal inflammation^[52,53]. As reported by Place *et al.*^[22], butyrate influences NF- κ B activity by preventing the proteasome-dependent degradation of I κ B α . This inhibition appears to arise from butyrate's ability to inhibit histone deacetylase (HDAC)^[54]. Specifically, the selective changes in gene expression induced by HDAC inhibitors, such as butyrate, arise from the enhanced acetylation of histone proteins and gene-regulatory transcription factors (*e.g.*, p53, Sp1 and Sp3)^[22].

NF- κ B is a central mediator of the immune and inflammatory response and, upon activation, it rapidly enhances the expression of pro-inflammatory genes such as those encoding cytokines and cell adhesion molecules^[55]. Dx effect on cytokine modulation in IBD is achieved through the translocation and activation of the glucocorticoid-receptor complex that can both bind to, and inactivate, key pro-inflammatory transcription factors, such as NF- κ B^[56]. Therefore, the greater effect observed in both *in vitro* and *in vivo* inflammation models by DxCb-SLN on TNF- α rather than IL-1 β secretion might be modulated by a gene transcriptional regulation of NF- κ B. Thus, according to our data we can speculate that an additive synergistic effect on NF- κ B modulation due to the co-administration of Dx and butyrate might be responsible for the higher anti-inflammatory effect observed compared to the use of each drug separately, even if further molecular investigations are needed to confirm this hypothesis.

DxCb-SLN may provide a novel approach to treating IBD by taking advantage of a combination treatment achieved by co-loading Dx and butyrate into the same nanoparticle, which is able to exert a more than additive anti-inflammatory effect. Moreover, the pronounced anti-inflammatory activity of the DxCb-SLN oral treatment may be also due to passive targeting of the inflamed IBD sites, with the potential to reduce systemic side effects of each single drug in addition to the reduced amount of each drug required to achieve such an important anti-inflammatory activity.

ACKNOWLEDGMENTS

We are grateful to the Obstetrics and Gynecology Unit, Martini Hospital, Torino, Italy, for providing human umbilical cords.

COMMENTS

Background

Dexamethasone has been used for decades in the treatment of inflammatory bowel disease (IBD) flares, even if such a life-long treatment might produce several adverse reactions that are mostly time- and dose-dependent, limiting its clinical usefulness. Hence, attempts to maintain the IBD therapeutic effects of corticosteroids while minimizing their systemic side effects might provide a major therapeutic improvement.

Research frontiers

Nanotechnology can be used to improve the pharmacokinetic and pharmacodynamic properties of such a powerful drug. The authors have developed a nanoformulation carrying dexamethasone and the short-chain fatty acid, butyrate, to improve anti-inflammatory activity while reducing drug doses.

Innovations and breakthroughs

The authors developed a new solid lipid nanoparticle formulation carrying dexamethasone and butyrate highlighting the efficacy of this strategy in strengthening the effect of each single drug in the treatment of inflammation.

Applications

This nanoformulation may open a new window on the treatment of chronic inflammatory conditions such as inflammatory bowel disease, where dose- and time-dependent side effects can limit the drug's therapeutic usefulness. Notably, dexamethasone cholesteryl butyrate-solid lipid nanoparticles significantly relieved and repaired colon inflammation in a colitis mouse model thanks to the nanoformulation, which displayed an additive synergism among the corticosteroid, dexamethasone, and the short-chain fatty acid, butyrate.

Terminology

Solid lipid nanoparticles are mainly composed of solid lipid core and lecithin, have very low toxicity profile, good affinity for biological membrane, ability to facilitate up-taking, and capacity to improve drug pharmacokinetics.

Peer-review

This is a very interesting article discussing a novel drug delivery using dexamethasone cholesteryl butyrate-solid lipid nanoparticles in *in vitro* and *in vivo* models.

REFERENCES

- Beattie RM, Croft NM, Fell JM, Afzal NA, Heuschkel RB. Inflammatory bowel disease. *Arch Dis Child* 2006; **91**: 426-432 [PMID: 16632672 DOI: 10.1136/adc.2005.080481]
- Gabay C, Kushner I. Acute-phase proteins and other systemic responses to inflammation. *N Engl J Med* 1999; **340**: 448-454 [PMID: 9971870 DOI: 10.1056/NEJM199902113400607]
- Sans M, Panés J, Ardite E, Elizalde JI, Arce Y, Elena M, Palacin A, Fernández-Checa JC, Anderson DC, Lobb R, Piqué JM. VCAM-1 and ICAM-1 mediate leukocyte-endothelial cell adhesion in rat experimental colitis. *Gastroenterology* 1999; **116**: 874-883 [PMID: 10092309]
- Szmitko PE, Wang CH, Weisel RD, de Almeida JR, Anderson TJ, Verma S. New markers of inflammation and endothelial cell activation: Part I. *Circulation* 2003; **108**: 1917-1923 [PMID: 14568885 DOI: 10.1161/01.CIR.0000089190.95415.9F]
- Coskun M, Vermeire S, Nielsen OH. Novel Targeted Therapies for Inflammatory Bowel Disease. *Trends Pharmacol Sci* 2017; **38**: 127-142 [PMID: 27916280 DOI: 10.1016/j.tips.2016.10.014]
- van Deventer SJ. The future of inflammatory bowel disease therapy. *Inflamm Bowel Dis* 2002; **8**: 301-305; discussion 306 [PMID: 12131615]
- Barnes PJ, Adcock I. Anti-inflammatory actions of steroids: molecular mechanisms. *Trends Pharmacol Sci* 1993; **14**: 436-441 [PMID: 7510080]
- Sands BE. Therapy of inflammatory bowel disease. *Gastroenterology* 2000; **118**: S68-S82 [PMID: 10868899]
- Hoy SM. Budesonide MMX®: a review of its use in patients with mild to moderate ulcerative colitis. *Drugs* 2015; **75**: 879-886 [PMID: 25920500 DOI: 10.1007/s40265-015-0396-8]
- Amidon S, Brown JE, Dave VS. Colon-targeted oral drug delivery systems: design trends and approaches. *AAPS PharmSciTech* 2015; **16**: 731-741 [PMID: 26070545 DOI: 10.1208/s12249-015-0350-9]
- Serpe L, Canaparo R, Foglietta F, Zara GP. Innovative formulations for the controlled and site-specific delivery of antiinflammatory drugs. *Curr Pharm Des* 2013; **19**: 7219-7236 [PMID: 23489201]
- Viscido A, Capannolo A, Latella G, Caprilli R, Frieri G. Nanotechnology in the treatment of inflammatory bowel diseases. *J Crohns Colitis* 2014; **8**: 903-918 [PMID: 24686095]
- Collnot EM, Ali H, Lehr CM. Nano- and microparticulate drug carriers for targeting of the inflamed intestinal mucosa. *J Control Release* 2012; **161**: 235-246 [PMID: 22306429 DOI: 10.1016/j.jconrel.2012.01.028]
- Takahashi M, Mutoh M, Kawamori T, Sugimura T, Wakabayashi K. Altered expression of beta-catenin, inducible nitric oxide synthase and cyclooxygenase-2 in azoxymethane-induced rat colon carcinogenesis. *Carcinogenesis* 2000; **21**: 1319-1327 [PMID: 10874009]
- d'Alessio P. Endothelium as a pharmacological target. *Curr Opin Investig Drugs* 2001; **2**: 1720-1724 [PMID: 11892934]
- Meager A. Cytokine regulation of cellular adhesion molecule expression in inflammation. *Cytokine Growth Factor Rev* 1999; **10**: 27-39 [PMID: 10379910]
- Serpe L, Canaparo R, Daperno M, Sostegni R, Martinasso G, Muntoni E, Ippolito L, Vivenza N, Pera A, Eandi M, Gasco MR, Zara GP. Solid lipid nanoparticles as anti-inflammatory drug delivery system in a human inflammatory bowel disease whole-blood model. *Eur J Pharm Sci* 2010; **39**: 428-436 [PMID: 20138213 DOI: 10.1016/j.ejps.2010.01.013]
- Schepbach W, Weiler F. The butyrate story: old wine in new bottles? *Curr Opin Clin Nutr Metab Care* 2004; **7**: 563-567 [PMID: 15295277]
- Vinolo MA, Rodrigues HG, Nachbar RT, Curi R. Regulation of inflammation by short chain fatty acids. *Nutrients* 2011; **3**: 858-876 [PMID: 22254083 DOI: 10.3390/nu3100858]
- Liu Q, Shimoyama T, Suzuki K, Umeda T, Nakaji S, Sugawara K. Effect of sodium butyrate on reactive oxygen species generation by human neutrophils. *Scand J Gastroenterol* 2001; **36**: 744-750 [PMID: 11444474]
- Hamer HM, Jonkers D, Venema K, Vanhoutvin S, Troost FJ, Brummer RJ. Review article: the role of butyrate on colonic function. *Aliment Pharmacol Ther* 2008; **27**: 104-119 [PMID: 17973645 DOI: 10.1111/j.1365-2036.2007.03562.x]
- Place RF, Noonan EJ, Giardina C. HDAC inhibition prevents NF-kappa B activation by suppressing proteasome activity: down-regulation of proteasome subunit expression stabilizes I kappa B alpha. *Biochem Pharmacol* 2005; **70**: 394-406 [PMID: 15950952 DOI: 10.1016/j.bcp.2005.04.030]
- Vinolo MA, Rodrigues HG, Hatanaka E, Sato FT, Sampaio SC, Curi R. Suppressive effect of short-chain fatty acids on production of proinflammatory mediators by neutrophils. *J Nutr Biochem* 2011; **22**: 849-855 [PMID: 21167700]
- Breuer RI, Soergel KH, Lashner BA, Christ ML, Hanauer SB, Vanaganas A, Harig JM, Keshavarzian A, Robinson M, Sellin JH, Weinberg D, Vidican DE, Flemal KL, Rademaker AW. Short chain fatty acid rectal irrigation for left-sided ulcerative colitis: a randomised, placebo controlled trial. *Gut* 1997; **40**: 485-491 [PMID: 9176076]
- Schepbach W. Treatment of distal ulcerative colitis with short-chain fatty acid enemas. A placebo-controlled trial. German-Austrian SCFA Study Group. *Dig Dis Sci* 1996; **41**: 2254-2259 [PMID: 8943981]
- Vernia P, Marcheggiano A, Caprilli R, Frieri G, Corrao G, Valpiani D, Di Paolo MC, Paoluzi P, Torsoli A. Short-chain fatty acid topical treatment in distal ulcerative colitis. *Aliment Pharmacol Ther* 1995; **9**: 309-313 [PMID: 7654893]
- Hamer HM, Jonkers DM, Vanhoutvin SA, Troost FJ, Rijkers G, de Bruïne A, Bast A, Venema K, Brummer RJ. Effect of butyrate

- enemas on inflammation and antioxidant status in the colonic mucosa of patients with ulcerative colitis in remission. *Clin Nutr* 2010; **29**: 738-744 [PMID: 20471725]
- 28 **Wan P**, Chen H, Guo Y, Bai AP. Advances in treatment of ulcerative colitis with herbs: from bench to bedside. *World J Gastroenterol* 2014; **20**: 14099-14104 [PMID: 25339799 DOI: 10.3748/wjg.v20.i39.14099]
- 29 **Eeckhaut V**, Ducatelle R, Sas B, Vermeire S, Van Immerseel F. Progress towards butyrate-producing probiotics: Butyricococcus pullicaecorum capsule and efficacy in TNBS models in comparison with therapeutics. *Gut* 2014; **63**: 367 [PMID: 23766442 DOI: 10.1136/gutjnl-2013-305293]
- 30 **Mariadason JM**. HDACs and HDAC inhibitors in colon cancer. *Epigenetics* 2008; **3**: 28-37 [PMID: 18326939]
- 31 **Pajak B**, Orzechowski A, Gajkowska B. Molecular basis of sodium butyrate-dependent proapoptotic activity in cancer cells. *Adv Med Sci* 2007; **52**: 83-88 [PMID: 18217395]
- 32 **Daniel P**, Brazier M, Cerutti I, Pieri F, Tardivel I, Desmet G, Baillet J, Chany C. Pharmacokinetic study of butyric acid administered in vivo as sodium and arginine butyrate salts. *Clin Chim Acta* 1989; **181**: 255-263 [PMID: 2667816]
- 33 **Brioschi A**, Zara GP, Calderoni S, Gasco MR, Mauro A. Cholesterylbutyrate solid lipid nanoparticles as a butyric acid prodrug. *Molecules* 2008; **13**: 230-254 [PMID: 18305415]
- 34 **Pellizzaro C**, Coradini D, Morel S, Ugazio E, Gasco MR, Daidone MG. Cholesteryl butyrate in solid lipid nanospheres as an alternative approach for butyric acid delivery. *Anticancer Res* 1999; **19**: 3921-3925 [PMID: 10628332]
- 35 **Ugazio E**, Marengo E, Pellizzaro C, Coradini D, Peira E, Daidone MG, Gasco MR. The effect of formulation and concentration of cholesteryl butyrate solid lipid nanospheres (SLN) on NIH-H460 cell proliferation. *Eur J Pharm Biopharm* 2001; **52**: 197-202 [PMID: 11522486]
- 36 **Manjunath K**, Reddy JS, Venkateswarlu V. Solid lipid nanoparticles as drug delivery systems. *Methods Find Exp Clin Pharmacol* 2005; **27**: 127-144 [PMID: 15834465 DOI: 10.1358/mf.2005.27.2.876286]
- 37 **Foglietta F**, Serpe L, Canaparo R, Vivenza N, Riccio G, Imbalzano E, Gasco P, Zara GP. Modulation of butyrate anticancer activity by solid lipid nanoparticle delivery: an in vitro investigation on human breast cancer and leukemia cell lines. *J Pharm Pharm Sci* 2014; **17**: 231-247 [PMID: 24934552]
- 38 **Minelli R**, Occhipinti S, Gigliotti CL, Barrera G, Gasco P, Conti L, Chiochetti A, Zara GP, Fantozzi R, Giovarelli M, Dianzani U, Dianzani C. Solid lipid nanoparticles of cholesteryl butyrate inhibit the proliferation of cancer cells in vitro and in vivo models. *Br J Pharmacol* 2013; **170**: 233-244 [PMID: 23713413]
- 39 **Minelli R**, Serpe L, Pettazzoni P, Minero V, Barrera G, Gigliotti C, Mesturini R, Rosa AC, Gasco P, Vivenza N, Muntoni E, Fantozzi R, Dianzani U, Zara GP, Dianzani C. Cholesteryl butyrate solid lipid nanoparticles inhibit the adhesion and migration of colon cancer cells. *Br J Pharmacol* 2012; **166**: 587-601 [PMID: 22049973 DOI: 10.1111/j.1476-5381.2011.01768.x]
- 40 **Serpe L**, Catalano MG, Cavalli R, Ugazio E, Bosco O, Canaparo R, Muntoni E, Frairia R, Gasco MR, Eandi M, Zara GP. Cytotoxicity of anticancer drugs incorporated in solid lipid nanoparticles on HT-29 colorectal cancer cell line. *Eur J Pharm Biopharm* 2004; **58**: 673-680 [PMID: 15451544 DOI: 10.1016/j.ejpb.2004.03.026]
- 41 **Serpe L**, Laurora S, Pizzimenti S, Ugazio E, Ponti R, Canaparo R, Briatore F, Barrera G, Gasco MR, Bernengo MG, Eandi M, Zara GP. Cholesteryl butyrate solid lipid nanoparticles as a butyric acid pro-drug: effects on cell proliferation, cell-cycle distribution and c-myc expression in human leukemic cells. *Anticancer Drugs* 2004; **15**: 525-536 [PMID: 15166628]
- 42 **Dianzani C**, Cavalli R, Zara GP, Gallicchio M, Lombardi G, Gasco MR, Panzanelli P, Fantozzi R. Cholesteryl butyrate solid lipid nanoparticles inhibit adhesion of human neutrophils to endothelial cells. *Br J Pharmacol* 2006; **148**: 648-656 [PMID: 16702992 DOI: 10.1038/sj.bjp.0706761]
- 43 **Liu FC**, Hoyt DB, Coimbra R, Junger WG. Proliferation assays with human, rabbit, rat, and mouse lymphocytes. *In Vitro Cell Dev Biol Anim* 1996; **32**: 520-523 [PMID: 8946221]
- 44 **Rachmilewitz D**, Karmeli F, Takabayashi K, Hayashi T, Leider-Trejo L, Lee J, Leoni LM, Raz E. Immunostimulatory DNA ameliorates experimental and spontaneous murine colitis. *Gastroenterology* 2002; **122**: 1428-1441 [PMID: 11984528]
- 45 **Yan Y**, Kolachala V, Dalmasso G, Nguyen H, Laroui H, Sitaraman SV, Merlin D. Temporal and spatial analysis of clinical and molecular parameters in dextran sodium sulfate induced colitis. *PLoS One* 2009; **4**: e6073 [PMID: 19562033 DOI: 10.1371/journal.pone.0006073]
- 46 **Takedatsu H**, Mitsuyama K, Torimura T. Nanomedicine and drug delivery strategies for treatment of inflammatory bowel disease. *World J Gastroenterol* 2015; **21**: 11343-11352 [PMID: 26525603 DOI: 10.3748/wjg.v21.i40.11343]
- 47 **Nakase H**, Okazaki K, Tabata Y, Uose S, Ohana M, Uchida K, Matsushima Y, Kawanami C, Oshima C, Ikada Y, Chiba T. Development of an oral drug delivery system targeting immune-regulating cells in experimental inflammatory bowel disease: a new therapeutic strategy. *J Pharmacol Exp Ther* 2000; **292**: 15-21 [PMID: 10604927]
- 48 **Geszke-Moritz M**, Moritz M. Solid lipid nanoparticles as attractive drug vehicles: Composition, properties and therapeutic strategies. *Mater Sci Eng C Mater Biol Appl* 2016; **68**: 982-994 [PMID: 27524099 DOI: 10.1016/j.msec.2016.05.119]
- 49 **Suchaoin W**, Bernkop-Schnürch A. Nanocarriers protecting toward an intestinal pre-uptake metabolism. *Nanomedicine (Lond)* 2017; **12**: 255-269 [PMID: 28093952 DOI: 10.2217/nmm-2016-0331]
- 50 **Song M**, Xia B, Li J. Effects of topical treatment of sodium butyrate and 5-aminosalicylic acid on expression of trefoil factor 3, interleukin 1beta, and nuclear factor kappaB in trinitrobenzene sulphonic acid induced colitis in rats. *Postgrad Med J* 2006; **82**: 130-135 [PMID: 16461476 DOI: 10.1136/pgmj.2005.037945]
- 51 **Guerron AD**, Rawat R, Sali A, Spurney CF, Pistilli E, Cha HJ, Pandey GS, Gernapudi R, Francia D, Farajian V, Escobar DM, Bossi L, Becker M, Zerr P, de la Porte S, Gordish-Dressman H, Partridge T, Hoffman EP, Nagaraju K. Functional and molecular effects of arginine butyrate and prednisone on muscle and heart in the mdx mouse model of Duchenne Muscular Dystrophy. *PLoS One* 2010; **5**: e11220 [PMID: 20574530]
- 52 **Berni Canani R**, Di Costanzo M, Leone L. The epigenetic effects of butyrate: potential therapeutic implications for clinical practice. *Clin Epigenetics* 2012; **4**: 4 [PMID: 22414433 DOI: 10.1186/1868-7083-4-4]
- 53 **Rieder F**, Karrasch T, Ben-Horin S, Schirbel A, Ehehalt R, Wehkamp J, de Haar C, Velin D, Latella G, Scaldaferrri F, Rogler G, Higgins P, Sans M. Results of the 2nd scientific workshop of the ECCO (III): basic mechanisms of intestinal healing. *J Crohns Colitis* 2012; **6**: 373-385 [PMID: 22405177]
- 54 **Felice C**, Lewis A, Armuzzi A, Lindsay JO, Silver A. Review article: selective histone deacetylase isoforms as potential therapeutic targets in inflammatory bowel diseases. *Aliment Pharmacol Ther* 2015; **41**: 26-38 [PMID: 25367825]
- 55 **Tak PP**, Firestein GS. NF-kappaB: a key role in inflammatory diseases. *J Clin Invest* 2001; **107**: 7-11 [PMID: 11134171]
- 56 **Auphan N**, DiDonato JA, Rosette C, Helmsberg A, Karin M. Immunosuppression by glucocorticoids: inhibition of NF-kappa B activity through induction of I kappa B synthesis. *Science* 1995; **270**: 286-290 [PMID: 7569976]

P- Reviewer: Battat R, Ozturk E, Vidal S S- Editor: Ma YJ
L- Editor: Filipodia E- Editor: Zhang FF





Published by **Baishideng Publishing Group Inc**
7901 Stoneridge Drive, Suite 501, Pleasanton, CA 94588, USA
Telephone: +1-925-223-8242
Fax: +1-925-223-8243
E-mail: bpgoffice@wjgnet.com
Help Desk: <http://www.f6publishing.com/helpdesk>
<http://www.wjgnet.com>



ISSN 1007 - 9327





Solid lipid nanoparticles carrying lipophilic derivatives of doxorubicin: preparation, characterization, and in vitro cytotoxicity studies

Elena Peira, Daniela Chirio, Luigi Battaglia, Alessandro Barge, Konstantin Chegaev, Casimiro Luca Gigliotti, Benedetta Ferrara, Chiara Dianzani & Marina Gallarate

To cite this article: Elena Peira, Daniela Chirio, Luigi Battaglia, Alessandro Barge, Konstantin Chegaev, Casimiro Luca Gigliotti, Benedetta Ferrara, Chiara Dianzani & Marina Gallarate (2016) Solid lipid nanoparticles carrying lipophilic derivatives of doxorubicin: preparation, characterization, and in vitro cytotoxicity studies, Journal of Microencapsulation, 33:4, 381-390, DOI: [10.1080/02652048.2016.1202342](https://doi.org/10.1080/02652048.2016.1202342)

To link to this article: <http://dx.doi.org/10.1080/02652048.2016.1202342>



Published online: 29 Jun 2016.



Submit your article to this journal [↗](#)



Article views: 86



View related articles [↗](#)




View Crossmark data [↗](#)



Citing articles: 1 View citing articles [↗](#)

RESEARCH ARTICLE

Solid lipid nanoparticles carrying lipophilic derivatives of doxorubicin: preparation, characterization, and *in vitro* cytotoxicity studies

Elena Peira^a, Daniela Chirio^a, Luigi Battaglia^a , Alessandro Barge^a, Konstantin Cheghev^a, Casimiro Luca Gigliotti^b, Benedetta Ferrara^a, Chiara Dianzani^a and Marina Gallarate^a

^aDipartimento di Scienza e Tecnologia del Farmaco, University of Turin, Torino, Italy; ^bDipartimento di Scienze della Salute, University of Eastern Piedmont Amedeo Avogadro, Novara, Italy

ABSTRACT

Doxorubicin (DOXO) lauroyl ester and amide were proposed as lipophilic derivatives and entrapped in SLNs. DOXO derivatives-loaded SLNs were spherical shaped, had 200–300 nm mean diameters and showed 80–94% w/w drug entrapment efficiencies. The effect of DOXO derivatives-loaded SLNs and free DOXO on cell growth was examined by MTT and colony-forming assays on four different tumour cell lines: a pancreatic, CFPAC-1, a lung, A549, and two ovarian, A2780 and A2780res (DOXO-resistant). The results obtained with MTT and colony-forming assay show that although DOXO displayed an inhibition of cell proliferation greater or similar to DOXO lauroyl amide-loaded SLNs on all cell types, the effect induced by DOXO lauroyl ester-loaded SLNs was higher and concentration-dependent, and it was the only one maintained at 10^{-5} mM concentration. Only DOXO lauroyl ester-loaded SLNs were able to induce a 40% inhibitory effect on A2780 res cell line up to 10^{-4} mM concentration.

ARTICLE HISTORY

Received 14 December 2015
Revised 6 June 2016
Accepted 9 June 2016
Published online 29 June 2016

KEYWORDS

Coacervation method;
cytotoxicity; doxorubicin;
SLN

Introduction

Doxorubicin (DOXO) is one of the most effective chemotherapeutics used against a wide spectrum of solid tumours in clinical cancer therapy for over 30 years. However, even when located in the tumour *interstitium*, similarly to other anticancer drugs, its efficacy against several solid tumour types can be limited, owing to the ability of cancer cells to develop drug-resistance mechanisms (MDR) and to evade chemotherapy. Transmembrane proteins act as drug-efflux pumps, actively reducing intracellular drug to levels lower than the effective cytotoxic concentration. Due to this efflux and to the resulting sub-therapeutic concentrations of active drug in cancer cells, progressively higher doses of the anti-cancer drug are required. The administration of increased DOXO doses enhances the risk of toxicity to normal cells as well as systemic toxicity to most major organs, especially life-threatening cardiotoxicity (Swain et al., 2003) and frequently occurring bone marrow suppression which force the treatment to become dose limiting. Consequently, the clinical application of DOXO is often limited by its severe toxicity and it is therefore pre-eminent to find effective approaches to overcome MDR in order to reduce adverse drug reactions.

Over the years, many studies were performed to develop drug delivery systems able to target the tumour site and overcome MDR (Barraud et al., 2005; Duggan and Keating, 2011; Petschauer et al., 2015). One of the effective approaches is to use nanoparticle (NP)-mediated drug delivery to increase drug accumulation in drug resistant cancer cells.

A possible application of NPs is the entrapment of poorly soluble drugs (Merisko-Liversidge and Liversidge, 2008) and the delivery of multi-agent enhancing therapeutic effects (Devalapally et al., 2007; Ganta and Amiji, 2009). However, the most attractive feature of multifunctional NPs for treating MDR cancers is the obtainment of targeting using target molecules such as antibodies, peptides or aptamers, that can help locate, bind or traffic NPs into the target

tumour (Iyer et al., 2013). Moreover, it is well known that nanosystems, such as properly designed NPs, can also passively reach tumours by EPR effect, which can be considered as passive targeting (Moghimi et al., 2001).

Among different NPs types, solid lipid nanoparticles (SLNs) have attracted increasing attention as potential drug delivery carriers consequently of their physical stability, their capacity to protect labile drugs from degradation, the easiness of preparation, and the lack of toxicity (Laquintana et al., 2009; Doktorovova et al., 2014; Thukral et al., 2014).

SLNs are disperse systems having size ranging from 1 to 1000 nm and represent an alternative to polymeric particulate carriers. They are composed of physiological or biocompatible lipids or lipid molecules with a history of safe use in therapy and they are generally suitable for intravenous administration, avoiding the toxicity problems caused by polymeric NPs.

SLNs technology represents a promising approach to lipophilic drug delivery, although in recent years, several papers report on SLNs potentially used as carriers of different water soluble drug, i.e. zidovudine, insulin, cisplatin, ciprofloxacin hydrochloride, to improve their therapeutic effects (Gasco et al., 1996; Singh et al., 2010; Trotta et al., 2010, 2011; Shah et al., 2012).

Moreover, recently, several authors described the ability of SLN formulations to increase both stability and efficacy of water-soluble substances other than drugs (i.e. vitamin C, caffeic acid) allowing their improved use (Güney et al., 2014; Dikmen et al., 2015).

In literature, many authors studied SLNs as systems able to deliver anticancer drugs to the tumour site (Wong et al., 2007). Miao et al. (2013) found that a SLN-based drug delivery system could increase the transport of paclitaxel or DOXO into cancer cells and enhance the cytotoxicity against both sensitive and their multi-drug resistant variant cells, compared with free drug solutions. It can be supposed that SLN lipid matrix can protect the entrapped drug from the P-gp efflux mechanism of the cell and

overcome MDR, revealing a potential application of this drug resistance reversal mechanism in drug resistant human cancer cells.

Some authors (Ma et al., 2009) found that SLNs loaded with DOXO were able to overcome Pgp-mediated MDR both *in vitro* in P388/ADR leukaemia cells and *in vivo* in the murine leukaemia mouse model. The results suggested that SLNs might offer potential to deliver anticancer drugs for the treatment of Pgp-mediated MDR in leukaemia.

Recently, a new solvent-free technique, defined as "coacervation" was developed to prepare fatty acids-based SLNs (Battaglia et al., 2010). In a fatty acid alkaline salt micellar solution, in the presence of an appropriate polymeric stabiliser, the pH is lowered by acidification and the fatty acid precipitates as SLNs owing to proton exchange between the acid solution and the sodium salt.

DOXO was studied as an anti-cancer drug to be entrapped in SLNs, but, owing to its hydrophilic nature that hampers its entrapment in SLNs, several strategies were performed to increase its lipophilicity and to favour its entrapment in the SLN core.

In previous studies, lipophilic counter ions were tested to perform lipophilic ion pairing of DOXO (Battaglia et al., 2014); among several screened counter ions, only sodium dioctylsulfosuccinate (AOT) allowed to obtain an ion pair entrapped in SLNs with high efficiency. Although cytotoxicity studies on glioma cell lines and *in vitro* BBB permeation studies revealed a higher performance of DOXO-AOT entrapped in SLNs than free DOXO, the possibility of ion pair dissociation after dilution (occurring after *i.v.* administration) is an actual risk that should not be underestimated.

The aim of this work is to prepare, characterise and evaluate the potential of SLNs to release DOXO lipophilic derivatives to tumour cells *in vitro* and to demonstrate that the entrapment of DOXO in SLNs does not negatively influence the cytotoxicity of the native drug.

For these reasons, in this experimental work we decided to synthesise lipophilic prodrugs of DOXO and entrap them in SLNs; lipophilic DOXO prodrugs and analogues have been described in the literature (de Graaf et al., 2004; Wang et al., 2006; Ibsen et al., 2010; Chhikara et al., 2011). Therefore, two different DOXO derivatives, lauroyl ester and lauroyl amide were prepared and proposed as model of DOXO lipophilic derivatives to be entrapped in fatty acid SLNs.

For the above-mentioned purpose, SLNs were prepared and extensively characterised *in vitro* with regard to their physicochemical properties, their capacity to load lipophilic derivatives and their cytotoxicity.

Methods

Chemicals

Na-BA was purchased from Nu-Chek Prep, Inc. (Elysian, MN). PVA 9000, acetonitrile, DMF, dioxane, DMSO, lauric acid, THF, trifluoroacetic acid and dichloromethane from Sigma (Dorset, UK); hydrochloric acid, sodium hydroxide and monobasic sodium phosphate from Merck (Darmstadt, Germany); methanol, thionyl chloride, diisopropyl ether, diethyl ether and ethanol from Carlo Erba (Val De Reuil, France); deionised water was obtained by a MilliQ system (Millipore, Bedford, MO).

Synthesis of DOXO derivatives

*C*₁₂-DOXO ester

KF (0.16 g, 2.70 mmol) was added to the solution of 14-bromo/chloro daunorubicin hydrobromide (0.30 g, 0.45 mmol) and lauric

acid (0.27 g, 1.35 mmol) in dry DMF, in one portion and the reaction, mixture was stirred at room temperature for 72 h. The solvent was removed under reduced pressure and the residue was purified by flash chromatography (eluent: gradient from 98/2 to 9/1 dichloromethane/methanol) to give a red solid. The obtained compound was dissolved in freshly distilled dry THF, and two equivalents of HCl 1.7 M solution in dry dioxane was added. The resulting mixture was stirred for 2 h at room temperature, then diluted with diisopropyl ether. Precipitated hydrochloride was filtered, washed extensively with diethyl ether and dried in a vacuum chamber to give a title compound as a red powder (yield 58% w/w). HPLC (Waters Acquity UPLC, Waters Corp., Milford, MA, column Xterra MS C18 2.1 × 150, 3.5 μm; flow rate = 0.3 ml/min; A = 0.1% v/v formic acid in water, B = 0.1% v/v formic acid in acetonitrile, gradient (B%, time (min)): 10,1; 90,9; 10,5): Rt = 10.7 min, 98% (Water Acquity PDA detector, λ 480 nm and 254 nm).

¹H NMR (300 MHz, CDCl₃) δ (ppm): 0.85 (t, 3H, CH₂CH₃); 1.18 (m, 3H, ⁵CHCH₃); 1.24 (m, 16H, 8CH₂); 1.57 (m, 2H, OCOCH₂CH₂); 1.70 (d, 1H), 1.89 (m, 1H) (²CH₂); 2.00 (d, 1H), 2.30 (d, 1H) (⁸CH₂); 2.39 (t, 2H, OCOCH₂); 2.75 (d, 1H), 2.97 (d, 1H) (¹⁰CH₂); 3.63 (m, 1H, ⁴CH); 3.94 (s, 3H, OCH₃); 4.25 (q, 1H, ⁵CH); 4.87 (bs, 1H, ⁴COH); 5.25 (m, 3H, ⁷CH + ¹⁴CH₂); 5.45 (bs, 1H, ⁹COH); 5.73 (s, 1H, ¹CH); 7.55 (m, 1H), 7.79 (m, 2H) (3CH Ar); 8.02 (bs, 3H, NH₃⁺); 13.13 (s, 1H, PhOH); 13.94 (s, 1H, PhOH).

ESI-MS *m/z* = 726.1 [M + H]⁺.

*C*₁₂-DOXO amide

Lauric acid (0.50 g, 2.5 mmol) was added to freshly distilled thionyl chloride (10 ml) to synthesise lauroyl chloride and stirred under reflux for 8 h. Thionyl chloride was then evaporated and product was used in the next step without further purification.

To synthesise DOXO lauroyl amide, DOXO hydrochloride (0.23 g, 0.40 mmol) was dissolved in water/acetonitrile mixture (10 ml/10 ml) and pH was adjusted to 7 by addition of diluted NaOH solution. A solution of lauroyl chloride (0.36 g, 1.64 mmol) in acetonitrile (15 ml) was added dropwise at room temperature. During the addition pH was monitored and maintained to 7 by addition of diluted NaOH aqueous solution. Reaction was monitored by TLC (silica gel, dichloromethane/methanol = 6/4) and when it was finished acetonitrile was removed under vacuum and aqueous phase was extracted with dichloromethane (3 × 15 ml). Organic layer was dried with Na₂SO₄ and solvent was removed under vacuum. Crude product was then purified by flash chromatography (eluent: 8/2 dichloromethane/methanol) to obtain a red solid (yield 80% w/w).

TLC: silica gel, dichloromethane/methanol = 6/4, R_f = 0.9; HPLC (Waters 1525EF pump, W717 autosampler and Waters 2996 PDA detector, column Xterra C8 4.6 × 150, 5 μm; flow rate = 1 ml/min; A = 0.1% v/v trifluoroacetic acid in water, B = 0.1% v/v trifluoroacetic acid in methanol, gradient (B%, time (min)): 0,30; 7,5,30; 25,0,100; 35,0,100): Rt = 29.3 min, 85% (λ 480 nm and 254 nm); ¹H NMR (300 MHz, CDCl₃) δ (ppm): 0.64–0.53 (m, 3H, CH₃); 0.76 (m, 16H, 8CH₂); 0.95 (d, 3H, ⁶CH₃); 1.41 (d, 2H, NHC(O)CH₂CH₂); 1.81–1.70 (m, 1H, ⁷eqH); 2.04 (dd, *J* = 9.35 Hz, *J* = 6.31 Hz, 1H, ⁷axH); 2.08–2.13 (m, 2H, NHC(O)CH₂); 2.46 (d, 1H, ³axH); 2.55 (d, *J* = 4.11, 1H, ³eqH); 2.96 (d, *J* = 19.8 Hz, ⁹axH); 3.22 (d, *J* = 19.2 Hz, ⁹eqH); 3.70 (s, 1H, ⁶H); 3.99 (s, 3H, OCH₃); 4.13–4.04 (m, 2H, ¹⁰H + ⁴H); 4.67 (s, 2H, ¹⁴CH₂); 5.20 (s, 1H, ⁵H); 5.41 (m, 1H, ²H); 5.76 (d, *J* = 6.3, 1H, OH); 6.80 (s, 1H, NH); 7.31 (d, *J* = 8.6 Hz, 1H, Ar ⁴CH); 7.70 (t, *J* = 8.2 Hz, 1H, Ar ³CH); 7.95 (d, *J* = 7.2 Hz, 1H, Ar ²CH); 13.18 (s, 1H, PhOH).

ESI-MS *m/z* = 726.73 [M + H]⁺, 748.64 [M + Na]⁺.

Determination of partition coefficient of C₁₂-DOXO derivatives

Octanol/water partition coefficient (P) of C₁₂-DOXO derivatives was determined using biphasic n-octanol/water system (octanol and water were mutually saturated). A volume of 2 ml C₁₂-DOXO ester or amide-saturated water solution, obtained by centrifuging an oversaturated suspension of both compounds, was added to 2 ml n-octanol in a separating funnel. The aqueous phase concentration of both C₁₂-DOXO derivatives was determined by HPLC. The mixture was then shaken for 10 minutes and left to rest overnight; after phase separation, C₁₂-DOXO derivative aqueous phase concentration was determined by HPLC. The C₁₂-DOXO derivative concentration in the organic phase was determined by the difference between its aqueous phase concentrations before and after phase separation. P was calculated as n-octanol/water C₁₂-DOXO derivatives molar concentration ratio at the equilibrium. The results were expressed as log P. Each experiment was repeated thrice.

C₁₂-DOXO derivatives loaded SLN preparation

SLNs were prepared using the coacervation method (Battaglia et al., 2010) which uses hydrophilic polymers as stabilisers able to confer hydrophilicity to SLN surface. Further to a preliminary cytotoxicity screening against hCMEC/D3 cells relating to different fatty acids, which evidenced that BA-SLNs did not cause any detectable cytotoxicity against hCMEC/D3 cells (Gallarate et al., 2014), BA was chosen as lipid matrix.

Briefly, appropriate amounts of Na-BA (1% w/w) and PVA 9000 (2% or 4% w/w), as steric stabiliser (Scholes et al., 1999), were dispersed in 5 ml deionised water and the mixture was then heated under stirring (300 rpm) just above the Krafft point of Na-BA (75 °C) to obtain a clear micellar solution.

A selected acidifying solution (100 µl 1M NaH₂PO₄ + 160 µl 1M HCl) was then added drop-wise until pH 3.5–4.0 was reached. The obtained suspension was then cooled in a water bath under stirring at 300 rpm up to complete precipitation of SLNs. SLNs were stored at 4 °C before characterisation.

Drug-loaded SLNs were prepared as described for blank SLNs (empty SLNs), introducing C₁₂-DOXO derivatives as follows:

400 µl of C₁₂-DOXO ester methanolic solution (10 mg/ml) was added:

- In the micellar hot solution before acidification and SLN formation;
- Directly into the SLN suspension heated just above the melting point of BA (80 °C).

In both methods (a) and (b) the sample was then cooled in a water bath under stirring at 300 rpm until the temperature reached 15 °C.

100 µl of C₁₂-DOXO amide ethanolic solution (40 mg/ml) was added in the same way as the ester derivative. SLN samples were prepared under sterile conditions working in a horizontal laminar flow hood to perform *in vitro* studies on cell lines.

SLN characterisation

C₁₂-DOXO derivatives localisation into SLN dispersion was determined using optical microscopy equipped with a fluorescent lamp (Leica DM 2500, Solms, Germany) at 630× magnification.

SLN particle sizes, polydispersion indexes (PDI) and Zeta potential were determined 1 h after preparation using dynamic light scattering technique-DLS (Brookhaven, NY). Size measurements were obtained at an angle of 90° at 25 °C. The dispersions were diluted with water or with the different growth media described later in cytotoxicity studies for size determination, or with 0.01 M

KCl for Zeta potential determination, in order to achieve the pre-scribed conductivity.

For size stability studies versus time, the samples were stored at 4 °C. All data were determined in triplicate.

%EE determination was performed as follows: 1 ml SLN suspension was centrifuged for 15 min at 62000g, the precipitate was washed twice with 1 ml 30:70 v/v ethanol:water to eliminate adsorbed drug. The solid residue was dissolved in 1:1 v/v DMSO:dichloromethane; 0.1 ml water was then added to precipitate the lipid matrix and the supernatant was injected in HPLC for C₁₂-DOXO derivative determination. C₁₂-DOXO derivative %EE was calculated as the ratio between drug amount in SLNs and that in the starting micellar solution × 100.

%EE was also determined after 1:100 dilutions in water. An aliquot of suspension was stirred for 1 h, centrifuged for 15 min at 62000g and then treated as previously described. The amount of untrapped drug was eliminated from drug-loaded SLN formulation by gel centrifugation on Bio-gel P-6DG (pore size 90–180 µm, nominal exclusion limit was 6000 Da).

HPLC analysis

C₁₂-DOXO amide

HPLC analysis was performed using a LC-6A pump (Shimadzu, Tokyo, Japan) with a reversed-phase column (Chromsystem™ ODS, 125 × 4.6 mm, 2.5 µm particle size) and a C-R6A integrator (Shimadzu, Tokyo, Japan). HPLC grade methanol/water (85/15 v/v) with pH 7 adjusted by NaOH 0.01 N was used as a mobile phase with a flow rate of 1 ml/min. UV-Vis detector was set at λ = 480 nm. R_t was 5 min.

C₁₂-DOXO ester

HPLC analysis was performed with YL9100 HPLC system equipped with a YL9110 quaternary pump, a YL 9101 vacuum degasser and a YL 9160 PDA detector linked to YL-Clarity software for data analysis (Young Lin, Hogye-dong, 258 Anyang, Korea) and with MERK 50986 LiChrospher 100 RP8 5 µm 80 × 4.6 mm column. Acetonitrile (A)-phosphate buffer (50 mM at pH = 2 adjusted by HCl 0.01 N) (B) with gradient system (30% A/70% B to 90% A/10% B in 15 min at flow rate: 1 ml/min; total run 25 min) was used as mobile phase. R_t was 14 min.

In vitro cytotoxicity studies

MTT assay

The following human tumour cells were used: CFPAC-1 (pancreatic adenocarcinoma cell line), A459 (lung cancer cell line), A2780 (ovarian cancer cell line) and A2780 res (A2780 resistant to DOXO cancer cell line). All of them were obtained from the American Type Culture Collection (ATCC, Manassas, VA). A2780 and A2780 res were grown as a monolayer culture in RPMI 1640 medium, CFPAC-1 in DMEM, A549 in DMEM + F12, all of them supplemented with 10% heat-inactivated foetal calf serum (FCS), 2 mmol/l L-glutamine and penicillin/streptomycin (100 units/ml), at 37 °C in 5% CO₂ humidified atmosphere.

A2780 and A2780 res cell lines (2 × 10³/well), CFPAC-1 and A549 (800/well) were seeded in 96-well plates and incubated at 37 °C, 5% CO₂, for 24 h. Then, they were treated with C₁₂-DOXO amide and C₁₂-DOXO ester-loaded SLNs prepared as reported above and diluted to obtain C₁₂-DOXO derivatives in the 10⁻²–10⁻⁵ mM range, based on %EE. After 72 h incubation, the amount of viable cells was evaluated by MTT (Sigma-Aldrich) inner salt reagent at 570 nm, as described by the manufacturer's protocol.

The controls (i.e. cells that had received no drug) were normalised to 100%, and the readings from treated cells were expressed as % viability. Eight replicates were used to determine each data point and five different experiments were performed.

Colony-forming assay

A2780 and A2780 res cell lines (2×10^3 /well), CFPAC-1 and A549 (800/well, determined according to cell growth rate), were seeded into six-well plates and the day after they were treated with the compounds diluted to obtain DOXO derivatives concentrations in the 10^{-2} – 10^{-6} mM range (based on %EE). The medium was changed after 72 h and cells were cultured for additional 7 days in a drug-free medium. Subsequently, cells were fixed and stained with a solution of 80% crystal violet (Sigma-Aldrich) and 20% methanol. Colonies were then photographed and counted with Gel Doc equipment (Bio-Rad Laboratories, Milan, Italy). Then the cells were perfectly washed and 30% v/v acetic acid was added to induce a completely dissolution of the crystal violet. Absorbance was recorded at 595 nm by a 96-well-plate ELISA reader. Five different experiments were performed.

Data analysis

Data are shown as mean \pm SEM (standard error mean = standard deviation/ $\sqrt{\text{number of replicates}}$). Statistical analyses were performed with GraphPad Prism 3.0 software (La Jolla, CA) using one-way ANOVA and Dunnett's test. Values of $p < 0.05$ were considered statistically significant.

Results

Water solubilities of C_{12} -DOXO amide and C_{12} -DOXO ester were 64.49 $\mu\text{g/ml}$ and 38.47 $\mu\text{g/ml}$, respectively. Log p values of C_{12} -DOXO amide and C_{12} -DOXO ester, 2.58 and 3.47 respectively, were significantly higher than that of DOXO (log $P=0.6$ reported by Chhikara et al., 2011), showing an increase in lipophilicity compared to the parent drug. Mean diameters (\pm standard error, SE), PDI and Zeta potential of SLNs, determined by DLS, are reported in Table 1.

Mean diameters are in the 200–300 nm range. Zeta potential of SLNs prepared by coacervation is around 0 mV (Chirio et al., 2011). Probably, PVA 9000 used as stabiliser locates itself externally, thus partially screening the surface charge. Zeta potential indicates the surface charge of SLNs: Zeta potential values of empty SLNs confirmed the external positioning of the stabilising polymer. Being Zeta potential also related to drug arrangement in the lipid matrix of these systems (Kushwaha et al., 2013), probably, the slightly positive Zeta potential of SLN C_{12} -DOXO ester is due to partial arrangement of the drug to the outside of SLN surface, conferring them a positive charge.

Although a high value of Zeta potential is generally required to improve the stability of disperse systems, in the present case SLNs are stable in spite of 0 mV Zeta potential due to the surface stabilisation of polymer that avoids aggregation.

Size measurements were performed also on samples diluted with the different growth media used in *in vitro* experiments in order to evaluate the possible changes of SLN sizes when tested

Table 1. Mean particle size, PDI and Zeta potential \pm SE ($n=3$) of empty SLNs and of SLNs loaded with C_{12} -DOXO derivatives.

Sample	Mean diameter (nm) after gel centrifugation	PDI	Zeta potential (mV)
Empty SLN	271.5 \pm 5.5	0.108 \pm 0.012	-2.20 \pm 0.84
SLN C_{12} -DOXO ester	287.4 \pm 6.1	0.135 \pm 0.024	2.70 \pm 1.08
SLN C_{12} -DOXO amide	318.9 \pm 0.8	0.173 \pm 0.031	-2.29 \pm 0.02

in vitro. The growth media do not seem to influence SLN dimensions, as all SLNs maintained their size ($\pm 5\%$). The formulations were analysed to verify their overtime size stability. Particles diameters measured at different times up to 70 days were practically unmodified (Figure 1).

In Figure 2(A and B) SLN microphotographs are reported. The observation of SLN suspensions under optical microscope confirmed the spherical shape of the particles. The use of fluorescent light allowed indentifying C_{12} -DOXO derivatives within the SLNs: the dispersions of fluorescent SLNs were observed in both suspensions.

In Table 2, the amount of C_{12} -DOXO derivatives in SLN, prepared by dispersion in 2% w/w PVA9000 aqueous solution, is expressed as %EE and as drug loading ($\mu\text{g } C_{12}$ -DOXO derivative/mg BA). %EE was calculated after SLN centrifugation and washing with ethanol:water 30:70 v/v.

SLNs showed a good C_{12} -DOXO derivatives loading capacity. In particular, %EE did not significantly vary by increasing the drug amount, while it was significantly influenced by PVA 9000 content. When the stabiliser percentage was increased from 2% w/w to 4% w/w in SLN loaded with C_{12} -DOXO ester (added after re-melting) a decrease in drug %EE from 80 to 70 $\pm 5\%$ (w/w) was noted; probably PVA 9000 formed micelles in aqueous phase able to solubilise the ester derivative.

When SLNs carrying both derivatives (added after SLN re-melting) were 1:100 diluted in physiological fluids, drug %EE remained almost unchanged ($\pm 5\%$). This is a successful improvement compared with the almost complete loss of %EE registered when DOXO-AOT ion pair was entrapped in SLNs (Battaglia et al., 2014).

On the contrary, when both derivatives were added to the micellar solution, after 1:100 dilution %EE decreased up to 65% w/w. Probably, when added to the micellar solution, derivatives are partially entrapped in PVA chains located on the surface of SLNs and therefore they might be released upon high dilutions.

After gel centrifugation of SLNs, in which the drug was added in the melted lipid, resulting %EE of C_{12} -DOXO ester was 73% w/w and that of C_{12} -DOXO amide was 65% w/w. The gel centrifugation method allows to eliminate the not-completely entrapped drug, that cannot be extracted by simple centrifugation and washing.

In vitro cytotoxicity studies

The effect of C_{12} -DOXO amide loaded SLNs, C_{12} -DOXO ester loaded SLNs and free DOXO on cell growth of three different

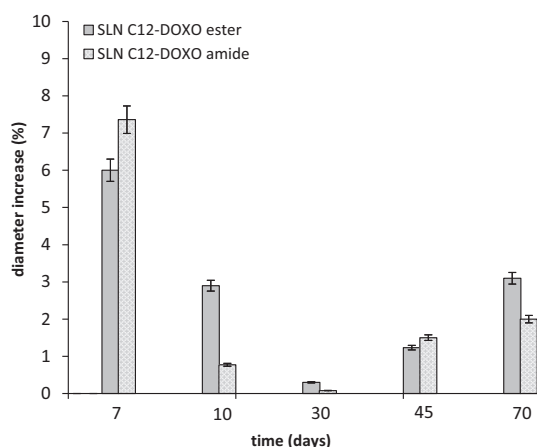


Figure 1. SLN diameter variation \pm SE ($n=3$) versus time.

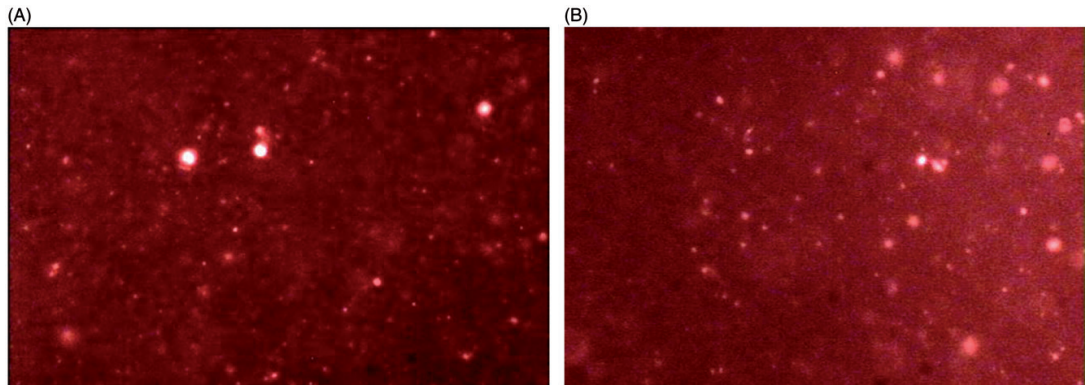


Figure 2. (A) Optical microscopy images of C_{12} -DOXO amide-loaded SLNs and (B) C_{12} -DOXO ester-loaded SLNs.

Table 2. %EE (w/w) and drug loading ($\mu\text{g}/\text{mg}$) \pm SE ($n = 3$) of C_{12} -DOXO derivative-loaded SLNs obtained using two different methods of preparation.

SLN loaded with C_{12} -DOXO derivatives	%EE (w/w)	Drug loading ($\mu\text{g}/\text{mg}$)
SLN C_{12} -DOXO ester added after re-melting	80 \pm 5	64 \pm 4
SLN C_{12} -DOXO ester added to the micellar solution	69 \pm 2	55 \pm 2
SLN C_{12} -DOXO amide added after re-melting	94 \pm 5	75 \pm 3
SLN C_{12} -DOXO amide added to the micellar solution	81 \pm 6	65 \pm 5

tumour cell lines was examined. Since, among different carcinoma types, ovarian, pancreatic and lung carcinoma are those with the worse prognosis, any therapeutic improvement is imperative: therefore, their cell types were selected as a model of tumour with high aggressive behaviour (Szepeshazi et al., 2013; Giovinazzo et al., 2016; Lixia et al., 2016). Initially, the ability of SLNs loaded with C_{12} -DOXO derivatives and of free DOXO to inhibit the growth of CFPAC-1, A549, A2780 and A2780res cells was compared. Cells were cultured in the presence and absence of titrated amounts (10^{-5} – 10^{-2} mM) of DOXO or both C_{12} -DOXO derivative loaded SLNs for 72 h, that is the same time point used for the subsequent clonogenic assay. The most significant time chosen was 72 h to detect cell growth inhibition, as preliminary *in vitro* release studies showed a very slow release of both DOXO derivatives from SLNs (data not reported). The amount of viable cells was then assessed by the MTT assay. MTT, a yellow tetrazole, is reduced to purple formazan in living cells. Tetrazolium dye reduction is dependent on NAD(P)H-dependent oxidoreductase enzymes largely in the cytosolic compartment of the cell. Therefore, reduction of MTT depends on the cellular metabolic activity due to NAD(P)H flux. Cells with a low metabolism such as thymocytes and splenocytes reduce very little MTT. In contrast, rapidly dividing cells exhibit high rates of MTT reduction.

The obtained results showed that DOXO displayed an inhibition of cell proliferation greater or similar to C_{12} -DOXO amide-loaded SLNs on all cell types (Figure 3). It has been revealed that the presence of the amide bond reduced the anticancer activity on A2780, A549 and CFPAC-1 cell lines, in accordance with previous literature data (Chhikara et al., 2011) suggesting that the presence of free amino group is required for anticancer activity of DOXO. Otherwise C_{12} -DOXO ester-loaded SLNs showed a stronger inhibitory effect than DOXO. The effect was concentration-dependent with some differences among the four cell lines. The most responsive cell line was A549, where C_{12} -DOXO ester-loaded SLNs were always more efficient than the free drug (Figure 3(B); inhibition rate: 90% versus 60% at 10^{-3} mM, 65% versus 40% at 10^{-4} mM). The two

formulations displayed a similar efficacy on CFPAC-1 in the range of concentrations 10^{-4} – 10^{-2} mM, but C_{12} -DOXO ester-loaded SLNs retained their activity at 10^{-5} mM (50% of inhibition) and became inefficient at 10^{-6} mM (data not reported), while the free drug was completely ineffective at 10^{-5} mM (Figure 3(A)). A2780 cell line was sensitive to both compound, but at 10^{-5} mM, only C_{12} -DOXO ester-loaded SLNs retained a weak inhibitory effect (Figure 3(C); 38% inhibition).

In order to deepen the evaluation on the efficacy of C_{12} -DOXO derivatives loaded SLNs, we decided to test their ability to exert an antitumor activity also on a particular ovarian cancer cell line resistant to DOXO (A2780res).

As expected, free DOXO was effective only at the highest concentration (10^{-2} mM; 40% inhibition), while C_{12} -DOXO ester-loaded SLN was more efficient since it was able to induce the same inhibitory effect (40%) also in the range of concentrations 10^{-2} – 10^{-4} mM (Figure 3(D)).

To investigate the possibility that empty SLNs may exert cell toxicity (not related to DOXO), the effects of empty SLNs (diluted as to obtain 10^{-5} – 10^{-2} mM DOXO-derivative concentration range) on cell growth of the four tumour cell lines were evaluated using the MTT assay. Results showed that SLNs did not affect cell growth even at the highest concentrations.

Table 3 shows the IC_{50} for all tested cell lines, revealing that C_{12} -DOXO ester-loaded SLNs were always more effective than the free drug except for A2780 cell line, as confirmed by MTT assay, where C_{12} -DOXO ester and free DOXO were similarly efficient at concentrations higher than 10^{-5} mM.

MTT test allows the evaluation of cell enzymatic activity after 72 h of incubation, but it does not give any information on cell ability to further proliferate even after the removal of the drug from culture medium.

Colony-forming (clonogenic) assay is the “gold standard” cellular-sensitivity assay and it is more representative of the *in vivo* condition (Langdon and Macleod, 2004). In order to validate the previous findings, clonogenic survival assays were performed. Clonogenic assay is an *in vitro* cell survival assay based on the ability of a single cell to grow into a colony. The colony is defined to consist of at least 50 cells. The assay essentially tests every cell in the population for its ability to undergo “unlimited” division. After plating at very-low density (800 or 2×10^3 cell per well), cells were treated with the samples for 72 h, then samples were removed by washing the cells with the cell medium and the cells were allowed to growth over extended period of time (7 days). Only a fraction of seeded cells retained the capacity to produce colonies.

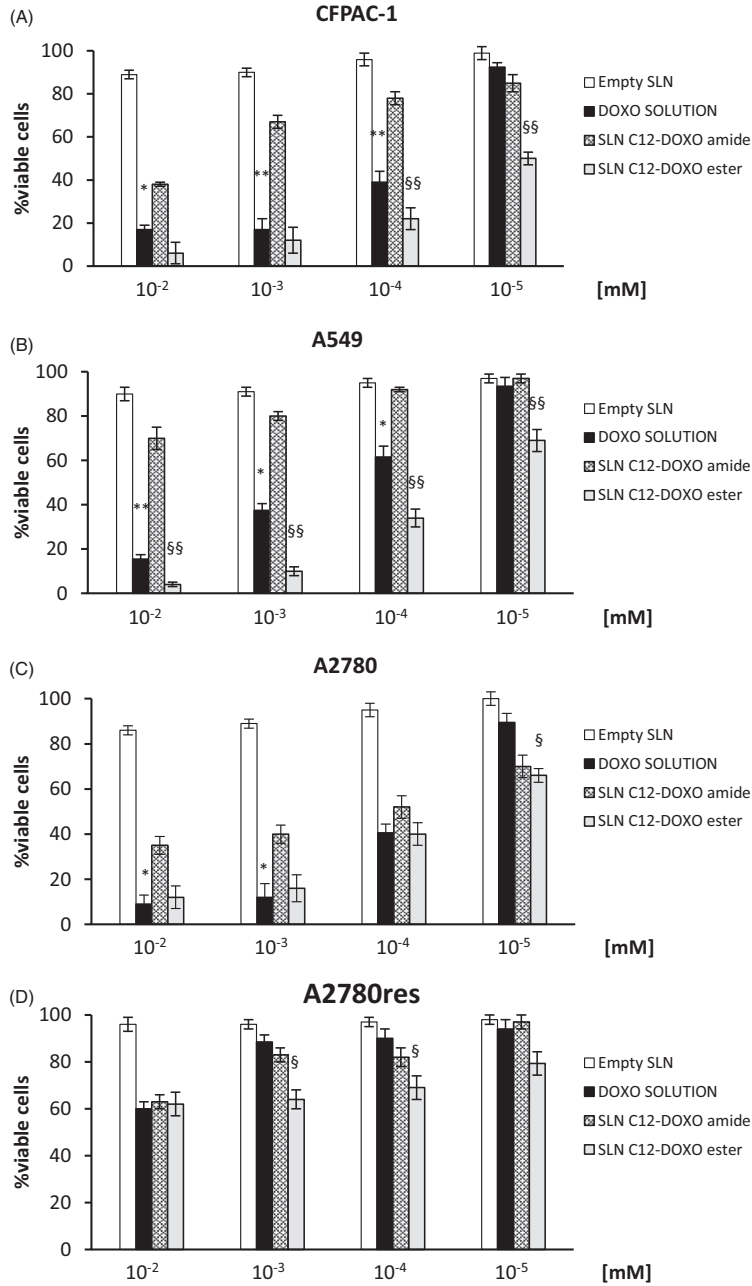


Figure 3. Inhibition of CFPAC-1 cells (A), A549 cells (B), A2780 cells (C), A2780res cells (D) proliferation following C₁₂-DOXO ester-loaded SLNs, C₁₂-DOXO amide loaded SLNs and DOXO treatment. Cells were treated with increasing concentrations (10⁻⁵–10⁻² mM) of C₁₂-DOXO ester-loaded SLNs, C₁₂-DOXO amide loaded SLNs, empty SLNs, and DOXO for 72 h; the result was expressed as the percentage of viable cells versus the control expressed as mean ± SEM (n = 5). One-way ANOVA and the Dunnett's test revealed statistically significance differences (*p < 0.05; **p < 0.01) of DOXO versus C₁₂-DOXO amide-loaded SLNs treated cells and (§p < 0.05; §§p < 0.01) of C₁₂-DOXO ester versus DOXO-treated cells.

Table 3. IC₅₀ ± SEM (n = 5) of C₁₂-DOXO derivatives loaded SLNs and DOXO solution.

	IC ₅₀ A2780 [mM]	IC ₅₀ A549 [mM]	IC ₅₀ A2780 res [mM]	IC ₅₀ CFPAC-1 [mM]
DOXO solution	5.5 · 10 ⁻⁵ ± 0.5	4.3 · 10 ⁻³ ± 0.1	5.8 · 10 ⁻² ± 0.6	5.3 · 10 ⁻⁵ ± 0.2
SLN C ₁₂ -DOXO amide	1.4 · 10 ⁻⁵ ± 0.6	7.1 · 10 ⁻⁴ ± 0.9	1.7 · 10 ⁻² ± 0.2	2.3 · 10 ⁻² ± 0.2
SLN C ₁₂ -DOXO ester	2.7 · 10 ⁻⁵ ± 0.1	2.9 · 10 ⁻⁶ ± 0.9**	7.5 · 10 ⁻⁶ ± 0.4**	8.8 · 10 ⁻⁶ ± 0.4*

One-way ANOVA and the Dunnett's tests revealed statistically significance differences (*p < 0.05; **p < 0.01) of C₁₂-DOXO ester-loaded SLNs versus DOXO treated cells.

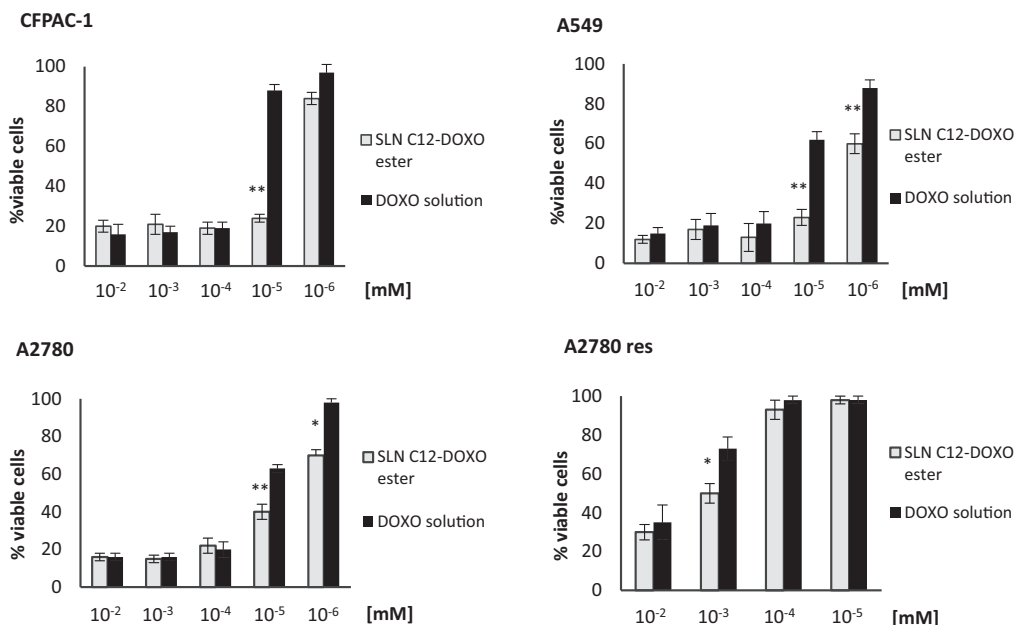


Figure 4. Effect of C₁₂-DOXO ester-loaded SLNs and DOXO treatment on cell clonogenicity was tested by colony forming assay. Cells (800 or 2 × 10³ per well) were seeded in six-well plates and treated with each sample at the indicated drug concentrations (10⁻⁶–10⁻² mM) for 72 h. The medium was then changed and cells were cultured for additional 7 days and subsequently fixed and stained with crystal violet (n = 5). One-way ANOVA and the Dunnett's tests revealed statistically significance differences (*p < 0.05; **p < 0.01) of C₁₂-DOXO ester-loaded SLNs versus DOXO-treated cells.

The results shown in Figure 4 were similar to those obtained with the MTT assay, but the inhibitory effect was more prominent, since noticeable even at 10⁻⁶ mM, in A549 and A2780. In fact, C₁₂-DOXO ester-loaded SLNs retained their ability to inhibit CFPAC-1 strongly, being able to induce the growth of only 20% of colony at 10⁻⁵ mM. DOXO was almost inefficient at the same concentration. A549 were also more sensitive to C₁₂-DOXO ester-loaded SLN than to DOXO, since it was still active at 10⁻⁶ mM, when only 60% of the colony were able to grow. A2780 resulted particularly sensitive to DOXO also in the clonogenic assay, but C₁₂-DOXO ester-loaded SLNs demonstrated a stronger efficacy at 10⁻⁵–10⁻⁶ mM. Finally, A2780 res showed a better response to C₁₂-DOXO ester loaded SLN than to DOXO to the concentration 10⁻³ mM, even if they were less responsive than the other cell types.

In Figure 5, representative photos of clonogenic assay carried out on the four cell lines are reported. In each non-resistant cell line, C₁₂-DOXO ester-loaded SLNs maintained their anti-proliferative effect up to 10⁻⁵ mM concentration, whereas, samples treated with free DOXO began to grow.

Discussion

BA SLNs, loaded with DOXO lauroyl ester or lauroyl amide, were prepared with the coacervation technique. Spherical-shaped SLNs with mean diameters in the 200–300 nm range were obtained.

SLNs showed a good C₁₂-DOXO derivatives loading capacity, but by introducing C₁₂-DOXO derivatives after SLN re-melting instead of adding them to the micellar solution allowed to obtain higher drug %EE, as reported in previous work (Chirio et al., 2014). Probably, the high drug lipophilicity does not allow its distribution within micelles, while promoting its solubilisation in the molten lipid.

Therefore, the preparation method consisting in the addition of both lipophilic DOXO derivatives in the re-molten lipid resulted to be the most suitable for our purposes, especially for *in vitro* cell toxicity studies, as well as for a possible future *in vivo* administration.

C₁₂-DOXO amide-loaded SLNs were not more effective than DOXO in inhibiting cell growth. Conjugation of 4'-amino group with fatty acid through an amide bond reduced or maintained almost unmodified the anticancer activity of the free drug in tested cancer cell lines. This suggests, as already demonstrated by Chhikara et al. (2011) that the presence of free amino group is required for anticancer activity of DOXO.

DOXO hinders the resealing of DNA double helix strands inhibiting the enzyme topoisomerase II during the replication and thereby arresting the reproduction of the cells. Replication inhibition is due to the structure of DOXO: the planar aromatic portion of the molecule intercalates between two base pairs of the DNA helix. The carbohydrate part of DOXO is involved in the binding to replicating DNA bases during its mechanism of action, and amine group should be freely available for interaction with the flanking base pairs.

Also, in this study, the requirement for availability of the sugar moiety in DOXO was confirmed. SLN-loaded C₁₂-DOXO amide was probably only partially hydrolysed even after long incubation time providing only a slow anti-proliferative activity in these specific cell lines.

The effect on inhibition of cell proliferation induced by C₁₂-DOXO ester-loaded SLNs was concentration-dependent, with some differences among the four cell lines and between the SLN-loaded pro-drug and the free drug. The results obtained with clonogenic assay were similar to those obtained with the MTT assay. In fact, C₁₂-DOXO ester-loaded SLNs retained the ability of the drug to inhibit CFPAC-1, A2780 and A549 strongly at 10⁻⁵ mM, while free

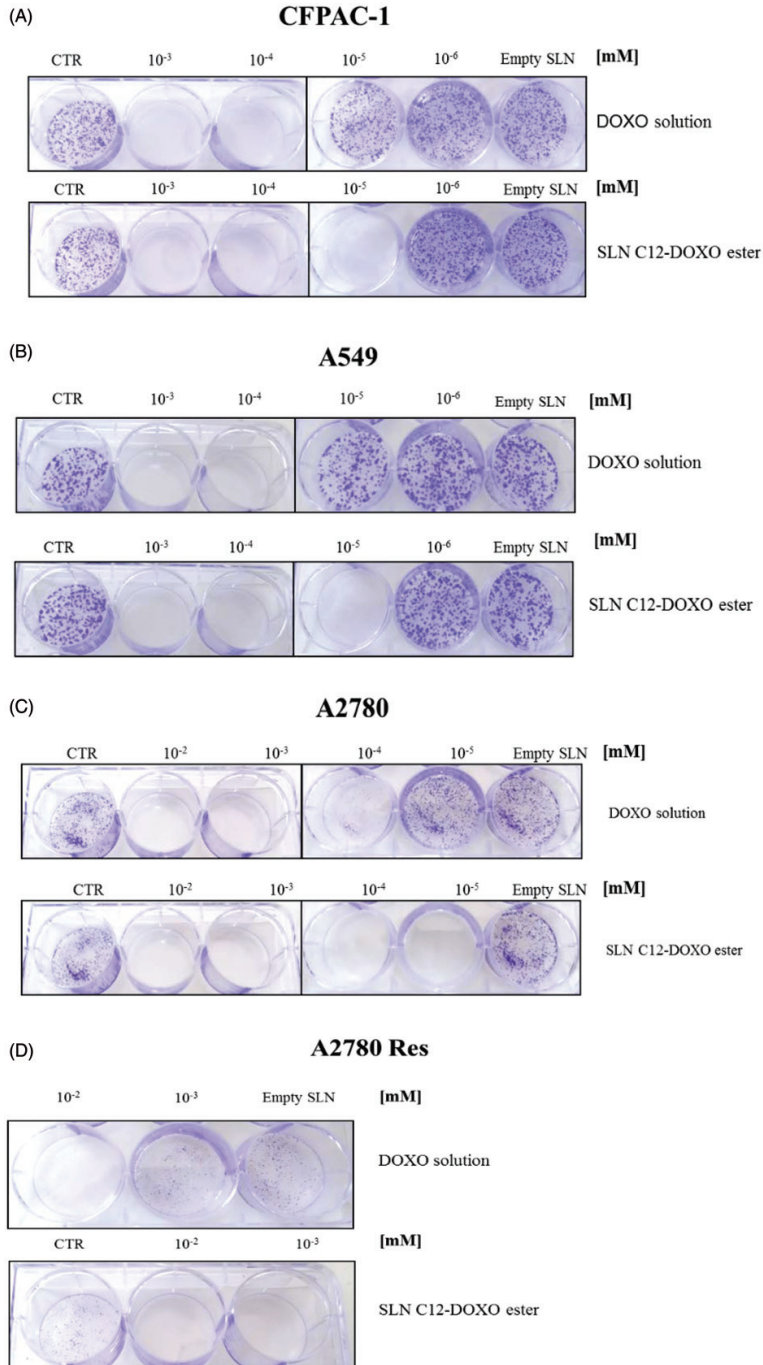


Figure 5. Effect of C_{12} -DOXO ester-loaded SLNs and DOXO treatment on cell clonogenicity was tested by colony forming assay. Clonogenic assay photos from a representative experiment. The amount of lipid in empty SLN sample corresponds to the dilution required to obtain 10^{-3} mM C_{12} -DOXO ester.

DOXO was almost inefficient or less efficient at the same concentration. The observation that the inhibition detected by the clonogenic assay was substantially higher than that detected by the MTT assay suggests that cells, which were still viable in the MTT assay, after 72 h of treatment, were severely damaged and unable

to proliferate in the clonogenic assay, partially confirming the slow release of DOXO-ester from SLNs. The positive result obtained also on A2780 cell lines, on which C_{12} -DOXO ester-loaded SLN and free DOXO were similarly efficient in MTT test, reinforces this hypothesis.

Even A2780 res, less responsive than the other cell types, showed a better response to C₁₂-DOXO ester-loaded SLNs than to free DOXO. Probably, the capacity of C₁₂-DOXO ester-loaded SLNs to partially inhibit the proliferation also of a resistant cell line might be ascribed to the overcoming of MDR due to the protection of the entrapped drug from the P-gp efflux mechanism of the cell. Further investigation on different resistant cancer cell lines are therefore needed to confirm such hypothesis.

From a formulative point of view, SLNs described in this paper proved to be able to incorporate lipophilic pro-drugs of DOXO with good %EE, which was maintained also after 1:100 dilution, other than what was noted in a previous work (Battaglia et al., 2014) for DOXO-AOT ion pairs.

The relevance of using DOXO derivatives strongly entrapped within the lipid matrix could be an important prerequisite for a future *in vivo* administration. Many problems are related to *in vivo* administration of nanoparticulate systems, such as the quickly binding to opsonin proteins that allows macrophages to easily recognise and remove them before they can perform their designed therapeutic function. Therefore, the developments of stealth SLNs as well as the modification of SLN surface with specific ligands to specific receptor over-expressed on different tumour cells are the mandatory following steps to begin *in vivo* studies. Moreover the effect on MDR of SLNs will be evaluated measuring the expression (by immunoblotting) and the activities (evaluating efflux of fluorescent substrates, ATPase activity) of Pgp and MRP. If the hypothesis that SLNs can overcome MDR will be confirmed, the effective concentration in the targeted cells will be increased, indirectly reducing the required administered drugs.

The results obtained *in vitro*, if supported by satisfactory pharmacokinetic and biodistribution patterns, with a possible targeting to the tumour site, might suggest the potential use of SLNs as DOXO delivery systems.

As one of the major DOXO adverse effect is cardiotoxicity, which may limit its use, the perspective to reduce its therapeutic dose by employing promising vehicles such as C₁₂-DOXO ester-loaded SLNs is an important goal of our future research.

Conclusion

SLNs are able to incorporate lipophilic pro-drugs of hydrophilic agents with unsatisfactory biodistribution patterns, and to increase cytotoxicity of parent drug. Although it is still necessary to assess the ability of SLN to revert MDR by *in vitro* studies, and to optimise SLN-loading capacity, C₁₂-DOXO ester-loaded SLNs are promising vehicles to increase DOXO cytotoxicity in perspective of reducing its therapeutic dose and consequently its systemic toxic side effect.

Disclosure statement

The authors report no declarations of interest.

ORCID

Luigi Battaglia  <http://orcid.org/0000-0002-5081-3638>

References

Barraud L, Merle P, Soma E, Lefrancois L, Guerret S, Chevallier M, Dubernet C, Couvreur P, Trepo C, Vitvitski L. Increase of doxorubicin sensitivity by doxorubicin-loading into nanoparticles for

hepatocellular carcinoma cells *in vitro* and *in vivo*. *J Hepatol*, 2005;42:736–43.

Battaglia L, Gallarate M, Cavalli R, Trotta M. Solid lipid nanoparticles produced through a coacervation method. *J Microencapsulation*, 2010;27:78–85.

Battaglia L, Gallarate M, Peira E, Chirio D, Muntoni E, Biasibetti E, Capucchio MT, Valazza A, Panciani PP, Lanotte M, et al. Solid lipid nanoparticles for potential doxorubicin delivery in glioblastoma treatment: Preliminary *in vitro* studies. *J Pharm Sci*, 2014;103:2157–65.

Chhikara BS, Jean NS, Mandal D, Kumar A, Parang K. Fatty acyl amide derivatives of doxorubicin: Synthesis and *in vitro* anti-cancer activities. *Eur J Med Chem*, 2011;46:2037–42.

Chirio D, Gallarate M, Peira E, Battaglia L, Serpe L, Trotta M. Formulation of curcumin-loaded solid lipid nanoparticles produced by fatty acids coacervation technique. *J Microencapsul*, 2011;28(6):537–48.

Chirio D, Gallarate M, Peira E, Battaglia L, Muntoni E, Riganti C, Biasibetti E, Capucchio MT, Valazza A, Panciani P, et al. Positive-charged solid lipid nanoparticles as paclitaxel drug delivery system in glioblastoma treatment. *Eur J Pharm Biopharm*, 2014;88(3):746–58.

de Graaf M, Nevalainen TJ, Scheeren HW, Pinedo HM, Haisma HJ, Boven E. A methylester of the glucuronide prodrug DOX-GA3 for improvement of tumor-selective chemotherapy. *Biochem Pharmacol*, 2004;68(11):2273–8.

Devalapally H, Duan Z, Seiden MV, Amiji MM. Paclitaxel and ceramide co-administration in biodegradable polymeric nanoparticulate delivery system to overcome drug resistance in ovarian cancer. *Int J Cancer*, 2007;121:1830–8.

Dikmen G, Güney G, Genc L. Characterization of solid lipid nanoparticles containing caffeic acid and determination of its effects on MCF-7 cells. *Recent Pat Anticancer Drug Discov*, 2015;10(2):224–32.

Doktorovova S, Souto EB, Silva AM. Nanotoxicology applied to solid lipid nanoparticles and nanostructured lipid carriers – A systematic review of *in vitro* data. *Eur J Pharm Biopharm*, 2014;87:1–18.

Duggan ST, Keating GM. Pegylated liposomal doxorubicin: A review of its use in metastatic breast cancer, ovarian cancer, multiple myeloma and AIDS-related Kaposi's sarcoma. *Drugs*, 2011;71:2531–58.

Gallarate M, Serpe L, Foglietta F, Zara GP, Giordano S, Peira E, Chirio D, Battaglia L. Solid lipid nanoparticles loaded with fluorescent-labelled Cyclosporine A: Anti-inflammatory activity *in vitro*. *Protein Pept Lett*, 2014;21(11):1157–62.

Ganta S, Amiji M. Coadministration of Paclitaxel and curcumin in nanoemulsion formulations to overcome multidrug resistance in tumor cells. *Mol Pharm*, 2009;6:928–39.

Gasco MR, Morel S, Ugazio E, Cavalli R. Thymopentin in solid lipid nanoparticles. *Int J Pharm*, 1996;132:259–61.

Giovinazzo H, Kumar P, Sheikh A, Brooks KM, Ivanovic M, Walsh M, Caron WP, Kowalsky RJ, Song G, Whitlow A, et al. Technetium Tc 99m sulfur colloid phenotypic probe for the pharmacokinetics and pharmacodynamics of PEGylated liposomal doxorubicin in women with ovarian cancer. *Cancer Chemother Pharmacol*, 2016;77:565–73.

Güney G, Kutlu HM, Genc L. Preparation and characterization of ascorbic acid loaded solid lipid nanoparticles and investigation of their apoptotic effects. *Colloids Surf B Biointerfaces*, 2014;121(1):270–80.

Ibsen S, Zahavy E, Wrasdilo W, Berns M, Chan M, Esener S. A novel Doxorubicin prodrug with controllable photolysis activation for cancer chemotherapy. *Pharm Res*, 2010;27(9):1848–60.

- Iyer AK, Singh A, Ganta SB, Amiji MM. Role of integrated cancer nanomedicine in overcoming drug resistance. *Adv Drug Deliv Rev*, 2013;65:1784–802.
- Kushwaha AK, Vuddanda PR, Priyanka K, Singh SK, Singh S. 2013. Development and evaluation of solid lipid nanoparticles of raloxifene hydrochloride for enhanced bioavailability. *BioMed Res Int*, 2013;2013:584549.
- Langdon SP, Macleod KG. 2004. Cancer cell culture: Methods and protocols. In: Langdon SP, ed. *Methods in molecular medicine*. Totowa, NJ: Humana Press Inc., pp. 159–64.
- Laquintana V, Trapani A, Denora N, Wang F, Gallo JM, Trapani G. New strategies to deliver anticancer drugs to brain tumors. *Expert Opin Drug Deliv*, 2009;6(10):1017–32.
- Lixia LV, Xiumei AN, Hongyan LI, Lanxiu MA. Effect of miR-155 knockdown on the reversal of doxorubicin resistance in human lung cancer A549/dox cells. *Oncol Lett*, 2016;11:1161–6.
- Ma P, Dong X, Swadley CL, Gupte A, Leggas M, Ledebur HC, Mumper RJ. Development of idarubicin and doxorubicin solid lipid nanoparticles to overcome Pgp-mediated multiple drug resistance in leukemia. *J Biomed Nanotechnol*, 2009;5:151–61.
- Merisko-Liversidge E.M, Liversidge GG. Drug nanoparticles: Formulating poorly water-soluble compounds. *Toxicol Pathol*, 2008;36:43–8.
- Miao J, Du YZ, Yuan H, Zhang XG, Hu FQ. Drug resistance reversal activity of anticancer drug loaded solid lipid nanoparticles in multi-drug resistant cancer cells. *Colloids Surf B Biointerfaces*, 2013;110:74–80.
- Moghimi SM, Hunter AC, Murray JC. Long-circulating and target-specific nanoparticles: Theory to practice. *Pharmacol Rev*, 2001;53:283–318.
- Petschauer JS, Madden AJ, Kirschbrown WP, Song G, Zamboni WC. The effects of nanoparticle drug loading on the pharmacokinetics of anticancer agents. *Nanomedicine (Lond)*, 2015;10:447–63.
- Scholes PD, Coombes AGA, Illum L, Davis SS, Watts JF, Ustariz C, Vert M, Davies MC. Detection and determination of surface levels of poloxamer and PVA surfactant on biodegradable nanospheres using SSIMS and XPS. *J Contr Rel*, 1999;59:261–78.
- Shah M, Agrawal Y K, Garala K, Ramkishan A. Solid lipid nanoparticles of a water soluble drug, ciprofloxacin hydrochloride. *Indian J Pharm Sci*, 2012;74(5):434–42.
- Singh S, Dobhal AK, Jain A, Pandit JK, Chakraborty S. Formulation and evaluation of solid lipid nanoparticles of a water soluble drug: Zidovudine. *Chem Pharm Bull*, 2010;58:650–5.
- Swain SM, Whaley FS, Ewer MS. Congestive heart failure in patients treated with doxorubicin: A retrospective analysis of three trials. *Cancer*, 2003;97:2869–79.
- Szepeshazi K, Schally AV, Block NL, Halmos G, Nadji M, Szalontay L, Vidaurre I, Abi-Chaker A, Rick FG. Powerful inhibition of experimental human pancreatic cancers by receptor targeted cytotoxic LH-RH analog AEZS-108. *Oncotarget*, 2013;4:751–60.
- Thukral DK, Dumoga S, Mishra AK. Solid lipid nanoparticles: Promising therapeutic nanocarriers for drug delivery. *Curr Drug Deliv*, 2014;11:771–91.
- Trotta M, Gallarate M, Battaglia L, Chirio D. Cisplatin loaded SLN produced by coacervation technique. *J Drug Deliv Sci Technol*, 2010;20:343–7.
- Trotta M, Gallarate M, Battaglia L, Peira E. Peptide loaded solid lipid nanoparticles prepared through coacervation technique. *Int J Chem Eng*, 2011;2011:132435.
- Wang Y, Li L, Jiang W, Yang Z, Zhang Z. Synthesis and preliminary antitumor activity evaluation of a DHA and doxorubicin conjugate. *Bioorg Med Chem Lett*, 2006;16(11):2974–7.
- Wong HL, Bendayan R, Rauth AM, Li Y, Wu XY. Chemotherapy with anticancer drugs encapsulated in solid lipid nanoparticles. *Adv Drug Deliv Rev*, 2007;59:491–504.

Latest News on Nanotechnology for
Melanoma Therapy and DiagnosisMartina Daga¹, Chiara Dianzani², Benedetta Ferrara², Valeria Nardoza¹, Roberta Cavalli², Giuseppina Barrera¹ and Stefania Pizzimenti^{1*}¹Department of Clinical and Biological Sciences, University of Turin, Italy²Department of Drug Science and Technology, University of Turin, Italy

Article Information

Received date: Apr 04, 2016

Accepted date: May 24, 2016

Published date: May 31, 2016

*Corresponding author

Stefania Pizzimenti, Department of
Clinical and Biological Sciences,
University of Turin, 10125 Turin, Italy,
Email: stefania.pizzimenti@unito.itDistributed under Creative Commons
CC-BY 4.0

Abstract

Melanoma skin cancer is an aggressive tumour with an increasing incidence. In recent years, the treatment options for the advanced disease have expanded dramatically with the employment of targeted therapy and the immunotherapy. However, the high rate of non-response, the toxicity, and the induced drug resistance remain unmet clinical problems. Scientists are expecting a further advance with the application of nanotechnology in melanoma treatment and diagnosis. In this review, we present an up-date on the latest pre-clinical studies (2015-2016) on nanomedicine with potential use in the clinical management of this disease.

Introduction

Melanoma skin cancer is an aggressive tumour whose incidence has been steadily increasing over the last 50 years, now representing 3% of total tumours. In 2012, more than 232,000 new cases of melanoma were diagnosed worldwide; in the same year, mortality estimation calculated 55,500 deaths from melanoma in the world [1], with an increasing stage-specific mortality rate [2]. The treatment of localized disease (stage I and II) is surgical excision, while, in the advanced disease, pharmacotherapy is included in the treatment [3]. Chemotherapy was the first therapeutical option: Dacarbazine (DTIC), an alkylating agent, was approved in 1974 by US Food and Drug Administration (FDA) for the treatment of metastatic melanoma. Later, other chemotherapeutic drugs were used, alone or in combination, in several clinical trials, such as Temozolomide (TMZ), a combination of Cisplatin, Vinblastine and Dacarbazine (CVD), or Carboplatin and Paclitaxel (CP). However, these regimes have been compared with DTIC alone and no significant improvements in overall survival were observed, or they elicited important toxic effects, such as myelosuppression, peripheral neuropathy and fatigue [4].

A recent report has calculated that less than 5% of patients achieve a complete response with DTIC, and the 5-year survival rate is only 2-6% [5]. Recent improvements in treatment effectiveness have been obtained with Immunotherapy and Targeted therapy (Table 1).

The immune system plays a very important role in melanoma progression. Indeed, melanoma can evade immune response which can be associated with immunosuppression [6]; thus, the possibility of re-activating a specific antitumour immune response has been widely explored. IL-2 and interferon were at first used as adjuvant therapy, but, more recently, very specific modulators of the immune response, such as the Cytotoxic T-Lymphocyte Antigen 4 (CTLA-4) and Programmed Death-1 (PD-1) inhibitors have been approved. CTLA-4 is a protein receptor present on the surface of cytotoxic T-lymphocytes, and acts as an inhibitory checkpoint that blocks T-cell activation; ipilimumab, the anti-CTLA-4 monoclonal antibody, is able to restore T cell activity [7]. Similar to CTLA-4, the PD-1 receptor is expressed on T-cells, and it normally binds to the PD-1 and 2 Ligands (PD-L1, PD-L2); moreover, it is present on antigen-presenting cells and suppresses T-cell activation; pembrolizumab and nivolumab are two anti-PD-1 antibodies that block the interaction between PD-1 and its ligands, PD-L1 and PD-L2, thus reactivating the T-cell response [8]. Very recently, the first live oncolytic virus therapy against melanoma has been approved by the FDA. Imlygic is a genetically modified oncolytic herpes virus, able to replicate within cancer cells, destroy them, and produce the immunostimulatory protein GM-CSF (Granulocyte-Macrophage Colony Stimulating Factor) [9].

In the last few years, the treatment options for the advanced disease have expanded dramatically, thanks to the identification of activating mutations in the genes involved in melanoma progression. New molecular targeted therapies have been set up, with the development of small molecular inhibitors that target these mutated proteins. In 2011, the FDA approved the first targeted drug for the advanced melanoma disease, the B-RAF inhibitor Vemurafenib [10]. B-RAF is a Serine/Threonine Kinase, belonging to Mitogen-Activated Protein Kinases (MAPKs), one of the main signal transduction pathways involved in cell proliferation. Vemurafenib, with the more recently

Table 1: FDA-approved drugs in Immunotherapy and Targeted therapy.

Targeted therapy		
Drug	Activity	FDA-Approved
Cotellic (Cobimetinib, Genentech)	MEK inhibitor	Nov 2015
Trametinib (Mekinist, GlaxoSmithKline)	MEK Inhibitor	May 2013
Dabrafenib (Tafinlar, GlaxoSmithKline)	Inhibitor of V600E-mutated form of BRAF	May 2013
Vemurafenib (Zelboraf, Roche)	Inhibitor of V600E-mutated form of BRAF	Aug 2011
Immunotherapy		
Drug	Activity	FDA-Approved
Talimogene laherparepvec "T-Vec" (Imlygic, Amgen)	Oncolytic effects and immunomodulating effect by producing GM-CSF (granulocyte-macrophage colony-stimulating factor)	Oct 2015
Pembrolizumab (Keytruda, Merck)	PD-1 inhibitor	Set 2014
Nivolumab (Opdivo, Bristol-Myers Squibb)	PD-1 inhibitor	Dec 2014
Peginterferon alfa-2b (Sylatron, Merck)	Peginterferon alfa-2b with immunomodulating action	Apr2011
Ipilimumab (Yervoy, Bristol-Myers Squibb)	CTLA-4 inhibitor	Mar 2011
IL-2 (Proleukin-Chiron)	IL-2 with immunomodulating action	Jan 1998
Interferon alfa-2b recombinant (Intron A, Schering-Plough)	Interferon alfa-2b with immunomodulating action	Dec 1995

FDA-approved dabrafenib, targets the V600E/K mutated form of BRAF, which is carried in 50-60% of cutaneous melanomas [11]. The treatment with the BRAFV600E/K inhibitors has been successfully used, prolonging both progression-free and overall survival, when compared with DTIC [12-14]. Another member of the MAPK pathway is the Mitogen-activated protein kinase (MEK), which is the primary downstream target of B-RAF. MEK is mutated in about 8% of melanomas [15]. MEK inhibitors, such as cobimetinib and trametinib are now available on the market for the treatment of advanced melanoma (Table 1). Moreover, several clinical trials are on-going for testing inhibitory molecules against other activating mutations which have been identified in melanoma, such as C-KIT or mTOR (i.e.: Trial ID NCT02501551, NCT01280565 and NCT01960829).

Both targeted therapies and immunotherapies are promising for advanced melanoma. However, toxicity and/or drug resistance remain unmet clinical problems. For instance, after vemurafenib treatment, most patients develop resistance after 6 to 7 months [12-14]; the concurrent administration of ipilimumab and nivolumab, although producing a 2-year survival of 79% caused severe immune toxicities in 53% of patients treated with this combination, leading 30% of patients to discontinue this therapy [16,17]. These important limitations strongly suggest investigating novel methods of drug delivery. With the recent and rapid developments in nanotechnology, the incorporation of therapeutic agents into Nanoparticles (NPs) can be the possible answer. The use of drug-loaded NPs can improve the solubility of poorly water-soluble drugs, optimize pharmacokinetics, increase drug half-life, improve bioavailability, achieve targeting specificity, diminish drug metabolism, with the ultimate goals of improving efficacy, overcoming drug resistance, and reducing toxicity.

Several types of NPs for cancer treatment are currently under investigation, including liposomes, Solid Lipid Nanoparticles (SLNs), polymeric micelles, nanospheres, dendrimers, nanotubes, mesoporous silica NPs, quantum dots, super paramagnetic iron oxide NPs, and gold NPs [18-21]. Several nanomedicines for cancer treatment have been FDA-approved, such as pegylated doxorubicin

(Doxil) in ovarian and breast cancer, albumin-bound paclitaxel nanospheres (Abraxane) and liposome-encapsulated doxorubicin (Myocet) in breast cancer [22]. For melanoma, nanomedicines are not yet FDA-approved, but there are several on-going trials (Table 2).

Beside the therapeutical option, another interesting application for the nanotechnological platforms consists of their use for diagnostic purposes. Several types of NPs, containing non-radioactive tracers, can be useful for visualizing the disease site, such as the presence of metastatic melanoma cells into the lymph nodes. Moreover, the possibility of combining the therapeutic and the diagnostic abilities, referred to as theranostic, is receiving growing interest [23-24]. Table 3 also reports the on-going trials having a diagnostic or theranostic purpose.

The opportunities offered by nanomedicine for melanoma treatment, diagnosis, and theranostic applications have been extensively reviewed [18-24-27]. In this review we present an update on the latest pre-clinical studies (2015-2016) of the use of nanotechnology in melanoma treatment and diagnosis.

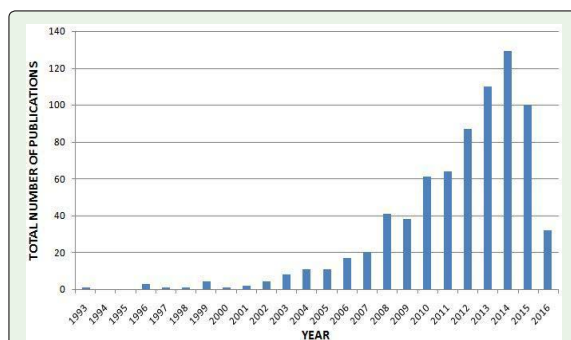


Figure 1: Number of Publications per year on Nanomedicine and Melanoma. Number of publications per year obtained on PubMed with the following query: "(Nanoparticle or Nanomedicine) and melanoma". A great increase is evident from the year 2008.

Table 2: Ongoing clinical trials involving NPs and melanoma (from www.clinicaltrials.gov and from www.isrctn.com).

Nanoformulations	Disease	Phase	Results	Trial ID
Cancer immunotherapy				
Pegylated Interferon-alpha-2a	Patients With Malignant Melanoma IIA-IIIb	III	ongoing, not recruiting	NCT00204529
Pegylated Interferon-alpha-2b	Melanoma stage I-III	0	recruiting	NCT00871533
Cytotoxic chemotherapy				
Albumin-bound paclitaxel (Nab-paclitaxel)	Pediatric Patients With Recurrent/ Refractory Solid Tumours, including melanoma	I - II	recruiting	NCT01962103
Targeted therapy				
Liposomes containing shRNA against human stathmin 1	Several metastatic tumours, including melanoma	I	ongoing, not recruiting	NCT01505153
Combined therapy				
Nab-paclitaxel and bevacizumab vs. ipilimumab	Patients With Stage IV Melanoma That Cannot Be Removed By Surgery	II	ongoing, not recruiting	NCT02158520
Nab-paclitaxel in combination with bevacizumab	Patients With Stage IV Melanoma That Cannot Be Removed By Surgery	II	ongoing, not recruiting	NCT01879306
Nab-paclitaxel in combination with bevacizumab	Patients With Stage IV Melanoma That Cannot Be Removed by Surgery	I	recruiting	NCT02020707
Rituxan and Nab-paclitaxel	Patients With Inoperable Stage III and IV Malignant Melanoma	II	recruiting	NCT02142335
nab-paclitaxel in combination with PLX7486 (tyrosine kinase inhibitor) and gemcitabine	Patients With Advanced Solid Tumours, including melanoma	I	recruiting	NCT01804530
Liposomal Cytarabine (DepoCytTM) in combination with lomustine and brain radiotherapy	Leptomeningeal Metastasis From Malignant Melanoma	I	recruiting	NCT01563614
Diagnosis and imaging				
Magnetic Nanoparticles	Using magnetic tracers to find the sentinel lymph nodes in patients with Melanoma skin cancer	III	recruiting	ISRCTN15768185
Silica-based nanoparticles labeled with the fluorophore cyanine 5.5, and functionalized with RGD	For Image-Guided Intraoperative Sentinel Lymph Node Mapping in Head and Neck Melanoma, and others cancers	0	recruiting	NCT02106598

The Use of Nanotechnology in Melanoma Treatment

The interest in nanotechnology for the treatment and diagnosis of melanoma has grown exponentially over the past five years (Figure 1). We found 79 publications in the period 2015-March 2016, about latest pre-clinical studies on nanotechnology applied to melanoma research. Most of the publications (65, representing the 82%) are about the identification of new type of anti-melanoma treatments. A small percentage (7 publications representing the 9%) is focused on diagnosis. Seven publications (9%) are devoted to the development of nanocarriers able to combine both therapy and diagnosis (theranostic) (Figure 2).

By considering the publications related to new nanotherapeutic approaches, we can further subdivide them according to the type of treatment: immunotherapy, the treatments that can restore or enhance the immune system’s ability to fight cancer; cytotoxic chemotherapy, which employs the common cytotoxic drugs; new anticancer agents, which explore the anti-tumoral properties of new molecules of different origins; targeted therapy, using drugs that interfere with specific molecules involved in tumor growth and survival; physically-driven therapy, which involves the use of photosensitizing agents; combined therapy, which combines the contemporary use of two or more therapeutical strategies; cellular targeting, which explores several strategies to enhance the active tumor targeting, such as the functionalization of nanocarriers or the stimuli-responsive nanoformulations; and theranostic, nanocarriers able to combine both therapy and diagnosis. In the 2015-2016 period, the nanoformulations were most commonly employed for immunotherapy (21%), followed by cellular targeting (18%), physically-driven therapy (15%), and new

anti-cancer (14%) studies (Figure 3). A graphical overview of these nanotherapeutic approaches for melanoma in 2015-16 is showed in Figure 4.

Cancer Immunotherapy

In recent years, we have witnessed tremendous progress in the development of the cancer immunotherapy, especially for melanoma tumours. Several immunomodulators are already in clinic (Table 1) and the scientists are expecting further advances with nanomedicine applications.

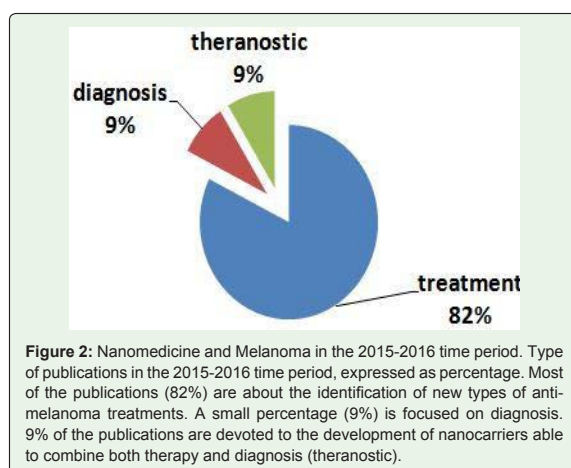


Figure 2: Nanomedicine and Melanoma in the 2015-2016 time period. Type of publications in the 2015-2016 time period, expressed as percentage. Most of the publications (82%) are about the identification of new types of anti-melanoma treatments. A small percentage (9%) is focused on diagnosis. 9% of the publications are devoted to the development of nanocarriers able to combine both therapy and diagnosis (theranostic).

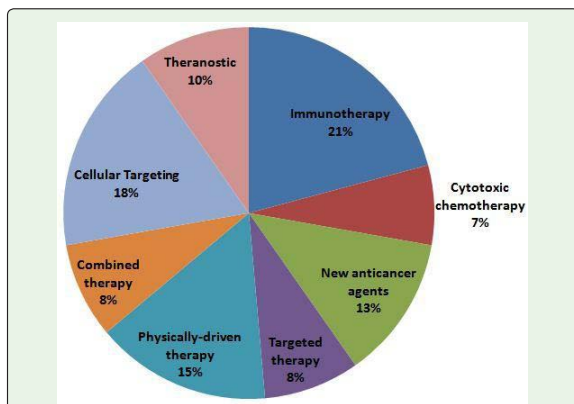


Figure 3: Different Nanotherapeutic approaches for Melanoma Treatment in the 2015-2016 time period. Number of publications in the period 2015-2016, expressed as percentage, relative to the different nanotherapeutic approaches for melanoma treatment.

Inhibition of the immunosuppressive cells: One of the possible strategies of cancer immunotherapy is to eradicate the immune suppressor cells, such as the regulatory T-lymphocytes (Treg) and the Myeloid-Derived Suppressor Cells (MDSCs), a heterogeneous population of immature myeloid cells that suppress effector T cell responses. Similar to anti-CTLA-4 drugs, Li and collaborators [28] developed NPs containing a siRNA targeting CLA-4 (NPsicTLA-4). They demonstrated, in the mouse model bearing B16 melanoma, that NPsicTLA-4 was able to activate the anti-tumour immune responses, as demonstrated by the increase of anti-tumour CD8+T cells, and the decrease of inhibitory T regulatory cells among tumour infiltrating lymphocytes [28]. An interesting strategy for the ablation of MDSCs was proposed by Jeanbart and collaborators [29], which have developed polymer micelles loaded with 6-Thioguanine (MC-TG), a cytotoxic drug used in the treatment of myelogenous leukemia, with the aim of killing MDSCs. After the injection of micelles in B16-F10 melanoma-bearing mice, they found a depletion of MDSC, as well as a higher efficacy of adoptive T cell therapy.

Toll-like receptors (TLR) agonists: Recently, tumour-specific immune activation was achieved with the agonist of Toll-Like Receptors (TLRs). Their engagement leads to innate and adaptive immune responses, which can have anti-tumoural effects [30]. For instance, it has been demonstrated that TLR agonists may indirectly kill chronic lymphocytic leukemia cells, by enhancing the activity of natural killer and tumor-reactive T cells [31]. Moreover, clinical trials demonstrated the successful treatment of cutaneous tumors, such as the basal cell carcinoma with imiquimod, an immunoresponse modifier affecting TLR-7, which is able to stimulate both the innate immune response and the cell-mediated immune system, via induction of cytokines [32].

With this aim, Zhu and collaborators [33] developed a new nanocarrier containing analogs of the unmethylated Cytosine-phosphate-Guanine (CpG), a class of potent adjuvants that activate TLR9, located in the endolysosome of many Antigen-Presenting Cells (APCs). This nanoformulation, obtained by self-assembling concatemer CpG analogs and Magnesium Pyrophosphate (Mg2PPI), had a rapidly uptake by APCs. In the endolysosomes compartment,

Mg2PPI was dissolved, due to the acidic environment, and CpG analogs were able to activate TLR9. Thus, APCs started to secrete proinflammatory and co-stimulatory factors, leading to the tumour growth inhibition in B16-F10 melanoma-bearing mice [33].

Cancer vaccines: The use of nanoparticle-based vaccines is a recent application of the field of nanomedicine [30]. A specific antigens, such as ovalbumin (OVA), or tumour-specific antigens with or without adjuvants, loaded in nanostructure, can be delivered to the “in situ” DCs for efficient antigen presentation and consequent stimulation of the antigen-specific response against cancer cells. Hong and collaborators [34] developed new antigen-encapsulating NPs, loaded with OVA, and coated with interLeukin-15 (IL-15) and its receptor IL-15R α (IL-15: IL-15R α), which functions as a vaccine adjuvant. After the treatment of DCs, they found an enhanced ability to stimulate antigen-specific CD8+T cell responses. Moreover, the treatment with (IL-15: IL-15R α)-coated NPs, in an animal model of murine melanoma, significantly increased the survival rate, in comparison with monovalent (IL-15: IL-15R α) treatment. Similar to IL-15, α -GalactosylCeramide (α -GalCer) has been regarded as a potent vaccine adjuvant. Dolen and collaborators [35] have encapsulated both in a single NP and they found that, in mice, a single immunization with OVA+ α -GalCer NPs provided substantial protection from melanoma tumour formation and even delayed the growth of already established tumours.

Poly Lactic-co-Glycolic Acid NPs (PLGA-NP) have been extensively studied for vaccine delivery and have been reported to target dendritic cells naturally through phagocytosis with efficient delivery of the vaccine components. OVA containing PLGA-NPs were loaded in thermoresponsive hydrogels, made of PolyEthyleneGlycol-PolyCaproLactone-PolyLactide-PolyCaproLactone-PolyEthyleneGlycol (PEG-PCL-PLA-PCL-PEG) [36]. The hydrogels stimulated both cellular and humoral responses, and stimulated effective anti-tumour responses in an animal melanoma tumour model. Tumour-Associated DCs (TADCs), compared to normal DCs, are less responsive to TLR stimulation, which has been related to STAT3 hyperactivity. Luo and collaborators [37] developed new nanovaccines with the aim to overcome DC dysfunction. They have co-encapsulated the Poly I:C (PIC), a TLR3 agonist, the OVA antigen,

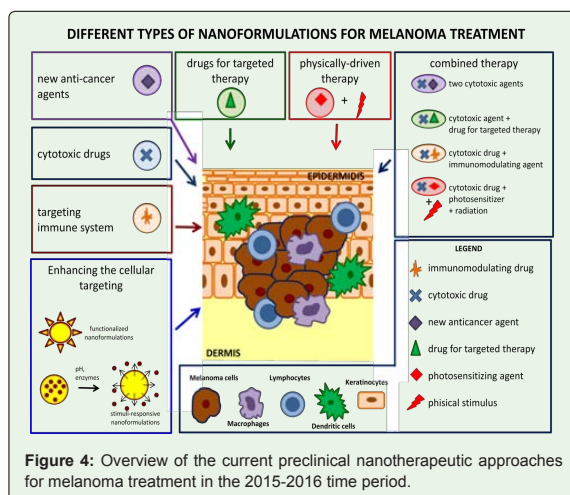


Figure 4: Overview of the current preclinical nanotherapeutic approaches for melanoma treatment in the 2015-2016 time period.

and the siRNA targeting STAT3, in PEG-b-Poly(L-Lysine)-b-Poly(L-Leucine) (PEG-PLL-PLLeu) polypeptide micelles. These micelles showed a strong tumour regression effect with prolonged survival, accompanied by anti-tumour immune responses in B16 melanoma-bearing mice. Silva and co-authors [38] co-delivered OVA and two TRL ligands, such as Poly(I:C) and CpG in mannose-functionalized NPs. The presence of this sugar, on the surface of the NPs, enhanced the up-take from the antigen-presenting cells, which have the mannose receptors. This nanovaccine decreased the growth rate of murine B16F10 melanoma tumours. A gene-carrier system based on chitosan NPs with immunomodulatory activity was developed by Yan and collaborators [39]. These NPs were loaded with a plasmid containing the fusion of two genes: the extracellular domain of the activating receptor NKG2D (Natural-Killer Group 2, member D) and the IL-15 gene. The protein showed the ability to activate NK and CD8+T cells, thus enhancing the antitumour activity of the immune system. Indeed, intramuscular injection of fused gene NPs suppressed tumour growth and prolonged survival of melanoma-bearing mice.

The use of specific antigens for melanoma can improve the efficacy of nanovaccines. Several authors, in 2015-2016, developed new nanovector containing specific melanoma antigens and adjuvants. PLGA-based NPs (PLGA-NPs), carrying the melanoma antigen (hgp10025-33) and, as adjuvant, the TRL4 agonist MonoPhosphoryl Lipid (MPLA), were recently reported [40]. Interestingly, the PLGA-NPs were coated with erythrocyte membranes, by virtue of their easy isolation and intrinsic biocompatibility [41]. PLGA-NPs were further modified by adding the mannose on the surface, to actively target APCs in the lymphatic organ. This nanovaccine demonstrated superiority to an ordinarily used vaccine formulation against tumour prevention, growth, and metastasis in B16-F10 bearing mice [40]. Zhuang and collaborators [42] proposed a Lipid-coated Zinc Phosphate hybrid NP (LZnP NP), able to co-deliver both the tumour specific antigens, represented by a multi-peptide (TRP2180-188 and HGP10025-33) and a TRL4 agonist (MPLA) as adjuvant. This nanoformulation, with the size of 30 nm, was intradermally injected in C57BL/6 mice. Ten days after the last immunization, C57BL/6 mice were inoculated subcutaneously B16-F10 melanoma cells. Mice exhibited antitumour immunity, as demonstrated by the secretion of cytokines and the increased CD8+T cell response. This antitumour effect elicited an inhibition of melanoma growth, more consistent when compared with the treatment of free antigens [42]. The gp100 melanocyte differentiation protein epitope was loaded into NPs, obtained by engineering the E2 subunit of pyruvate dehydrogenase [43]. Moreover, this non-viral cage contained CpG DNA molecules, able to increase the antigen-specific anti-tumour responses following immunization, since CpG sequences are similar to those found in bacterial DNA. They succeeded in obtaining higher CD8+T cell activation, as well as an increased survival of animals bearing B16 melanoma by 40%, compared to PBS-treated animals [43].

The melanoma immunotherapy can also take advantage of the treatment with plant-derived Viral NPs (VNPs), since they are natural nanomaterials, biodegradable and biocompatible. They can be used as a carrier for drug delivery or for imaging applications, or they can use as an adjuvant immunostimulatory molecules, able to activate the anti-tumoural T-cell response [44]. For instance, it has been shown that the self-assembling virus-like NPs from Cow Pea Mosaic Virus (CPMV) [45] and the Papaya Mosaic Virus nanoparticle (PapMV) [46] suppress melanoma metastatic cancer in animals.

Cytotoxic Chemotherapy

In melanoma, the response rates to the common cytotoxic drugs are very low. Thus, the scientists do hope to develop effective anticancer treatments thanks to nanotechnology, which will increase the effectiveness of anti-cancer treatments. Gold NPs (AuNPs) conjugated with doxorubicin (Au-Dox) are receiving great attention. Zhang and collaborators [47] demonstrated that the intratumoural injection of ultra-small Au-Dox is effective against melanoma in immunocompetent mice bearing murine B16 melanoma cells and in nude mice bearing human SK-MEL-28 xenograft. Moreover, Tawagi and collaborators [48] compared the toxicity of Au-Dox in B16 melanoma cell lines and cardiomyocytes, measured by real-time growth assays and Fluorescence Lifetime Imaging Microscopy (FLIM). They demonstrated that cardiomyocytes were more sensitive than B16 cells to Dox alone, but were dramatically less sensitive to Au-Dox. On the contrary, Au-Dox was more effective in inducing cell death of B16 melanoma cells, compared to Dox alone. The different patterns of Au-Dox in the two cell types can explain the differential toxicity: while Au-Dox concentrated in the nuclei of B16 cells, it remained endosomal in cardiomyocytes. Kaiser and collaborators [49] demonstrated an enhanced antitumoural activity of docetaxel, when loaded in Acid-Prepared Mesoporous Spheres (APMS-TEG). This nano-formulation was effective in MelJuSo, UACC903, and WM1205 melanoma cell lines at a nanomolar concentration, thus suggesting a potential use in clinic. A Graphene Oxide (GO) sheet conjugated with paclitaxel (PTX) was successfully employed in B16 melanoma-bearing C57 mice [50].

An interesting study has determined the influence of nanoparticle size on targeting lymph node metastases [51]. The authors delivered micelles, loaded with the platinum anticancer drug, with different diameters, in a syngenic melanoma model. The targeting of lymph node metastases was compared with results obtained with the clinically used Doxil having a diameter of 80 nm. They found that the sub-50 nm micelles were more efficient in reaching lymph node metastasis, having a higher capability in extravasating from the blood and penetrating into the metastatic tumour.

New Anticancer Agents

The anti-melanoma properties of several plant extracts, or derivatives, have been explored in the last two years.

Dwivedi and collaborators [52] have studied the antitumoural effect of artemisone, an artemisinin derivative, isolated from the plant *Artemisia annua* and currently used as an antimalarial drug, on melanoma cells in vitro. They loaded Artemisone in nano-vesicular niosomes and in solid lipid NPs, demonstrating in both cases enhanced antiproliferative effects against human melanoma A375 cells, with respect to the free drug. Moreover, these nanoformulations had negligible toxicity towards normal skin cells. Later, they performed in vitro skin permeation studies with both nanoformulations. They found out that, in the stratum corneum-epidermis, artemisone-SLN was found at higher concentration compared to than the artemisone-niosomes, and that, in the epidermis-dermis, artemisone was only detected after application of the SLN formulation. These results suggest the possible topical delivery of artemisone-SLN in treatment of melanoma [53].

Hu and collaborators [54] have developed new NPs loaded

with saikosaponin, a biologically active compound extract from the *Bupleurum chinense*, with anti-melanoma activity “*in vitro*” and “*in vivo*”. They were able to demonstrate that saikosaponin-d NPs enhanced the antiproliferative activity against melanoma cells, and induced apoptosis through the mitochondrial pathway.

The plant-derived curcumin, loaded into chitosan-coated NPs was orally administered to the B16F10 metastatic melanoma bearing mice, obtaining an enhanced anti-tumoural activity [55].

Gismondi and collaborators [56] developed novel Detonation NanoDiamonds (DNDs), which are new nanoparticles produced by detonation of explosive Carbon materials. They loaded the Citropten (5,7-dimethoxycoumarin) agent, a plant secondary metabolite into DNDs, and demonstrated that this nanovehicle was able to reduce B16-F10 tumour cell growth.

The herb-derived compound triptolide (TP), with anti-angiogenic properties, was loaded into methoxy poly(ethylene glycol)-block-poly(ϵ -caprolactone) micelles by Wang and collaborators [57]. In B16-F10 melanoma-bearing mice they demonstrated that the nanovehicle enhanced the TP accumulation in tumour tissues, increased the survival time and inhibited angiogenesis.

4-Hydroxynonenal, an endogenous compound derived from lipid peroxidation was studied as an anti-melanoma agent [58]. A new type of lipid nanocapsule, based on β -Cyclodextrin-poly(4-acryloylmorpholine) conjugates, was designed to enhance its solubility and stability. HNE loaded in the nanocapsules was more effective than free HNE in inhibiting proliferation of several tumour cancer cells, including melanoma. Moreover, the effect of these new nanocapsules on a three-dimensional human reconstructed model of skin melanoma was evaluated. Two diverse treatments were performed: one in the medium, mimicking the parenteral administration, and the other onto the epidermal surface, mimicking the topical treatment. Both treatments were more effective than free HNE on melanoma cell growth inhibition. Interestingly, the encouraging results obtained with the topical administration on the epidermal surface could open new perspectives in melanoma treatments [58].

Other chemical compounds loaded into NPs were successfully employed for melanoma treatment, such as the novel synthetic tubulin inhibitor, 2-(1H-indol-5-yl)thiazol-4-yl)3,4,5-trimethoxyphenyl methanone (abbreviated as LY293) [59], and the Cerium oxide CeO₂ [60].

Targeted Therapy

Most recent preclinical studies in the field of targeted therapy explored the use of nucleic acid for melanoma treatment.

Li and collaborators [61] developed new NPs able to carry the DNA for the pro-apoptotic gene PUMA (p53 up-regulated modulator of apoptosis). In particular they used the cationic Polymer Polyethylenimine (PEI), widely employed for non-viral transfection, crosslinked with Sulfosuccinimidyl-4-(N-maleimidomethyl) cyclohexane-1-carboxylate (Sulfo-SMCC) conjugating Trans-Activating Transcriptional activator (TAT). This nanovehicle enhanced the transfection efficiency of PUMA gene in malignant melanoma A375 cell, resulting in increased apoptosis.

Polycation based NPs (jetPEI) were used as carrier for the delivery of a plasmid expressing the short hairpin RNA (shRNA) against the CXC motif Chemokine Receptor 4 (CXCR4) [62], as an anti-

metastatic target. They succeeded in obtaining a significant reduction in the number of pulmonary metastatic nodules (50%) in animals that received a retro orbital injection of jetPEI CXCR4 1 shRNA.

Hundt and collaborators [63] set up a method to monitor by MR imaging the antiangiogenic gene therapy in M21 melanoma-bearing mice. As the antiangiogenic gene, they chose the dominant-negative mutant form of Raf-1 (Raf-1-). The plasmid containing Raf-1- was loaded into RGD-targeted sNPs and was given to the animals. They found that the targeted gene delivery therapy induces significant changes in Magnetic Resonance Imaging (MRI) and that there was an excellent correlation between MRI and histological results, which were direct effect of the gene delivery therapy.

Beside the employment of the nucleic acids, specific inhibitors were also studied, such as the Sn-2 lipase-labile, an inhibitor of the oncogene *c-myc* [64] and glycomimetic (P-3F(ax)-Neu5Ac), an inhibitor of the sialic acid, frequently over expressed on cancer cell surfaces and contributing to the metastatic process [65].

A nanovehicle for the imatinib mesylate, a tyrosine-kinase inhibitor already in clinical use for several tumours, was developed by Labala and collaborators [66]. This nanoformulation consists of a layer-by-layer polyelectrolyte coated AuNP (LbL-AuNP) and it was specifically designed for the ionophoretic transport into skin.

Physically-Driven Therapy

Therapies inducing hyperthermia: Photo Thermal Therapy (PTT) involves the use of light and a photosensitizer to generate heat for therapeutic purposes. Gold-based NPs are widely used for this purpose, since after the irradiation, they generate a localized heat so as to damage a region of interest [67]. A Gold-Ferrite Nano Composite (GFNC) was obtained by Heidari and collaborators [68], as a photo thermal agent in melanoma-bearing mice. They have demonstrated a higher necrotic surface tumour area in mice receiving GFNC injection and laser irradiation. Wang and collaborators [69] developed gold nanoshell capsules, which easily penetrate melanoma cells. After a mild laser irradiation, they observed a consistent ablation of malignant melanomas.

Magnetic Field Hyperthermia (MFH) treatment has received great attention from the scientific community, since this therapeutic option elicits the heating of magnetic NPs by time-varying magnetic fields. Blanco-Andujar and collaborators [70] demonstrated that human melanoma cells undergo apoptosis upon exposure to citric acid-coated iron-oxide NPs, followed by a Magnetic Field Hyperthermia (MFH) treatment.

The ability of Radio Frequency (RF) radiation to heat human tissues has been known for a long time, and now this knowledge can be exploited in cancer therapy. Haghniaz and collaborators [71] have explored the potential use of Dextran-coated (Dex) Lanthanum Strontium Manganese Oxide (LSMO) NPs, as a hyperthermia agent in the treatment of cancer. B16-F1 melanoma cells were exposed to Dex-LSMO NPs and heated using a radiofrequency generator, finding that the cell death increased in a time-dependent and temperature-dependent manner.

Photo dynamic therapy (PDT): Photo Dynamic Therapy (PDT) uses nontoxic photosensitizing agents and a light source to treat cancers. Under light exposure, these chemical compounds are excited and are able to produce ROS, able to kill cancer cells. Ogawara and

collaborators [72] developed a new nanoformulation for cancer PDT. They encapsulated Photoporphyrin IX DiMethyl Ester (PppIX-DME), a hydrophobic porphyrin derivative, into polymeric NPs composed of polyethylene glycol and polylactic acid block copolymer (PN-Por). An “*in vitro*” phototoxicity study clearly indicated the significant phototoxicity of PN-Por for three types of tumour cells, (including B16-BL6 melanoma cancer cells), in a PppIX-DME concentration-dependent fashion [72]. Thus, the use of Zinc Oxide (ZnO) NPs in anticancer treatment has become a promising strategy, due to their excellent photo-oxidation activity.

Under light activation, ZnO, or a derivative, is able to induce ROS production, thus killing cells via oxidative stress. However, ZnO has a low photocatalytic decomposition rate and Arooj and collaborators [73] demonstrated that metal ions such as Silver (Ag) improve their activity. Under daylight exposure, ZnO: Ag nanocomposites induced cell death of human malignant melanoma (HT144) more efficiently than ZnO alone. Interestingly, these ZnO: Ag nanocomposites killed melanoma HT144 cells more efficiently than normal Human Corneal Epithelial Cells (HCEC). Wang and collaborators [74] succeeded in treating cultured melanoma cells and a B16 murine melanoma model with Near-Infrared (NIR) Plasmonic copper sulfide (Cu₂-xS) Nano Crystals (NCs), followed by NIR irradiation. Interestingly, they concluded that the therapeutic effect was due to a combination of the photo thermal heat mechanism (Photo Thermal Therapy, PTT) and the photodynamic activity, via the production of high levels of ROS.

Araki and collaborators [75] explored the possibility that the Photo Dynamic Therapy (PDT) towards the tumour vasculature (Photo-triggered tumour Vascular Treatment, PVT) may enhance the vascular permeability, leading to augmented Enhanced Permeability and Retention (EPR). B16 tumour-bearing mice, with low permeable vasculature, were treated with liposomal paclitaxel (PL-PTX) and a hydrophobic porphyrin derivative in polyethylene glycol-block-poly-lactic acid NPs was used as a photosensitizer. The authors demonstrated that the PVT treatment enhanced the anti-tumour activity elicited by PL-PTX, thus augmenting the EPR effect in a model of low permeable tumour vasculature.

Non-thermal atmospheric-pressure plasma: Non-thermal atmospheric-pressure plasma, also named cold plasma, is defined as a partly ionized gas and it is a new innovative approach to medicine [76]. Recently, its anti-tumoural activity has emerged and gained attention. However, its action is not specific. Choi and collaborators [77] succeeded in enhancing the capability of the cold plasma in specifically killing melanoma cells. They have targeted NEU (human epidermal growth factor receptor 2) protein, which is frequently over-expressed in the cell membrane of melanoma cells, using anti-NEU antibody-labeled gold NPs. The labeled NPs preferentially targeted melanoma cells rather than normal keratinocytes. Both cells were exposed to the cold plasma and they found the death rate of melanoma cells was significantly higher than that of normal keratinocyte cells.

Combined Therapy

Several combination therapies have been FDA-approved for melanoma treatment (i.e. nivolumab plus ipilimumab; trametinib plus dabrafenib), and studies on other combinatory regimens are on-going in many trials. Thus, the researchers continue exploring several types of combinations in pre-clinical studies, involving nanotechnological carriers.

Combining two chemical agents: Ruttala and collaborators [78] have developed a liposome carrier containing two chemotherapeutic agents, paclitaxel (PTX) and curcumin (CUR). Via a thin-film hydration technique, they encapsulated the PTX-loaded Albumin NPs (APN) in PEGylated hybrid liposomes containing CUR (CL-APN). This co-loaded delivery system has shown a higher cytotoxic effect on several tumour cell lines, including B16-F10 melanoma cells, compared to single free chemotherapeutic drugs or single drugs encapsulated in the respective nanocarrier.

Recently, glutamate receptor antagonists, mainly used in the treatment of many neuronal diseases, have been proposed as anticancer agents. Tan and collaborators [79] developed Mesoporous Silica NPs (MSNPs) loaded with both an ionotropic Glutamate (iGlu) receptor antagonist, the 4-Hydroxyphenylacetyl spermine (L1), and Dox. Moreover, Dox was trapped within the MSNPs by a redox-cleavable linker, thus being able to be released upon exposure to glutathione. The authors demonstrated an enhanced antitumoural effect of L1 and Dox co-delivering on B16-F10 melanoma cells *in vitro*.

Combining chemical agent with targeted therapy: A porous silicon-based Micro/Nano Composite (MNC) has been designed, able to co-deliver a chemotherapeutic drug, such as Docetaxel, and a small interfering RNA (siRNA) against BRAF. The MNC was more effective in inhibiting tumour growth and reducing lung metastasis in a mouse melanoma model [80].

Doddapaneni and collaborators [81] designed a novel PEG-PCL polymer able to contain three drugs against melanoma: docetaxel (targeting microtubules), everolimus and LY294002 (two inhibitors of mammalian target of rapamycin, mTOR). They were able to modify the surface charge of the NPs, obtaining neutral, partially charged, or fully charged surface, with the aim of having preferential uptake and accumulation in the lymphatic system, in mice injected subcutaneously. Two metastatic melanoma mouse models with the two major mutations (NRASQ61K and RXR α) found in human melanoma, were used for the *in vivo* studies. After NPs injection, they found that the partially charged NPs have the highest potential in treating metastatic melanoma, demonstrating that the surface charge is a critical parameter for the lymphatic uptake [81].

Combining chemical agent with radiotherapy: Li and collaborators [82] succeeded in establishing a Pluronic® F127-based thermosensitive hydrogel (Au-Dox-Gel) containing gold NPs (AuNPs), used as radio sensitizer and Dox, the chemotherapeutic drug, to improve cancer chemo radiotherapy. Indeed, after radiation, tumour sizes in melanoma B16 bearing mice were significantly decreased by Au-Dox-Gel compared to control mice.

Combining chemical agent with immunotherapy: Chemotherapy with immunotherapy is a regimen generally referred to as ‘BioChemoTherapy’ (BCT). In this respect, Zhao and collaborators [83] have co-delivered two types of NPs in B16-F10 melanoma-bearing mice, one carrying the vaccine antigen and the second loaded with the chemotherapeutic agent. As anti-cancer drug, they have used the triterpenoid methyl-2-cyano-3,12-dioxooleana-1,9(11)-dien-28-oate (CDDO-Me) loaded in PLGA-NPs. The antitumoural mechanisms of CDDO-Me include induction of apoptosis and modulation of several signal transduction pathways involved in tumour cell proliferation, but it can also block furthermore the

immune suppressive function of Myeloid-Derived Suppressor Cells (MDSCs) and improve the immune response to cancer. The second nanovector consisted of the self-antigen tyrosinase-related protein 2 (Trp2) peptide, a melanocyte differentiation antigen, loaded in a Lipid-Calcium-Phosphate NanoParticle (LCP-NP). The authors demonstrated that the intravenous delivery of CDDO-Me loaded in PLGA-NP, combined with the subcutaneous Trp2 vaccination, resulted in an increase of anticancer activity compared to Trp2 vaccine alone in B16-F10 melanoma-bearing mice [83].

Enhancing the Cellular Targeting

Two main strategies are in use to enhance active tumour targeting. The first consists of the decoration of the surface of the nanocarrier with ligands (i.e. antibodies, aptamers, peptides, sugars) to allow for the homing of the drug to a specific target site. The second approach is the stimuli-responsive delivery strategies, in which the drug release can be achieved within a tumour in response to a cancer-specific stimulus.

Functionalized nanocarriers: A well-known peptide used in targeting nanocarriers is the arginine-glycine-aspartic (RGD) peptide, which is the minimal binding domain of fibronectin necessary to recognize cell surface $\alpha v\beta 3/\alpha v\beta 5$ integrins, frequently over expressed on cancer cells and tumour vasculature. Zhao and collaborators [84] enhanced the hydrosolubility of the anti-cancer agent curcumin with a PEG-PLA micelle-based drug delivery system. These PEG-PLA micelles were functionalized with the $\alpha v\beta 3$ integrin-targeted peptide RGD. The authors showed that RGD-functionalized PEG-PLA micelles containing curcumin had a stronger inhibition of tumour growth in B16 tumour-bearing mice, compared with non-RGD modified PEG-PLA micelles. Similar results were obtained by Makino and collaborators [85] in B16-F10 melanoma-bearing mice with PEG micelles loaded with platinum anticancer drug and decorated with the RGD peptide. Moreover, they demonstrated the cyclic RGD peptide (cRGDs) have antitumour activities themselves, since it has been shown that they can inhibit tumour growth and metastasis by interfering with the angiogenesis or the integrin-dependent metastatic processes.

Hyaluronan (HA) is another interesting molecule which has been explored for active targeting. This non-sulfated polysaccharide is being recognized as an important regulator of cancer progression and is a ligand for CD44, a transmembrane glycoprotein abundantly expressed in many malignant tumours and present on many types of Cancer Stem Cells (CSCs) [86]. An enhancement of anti-melanoma activity was then observed after HA-decorated nanocarrier treatments in melanoma-bearing mice [87,88].

Interesting results on enhanced anti-melanoma activity have been obtained with several other molecules used for active targeting, such as anisamide, a small molecule of benzamide specific ligand for the Sigma-1 receptor, highly expressed by tumour cells [89]; the tumour-penetrating peptide RPARPAR [90], able to bind to the cell surface Neutrophilin-1 receptor (NRP-1), with essential roles in vascular biology and which is over expressed in angiogenic endothelial cells and in tumour cells; the tumour homing peptide GKRK [90], ligand for the receptor p32, a mitochondrial chaperone protein, aberrantly expressed at the surface of activated cells such as tumour blood and lymphatic endothelial cells, tumour cells, and

tumour-associated macrophages; and the Polydopamine (PDA), a mimic of the specialized adhesive foot protein Mefp-5 (mytilus edulis foot protein-5) secreted by mussels [91].

Stimuli-responsive particles: In the most recent period, scientists have focused their attention on pH-responsive nanocarrier and enzyme-responsive nanovehicles.

pH-responsive nanovehicles, from acetalated cyclodextrins loaded with docetaxel, have demonstrated a dramatically enhanced efficacy in a melanoma-bearing nude mouse model [92]. Xu and collaborators [93] have developed a pH-sensitive carrier, able to simultaneously deliver Dox and Bcl2 siRNA, specifically designed for local treatment of lung metastasis. Dox was conjugated onto Polyethylenimine (PEI) by using Cis-aconitic Anhydride (CA, a pH-sensitive linker) to obtain PEI-CA-Dox conjugates. At acidic pH the drug was released faster. Then, the anionic siRNA spontaneously formed a complex with the cationic PEI-CA-Dox NPs. This nanoformulation showed higher anti-cancer activity in B16F10 melanoma cells in vitro, with respect to the treatment with either Dox or Bcl2 siRNA alone. Interestingly, when it was directly sprayed into the lungs (with acidic pH), of B16-F10 melanoma-bearing mice, the PEI-CA-Dox/Bcl2 siRNA complex NPs exhibited enhanced antitumour efficacy compared with the single delivery of Dox or Bcl2 siRNA.

Among the enzymes, the Matrix MetalloProteases (MMPs) and gelatinases have been selected as the external stimulus for the nanocarrier opening, since these enzymes are more highly represented in the cancer microenvironment. Jallouk and collaborators [94] have designed a new perfluorocarbon NP delivery system activated by MMP-9 cleavage, able to carry mellitin derivatives (cytolytic peptides derived from bee venom) and obtaining enhanced tumour growth suppression in a mouse model of melanoma. Similar results were obtained with a novel gelatinase-stimuli nanoparticle, loaded with pemetrexed, a new antifolate medicine with antitumoural and antimetastatic activity [95].

Finally, a combination of the two types of active targeting treatments was presented by You and collaborators [96], which designed a complex nanocarrier with three layer: the innermost core of PCL loaded with the anti-cancer drug camptothecin (CPT), the medium layer containing the folate receptor, for the active targeting via functionalization, and the outer part consisting of a PEG layer sensitive to MMP2 and MMP9. In presence of the tumour cells, the PEG layer would detach from the NPs, due to the higher level of MMP2 and MMP9 in the cancer microenvironment, resulting in the exposure of folate to enhance the cellular internalization via folate receptor-mediated endocytosis, which accelerated the release rate of CPT in vivo. These nanovectors showed an enhanced anti-cancer activity on melanoma B16 bearing mice.

The Use of Nanotechnology for Imaging and Diagnosis

The presence of Lymph Node (LNs) metastasis is an important prognostic factor in melanoma. Nanotechnology can help in noninvasive, specific and sensitive detection of LN metastasis. Ultra small tumour-targeting inorganic (Silica) nanoparticles have been recently proposed as an intraoperative tool for guiding resection of sentinel lymph node metastases [97]. The specificity and sensitivity of contrast-enhanced MRI lymphography can be improved with the use of Gadolinium (Gd)-loaded NPs, as demonstrated by Partridge and

collaborators [98] in mice bearing B16-F10 melanoma. Interestingly, Zhou and collaborators [99] have demonstrated that Gd-embedded Iron oxide nanoplates (GdIOP), functionalized with Zwitterionic Dopamine Sulfonate (ZDS) molecules, were uptaken differently by B16 melanoma cells and by immune cells, such as macrophages and dendritic cells in B16 melanoma-bearing mice. After the addition of GdIOP NPs, they demonstrated that they were efficiently uptaken by immune cells, whereas melanoma B16 tumour cells showed a lower intake. Under T1-T2 dual-modal MRI, this difference generated pseudo contrast images, with potential use for the detection of tumour metastasis in LNs.

A possible application of nanotechnology is to detect angiogenesis *in vivo*. Melemenidis and collaborators [100] have developed RGD-targeted NPs of Iron Oxide (NPIO) for MRI of tumour angiogenesis, after injection, mice bearing subcutaneous melanoma (B16-F10) tumours underwent *in vivo* MRI. The authors demonstrated the specific binding of RGD-targeted NPs loaded with NPIO with the $\alpha v\beta 3$ expressing neo-vessels of the tumours.

Meir and collaborators [101] have found an interesting method to trace immune cells, with the aim to study their fate in cancer immunotherapy. T-cells were transduced to express a melanoma-specific T-cell receptor and then labeled with gold NPs (GNPs) as an X-ray Computed Tomography (CT) contrast agent. After injection, in mice bearing human melanoma xenografts, whole-body CT imaging allowed examination of the distribution, migration, and kinetics of T-cells.

Another interesting application of nanotechnology is the possibility of detecting and quantifying Circulating Tumour Cells (CTCs), since their presence at an early stage of cancer progression is of significant prognostic value, even in melanoma cancer [102]. However, most of the common methods to detect melanoma markers often lack sensitivity or selectivity and often produce false-positive results. Seenivasan and collaborators [103] proposed an electrochemical immunosensing method to detect melanoma cells, based on the affinity between cell surface MelanoCortin 1 Receptor (MC1R) antigen and anti-MC1R Antibody (MC1R-Ab). The MC1R-Abs were immobilized in amino-functionalized silica NPs and they achieved the very low detection limit of 20 cells/ml for melanoma cells.

Theranostic Applications on Melanoma

The possibility to load more than one molecule into a single nanocarrier opens the way to theranostic applications, since it allows the co-delivery of an anti-tumour agent and a tracer for imaging, useful for diagnosis. Bazylińska and collaborators [104] succeeded in developing a new nanoemulsion able to carry both DNA, useful for the gene transfer strategy in cancer treatment, and IR-780 indocyanine, a fluorescent marker for bioimaging analysis. They obtained good bioimaging of intracellular localization by Confocal Laser Scanning Microscopy (CLSM) and Total Internal Reflection Fluorescence Microscopy (TIRFM) in a melanoma MEWO cell line. Later, the same group developed new theranostic nanocarriers loaded with both colchicine, a cytostatic drug, and coumarin-6, as fluorescent tracer. These labeled nanovehicles were efficiently up-taken by several cell lines of different origins, including melanoma MEWO cells. The good fluorescent signal, as well as the biocompatibility, and the enhanced

antitumoural activity of colchicines of this nanoformulation suggest the potential use as nanotheranostic agents [105].

Vannucci and collaborators [106] developed PEG-based NPs functionalized with both the Human protein Ferritin (HFt), and the α -Melanocyte-Stimulating Hormone (α -MSH) and also contained fluorophore and magnetic resonance imaging tracers to detect “*in vivo*” localization of NP. After the treatment in a spontaneous metastatic mouse melanoma model, targeted HFt-MSH-PEG NPs accumulated mostly in the primary melanoma lesions, as well as at the metastasis level, with high selectivity with respect to other organs.

Interestingly, some metals, such as Au and Gd, can have both functions, thus they can have an anti-cancer activity and can be used as tracer for imaging. Gd is a paramagnetic metal, normally used in contrast agents for MRI. Moreover, it can enhance the efficacy of radiation therapy. Thus, the incorporation of Gd into nanoparticle allows for the simultaneous use of imaging to guide the radiation beams and to locate the tumour, as well as to enhance the toxic effect of radiation. Kobt and collaborator [107] have successfully treated animals bearing B16-F10 tumours with Gd-based NPs, AGuIX. After radiation therapy, in the AGuIX treated animals they observed an increase of tumour cell death, and improvement of the life spans of animals bearing multiple brain melanoma metastases. Kang and collaborators [108] have incorporated thermosensitive phospholipids, loaded with the drug docetaxel, onto the surface of gold NPs (AuNPs) or gold NanoRod (AuNR). Both nanovehicles showed enhanced tumour-cell suppression properties towards the melanoma B10-F10 cell line. A potential theranostic use is suggested by the authors. Indeed, two synergistic anticancer actions can be achieved after infrared photo thermal treatment and, thanks to the Au particles, they can have bioimaging applications.

An enhanced theranostic activity was achieved by conjugating functionalized gold NPs with Single-Wall Carbon NanoTubes (SWCNT) [109]. The authors demonstrated a selective imaging and efficient photo thermal therapy on UACC903 human melanoma cancer cells.

Wang and collaborators [110] have developed very complex multifunctional hybrid NPs, composed of gold nanocrystals coated on a magnetite-fluorescent porous carbon core-shell. The biomedical application of this theranostic nanocarrier includes the possibility of bioimaging in multicolor mode, the magnetic/NIR-responsive drug release, and the enhanced photo thermal therapy. Mouse melanoma B16-F10 cells have been used for this study, thus suggesting their potential use in melanoma treatment.

Conclusion

There is no doubt that nanotechnology may offer new therapeutic opportunities for the treatment of metastatic melanoma. Given the clinical success of immunomodulatory drugs, it is likely we will observe more and more pre-clinical studies on strengthening their effectiveness, thanks to nanotechnology platforms. Moreover, considering the currently on-going clinical trials, the combined therapy also seems promising in therapeutic advantages. However, it's difficult to identify the most promising nanomedicine to treat melanoma, relying on pre-clinical studies, since these studies present several concerns and limitations. The physico-chemical properties of delivery systems can modify pharmacokinetics, tumor accumulation, and biodistribution. Xenografts represent a useful

model to study these parameters for nanoformulations, however, tumor characteristics can vary with cell line and size, as well as the density and vascularization. Therefore, tumor uptake by the EPR effect is expected to be strongly dependent on the cell line used. On the other hand, the studies running on the murine melanoma model do not completely reflect the complexity of the human melanoma cell population. From this point of view, besides the implementation of nanotechnological therapies, it could be important to develop immunocompetent human models for melanoma research, such as three-dimensional human skin reconstruct models containing human melanoma cells, with the addition of the immune system cells.

Another concern regards the toxicity studies of NPs with clinical potential. Current research lacks a unifying protocol for the toxicological profiling of NPs, and studies on the long-term effects on human health are also needed [111]. As previously reported, in these years the majority of studies on melanoma therapy was regarding new platforms for immunotherapy. In melanoma treatments targeting the immune response of patients, it is necessary to pay particular attention to a possible interaction between nanoparticles and the immune system. Although it has been said that nanoparticles are unlikely to act as a hapten, inducing a specific IgE production, they can induce allergic sensitization (contact dermatitis) and they are likely to act as an adjuvant in inducing a specific pattern of cytokines, antibodies and cells that favor allergic sensitization to environmental allergens [112]. Moreover, the stimulation of inflammatory cytokines has been demonstrated to be a key point in nanoparticle-induced immunostimulatory reactions [113]. Since an adverse effect of immunostimulatory drugs is the risk of developing autoimmune disease, these aspects are very important considerations for the choice of a drug delivery platform. Therefore, further studies are needed in nanotoxicology, to provide safer nanoformulation for the melanoma treatment.

References

- World Cancer Report 2014. World Health Organization. 2014.
- Dickson PV, Gershenwald JE. Staging and Prognosis of Cutaneous Melanoma. *Surg Oncol Clin N Am*. 2011; 20: 1-17.
- PDQ Adult Treatment Editorial Board. Melanoma Treatment (PDQ®): Health Professional Version. PDQ Cancer Information Summaries. 2016.
- Batus M, Waheed S, Ruby C, Petersen L, Bines SD, Kaufman HL. Optimal management of metastatic melanoma: current strategies and future directions. *Am J Clin Dermatol*. 2013; 14: 179-194.
- Kim C, Lee CW, Kovacic L, Shah A, Klasa R, Savage KJ. Long-term survival in patients with metastatic melanoma treated with DTIC or temozolomide. *Oncologist*. 2010; 15: 765-771.
- Jacobs JF, Nierkens S, Figdor CG, de Vries IJ, Adema GJ. Regulatory T cells in melanoma: the final hurdle towards effective immunotherapy? *Lancet Oncol*. 2012; 13: e32-42.
- Hodi FS, O'Day SJ, McDermott DF, Weber RW, Sosman JA, Haanen JB, et al. Improved survival with ipilimumab in patients with metastatic melanoma. *N Engl J Med*. 2010; 363: 711-723.
- Carbognin L, Pilotto S, Milella M, Vaccaro V, Brunelli M, Calio A, et al. Differential Activity of Nivolumab, Pembrolizumab and MPDL3280A according to the Tumor Expression of Programmed Death-Ligand-1 (PD-L1): Sensitivity Analysis of Trials in Melanoma, Lung and Genitourinary Cancers. *PLoS One*. 2015; 10: e0130142.
- Pol J, Kroemer G, Galluzzi L. First oncolytic virus approved for melanoma immunotherapy. *Oncoimmunology*. 2015; 5: e1115641.
- Flaherty KT, Hodi FS, Fisher DE. From genes to drugs: targeted strategies for melanoma. *Nat Rev Cancer*. 2012; 12: 349-361.
- Flaherty KT. Targeting metastatic melanoma. *Annu Rev Med*. 2012; 63: 171-183.
- Hauschild A, Grob JJ, Demidov LV, Jouary T, Gutzmer R, Millward M, et al. Dabrafenib in BRAF-mutated metastatic melanoma: a multicentre, open-label, phase 3 randomised controlled trial. *Lancet*. 2012; 380: 358-365.
- Chapman PB, Hauschild A, Robert C, Haanen JB, Ascierto P, Larkin J, et al. Improved survival with vemurafenib in melanoma with BRAF V600E mutation. *N Engl J Med*. 2011; 364: 2507-2516.
- Sosman JA, Kim KB, Schuchter L, Gonzalez R, Pavlick AC, Weber JS, et al. Survival in BRAF V600-Mutant Advanced Melanoma Treated with Vemurafenib. *N Engl J Med*. 2012; 366: 707-714.
- Nikolaev SI, Rimoldi D, Iseli C, Valsesia A, Robyr D, Gehrig C, et al. Exome sequencing identifies recurrent somatic MAP2K1 and MAP2K2 mutations in melanoma. *Nat Genet*. 2011; 44: 133-139.
- Weber JS, Kudchadkar RR, Yu B, Gallenstein D, Horak CE, Inzunza HD, et al. Safety, Efficacy, and Biomarkers of Nivolumab With Vaccine in Ipilimumab-Refractory or -Naive Melanoma. *J Clin Oncol*. 2013; 31: 4311-4318.
- Wolchok JD, Kluger H, Callahan MK, Postow MA, Rizvi NA, Lesokin AM, et al. Nivolumab plus Ipilimumab in Advanced Melanoma. *N Engl J Med*. 2013; 369: 122-133.
- Dianzani C, Zara GP, Maina G, Pettazzoni P, Pizzimenti S, Rossi F, et al. Drug delivery nanoparticles in skin cancers. *Biomed Res Int*. 2014; 895986.
- Jain RK, Stylianopoulos T. Delivering nanomedicine to solid tumors. *Nat Rev Clin Oncol*. 2010; 7: 653-664.
- Bei D, Meng J, Youan BB. Engineering nanomedicines for improved melanoma therapy: progress and promises. *Nanomedicine (Lond)*. 2010; 5: 1385-1399.
- Tran MA, Watts RJ, Robertson GP. Use of liposomes as drug delivery vehicles for treatment of melanoma. *Pigment Cell Melanoma Res*. 2009; 22: 388-399.
- Ventola CL. The nanomedicine revolution: Part 2: current and future clinical applications. *P T*. 2012; 37: 582-591.
- Xie J, Lee S, Chen X. Nanoparticle-based theranostic agents. *Adv Drug Deliv Rev*. 2010; 62: 1064-1079.
- Pizzimenti S, Dianzani C, Zara GP, Ferretti C, Rossi F, et al. Challenges and opportunities of nanoparticle-based theranostics in skin cancer. In Hamblin & Avci & Prow (Eds.), *Nanoscience in Dermatology*, 1st Edition. Academic Press Elsevier. 2016.
- Brys AK, Gowda R, Loriaux DB, Robertson GP, Mosca PJ. Nanotechnology-based strategies for combating toxicity and resistance in melanoma therapy. *Biotechnol Adv*. 2016.
- Chen J, Shao R, Zhang XD, Chen C. Applications of nanotechnology for melanoma treatment, diagnosis, and theranostics. *Int J Nanomedicine*. 2013; 8: 2677-2688.
- Rigon RB, Oyafuso MH, Fujimura AT, Gonzalez ML, do Prado AH, Daffon Gremiao MP, et al. Nanotechnology-Based Drug Delivery Systems for Melanoma Antitumoral Therapy: A Review. *Bio Med Research International*. 2015; 841817.
- Li SY, Liu Y, Xu CF, Shen S, Sun R, Du XJ, et al. Restoring anti-tumour functions of T cells via nanoparticle-mediated immune checkpoint modulation. *J Control Release*. 2016; 231: 17-28.
- Jeanbart L, Kourtis IC, van der Vlies AJ, Swartz MA, Hubbell JA. 6-Thioguanine-loaded polymeric micelles deplete myeloid-derived suppressor cells and enhance the efficacy of T cell immunotherapy in tumour-bearing mice. *Cancer Immunol Immunother*. 2015; 64: 1033-1046.
- Sheng WY, Huang L. Cancer immunotherapy and nanomedicine. *Pharm Res*. 2011; 28: 200-214.

31. Spaner DE, Masellis A. Toll-like receptor agonists in the treatment of chronic lymphocytic leukemia. *Leukemia*. 2007; 21: 53-60.
32. Stockfleth E, Trefzer U, Garcia-Bartels C, Wegner T, Schmook T, Sterry W. The use of Toll-like receptor-7 agonist in the treatment of basal cell carcinoma: an overview. *Br J Dermatol*. 2003; 149: 53-56.
33. Zhu G, Liu Y, Yang X, Kim YH, Zhang H, Jia R, et al. DNA-inorganic hybrid nanovaccine for cancer immunotherapy. *Nanoscale*. 2016; 8: 6684-6692.
34. Hong E, Usiskin JM, Bergamaschi C, Hanlon DJ, Edelson RL, Justesen S, et al. Configuration-dependent Presentation of Multivalent IL-15:IL-15R α Enhances the Antigen-specific T cell Response and Anti-tumour Immunity. *J Biol Chem*. 2016; 291: 8931-8950.
35. Dolen Y, Kreutz M, Gileadi U, Tel J, Vasaturo A, van Dinther EA, et al. Co-delivery of PLGA encapsulated invariant NKT cell agonist with antigenic protein induce strong T cell-mediated antitumour immune responses. *Oncoimmunology*. 2015; 5: e1068493.
36. Bobbala S, Tamboli V, McDowell A, Mitra AK, Hook S. Novel Injectable Pentablock Copolymer Based Thermoresponsive Hydrogels for Sustained Release Vaccines. *AAPS J*. 2016; 18: 261-269.
37. Luo Z, Wang C, Yi H, Li P, Pan H, Liu L, et al. Nanovaccine loaded with poly I:C and STAT3 siRNA robustly elicits anti-tumour immune responses through modulating tumour-associated dendritic cells in vivo. *Biomaterials*. 2015; 38: 50-60.
38. Silva JM, Zupancic E, Vandermeulen G, Oliveira VG, Salgado A, Videira M, et al. In vivo delivery of peptides and Toll-like receptor ligands by mannose-functionalized polymeric nanoparticles induces prophylactic and therapeutic anti-tumour immune responses in a melanoma model. *J Control Release*. 2015; 198: 91-103.
39. Yan C, Jie L, Yongqi W, Weiming X, Juqun X, Yanbing D, et al. Delivery of human NKG2D-IL-15 fusion gene by chitosan nanoparticles to enhance antitumour immunity. *Biochem Biophys Res Commun*. 2015; 463: 336-343.
40. Guo Y, Wang D, Song Q, Wu T, Zhuang X, Bao Y, et al. Erythrocyte Membrane-Enveloped Polymeric Nanoparticles as Nanovaccine for Induction of Antitumour Immunity against Melanoma. *ACS Nano*. 2015; 9: 6918-6933.
41. Tan S, Wu T, Zhang D, Zhang Z. Cell or Cell membrane-based drug delivery systems. *Theranostics*. 2015; 5: 863-881.
42. Zhuang X, Wu T, Zhao Y, Hu X, Bao Y, Guo Y, et al. Lipid-enveloped zinc phosphate hybrid nanoparticles for codelivery of H-2K(b) and H-2D(b)-restricted antigenic peptides and monophosphoryl lipid A to induce antitumour immunity against melanoma. *J Control Release*. 2016; 228: 26-37.
43. Molino NM, Neek M, Tucker JA, Nelson EL, Wang SW. Viral-mimicking protein nanoparticle vaccine for eliciting anti-tumour responses. *Biomaterials*. 2016; 86: 83-91.
44. Yildiz I, Shukla S, Steinmetz NF. Applications of viral nanoparticles in medicine. *Curr Opin Biotechnol*. 2011; 22: 901-908.
45. Lizotte PH, Wen AM, Sheen MR, Fields J, Rojanasopondist P, Steinmetz NF, et al. In situ vaccination with cowpea mosaic virus nanoparticles suppresses metastatic cancer. *Nat Nanotechnol*. 2016; 11: 295-303.
46. Lebel ME, Chartrand K, Tarrab E, Savard P, Leclerc D, Lamarre A. Potentiating Cancer Immunotherapy Using Papaya Mosaic Virus-Derived Nanoparticles. *Nano Lett*. 2016; 16: 1826-1832.
47. Zhang X, Teodoro JG, Nadeau JL. Intratumoural gold-doxorubicin is effective in treating melanoma in mice. *Nanomedicine*. 2015; 11: 1365-1375.
48. Tawagi E, Massmann C, Chibli H, Nadeau JL. Differential toxicity of gold-doxorubicin in cancer cells vs. cardiomyocytes as measured by real-time growth assays and fluorescence lifetime imaging microscopy (FLIM). *Analyst*. 2015; 140: 5732-5741.
49. Kaiser S, MacPherson MB, James TA, Emery A, Spiess P, van der Vliet A, et al. Exploratory use of docetaxel loaded acid-prepared mesoporous spheres for the treatment of malignant melanoma. *Cancer Nanotechnol*. 2015; 6: 1.
50. Xu H, Fan M, Elhissi AM, Zhang Z, Wan KW, Ahmed W, et al. PEGylated graphene oxide for tumour-targeted delivery of paclitaxel. *Nanomedicine (Lond)*. 2015; 10: 1247-1262.
51. Cabral H, Makino J, Matsumoto Y, Mi P, Wu H, Nomoto T, et al. Systemic Targeting of Lymph Node Metastasis through the Blood Vascular System by Using Size-Controlled Nanocarriers. *ACS Nano*. 2015; 9: 4957-4967.
52. Dwivedi A, Mazumder A, du Plessis L, du Preez JL, Haynes RK, du Plessis J. In vitro anti-cancer effects of artemisone nano-vesicular formulations on melanoma cells. *Nanomedicine*. 2015; 11: 2041-2050.
53. Dwivedi A, Mazumder A, Fox LT, Brummer A, Gerber M, du Preez JL, et al. In vitro skin permeation of artemisone and its nano-vesicular formulations. *Int J Pharm*. 2016; 503: 1-7.
54. Hu SC, Lee IT, Yen MH, Lin CC, Lee CW, Yen FL. Anti-melanoma activity of *Bupleurum chinense*, *Bupleurum kaioi* and nanoparticle formulation of their major bioactive compound saikosaponin-d. *J Ethnopharmacol*. 2016; 179: 432-442.
55. Loch-Neckel G, Santos-Bubniak L, Mazarino L, Jacques AV, Moccelin B, Santos-Silva MC, et al. Orally Administered chitosan-Coated Polycaprolactone Nanoparticles Containing Curcumin Attenuate Metastatic Melanoma in the Lungs. *J Pharm Sci*. 2015; 104: 3524-3534.
56. Gismondi A, Nanni V, Reina G, Orlanducci S, Terranova ML, Canini A. Nanodiamonds coupled with 5,7-dimethoxycoumarin, a plant bioactive metabolite, interfere with the mitotic process in B16F10 cells altering the actin organization. *Int J Nanomedicine*. 2016; 11: 557-574.
57. Wang C, Shan Y, Yang J, Xu X, Zhuang B, Fan Y, et al. Inhibition of Cancer Angiogenesis Using Triptolide Nanoparticles. *J Biomed Nanotechnol*. 2015; 11: 805-815.
58. Pizzimenti S, Daga M, Ciamporcerio E, Toaldo C, Pettazzoni P, Osella-Abate S, et al. Improved Anti-Tumoural Therapeutic Efficacy of 4-Hydroxynonenal Incorporated in Novel Lipid Nanocapsules in 2D and 3D Models. *J Biomed Nanotechnol*. 2015; 11: 2169-2185.
59. Mundra V, Peng Y, Kumar V, Li W, Miller DD, Mahato RI. Systemic delivery of nanoparticle formulation of novel tubulin inhibitor for treating metastatic melanoma. *Drug Deliv Transl Res*. 2015; 5: 199-208.
60. Pestic M, Podolski-Renic A, Stojkovic S, Matovic B, Zmejkoski D, Kojic V, et al. Anti-cancer effects of cerium oxide nanoparticles and its intracellular redox activity. *Chem Biol Interact*. 2015; 232: 85-93.
61. Li F, Wang Z, Huang Y, Xu H, He L, Deng Yan, et al. Delivery of PUMA Apoptosis Gene Using Polyethyleneimine-SMCC-TAT/DNA Nanoparticles: Biophysical Characterization and In Vitro Transfection Into Malignant Melanoma Cells. *J Biomed Nanotechnol*. 2015; 11: 1776-1782.
62. Andre ND, Silva VA, Ariza CB, Watanabe MA, De Lucca FL. In vivo knockdown of CXCR4 using jetPEI/CXCR4 shRNA nanoparticles inhibits the pulmonary metastatic potential of B16-F10 melanoma cells. *Mol Med Rep*. 2015; 12: 8320-8326.
63. Hundt W, Steinbach S, Mayer D, Burbelko M, Kiessling A, Figiel J, et al. Magnetic resonance-imaging of the effect of targeted antiangiogenic gene delivery in a melanoma tumour model. *Eur Radiol*. 2015; 25: 1107-1118.
64. Pan D, Kim B, Hu G, Gupta DS, Senpan A, Yang X, et al. A strategy for combating melanoma with oncogenic c-Myc inhibitors and targeted nanotherapy. *Nanomedicine (Lond)*. 2015; 10: 241-251.
65. Bull C, Boltje TJ, van Dinther EA, Peters T, de Graaf AM, Leusen JH, et al. Targeted delivery of a sialic acid-blocking glycomimetic to cancer cells inhibits metastatic spread. *ACS Nano*. 2015; 9: 733-745.
66. Labala S, Mandapalli PK, Kurumaddali A, Venuganti VV. Layer-by-layer polymer coated gold nanoparticles for topical delivery of imatinib mesylate to treat melanoma. *Mol Pharm*. 2015; 12: 878-888.
67. Curry T, Kopelman R, Shilo M, Popovtzer R. Multifunctional theranostic gold nanoparticles for targeted CT imaging and photothermal therapy. *Contrast Media Mol Imaging*. 2014; 9: 53-61.

68. Heidari M, Sattarahmady N, Azarpira N, Heli H, Mehdizadeh AR, Zare T. Photothermal cancer therapy by gold-ferrite nanocomposite and near-infrared laser in animal model. *Lasers Med Sci*. 2016; 31: 221-227.
69. Wang H, Zhao R, Li Y, Liu H, Li F, Zhao Y, et al. Aspect ratios of gold nanoshell capsules mediated melanoma ablation by synergistic photothermal therapy and chemotherapy. *Nanomedicine*. 2016; 12: 439-448.
70. Blanco-Andujar C, Ortega D, Southern P, Nesbitt SA, Thanh NT, Pankhurst QA. Real-time tracking of delayed-onset cellular apoptosis induced by intracellular magnetic hyperthermia. *Nanomedicine (Lond)*. 2016; 11: 121-136.
71. Haghniaz R, Umrani RD, Paknikar KM. Temperature-dependent and time-dependent effects of hyperthermia mediated by dextran-coated La_{0.7} Sr_{0.3} MnO₃: in vitro studies. *Int J Nanomedicine*. 2015; 10: 1609-1623.
72. Ogawara K, Shiraishi T, Araki T, Watanabe T, Ono T, Higaki K. Efficient anti-tumour effect of photodynamic treatment with polymeric nanoparticles composed of polyethylene glycol and polylactic acid block copolymer encapsulating hydrophobic porphyrin derivative. *Eur J Pharm Sci*. 2016; 82: 154-160.
73. Arooj S, Nazir S, Nadhman A, Ahmad N, Muhammad B, Ahmad I, et al. Novel ZnO:Ag nanocomposites induce significant oxidative stress in human fibroblast malignant melanoma (Ht144) cells. *Beilstein J Nanotechnol*. 2015; 6: 570-582.
74. Wang S, Riedinger A, Li H, Fu C, Liu H, Liu L, et al. Plasmonic copper sulfide nanocrystals exhibiting near-infrared photothermal and photodynamic therapeutic effects. *ACS Nano*. 2015; 9: 1788-1800.
75. Araki T, Ogawara K, Suzuki H, Kawai R, Watanabe T, Ono T, et al. Augmented EPR effect by photo-triggered tumour vascular treatment improved therapeutic efficacy of liposomal paclitaxel in mice bearing tumours with low permeable vasculature. *J Control Release*. 2015; 200: 106-114.
76. Babington P, Rajjoub K, Canady J, Siu A, Keidar M, Sherman JH. Use of cold atmospheric plasma in the treatment of cancer. *Biointerphases*. 2015; 10: 029403.
77. Choi BB, Kim MS, Kim UK, Hong JW, Lee HJ, Kim GC. Targeting NEU Protein in Melanoma Cells with Non-Thermal Atmospheric Pressure Plasma and Gold Nanoparticles. *J Biomed Nanotechnol*. 2015; 11: 900-905.
78. Ruttala HB, Ko YT. Liposomal co-delivery of curcumin and albumin/paclitaxel nanoparticle for enhanced synergistic antitumour efficacy. *Colloids Surf B Biointerfaces*. 2015; 128: 419-426.
79. Tan SY, Ang CY, Luo Z, Li P, Nguyen KT, Zhao Y. An iGlu receptor antagonist and its simultaneous use with an anticancer drug for cancer therapy. *Chemistry*. 2015; 21: 6123-6131.
80. Mi Y, Mu C, Wolfram J, Deng Z, Hu TY, Liu X, et al. A Micro/Nano Composite for Combination Treatment of Melanoma Lung Metastasis. *Adv Healthc Mater*. 2016; 5: 936-946.
81. Doddapaneni BS, Kyrachenko S, Chagani SE, Alany RG, Rao DA, Indra AK, et al. A three-drug nanoscale drug delivery system designed for preferential lymphatic uptake for the treatment of metastatic melanoma. *J Control Release*. 2015; 220: 503-514.
82. Li T, Zhang M, Wang J, Wang T, Yao Y, Zhang X, et al. Thermosensitive Hydrogel Co-loaded with Gold Nanoparticles and Doxorubicin for Effective Chemoradiotherapy. *AAPS J*. 2016; 18: 146-155.
83. Zhao Y, Huo M, Xu Z, Wang Y, Huang L. Nanoparticle delivery of CDDO-Me remodels the tumour microenvironment and enhances vaccine therapy for melanoma. *Biomaterials*. 2015; 68: 54-66.
84. Zhao L, Yang C, Dou J, Xi Y, Lou H, Zhai G. Development of RGD-Functionalized PEG-PLA Micelles for Delivery of Curcumin. *J Biomed Nanotechnol*. 2015; 11: 436-446.
85. Makino J, Cabral H, Miura Y, Matsumoto Y, Wang M, Kinoh H, et al. cRGD-installed polymeric micelles loading platinum anticancer drugs enable cooperative treatment against lymph node metastasis. *J Control Release*. 2015; 220: 783-791.
86. Chanmee T, Ontong P, Kimata K, Itano N. Key Roles of Hyaluronan and Its CD44 Receptor in the Stemness and Survival of Cancer Stem Cells. *Front Oncol*. 2015; 5: 180.
87. Shen H, Shi S, Zhang Z, Gong T, Sun X. Coating Solid Lipid Nanoparticles with Hyaluronic Acid Enhances Antitumour Activity against Melanoma Stem-like Cells. *Theranostics*. 2015; 5: 755-771.
88. Viale M, Rossi M, Russo E, Cilli M, Aprile A, Profumo A, et al. Fibrin gels loaded with cisplatin and cisplatin-hyaluronate complexes tested in a subcutaneous human melanoma model. *Invest New Drugs*. 2015; 33: 1151-1161.
89. Dasargyri A, Hervella P, Christiansen A, Proulx ST, Detmar M, Leroux JC. Findings questioning the involvement of Sigma-1 receptor in the uptake of anisamide-decorated particles. *J Control Release*. 2016; 224: 229-238.
90. Willmore AM, Simon-Gracia L, Toome K, Paiste P, Kotamraju VR, Molder T, et al. Targeted silver nanoparticles for ratiometric cell phenotyping. *Nanoscale*. 2016; 8: 9096-9101.
91. Xiong W, Peng L, Chen H, Li Q. Surface modification of MPEG-b-PCL-based nanoparticles via oxidative self-polymerization of dopamine for malignant melanoma therapy. *Int J Nanomedicine*. 2015; 10: 2985-2996.
92. Zhang D, Wei Y, Chen K, Gong H, Han S, Guo J, et al. Engineering of Biocompatible pH-Responsive Nanovehicles from Acetalated Cyclodextrins as Effective Delivery Systems for Tumour Therapy. *J Biomed Nanotechnol*. 2015; 11: 923-941.
93. Xu C, Wang P, Zhang J, Tian H, Park K, Chen X. Pulmonary Codelivery of Doxorubicin and siRNA by pH-Sensitive Nanoparticles for Therapy of Metastatic Lung Cancer. *Small*. 2015; 11: 4321-4333.
94. Jallouk AP, Palekar RU, Marsh JN, Pan H, Pham CT, Schlesinger PH, et al. Delivery of a Protease-Activated Cytolytic Peptide Prodrug by Perfluorocarbon Nanoparticles. *Bioconjug Chem*. 2015; 26: 1640-1650.
95. Lu N, Li R, Liu Q, Hu B, Xu X, Ji C, et al. Antitumour and antimetastatic effects of pemetrexed-loaded targeted nanoparticles in B16 bearing mice. *Drug Deliv*. 2015; 26: 1-9.
96. Yu H, Chen J, Liu S, Lu Q, He J, Zhou Z, et al. Enzyme sensitive, surface engineered nanoparticles for enhanced delivery of camptothecin. *J Control Release*. 2015; 216: 111-120.
97. Bradbury MS, Pauliah M, Zanzonico P, Wiesner U, Patel S. Intraoperative mapping of sentinel lymph node metastases using a clinically translated ultrasmall silica nanoparticle. *Wiley Interdiscip Rev Nanomed Nanobiotechnol*. 2015.
98. Partridge SC, Kurland BF, Liu CL, Ho RJ, Ruddell A. Tumour-induced lymph node alterations detected by MRI lymphography using gadolinium nanoparticles. *Sci Rep*. 2015; 5: 15641.
99. Zhou Z, Liu H, Chi X, Chen J, Wang L, Sun C, et al. A Protein-Corona-Free T(1)-T(2) Dual-Modal Contrast Agent for Accurate Imaging of Lymphatic Tumour Metastasis. *ACS Appl Mater Interfaces*. 2015; 7: 28286-28293.
100. Melemenidis S, Jefferson A, Ruparelia N, Akhtar AM, Xie J, Allen D, et al. Molecular magnetic resonance imaging of angiogenesis in vivo using polyvalent cyclic RGD-iron oxide microparticle conjugates. *Theranostics*. 2015; 5: 515-529.
101. Meir R, Shamalov K, Betzer O, Motiei M, Horovitz-Fried M, Yehuda R, et al. Nanomedicine for Cancer Immunotherapy: Tracking Cancer-Specific T-Cells in Vivo with Gold Nanoparticles and CT Imaging. *ACS Nano*. 2015; 9: 6363-6372.
102. Huang SK, Hoon DS. Liquid biopsy utility for the surveillance of cutaneous malignant melanoma patients. *Mol Oncol*. 2016; 10: 450-463.
103. Seenivasan R, Maddodi N, Setaluri V, Gunasekaran S. An electrochemical immunosensing method for detecting melanoma cells. *Biosens Bioelectron*. 2015; 68: 508-515.
104. Bazylinska U, Saczko J. Nanoemulsion-templated polyelectrolyte multifunctional nanocapsules for DNA entrapment and bioimaging. *Colloids Surf B Biointerfaces*. 2016; 137: 191-202.

105. Bazylińska U, Zielinski W, Kulbacka J, Samoc M, Wilk KA. New diamidequat-type surfactants in fabrication of long-sustained theranostic nanocapsules: Colloidal stability, drug delivery and bioimaging. *Colloids Surf B Biointerfaces*. 2016; 137: 121-132.
106. Vannucci L, Falvo E, Failla CM, Carbo M, Fornara M, Canese Rossella, et al. In Vivo Targeting of Cutaneous Melanoma Using an Melanoma Stimulating Hormone-Engineered Human Protein Cage with Fluorophore and Magnetic Resonance Imaging Tracers. *J Biomed Nanotechnol*. 2015; 11: 81-92.
107. Kotb S, Detappe A, Lux F, Appaix F, Barbier EL, Tran VL, et al. Gadolinium-Based Nanoparticles and Radiation Therapy for Multiple Brain Melanoma Metastases: Proof of Concept before Phase I Trial. *Theranostics*. 2016; 6: 418-427.
108. Kang JH, Ko YT. Lipid-coated gold nanocomposites for enhanced cancer therapy. *Int J Nanomedicine*. 2015; 10: 33-45.
109. Tchounwou C, Sinha SS, Viraka Nellore BP, Pramanik A, Kanchanapally R, Jones S, et al. Hybrid Theranostic Platform for Second Near-IR Window Light Triggered Selective Two-Photon Imaging and Photothermal Killing of Targeted Melanoma Cells. *ACS Appl Mater Interfaces*. 2015; 7: 20649-20656.
110. Wang H, Cao G, Gai Z, Hong K, Banerjee P, Zhou S. Magnetic/NIR-responsive drug carrier, multicolor cell imaging, and enhanced photothermal therapy of gold capped magnetite-fluorescent carbon hybrid nanoparticles. *Nanoscale*. 2015; 7: 7885-7895.
111. Yildirimer L, Thanh NT, Loizidou M, Seifalian AM. Toxicology and clinical potential of nanoparticles. *Nano Today*. 2011; 6: 585-607.
112. Di Gioacchino M, Petrarca C, Lazzarin F, Di Giampaolo L, Sabbioni E, Boscolo P, et al. Immunotoxicity of nanoparticles. *Int J Immunopathol Pharmacol*. 2011; 24: 65S-71S.
113. Scholer N, Hahn H, Muller R, Liesenfeld O. Effect of lipid matrix and size of solid lipid nanoparticles (SLN) on the viability and cytokine production of macrophages. *Int J Pharm*. 2002; 231: 167-176.

This is the author's final version of the contribution published as:

Barrera, Giuseppina; Daga, Martina; Ferrara, Benedetta; Dianzani, Chiara; Pizzimenti, Stefania; Argenziano, Monica; Cavalli, Roberta; Trotta, Francesco. Drug delivery nanoparticles in treating chemoresistant tumor cells. *CURRENT MEDICINAL CHEMISTRY*. 23 (999) pp: 1-1.
DOI: 10.2174/0929867323666161205122225

The publisher's version is available at:

<http://www.eurekaselect.com/openurl/content.php?genre=article&doi=10.2174/0929867323666161205122225>

When citing, please refer to the published version.

Link to this full text:

<http://hdl.handle.net/2318/1634214>

Drug delivery nanoparticles in treating chemoresistant tumor cells.

Giuseppina Barrera¹, Martina Daga¹, Benedetta Ferrara², Chiara Dianzani², Stefania Pizzimenti¹, Monica Argenziano², Roberta Cavalli² and Francesco Trotta³.

- 1. Department of Clinical and Biological Sciences, University of Turin, Corso Raffaello 30, 10125 Turin (Italy).**
- 2. Department of Drug Science and Technology, University of Turin, Via P. Giuria 9, 10125 Turin, Italy,**
- 3. Department of Chemistry, University of Turin, Via Pietro Giuria 7, 10125 Turin, Italy**

Abstract

Intrinsic or acquired chemoresistance represents the main obstacle to the successful treatment of cancer patients. Several mechanisms are involved in multidrug resistance: decreased uptake of hydrophilic drugs, increase of energy dependent efflux, alteration of the redox state, alteration of apoptotic pathways, and modification of the tumor microenvironment. In recent years, several types of nanoparticles have been developed to overcome these obstacles and improve the accumulation and release of drugs at the pathological site. In this review we describe the main mechanisms involved in multidrug resistance and the nanovehicles which have been proposed to target specific aspects of this phenomenon.

1. Introduction

Drug resistance, which occurs in nearly all types of cancer, is a major problem in the treatment of cancer patients. Drug resistance can be classified in two ways: the intrinsic resistance, when tumors are resistant prior to treatment, therefore the drugs are not effective even with initial early diagnosis and treatment, and the acquired resistance which occurs after prolonged cycles of chemotherapy, despite an initial positive response [1]. Unfortunately, resistance appears not only to conventional chemotherapy but also to targeted therapies, the so-called “smart drugs” such as kinase inhibitors and tamoxifen that binds to the estrogen receptor [2].

Various mechanisms have been proposed to elucidate pathways and targets of multidrug resistance (MDR) [1]. They can be summarized by three major mechanisms: 1) decreased uptake of hydrophilic drugs, such as folate antagonists, nucleoside analogues and cisplatin, which require transporters to enter cells; 2) various molecular changes in cells, that affect the capacity of cytotoxic drugs to kill cells, including alterations in redox status, increased repair of DNA damage, alteration of apoptotic machinery etc., and 3) increased energy-dependent efflux of hydrophobic drugs, that can easily enter the cells by diffusion through the plasma membrane. This phenomenon occurs

predominantly via ABC superfamily transporters and elevated expression levels of these drug efflux pumps [3].

1.1 ABC Transporter family

The first mechanism found to explain MDR is the increased efflux of hydrophobic cytotoxic drugs, mediated by members of energy-dependent transporters, the ABC transporter family [4]. The human ATP-binding cassette (ABC) transporters are a large group of membrane protein complexes which consist of 48 members, classified into seven subfamilies from ABC-A through to ABC-G based on their sequence similarities [5]. Among the 48 ABC transporters, the protein complexes located on the plasma membrane significantly affect the intracellular concentration of diverse drugs, drug conjugates and metabolites by export. Several ABC proteins have been characterized to confer resistance to anticancer drugs. Among them, P-glycoprotein (MDR, Pgp or ABCB1), multidrug resistance protein 1 (MRP1 or ABCC1) and ABCG2 (also known as Breast Cancer Resistance Protein: BCRP) are the most frequently associated with MDR [6]. Increased expression of Pgp, as well as of other ABC proteins, can be induced by exposure of the cells to the drugs, due to genomic mutations or epigenetic modifications of its promoter [7]. The overexpression of these pumps obviously reduce the intracellular concentration of numerous endo- and exo-toxins which are structurally and biochemically distinct, resulting in MDR. To overcome ABC transporter-mediated MDR and sensitize cancer cells to chemotherapeutic agents, some inhibitors of ABC superfamily transporter have been used in association with chemotherapeutic drugs. Although the combined therapies displayed some encouraging clinical results, there is no effective MDR reversing agent approved for an appreciable sensitization of malignant tumors to chemotherapeutic drugs without toxic effects to date. Combined treatment with the first-generation MDR inhibitors such as verapamil and cyclosporine A and anticancer drugs (e.g., mitoxantrone and daunorubicin) led to toxic side effects showing only limited function or no benefits [8; 9].

1.2 Alteration of signaling pathways

Several signaling pathways have been found to be involved in chemoresistance of cancer cells. A pathway frequently activated, during life of the cancer cells, is the Hedgehog (Hh) pathway [10]. The Hh signaling pathway is one of the important signaling pathways that play key roles in the processes of embryonic development, carcinogenesis, maintenance of cancer stem cells (CSCs), and the acquisition of epithelial-to-mesenchymal transition (EMT) leading to metastasis [10]. The functional transcription activators of the Hh pathway include the GLI proteins. Inhibition of the activity of GLI can interfere with almost all DNA repair types in human cancer and can render tumor cells more vulnerable to lethal DNA damages induced by chemotherapy and radiotherapy [10]. Moreover, the activation of GLI-mediated transcription (through ligand-dependent or ligand-

independent modes), also induces chemo-resistance also by increasing drug efflux in an ABC transporter-dependent manner [11]. Thus, Hh signaling is an important therapeutic target to overcome MDR and consequently increases the chemotherapeutic response in the treatment of cancer.

Another signaling pathway which has been found to be involved in chemoresistance is the Keap1/Nrf2 pathway [12]. Nrf2 (NF-E2-related factor 2) transcription factor is the master regulator of the antioxidant response of the cells to oxidative stress stimuli through the activation of the synthesis of cytoprotective genes. Under physiological conditions, Nrf2 is present in the cytoplasm where it is bound by Keap1 (Kelch-like ECH-associated protein 1). Keap1 forms a complex with Cul3 and Rbx1, and this E3 ubiquitin ligase complex is able to bind and ubiquitinate Nrf2, resulting in Nrf2 proteasomal degradation [13]. When oxidative stress is present within the cell, the cysteine residues of Keap1 become oxidized, resulting in a conformational change of the Keap1-Nrf2 complex which prevents Nrf2 ubiquitination. The stabilized Nrf2 accumulates in nuclei, heterodimerizes with small Maf proteins and activates target genes for cytoprotection through the antioxidant response element (ARE)/electrophile response element (EpRE) [14]. Nrf2 has a dual role in cancer: the canonical protective role in carcinogenesis, and the non-canonical 'dark-side' of Nrf2 in promoting chemoresistance [15]. A Nrf2 role in cisplatin resistance of bladder cancer cells has been indicated by Hayden et al. (2014), which demonstrated that Nrf2 overexpression is associated with clinically relevant cisplatin resistance, that becomes reversible after Nrf2 silencing in experimental models [16]. In ovarian cancer, an aberrant activation of Nrf2 is observed, which confers resistance to cisplatin-induced apoptosis [17].

Increasing evidence has demonstrated the involvement of Yes-associated protein (YAP) with chemoresistance in diverse types of cancers. YAP, a transcriptional co-activator, is a key component of the Hippo tumor-suppressor pathway [18]. Hippo pathway-mediated YAP phosphorylation on Ser127 mainly leads to its cytoplasm sequestration or ubiquitination and degradation [19]. Conversely, unphosphorylated YAP translocates into the nucleus where it binds to the TEAD transcription factor, triggering the expression of several genes involved in organ size control, cell proliferation and survival (i.e. CTGF and survivin) [20]. Indeed, YAP expression inhibition results in reduced cell proliferation and enhanced cell death through modulation of downstream transcriptional targets [21]. Moreover, YAP expression and nuclear localization strongly correlate with poor patient outcome and the progression of several tumors, including bladder and ovarian cancer [22]. In particular, for these two types of tumors, YAP protein has been demonstrated to play a role in cisplatin resistance of cancer cells. Overexpression of Yap2 in immortalized ovarian surface epithelium cells resulted in increased cell proliferation, resistance to

cisplatin-induced apoptosis, faster cell migration, and anchorage independent growth, while YAP knockdown resulted in increased sensitivity to cisplatin-induced death [23]. Recently it has been demonstrated that constitutive expression and activation of YAP is inversely correlated with *in vitro* and *in vivo* cisplatin sensitivity of urothelial cell carcinoma cells [24]. YAP overexpression protects, while YAP knockdown sensitizes cancer cells to chemotherapy and radiation effects via increased accumulation of DNA damage and apoptosis [24].

Through a screening approach, Matz et al (2014) created a library of barcoded pathway-activating mutant complementary DNAs to identify those that enhanced the survival of cancer cells in the presence of 13 clinically relevant, targeted therapies. The Authors found that RAS-MAPK (mitogen-activated protein kinase), Notch1, PI3K (phosphoinositide 3-kinase)-mTOR (mechanistic target of rapamycin), and ER (estrogen receptor) signaling pathways often conferred resistance to specific drugs. In particular, they demonstrated that the activation of the Notch1 pathway promoted acquired resistance to tamoxifen (an ER-targeted therapy) in breast cancer cells and that the inhibition of Notch signaling restored tamoxifen sensitivity. Moreover, Notch1 knockdown fully sensitized drug-resistant melanoma cells to MAPK inhibitors, indicating that, Notch1 signaling may be a therapeutic target in some drug-resistant breast cancers and melanomas [25].

1.3 Control of redox state.

The redox status regulation plays an important role in cancer cell survival to the therapy. Many types of cancer cells display a large amount of reactive oxygen species (ROS), due to an aberrant metabolism, mitochondrial dysfunction or activation of oncogenes. This characteristic makes cancer cells more vulnerable to damage by further ROS production induced by exogenous agents [26]. In this context, ROS may exert a cytotoxic effect, leading to the death of malignant cells and thus limiting cancer progression [27]. On the basis of these observations, several ROS-generating agents are currently in clinical trials as single agents or in combination therapy [28]. Alteration of redox status, namely the increase of antioxidant defenses in cancer cells, has been indicated as responsible for radio- and chemoresistance. Indeed, some cancer cells, in particular those in advanced stages of disease, have become highly adapted to intrinsic oxidative stress by up-regulating their antioxidant systems [29]. This redox adaptation provides a mechanism of resistance to many anticancer agents, due to increased tolerance of exogenous stress and increased capacity for drug inactivation, mainly linked to the GSH increase [30].

1.4 miRNA and chemoresistance.

Several reports have recently highlighted the involvement of endogenous non-coding RNAs, known as microRNAs (miRNAs), in the evolution of drug resistance in cancer cells. MiRNAs are small non-coding RNAs 19-25 nucleotides in size involved in many biological processes such as

survival, apoptosis, cell cycle and gene expression regulation [31]. MiRNAs are evolutionarily conserved and work by silencing gene expression. They are involved in many different cancer types and can act as both tumor suppressors and oncogenes [32]. Accumulating evidence is revealing an important role of miRNAs in anticancer drug resistance and their expression profiling can be correlated with the development of resistance [33]. Some miRNAs, such as miRNA 21, have been involved in the resistance toward doxacetol in prostate cancer cells [34] and its aberrant expression is critically correlated with the disease stage, drug resistance, and survival of pancreatic cancer patients [35]. The miR-21 is one of the most commonly implicated miRNAs in cancer as its expression is highly up-regulated in a variety of solid tumors, including breast, gastric, colon, lung, pancreatic and ovarian cancers [36]. Several downstream pathways of miR-21 have been identified including phosphatase and tensin homolog (PTEN)/phosphoinositide 3-kinase/protein kinase B (PI3K/Akt), programmed cell death protein 4 (PDCD4, neoplastic transformation inhibitor protein), NF- κ B pathways and the HIF-1 α pathway, a key downstream target of miR-21 in regulating tumor angiogenesis [37]. Inhibition of miR-21 by curcumin increased pancreatic cancer cell sensitivity to gemcitabine [38]. Roy et al. showed that difluorinated-curcumin decreased miR-21 in 5-FU and oxaliplatin resistant colon cancer cell lines through upregulation of phosphatase and tensin homolog (PTEN) and thus reduced the activity status of the PI3K/Akt pathway [39] which is involved, when activated, in the drug resistance of colon cancer cells [40]. In addition to miRNA 21, other miRNAs, such as, Let 7, miRNA 15, miRNA 16 and miRNA 34, have been found to be involved in chemoresistance [41]. This indicates that miRNA-based therapy may provide a new strategy to overcome drug resistance in future.

1.5 Tumor microenvironment

Another aspect involved in chemoresistance is the abnormal tumor microenvironment which induces a collection of cellular stress responses and plays a major role in determining the metabolic status and chemosensitivity in cancer cells [42]. Tumor vasculature is structurally and functionally abnormal, and combined with intrinsically altered tumor cell metabolism, produces heterogeneity in oxygenation, pH, exposure to increased interstitial fluid pressure and the concentrations of glucose and many other metabolites that promote tumor progression and metastatization [43]. For example, in certain microenvironmental contexts, extreme hypoxia causes endoplasmic reticulum stress and activates the unfolded protein response, which provides a further adaptive mechanism that allows tumor cells to survive under adverse metabolic conditions [44]. Moreover, since oxygen is a potent radiosensitizer, hypoxia inhibits effective radiation killing in vitro [45]. and has a direct effect on the effectiveness of drugs, such as mephalan, bleomycin, and etoposide, which require molecular oxygen for maximal efficiency [46].

The impairment of the ability of the tumor vasculature to deliver nutrients and remove waste products leads to the increase of environmental acidosis [47], which is involved in chemoresistance too. Indeed, in an acidic extracellular environment, the cellular uptake of some chemotherapeutic drugs, such as doxorubicin, mitoxantrone, or vinblastine, is significantly reduced [48].

In recent years, several types of nanoparticles have been produced in order to overcome the alterations above described which make cancer cells highly resistant to cancer therapy.

2. Nanoparticles in chemoresistant cells.

As described above, several mechanisms are involved in induced or intrinsic resistance. Therefore nanomedicine developed drug-loaded nanocarriers able to target specific aspects of chemoresistant cancer cells. In this section we report the more recent issues describing the nanoparticles employed in overcoming the diverse behaviors of chemoresistant tumors.

2.1 Targeting ABC transporters

As previously illustrated, the overexpression of ABCs is a well-known mechanism of MDR in cancer and is associated with therapeutic failure. Since their discovery, ABCs have emerged as attractive therapeutic targets and the search for compounds that inhibit their expression and/or their functional activity has gained growing interest [49]. However, the pharmacological ABC inhibitors present high toxicity and the clinical results have been somewhat disappointing.

Some attempts have been performed to conjugate nontoxic compounds, or lowest doses of toxic compounds, which have been demonstrated an inhibitory activity on some member of ABC transporters, with antineoplastic drugs (Fig.1). In example, Khdair et al. (2009) utilized aerosol OT (AOT)-alginate nanoparticles as a carrier for the simultaneous cellular delivery of methylene blue, an inhibitor of P-gp, and doxorubicin. After photoactivation, nanoparticle-mediated combination therapy resulted in a significant induction of both apoptosis and necrosis in adriamycin-resistant cancer cells compared to single drug treatment [50]. Song et al. (2000) loaded poly(D,L-lactide-co-glycolide acid) (PLGA) nanoparticles with vincristine and verapamil hydrochloride (VRP), a calcium channel blocker, able to reverse completely the resistance caused by Pgp in vitro (Huang et al., 1999). Results demonstrated that the co-encapsulation of an anticancer drug and chemosensitizer had high therapeutic effectiveness on MCF-7/ADR breast cancer cells and suggest that this strategy might cause lower normal tissue drug toxicity and fewer drug-drug interactions [51]. Transferrin coated liposomes co-encapsulating verapamil and doxorubicin have been tested by Wu et al (2009), which demonstrated that this association exhibited 5 and 3-fold higher cytotoxicity in doxorubicin-resistant human erythroleukemia K562 cells, compared to non-targeted liposomes and transferrin targeted liposomes with doxorubicin alone, respectively [52]. Other studies have been performed to reduce drug efflux from cancer cells, by utilizing specific platforms for the drug

delivery. Nanodiamonds (NDs) are promising candidates in this field, demonstrating significant potential as gene/drug delivery platform for cancer therapy. The effectiveness of the ND platform has been demonstrated in daunorubicin delivery in K562 resistant cells [53] and in mitoxantrone delivery in the MDA-MB-231 triple negative breast cancer cell line that was lentivirally transduced for resistance against mitoxantrone [54]. In addition, NDs have been utilized to deliver epirubicin in hepatic cancer stem cells, demonstrating a high effectiveness in overcoming chemoresistance by promoting endocytic uptake and enhancing tumor cell retention [55]. These works demonstrated that ND-drug complexes have favorable drug delivery properties and are capable of improving drug retention and efficacy. Recently, Kovács D. et al. (2015) demonstrated that silver nanoparticles (AgNPs) display an anti-proliferative effect and induce apoptosis mediated cell death both in drug sensitive and in MDR cancer cells and that this action is due to the inhibition of the efflux activity of MDR cancer cells which enhance drug accumulation. Furthermore, AgNPs synergistically potentiate six different antineoplastic agents on drug resistant cells [56].

2.2 Targeting signal transduction pathways

Since several signal transduction pathways are activated in cancer cells, some studies have been devoted to investigating whether the delivery of specific inhibitors of a signaling pathway could overcome the MDR. Fan et al. (2010) utilized micellar nanoparticles self-assembled from copolymer folate-chitosan (FA-CS) as carriers to co-deliver doxorubicin and pyrrolidinedithio carbamate (PDTC), an antioxidant and chelator of heavy metals that blocks NF- κ B activity by suppressing the release of I κ B from NF- κ B [57]. These NPs were designed to achieve targeted doxorubicin delivery via endocytosis, with a low pH responsive endosomal or extracellular drug release, and to overcome resistance via inhibition of NF- κ B by PDTC. Results confirmed that the co-delivery of the NF- κ B inhibitor PDTC and doxorubicin, effectively overcame drug resistance.

Another approach was the use of metallic nanoparticles to increase the cytotoxic effect of chemotherapeutic drugs. Xiong et al. (2014) have demonstrated that 20 nm gold nanoparticles (AuNPs) carrying cisplatin prevent cisplatin-induced activation of Akt and NF- κ B signaling axis in ovarian cancer cells that are critical for epithelial-mesenchymal transition, stem cell maintenance and drug resistance. In vivo, AuNPs sensitize orthotopically implanted ovarian tumor to a low dose of cisplatin and significantly inhibit tumor growth [58]. Other effects displayed by AuNPs is related to the modification of gene expression as detected in CaCo2 colon cancer cells by Bajak et al. (2015). The modifications affected some Nrf2 responsive genes (several metallothioneins, HMOX, G6PD, OSGIN1 and GPX2) that were highly up regulated and members of the selenoproteins that were also differentially expressed. These findings indicate that exposure to AuNPs induces

oxidative stress signaling pathways, and might enhance the anti-cancer properties of chemotherapeutic drugs [59].

The inhibition of the Nrf2 pathway could represent a way to sensitize cancer cells to anticancer drugs by increasing intracellular oxidative stress. Luteolin, as a flavonoid compound, can inhibit Nrf2 and sensitize cancer cells to chemotherapeutic agents. Sabzichi et al. (2014) demonstrated that luteolin loaded in phytosomes, as an advanced nanoparticle carrier, sensitized MDA-MB 231 cells to doxorubicin [60].

2.3 Targeting redox state

The extent of antioxidant capacity is actually reported to correlate with the aggressiveness of tumors and it can go beyond the antioxidant capacity of normal cells [61]. In normal cells the glutathione (GSH) concentration is 100 to 1000 times higher than that in the extracellular fluids and circulation and it is further increased in chemoresistant tumor cells. GSH has been recognized as an ideal and ubiquitous internal stimulus for rapid destabilization of nano-carriers inside cells to accomplish efficient intracellular drug release. For this reason GSH-responsive nanoparticles (GSH-NPs), which respond to the intracellular concentration of GSH, have been developed [62]. Since in most chemo-resistant and radio-resistant cancer cells the level of intracellular GSH was higher than in the chemo-sensitive or radio-sensitive cancer cells, it has been speculated that GSH-NPs could preferentially drive the drugs in the resistant cancer cells. To pursue this purpose, a new class of cyclodextrin GSH-responsive nanosponges (GSH-NSs) that are able to host and to release anticancer drugs in the presence of GSH, at concentrations similar to those found in chemoresistant cancer cells, have been synthesized (Fig.2) [63].

However, even if the antioxidant capacity of chemoresistant cancer cells could constitute a cue for the choice of particles sensitive to the high GSH concentrations, on the other hand, the increase of oxidative stress in this type of cancer cells can contribute to their killing. There is rapidly accumulating evidence sustaining the fact that some types of nanoparticles induce oxidative stress that consequently results in signaling pathway stimulation and apoptotic cell death of cancer cells.

Cadmium telluride quantum dots (CdTe-QDs) have recently been shown to effectively induce apoptosis in hepatocellular carcinoma HepG2 cells by activating MAPKs, including JNK, Erk1/2 and p38, as a result of oxidative stress induced in HepG2 cells [64]. Analogously, cadmium sulfide quantum dots (bsCdSQDs) stabilized with a biosurfactant induces ROS-mediated apoptotic cell death in human prostate cancer LNCaP cells [65]. The ROS mediated activation of ERK1/2, JNK and p38 MAPK and apoptosis induction was also observed by treating hepatoma SMMC-7721 cells with cerium oxide nanoparticles. The use of

ROS scavengers dramatically reduced activated kinases and simultaneously there was a decrease in the apoptotic rate [66]. It has been found that the metal based nanoparticles, such as tungsten carbide-cobalt (WC-Co) nanoparticles, zinc oxide (ZnO) nanoparticles, cobalt nanoparticles, titanium dioxide (TiO₂) nanoparticles, nickel oxide nanoparticles, cuprous oxide nanoparticles, silver nanoparticles and zinc nanoparticles can induce oxidative stress and increase the ROS level in a number of different tumor cells [67]. This effect could increase the cytotoxicity of prooxidant cytotoxic drugs.

2.4 Targeting microenvironmental stressors

Due to the specific micro environment of the tumor, some of the unique factors such as low pH and hypoxia can be used as a trigger to overcome MDR. The acidosis in tumor cells, due to the high production of lactate by Warburg effect, and the related acidosis of the environmental tissue due to the impairment of the ability of the tumor vasculature to remove waste products, have been considered for developing of nanoparticles able to release the drug in an acidic environment. Aryal et al. synthesized a Bi(PEG-PLA)-Pt(IV) polymer-cisplatin prodrug conjugate which had a well controlled cisplatin loading yield and showed excellent acid-responsive drug release kinetics, leading to enhanced *in vitro* cytotoxicity against tumor cells as compared to free cisplatin [68]. Long-circulating and pH-sensitive liposomes containing cisplatin (SpHL-CDDP) have been developed by Leite et al. (2012), which demonstrated that the intravenous administration of SpHL-CDDP in solid Ehrlich tumor-bearing mice caused a significant reduction in the tumor volume and a higher tumor growth inhibition ratio with respect to the administration of CDDP alone [69]. Wu et al. (2012) have synthesized mixed micelles of polyethylene glycol based on DSPE-PEG2000, DSPE-PEG3400 and a pH-sensitive polymer PHIS-PEG2000. This mixed micelles showed a pH-dependent drug release property with much faster release at around pH 5.5 compared to micelles without PHIS-PEG2000 [70]. Other core-crosslinked pH-sensitive degradable micelles were synthesized based on poly(ethylene glycol)-b-poly(mono-2,4,6-trimethoxy benzylidene-pentaerythritol carbonate-co-acryloyl carbonate) (PEG-b-P(TMBPEC-co-AC) copolymer that contains acid-labile acetal and photo-cross-linkable acryloyl groups in the hydrophobic polycarbonate block for intracellular paclitaxel (PTX) release. The *in vitro* release studies showed that rapid drug release was obtained under mildly acidic conditions, whereas PTX release at pH 7.4 was greatly inhibited [71]. A pH-sensitive mixed copolymer micelles system, composed of hyaluronic acid-g-poly(l-histidine) (HA-PHis) and d-α-tocopheryl polyethylene glycol 2000 (TPGS2k), an inhibitor of the efflux pumps, was developed to co-deliver doxorubicin and TPGS2k into drug-resistant breast cancer MCF-7 cells. The pH dependent drug release profile due to the protonation of poly(l-histidine) and the higher cellular uptake conferred to these micelles an

enhanced MDR reversal effect [72]. Another system to release drug in an acidic environment has been recently proposed by Nogueira et al. (2016), which prepared chitosan-based nanoparticles encapsulating methotrexate modified with the pH-sensitive surfactant 77KS [73]. The presence of 77KS gives a pH-sensitive behavior to nanoparticles, which allowed accelerated release of methotrexate with decreasing pH as well as pH-dependent membrane-lytic activity.

As previously described, hypoxia is a characteristic of tumor tissues, which can confer, through hypoxia-inducible factors (HIFs), pro-survival and pro-angiogenic stimuli. Moreover hypoxia induces macrophage recruitment and transforms them in tumor-associated macrophages (TAMs) which, in turn, promote wound healing, tissue repair and production of anti-inflammatory cytokines like IL-10 [74]. To overcome the hypoxia in the cancer tissue [75] Song et al. (2016) synthesized MnO₂ nanoparticles by reducing manganese permanganate (KMnO₄) to MnO₂ with cationic polyelectrolyte poly-(allylamine hydrochloride) (PAH) [76]. The high reactivity of manganese dioxide nanoparticles (MnO₂ NPs) toward hydrogen peroxide (H₂O₂), for the simultaneous production of O₂ and regulation of pH, alleviates tumor hypoxia. Moreover, the Authors conjugated to MnO₂ NPs, hyaluronic acid (HA-MnO₂ NPs) which has an immune toxicological effect on macrophages and induces their activation and the production of endogenous ROS, and coated HA-MnO₂ NPs with mannan that targets the mannose receptor on the surface of TAMs. These modifications further enhanced the ability of MnO₂ NPs to lessen tumor hypoxia and modulate chemoresistance. Indeed, combination treatment of breast tumors with Man-HA-MnO₂ NPs and doxorubicin significantly inhibited tumor growth and tumor cell proliferation as compared with chemotherapy alone.

2.5 Delivery of RNA molecules

The use of RNA molecules to counteract chemoresistance involves both miRNAs, and small interfering RNA (siRNA). siRNA are target-specific double-strand RNA molecules synthesized to suppress gene expression through the process of RNA interfering [77]. As previously illustrated, miRNAs are small non-coding RNA molecules (containing about 22 nucleotides) found in plants, animals and some viruses, that functions in RNA silencing and post-transcriptional regulation of gene expression [78]. MiRNAs in cancer can function as oncogenes or tumor suppressors. In cancer, overexpression of some miRNAs, such as miR-21, may promote cancer development by negatively regulating tumor suppressor genes and/or genes that control cell differentiation or apoptosis. On the contrary, underexpression of other miRNAs, such as let-7, function as tumor suppressor genes and may inhibit cancers by regulating oncogenes and/or genes that control cell differentiation or apoptosis [79].

The use of miRNA and siRNA in cancer therapy or to counteract chemoresistance is hindered by two main factors: 1) they are unstable in blood since they are substrates of blood nucleases; 2) they have large molecular weights and are hydrophilic, thus they have very poor ability to cross the lipophilic phospholipids bilayers of cell membranes.

To overcome these obstacles, various nanoparticle types have been developed for the delivery miRNA or siRNA into the tumor mass. In the chemoresistance context, siRNA have been utilized to silence genes involved in chemoresistance, whereas the miRNA or anti-miRNAs were utilized to block the action of cellular oncogenes or oncogenic miRNAs, respectively.

2.5.1 Small interfering RNA delivery

Although the use of siRNA is an attractive option for post-transcriptional silencing of a target genes, some limitations to clinical application of siRNA drugs in oncology depend on their physicochemical properties, the large molecular weight and polyanionic nature of siRNA which limits its' passive uptake by cells [80]. In addition extracellular barriers exist that prevent an efficient delivery of siRNA and transfection in solid tumors [81]. Moreover, because of plasmatic nucleases, siRNA cannot be directly injected into systemic circulation. Consequently, the encapsulation of siRNA with nanoparticles can shield the siRNA from plasmatic nucleases and immune responses, thus assisting in successful siRNA delivery (Fig. 3).

Lipid-based particles (or liposomes) have been used for decades for the delivery of gene medicines including plasmids, antisense oligonucleotides, and siRNAs. A number of lipid-based particle systems have been developed for delivery of siRNAs or miRNA mimics and used in clinical trials [82]. Wang et al. (2011) demonstrated an increase of siRNA delivery, using lipoplex of siRNA with pegylated cationic liposomes (PCat) [83]. In particular, by targeting survivin, an inducible chemoresistance gene, in combination with paclitaxel treatment, the Authors demonstrated that the silencing of survivin enhanced paclitaxel anticancer activity in a human pancreatic Hs766T xenograft model [84]. However, there are many problems with lipid-based delivery systems *in vivo*, such as rapid clearance by the liver, lack of target tissue specificity and a low entrapment efficiency [85]. To increase entrapment efficiency, Landen Jr. et al. developed a method of formulating 1,2-dioleoyl-sn-glycero-3-phosphatidylcholine-(DOPC-) encapsulated siRNA liposomes [86]. DOPC-encapsulated siRNA targeted the oncoprotein EphA2, a tyrosine kinase receptor in the ephrin family, which is highly overexpressed in ovarian cancer and correlates with low response to therapy [87]. This system was highly effective in reducing EphA2 expression 48h after administration of a single dose in an orthotopic model of ovarian carcinoma [86].

PLGA is a copolymer which is used in a host of Food and Drug Administration (FDA) approved therapeutic devices, owing to its biodegradability and biocompatibility. Recently PLGA is being

used as a nanocarrier for plasmid DNA and siRNA delivery. The advantages conferred by PLGA-based siRNA delivery include high plasma stability and endocytic uptake [88]. Modification of PLGA leading to the targeting of specific aspects of resistant tumors can increase the accumulation of these particles in tumor sites. For example pH-labile linkage-bridged block copolymer of poly(ethylene glycol) with poly(lacide-co-glycolide) (PEG-Dlinkm-PLGA) was used for siRNA delivery. The obtained siRNA-encapsulating PEG-Dlinkm-PLGA nanoparticle gained efficiently prolonged circulation in the blood and preferential accumulation in tumor sites via the PEGylation [89]. Recent studies have shown that the suppression of gene products involved in the DNA repair pathway, such as REV1/REV31 can sensitize intrinsically resistant tumors to chemotherapy and reduce the frequency of acquired drug resistance of relapsed tumors. Thus, a combination of conventional DNA-damaging chemotherapy with siRNA-based therapeutics has been proposed by Xu et al., (2013). The Authors found that nanoparticles (NPs) self-assembled from biodegradable PLGA-PEG block copolymers delivering a cisplatin prodrug in combination with *REV1/REV3L*-specific siRNAs revealed a synergistic effect on tumor inhibition in a human lymph node carcinoma of the xenograft mouse model and they were strikingly more effective than platinum monotherapy [90].

Chitosan-encapsulated TWIST-siRNA nanoparticles were constructed and used to silence the TWIST gene [91], which has been involved in chemoresistance and poor prognosis of nasopharyngeal carcinoma [92]. It has been shown that nanoparticles successfully knock-down TWIST expression in a human nasopharyngeal cell line (CNE2), and significantly sensitized CNE2 cells to irradiation.

2.5.2 miRNA delivery

MiRNAs play critical roles in modulating the oncogenic driver pathways involved in the acquisition of resistance to cancer treatments. Despite promising results in the development of miRNA therapeutics and successes on *in vitro* studies, limited progress has been made with *in vivo* studies or clinical trials. To increase the resistance to serum nuclease, avoid the activation of the innate immune system, and reduce off-target effects, chemical modifications of miRNA molecules [93] and different types of nano-vehicles have been proposed to treat different cancer types [94].

Triple negative breast cancers (TNBCs) are a specific subtype of epithelial breast tumours that are immunohistochemically negative for the protein expression of the estrogen receptor (ER), the progesterone receptor (PR) and lack overexpression/gene amplification of HER2 [95]. Treatment of TNBC with chemotherapeutics such as taxanes is initially very effective in most patients. However, the majority of these tumors develop resistance [96]. To treat and overcome resistance of TNBC several nano-vehicles have been proposed. Wang et al. (2015) have loaded hyaluronic acid (HA)-

decorated polyethylenimine-poly(d,l-lactide-co-glycolide) (PEI-PLGA) nanoparticles with doxorubicin and miR-542-3p, a potent tumor suppressor molecule, which targets tumor suppressor p53 and apoptosis inhibitor survival [97]. The co-delivery of doxorubicin and miR-542-3p increased both drug uptake and cytotoxicity in triple negative breast cancer cells.

Recently an hydrophilic poly(ethylene glycol)-conjugated poly(lactic-co-glycolic acid) nanoparticle (PLGA-PEG-NP) delivery system has been demonstrated the ability to successfully deliver antisense-miR-21. miR-21 is an oncogenic miRNA involved in tumor initiation, progression, invasion and metastasis in several cancers, including triple negative breast cancer (TNBC). Antisense-miR-21-loaded nanoparticles (NPs) were able to increase the apoptotic effect of orlistat-loaded NPs in triple negative breast cancer cells [98].

An important finding in systemic delivery of anti-miRNA has been reported by Shu D. et al. (2015) which proposed an application of RNA nanotechnology for specific and efficient delivery of anti-miR-21 to block the growth of triple negative breast cancer in orthotopic mouse models [99]. These therapeutic RNA nanoparticles contain an 8-nt sequence complementary to the seed region of miR-21, and a 39-nt sequence complementary to epidermal growth factor receptor (EGFR). They simultaneously target EGFR for internalizing RNA nanoparticles into cancer cells via receptor mediated endocytosis and are able to inhibit miR-21 activity. In addition, these particles demonstrate a resistance toward RNase and are thermodynamically stable, thus remaining intact after systemic injection into mice.

Another tumor which displays a great resistance to chemotherapeutic treatment is glioblastoma. Despite important advances in cancer treatment, which resulted in significant improvement of clinical outcomes, glioblastoma relapse is very frequent and patient survival is 12 to 15 months after diagnosis [100]. Successful *in vivo* delivery of anti-miRNA oligonucleotides to brain tumors requires the carriers not only possessing bioavailability but also overcoming the blood-brain barrier and enhance target cell uptake, while sparing the normal tissues. In this regard, Costa et al. (2015) proposed stable nucleic acid lipid particles (SNALPs) coupled with chlorotoxin (CTX), a scorpion-derived peptide that was reported as a reliable and specific marker for gliomas [101] to the surface of stabilized liposomes, for delivery of anti-miR-21 oligonucleotides to glioblastoma cells [102]. This delivery system enhanced uptake in brain tumors and increased miR-21 silencing, while showing no signs of systemic immunogenicity. Moreover, the systemic treatment with targeted nanoparticle-formulated anti-miR-21 oligonucleotides and sunitinib (a tyrosine kinase inhibitor) decreased tumor cell proliferation and tumor size and enhanced apoptosis in glioblastoma-bearing mice.

2.6 Co-delivery of chemotherapeutic drugs

Multi-targeted strategies are necessary to overcome multidrug resistance mechanisms and several studies have investigated effective combinatorial approaches for cancer treatments. The use of gemcitabine (2,2'-difluorodeoxycytidine; dFdC) in combination with carboplatin to treat patients with advanced, refractory, or recurrent ovarian cancer as well as patients who showed initial

resistance to platin-based treatments has been recently approved by the U.S. Food and Drug Administration (FDA) [103]. However, cancer cells often show a defective transport of gemcitabine. To overcome the transporter defects in ovarian cancer cells, Hung et al. (2015) constructed NPs from poly(d,l-lactic-co-glycolic acid)-block (PLGA-b)-poly(ethylene glycol) (PEG) polymer (PLGA-b-PEG-OH) containing gemcitabine, cisplatin or both compounds [104]. and demonstrated that this construct highly increased the chemotherapeutic efficacy of gemcitabine. Moreover, the delivery of a gemcitabine-cisplatin combination in such nanoparticle formulation increased their synergistic interactions.

Magnetite doped mesoporous silica nanoparticles (MSNs), in which both internal porous and external surface of MSN were respectively exploited to load two different kinds of cytotoxic agents, camptothecin and arsenic trioxide, have been prepared by Muhammad Fet al. (2014) [105]. MSNs were used to inhibit proliferation of BxPC-3 pancreatic cancer cells, which are associated with a low responsiveness to conventional chemotherapies. Results obtained (da molti autori, ci sono moltissimi lavori in letteratura) demonstrated that the cell inhibition performance of dual drug nanoformulation was significantly higher than single drug formulation, possibly due to additional or synergistic effects.

3. Conclusion and future prospective

Studies on the mechanisms involved in chemoresistance are progressing rapidly and new targets for the nanomedicine application are continuously being found. In addition, advancement in the field of nanomedicine has led to the development of several types of nanoparticles able to overcome multidrug resistance mechanisms and re-sensitize cancer cells to the anticancer drug. Multivalent constructs may include both drugs acting on cancer cells in combination with inhibitors of drug efflux, or siRNA against genes involved in specific pathways, in combination with anticancer drugs. Results obtained have demonstrated that nano-drug delivery systems are a versatile platform for delivery of anticancer drugs and for overcoming cancer drug resistance mechanisms, maximizing chemotherapeutic efficacy. However, many multifunctional nano-platforms are still in the initial stage of development and a number of safety issues and therapeutic efficacy issues of the nanomaterials should also be addressed before they enter into clinical trials. During the transition □benchtop-to-clinic□ is also necessary to increase manufacturing reproducibility and overcome the lack of collaboration in innovative research between academia and the pharmaceutical industry.

4. References

[1] Rebutti, M.; Michiels, C. Molecular aspects of cancer cell resistance to chemotherapy. *Biochem. Pharmacol.*, **2013**, 85, 1219-26.

[2] Raguz, S.; Yague, E. Resistance to chemotherapy: new treatments novel insights into an old problem. *Br. J. Cancer*, **2008**, 99, 387-391.

[3] Szakács, G.; Paterson, J.K.; Ludwig, J.A.; Booth-Genthe, C.; Gottesman, M.M. Targeting multidrug resistance in cancer. *Nat. Rev. Drug. Discov.*, **2006**, 5(3), 219-34.

[4] Gottesman, M.M.; Fojo, T; Bates, S.E. Multidrug resistance in cancer: role of ATP-dependent transporters. *Nat. Rev. Cancer*, **2002**, 2, 48-58.

[5] Ween, M.P; Armstrong, M.A.; Oehler, M.K.; Ricciardelli, C. The role of ABC transporters in ovarian cancer progression and chemoresistance. *Crit. Rev. Oncol. Hematol*, **2015**, 96, 220-256.

[6] Wu, C.P.; Hsieh, C.H.; Wu, Y.S. The emergence of drug transporter-mediated multidrug resistance to cancer chemotherapy. *Mol. Pharm.*, **2011**, 8, 1996-2011.

[7] Chen, K.G.; Sikic, B.I. Molecular pathways: regulation and therapeutic implications of multidrug resistance. *Clin. Cancer Res.*, **2012**, 18, 1863-1869.

[8] Daenen, S.; van der Holt, B.; Verhoef, G.E.; Lowenberg, B.; Wijermans, P.W.; Huijgens, P.C. et al. Addition of cyclosporin A to the combination of mitoxantrone and etoposide to overcome resistance to chemotherapy in refractory or relapsing acute myeloid leukaemia: a randomised phase II trial from HOVON, the Dutch-Belgian Haemato-Oncology Working Group for adults. *Leuk. Res.*, **2004**, 28, 1057-1067.

[9] List, A.F.; Kopecky, K.J.; Willman, C.L.; Head, D.R.; Persons, D.L.; Slovak, M.L. et al. Benefit of cyclosporine modulation of drug resistance in patients with poor-risk acute myeloid leukemia: a Southwest Oncology Group study. *Blood*, **2001**, 98, 3212-3220.

- [10] Meng, E.; Hanna, A.; Samant, R.S.; Shevde, L.A. The Impact of Hedgehog Signaling Pathway on DNA Repair Mechanisms in Human Cancer. *Cancers*, **2015**, 7(3), 1333-48.
- [11] Shevde, L.A.; Samant, R.S. Non-classical hedgehog-GLI signaling and its clinical implications. *Int. J. Cancer*, **2014**, 135, 1-6.
- [12] Furfaro, A.L.; Traverso, N.; Domenicotti, C.; Piras, S.; Moretta, L.; Marinari, U.M.; Pronzato, M.A.; Nitti, M. The Nrf2/HO-1 Axis in Cancer Cell Growth and Chemoresistance. *Oxid. Med. Cell. Longev.*, **2016**, 1958174.
- [13] Taguchi, K.; Motohashi, H.; Yamamoto, M. Molecular mechanisms of the Keap1-Nrf2 pathway in stress response and cancer evolution. *Genes Cells*, **2011**, 16, 123-40.
- [14] Itoh, K.; Tong, K.I.; Yamamoto, M. Molecular mechanism activating Nrf2-Keap1 pathway in regulation of adaptive response to electrophiles. *Free Radic. Biol. Med.*, **2004**, 36, 1208-1213.
- [15] No, J.H.; Kim, Y.B.; Song, Y.S. Targeting nrf2 signaling to combat chemoresistance. *J. Cancer Prev.*, **2014**, 19, 111-7.
- [16] Hayden, A.; Douglas, J.; Sommerlad, M.; Andrews, L.; Gould, K.; Hussain, S.; Thomas, G.J.; Packham, G.; Crabb, S.J. The Nrf2 transcription factor contributes to resistance to cisplatin in bladder cancer. *Urol. Oncol.*, **2014**, 32, 806-14.
- [17] Van der Wijst, M.G.; Brown, R.; Rots, M.G. Nrf2, the master redox switch: the Achilles' heel of ovarian cancer? *Biochim. Biophys. Acta.*, **2014**, 1846, 494-509.
- [18] Harvey, K.F.; Zhang, X.; Thomas, D.M. The Hippo pathway and human cancer. *Nat. Rev. Cancer*, **2013**, 13, 246-257.
- [19] Zhao, B.; Li, L.; Tumaneng, K.; Wang, C.Y.; Guan, K.L. A coordinated phosphorylation by Lats and CK1 regulates YAP stability through SCF (beta-TRCP). *Genes Dev.*, **2010**, 24, 72-85.

[20] Zhao, B.; Ye, X.; Yu, J.; Li, L.; Li, W.; Li, S.; Yu, J.; Lin, J.D.; Wang, C.Y.; Chinnaiyan, A.M.; Lai, Z.C.; Guan, K.L. TEAD mediates YAP-dependent gene induction and growth control. *Genes Dev.*, **2008**, *22*, 1962-1971.

[21] Steinhardt, A.A.; Gayyed, M.F.; Klein, A.P.; Dong, J.; Maitra, A.; Pan, D.; Montgomery, E.A.; Anders, R.A. Expression of Yes-associated protein in common solid tumors. *Hum. Pathol.*, **2008**, *39*, 1582-9.

[22] Fernandez-L, A.; Kenney, A.M. The Hippo in the room: a new look at a key pathway in cell growth and transformation. *Cell Cycle*, **2010**, *9*, 2292-9.

[23] Hall, C.A.; Wang, R.; Miao, J.; Oliva, E.; Shen, X.; Wheeler, T.; Hilsenbeck, S.G.; Orsulic, S.; Goode, S. Hippo pathway effector YAP is an ovarian cancer oncogene. *Cancer Res.*, **2010**, *70*, 8517-25.

[24] Ciamporcero, E.; Shen, H.; Ramakrishnan, S.; Yu Ku, S.; Chintala, S.; Shen, L.; Adelaiye, R.; Miles, K.M.; Ullio, C.; Pizzimenti, S.; Daga, M.; Azabdaftari, G.; Attwood, K.; Johnson, C.; Zhang, J.; Barrera, G.; Pili, R. YAP activation protects urothelial cell carcinoma from treatment-induced DNA damage. *Oncogene*, **2015**, *35*, 1541-1553.

[25] Martz, C.A.; Ottina, K.A.; Singleton, K.R. et al. Systematic identification of signaling pathways with potential to confer anticancer drug resistance. *Sci. Signal.*, **2014**, *7*, ra121.

[26] Pelicano, H.; Carney, D.; Huang, P. ROS stress in cancer cells and therapeutic implications. *Drug Resist.*, **2004**, *7*, 97-110.

[27] Fruehauf, J. P.; Meyskens, F. L., Jr. Reactive oxygen species: a breath of life or death? *Clin. Cancer Res.*, **2007**, *13*, 789-794.

[28] Cabello, C. M.; Bair, W. B., 3rd; Wondrak, G. T. Experimental therapeutics: targeting the redox Achilles heel of cancer. *Curr. Opin. Investig. Drugs*, **2007**, *8*, 1022-1037.

[29] Barrera, G. Oxidative stress and lipid peroxidation products in cancer progression and therapy. *ISRN Oncol.*, **2012**, *201*, 137289.

- [30] Trachootham, D.; Alexandre, J.; Huang, P. Targeting cancer cells by ROS-mediated mechanisms: a radical therapeutic approach? *Nat. Rev. Drug Discov.*, **2009**, 8, 579-591.
- Bartel, D.P. MicroRNAs: genomics, biogenesis, mechanism, and function. *Cell*, **2004**, 116, 281-97.
- [31] Calin, G.A.; Croce, C.M. MicroRNA signatures in human cancers. *Nat. Rev. Cancer*, **2006**, 6, 857-66.
- [32] Ventura, A.; Jacks, T. MicroRNAs and cancer: short RNAs go a long way. *Cell*, **2009**, 136, 586-91.
- [33] Kutanzi, K.R. et al. MicroRNA-mediated drug resistance in breast cancer *Clin. Epigenetics*, **2011**, 2, 171-185.
- [34] Kopczyńska, E. Role of microRNAs in the resistance of prostate cancer to docetaxel and paclitaxel. *Contemp. Oncol.*, **2016**, 19(6), 423-7.
- [35] Li, Y.; Sarkar, F.H. MicroRNA Targeted Therapeutic Approach for Pancreatic Cancer. *Int. J. Biol. Sci.*, **2016**, 12(3), 326-37.
- [36] Si, M.L.; Zhu, S.; Wu, H. et al. miR-21-mediated tumor growth. *Oncogene*, **2007**, 26, 2799-803.
- [37] Liu, L.Z.; Li, C.; Chen, Q. MiR-21 induced angiogenesis through AKT and ERK activation and HIF-1 α expression. *PLoS One*, **2011**, 6, 1-9.
- [38] Ali, S.; Ahmad, A.; Banerjee, S. et al. Gemcitabine sensitivity can be induced in pancreatic cancer cells through modulation of miR-200 and miR-21 expression by curcumin or its analogue CDF. *Cancer Res.*, **2010**, 70, 3606-17.
- [39] Roy, S.; Yu, Y.; Padhye, S.B. et al. Difluorinated-curcumin (CDF) restores PTEN expression in colon cancer cells by down-regulating miR-21. *PLoS One*, **2013**, 8, e68543h.

- [40] Chen, J.; Huang, X.F.; Qiao, L. et al. Insulin caused drug resistance to oxaliplatin in colon cancer cell line HT29. *J. Gastrointest. Oncol.*, **2011**, 2, 27-33.
- [41] Dehghanzadeh, R.; Jadidi-Niaragh, F.; Gharibi, T.; Yousefi, M. MicroRNA-induced drug resistance in gastric cancer. *Biomed. Pharmacother.*, **2015**, 74, 191-9.
- [42] Cairns, R.A.; Harris, I.S.; Mak, T.W. Regulation of cancer cell metabolism. *Nature Reviews Cancer*, **2011**, 11, 85-95.
- [43] Lunt, S. J.; Chaudary, N. & Hill, R. P. The tumor microenvironment and metastatic disease. *Clin. Exp. Metastasis*, **2009**, 26, 19-34.
- [44] Bi, M. et al. ER stress-regulated translation increases tolerance to extreme hypoxia and promotes tumor growth. *EMBO J.*, **2015**, 24, 3470-3481.
- [45] Mohindra, J.K.; Rauth, A.M. Increased cell killing by metronidazole and nitrofurazone of hypoxic compared to aerobic mammalian cells. *Cancer Res.*, **1976**, 36, 930-6
- [46] Koch, S.; Mayer, F.; Honecker, F.; Schittenhelm, M.; Bokemeyer, C. Efficacy of cytotoxic agents used in the treatment of testicular germ cell tumours under normoxic and hypoxic conditions in vitro. *Br. J. Cancer*, **2003**, 89, 2133-9.
- [47] Griffiths, J.R.; McIntyre, D.J.; Howe, F.A.; Stubbs, M. Why are cancers acidic? A carrier-mediated diffusion model for H⁺ transport in the interstitial fluid. *Novartis Found Symp*, **2001**; 240, 46-62; discussion 62-47, 152-3.
- [48] Mahoney, B.P.; Raghunand, N.; Baggett, B.; Gillies, R.J. Tumor acidity, ion trapping and chemotherapeutics. I. Acid pH affects the distribution of chemotherapeutic agents in vitro. *Biochem. Pharmacol.*, **2003**, 66, 1207-18.
- [49] Mimeault, M.; Batra, S.K. Potential molecular therapeutic targets in cancer stem/progenitor cells: are ATP-binding cassette membrane transporters appropriate targets to eliminate cancer-initiating cells? In: *Stem Cell Biology in Health and Disease*; T. Dittmar, K.S. Zanker, Eds.; Springer Science + Business Media B.V: Dordrecht, 2010; Vol. 17, pp. 385-421.

[50] Khdair, A.; Handa, H.; Mao, G.; Panyam, J. Nanoparticle-mediated combination chemotherapy and photodynamic therapy overcomes tumor drug resistance in vitro. *Eur. J. Pharm. Biopharm.*, **2009**, 71, 214–222.

[51] Song, X.; Cai, Z.; Zheng, Y.; He, G.; Cui, F.; Gong, D. et al. Reversion of multidrug resistance by co-encapsulation of vincristine and verapamil in PLGA nanoparticles. *Eur. J. Pharm. Sci.*, **2009**, 37, 300–305.

[52] Wu, J.; Lu, Y.; Lee, A.; Pan, X.; Yang, X.; Zhao, X. et al. Reversal of multidrug resistance by transferrin-conjugated liposomes co-encapsulating doxorubicin and verapamil. *J. Pharmacol. Pharm. Sci.*, **2007**, 10, 350–357.

[53] Man, H.B.; Kim, H.; Kim, H.J.; Robinson, E.; Liu, W.K.; Chow, E.K.; Ho, D. Synthesis of nanodiamond-daunorubicin conjugates to overcome multidrug chemoresistance in leukemia. *Nanomedicine*, **2014**, 10(2), 359–69.

[54] Toh, T.B.; Lee, D.K.; Hou, W.; Abdullah, L.N.; Nguyen, J.; Ho, D.; Chow, E.K. Nanodiamond-mitoxantrone complexes enhance drug retention in chemoresistant breast cancer cells. *Mol. Pharm.*, **2014**, 11(8), 2683–91.

[55] Wang, X.; Low, X.C.; Hou, W.; Abdullah, L.N.; Toh, T.B.; Mohd Abdul Rashid, M.; Ho, D.; Chow, E.K. Epirubicin-adsorbed nanodiamonds kill chemoresistant hepatic cancer stem cells. *ACS Nano*, **2014**, 8(12), 12151–66.

[56] Kovács, D.; Széke, K.; Igaz, N.; Spengler, G.; Molnár, J.; Tóth, T.; Madarász, D.; Rázga, Z.; Kónya, Z.; Boros, I.M.; Kiricsi, M. Silver nanoparticles modulate ABC transporter activity and enhance chemotherapy in multidrug resistant cancer. *Nanomedicine*, **2016**, 12(3), 601–610.

[57] Fan, L.; Li, F.; Zhang, H.T.; Wang, Y.K.; Cheng, C.; Li, X.Y. et al. Co-delivery of PDTC and doxorubicin by multifunctional micellar nanoparticles to achieve active targeted drug delivery and overcome multidrug resistance. *Biomaterials*, **2010**, 31, 5634–5642.

- [58] Xiong, X.; Arvizo, R.R.; Saha, S.; Robertson, D.J.; McMeekin, S.; Bhattacharya, R.; Mukherjee, P. Sensitization of ovarian cancer cells to cisplatin by gold nanoparticles. *Oncotarget*, **2014**, 5(15), 6453-65.
- [59] Bajak, E.; Fabbri, M.; Ponti, J.; Gioria, S.; Ojea-Jiménez, I.; Collotta, A.; Mariani, V.; Gilliland, D.; Rossi, F.; Gribaldo, L. Changes in Caco-2 cells transcriptome profiles upon exposure to gold nanoparticles. *Toxicol. Lett.*, **2015**, 233(2), 187-99.
- [60] Sabzichi, M.; Hamishehkar, H.; Ramezani, F.; Sharifi, S.; Tabasinezhad, M.; Pirouzpanah, M.; Ghanbari, P.; Samadi, N. Luteolin-loaded phytosomes sensitize human breast carcinoma MDA-MB 231 cells to doxorubicin by suppressing Nrf2 mediated signalling. *Asian. Pac. J. Cancer Prev.*, **2014**, 15(13), 5311-6.
- [61] Kobayashi, C.I.; Suda, T. Regulation of reactive oxygen species in stem cells and cancer stem cells. *J. Cell. Physiol.*, **2012**, 227(2), 421-30.
- [62] Cheng, R.; Feng, F.; Meng, F.; Deng, C.; Feijen, J.; Zhong, Z. Glutathione-responsive nano-vehicles as a promising platform for targeted intracellular drug and gene delivery. *J. Control Release*, **2011**, 152, 2-12.
- [63] Trotta, F.; Caldera, F.; Dianzani, C.; Argenziano, M.; Barrera, G.; Cavalli, R. Glutathione Bioresponsive Cyclodextrin Nanosponges. *Chempluschem*. DOI: 10.1002/cplu.201500531.
- [64] Nguyen, K.C.; Willmore, W.G.; Tayabali, A.F. Cadmium telluride quantum dots cause oxidative stress leading to extrinsic and intrinsic apoptosis in hepatocellular carcinoma HepG2 cells. *Toxicology*, **2013**, 306, 114-23.
- [65] Singh, B.R.; Singh, B.N.; Khan, W.; Singh, H.B.; Naqvi, A.H. ROS-mediated apoptotic cell death in prostate cancer LNCaP cells induced by biosurfactant stabilized CdS quantum dots. *Biomaterials*, **2012**, 33, 5753-67.

- [66] Cheng, G.; Guo, W.; Han, L. et al. Cerium oxide nanoparticles induce cytotoxicity in human hepatoma SMMC-7721 cells via oxidative stress and the activation of MAPK signaling pathways. *Toxicol. In Vitro*, **2013**, *27*, 1082-8.
- [67] Nogueira, D.R.; Rolim, C.M.; Farooqi, A.A. Nanoparticle induced oxidative stress in cancer cells: adding new pieces to an incomplete jigsaw puzzle. *Asian. Pac. J. Cancer Prev.*, **2014**, *15*(12), 4739-43.
- [68] Aryal, S.; Hu, C.M.; Zhang, L. Polymer--cisplatin conjugate nanoparticles for acid-responsive drug delivery. *ACS Nano.*, **2010**, *4*(1), 251-8.
- [69] Leite, E.A.; Souza, C.M.; Carvalho-Júnior, A.D.; Coelho, L.G.; Lana, A.M.; Cassali, G.D.; Oliveira, M.C. Encapsulation of cisplatin in long-circulating and pH-sensitive liposomes improves its antitumor effect and reduces acute toxicity. *Int. J. Nanomedicine*, **2012**, *7*, 5259-69.
- [70] Wu, H.; Zhu, L.; Torchilin, V.P. pH-sensitive poly (histidine)-PEG/DSPE-PEG co-polymer micelles for cytosolic drug delivery. *Biomaterials*, **2013**, *34*, 1213-1222.
- [71] Wu, Y.; Chen, W.; Meng, F.; Wang, Z.; Cheng, R.; Deng, C.; Liu, H.; Zhong, Z. Core-crosslinked pH-sensitive degradable micelles: A promising approach to resolve the extracellular stability versus intracellular drug release dilemma. *J. Control Release*, **2012**, *164*(3), 338-45.
- [72] Qiu, L.; Qiao, M.; Chen, Q.; Tian, C.; Long, M.; Wang, M. et al. Enhanced effect of pH-sensitive mixed copolymer micelles for overcoming multidrug resistance of doxorubicin. *Biomaterials*, **2014**, *35*, 9877-9887.
- [73] Nogueira, D.R.; Scheeren, L.E.; Macedo, L.B.; Marcolino, A.I.; Pilar Vinardell, M.; Mitjans, M.; Rosa Infante, M.; Farooqi, A.A.; Rolim, C.M. Inclusion of a pH-responsive amino acid-based amphiphile in methotrexate-loaded chitosan nanoparticles as a delivery strategy in cancer therapy. *Amino Acids*, **2016**, *48*(1), 157-68.
- [74] Hao, N. B.; Lu, M. H.; Fan, Y. H.; Cao, Y. L.; Zhang, Z. R.; Yang, S. M. Macrophages in Tumor Microenvironments and the Progression of Tumors. *Clin. Dev. Immunol.*, **2012**, 948098.

- [75] Martinez, F. O.; Sica, A.; Mantovani, A.; Locati, M. Macrophage Activation and Polarization. *Front. Biosci.*, **2008**, 13, 453-461.
- [76] Song, M.; Liu, T.; Shi, C.; Zhang, X.; Chen, X. Bioconjugated Manganese Dioxide Nanoparticles Enhance Chemotherapy Response by Priming Tumor-Associated Macrophages toward M1-like Phenotype and Attenuating Tumor Hypoxia. *ACS Nano.*, **2016**, 10(1), 633-47.
- [77] Elbashir, S.M. et al. Duplexes of 21-nucleotide RNAs mediate RNA interference in cultured mammalian cells. *Nature*, **2001**, 411, 494-498.
- [78] Ambros, V. The functions of animal microRNAs. *Nature*, **2004**, 431(7006), 350-5.
- [79] Zhang, B.; Pan, X.; Cobb, G.P.; Anderson, T.A. microRNAs as oncogenes and tumor suppressors. *Dev. Biol.*, **2007**, 302(1), 1-12.
- [80] Young, S.W.; Stenzel, M.; Jia-Lin, Y. Nanoparticle-siRNA: A potential cancer therapy? *Crit. Rev. Oncol. Hematol.*, **2016**, 98, 159-69.
- [81] Zhang, Y.; Satterlee, A.; Huang, L. In vivo gene delivery by nonviral vectors: overcoming hurdles? *Mol. Ther.*, **2012**, 20(7), 1298-304.
- [82] Shields, N.; Dodd, K. J.; Abblitt, C. Do children with Down Syndrome perform sufficient physical activity to maintain good health? A pilot study. *Adapt. Phys. Act. Q.*, **2009**, 26(4), 307-20
- [83] Wong, H.L.; Shen, Z.; Lu, Z.; Wientjes, M.G.; Au, J.L. Paclitaxel tumor-priming enhances siRNA delivery and transfection in 3-dimensional tumor cultures. *Mol. Pharm.*, **2011**, 8, 833-840.
- [84] Wang, J.; Lu, Z.; Wang, J.; Cui, M.; Yeung, B.Z.; Cole, D.J.; Wientjes, M.G.; Au, J.L. Paclitaxel tumor priming promotes delivery and transfection of intravenous lipid-siRNA in pancreatic tumors. *J. Control Release*, **2015**, 216, 103-10.
- [85] Wu, S.Y.; McMillan, N.A.J. Lipidic systems for in vivo siRNA delivery. *AAPS Journal*, **2009**, 11(4), 639-652.

- [86] Landen, C.N.Jr., Chavez-Reyes, A.; Bucana, C. et al. Therapeutic EphA2 gene targeting in vivo using neutral liposomal small interfering RNA delivery. *Cancer Research*, **2005**, 65(15), 6910-6918.
- [87] Thaker, P.H.; Deavers, M.; Celestino, J. et al. EphA2 expression is associated with aggressive features in ovarian carcinoma. *Clin. Cancer Res.*, **2004**, 10, 5145-50.
- [88] Lee, J.M.; Yoon, T.J.; Cho, Y.S. Recent developments in nanoparticle-based siRNA delivery for cancer therapy. *BioMed. Res. Int.*, **2013**, p. 10.
- [89] Xu, C.F.; Zhang, H.B.; Sun, C.Y.; Liu, Y.; Shen, S.; Yang, X.Z.; Zhu, Y.H.; Wang, J. Tumor acidity-sensitive linkage-bridged block copolymer for therapeutic siRNA delivery. *Biomaterials*, **2016**, 88, 48-59.
- [90] Xu, X.; Xie, K.; Zhang, X.Q.; Pridgen, E.M.; Park, G.Y.; Cui, D.S.; Shi, J.; Wu, J.; Kantoff, P.W.; Lippard, S.J.; Langer, R.; Walker, G.C.; Farokhzad, O.C. Enhancing tumor cell response to chemotherapy through nanoparticle-mediated codelivery of siRNA and cisplatin prodrug. *Proc. Natl. Acad. Sci. USA*, **2013**, 110(46), 18638-43.
- [91] Zhuo, X.; Chang, A.; Huang, C.; Yang, L.; Zhao, H.; Wu, Y.; Zhou, Q. Nanoparticle-mediated down-regulation of TWIST increases radiosensitivity of nasopharyngeal carcinoma cells via ERK pathway. *Am. J. Cancer Res.*, **2015**, 5(4), 1571-9.
- [92] Chen, Y.; Li, L.; Zeng, J.; Wu, K.; Zhou, J.; Guo, P.; Zhang, D.; Xue, Y.; Liang, L.; Wang, X.; Chang, L.S.; He, D. Twist confers chemoresistance to anthracyclines in bladder cancer through upregulating P-glycoprotein. *Chemotherapy*, **2012**, 58, 264-272.
- [93] Li, F.; Mahato, R.I. RNA interference for improving the outcome of islet transplantation. *Adv. Drug Delivery Rev.*, **2011**, 63(1-2), 47-68.
- [94] Li, F.; Mahato, R.I. MicroRNAs and drug resistance in prostate cancers. *Mol. Pharm.*, **2014**, 11(8), 2539-52.

- [95] Schneider, B.P.; Winer, E.P.; Foulkes, W.D.; Garber, J.; Perou, C.M.; Richardson, A. Triple-negative breast cancer: risk factors to potential targets. *Clin. Cancer Res.*, **2008**, *14*, 8010–8018.
- [96] Liedtke, C.; Mazouni, C.; Hess, K.R.; André, F.; Tordai, A.; Mejia, J.A. Response to neoadjuvant therapy and long-term survival in patients with triple-negative breast cancer. *J. Clin. Oncol.*, **2008**, *26*, 1275–1281.
- [97] Wang, S.; Zhang, J.; Wang, Y.; Chen, M. Hyaluronic acid-coated PEI-PLGA nanoparticles mediated co-delivery of doxorubicin and miR-542-3p for triple negative breast cancer therapy. *Nanomedicine*, **2015**, *12*, 411-420.
- [98] Bhargava-Shah, A.; Foygel, K.; Devulapally, R.; Paulmurugan, R. Orlistat and antisense-miRNA-loaded PLGA-PEG nanoparticles for enhanced triple negative breast cancer therapy. *Nanomedicine*, **2016**, *11*(3), 235-47.
- [99] Shu, D.; Li, H.; Shu, Y.; Xiong, G.; Carson, W.E.; Haque, F.; Xu, R.; Guo, P. Systemic Delivery of Anti-miRNA for Suppression of Triple Negative Breast Cancer Utilizing RNA Nanotechnology. *ACS Nano.*, **2015**, *9*(10), 9731-40.
- [100] Wen, P.Y.; Kesari, S. Malignant gliomas in adults. *N. Engl. J. Med.*, **2008**, *359*, 492–507.
- [101] Mamelak, A.N.; Jacoby, D.B. Targeted delivery of antitumoral therapy to glioma and other malignancies with synthetic chlorotoxin (TM-601). *Expert Opin. Drug Deliv.*, **2007**, *4*, 175–186.
- [102] Costa, P.M.; Cardoso, A.L.; Custódia, C.; Cunha, P.; Pereira de Almeida, L.; Pedroso de Lima, M.C. MiRNA-21 silencing mediated by tumor-targeted nanoparticles combined with sunitinib: A new multimodal gene therapy approach for glioblastoma. *J. Control Release*, **2015**, *207*, 31-9.
- [103] Pazdur, R. National Cancer Institute at the National Institutes of Health. FDA Approval for Gemcitabine Hydrochloride. <http://www.cancer.gov/cancertopics/druginfo/fda-gemcitabine-hydrochloride> (Accessed 2011).

[104] Hung, S.W.; Marrache, S.; Cummins, S.; Bhutia, Y.D.; Mody, H.; Hooks, S.B.; Dhar, S.; Govindarajan, R. Defective hCNT1 transport contributes to gemcitabine chemoresistance in ovarian cancer subtypes: overcoming transport defects using a nanoparticle approach. *Cancer Lett.*, **2015**, 359(2), 233-40.

[105] Muhammad, F.; Zhao, J.; Wang, N.; Guo, M.; Wang, A.; Chen, L.; Guo, Y.; Li, Q.; Zhu, G. Lethal drug combination: arsenic loaded multiple drug mesoporous silica for theranostic applications. *Colloids Surf. B Biointerfaces*, **2014**, 123 506-14.

Bibliography

- Aalberts, Marian, Federica M.F van Dissel-Emiliani, Nick P.H van Adrichem, Merel van Wijnen, Marca H.M Wauben, Tom A.E Stout, and Willem Stoorvogel. 2012. "Identification of Distinct Populations of Prostatomes That Differentially Express Prostate Stem Cell Antigen, Annexin A1, and GLIPR2 in Humans1." *Biology of Reproduction* 86 (3). doi:10.1095/biolreprod.111.095760.
- Adair, James H., Mylisa P. Parette, Erhan İ. Altinoğlu, and Mark Kester. 2010. "Nanoparticulate Alternatives for Drug Delivery." *ACS Nano* 4 (9): 4967–70. doi:10.1021/nn102324e.
- Adamska, Aleksandra, Alice Domenichini, and Marco Falasca. 2017. "Pancreatic Ductal Adenocarcinoma: Current and Evolving Therapies." *International Journal of Molecular Sciences*. doi:10.3390/ijms18071338.
- Ahmed, Rana Z, Gunjan Patil, and Zahid Zaheer. 2013. "Nanosponges - a Completely New Nano-Horizon: Pharmaceutical Applications and Recent Advances." *Drug Development and Industrial Pharmacy* 39 (9): 1263–72. doi:10.3109/03639045.2012.694610.
- Alivisatos, Paul. 2004. "The Use of Nanocrystals in Biological Detection." *Nature Biotechnology*. doi:10.1038/nbt927.
- Amer, Magid H. 2014. "Gene Therapy for Cancer: Present Status and Future Perspective." *Molecular and Cellular Therapies* 2 (1): 27. doi:10.1186/2052-8426-2-27.
- American Pharmaceutical Partners. n.d. "Product Information. Abraxane (Paclitaxel Protein-Bound)."
- Anand, Preetha, Ajaikumar B Kunnumakara, Chitra Sundaram, Kuzhuvelil B Harikumar, Sheeja T Tharakan, Oiki S Lai, Bokyoung Sung, and Bharat B Aggarwal. 2008. "Cancer Is a Preventable Disease That Requires Major Lifestyle Changes." *Pharmaceutical Research*. doi:10.1007/s11095-008-9661-9.
- Andaloussi, Samir EL, Imre Mäger, Xandra O Breakefield, and Matthew J A Wood. 2013. "Extracellular Vesicles: Biology and Emerging Therapeutic Opportunities." *Nature Reviews. Drug Discovery* 12 (5): 347–57. doi:10.1038/nrd3978.
- Andre, Fabrice, Noel EC Scharz, Mojgan Movassagh, Caroline Flament, Patricia Pautier, Philippe Morice, Christophe Pomel, et al. 2002. "Malignant Effusions and Immunogenic Tumour-Derived Exosomes." *The Lancet* 360

- (9329): 295–305. doi:10.1016/S0140-6736(02)09552-1.
- Asea, Alexander, Claudel Jean-Pierre, Punit Kaur, Preethi Rao, Iara M. Linhares, Daniel Skupski, and Steven S. Witkin. 2008. "Heat Shock Protein-Containing Exosomes in Mid-Trimester Amniotic Fluids." *Journal of Reproductive Immunology* 79 (1): 12–17. doi:10.1016/j.jri.2008.06.001.
- Ashkar, S, G F Weber, V Panoutsakopoulou, M E Sanchirico, M Jansson, S Zawaideh, S R Rittling, D T Denhardt, M J Glimcher, and H Cantor. 2000. "Eta-1 (Osteopontin): An Early Component of Type-1 (Cell-Mediated) Immunity." *Science (New York, N.Y.)* 287 (5454): 860–64. <http://www.ncbi.nlm.nih.gov/pubmed/10657301>.
- Atai, Nadia A., Manju Bansal, Cheungh Lo, Joost Bosman, Wikky Tigchelaar, Klazien S. Bosch, Ard Jonker, et al. 2011. "Osteopontin Is up-Regulated and Associated with Neutrophil and Macrophage Infiltration in Glioblastoma." *Immunology* 132 (1): 39–48. doi:10.1111/j.1365-2567.2010.03335.x.
- Baaten, Bas J G, Roberto Tinoco, Alex T Chen, and Linda M Bradley. 2012. "Regulation of Antigen-Experienced T Cells: Lessons from the Quintessential Memory Marker CD44." *Frontiers in Immunology* 3: 23. doi:10.3389/fimmu.2012.00023.
- Babic, Michal, Daniel Horák, Miroslava Trchová, Pavla Jendelová, Katerina Glogarová, Petr Lesný, Vít Herynek, Milan Hájek, and Eva Syková. 2008. "Poly(L-Lysine)-Modified Iron Oxide Nanoparticles for Stem Cell Labeling." *Bioconjugate Chemistry* 19 (3): 740–50. doi:10.1021/bc700410z.
- Babst, Markus, David J. Katzmann, Eden J. Estepa-Sabal, Timo Meerloo, and Scott D. Emr. 2002. "Escrt-III." *Developmental Cell* 3 (2): 271–82. doi:10.1016/S1534-5807(02)00220-4.
- Bacac, Marina, and Ivan Stamenkovic. 2008. "Metastatic Cancer Cell." *Annual Review of Pathology* 3: 221–47. doi:10.1146/annurev.pathmechdis.3.121806.151523.
- Bailar, J C, and H L Gornik. 1997. "Cancer Undefeated." *The New England Journal of Medicine* 336 (22): 1569–74. doi:10.1056/NEJM199705293362206.
- Baldi, Giovanni, Costanza Ravagli, Filippo Mazzantini, George Loudos, Jaume Adan, Marc Masa, Dimitrios Psimadas, et al. 2014. "In Vivo Anticancer Evaluation of the Hyperthermic Efficacy of Anti-Human Epidermal Growth Factor Receptor-Targeted PEG-Based Nanocarrier Containing Magnetic Nanoparticles." *International Journal of Nanomedicine* 9: 3037–56. doi:10.2147/IJN.S61273.
- Bandopadhyay, Monalisa, Anuradha Bulbule, Ramesh Butti, Goutam

- Chakraborty, Priyanka Ghorpade, Pompom Ghosh, Mahadeo Gorain, et al. 2014. "Osteopontin as a Therapeutic Target for Cancer." *Expert Opinion on Therapeutic Targets* 18 (8): 883–95. doi:10.1517/14728222.2014.925447.
- Barth, Rolf F, Jeffrey A Coderre, M Graça H Vicente, and Thomas E Blue. 2005. "Boron Neutron Capture Therapy of Cancer: Current Status and Future Prospects." *Clinical Cancer Research : An Official Journal of the American Association for Cancer Research* 11 (11): 3987–4002. doi:10.1158/1078-0432.CCR-05-0035.
- Beachy, Philip A, Sunil S Karhadkar, and David M Berman. 2004. "Tissue Repair and Stem Cell Renewal in Carcinogenesis." *Nature* 432 (7015): 324–31. doi:10.1038/nature03100.
- Beausoleil, Michel S, Erika B Schulze, David Goodale, Carl O Postenka, and Alison L Allan. 2011. "Deletion of the Thrombin Cleavage Domain of Osteopontin Mediates Breast Cancer Cell Adhesion, Proteolytic Activity, Tumorigenicity, and Metastasis." *BMC Cancer* 11 (1): 25. doi:10.1186/1471-2407-11-25.
- Becker, Andrew E, Yasmin G Hernandez, Harold Frucht, and Aimee L Lucas. 2014. "Pancreatic Ductal Adenocarcinoma: Risk Factors, Screening, and Early Detection." *World Journal of Gastroenterology* 20 (32): 11182–98. doi:10.3748/wjg.v20.i32.11182.
- Beilin, Orit, Dimitrios M Karussis, Amos D Korczyn, David Gurwitz, Ramona Aronovich, Daniel Hantai, Nikolaos Grigoriadis, Rachel Mizrachi-Kol, and Joab Chapman. 2005. "Increased Thrombin Inhibition in Experimental Autoimmune Encephalomyelitis." *Journal of Neuroscience Research* 79 (3): 351–59. doi:10.1002/jnr.20270.
- Bellavista, Elena, Aurelia Santoro, Daniela Galimberti, Cristoforo Comi, Fabio Luciani, and Michele Mishto. 2014. "Current Understanding on the Role of Standard and Immunoproteasomes in Inflammatory/Immunological Pathways of Multiple Sclerosis." *Autoimmune Diseases* 2014: 1–12. doi:10.1155/2014/739705.
- Belpomme, D, P Irigaray, L Hardell, R Clapp, L Montagnier, S Epstein, and A J Sasco. 2007. "The Multitude and Diversity of Environmental Carcinogens." *Environmental Research*. doi:10.1016/j.envres.2007.07.002.
- Ben-Nissan, Gili, and Michal Sharon. 2014. "Regulating the 20S Proteasome Ubiquitin-Independent Degradation Pathway." *Biomolecules* 4 (3): 862–84. doi:10.3390/biom4030862.
- Benton, Michael J, Michelle L Malott, Scott S Knight, Charles M Cooper, and William H Benson. 1995. "Influence of Sediment Composition on

- Apparent Toxicity in a Solid-phase Test Using Bioluminescent Bacteria.” *Environmental Toxicology and Chemistry* 14 (3): 411–14. doi:10.1002/etc.5620140309.
- Berrington de Gonzalez, A, S Sweetland, and E Spencer. 2003. “A Meta-Analysis of Obesity and the Risk of Pancreatic Cancer.” *British Journal of Cancer* 89 (3): 519–23. doi:10.1038/sj.bjc.6601140.
- Bharali, Dhruva J, Marianne Khalil, Mujgan Gurbuz, Tessa M Simone, and Shaker A Mousa. 2009. “Nanoparticles and Cancer Therapy: A Concise Review with Emphasis on Dendrimers.” *International Journal of Nanomedicine*. doi:10.2147/IJN.S4241.
- Bilensoy, Erem, Oya Gürkaynak, Mevlut Ertan, Murat Sen, and A Atilla Hincal. 2008. “Development of Nonsurfactant Cyclodextrin Nanoparticles Loaded with Anticancer Drug Paclitaxel.” *Journal of Pharmaceutical Sciences* 97 (4): 1519–29. doi:10.1002/jps.21111.
- Blanchard, N, D Lankar, F Faure, A Regnault, C Dumont, G Raposo, and C Hivroz. 2002. “TCR Activation of Human T Cells Induces the Production of Exosomes Bearing the TCR/CD3/ Complex.” *The Journal of Immunology* 168 (7): 3235–41. doi:10.4049/jimmunol.168.7.3235.
- Bocci, Guido, Antonello Di Paolo, and Romano Danesi. 2013. “The Pharmacological Bases of the Antiangiogenic Activity of Paclitaxel.” *Angiogenesis* 16 (3): 481–92. doi:10.1007/s10456-013-9334-0.
- Boggio, Elena, Chiara Dianzani, Casimiro Luca Gigliotti, Maria Felicia Soluri, Nausicaa Clemente, Giuseppe Cappellano, Erika Toth, et al. 2016. “Thrombin Cleavage of Osteopontin Modulates Its Activities in Human Cells In Vitro and Mouse Experimental Autoimmune Encephalomyelitis In Vivo.” *Journal of Immunology Research* 2016: 1–13. doi:10.1155/2016/9345495.
- Borges, F, L Reis, and N Schor. 2013. “Extracellular Vesicles: Structure, Function and Potential Clinical Uses in Renal Diseases.” *Brazilian Journal of Medical and Biological Research* 46 (10): 824–30. doi:10.1590/1414-431X20132964.
- Bose, D, MH Katz, and JB Fleming. 2012. “The MD Anderson Cancer Center Surgical Oncology Handbook.” In *Pancreatic Adenocarcinoma*.
- Brandi, Giovanni, Guido Biasco, Maria Grazia Mirarchi, Rita Golfieri, Antonello Di Paolo, Alberto Borghi, Silvia Fanello, et al. 2011. “A Phase I Study of Continuous Hepatic Arterial Infusion of Irinotecan in Patients with Locally Advanced Hepatocellular Carcinoma.” *Digestive and Liver Disease : Official Journal of the Italian Society of Gastroenterology and the Italian Association for the Study of the Liver* 43 (12): 1015–21.

doi:10.1016/j.dld.2011.08.005.

- Brocke, S, C Piercy, L Steinman, I L Weissman, and T Veromaa. 1999. "Antibodies to CD44 and Integrin alpha4, but Not L-Selectin, Prevent Central Nervous System Inflammation and Experimental Encephalomyelitis by Blocking Secondary Leukocyte Recruitment." *Proceedings of the National Academy of Sciences of the United States of America* 96 (12): 6896–6901. <http://www.ncbi.nlm.nih.gov/pubmed/10359810>.
- Brown, Amanda. 2012. "Osteopontin: A Key Link between Immunity, Inflammation and the Central Nervous System." *Translational Neuroscience* 3 (3). doi:10.2478/s13380-012-0028-7.
- Brown, Darren M, and Erkki Ruoslahti. 2004. "Metadherin, a Cell Surface Protein in Breast Tumors That Mediates Lung Metastasis." *Cancer Cell* 5 (4): 365–74. doi:10.1016/S1535-6108(04)00079-0.
- Budczies, Jan, Moritz Von Winterfeld, Frederick Klauschen, Manfred Dietel, Ioannis Anagnostopoulos, and Wilko Weichert. 2014. "The Landscape of Metastatic Progression Patterns across Major Human Cancers." *Oncotarget* 6 (1): 570–83. doi:10.18632/oncotarget.2677.
- Burke, Thomas G., Awadesh K. Mishra, Mansukh C. Wani, and Monroe E. Wall. 1993. "Lipid Bilayer Partitioning and Stability of Camptothecin Drugs." *Biochemistry* 32 (20): 5352–64. doi:10.1021/bi00071a010.
- Burris, H A, A Awada, J G Kuhn, J R Eckardt, P W Cobb, D A Rinaldi, S Fields, L Smith, and D D Von Hoff. 1994. "Phase I and Pharmacokinetic Studies of Topotecan Administered as a 72 or 120 H Continuous Infusion." *Anti-Cancer Drugs* 5 (4): 394–402. <http://www.ncbi.nlm.nih.gov/pubmed/7949242>.
- Buschow, Sonja I, Esther N M Nolte-‘t Hoen, Guillaume van Niel, Maaïke S Pols, Toine ten Broeke, Marjolein Lauwen, Ferry Ossendorp, et al. 2009. "MHC II in Dendritic Cells Is Targeted to Lysosomes or T Cell-Induced Exosomes Via Distinct Multivesicular Body Pathways." *Traffic* 10 (10): 1528–42. doi:10.1111/j.1600-0854.2009.00963.x.
- Caby, Marie-Pierre, Danielle Lankar, Claude Vincendeau-Scherrer, Graça Raposo, and Christian Bonnerot. 2005. "Exosomal-like Vesicles Are Present in Human Blood Plasma." *International Immunology* 17 (7): 879–87. doi:10.1093/intimm/dxh267.
- Cai, Huaqing, Karin Reinisch, and Susan Ferro-Novick. 2007. "Coats, Tethers, Rabs, and SNAREs Work Together to Mediate the Intracellular Destination of a Transport Vesicle." *Developmental Cell* 12 (5): 671–82. doi:10.1016/j.devcel.2007.04.005.

- Caldera, Fabrizio, Maria Tannous, Roberta Cavalli, Marco Zanetti, and Francesco Trotta. 2017. "Evolution of Cyclodextrin Nanosponges." *International Journal of Pharmaceutics* 531 (2): 470–79. doi:10.1016/j.ijpharm.2017.06.072.
- Calle, Eugenia E, Carmen Rodriguez, Kimberly Walker-Thurmond, and Michael J Thun. 2003. "Overweight, Obesity, and Mortality from Cancer in a Prospectively Studied Cohort of U.S. Adults." *New England Journal of Medicine* 348 (17): 1625–38. doi:10.1056/NEJMoa021423.
- Calogero, Raffaele Adolfo, Francesca Cordero, Guido Forni, and Federica Cavallo. 2007. "Inflammation and Breast Cancer. Inflammatory Component of Mammary Carcinogenesis in ErbB2 Transgenic Mice." *Breast Cancer Research* 9 (4): 211. doi:10.1186/bcr1745.
- "Cancer, Fact Sheet." 2017. <http://who.int/mediacentre/factsheets/fs297/en/>.
- Cannella, B, and C S Raine. 1995. "The Adhesion Molecule and Cytokine Profile of Multiple Sclerosis Lesions." *Annals of Neurology* 37 (4): 424–35. doi:10.1002/ana.410370404.
- Carlo, E Di, M G Diodoro, K Boggio, A Modesti, M Modesti, P Nanni, G Forni, and P Musiani. 1999. "Analysis of Mammary Carcinoma Onset and Progression in HER-2/neu Oncogene Transgenic Mice Reveals a Lobular Origin." *Laboratory Investigation; a Journal of Technical Methods and Pathology* 79 (10): 1261–69. <http://www.ncbi.nlm.nih.gov/pubmed/10532589>.
- Castello, Luigi Mario, Davide Raineri, Livia Salmi, Nausicaa Clemente, Rosanna Vaschetto, Marco Quaglia, Massimiliano Garzaro, et al. 2017. "Osteopontin at the Crossroads of Inflammation and Tumor Progression." *Mediators of Inflammation* 2017: 1–22. doi:10.1155/2017/4049098.
- Cavalli, R, M Argenziano, and C Dianzani. 2014. "Disulfide Nanosponges as Innovative Glutathione-Responsive Nanocarrier for Doxorubicin Delivery." In *41st CRS Meeting, Chicago*, 13–16. Chicago.
- Cavalli, Roberta, M Rosa Gasco, Patrizia Chetoni, Susi Burgalassi, and M Fabrizio Saettone. 2002. "Solid Lipid Nanoparticles (SLN) as Ocular Delivery System for Tobramycin." *International Journal of Pharmaceutics* 238 (1–2): 241–45. doi:10.1016/S0378-5173(02)00080-7.
- Cavalli, Roberta, Francesco Trotta, and Wander Tumiatti. 2006. "Cyclodextrin-Based Nanosponges for Drug Delivery." *Journal of Inclusion Phenomena and Macrocyclic Chemistry* 56 (1–2): 209–13. doi:10.1007/s10847-006-9085-2.
- Cel-Sci. n.d. "Limitations of Current Immunotherapies." http://www.cel-sci.com/limitations_of_current_immunotherapies.html.

- Cevc, Gregor. 1996. "Transfersomes, Liposomes and Other Lipid Suspensions on the Skin: Permeation Enhancement, Vesicle Penetration, and Transdermal Drug Delivery." *Critical Reviews™ in Therapeutic Drug Carrier Systems* 13 (3–4): 257–388.
doi:10.1615/CritRevTherDrugCarrierSyst.v13.i3-4.30.
- Chabas, D, S E Baranzini, D Mitchell, C C Bernard, S R Rittling, D T Denhardt, R A Sobel, et al. 2001. "The Influence of the Proinflammatory Cytokine, Osteopontin, on Autoimmune Demyelinating Disease." *Science (New York, N.Y.)* 294 (5547): 1731–35. doi:10.1126/science.1062960.
- Chairoungdua, Arthit, Danielle L Smith, Pierre Pochard, Michael Hull, and Michael J Caplan. 2010. "Exosome Release of β -Catenin: A Novel Mechanism That Antagonizes Wnt Signaling." *The Journal of Cell Biology* 190 (6): 1079–91. doi:10.1083/jcb.201002049.
- Chambers, Ann F, Alan C Groom, and Ian C MacDonald. 2002. "Dissemination and Growth of Cancer Cells in Metastatic Sites." *Nature Reviews Cancer*. doi:10.1038/nrc865.
- Chiocchetti, Annalisa, Cristoforo Comi, Manuela Indelicato, Luca Castelli, Riccardo Mesturini, Thea Bensi, Maria C Mazzarino, et al. 2005. "Osteopontin Gene Haplotypes Correlate with Multiple Sclerosis Development and Progression." *Journal of Neuroimmunology* 163 (1–2): 172–78. doi:10.1016/j.jneuroim.2005.02.020.
- Cho, Hyun-Ju, Hyun-Jai Cho, and Hyo-Soo Kim. 2009. "Osteopontin: A Multifunctional Protein at the Crossroads of Inflammation, Atherosclerosis, and Vascular Calcification." *Current Atherosclerosis Reports* 11 (3): 206–13. <http://www.ncbi.nlm.nih.gov/pubmed/19361352>.
- Choi, Angela O, Sung Ju Cho, Julie Desbarats, Jasmina Lovrić, and Dusica Maysinger. 2007. "Quantum Dot-Induced Cell Death Involves Fas Upregulation and Lipid Peroxidation in Human Neuroblastoma Cells." *Journal of Nanobiotechnology* 5: 1. doi:10.1186/1477-3155-5-1.
- Chourpa, I, J M Millot, G D Sockalingum, J F Riou, and M Manfait. 1998. "Kinetics of Lactone Hydrolysis in Antitumor Drugs of Camptothecin Series as Studied by Fluorescence Spectroscopy." *Biochimica et Biophysica Acta* 1379 (3): 353–66. <http://www.ncbi.nlm.nih.gov/pubmed/9545598>.
- Chow, Shein Chung. 2013. "Assessing Biosimilarity and Interchangeability of Biosimilar Products." *Statistics in Medicine* 32 (3): 361–63. doi:10.1002/sim.5577.
- Christensen, Brian, Torben E Petersen, and Esben S Sørensen. 2008. "Post-Translational Modification and Proteolytic Processing of Urinary Osteopontin." *The Biochemical Journal* 411 (1): 53–61.

doi:10.1042/BJ20071021.

- Clark, E A, T R Golub, E S Lander, and R O Hynes. 2000. "Genomic Analysis of Metastasis Reveals an Essential Role for RhoC." *Nature* 406 (6795): 532–35. doi:10.1038/35020106.
- Clemente, Nausicaa, Cristoforo Comi, Davide Raineri, Giuseppe Cappellano, Domizia Vecchio, Elisabetta Orilieri, Casimiro L Gigliotti, et al. 2017. "Role of Anti-Osteopontin Antibodies in Multiple Sclerosis and Experimental Autoimmune Encephalomyelitis." *Frontiers in Immunology* 8: 321. doi:10.3389/fimmu.2017.00321.
- Clemente, Nausicaa, Davide Raineri, Giuseppe Cappellano, Elena Boggio, Francesco Favero, Maria Felicia Soluri, Chiara Dianzani, Cristoforo Comi, Umberto Dianzani, and Annalisa Chiocchetti. 2016. "Osteopontin Bridging Innate and Adaptive Immunity in Autoimmune Diseases." *Journal of Immunology Research* 2016: 7675437. doi:10.1155/2016/7675437.
- Cocucci, Emanuele, Gabriella Racchetti, and Jacopo Meldolesi. 2009. "Shedding Microvesicles: Artefacts No More." *Trends in Cell Biology* 19 (2): 43–51. doi:10.1016/j.tcb.2008.11.003.
- Comi, Cristoforo, Giuseppe Cappellano, Annalisa Chiocchetti, Elisabetta Orilieri, Sara Buttini, Laura Ghezzi, Daniela Galimberti, et al. 2012. "The Impact of Osteopontin Gene Variations on Multiple Sclerosis Development and Progression." *Clinical and Developmental Immunology* 2012: 1–6. doi:10.1155/2012/212893.
- Conroy, Thierry, Françoise Desseigne, Marc Ychou, Olivier Bouché, Rosine Guimbaud, Yves Bécouarn, Antoine Adenis, et al. 2011. "FOLFIRINOX versus Gemcitabine for Metastatic Pancreatic Cancer." *New England Journal of Medicine* 364 (19): 1817–25. doi:10.1056/NEJMoa1011923.
- Conti, Laura, Roberto Ruiu, Giuseppina Barutello, Marco Macagno, Silvio Bandini, Federica Cavallo, and Stefania Lanzardo. 2014. "Microenvironment, Oncoantigens, and Antitumor Vaccination: Lessons Learned from BALB-neuT Mice." *BioMed Research International* 2014: 1–16. doi:10.1155/2014/534969.
- Cook, Amy C, Alan B Tuck, Susan McCarthy, Joel G Turner, Rosalyn B Irby, Gregory C Bloom, Timothy J Yeatman, and Ann F Chambers. 2005. "Osteopontin Induces Multiple Changes in Gene Expression That Reflect the Six 'hallmarks of Cancer' in a Model of Breast Cancer Progression." *Molecular Carcinogenesis* 43 (4): 225–36. doi:10.1002/mc.20105.
- Cooper, Geoffrey M. 2000. *The Cell: A Molecular Approach 2nd Edition*. Sinauer Associates. doi:NBK9839.
- Costa-Silva, Bruno, Nicole M Aiello, Allyson J Ocean, Swarnima Singh, Haiying

- Zhang, Basant Kumar Thakur, Annette Becker, et al. 2015. "Pancreatic Cancer Exosomes Initiate Pre-Metastatic Niche Formation in the Liver." *Nature Cell Biology* 17 (6): 816–26. doi:10.1038/ncb3169.
- Coulson, A, A Levy, and M Gossell-Williams. 2014. "Monoclonal Antibodies in Cancer Therapy: Mechanisms, Successes and Limitations." *West Indian Medical Journal*. doi:10.7727/wimj.2013.241.
- Coux, O, K Tanaka, and A L Goldberg. 1996. "Structure and Functions of the 20S and 26S Proteasomes." *Annual Review of Biochemistry* 65: 801–47. doi:10.1146/annurev.bi.65.070196.004101.
- Craik, David J, David P Fairlie, Spiros Liras, and David Price. 2013. "The Future of Peptide-Based Drugs." *Chemical Biology and Drug Design* 81 (1): 136–47. doi:10.1111/cbdd.12055.
- Crouch, S P M, R Kozlowski, K J Slater, and J Fletcher. 1993. "The Use of ATP Bioluminescence as a Measure of Cell Proliferation and Cytotoxicity." *Journal of Immunological Methods* 160 (1): 81–88. doi:10.1016/0022-1759(93)90011-U.
- Daga, Martina, Chiara Ullio, Monica Argenziano, Chiara Dianzani, Roberta Cavalli, Francesco Trotta, Carlo Ferretti, et al. 2016. "GSH-Targeted Nanosponges Increase Doxorubicin-Induced Toxicity 'in Vitro' and 'in Vivo' in Cancer Cells with High Antioxidant Defenses." *Free Radical Biology & Medicine* 97 (August): 24–37. doi:10.1016/j.freeradbiomed.2016.05.009.
- Dai, J, L Peng, K Fan, H Wang, R Wei, G Ji, J Cai, et al. 2009. "Osteopontin Induces Angiogenesis through Activation of PI3K/AKT and ERK1/2 in Endothelial Cells." *Oncogene* 28 (38): 3412–22. doi:10.1038/onc.2009.189.
- Das, Riku, Ganapati H Mahabeleshwar, and Gopal C Kundu. 2003. "Osteopontin Stimulates Cell Motility and Nuclear Factor kappaB-Mediated Secretion of Urokinase Type Plasminogen Activator through Phosphatidylinositol 3-kinase/Akt Signaling Pathways in Breast Cancer Cells." *The Journal of Biological Chemistry* 278 (31): 28593–606. doi:10.1074/jbc.M303445200.
- Davalos, Dimitrios, Jae Kyu Ryu, Mario Merlini, Kim M. Baeten, Natacha Le Moan, Mark A. Petersen, Thomas J. Deerinck, et al. 2012. "Fibrinogen-Induced Perivascular Microglial Clustering Is Required for the Development of Axonal Damage in Neuroinflammation." *Nature Communications* 3 (November): 1227. doi:10.1038/ncomms2230.
- Davis, Mark E, Zhuo Chen, and Dong M Shin. 2008. "Nanoparticle Therapeutics: An Emerging Treatment Modality for Cancer." *Nature*

Reviews Drug Discovery. doi:10.1038/nrd2614.

- Delaney, Geoff, Susannah Jacob, Carolyn Featherstone, and Michael Barton. 2005. "The Role of Radiotherapy in Cancer Treatment: Estimating Optimal Utilization from a Review of Evidence-Based Clinical Guidelines." *Cancer* 104 (6): 1129–37. doi:10.1002/cncr.21324.
- Denzer, K, M van Eijk, M J Kleijmeer, E Jakobson, C de Groot, and H J Geuze. 2000. "Follicular Dendritic Cells Carry MHC Class II-Expressing Microvesicles at Their Surface." *Journal of Immunology (Baltimore, Md. : 1950)* 165 (3): 1259–65. <http://www.ncbi.nlm.nih.gov/pubmed/10903724>.
- Deregibus, M. C., V. Cantaluppi, R. Calogero, M. Lo Iacono, C. Tetta, L. Biancone, S. Bruno, B. Bussolati, and G. Camussi. 2007. "Endothelial Progenitor Cell Derived Microvesicles Activate an Angiogenic Program in Endothelial Cells by a Horizontal Transfer of mRNA." *Blood* 110 (7): 2440–48. doi:10.1182/blood-2007-03-078709.
- Desai, Bhavik, Michael J Rogers, and Meenakshi A Chellaiah. 2007. "Mechanisms of Osteopontin and CD44 as Metastatic Principles in Prostate Cancer Cells." *Molecular Cancer* 6 (March): 18. doi:10.1186/1476-4598-6-18.
- Deun, Jan Van, Pieter Mestdagh, Raija Sormunen, Veronique Cocquyt, Karim Vermaelen, Jo Vandesompele, Marc Bracke, Olivier De Wever, and An Hendrix. 2014. "The Impact of Disparate Isolation Methods for Extracellular Vesicles on Downstream RNA Profiling." *Journal of Extracellular Vesicles* 3 (1): 24858. doi:10.3402/jev.v3.24858.
- Dianzani, Chiara, Elena Bellavista, Juliane Liepe, Claudia Verderio, Morena Martucci, Aurelia Santoro, Annalisa Chiocchetti, et al. 2017. "Extracellular Proteasome-Osteopontin Circuit Regulates Cell Migration with Implications in Multiple Sclerosis." *Scientific Reports* 7: 43718. doi:10.1038/srep43718.
- Distler, M, D Aust, J Weitz, C Pilarsky, and Robert Grützmann. 2014. "Precursor Lesions for Sporadic Pancreatic Cancer: PanIN, IPMN, and MCN." *BioMed Research International* 2014: 1–11. doi:10.1155/2014/474905.
- Drewnowski, A, and B M Popkin. 1997. "The Nutrition Transition: New Trends in the Global Diet." *Nutr Rev.* 55 (0029–6643 (Print)): 31–43. doi:10.1111/j.1753-4887.1997.tb01593.x.
- Duchêne, Dominique. 2011. "Cyclodextrins and Their Inclusion Complexes." In *Cyclodextrins in Pharmaceuticals, Cosmetics, and Biomedicine*, 1–18. Hoboken, NJ, USA: John Wiley & Sons, Inc. doi:10.1002/9780470926819.ch1.

- Duffy, M J, P M McGowan, and W M Gallagher. 2008. "Cancer Invasion and Metastasis: Changing Views." *The Journal of Pathology*. doi:10.1002/path.2282.
- Dutta, Suman, Onrapak Reamtong, Wittaya Panvongsa, Sarunya Kitdumrongthum, Keatdamrong Janpipatkul, Polkit Sangvanich, Pawinee Piyachaturawat, and Arthit Chairoungdua. 2015. "Proteomics Profiling of Cholangiocarcinoma Exosomes: A Potential Role of Oncogenic Protein Transferring in Cancer Progression." *Biochimica et Biophysica Acta (BBA) - Molecular Basis of Disease* 1852 (9): 1989–99. doi:10.1016/j.bbadis.2015.06.024.
- Ebstein, Frédéric, Peter-Michael Kloetzel, Elke Krüger, and Ulrike Seifert. 2012. "Emerging Roles of Immunoproteasomes beyond MHC Class I Antigen Processing." *Cellular and Molecular Life Sciences : CMLS* 69 (15): 2543–58. doi:10.1007/s00018-012-0938-0.
- Egerer, Karl, Ulrike Kuckelkorn, Paul E Rudolph, Jens C Rückert, Thomas Dörner, Gerd-R Burmester, Peter-M Kloetzel, and Eugen Feist. 2002. "Circulating Proteasomes Are Markers of Cell Damage and Immunologic Activity in Autoimmune Diseases." *The Journal of Rheumatology* 29 (10): 2045–52. <http://www.ncbi.nlm.nih.gov/pubmed/12375310>.
- Euliss, Larken E, Stephanie G Grancharov, Stephen O'Brien, Timothy J Deming, Galen D Stucky, C B Murray, and G A Held. 2003. "Cooperative Assembly of Magnetic Nanoparticles and Block Copolypeptides in Aqueous Media." *Nano Letters* 3 (11): 1489–93. doi:10.1021/nl034472y.
- Everhart, J, and D Wright. n.d. "Diabetes Mellitus as a Risk Factor for Pancreatic Cancer. A Meta-Analysis." *JAMA* 273 (20): 1605–9. <http://www.ncbi.nlm.nih.gov/pubmed/7745774>.
- Fard, J K, Samira Jafari, Mohammad Ali Eghbal, Javad Khalili Fard, Samira Jafari, and Mohammad Ali Eghbal. 2015. "A Review of Molecular Mechanisms Involved in Toxicity of Nanoparticles." *Advanced Pharmaceutical Bulletin* 5 (4): 447–54. doi:10.15171/apb.2015.061.
- Farid, Suzanne S. 2007. "Process Economics of Industrial Monoclonal Antibody Manufacture." *Journal of Chromatography B: Analytical Technologies in the Biomedical and Life Sciences*. doi:10.1016/j.jchromb.2006.07.037.
- Fassberg, J, and V J Stella. 1992. "A Kinetic and Mechanistic Study of the Hydrolysis of Camptothecin and Some Analogues." *Journal of Pharmaceutical Sciences* 81 (7): 676–84. <http://www.ncbi.nlm.nih.gov/pubmed/1403703>.
- Fauré, J, G Lachenal, M Court, J Hirrlinger, C Chatellard-Causse, B Blot, J Grange, et al. 2006. "Exosomes Are Released by Cultured Cortical

- Neurones." *Molecular and Cellular Neuroscience* 31 (4): 642–48.
doi:10.1016/j.mcn.2005.12.003.
- Ferlay, J, I Soerjomataram, M Ervik, R Dikshit, S Eser, C Mathers, M Rebelo, D M Parkin, D Forman, and F Bray. 2013. "GLOBOCAN 2012 v1.0, Cancer Incidence and Mortality Worldwide: IARC CancerBase. No. 11 [Internet]." *Lyon, France: International Agency for Research on Cancer.*
doi:10.1016/j.ucl.2013.01.011.
- Ferrington, Deborah A, and Dale S Gregerson. 2012. "Immunoproteasomes: Structure, Function, and Antigen Presentation." *Progress in Molecular Biology and Translational Science* 109: 75–112. doi:10.1016/B978-0-12-397863-9.00003-1.
- Fischer, Janine, Marc H Proscenc, Martin Wolff, Norbert Hort, Regine Willumeit, and Frank Feyerabend. 2010. "Interference of Magnesium Corrosion with Tetrazolium-Based Cytotoxicity Assays." *Acta Biomaterialia* 6 (5): 1813–23. doi:10.1016/j.actbio.2009.10.020.
- Fok, T C, H Lapointe, A B Tuck, A F Chambers, L Jackson-Boeters, T D Daley, and M R Darling. 2014. "Expression and Localization of Osteopontin, Homing Cell Adhesion molecule/CD44, and Integrin $\alpha\beta 3$ in Mucoepidermoid Carcinoma and Acinic Cell Adenocarcinoma of Salivary Gland Origin." *Oral Surgery, Oral Medicine, Oral Pathology and Oral Radiology* 118 (3): 320–29. doi:10.1016/j.oooo.2014.05.004.
- Folkman, J. 1971. "Tumor Angiogenesis: Therapeutic Implications." *The New England Journal of Medicine* 285 (21): 1182–86.
doi:10.1056/NEJM197111182852108.
- Force, Jeremy, and April Salama. 2017. "First-Line Treatment of Metastatic Melanoma: Role of Nivolumab." *ImmunoTargets and Therapy* Volume 6 (February): 1–10. doi:10.2147/ITT.S110479.
- Fotakis, George, and John A Timbrell. 2006. "In Vitro Cytotoxicity Assays: Comparison of LDH, Neutral Red, MTT and Protein Assay in Hepatoma Cell Lines Following Exposure to Cadmium Chloride." *Toxicology Letters* 160 (2): 171–77. doi:10.1016/j.toxlet.2005.07.001.
- Franchini, Massimo, and Pier Mannuccio Mannucci. 2012. "Thrombin and Cancer: From Molecular Basis to Therapeutic Implications." *Seminars in Thrombosis and Hemostasis* 38 (1): 95–101. doi:10.1055/s-0031-1300955.
- Friedman, Adam D, Sarah E Claypool, and Rihe Liu. 2013. "The Smart Targeting of Nanoparticles." *Current Pharmaceutical Design* 19 (35): 6315–29.
doi:10.2174/13816128113199990375.
- Fuchs, C S, G A Colditz, M J Stampfer, E L Giovannucci, D J Hunter, E B Rimm, W C Willett, and F E Speizer. 1996. "A Prospective Study of Cigarette

- Smoking and the Risk of Pancreatic Cancer." *Archives of Internal Medicine* 156 (19): 2255–60. <http://www.ncbi.nlm.nih.gov/pubmed/8885826>.
- Furger, K A, R K Menon, A B Tuck, V H Bramwell, and A F Chambers. 2001. "The Functional and Clinical Roles of Osteopontin in Cancer and Metastasis." *Current Molecular Medicine* 1 (5): 621–32. <http://www.ncbi.nlm.nih.gov/pubmed/11899236>.
- Gapstur, S M, P H Gann, W Lowe, K Liu, L Colangelo, and A Dyer. 2000. "Abnormal Glucose Metabolism and Pancreatic Cancer Mortality." *JAMA* 283 (19): 2552–58. <http://www.ncbi.nlm.nih.gov/pubmed/10815119>.
- Garcia-Carbonero, Rocio, and Jeffrey G Supko. 2002. "Current Perspectives on the Clinical Experience, Pharmacology, and Continued Development of the Camptothecins." *Clinical Cancer Research : An Official Journal of the American Association for Cancer Research* 8 (3): 641–61. <http://www.ncbi.nlm.nih.gov/pubmed/11895891>.
- Gigliotti, Casimiro Luca, Benedetta Ferrara, Sergio Occhipinti, Elena Boggio, Giuseppina Barrera, Stefania Pizzimenti, Mirella Giovarelli, et al. 2017. "Enhanced Cytotoxic Effect of Camptothecin Nanosponges in Anaplastic Thyroid Cancer Cells in Vitro and in Vivo on Orthotopic Xenograft Tumors." *Drug Delivery* 24 (1): 670–80. doi:10.1080/10717544.2017.1303856.
- Gigliotti, Casimiro Luca, Rosalba Minelli, Roberta Cavalli, Sergio Occhipinti, Giuseppina Barrera, Stefania Pizzimenti, Giuseppe Cappellano, et al. 2016. "In Vitro and In Vivo Therapeutic Evaluation of Camptothecin-Encapsulated β -Cyclodextrin Nanosponges in Prostate Cancer." *Journal of Biomedical Nanotechnology* 12 (1): 114–27. <http://www.ncbi.nlm.nih.gov/pubmed/27301177>.
- Gilligan, Timothy D, Jerome Seidenfeld, Ethan M Basch, Lawrence H Einhorn, Timothy Fancher, David C Smith, Andrew J Stephenson, et al. 2010. "American Society of Clinical Oncology Clinical Practice Guideline on Uses of Serum Tumor Markers in Adult Males with Germ Cell Tumors." *Journal of Clinical Oncology : Official Journal of the American Society of Clinical Oncology* 28 (20): 3388–3404. doi:10.1200/JCO.2009.26.4481.
- Gomez-Roldan, Victoria, Soraya Fermas, Philip B Brewer, Virginie Puech-Pagès, Elizabeth A Dun, Jean-Paul Pillot, Fabien Letisse, et al. 2008. "Strigolactone Inhibition of Shoot Branching." *Nature* 455 (7210): 189–94. doi:10.1038/nature07271.
- Gotoh, Masahiro, Michiie Sakamoto, Kengo Kanetaka, Makoto Chuuma, and Setsuo Hirohashi. 2002. "Overexpression of Osteopontin in Hepatocellular Carcinoma." *Pathology International* 52 (1): 19–24.

<http://www.ncbi.nlm.nih.gov/pubmed/11940202>.

- Gourgou-Bourgade, Sophie, Caroline Bascoul-Mollevi, Françoise Desseigne, Marc Ychou, Olivier Bouché, Rosine Guimbaud, Yves Bécouarn, et al. 2013. "Impact of FOLFIRINOX Compared with Gemcitabine on Quality of Life in Patients with Metastatic Pancreatic Cancer: Results from the PRODIGE 4/ACCORD 11 Randomized Trial." *Journal of Clinical Oncology : Official Journal of the American Society of Clinical Oncology* 31 (1): 23–29. doi:10.1200/JCO.2012.44.4869.
- Gradishar, William J, Sergei Tjulandin, Neville Davidson, Heather Shaw, Neil Desai, Paul Bhar, Michael Hawkins, and Joyce O'Shaughnessy. 2005. "Phase III Trial of Nanoparticle Albumin-Bound Paclitaxel Compared with Polyethylated Castor Oil-Based Paclitaxel in Women with Breast Cancer." *Journal of Clinical Oncology* 23 (31): 7794–7803. doi:10.1200/JCO.2005.04.937.
- Grassinger, Jochen, David N Haylock, Melonie J Storan, Gemma O Haines, Brenda Williams, Genevieve A Whitty, Andrew R Vinson, et al. 2009. "Thrombin-Cleaved Osteopontin Regulates Hemopoietic Stem and Progenitor Cell Functions through Interactions with α 9 β 1 and α 4 β 1 Integrins." *Blood* 114 (1): 49–59. doi:10.1182/blood-2009-01-197988.
- Grayson, Scott M, and Jean M J Fréchet. 2001. "Convergent Dendrons and Dendrimers: From Synthesis to Applications." *Chemical Reviews*. doi:10.1021/cr990116h.
- Green, M R, G M Manikhas, S Orlov, B Afanasyev, A M Makhson, P Bhar, and M J Hawkins. 2006. "Abraxane(R), a Novel Cremophor(R)-Free, Albumin-Bound Particle Form of Paclitaxel for the Treatment of Advanced Non-Small-Cell Lung Cancer." *Annals of Oncology* 17 (8): 1263–68. doi:10.1093/annonc/mdl104.
- Green, Philip M., Steven B. Ludbrook, David D. Miller, Carmel M.T. Horgan, and Simon T. Barry. 2001. "Structural Elements of the Osteopontin SVVYGLR Motif Important for the Interaction with α 4 Integrins." *FEBS Letters* 503 (1): 75–79. doi:10.1016/S0014-5793(01)02690-4.
- Greenhalf, W, C Grocock, M Marcus, and J Neoptolemos. 2009. "Screening of High-Risk Families for Pancreatic Cancer." *Pancreatology* 9 (3): 215–22. doi:10.1159/000210262.
- Groettrup, Marcus, Christopher J Kirk, and Michael Basler. 2010. "Proteasomes in Immune Cells: More than Peptide Producers?" *Nature Reviews. Immunology* 10 (1): 73–78. doi:10.1038/nri2687.
- Gross, Julia Christina, Varun Chaudhary, Kerstin Bartscherer, and Michael

- Boutros. 2012. "Active Wnt Proteins Are Secreted on Exosomes." *Nature Cell Biology* 14 (10): 1036–45. doi:10.1038/ncb2574.
- Gupta, Ajay Kumar, and Adam S G Curtis. 2004. "Lactoferrin and Ceruloplasmin Derivatized Superparamagnetic Iron Oxide Nanoparticles for Targeting Cell Surface Receptors." *Biomaterials* 25 (15): 3029–40. doi:10.1016/j.biomaterials.2003.09.095.
- Gupta, Ajay Kumar, and Mona Gupta. 2005. "Synthesis and Surface Engineering of Iron Oxide Nanoparticles for Biomedical Applications." *Biomaterials*. doi:10.1016/j.biomaterials.2004.10.012.
- György, Bence, Tamás G Szabó, Mária Pásztói, Zsuzsanna Pál, Petra Misják, Borbála Aradi, Valéria László, et al. 2011. "Membrane Vesicles, Current State-of-the-Art: Emerging Role of Extracellular Vesicles." *Cellular and Molecular Life Sciences* 68 (16): 2667–88. doi:10.1007/s00018-011-0689-3.
- Halperin, Daniel M, and Gauri R Varadhachary. 2014. "Resectable, Borderline Resectable, and Locally Advanced Pancreatic Cancer: What Does It Matter?" *Current Oncology Reports* 16 (2): 366. doi:10.1007/s11912-013-0366-9.
- Hanahan, D, G Bergers, and E Bergsland. 2000. "Less Is More, Regularly: Metronomic Dosing of Cytotoxic Drugs Can Target Tumor Angiogenesis in Mice." *The Journal of Clinical Investigation* 105 (8): 1045–47. doi:10.1172/JCI9872.
- Hansel, Trevor T, Harald Kropshofer, Thomas Singer, Jane A Mitchell, and Andrew J T George. 2010. "The Safety and Side Effects of Monoclonal Antibodies." *Nat Rev Drug Discov* 9 (4): 325–38. doi:10.1038/nrd3003.
- Harding, C, J Heuser, and P Stahl. 1984. "Endocytosis and Intracellular Processing of Transferrin and Colloidal Gold-Transferrin in Rat Reticulocytes: Demonstration of a Pathway for Receptor Shedding." *European Journal of Cell Biology* 35 (2): 256–63. <http://www.ncbi.nlm.nih.gov/pubmed/6151502>.
- Harris, Lyndsay, Herbert Fritsche, Robert Mennel, Larry Norton, Peter Ravdin, Sheila Taube, Mark R Somerfield, Daniel F Hayes, Robert C Bast, and American Society of Clinical Oncology. 2007. "American Society of Clinical Oncology 2007 Update of Recommendations for the Use of Tumor Markers in Breast Cancer." *Journal of Clinical Oncology : Official Journal of the American Society of Clinical Oncology* 25 (33): 5287–5312. doi:10.1200/JCO.2007.14.2364.
- Hasegawa, Masahiro, Tatsuya Segawa, Masahiro Maeda, Toshimichi Yoshida, and Akihiro Sudo. 2011. "Thrombin-Cleaved Osteopontin Levels in

- Synovial Fluid Correlate with Disease Severity of Knee Osteoarthritis." *The Journal of Rheumatology* 38 (1): 129–34. doi:10.3899/jrheum.100637.
- Heijnen, H F, A E Schiel, R Fijnheer, H J Geuze, and J J Sixma. 1999. "Activated Platelets Release Two Types of Membrane Vesicles: Microvesicles by Surface Shedding and Exosomes Derived from Exocytosis of Multivesicular Bodies and Alpha-Granules." *Blood* 94 (11): 3791–99. <http://www.ncbi.nlm.nih.gov/pubmed/10572093>.
- Henry, L, T Lavabre-Bertrand, L Vercambre, J Ramos, S Carillo, I Guiraud, P Poudroux, et al. 2009. "Plasma Proteasome Level Is a Reliable Early Marker of Malignant Transformation of Liver Cirrhosis." *Gut* 58 (6): 833–38. doi:10.1136/gut.2008.157016.
- Henry, Laurent, Cécile Fabre, Isabelle Guiraud, Sophie Bastide, Pascale Fabbro-Peray, Jean Martinez, Thierry Lavabre-Bertrand, Laurent Meunier, and Pierre-Emmanuel Stoebner. 2013. "Clinical Use of P-Proteasome in Discriminating Metastatic Melanoma Patients: Comparative Study with LDH, MIA and S100B Protein." *International Journal of Cancer* 133 (1): 142–48. doi:10.1002/ijc.27991.
- Henry, N. Lynn, and Daniel F. Hayes. 2012. "Cancer Biomarkers." *Molecular Oncology* 6 (2): 140–46. doi:10.1016/j.molonc.2012.01.010.
- Hertzberg, R P, M J Caranfa, and S M Hecht. 1989. "On the Mechanism of Topoisomerase I Inhibition by Camptothecin: Evidence for Binding to an Enzyme-DNA Complex." *Biochemistry* 28 (11): 4629–38. <http://www.ncbi.nlm.nih.gov/pubmed/2548584>.
- Hess, C, S Sadallah, A Hefti, R Landmann, and J A Schifferli. 1999. "Ectosomes Released by Human Neutrophils Are Specialized Functional Units." *Journal of Immunology (Baltimore, Md. : 1950)* 163 (8): 4564–73. <http://www.ncbi.nlm.nih.gov/pubmed/10510400>.
- Hess, Kenneth R, Gauri R Varadhachary, Sarah H Taylor, Wei Wei, Martin N Raber, Renato Lenzi, and James L Abbruzzese. 2006. "Metastatic Patterns in Adenocarcinoma." *Cancer* 106 (7): 1624–33. doi:10.1002/cncr.21778.
- Hezel, Aram F, Alec C Kimmelman, Ben Z Stanger, Nabeel Bardeesy, and Ronald a Depinho. 2006. "Genetics and Biology of Pancreatic Ductal Adenocarcinoma Genetics and Biology of Pancreatic Ductal Adenocarcinoma." *Genes & Development* 1: 1218–49. doi:10.1101/gad.1415606.
- Hidalgo, Manuel. 2010. "Pancreatic Cancer." *The New England Journal of Medicine* 362 (17): 1605–17. doi:10.1056/NEJMra0901557.
- Hocking, Christopher M, and Timothy J Price. 2014. "Panitumumab in the Management of Patients with KRAS Wild-Type Metastatic Colorectal

- Cancer." *Therapeutic Advances in Gastroenterology* 7 (1): 20–37.
doi:10.1177/1756283X13498660.
- Hoff, Daniel D Von, Thomas Ervin, Francis P Arena, E Gabriela Chiorean, Jeffrey Infante, Malcolm Moore, Thomas Seay, et al. 2013. "Increased Survival in Pancreatic Cancer with Nab-Paclitaxel plus Gemcitabine." *The New England Journal of Medicine* 369 (18): 1691–1703.
doi:10.1056/NEJMoa1304369.
- Holash, J, P C Maisonpierre, D Compton, P Boland, C R Alexander, D Zagzag, G D Yancopoulos, and S J Wiegand. 1999. "Vessel Cooption, Regression, and Growth in Tumors Mediated by Angiopoietins and VEGF." *Science (New York, N.Y.)* 284 (5422): 1994–98.
<http://www.ncbi.nlm.nih.gov/pubmed/10373119>.
- Holme, P A, N O Solum, F Brosstad, M Røger, and M Abdelnoor. 1994. "Demonstration of Platelet-Derived Microvesicles in Blood from Patients with Activated Coagulation and Fibrinolysis Using a Filtration Technique and Western Blotting." *Thrombosis and Haemostasis* 72 (5): 666–71.
<http://www.ncbi.nlm.nih.gov/pubmed/7900071>.
- Hood, Joshua L, Roman Susana San, and Samuel A Wickline. 2011. "Exosomes Released by Melanoma Cells Prepare Sentinel Lymph Nodes for Tumor Metastasis." *Cancer Research* 71 (11): 3792–3801. doi:10.1158/0008-5472.CAN-10-4455.
- Horák, Daniel, Bohuslav Rittich, Alena Španová, and Milan J Beneš. 2005. "Magnetic Microparticulate Carriers with Immobilized Selective Ligands in DNA Diagnostics." In *Polymer*, 46:1245–55.
doi:10.1016/j.polymer.2004.11.049.
- Hristov, M. 2004. "Apoptotic Bodies from Endothelial Cells Enhance the Number and Initiate the Differentiation of Human Endothelial Progenitor Cells in Vitro." *Blood* 104 (9): 2761–66. doi:10.1182/blood-2003-10-3614.
- Hu-Lieskovan, Siwen, Jeremy D Heidel, Derek W Bartlett, Mark E Davis, and Timothy J Triche. 2005. "Sequence-Specific Knockdown of EWS-FLI1 by Targeted, Nonviral Delivery of Small Interfering RNA Inhibits Tumor Growth in a Murine Model of Metastatic Ewing's Sarcoma." *Cancer Research* 65 (19): 8984–92. doi:10.1158/0008-5472.CAN-05-0565.
- Hu, D D, E C Lin, N L Kovach, J R Hoyer, and J W Smith. 1995. "A Biochemical Characterization of the Binding of Osteopontin to Integrins Alpha v Beta 1 and Alpha v Beta 5." *The Journal of Biological Chemistry* 270 (44): 26232–38. <http://www.ncbi.nlm.nih.gov/pubmed/7592829>.
- Huang, Xiaohua, Prashant K Jain, Ivan H El-Sayed, and Mostafa A El-Sayed. 2007. "Gold Nanoparticles: Interesting Optical Properties and Recent

- Applications in Cancer Diagnostics and Therapy.” *Nanomedicine (London, England)* 2 (5): 681–93. doi:10.2217/17435889.2.5.681.
- Humber, C E, J F Tierney, R P Symonds, M Collingwood, J Kirwan, C Williams, and J A Green. 2007. “Chemotherapy for Advanced, Recurrent or Metastatic Endometrial Cancer: A Systematic Review of Cochrane Collaboration.” *Annals of Oncology : Official Journal of the European Society for Medical Oncology* 18 (3): 409–20. doi:10.1093/annonc/mdl417.
- Hur, Eun Mi, Sawsan Youssef, M Edward Haws, Susan Y Zhang, Raymond A Sobel, and Lawrence Steinman. 2007. “Osteopontin-Induced Relapse and Progression of Autoimmune Brain Disease through Enhanced Survival of Activated T Cells.” *Nature Immunology* 8 (1): 74–83. doi:10.1038/ni1415.
- Hurwitz, Herbert, Louis Fehrenbacher, William Novotny, Thomas Cartwright, John Hainsworth, William Heim, Jordan Berlin, et al. 2004. “Bevacizumab plus Irinotecan, Fluorouracil, and Leucovorin for Metastatic Colorectal Cancer.” *The New England Journal of Medicine* 350 (23): 2335–42. doi:10.1056/NEJMoa032691.
- Iczkowski, Kenneth A. 2010. “Cell Adhesion Molecule CD44: Its Functional Roles in Prostate Cancer.” *American Journal of Translational Research* 3 (1): 1–7. <http://www.ncbi.nlm.nih.gov/pubmed/21139802>.
- Iero, M, R Valenti, V Huber, P Filipazzi, G Parmiani, S Fais, and L Rivoltini. 2008. “Tumour-Released Exosomes and Their Implications in Cancer Immunity.” *Cell Death and Differentiation* 15 (1): 80–88. doi:10.1038/sj.cdd.4402237.
- Iezzi, Manuela, Raffaele A. Calogero, Michela Spadaro, Piero Musiani, Guido Forni, and Federica Cavallo, eds. 2012. “BALB-neuT Female Mice as a Dynamic Model of Mammary Cancer.” In *Translational Animal Models in Drug Discovery and Development*, 139–66. BENTHAM SCIENCE PUBLISHERS. doi:10.2174/978160805469511201010139.
- Inoue, Makoto, and Mari L Shinohara. 2011. “Intracellular Osteopontin (iOPN) and Immunity.” *Immunologic Research* 49 (1–3): 160–72. doi:10.1007/s12026-010-8179-5.
- Irby, R B, S M McCarthy, and T J Yeatman. 2004. “Osteopontin Regulates Multiple Functions Contributing to Human Colon Cancer Development and Progression.” *Clinical & Experimental Metastasis* 21 (6): 515–23. <http://www.ncbi.nlm.nih.gov/pubmed/15679049>.
- Irving, Bob. 2007. “Nanoparticle Drug Delivery Systems.” *Innovations in Pharmaceutical Technology*, no. 24.
- Ito, Naomi, Hideaki Obata, and Shigeru Saito. 2009. “Spinal Microglial Expression and Mechanical Hypersensitivity in a Postoperative Pain

- Model: Comparison with a Neuropathic Pain Model." *Anesthesiology* 111 (3): 640–48. doi:10.1097/ALN.0b013e3181b05f42.
- Jack Hu, Che-Ming, and Liangfang Zhang. 2009. "Therapeutic Nanoparticles to Combat Cancer Drug Resistance." *Current Drug Metabolism* 10: 836–41. doi:10.2174/138920009790274540.
- Jaffee, Elizabeth M, Ralph H Hruban, Marcia Canto, and Scott E Kern. 2002. "Focus on Pancreas Cancer." *Cancer Cell* 2 (1): 25–28. <http://www.ncbi.nlm.nih.gov/pubmed/12150822>.
- Jansson, M., V. Panoutsakopoulou, J. Baker, L. Klein, and H. Cantor. 2002. "Cutting Edge: Attenuated Experimental Autoimmune Encephalomyelitis in Eta-1/Osteopontin-Deficient Mice." *The Journal of Immunology* 168 (5): 2096–99. doi:10.4049/jimmunol.168.5.2096.
- Jenning, Volkhard, Anja Gysler, Monika Schäfer-Korting, and Sven H Gohla. 2000. "Vitamin A Loaded Solid Lipid Nanoparticles for Topical Use: Occlusive Properties and Drug Targeting to the Upper Skin." *European Journal of Pharmaceutics and Biopharmaceutics* 49 (3): 211–18. doi:10.1016/S0939-6411(99)00075-2.
- Jokerst, Jesse V, and Sanjiv S Gambhir. 2011. "Molecular Imaging with Theranostic Nanoparticles." *Accounts of Chemical Research* 44 (10): 1050–60. doi:10.1021/ar200106e.
- Jordan, Andreas, Regina Scholz, Klaus Maier-Hauff, Manfred Johannsen, Peter Wust, Jacek Nadobny, Hermann Schirra, et al. 2001. "Presentation of a New Magnetic Field Therapy System for the Treatment of Human Solid Tumors with Magnetic Fluid Hyperthermia." *Journal of Magnetism and Magnetic Materials* 225 (1–2): 118–26. doi:10.1016/S0304-8853(00)01239-7.
- Juliano, R. 2013. "Nanomedicine: Is the Wave Cresting?" *Nat Rev Drug Discov* 12: 171–172.
- Karmazanovsky, G, V Fedorov, V Kubyshkin, and A Kotchatkov. n.d. "Pancreatic Head Cancer: Accuracy of CT in Determination of Resectability." *Abdominal Imaging* 30 (4): 488–500. doi:10.1007/s00261-004-0279-z.
- Kedrin, Dmitriy, Jacco van Rheenen, Lorena Hernandez, John Condeelis, and Jeffrey E Segall. 2007. "Cell Motility and Cytoskeletal Regulation in Invasion and Metastasis." *Journal of Mammary Gland Biology and Neoplasia* 12 (2–3): 143–52. doi:10.1007/s10911-007-9046-4.
- Kerbel, Robert S, and Barton A Kamen. 2004. "The Anti-Angiogenic Basis of Metronomic Chemotherapy." *Nature Reviews. Cancer* 4 (6): 423–36. doi:10.1038/nrc1369.
- Khan, Ibrahim, Khalid Saeed, and Idrees Khan. 2017. "Nanoparticles:

- Properties, Applications and Toxicities." *Arabian Journal of Chemistry*. doi:10.1016/j.arabjc.2017.05.011.
- Kievit, Forrest M, and Miqin Zhang. 2011. "Surface Engineering of Iron Oxide Nanoparticles for Targeted Cancer Therapy." *Accounts of Chemical Research* 44 (10): 853–62. doi:10.1021/ar2000277.
- Kimling, J., M. Maier, B. Okenve, V. Kotaidis, H. Ballot, and A. Plech. 2006. "Turkevich Method for Gold Nanoparticle Synthesis Revisited." *The Journal of Physical Chemistry B* 110 (32): 15700–707. doi:10.1021/jp061667w.
- Kindler, Hedy Lee, Donna Niedzwiecki, Donna Hollis, Susan Sutherland, Deborah Schrag, Herbert Hurwitz, Federico Innocenti, et al. 2010. "Gemcitabine plus Bevacizumab Compared with Gemcitabine plus Placebo in Patients with Advanced Pancreatic Cancer: Phase III Trial of the Cancer and Leukemia Group B (CALGB 80303)." *Journal of Clinical Oncology : Official Journal of the American Society of Clinical Oncology* 28 (22): 3617–22. doi:10.1200/JCO.2010.28.1386.
- Kirpotin, Dmitri B, Daryl C Drummond, Yi Shao, M Refaat Shalaby, Keelung Hong, Ulrik B Nielsen, James D Marks, Christopher C Benz, and John W Park. 2006. "Antibody Targeting of Long-Circulating Lipidic Nanoparticles Does Not Increase Tumor Localization but Does Increase Internalization in Animal Models." *Cancer Research* 66 (13): 6732–40. doi:10.1158/0008-5472.CAN-05-4199.
- Kleeff, Jorg, Murray Korc, Minoti Apte, Carlo La Vecchia, Colin D Johnson, Andrew V Biankin, Rachel E Neale, et al. 2016. "Pancreatic Cancer." *Nature Reviews. Disease Primers* 2: 16022. doi:10.1038/nrdp.2016.22.
- Koltai, Hinanit, Evgenia Dor, Joseph Hershenhorn, Daniel M. Joel, Smadar Weinger, Sivarama Lekalla, Hagit Shealtiel, et al. 2010. "Strigolactones' Effect on Root Growth and Root-Hair Elongation May Be Mediated by Auxin-Efflux Carriers." *Journal of Plant Growth Regulation* 29 (2): 129–36. doi:10.1007/s00344-009-9122-7.
- Kon, Shigeyuki, Yasuyuki Yokosaki, Masahiro Maeda, Tatsuya Segawa, Yuko Horikoshi, Hiroe Tsukagoshi, Mohammad M Rashid, et al. 2002. "Mapping of Functional Epitopes of Osteopontin by Monoclonal Antibodies Raised against Defined Internal Sequences." *Journal of Cellular Biochemistry* 84 (2): 420–32. <http://www.ncbi.nlm.nih.gov/pubmed/11787071>.
- Koo, Otilia M, Israel Rubinstein, and Hayat Onyuksel. 2005. "Camptothecin in Sterically Stabilized Phospholipid Micelles: A Novel Nanomedicine." *Nanomedicine : Nanotechnology, Biology, and Medicine* 1 (1): 77–84. doi:10.1016/j.nano.2004.11.002.

- Krishna, R, and J K Pandit. 1996. "Carboxymethylcellulose-Sodium Based Transdermal Drug Delivery System for Propranolol." *The Journal of Pharmacy and Pharmacology* 48 (4): 367–70.
- Kruger, Thomas E., Andrew H. Miller, Andrew K. Godwin, and Jinxi Wang. 2014. "Bone Sialoprotein and Osteopontin in Bone Metastasis of Osteotropic Cancers." *Critical Reviews in Oncology/Hematology* 89 (2): 330–41. doi:10.1016/j.critrevonc.2013.08.013.
- Kumbıçak, Umit, Tolga Cavaş, Nilüfer Cinkılıç, Zübeyde Kumbıçak, Ozgür Vatan, and Dilek Yılmaz. 2014. "Evaluation of in Vitro Cytotoxicity and Genotoxicity of Copper-Zinc Alloy Nanoparticles in Human Lung Epithelial Cells." *Food and Chemical Toxicology : An International Journal Published for the British Industrial Biological Research Association* 73 (August): 105–12. doi:10.1016/j.fct.2014.07.040.
- Kunii, Yasuto, Shin-ichi Niwa, Yoshiaki Hagiwara, Masahiro Maeda, Tsutomu Seitoh, and Toshimitsu Suzuki. 2009. "The Immunohistochemical Expression Profile of Osteopontin in Normal Human Tissues Using Two Site-Specific Antibodies Reveals a Wide Distribution of Positive Cells and Extensive Expression in the Central and Peripheral Nervous Systems." *Medical Molecular Morphology* 42 (3): 155–61. doi:10.1007/s00795-009-0459-6.
- Lachenal, Gaele, Karin Pernet-Gallay, Mathilde Chivet, Fiona J Hemming, Agnès Belly, Gilles Bodon, Béatrice Blot, Georg Haase, Yves Goldberg, and Rémy Sadoul. 2011. "Release of Exosomes from Differentiated Neurons and Its Regulation by Synaptic Glutamatergic Activity." *Molecular and Cellular Neuroscience* 46 (2): 409–18. doi:10.1016/j.mcn.2010.11.004.
- Lalor, Patricia F, W K Lai, S M Curbishley, S Shetty, and D H Adams. 2006. "Human Hepatic Sinusoidal Endothelial Cells Can Be Distinguished by Expression of Phenotypic Markers Related to Their Specialised Functions in Vivo." *World Journal of Gastroenterology* 12 (34): 5429–39. doi:10.3748/wjg.v12.i34.5429.
- Lamour, Virginie, Aurélie Henry, Jérôme Kroonen, Marie-Julie Nokin, Zofia von Marschall, Larry W Fisher, Tieu-Lan Chau, et al. 2015. "Targeting Osteopontin Suppresses Glioblastoma Stem-like Cell Character and Tumorigenicity in Vivo." *International Journal of Cancer* 137 (5): 1047–57. doi:10.1002/ijc.29454.
- Lamparski, Henry G, Anita Metha-Damani, Jenq-Yuan Yao, Sanjay Patel, Di-Hwei Hsu, Curtis Ruegg, and Jean-Bernard Le Pecq. 2002. "Production and Characterization of Clinical Grade Exosomes Derived from Dendritic Cells." *Journal of Immunological Methods* 270 (2): 211–26.

<http://www.ncbi.nlm.nih.gov/pubmed/12379326>.

- Leali, Daria, Patrizia Dell’Era, Helena Stabile, Barbara Sennino, Ann F Chambers, Antonella Naldini, Silvano Sozzani, Beatrice Nico, Domenico Ribatti, and Marco Presta. 2003. “Osteopontin (Eta-1) and Fibroblast Growth Factor-2 Cross-Talk in Angiogenesis.” *Journal of Immunology (Baltimore, Md. : 1950)* 171 (2): 1085–93.
<http://www.ncbi.nlm.nih.gov/pubmed/12847283>.
- Lemire, J, A Alhasawi, V P Appanna, S Tharmalingam, and V D Appanna. 2017. “Metabolic Defence against Oxidative Stress: The Road Less Travelled so Far.” *Journal of Applied Microbiology* 123 (4): 798–809.
doi:10.1111/jam.13509.
- Leone, M A, S Bonisconi, L Collimedaglia, F Tesser, S Calzoni, A Stecco, P Naldi, and F Monaco. 2008. “Factors Predicting Incomplete Recovery from Relapses in Multiple Sclerosis: A Prospective Study.” *Multiple Sclerosis (Houndmills, Basingstoke, England)* 14 (4): 485–93.
doi:10.1177/1352458507084650.
- Li, Donghui, Keping Xie, Robert Wolff, and James L Abbruzzese. 2004. “Pancreatic Cancer.” *Lancet (London, England)* 363 (9414): 1049–57.
doi:10.1016/S0140-6736(04)15841-8.
- Liaw, L, D E Birk, C B Ballas, J S Whitsitt, J M Davidson, and B L Hogan. 1998. “Altered Wound Healing in Mice Lacking a Functional Osteopontin Gene (spp1).” *Journal of Clinical Investigation* 101 (7): 1468–78.
doi:10.1172/JCI1122.
- Liepe, Juliane, Hermann-Georg Holzhütter, Elena Bellavista, Peter M Kloetzel, Michael PH Stumpf, and Michele Mishto. 2015. “Quantitative Time-Resolved Analysis Reveals Intricate, Differential Regulation of Standard- and Immuno-Proteasomes.” *eLife* 4 (September).
doi:10.7554/eLife.07545.
- Liu, Jie, Qishen Liu, Yali Wan, Zhigang Zhao, Honggang Yu, Hesheng Luo, and Zhongzhi Tang. 2014. “Osteopontin Promotes the Progression of Gastric Cancer through the NF- κ B Pathway Regulated by the MAPK and PI3K.” *International Journal of Oncology* 45 (1): 282–90.
doi:10.3892/ijco.2014.2393.
- Lobb, Richard J, Melanie Becker, Shu Wen Wen, Christina S F Wong, Adrian P Wiegman, Antoine Leimgruber, and Andreas Möller. 2015. “Optimized Exosome Isolation Protocol for Cell Culture Supernatant and Human Plasma.” *Journal of Extracellular Vesicles* 4 (1): 27031.
doi:10.3402/jev.v4.27031.
- Lochan, Rajiv, Helen L Reeves, Anne K Daly, and Richard M Charnley. 2011.

- “The Role of Tobacco-Derived Carcinogens in Pancreas Cancer.” *ISRN Oncology* 2011: 1–9. doi:10.5402/2011/249235.
- Locker, Gershon Y, Stanley Hamilton, Jules Harris, John M Jessup, Nancy Kemeny, John S Macdonald, Mark R Somerfield, Daniel F Hayes, Robert C Bast, and ASCO. 2006. “ASCO 2006 Update of Recommendations for the Use of Tumor Markers in Gastrointestinal Cancer.” *Journal of Clinical Oncology : Official Journal of the American Society of Clinical Oncology* 24 (33): 5313–27. doi:10.1200/JCO.2006.08.2644.
- Löhr, M, P Maisonneuve, and A B Lowenfels. 2000. “K-Ras Mutations and Benign Pancreatic Disease.” *International Journal of Pancreatology : Official Journal of the International Association of Pancreatology* 27 (2): 93–103. doi:10.1385/IJGC:27:2:093.
- Lu, C., T. Bonome, Y. Li, A. A. Kamat, L. Y. Han, R. Schmandt, R. L. Coleman, et al. 2007. “Gene Alterations Identified by Expression Profiling in Tumor-Associated Endothelial Cells from Invasive Ovarian Carcinoma.” *Cancer Research* 67 (4): 1757–68. doi:10.1158/0008-5472.CAN-06-3700.
- Mäder, K, and W Mehnert. 2001. “Solid Lipid Nanoparticles: Production, Characterization and Applications.” *Advanced Drug Delivery Reviews* 47 (2–3): 165–96. doi:10.1016/S0169-409X(01)00105-3.
- Mahmoudi, Morteza, Heinrich Hofmann, Barbara Rothen-Rutishauser, and Alke Petri-Fink. 2012. “Assessing the in Vitro and in Vivo Toxicity of Superparamagnetic Iron Oxide Nanoparticles.” *Chemical Reviews*. doi:10.1021/cr2002596.
- Mallegol, Julia, Guillaume Van Niel, Corinne Lebreton, Yves Lepelletier, Céline Candalh, Christophe Dugave, Joan K Heath, Graça Raposo, Nadine Cerf-Bensussan, and Martine Heyman. 2007. “T84-Intestinal Epithelial Exosomes Bear MHC Class II/Peptide Complexes Potentiating Antigen Presentation by Dendritic Cells.” *Gastroenterology* 132 (5): 1866–76. doi:10.1053/j.gastro.2007.02.043.
- MARTIN, FRANCIS J. 1998. “Clinical Pharmacology and Antitumor Efficacy of DOXIL (Pegylated Liposomal Doxorubicin).” In *Medical Applications of Liposomes*, 635–88. Elsevier. doi:10.1016/B978-044482917-7/50035-1.
- Martin, Tracey A, Lin Ye, Andrew J Sanders, Jane Lane, and Weng G Jiang. 2013. *Cancer Invasion and Metastasis: Molecular and Cellular Perspective. Metastatic Cancer: Clinical and Biological Perspectives*. doi:10.1607626.
- Martino, M de, K Hoetzenecker, H J Ankersmit, G A Roth, A Haitel, M Waldert, and T Klatter. 2012. “Serum 20S Proteasome Is Elevated in Patients with Renal Cell Carcinoma and Associated with Poor Prognosis.” *British Journal of Cancer* 106 (5): 904–8. doi:10.1038/bjc.2012.20.

- Masyuk, A. I., B. Q. Huang, C. J. Ward, S. A. Gradilone, J. M. Banales, T. V. Masyuk, B. Radtke, P. L. Splinter, and N. F. LaRusso. 2010. "Biliary Exosomes Influence Cholangiocyte Regulatory Mechanisms and Proliferation through Interaction with Primary Cilia." *AJP: Gastrointestinal and Liver Physiology* 299 (4): G990–99. doi:10.1152/ajpgi.00093.2010.
- Mathivanan, Suresh, Hong Ji, and Richard J Simpson. 2010. "Exosomes: Extracellular Organelles Important in Intercellular Communication." *Journal of Proteomics* 73 (10): 1907–20. doi:10.1016/j.jprot.2010.06.006.
- Medico, E, A Gentile, C Lo Celso, T A Williams, G Gambarotta, L Trusolino, and P M Comoglio. 2001. "Osteopontin Is an Autocrine Mediator of Hepatocyte Growth Factor-Induced Invasive Growth." *Cancer Research* 61 (15): 5861–68. <http://www.ncbi.nlm.nih.gov/pubmed/11479227>.
- Medintz, Igor L, H Tetsuo Uyeda, Ellen R Goldman, and Hedi Mattoussi. 2005. "Quantum Dot Bioconjugates for Imaging, Labelling and Sensing." *Nature Materials*. doi:10.1038/nmat1390.
- Michalet, X, F F Pinaud, L A Bentolila, J M Tsay, S Doose, J J Li, G Sundaresan, A M Wu, S S Gambhir, and S Weiss. 2005. "Quantum Dots for Live Cells, in Vivo Imaging, and Diagnostics." *Science (New York, N.Y.)* 307 (5709): 538–44. doi:10.1126/science.1104274.
- Michaud, D S, E Giovannucci, W C Willett, G A Colditz, M J Stampfer, and C S Fuchs. n.d. "Physical Activity, Obesity, Height, and the Risk of Pancreatic Cancer." *JAMA* 286 (8): 921–29. <http://www.ncbi.nlm.nih.gov/pubmed/11509056>.
- Minagar, Alireza, Wanlong Ma, Xi Zhang, Xiuqiang Wang, Ke Zhang, J Steven Alexander, Eduardo Gonzalez-Toledo, and Maher Albitar. 2012. "Plasma Ubiquitin-Proteasome System Profile in Patients with Multiple Sclerosis: Correlation with Clinical Features, Neuroimaging, and Treatment with Interferon-Beta-1b." *Neurological Research* 34 (6): 611–18. doi:10.1179/1743132812Y.0000000055.
- Minelli, R, S Occhipinti, C L Gigliotti, G Barrera, P Gasco, L Conti, A Chiocchetti, et al. 2013. "Solid Lipid Nanoparticles of Cholesteryl Butyrate Inhibit the Proliferation of Cancer Cells in Vitro and in Vivo Models." *British Journal of Pharmacology* 170 (2): 233–44. doi:10.1111/bph.12255.
- Minelli, R, L Serpe, P Pettazoni, V Minero, G Barrera, Cl Gigliotti, R Mesturini, et al. 2012. "Cholesteryl Butyrate Solid Lipid Nanoparticles Inhibit the Adhesion and Migration of Colon Cancer Cells." *British Journal of Pharmacology* 166 (2): 587–601. doi:10.1111/j.1476-5381.2011.01768.x.
- Minelli, Rosalba, Roberta Cavalli, Leigh Ellis, Piergiorgio Pettazoni, Francesco Trotta, Eric Ciamporcero, Giuseppina Barrera, Roberto Fantozzi, Chiara

- Dianzani, and Roberto Pili. 2012. "Nanosponge-Encapsulated Camptothecin Exerts Anti-Tumor Activity in Human Prostate Cancer Cells." *European Journal of Pharmaceutical Sciences : Official Journal of the European Federation for Pharmaceutical Sciences* 47 (4): 686–94. doi:10.1016/j.ejps.2012.08.003.
- Mishto, Michele, Elena Bellavista, Claudia Ligorio, Kathrin Textoris-Taube, Aurelia Santoro, Mara Giordano, Sandra D'Alfonso, et al. 2010. "Immunoproteasome LMP2 60HH Variant Alters MBP Epitope Generation and Reduces the Risk to Develop Multiple Sclerosis in Italian Female Population." Edited by Christoph Kleinschnitz. *PLoS ONE* 5 (2): e9287. doi:10.1371/journal.pone.0009287.
- Moore, Malcolm J, David Goldstein, John Hamm, Arie Figer, Joel R Hecht, Steven Gallinger, Heather J Au, et al. 2007. "Erlotinib plus Gemcitabine Compared with Gemcitabine Alone in Patients with Advanced Pancreatic Cancer: A Phase III Trial of the National Cancer Institute of Canada Clinical Trials Group." *Journal of Clinical Oncology : Official Journal of the American Society of Clinical Oncology* 25 (15): 1960–66. doi:10.1200/JCO.2006.07.9525.
- Moran, A, C O'Hara, S Khan, L Shack, E Woodward, E R Maher, F Laloo, and D G R Evans. 2012. "Risk of Cancer Other than Breast or Ovarian in Individuals with BRCA1 and BRCA2 Mutations." *Familial Cancer* 11 (2): 235–42. doi:10.1007/s10689-011-9506-2.
- Morelli, A E. 2006. "The Immune Regulatory Effect of Apoptotic Cells and Exosomes on Dendritic Cells: Its Impact on Transplantation." *American Journal of Transplantation* 6 (2): 254–61. doi:10.1111/j.1600-6143.2005.01197.x.
- Moreno-Aspitia, Alvaro, and Edith A Perez. 2005. "Nanoparticle Albumin-Bound Paclitaxel (ABI-007): A Newer Taxane Alternative in Breast Cancer." *Future Oncology (London, England)* 1 (6): 755–62. doi:10.2217/14796694.1.6.755.
- Morimoto, Junko, Shigeyuki Kon, Yutaka Matsui, and Toshimitsu Uede. 2010. "Osteopontin; as a Target Molecule for the Treatment of Inflammatory Diseases." *Current Drug Targets* 11 (4): 494–505. <http://www.ncbi.nlm.nih.gov/pubmed/20196720>.
- Mosallaei, Navid, Mahmoud Reza Jaafari, Mohammad Yahya Hanafi-Bojd, Shiva Golmohammadzadeh, and Bizhan Malaekheh-Nikouei. 2013. "Docetaxel-Loaded Solid Lipid Nanoparticles: Preparation, Characterization, in Vitro, and in Vivo Evaluations." *Journal of Pharmaceutical Sciences* 102 (6): 1994–2004. doi:10.1002/jps.23522.

- Mu, Wei, Sanyukta Rana, and Margot Zöller. 2013. "Host Matrix Modulation by Tumor Exosomes Promotes Motility and Invasiveness." *Neoplasia (New York, N.Y.)* 15 (8): 875–87.
<http://www.ncbi.nlm.nih.gov/pubmed/23908589>.
- Mudshinge, Sagar R, Amol B Deore, Sachin Patil, and Chetan M Bhalgat. 2011. "Nanoparticles: Emerging Carriers for Drug Delivery." *Saudi Pharmaceutical Journal*. doi:10.1016/j.jsps.2011.04.001.
- Mühlen, Anette zur, Cora Schwarz, and Wolfgang Mehnert. 1998. "Solid Lipid Nanoparticles (SLN) for Controlled Drug Delivery--Drug Release and Release Mechanism." *European Journal of Pharmaceutics and Biopharmaceutics* 45 (2): 149–55. doi:10.1016/S0939-6411(97)00150-1.
- Müller, R H, K Mäder, and S Gohla. 2000. "Solid Lipid Nanoparticles (SLN) for Controlled Drug Delivery - a Review of the State of the Art." *European Journal of Pharmaceutics and Biopharmaceutics : Official Journal of Arbeitsgemeinschaft Für Pharmazeutische Verfahrenstechnik e.V* 50 (1): 161–77. doi:10.1016/S0939-6411(00)00087-4.
- Müller, R H, M Radtke, and S A Wissing. 2002. "Solid Lipid Nanoparticles (SLN) and Nanostructured Lipid Carriers (NLC) in Cosmetic and Dermatological Preparations." In *Advanced Drug Delivery Reviews*. Vol. 54. doi:10.1016/S0169-409X(02)00118-7.
- Muralidharan-Chari, Vandhana, James Clancy, Carolyn Plou, Maryse Romao, Philippe Chavrier, Graca Raposo, and Crislyn D'Souza-Schorey. 2009. "ARF6-Regulated Shedding of Tumor Cell-Derived Plasma Membrane Microvesicles." *Current Biology* 19 (22): 1875–85. doi:10.1016/j.cub.2009.09.059.
- Murry, C E, C M Giachelli, S M Schwartz, and R Vracko. 1994. "Macrophages Express Osteopontin during Repair of Myocardial Necrosis." *The American Journal of Pathology* 145 (6): 1450–62.
<http://www.ncbi.nlm.nih.gov/pubmed/7992848>.
- Murugaiyan, Gopal, Akanksha Mittal, and Howard L Weiner. 2008. "Increased Osteopontin Expression in Dendritic Cells Amplifies IL-17 Production by CD4+ T Cells in Experimental Autoimmune Encephalomyelitis and in Multiple Sclerosis." *Journal of Immunology (Baltimore, Md. : 1950)* 181 (11): 7480–88. <http://www.ncbi.nlm.nih.gov/pubmed/19017937>.
- "Nanotechnology in Therapeutics." n.d.
http://www.nanopinion.eu/sites/default/files/therapeutics_april_2009.pdf.
- Nareika, Alena, Yeong Bin Im, Bryan A Game, Elizabeth H Slate, John J Sanders, Steven D London, Maria F Lopes-Virella, and Yan Huang. 2008. "High

Glucose Enhances Lipopolysaccharide-Stimulated CD14 Expression in U937 Mononuclear Cells by Increasing Nuclear Factor κ B and AP-1 Activities." *Journal of Endocrinology* 196 (1): 45–55. doi:10.1677/JOE-07-0145.

- Nazir, Samina, Tajammul Hussain, Attiya Ayub, Umer Rashid, and Alexander John MacRobert. 2014. "Nanomaterials in Combating Cancer: Therapeutic Applications and Developments." *Nanomedicine : Nanotechnology, Biology, and Medicine* 10 (1): 19–34. doi:10.1016/j.nano.2013.07.001.
- Neuberger, Tobias, Bernhard Schöpf, Heinrich Hofmann, Margarete Hofmann, and Brigitte von Rechenberg. 2005. "Superparamagnetic Nanoparticles for Biomedical Applications: Possibilities and Limitations of a New Drug Delivery System." *Journal of Magnetism and Magnetic Materials* 293 (1): 483–96. doi:10.1016/j.jmmm.2005.01.064.
- Nguyen, Don X, Paula D Bos, and Joan Massagué. 2009. "Metastasis: From Dissemination to Organ-Specific Colonization." *Nature Reviews Cancer*. doi:10.1038/nrc2622.
- Nishida, Naoyo, Hirohisa Yano, Takashi Nishida, Toshiharu Kamura, and Masamichi Kojiro. 2006. "Angiogenesis in Cancer." *Vascular Health and Risk Management*. doi:10.2147/vhrm.2006.2.3.213.
- Nishiyama, Nobuhiro, and Kazunori Kataoka. 2006. "Current State, Achievements, and Future Prospects of Polymeric Micelles as Nanocarriers for Drug and Gene Delivery." *Pharmacology & Therapeutics* 112 (3): 630–48. doi:10.1016/j.pharmthera.2006.05.006.
- Nolte-'t Hoen, E N M, E J van der Vlist, M de Boer-Brouwer, G J A Arkesteijn, W Stoorvogel, and M H M Wauben. 2013. "Dynamics of Dendritic Cell-Derived Vesicles: High-Resolution Flow Cytometric Analysis of Extracellular Vesicle Quantity and Quality." *Journal of Leukocyte Biology* 93 (3): 395–402. doi:10.1189/jlb.0911480.
- Obenauf, Anna C, and Joan Massagué. 2015. "Surviving at a Distance: Organ-Specific Metastasis." *Trends in Cancer*. doi:10.1016/j.trecan.2015.07.009.
- Obregon, Carolina, Barbara Rothen-Rutishauser, Stephen Kiama Gitahi, Peter Gehr, and Laurent P Nicod. 2006. "Exovesicles from Human Activated Dendritic Cells Fuse with Resting Dendritic Cells, Allowing Them to Present Alloantigens." *The American Journal of Pathology* 169 (6): 2127–36. doi:10.2353/ajpath.2006.060453.
- Oettle, Helmut, Stefan Post, Peter Neuhaus, Klaus Gellert, Jan Langrehr, Karsten Ridwelski, Harald Schramm, et al. 2007. "Adjuvant Chemotherapy With Gemcitabine vs Observation in Patients Undergoing Curative-Intent Resection of Pancreatic Cancer." *JAMA* 297 (3): 267.

doi:10.1001/jama.297.3.267.

- Ogawa, Yuko, Yuri Miura, Akira Harazono, Masami Kanai-Azuma, Yoshihiro Akimoto, Hayato Kawakami, Teruhide Yamaguchi, et al. 2011. "Proteomic Analysis of Two Types of Exosomes in Human Whole Saliva." *Biological & Pharmaceutical Bulletin* 34 (1): 13–23. doi:10.1248/bpb.34.13.
- Orimo, Akira, and Robert A Weinberg. 2006. "Stromal Fibroblasts in Cancer: A Novel Tumor-Promoting Cell Type." *Cell Cycle (Georgetown, Tex.)* 5 (15): 1597–1601. doi:10.4161/cc.5.15.3112.
- Ostenfeld, Marie Stampe, Dennis K Jeppesen, Jens R Laurberg, Anders T Boysen, Jesper B Bramsen, Bjarke Primdal-Bengtson, An Hendrix, et al. 2014. "Cellular Disposal of miR23b by RAB27-Dependent Exosome Release Is Linked to Acquisition of Metastatic Properties." *Cancer Research* 74 (20): 5758–71. doi:10.1158/0008-5472.CAN-13-3512.
- Ostrowski, Matias, Nuno B Carmo, Sophie Krumeich, Isabelle Fanget, Graça Raposo, Ariel Savina, Catarina F Moita, et al. 2010. "Rab27a and Rab27b Control Different Steps of the Exosome Secretion Pathway." *Nature Cell Biology* 12 (1): 19–30. doi:10.1038/ncb2000.
- Paku, S, B Döme, R Tóth, and J Timár. 2000. "Organ-Specificity of the Extravasation Process: An Ultrastructural Study." *Clinical and Experimental Metastasis* 18 (6): 481–92. doi:10.1023/A:1011858925376.
- Palay, Sanford L. 1960. "The Fine Structure of Secretory Neurons in the Preoptic Nucleus of the Goldfish (*Carassius Auratus*)." *The Anatomical Record* 138 (4): 417–43. doi:10.1002/ar.1091380404.
- Pan, Yu, Sabine Neuss, Annika Leifert, Monika Fischler, Fei Wen, Ulrich Simon, Günter Schmid, Wolfgang Brandau, and Willi Jahnen-Dechent. 2007. "Size-Dependent Cytotoxicity of Gold Nanoparticles." *Small (Weinheim an Der Bergstrasse, Germany)* 3 (11): 1941–49. doi:10.1002/smll.200700378.
- Park, John W. 2002. "Liposome-Based Drug Delivery in Breast Cancer Treatment." *Breast Cancer Research : BCR* 4 (3): 95–99. doi:10.1186/bcr432.
- Park, K.-H., B.-J. Kim, J. Kang, T.-S. Nam, J. M. Lim, H. T. Kim, J. K. Park, Y. G. Kim, S.-W. Chae, and U.-H. Kim. 2011. "Ca²⁺ Signaling Tools Acquired from Prostatomes Are Required for Progesterone-Induced Sperm Motility." *Science Signaling* 4 (173): ra31-ra31. doi:10.1126/scisignal.2001595.
- Parkin, Donald Maxwell. 2006. "The Global Health Burden of Infection-Associated Cancers in the Year 2002." *International Journal of Cancer* 118 (12): 3030–44. doi:10.1002/ijc.21731.
- Patani, Neill, Fadi Jouhra, Wen Jiang, and Kefah Mokbel. n.d. "Osteopontin

- Expression Profiles Predict Pathological and Clinical Outcome in Breast Cancer." *Anticancer Research* 28 (6B): 4105–10.
<http://www.ncbi.nlm.nih.gov/pubmed/19192668>.
- Peinado, Héctor, Maša Alečković, Simon Lavotshkin, Irina Matei, Bruno Costa-Silva, Gema Moreno-Bueno, Marta Hergueta-Redondo, et al. 2012. "Melanoma Exosomes Educate Bone Marrow Progenitor Cells toward a pro-Metastatic Phenotype through MET." *Nature Medicine* 18 (6): 883–91. doi:10.1038/nm.2753.
- Philip, Philip A, Jacqueline Benedetti, Christopher L Corless, Ralph Wong, Eileen M O'Reilly, Patrick J Flynn, Kendrith M Rowland, et al. 2010. "Phase III Study Comparing Gemcitabine plus Cetuximab versus Gemcitabine in Patients with Advanced Pancreatic Adenocarcinoma: Southwest Oncology Group-Directed Intergroup Trial S0205." *Journal of Clinical Oncology : Official Journal of the American Society of Clinical Oncology* 28 (22): 3605–10. doi:10.1200/JCO.2009.25.7550.
- Pintado, Cristina, María P Gavilán, Elena Gavilán, Luisa García-Cuervo, Antonia Gutiérrez, Javier Vitorica, Angélica Castaño, Rosa M Ríos, and Diego Ruano. 2012. "Lipopolysaccharide-Induced Neuroinflammation Leads to the Accumulation of Ubiquitinated Proteins and Increases Susceptibility to Neurodegeneration Induced by Proteasome Inhibition in Rat Hippocampus." *Journal of Neuroinflammation* 9 (May): 87. doi:10.1186/1742-2094-9-87.
- Pisani, Paola, D Maxwell Parkin, Nubia Muñoz, and Jacques Ferlay. 1997. "Cancer and Infection: Estimates of the Attributable Fraction in 1990." *Cancer Epidemiology Biomarkers and Prevention*.
- Pisitkun, T., R.-F. Shen, and M. A. Knepper. 2004. "Identification and Proteomic Profiling of Exosomes in Human Urine." *Proceedings of the National Academy of Sciences* 101 (36): 13368–73. doi:10.1073/pnas.0403453101.
- Pitot, H C, R M Goldberg, J M Reid, J A Sloan, P A Skaff, C Erlichman, J Rubin, et al. 2000. "Phase I Dose-Finding and Pharmacokinetic Trial of Irinotecan Hydrochloride (CPT-11) Using a Once-Every-Three-Week Dosing Schedule for Patients with Advanced Solid Tumor Malignancy." *Clinical Cancer Research : An Official Journal of the American Association for Cancer Research* 6 (6): 2236–44.
<http://www.ncbi.nlm.nih.gov/pubmed/10873073>.
- Pizzimenti, S., C. Dianzani, G.P. Zara, C. Ferretti, F. Rossi, C.L. Gigliotti, M. Daga, E.S. Ciamporcerro, G. Maina, and G. Barrera. 2016. "Challenges and Opportunities of Nanoparticle-Based Theranostics in Skin Cancer." In *Nanoscience in Dermatology*, 177–88. Elsevier. doi:10.1016/B978-0-12-

802926-8.00014-8.

- Plummer, Martyn, Catherine de Martel, Jerome Vignat, Jacques Ferlay, Freddie Bray, and Silvia Franceschi. 2016. "Global Burden of Cancers Attributable to Infections in 2012: A Synthetic Analysis." *The Lancet Global Health* 4 (9): e609--e616. doi:10.1016/S2214-109X(16)30143-7.
- Pollock, C B, H Koltai, Y Kapulnik, C Prandi, and R I Yarden. 2012. "Strigolactones: A Novel Class of Phytohormones That Inhibit the Growth and Survival of Breast Cancer Cells and Breast Cancer Stem-like Enriched Mammosphere Cells." *Breast Cancer Research and Treatment* 134 (3): 1041--55. doi:10.1007/s10549-012-1992-x.
- Pollock, Claire B, Sara McDonough, Victor S Wang, Hyojung Lee, Lymor Ringer, Xin Li, Cristina Prandi, et al. 2014. "Strigolactone Analogues Induce Apoptosis through Activation of p38 and the Stress Response Pathway in Cancer Cell Lines and in Conditionally Reprogrammed Primary Prostate Cancer Cells." *Oncotarget* 5 (6): 1683--98. doi:10.18632/oncotarget.1849.
- Polman, Chris H, Paul W O'Connor, Eva Havrdova, Michael Hutchinson, Ludwig Kappos, David H Miller, J Theodore Phillips, et al. 2006. "A Randomized, Placebo-Controlled Trial of Natalizumab for Relapsing Multiple Sclerosis." *The New England Journal of Medicine* 354 (9): 899--910. doi:10.1056/NEJMoa044397.
- Postow, M. A., J. J. Luke, M. J. Bluth, N. Ramaiya, K. S. Panageas, D. P. Lawrence, N. Ibrahim, et al. 2013. "Ipilimumab for Patients With Advanced Mucosal Melanoma." *The Oncologist* 18 (6): 726--32. doi:10.1634/theoncologist.2012-0464.
- Prasad, Preethy, Adam Shuhendler, Ping Cai, Andrew M Rauth, and Xiao Yu Wu. 2013. "Doxorubicin and Mitomycin C Co-Loaded Polymer-Lipid Hybrid Nanoparticles Inhibit Growth of Sensitive and Multidrug Resistant Human Mammary Tumor Xenografts." *Cancer Letters* 334 (2): 263--73. doi:10.1016/j.canlet.2012.08.008.
- Putz, Ulrich, Jason Howitt, Anh Doan, Choo-Peng Goh, Ley-Hian Low, John Silke, and Seong-Seng Tan. 2012. "The Tumor Suppressor PTEN Is Exported in Exosomes and Has Phosphatase Activity in Recipient Cells." *Science Signaling* 5 (243): ra70. doi:10.1126/scisignal.2003084.
- Qi, Lifeng, and Xiaohu Gao. 2008. "Emerging Application of Quantum Dots for Drug Delivery and Therapy." *Expert Opinion on Drug Delivery* 5: 263--67. doi:10.1517/17425247.5.3.263.
- Quaglino, Elena, Cristina Mastini, Guido Forni, and Federica Cavallo. 2008. "ErbB2 Transgenic Mice: A Tool for Investigation of the Immune Prevention and Treatment of Mammary Carcinomas." *Current Protocols in*

- Immunology* Chapter 20 (August): Unit 20.9.1-20.9-10.
doi:10.1002/0471142735.im2009s82.
- Qureshi, Nilofer, David C Morrison, and Julia Reis. 2012. "Proteasome Protease Mediated Regulation of Cytokine Induction and Inflammation." *Biochimica et Biophysica Acta* 1823 (11): 2087–93.
doi:10.1016/j.bbamcr.2012.06.016.
- Rabolli, Virginie, Leen C J Thomassen, Catherine Princen, Dorota Napierska, Laetitia Gonzalez, Micheline Kirsch-Volders, Peter H Hoet, et al. 2010. "Influence of Size, Surface Area and Microporosity on the in Vitro Cytotoxic Activity of Amorphous Silica Nanoparticles in Different Cell Types." *Nanotoxicology* 4 (3): 307–18.
doi:10.3109/17435390.2010.482749.
- Ramagopal, Udupi A., Weifeng Liu, Sarah C. Garrett-Thomson, Jeffrey B. Bonanno, Qingrong Yan, Mohan Srinivasan, Susan C. Wong, et al. 2017. "Structural Basis for Cancer Immunotherapy by the First-in-Class Checkpoint Inhibitor Ipilimumab." *Proceedings of the National Academy of Sciences* 114 (21): E4223–32. doi:10.1073/pnas.1617941114.
- Rana, Sanyukta, Shijing Yue, Daniela Stadel, and Margot Zöller. 2012. "Toward Tailored Exosomes: The Exosomal Tetraspanin Web Contributes to Target Cell Selection." *The International Journal of Biochemistry & Cell Biology* 44 (9): 1574–84. doi:10.1016/j.biocel.2012.06.018.
- Raposo, G. 1996. "B Lymphocytes Secrete Antigen-Presenting Vesicles." *Journal of Experimental Medicine* 183 (3): 1161–72.
doi:10.1084/jem.183.3.1161.
- Raposo, Graça, and Willem Stoorvogel. 2013. "Extracellular Vesicles: Exosomes, Microvesicles, and Friends." *Journal of Cell Biology*.
doi:10.1083/jcb.201211138.
- Rasmussen, A., M. G. Mason, C. De Cuyper, P. B. Brewer, S. Herold, J. Agusti, D. Geelen, et al. 2012. "Strigolactones Suppress Adventitious Rooting in Arabidopsis and Pea." *PLANT PHYSIOLOGY* 158 (4): 1976–87.
doi:10.1104/pp.111.187104.
- Rittling, S R, and A F Chambers. 2004. "Role of Osteopontin in Tumour Progression." *British Journal of Cancer* 90 (10): 1877–81.
doi:10.1038/sj.bjc.6601839.
- Robert, Caroline, Georgina V Long, Benjamin Brady, Caroline Dutriaux, Michele Maio, Laurent Mortier, Jessica C Hassel, et al. 2015. "Nivolumab in Previously Untreated Melanoma without BRAF Mutation." *The New England Journal of Medicine* 372 (4): 320–30.
doi:10.1056/NEJMoa1412082.

- Rossi, Barbara, Silvia Caponi, Franca Castiglione, Silvia Corezzi, Aldo Fontana, Marco Giarola, Gino Mariotto, et al. 2012. "Networking Properties of Cyclodextrin-Based Cross-Linked Polymers Probed by Inelastic Light-Scattering Experiments." *The Journal of Physical Chemistry. B* 116 (17): 5323–27. doi:10.1021/jp302047u.
- Rudick, Richard A., William H. Stuart, Peter A. Calabresi, Christian Confavreux, Steven L. Galetta, Ernst-Wilhelm Radue, Fred D. Lublin, et al. 2006. "Natalizumab plus Interferon Beta-1a for Relapsing Multiple Sclerosis." *New England Journal of Medicine* 354 (9): 911–23. doi:10.1056/NEJMoa044396.
- Savina, Ariel, Michel Vidal, and Maria I Colombo. 2002. "The Exosome Pathway in K562 Cells Is Regulated by Rab11." *Journal of Cell Science* 115 (Pt 12): 2505–15. <http://www.ncbi.nlm.nih.gov/pubmed/12045221>.
- Scatena, M, M Almeida, M L Chaisson, N Fausto, R F Nicosia, and C M Giachelli. 1998. "NF-kappaB Mediates alphavbeta3 Integrin-Induced Endothelial Cell Survival." *The Journal of Cell Biology* 141 (4): 1083–93. <http://www.ncbi.nlm.nih.gov/pubmed/9585425>.
- Schiewe, M H, and et Al. 1985. "Use of Bacterial Bioluminescence Assay to Assess Toxicity of Contaminated Marine Sediments." *Canadian Journal of Fisheries and Aquatic Sciences* 42 (7): 1244–48. doi:10.1139/f85-154.
- Schlüter, Kerstin, Peter Gassmann, Andreas Enns, Timo Korb, Andre Hemping-Bovenkerk, Jens Hölzen, and Jörg Haier. 2006. "Organ-Specific Metastatic Tumor Cell Adhesion and Extravasation of Colon Carcinoma Cells with Different Metastatic Potential." *The American Journal of Pathology* 169 (3): 1064–73. doi:10.2353/ajpath.2006.050566.
- Schwartz, Alan L., and Aaron Ciechanover. 2009. "Targeting Proteins for Destruction by the Ubiquitin System: Implications for Human Pathobiology." *Annual Review of Pharmacology and Toxicology* 49 (1): 73–96. doi:10.1146/annurev.pharmtox.051208.165340.
- Senger, Donald R, Carole A Perruzzi, Michael Streit, Victor E Koteliensky, Antonin R de Fougerolles, and Michael Detmar. 2002. "The alpha(1)beta(1) and alpha(2)beta(1) Integrins Provide Critical Support for Vascular Endothelial Growth Factor Signaling, Endothelial Cell Migration, and Tumor Angiogenesis." *The American Journal of Pathology* 160 (1): 195–204. <http://www.ncbi.nlm.nih.gov/pubmed/11786413>.
- Shao, Huilin, Jaehoon Chung, Leonora Balaj, Alain Charest, Darell D Bigner, Bob S Carter, Fred H Hochberg, Xandra O Breakefield, Ralph Weissleder, and Hakho Lee. 2012. "Protein Typing of Circulating Microvesicles Allows Real-Time Monitoring of Glioblastoma Therapy." *Nature Medicine* 18 (12):

1835–40. doi:10.1038/nm.2994.

- Shao, Zhifei, John Morser, and Lawrence L K Leung. 2014. "Thrombin Cleavage of Osteopontin Disrupts a pro-Chemotactic Sequence for Dendritic Cells, Which Is Compensated by the Release of Its pro-Chemotactic C-Terminal Fragment." *The Journal of Biological Chemistry* 289 (39): 27146–58. doi:10.1074/jbc.M114.572172.
- Sharma, Sreenath V, Daphne W Bell, Jeffrey Settleman, and Daniel A Haber. 2007. "Epidermal Growth Factor Receptor Mutations in Lung Cancer." *Nature Reviews. Cancer* 7 (3): 169–81. doi:10.1038/nrc2088.
- Shende, Pravin, Yogesh A Kulkarni, R S Gaud, Kiran Deshmukh, Roberta Cavalli, Francesco Trotta, and Fabrizio Caldera. 2015. "Acute and Repeated Dose Toxicity Studies of Different β -Cyclodextrin-Based Nanosponge Formulations." *Journal of Pharmaceutical Sciences* 104 (5): 1856–63. doi:10.1002/jps.24416.
- Shi, Xiangyang, Suhe Wang, Sasha Meshinchi, Mary E Van Antwerp, Xiangdong Bi, Inhan Lee, and James R Baker. 2007. "Dendrimer-Entrapped Gold Nanoparticles as a Platform for Cancer-Cell Targeting and Imaging." *Small (Weinheim an Der Bergstrasse, Germany)* 3 (7): 1245–52. doi:10.1002/smll.200700054.
- Shinohara, Mari L., June-Ho Kim, Virgilio A. Garcia, and Harvey Cantor. 2008. "Engagement of the Type I Interferon Receptor on Dendritic Cells Inhibits T Helper 17 Cell Development: Role of Intracellular Osteopontin." *Immunity* 29 (1): 68–78. doi:10.1016/j.immuni.2008.05.008.
- Shinohara, Mari L, Hye-Jung Kim, June-Ho Kim, Virgilio A Garcia, and Harvey Cantor. 2008. "Alternative Translation of Osteopontin Generates Intracellular and Secreted Isoforms That Mediate Distinct Biological Activities in Dendritic Cells." *Proceedings of the National Academy of Sciences of the United States of America* 105 (20): 7235–39. doi:10.1073/pnas.0802301105.
- Shinohara, Mari L, Linrong Lu, Jing Bu, Miriam B F Werneck, Koichi S Kobayashi, Laurie H Glimcher, and Harvey Cantor. 2006. "Osteopontin Expression Is Essential for Interferon-Alpha Production by Plasmacytoid Dendritic Cells." *Nature Immunology* 7 (5): 498–506. doi:10.1038/ni1327.
- Simons, Mikael, and Graça Raposo. 2009. "Exosomes – Vesicular Carriers for Intercellular Communication." *Current Opinion in Cell Biology* 21 (4): 575–81. doi:10.1016/j.ceb.2009.03.007.
- Sixt, Stephan U, and Burkhardt Dahlmann. 2008. "Extracellular, Circulating Proteasomes and Ubiquitin - Incidence and Relevance." *Biochimica et Biophysica Acta* 1782 (12): 817–23. doi:10.1016/j.bbadis.2008.06.005.

- Skog, Johan, Tom Würdinger, Sjoerd van Rijn, Dimphna H Meijer, Laura Gainche, Miguel Sena-Esteves, William T Curry, Bob S Carter, Anna M Krichevsky, and Xandra O Breakefield. 2008. "Glioblastoma Microvesicles Transport RNA and Proteins That Promote Tumour Growth and Provide Diagnostic Biomarkers." *Nature Cell Biology* 10 (12): 1470–76. doi:10.1038/ncb1800.
- Slingerland, Marije, Henk-Jan Guchelaar, and Hans Gelderblom. 2012. "Liposomal Drug Formulations in Cancer Therapy: 15 Years along the Road." *Drug Discovery Today* 17 (3–4): 160–66. doi:10.1016/j.drudis.2011.09.015.
- Smith, Andrew M, Shivang Dave, Shuming Nie, Lawrence True, and Xiaohu Gao. 2006. "Multicolor Quantum Dots for Molecular Diagnostics of Cancer." *Expert Review of Molecular Diagnostics* 6 (2): 231–44. doi:10.1586/14737159.6.2.231.
- Solomon, Sheila, Siddhartha Das, Randall Brand, and David C Whitcomb. n.d. "Inherited Pancreatic Cancer Syndromes." *Cancer Journal (Sudbury, Mass.)* 18 (6): 485–91. doi:10.1097/PPO.0b013e318278c4a6.
- Sonavane, Ganeshchandra, Keishiro Tomoda, and Kimiko Makino. 2008. "Biodistribution of Colloidal Gold Nanoparticles after Intravenous Administration: Effect of Particle Size." *Colloids and Surfaces. B, Biointerfaces* 66 (2): 274–80. doi:10.1016/j.colsurfb.2008.07.004.
- Sparreboom, Alex, Charity D Scripture, Vuong Trieu, Paul J Williams, Tapas De, Andrew Yang, Bridget Beals, William D Figg, Michael Hawkins, and Neil Desai. 2005. "Comparative Preclinical and Clinical Pharmacokinetics of a Cremophor-Free, Nanoparticle Albumin-Bound Paclitaxel (ABI-007) and Paclitaxel Formulated in Cremophor (Taxol)." *Clinical Cancer Research* 11 (11): 4136–43. doi:10.1158/1078-0432.CCR-04-2291.
- Steinman, Lawrence. 2005. "Blocking Adhesion Molecules as Therapy for Multiple Sclerosis: Natalizumab." *Nature Reviews. Drug Discovery* 4 (6): 510–18. doi:10.1038/nrd1752.
- . 2009. "A Molecular Trio in Relapse and Remission in Multiple Sclerosis." *Nature Reviews. Immunology* 9 (6): 440–47. doi:10.1038/nri2548.
- Stewart, B W, and C P Wild. 2014. "World Cancer Report 2014." *World Health Organization*, 1–2. doi:9283204298.
- Stolzenberg-Solomon, Rachael Z, Barry I Graubard, Suresh Chari, Paul Limburg, Philip R Taylor, Jarmo Virtamo, and Demetrius Albanes. 2005. "Insulin, Glucose, Insulin Resistance, and Pancreatic Cancer in Male Smokers." *JAMA* 294 (22): 2872–78. doi:10.1001/jama.294.22.2872.

- Strachan, T. 1999. *Human Molecular Genetics*.
- Stromnes, Ingunn M, and Joan M Goverman. 2007. "Osteopontin-Induced Survival of T Cells." *Nature Immunology* 8 (1): 19–20. doi:10.1038/ni0107-19.
- Subbiah, R, M Veerapandian, and K S. Yun. 2010. "Nanoparticles: Functionalization and Multifunctional Applications in Biomedical Sciences." *Current Medicinal Chemistry* 17 (36): 4559–77. doi:10.2174/092986710794183024.
- Suppasansatorn, Panassaya, Guocheng Wang, Barbara R Conway, Weidong Wang, and Yongfeng Wang. 2006. "Skin Delivery Potency and Antitumor Activities of Temozolomide Ester Prodrugs." *Cancer Letters* 244 (1): 42–52. doi:10.1016/j.canlet.2005.11.029.
- Surapaneni, Madhu S, Sudip K Das, and Nandita G Das. 2012. "Designing Paclitaxel Drug Delivery Systems Aimed at Improved Patient Outcomes: Current Status and Challenges." *ISRN Pharmacology* 2012: 623139. doi:10.5402/2012/623139.
- Svenson, Sönke, and Donald A Tomalia. 2012. "Dendrimers in Biomedical Applications–Reflections on the Field." *Advanced Drug Delivery Reviews*. doi:10.1016/j.addr.2012.09.030.
- Swaminathan, Shankar, Roberta Cavalli, and Francesco Trotta. 2016. "Cyclodextrin-Based Nanosponges: A Versatile Platform for Cancer Nanotherapeutics Development." *Wiley Interdisciplinary Reviews: Nanomedicine and Nanobiotechnology*. doi:10.1002/wnan.1384.
- Swaminathan, Shankar, Linda Pastero, Loredana Serpe, Francesco Trotta, Pradeep Vavia, Dino Aquilano, Michele Trotta, GianPaolo Zara, and Roberta Cavalli. 2010. "Cyclodextrin-Based Nanosponges Encapsulating Camptothecin: Physicochemical Characterization, Stability and Cytotoxicity." *European Journal of Pharmaceutics and Biopharmaceutics* 74 (2): 193–201. doi:10.1016/j.ejpb.2009.11.003.
- Takahashi, Fumiyouki, Shigeru Akutagawa, Hisao Fukumoto, Shoji Tsukiyama, Yuichiro Ohe, Kazuhisa Takahashi, Yoshinosuke Fukuchi, Nagahiro Saijo, and Kazuto Nishio. 2002. "Osteopontin Induces Angiogenesis of Murine Neuroblastoma Cells in Mice." *International Journal of Cancer* 98 (5): 707–12. doi:10.1002/ijc.10261.
- Takemura, Genzou, and Hisayoshi Fujiwara. n.d. "Doxorubicin-Induced Cardiomyopathy from the Cardiotoxic Mechanisms to Management." *Progress in Cardiovascular Diseases* 49 (5): 330–52. doi:10.1016/j.pcad.2006.10.002.
- Takimoto, C H, J Wright, and S G Arbutk. 1998. "Clinical Applications of the

- Camptothecins." *Biochimica et Biophysica Acta* 1400 (1–3): 107–19.
<http://www.ncbi.nlm.nih.gov/pubmed/9748525>.
- Tarin, David. 2011. "Cell and Tissue Interactions in Carcinogenesis and Metastasis and Their Clinical Significance." *Seminars in Cancer Biology*. doi:10.1016/j.semcancer.2010.12.006.
- Taverna, Simona, Anna Flugy, Laura Saieva, Elise C Kohn, Alessandra Santoro, Serena Meraviglia, Giacomo De Leo, and Riccardo Alessandro. 2012. "Role of Exosomes Released by Chronic Myelogenous Leukemia Cells in Angiogenesis." *International Journal of Cancer* 130 (9): 2033–43. doi:10.1002/ijc.26217.
- Thalmann, G N, R A Sikes, R E Devoll, J A Kiefer, R Markwalder, I Klima, C M Farach-Carson, U E Studer, and L W Chung. 1999. "Osteopontin: Possible Role in Prostate Cancer Progression." *Clinical Cancer Research : An Official Journal of the American Association for Cancer Research* 5 (8): 2271–77. <http://www.ncbi.nlm.nih.gov/pubmed/10473115>.
- Théry, Clotilde, Sebastian Amigorena, Graça Raposo, and Aled Clayton. 2006. "Isolation and Characterization of Exosomes from Cell Culture Supernatants and Biological Fluids." *Current Protocols in Cell Biology* Chapter 3 (April): Unit 3.22. doi:10.1002/0471143030.cb0322s30.
- Théry, Clotilde, Matias Ostrowski, and Elodie Segura. 2009. "Membrane Vesicles as Conveyors of Immune Responses." *Nature Reviews. Immunology* 9 (8): 581–93. doi:10.1038/nri2567.
- Tian, Tian, Yuanyuan Wang, Haitao Wang, Zhaoqi Zhu, and Zhongdang Xiao. 2010. "Visualizing of the Cellular Uptake and Intracellular Trafficking of Exosomes by Live-Cell Microscopy." *Journal of Cellular Biochemistry* 111 (2): 488–96. doi:10.1002/jcb.22733.
- Tiwari, Ruchi Tiwari, Birendra Sriwastawa, L Bhati, S Pandey, P Pandey, and Saurabh K Bannerjee. 2012. "Drug Delivery Systems: An Updated Review." *International Journal of Pharmaceutical Investigation* 2 (1): 2. doi:10.4103/2230-973X.96920.
- Tomalia, D A, L A Reyna, and S Svenson. 2007. "Dendrimers as Multi-Purpose Nanodevices for Oncology Drug Delivery and Diagnostic Imaging." *Biochemical Society Transactions* 35 (1): 61–67. doi:10.1042/BST0350061.
- Torchilin, Vladimir P. 2005. "Recent Advances with Liposomes as Pharmaceutical Carriers." *Nature Reviews. Drug Discovery* 4 (2): 145–60. doi:10.1038/nrd1632.
- Trams, Eberhard G., Carl J. Lauter, Jr. Norman Salem, and Ursula Heine. 1981. "Exfoliation of Membrane Ecto-Enzymes in the Form of Micro-Vesicles." *Biochimica et Biophysica Acta (BBA) - Biomembranes* 645 (1): 63–70.

doi:10.1016/0005-2736(81)90512-5.

- Treps, L, S Edmond, E Harford-Wright, E M Galan-Moya, A Schmitt, S Azzi, A Citerne, N Bidère, D Ricard, and J Gavard. 2016. "Extracellular Vesicle-Transported Semaphorin3A Promotes Vascular Permeability in Glioblastoma." *Oncogene* 35 (20): 2615–23. doi:10.1038/onc.2015.317.
- Trotta, Francesco. 2011. "Cyclodextrin Nanosponges and Their Applications." In *Cyclodextrins in Pharmaceuticals, Cosmetics, and Biomedicine*, 323–42. Hoboken, NJ, USA: John Wiley & Sons, Inc. doi:10.1002/9780470926819.ch17.
- Trotta, Francesco, Fabrizio Caldera, Chiara Dianzani, Monica Argenziano, Giuseppina Barrera, and Roberta Cavalli. 2016. "Glutathione Bioresponsive Cyclodextrin Nanosponges." *ChemPlusChem* 81 (5): 439–43. doi:10.1002/cplu.201500531.
- Trotta, Francesco, Chiara Dianzani, Fabrizio Caldera, Barbara Mognetti, and Roberta Cavalli. 2014. "The Application of Nanosponges to Cancer Drug Delivery." *Expert Opinion on Drug Delivery* 11 (6): 931–41. doi:10.1517/17425247.2014.911729.
- Trotta, Francesco, Marco Zanetti, and Roberta Cavalli. 2012. "Cyclodextrin-Based Nanosponges as Drug Carriers." *Beilstein Journal of Organic Chemistry* 8 (November): 2091–99. doi:10.3762/bjoc.8.235.
- Tuck, A B, and A F Chambers. 2001. "The Role of Osteopontin in Breast Cancer: Clinical and Experimental Studies." *Journal of Mammary Gland Biology and Neoplasia* 6 (4): 419–29. <http://www.ncbi.nlm.nih.gov/pubmed/12013531>.
- Tuck, A B, B E Elliott, C Hota, E Tremblay, and A F Chambers. 2000. "Osteopontin-Induced, Integrin-Dependent Migration of Human Mammary Epithelial Cells Involves Activation of the Hepatocyte Growth Factor Receptor (Met)." *Journal of Cellular Biochemistry* 78 (3): 465–75. <http://www.ncbi.nlm.nih.gov/pubmed/10861844>.
- Tuck, Alan B, Denise M Arsenault, Frances P O'Malley, Charulata Hota, Michael C Ling, Sylvia M Wilson, and Ann F Chambers. 1999. "Osteopontin Induces Increased Invasiveness and Plasminogen Activator Expression of Human Mammary Epithelial Cells." *Oncogene* 18 (29): 4237–46. doi:10.1038/sj.onc.1202799.
- Tuck, Alan B, Charulata Hota, Sylvia M Wilson, and Ann F Chambers. 2003. "Osteopontin-Induced Migration of Human Mammary Epithelial Cells Involves Activation of EGF Receptor and Multiple Signal Transduction Pathways." *Oncogene* 22 (8): 1198–1205. doi:10.1038/sj.onc.1206209.
- Urosevic, Jelena, Xabier Garcia-Albéniz, Evarist Planet, Sebastián Real, María

- Virtudes Céspedes, Marc Guiu, Esther Fernandez, et al. 2014. "Colon Cancer Cells Colonize the Lung from Established Liver Metastases through p38 MAPK Signalling and PTHLH." *Nature Cell Biology* 16 (7): 685–94. doi:10.1038/ncb2977.
- Urruticoechea, a, R Alemany, J Balart, a Villanueva, F Viñals, and G Capellá. 2010. "Recent Advances in Cancer Therapy: An Overview." *Current Pharmaceutical Design* 16: 3–10. doi:10.2174/138161210789941847.
- Vaschetto, Rosanna, Stefania Nicola, Carlo Olivieri, Elena Boggio, Fabio Piccolella, Riccardo Mesturini, Federica Damnotti, et al. 2008. "Serum Levels of Osteopontin Are Increased in SIRS and Sepsis." *Intensive Care Medicine* 34 (12): 2176–84. doi:10.1007/s00134-008-1268-4.
- Vavia PR, Swaminathan S., Trotta F, Cavalli R. 2006. "Applications of Nanosponges in Drug Delivery." In , 14–17.
- Vella, LJ, RA Sharples, VA Lawson, CL Masters, R Cappai, and AF Hill. 2007. "Packaging of Prions into Exosomes Is Associated with a Novel Pathway of PrP Processing." *The Journal of Pathology* 211 (5): 582–90. doi:10.1002/path.2145.
- Vemuri, Sriram, and C T Rhodes. 1995. "Preparation and Characterization of Liposomes as Therapeutic Delivery Systems: A Review." *Pharmaceutica Acta Helveticae*. doi:10.1016/0031-6865(95)00010-7.
- Venditto, Vincent J, and Eric E Simanek. 2010. "Cancer Therapies Utilizing the Camptothecins: A Review of the in Vivo Literature." *Molecular Pharmaceutics* 7 (2): 307–49. doi:10.1021/mp900243b.
- Voges, D, P Zwickl, and W Baumeister. 1999. "The 26S Proteasome: A Molecular Machine Designed for Controlled Proteolysis." *Annual Review of Biochemistry* 68: 1015–68. doi:10.1146/annurev.biochem.68.1.1015.
- Vogt, Mario H J, Luba Lopatinskaya, Monique Smits, Chris H Polman, and Lex Nagelkerken. 2003. "Elevated Osteopontin Levels in Active Relapsing-Remitting Multiple Sclerosis." *Annals of Neurology* 53 (6): 819–22. doi:10.1002/ana.10606.
- Walsh, Gary. 2014. "Biopharmaceutical Benchmarks 2014." *Nature Biotechnology* 32 (10): 992–1000. doi:10.1038/nbt.3040.
- Warshaw, A L, and C Fernández-del Castillo. 1992. "Pancreatic Carcinoma." *The New England Journal of Medicine* 326 (7): 455–65. doi:10.1056/NEJM199202133260706.
- Webber, J P, L K Spary, A J Sanders, R Chowdhury, W G Jiang, R Steadman, J Wymant, et al. 2015. "Differentiation of Tumour-Promoting Stromal Myofibroblasts by Cancer Exosomes." *Oncogene* 34 (3): 290–302. doi:10.1038/onc.2013.560.

- Weber, Georg F. 2008. "Molecular Mechanisms of Metastasis." *Cancer Letters* 270 (2): 181–90. doi:10.1016/j.canlet.2008.04.030.
- Weber, Jeffrey S, Sandra P D'Angelo, David Minor, F Stephen Hodi, Ralf Gutzmer, Bart Neyns, Christoph Hoeller, et al. 2015. "Nivolumab versus Chemotherapy in Patients with Advanced Melanoma Who Progressed after Anti-CTLA-4 Treatment (CheckMate 037): A Randomised, Controlled, Open-Label, Phase 3 Trial." *The Lancet. Oncology* 16 (4): 375–84. doi:10.1016/S1470-2045(15)70076-8.
- Weichselbaum, Ralph R, and Donald Kufe. 1997. "Gene Therapy of Cancer." *The Lancet* 349 (May): S10–12. doi:10.1016/S0140-6736(97)90013-1.
- Whitcomb, D C, M C Gorry, R A Preston, W Furey, M J Sossenheimer, C D Ulrich, S P Martin, et al. 1996. "Hereditary Pancreatitis Is Caused by a Mutation in the Cationic Trypsinogen Gene." *Nature Genetics* 14 (2): 141–45. doi:10.1038/ng1096-141.
- Wilson, Heather L, Sheila E Francis, Steven K Dower, and David C Crossman. 2004. "Secretion of Intracellular IL-1 Receptor Antagonist (Type 1) Is Dependent on P2X7 Receptor Activation." *Journal of Immunology (Baltimore, Md. : 1950)* 173 (2): 1202–8. <http://www.ncbi.nlm.nih.gov/pubmed/15240711>.
- Wolinsky, Jesse B, and Mark W Grinstaff. 2008. "Therapeutic and Diagnostic Applications of Dendrimers for Cancer Treatment." *Advanced Drug Delivery Reviews* 60 (9): 1037–55. doi:10.1016/j.addr.2008.02.012.
- Wollert, Thomas, and James H. Hurley. 2010. "Molecular Mechanism of Multivesicular Body Biogenesis by ESCRT Complexes." *Nature* 464 (7290): 864–69. doi:10.1038/nature08849.
- Wung, John K, George Perry, Aaron Kowalski, Peggy L R Harris, Glenda M Bishop, Mehul A Trivedi, Sterling C Johnson, Mark A Smith, David T Denhardt, and Craig S Atwood. 2007. "Increased Expression of the Remodeling- and Tumorigenic-Associated Factor Osteopontin in Pyramidal Neurons of the Alzheimer's Disease Brain." *Current Alzheimer Research* 4 (1): 67–72. <http://www.ncbi.nlm.nih.gov/pubmed/17316167>.
- Yamaguchi, Hideki, Jeffrey Wyckoff, and John Condeelis. 2005. "Cell Migration in Tumors." *Current Opinion in Cell Biology*. doi:10.1016/j.ceb.2005.08.002.
- Yamaguchi, Yasuto, Zhifei Shao, Shadi Sharif, Xiao-Yan Du, Timothy Myles, Milton Merchant, Griffith Harsh, et al. 2013. "Thrombin-Cleaved Fragments of Osteopontin Are Overexpressed in Malignant Glial Tumors and Provide a Molecular Niche with Survival Advantage." *The Journal of Biological Chemistry* 288 (5): 3097–3111. doi:10.1074/jbc.M112.362954.

- Yang, Jing, and Robert A Weinberg. 2008. "Epithelial-Mesenchymal Transition: At the Crossroads of Development and Tumor Metastasis." *Developmental Cell* 14 (6): 818–29. doi:10.1016/j.devcel.2008.05.009.
- Yano, Junichi, Kazuko Hirabayashi, Shin-Ichiro Nakagawa, Tohru Yamaguchi, Masaki Nogawa, Isao Kashimori, Haruna Naito, et al. 2004. "Antitumor Activity of Small Interfering RNA/cationic Liposome Complex in Mouse Models of Cancer." *Clinical Cancer Research : An Official Journal of the American Association for Cancer Research* 10 (22): 7721–26. doi:10.1158/1078-0432.CCR-04-1049.
- Yarden, Y, and M X Sliwkowski. 2001. "Untangling the ErbB Signalling Network." *Nature Reviews. Molecular Cell Biology* 2 (2): 127–37. doi:10.1038/35052073.
- Yednock, T A, C Cannon, L C Fritz, F Sanchez-Madrid, L Steinman, and N Karin. 1992. "Prevention of Experimental Autoimmune Encephalomyelitis by Antibodies against Alpha 4 Beta 1 Integrin." *Nature* 356 (6364): 63–66. doi:10.1038/356063a0.
- Yokasaki, Y, and D Sheppard. 2000. "Mapping of the Cryptic Integrin-Binding Site in Osteopontin Suggests a New Mechanism by Which Thrombin Can Regulate Inflammation and Tissue Repair." *Trends in Cardiovascular Medicine* 10 (4): 155–59. <http://www.ncbi.nlm.nih.gov/pubmed/11239795>.
- Yokosaki, Y, M Kido, N Nagata, Y Nikaido, T Tsuda, J Miyake, and H Manabe. 1995. "Hypoglycemia Associated with Localized Fibrous Mesothelioma of the Pleura." *Journal of UOEH* 17 (3): 191–97. <http://www.ncbi.nlm.nih.gov/pubmed/7569471>.
- Yu, Lili, Lin Yao, and Kuan Yang. 2016. "Redox- and pH-Responsive Hydrogels: Formulation and Controlled Drug Delivery." *Journal of Porous Materials* 23 (6): 1581–89. doi:10.1007/s10934-016-0219-7.
- Zhang, L, D Pornpattananangkul, C.-M. Hu, and C.-M. Huang. 2010. "Development of Nanoparticles for Antimicrobial Drug Delivery." *Current Medicinal Chemistry* 17 (6): 585–94. doi:10.2174/092986710790416290.
- Zhang, Liangfang, and Steve Granick. 2006. "How to Stabilize Phospholipid Liposomes (Using Nanoparticles)." *Nano Letters*. doi:10.1021/nl052455y.
- Zhang, Li, and Na Zhang. 2013. "How Nanotechnology Can Enhance Docetaxel Therapy." *International Journal of Nanomedicine* 8: 2927–41. doi:10.2147/IJN.S46921.
- Zheng, Jianzheng, Anushka Dasgupta, and Oscar A Bizzozero. 2012. "Changes in 20S Subunit Composition Are Largely Responsible for Altered Proteasomal Activities in Experimental Autoimmune Encephalomyelitis."

Journal of Neurochemistry 121 (3): 486–94. doi:10.1111/j.1471-4159.2012.07699.x.

- Zhou, Youwen, Derek L Dai, Magdalena Martinka, Mingwan Su, Yi Zhang, Eric I Campos, Irene Dorocicz, et al. 2005. "Osteopontin Expression Correlates with Melanoma Invasion." *The Journal of Investigative Dermatology* 124 (5): 1044–52. doi:10.1111/j.0022-202X.2005.23680.x.
- Zhu, Baoqian, Keiko Suzuki, Harvey A Goldberg, Susan R Rittling, David T Denhardt, Christopher A G McCulloch, and Jaro Sodek. 2004. "Osteopontin Modulates CD44-Dependent Chemotaxis of Peritoneal Macrophages through G-Protein-Coupled Receptors: Evidence of a Role for an Intracellular Form of Osteopontin." *Journal of Cellular Physiology* 198 (1): 155–67. doi:10.1002/jcp.10394.
- Zoeger, Annette, Michael Blau, Karl Egerer, Eugen Feist, and Burkhardt Dahlmann. 2006. "Circulating Proteasomes Are Functional and Have a Subtype Pattern Distinct from 20S Proteasomes in Major Blood Cells." *Clinical Chemistry* 52 (11): 2079–86. doi:10.1373/clinchem.2006.072496.
- Zohar, R, N Suzuki, K Suzuki, P Arora, M Glogauer, C A McCulloch, and J Sodek. 2000. "Intracellular Osteopontin Is an Integral Component of the CD44-ERM Complex Involved in Cell Migration." *Journal of Cellular Physiology* 184 (1): 118–30. doi:10.1002/(SICI)1097-4652(200007)184:1<118::AID-JCP13>3.0.CO;2-Y.

Acknowledgments

During the PhD academic period at department of pharmacology of Turin, I could improve my scientific knowledge, becoming confident with the research approach and constantly learning how to develop a project in this field.

I could appreciate the laboratory life, the work in a research group and the relationships with the colleagues, both in science and life.

I would like to thank Dr Chiara Dianzani, since she was responsible of my growth in the research and laboratory life. She taught me how to manage in the scientific world and how to greatly appreciate our work, with constance, interest and passion.

I would also thank Prof Roberto Fantozzi, who helped me at growing in the pharmacological field.

I also would thank all the people working in the laboratory of pharmacology: researchers, PhD students, fellows and undergraduated students. I really enjoyed working in such a warm and friendly environment.

I would thank the CRRET laboratory at UPEC, where I spent 6 months of my PhD under the supervision of Prof Josè Courty, since it was a very exciting research period, in which I could really improve my experience enjoying the abroad life.

Finally, I would thank my family, that gave me all the necessary support to realize my objectives, helping me in every situation and being always present for me.

I would thank Fausto, who supported me with experience and patience, both in work and life.

I also thank my friends, who were always near me during this great period of my life.